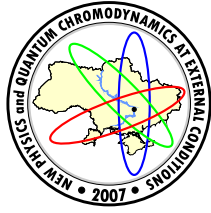


# Contents

<b>Plenary Talks</b>	5
<i>Bordag M., Skalozub V.</i>	
One-loop gluon polarization tensor in color magnetic background at finite temperature .....	6
<i>Borisenko O.</i>	
Deconfinement phase transition in 3D $U(1)$ LGT .....	17
<i>Faber M., Jordan G., Höllwieser R.</i>	
Topology, Center Vortices, Confinement and Chiral Symmetry Breaking in $SU(2)$ Lattice-QCD .....	27
<i>Ilgenfritz E.-M.</i>	
Confinement encoded in Landau gauge gluon and ghost propagators .....	38
<i>Korchin A.Yu., Ivashyn S.A.</i>	
$K$ -meson production in electron-positron annihilation .....	48
<i>Pankov A.A., Tsytrinov A.V.</i>	
Indirect collider tests for large extra dimensions .....	58
<i>Polikarpov M.I.</i>	
Confinement on the lattice, numerical results and theory .....	66
<i>Sinyukov Yu.M., Karpenko Iu., Nazarenko A.V.</i>	
Interferometry analysis and initial conditions in A+A collisions .....	75
<i>Shishkina T.V.</i>	
Search for effects beyond the Standard Model in photon scatterings and in nonminimal gauge theories on linear colliders of new generation .....	86
<i>Shul'ga N.F., Tyutyunnik D.N.</i>	
Coherent Effects in Radiation at Collisions of Short Bunches of High Energy Particles .....	99
<i>Vysotsky M.I.</i>	
New (virtual) physics in the era of the LHC .....	104
<b>Section Talks</b> 107	
<i>Anchishkin D.V.</i>	
Annihilation Mechanism of Dilepton Production in Relativistic Heavy-Ion Collisions: Granular Fireball	108
<i>Bugaev K.A.</i>	
The Role of Surface Tension for the Equation of State of Quark-Gluon Bags .....	115
<i>Demchik V.I., Skalozub V.V.</i>	
The spontaneous generation of magnetic field at high temperature on a lattice .....	124
<i>Ferludin A., Khandoga N., Skalozub V.</i>	
The Green function of neutral gluons in color magnetic background field at finite temperature .....	130
<i>Gulov A.V., Skalozub V.V.</i>	
$Z'$ signals from the LEP2 data .....	136
<i>Kokoulin E.S., Kutov A.</i>	
Multiparticle production at high multiplicities .....	142
<i>Kulikov D.A., Tutik R.S.</i>	
Relativistic wave equation for one spin-1/2 and one spin-0 particle .....	148
<i>Kulikov D.A., Tutik R.S., Yaroshenko A.P.</i>	
Wave functions of the relativistic three-body oscillator constructed with the extension of the $SL(2, C)$ group .....	152
<i>Molodtsov S.V., Dorokhov A.E., Zinovjev G.M.</i>	
Gluon condensate behaviour at filling the Fermi sphere up .....	157
<i>Molodtsov S.V., Zinovjev G.M.</i>	
Towards screening of color field in instanton liquid .....	168
<i>Nurmagambetov A.J.</i>	
Strings and QCD: Problems and perspectives .....	179
<i>Sevbitov S.N., Shishkina T.V.</i>	
Study of weak charged current polarized lepton-nucleon deep inelastic scattering .....	186

<i>Skalozub V.V., Demchik V.I.</i>	
Electroweak phase transition in a hypermagnetic field .....	191
<i>Sokolovsky A.I., Stupka A.A.</i>	
Electrodynamics of continuous media taking into account correlations of electromagnetic field .....	194
<i>Solovtsov I.L.</i>	
Nonperturbative calculations in QCD .....	200
<i>Solovtsova O.P.</i>	
Advantages of APT in QCD study of hadronic tau decays .....	209
<i>Strelchenko A.</i>	
On the one-loop renormalization of noncommutative gauge theories .....	217
<i>Tutik R.S., Dobrovolska I.V.</i>	
The logarithmic perturbation theory for bound states in spherical-symmetric potentials via the $\hbar$ -expansions .....	223
<i>Vanyashin V.S.</i>	
Plasma photons are able to emit axions .....	230
<i>Voloshin S., Borisenko O.</i>	
Monopole contribution to the Wilson loop in the 3D $SU(2)$ lattice gauge model .....	231

## Plenary Talks



## ONE-LOOP GLUON POLARIZATION TENSOR IN COLOR MAGNETIC BACKGROUND AT FINITE TEMPERATURE

M. Bordag<sup>\*,a</sup>, V. Skalozub<sup>‡,b</sup>

<sup>\*</sup>University of Leipzig, Institute for Theoretical Physics, Leipzig, Germany

<sup>‡</sup>Dnipropetrovsk National University, Dnipropetrovsk, Ukraine

In the framework of SU(2) gluodynamics, we derive the tensor structure of the charged gluon polarization tensor in an Abelian homogeneous magnetic field at finite temperature and calculate it in one-loop approximation in the Lorentz background field gauge. The imaginary time formalism and the Schwinger operator method are used. The polarization tensor turns out to be non transversal. It can be written as a sum of ten tensor structures with corresponding form factors. We represent the form factors in terms of double parametric integrals and the temperature sum which can be computed numerically. As applications we calculate the Debye mass of charged gluons in the background field at high temperature.

### 1 Introduction

The investigations of QCD at high temperature carried out in recent years have elucidated an important role of color magnetic fields. In Refs. [1, 2] it was discovered in lattice simulations that sufficiently strong constant Abelian magnetic fields described by the potential of the form  $A_\mu^a = B\delta_{\mu 2}\delta^{a3}$ , where  $B$  is field strength,  $a$  is the index of internal symmetry,  $\mu$  – Lorentz index, shift the deconfinement phase transition temperature  $T_c$ . On the other hand, in Refs. [3, 4] from the analysis of lattice simulations and in Refs. [2, 6, 7] from perturbative resummations of daisy graphs in the background field at high temperature it was found that Abelian chromomagnetic fields of order  $gB \sim g^4T^2$ , where  $g$  is a the gauge coupling, are spontaneously created.

These results served as motivations for investigations began in our papers Refs.[8, 9], which goal is to determine the operator structure of the gluon polarization tensor in the constant Abelian chromomagnetic background field at finite temperature. This is necessary for investigations of the quark-gluon plasma (QGP), first of all, when resummations of perturbative series are carried out.

In the presence of the background field, for many reasons it is convenient to use the decomposition of gauge fields in the internal space of the form  $W_\mu^\pm = 1/\sqrt{2}(A^1 \pm iA_\pm^2)$ ,  $A_\mu = A_\mu^3$  and consider the former “charged” and the latter “neutral” gluons separately because of sufficiently different properties of them. That concerns not only physics but also the calculation procedures required for investigations. In recent paper Ref. [10] a detailed investigation of the neutral gluons has been done. The tensor structure of the gluon polarization tensor (PT) as well as the one-loop contributions to its form factors at zero and finite temperature have been obtained and partially investigated therein.

As the next step the investigation of the charged gluon case is in order. This is the goal of the present report. We determine the tensor structure of the charged gluon PT at finite temperature in the constant Abelian background field and calculate it in one-loop approximation. The PT consists of ten tensors and corresponding form factors. In actual one-loop calculations the Feynman-Lorentz background field gauge is used. We calculate the form factors as the two parametric integrals over the proper time variables and the Matsubara temperature sum. This representation is convenient for numeric investigations and asymptotic expansions. As an application of the results obtained we compute the Debye mass of charged gluons in the background field at high temperature.

### 2 Basic notations

We start from the operator structures  $T_{\lambda\lambda'}^{(i)}$  which are allowed by the weak transversality condition,

$$p_\lambda T_{\lambda\lambda'}^{(i)} p_{\lambda'} = 0 , \quad (1)$$

which follows from the corresponding relation the PT has to obey. These structures appear in the expansion in terms of form factors which will be given below.

e-mail: <sup>a</sup>michael.bordag@itp.uni-leipzig.de; <sup>b</sup>skalozub@dsu.dp.ua

© Bordag M., Skalozub V., 2007.

In the magnetic background field, the polarization tensor can be constructed out of the vectors  $l_\mu$ ,  $h_\mu$  and  $d_\mu$ ,

$$l_\mu = \begin{pmatrix} 0 \\ 0 \\ p_3 \\ p_4 \end{pmatrix}, \quad h_\mu = \begin{pmatrix} p_1 \\ p_2 \\ 0 \\ 0 \end{pmatrix}, \quad d_\mu = \begin{pmatrix} p_2 \\ -p_1 \\ 0 \\ 0 \end{pmatrix}, \quad (2)$$

where the third vector is  $d_\mu = F_{\mu\nu}p_\nu$  and we note  $p_\lambda = l_\lambda + h_\lambda$ , and the matrixes

$$\delta_{\mu\lambda}^{||} = \begin{pmatrix} 0 & 0 & 0 & 0 \\ 0 & 0 & 0 & 0 \\ 0 & 0 & 1 & 0 \\ 0 & 0 & 0 & 1 \end{pmatrix}, \quad \delta_{\mu\lambda}^\perp = \begin{pmatrix} 1 & 0 & 0 & 0 \\ 0 & 1 & 0 & 0 \\ 0 & 0 & 0 & 0 \\ 0 & 0 & 0 & 0 \end{pmatrix}, \quad F_{\mu\lambda} = \begin{pmatrix} 0 & 1 & 0 & 0 \\ -1 & 0 & 0 & 0 \\ 0 & 0 & 0 & 0 \\ 0 & 0 & 0 & 0 \end{pmatrix}. \quad (3)$$

Hence, the operator structures can also be constructed out of these quantities only. Further, for dimensional reasons the structures can be at most quadratic in the momenta and the following PT must be Hermite. Writing down all the allowed combinations, the set of linear independent ones is

$$\begin{aligned} T_{\lambda\lambda'}^{(1)} &= l^2 \delta_{\lambda\lambda'}^{||} - l_\lambda l_{\lambda'}, & T_{\lambda\lambda'}^{(2)} &= h^2 \delta_{\lambda\lambda'}^\perp + 2iF_{\lambda\lambda'} - h_\lambda h_{\lambda'} = d_\lambda d_{\lambda'} + iF_{\lambda\lambda'} \\ T_{\lambda\lambda'}^{(3)} &= h^2 \delta_{\lambda\lambda'}^{||} + l^2 \delta_{\lambda\lambda'}^\perp - l_\lambda h_{\lambda'} - h_\lambda l_{\lambda'}, & T_{\lambda\lambda'}^{(4)} &= i(l_\lambda d_{\lambda'} - d_\lambda l_{\lambda'}) + il^2 F_{\lambda\lambda'} - \delta_{\lambda\lambda'}^{||} \\ T_{\lambda\lambda'}^{(5)} &= h^2 \delta_{\lambda\lambda'}^{||} - l^2 \delta_{\lambda\lambda'}^\perp, & T_{\lambda\lambda'}^{(6a)} &= \delta_{\lambda\lambda'}^{||} + l^2 iF_{\lambda\lambda'}, & T_{\lambda\lambda'}^{(6b)} &= 3\delta_{\lambda\lambda'}^\perp + h^2 iF_{\lambda\lambda'}, \end{aligned} \quad (4)$$

where also the identity  $i(d_\lambda h_{\lambda'} - h_\lambda d_{\lambda'}) = ih^2 F_{\lambda\lambda'} + \delta_{\lambda\lambda'}^\perp$  was used. In our previous paper [8] we mentioned instead of the two structures  $T_{\lambda\lambda'}^{(6a)}$  and  $T_{\lambda\lambda'}^{(6b)}$  only their sum,

$$T_{\lambda\lambda'}^{(6)} = T_{\lambda\lambda'}^{(6a)} + T_{\lambda\lambda'}^{(6b)}. \quad (5)$$

In the end it will turn out that for the considered one-loop contribution this is sufficient. However, for the calculations in this section it is convenient to keep temporarily separately both,  $T_{\lambda\lambda'}^{(6a)}$  and  $T_{\lambda\lambda'}^{(6b)}$ .

Another remark on the properties of the structures  $T_{\lambda\lambda'}^{(i)}$  is that the first four are transversal,  $p_\lambda T_{\lambda\lambda'}^{(i)} = T_{\lambda\lambda'}^{(i)} p_{\lambda'} = 0$  holds for  $i = 1, 2, 3, 4$  in addition to (1). The first three structures are just a decomposition of the kernel of the quadratic part of the action, Eq. (24) in [8],

$$T_{\lambda\lambda'}^{(1)} + T_{\lambda\lambda'}^{(2)} + T_{\lambda\lambda'}^{(3)} = K_{\lambda\lambda'}(p). \quad (6)$$

In the case of finite temperature, in addition to the magnetic field, we have to account also for the vector  $u_\lambda$  which describes the speed of the heat bath. In the following we assume it to be orthogonal to  $h_\lambda$ . In fact we use  $u_\lambda = (0, 0, 0, 1)$ . With this vector additional tensor structures obeying the weak transversality condition (1) can be constructed,

$$\begin{aligned} T_{\lambda\lambda'}^{(7)} &= (u_\lambda l_{\lambda'} + l_\lambda u_{\lambda'}) (up) - \delta_{\lambda\lambda'}^{||} (up)^2 - u_\lambda u_{\lambda'} l^2, \\ T_{\lambda\lambda'}^{(8)} &= (u_\lambda h_{\lambda'} + h_\lambda u_{\lambda'}) (up) - \delta_{\lambda\lambda'}^\perp (up)^2 - u_\lambda u_{\lambda'} h^2, \\ T_{\lambda\lambda'}^{(9)} &= u_\lambda i d_{\lambda'} - i d_\lambda u_{\lambda'} + 2iF_{\lambda\lambda'} (up), \\ T_{\lambda\lambda'}^{(10a)} &= \delta_{\lambda\lambda'}^{||} (up)^2 - u_\lambda u_{\lambda'} l^2, \quad T_{\lambda\lambda'}^{(10b)} = \delta_{\lambda\lambda'}^\perp (up)^2 - u_\lambda u_{\lambda'} h^2. \end{aligned} \quad (7)$$

These structures are linear independent. Below, however, it will turn out that  $T^{(10a)}$  and  $T^{(10b)}$  appear at the one-loop level which we consider here only in intermediate steps and drop out from the final result.

In addition to (7) there exists a further structure,

$$T_{\lambda\lambda'}^D = u_\lambda u_{\lambda'} \quad (8)$$

which fulfills (1) for  $p_4 = 0$  (in an obvious, trivial way). Having in mind that the condition (1) holds only if the external moment  $p$  of the polarization tensor fits into the Matsubara formalism, i.e., if it is given by  $p_4 = 2\pi Tl$  ( $l$  integer) than (9) makes sense as a structure being present for  $l = 0$  only (or, formally, being proportional to  $\delta_{l,0}$ ). It is just this structure which delivers the Debye mass term. It must be mentioned that  $T_{\lambda\lambda'}^D$  is contained as special case also in  $T_{\lambda\lambda'}^{(8)}$ ,  $T_{\lambda\lambda'}^{(9)}$ ,  $T_{\lambda\lambda'}^{(10a)}$  or in  $T_{\lambda\lambda'}^{(10b)}$  but due to its exceptional role it makes sense to keep it as separate contribution.

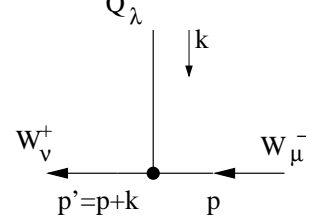
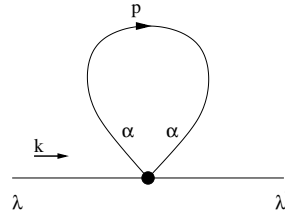
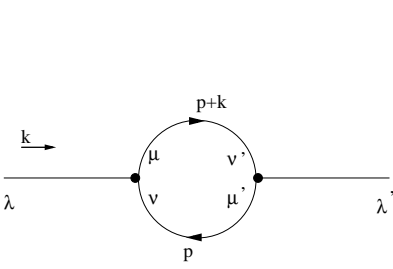


**Figure 1.** The basic Feynman graph for the polarization tensor.

Before writing down the expansion of the polarization tensor in terms of form factors we mention one property which follows directly from the basic commutator relation the momentum  $p_\mu$  obeys, namely  $p_\lambda p^2 = (p^2 \delta_{\lambda\lambda'} + 2iF_{\lambda\lambda'})p_{\lambda'}$ . As a consequence, for a function of  $p^2$  the relations

$$p_\lambda f(p^2) = f(p^2 + 2iF)_{\lambda\lambda'} p_{\lambda'}, \quad f(p^2) p_\lambda = p_{\lambda'} f(p^2 + 2iF)_{\lambda'\lambda} \quad (9)$$

hold where now  $f$  must be viewed as a function of a matrix so that it itself becomes a matrix carrying the indices  $\lambda$  and  $\lambda'$ . The same is true with  $h^2$  in place of  $p^2$ .

The decomposition of the polarization tensor can be written in the form

$$\Pi_{\lambda\lambda'}(p) = \sum_i \Pi^{(i)}(l^2, h^2 + 2iF)_{\lambda\lambda''} T_{\lambda''\lambda'}^{(i)} + \Pi^D T_{\lambda\lambda'}^D. \quad (10)$$

The sum includes in general all structures  $T_{\lambda\lambda'}^{(i)}$  defined in (4) and in (7). The form factors  $\Pi^{(i)}(l^2, h^2 + 2iF)_{\lambda\lambda'}$  depend on  $l^2$  and  $h^2$  only (besides their dependence on the matrices in (3)). In (10) the form factors can be placed also on the right from the operator structures applying both relations (9).

### 3 Calculation of the polarization tensor

The basic Feynman graph for the polarization tensor is shown in Fig. 1 and the notations of the vertex factors in Fig. 2. The analytic expression in momentum space reads

$$\begin{aligned} \Pi_{\lambda\lambda'}(p) = & \int \frac{dk}{(2\pi)^4} \{ \Gamma_{\lambda\nu\rho} G_{\nu\nu'}(p-k) \Gamma_{\lambda'\nu'\rho'} G_{\rho\rho'}(k) \\ & + (p-k)_\lambda G(p-k) k_{\lambda'} G(k) + k_\lambda G(p-k) (p-k)_{\lambda'} G(k) \} + \Pi_{\lambda\lambda'}^{\text{tadpol}}, \end{aligned} \quad (11)$$

where the second line results from the ghost contribution and the tadpole contribution is given by

$$\begin{aligned} \Pi^{\text{tadpol}} = & \int \frac{dk}{(2\pi)^4} \{ \delta_{\lambda\lambda'} G_{\rho\rho}(k) - G(k)_{\lambda\lambda'} \} \\ & + \int \frac{dp'}{(2\pi)^4} \{ \delta_{\lambda\lambda'} G_{\rho\rho}(p') + G_{\lambda'\lambda}(p') - 2G_{\lambda\lambda'}(p') \}. \end{aligned} \quad (12)$$

The vertex factor is

$$\Gamma_{\lambda\nu\rho} = (k-2p)_\rho \delta_{\lambda\nu} + \delta_{\rho\nu} (p-2k)_\lambda + \delta_{\rho\lambda} (p+k)_\nu. \quad (13)$$

For the following we rearrange it in the form

$$\begin{aligned} \Gamma_{\lambda\nu\rho} = & \underbrace{(p-2k)_\lambda \delta_{\nu\rho}}_{\Gamma_\lambda^{(1)}} + \underbrace{2(p_\nu \delta_{\lambda\rho} - p_\rho \delta_{\lambda\nu})}_{\Gamma_{\lambda\nu\rho}^{(2)}} + \underbrace{(-(p-k)_\nu \delta_{\lambda\rho} + k_\rho \delta_{\lambda\nu})}_{\Gamma_{\lambda\nu\rho}^{(3)}}, \end{aligned} \quad (14)$$

where  $\Gamma_{\lambda\nu\rho}^{(3)}$  will be temporary further subdivided into two parts,

$$\Gamma_{\lambda\nu\rho}^{(31)} = -(p-k)_\nu \delta_{\lambda\rho} \quad \text{and} \quad \Gamma_{\lambda\nu\rho}^{(32)} = k_\rho \delta_{\lambda\nu}. \quad (15)$$

The momentum integration in the polarization tensor is carried out using the formalism introduced by Schwinger, [11]. There the propagators (in Feynman gauge,  $\xi = 1$ ) are represented as parametric integrals,

$$G(p-k) = \int_0^\infty ds e^{-s(p-k)^2}, \quad G(k) = \int_0^\infty dt e^{-tk^2} \quad (16)$$

for the scalar lines and

$$G_{\nu\nu'}(p-k) = \int_0^\infty ds e^{-s(p-k)^2} E_{\nu\nu'}, \quad G_{\rho\rho'}(k) = \int_0^\infty dt e^{-tk^2} \delta_{\rho\rho'} \quad (17)$$

for the vector lines with

$$E_{\nu\nu'} \equiv e^{-2isF} = \delta_{\lambda\lambda'}^{||} - iF_{\lambda\lambda'} \sinh(2s) + \delta_{\lambda\lambda'}^{\perp} \cosh(2s). \quad (18)$$

In this formalism the momentum integration is written as an averaging procedure in some auxiliary space and for the basic exponential

$$\hat{\Theta} = e^{-s(p-k)^2} e^{-tk^2} \quad (19)$$

it holds

$$\int \frac{dk}{(2\pi)^4} \hat{\Theta} = \langle \hat{\Theta} \rangle = \Theta(l^2, h^2) \quad (20)$$

with

$$\Theta(l^2, h^2) = \frac{\exp[-H]}{(4\pi)^2(s+t)\sqrt{N}}, \quad (21)$$

which is the result of the corresponding calculations (see [11] for details). The following notations are used,

$$H = \frac{st}{s+t} l^2 + m(s, t) h^2 \quad (22)$$

and

$$m(s, t) \equiv s - \operatorname{arctanh} \frac{p}{q} = \frac{1}{2} \ln \frac{1+2t-e^{-2s}}{1-(1-2t)e^{-2s}} \quad (23)$$

as well as

$$N = (q^2 - p^2)/4 = t^2 + t \sinh(2s) + p/2 \quad (24)$$

with the notations

$$p = \cosh(2s) - 1, \quad q = 2t + \sinh(2s), \quad (25)$$

which will be met frequently in the following. With these notations the self energy graph for scalar lines becomes represented by the parametric integrals in the form

$$\Pi_{(T=0)}^{\text{scalar}} = \int \frac{dk}{(2\pi)^4} G(p-k) G(k) = \int ds dt \Theta(l^2, h^2). \quad (26)$$

These formulas are derived for  $T = 0$ . To include nonzero temperature, within the Matsubara formalism we are using we have to substitute the integration over the continuous momentum  $k_4$  by a discrete sum over  $l$  in  $k_4 = 2\pi lT$ ,

$$\int_{-\infty}^{\infty} \frac{dk_4}{2\pi} \rightarrow T \sum_{l=-\infty}^{\infty} . \quad (27)$$

In order to incorporate this into the parametric integral we represent

$$T \sum_{l=-\infty}^{\infty} = T \sum_{l=-\infty}^{\infty} \int_{-\infty}^{\infty} dk_4 \delta(k_4 - 2\pi lT) = T \sum_{l=-\infty}^{\infty} \int_{-\infty}^{\infty} d\sigma e^{-i\sigma 2\pi lT} \int_{-\infty}^{\infty} \frac{dk_4}{2\pi} e^{i\sigma k_4} \quad (28)$$

in this way keeping the original formalism on the expense of accommodating the additional factor  $\exp(i\sigma k_4)$  and carrying out the integration over  $\sigma$  and the summation over  $l$  afterwards. Under the above assumption that the speed of the heat bath is orthogonal to  $h_\lambda$ , the additional factor  $\exp(i\sigma k_4)$  can be incorporated into Schwinger's formalism quite trivially because the integration over  $k_4$  (in the same way as that over  $k_3$ ) decouples from the other ones in the sense that the corresponding integrals factorize. For the integration over  $k_4$  we have

$$\int_{-\infty}^{\infty} \frac{dk_4}{2\pi} e^{i\sigma k_4} e^{-s(p_4 - k_4)^2 - tk_4^2} = \frac{\exp\left(-\frac{\sigma^2}{4(s+t)} + i\frac{\sigma s p_4}{s+t} - \frac{st}{s+t} p_4^2\right)}{\sqrt{4\pi(s+t)}} \quad (29)$$

and

$$\begin{aligned} T \sum_{l=-\infty}^{\infty} \int_{-\infty}^{\infty} d\sigma \int_{-\infty}^{\infty} \frac{dk_4}{2\pi} e^{-\sigma k_4} e^{-s(p_4-k_4)^2-tk_4^2} \\ = T \sum_{l=-\infty}^{\infty} \exp \left( -(2\pi l T)^2 + 4\pi l T s (up) - \frac{s^2}{s+t} (up)^2 - \frac{st}{s+t} p_4^2 \right). \end{aligned} \quad (30)$$

In this formula we used  $(up) = p_4$  because this form of writing will be more convenient below.

Combining these with (20), (21) and (20) we obtain for a graph consisting of scalar lines

$$\begin{aligned} \Pi^{\text{scalar}} &\equiv T \sum_{l=-\infty}^{\infty} \int \frac{d^3 k}{(2\pi)^3} G(p-k) G(k) \\ &= T \sum_{l=-\infty}^{\infty} \int ds dt e^{-(2\pi l T)^2(s+t)+4\pi l T s (up)-\frac{s^2}{s+t} (up)^2} \sqrt{4\pi(s+t)} \Theta(l^2, h^2). \end{aligned} \quad (31)$$

This representation is still not in a form which is sufficiently convenient for the following, for instance, it contains still the ultraviolet divergence which appears from small  $s, t$  and large  $l$ . Using the well known resummation formula

$$\sum_l \exp(-z l^2 + al) = \sqrt{\frac{\pi}{z}} \sum_N \exp \left( -\frac{\pi^2 N^2}{z} + i\pi N \frac{a}{z} + \frac{a^2}{4z^2} \right) \quad (32)$$

(both sums run over the integers) we obtain with  $z \rightarrow (2\pi T)^2$ ,  $a \rightarrow 4\pi T (up)$

$$\Pi^{\text{scalar}} = \sum_N \int ds dt \Theta_T(l^2, h^2). \quad (33)$$

Here we introduced the basic average

$$\Theta_T(l^2, h^2) = \exp \left\{ -\frac{N^2}{4(s+t)T^2} + 2s(\tilde{u}p) \right\} \Theta(l^2, h^2), \quad (34)$$

where  $\Theta(l^2, h^2)$  given by Eq.(21) and where the notation

$$\tilde{u}_\lambda = \frac{iN}{2(s+t)T} u_\lambda \quad (35)$$

was introduced. This average is what comes at finite temperature in place of (20),

$$T \sum_{l=-\infty}^{\infty} \int \frac{d^3 k}{(2\pi)^3} = \langle \hat{\Theta} \rangle_T = \Theta_T(l^2, h^2). \quad (36)$$

In (34) the ultraviolet divergence is in the  $N = 0$  contribution taken at  $B = 0$ . The well known basic properties of the representations as sum over  $l$  or as sum over  $N$  are that the sum over  $l$  is convenient for high temperature ( $l = 0$  – the so called static mode, gives the leading contribution for  $T \rightarrow \infty$ ) and the sum over  $N$  gives the low temperature expansion, for instance the  $N = 0$  term is the contribution at  $T = 0$ .

We continue with the remark that since below  $\Theta(l^2, h^2)$  will become part of the form factors it is meaningful to write it as a function of  $h^2 + 2iF$ . This can be done by means of the relation

$$\Theta(l^2, h^2) = \Theta(l^2, h^2 + 2iF) Z \quad (37)$$

with

$$Z = -E^\top \frac{D}{D^\top} = \delta^{||} + \frac{\alpha}{4N} iF + \frac{\beta}{4N} \delta^\perp, \quad (38)$$

where the notations

$$\alpha = (p^2 + q^2) \sinh(2s) - 2pq \cosh(2s), \quad \beta = (p^2 + q^2) \cosh(2s) - 2pq \sinh(2s), \quad (39)$$

and

$$A = E - 1, \quad D = A - 2itF \quad (40)$$

are introduced.

From Schwinger's formalism we need also the commutator relation

$$p_\mu \Theta(l^2, h^2) = \Theta(l^2, h^2) \bar{p}_\mu \quad (41)$$

with

$$\bar{p}_\mu = (Ep)_\mu - (Ak)_\mu. \quad (42)$$

Here we used obvious short notations like  $(Ep)_\mu = E_{\mu\mu'} p_{\mu'}$ . Finally, we need the average formulas for vectors,

$$\langle \hat{\Theta} k_\lambda \rangle_T = \langle \hat{\Theta} \rangle_T \left( \frac{A}{D} p + \tilde{u} \right)_\lambda, \quad \langle \hat{\Theta} k_\lambda k_{\lambda'} \rangle_T = \langle \Theta \rangle_T \left[ \left( \frac{A}{D} p + \tilde{u} \right)_\lambda \left( \frac{A}{D} p + \tilde{u} \right)_{\lambda'} + \left( \frac{iF}{D^\top} \right)_{\lambda\lambda'} \right], \quad (43)$$

together with the explicit representation

$$\frac{A}{D} = \frac{s}{s+t} \delta^{||} - \frac{tp}{2N} iF + \frac{p+t \sinh(2s)}{2N} \delta^\perp. \quad (44)$$

All other quantities can be calculated from these, for example,

$$\frac{iF}{D^\top} = \frac{1}{2} \left( \frac{-2iF}{D} \right)^\top = \frac{1}{2t} \left( 1 - \frac{A}{D} \right)^\top = \frac{1}{2} \left( \frac{\delta^{||}}{s+t} + \frac{p}{2N} iF + \frac{q}{2N} \delta^\perp \right). \quad (45)$$

Perhaps it is useful to remark that all these matrices commute one with the other, that the transposition changes the sign of  $F$  and that the simple algebra  $\delta^{||2} = \delta^{||}$ ,  $\delta^{\perp 2} = \delta^\perp$ ,  $F^2 = -\delta^\perp$ ,  $\delta^{||} \delta^\perp = \delta^{||} F = 0$  and  $\delta^\perp F = F$  holds.

The averages in (43) are calculated at  $T \neq 0$ . For  $T = 0$  they reduce to the formulas known from [11]. For  $T \neq 0$  one needs to consider the corresponding generalizations of Eq.(29),

$$\int_{-\infty}^{\infty} \frac{dk_4}{2\pi} k_4 e^{i\sigma k_4} e^{-s(p_4 - k_4)^2 - tk_4^2}. \quad (46)$$

Replacing the additional factor  $k_4$  by  $i\frac{\partial}{\partial\sigma}$ , after integration over  $\sigma$  an additional factor  $2\pi l/T$  appears in a formula which generalized Eq.(31). It remains to do the resummation from  $l$  to  $N$ . Taking the derivative with respect to  $a$  from Eq.(32) after some calculations the first line in (43) for  $\lambda = 4$  appears. The derivation of (43) is then finished by the remark that for  $\lambda = 1, 2, 3$  no additional contributions appear. In a similar way also the second line in Eq.(43) can be derived.

Now we turn to the calculation of the polarization tensor (11). Using (17), (19), (20) and (41) it can be written in the form

$$\Pi_{\lambda\lambda'} = \sum_N \int ds dt \langle \hat{\Theta}_T [\Gamma_{\lambda\nu\rho} E_{\nu\nu'} \Gamma_{\lambda'\nu'\rho} + (\bar{p} - k)_\lambda k_{\lambda'} + k_\lambda (p - k)_{\lambda'}] \rangle + \Pi_{\lambda\lambda'}^{\text{tadpol}}, \quad (47)$$

where in  $\Gamma_{\lambda\nu\rho}$  one needs to substitute  $p$  by  $\bar{p}$ .

In the next step we divide the whole expression into parts according to the division made in (14) and (15),

$$\Pi_{\lambda\lambda'} = \sum_N \int ds dt \langle \hat{\Theta}_T \left[ \sum_{i,j} \hat{M}_{\lambda\lambda'}^{i,j} + \hat{M}_{\lambda\lambda'}^{\text{gh}} \right] \rangle + \Pi_{\lambda\lambda'}^{\text{tadpol}} \quad (48)$$

with

$$\hat{M}_{\lambda\lambda'}^{i,j} = \Gamma_{\lambda\nu\rho}^{(i)} E_{\nu\nu'} \Gamma_{\lambda'\nu'\rho}^{(j)} \quad (49)$$

and  $\hat{M}_{\lambda\lambda'}^{\text{gh}}$  is the corresponding contribution from the ghost loop.

The sums in (48) include also the decomposition (15).

The explicit expressions in this formula are of the type (we write that for the case of  $M_{\lambda\lambda'}^{1,1}$  as an example),

$$\hat{M}^{1,1} = (\bar{p} - 2k)_\lambda (p - 2k)_{\lambda'} \text{tr} E. \quad (50)$$

Using (42) we rewrite this expression in the form

$$\hat{M}^{1,1} = (Ep - (E+1)k)_\lambda (p - 2k)_{\lambda'} \text{tr} E, \quad (51)$$

Now we apply the average formulas (43) and we pass from  $\Theta(l^2, h^2)$  to  $\Theta(l^2, h^2 + 2iF)$  by means of (37) which brings a factor  $Z$  to the  $M^{i,j}$  which couples to the index  $\lambda$ , in detail,  $ZM^{i,j}$  stands for  $Z_{\lambda\lambda''} M_{\lambda''\lambda'}^{i,j}$ . In this way we come to

$$\langle \hat{\Theta} \hat{M}^{i,j} \rangle_T = \Theta_T(l^2, h^2 + 2iF) M^{i,j} \quad (52)$$

with

$$M^{1,1} = \left( (Pp - 2\tilde{u})_{\lambda} (P^{\top}p - 2\tilde{u})_{\lambda'} + 2Z \frac{2iF}{D^{\top}} \right) \text{tr}E \quad (53)$$

Here, again, new notations were introduced, namely

$$\begin{aligned} P &= \left( 1 - 2 \frac{A}{D} \right)^{\top} = Z \left( E - (E+1) \frac{A}{D} \right) = -\frac{s-t}{s+t} \delta^{\parallel} - \frac{tp}{N} iF - \frac{p/2-t^2}{N} \delta^{\perp} \equiv r_3 \delta^{\parallel} + \alpha_3 iF + \beta_3 \delta^{\perp}, \\ R &= 2(E - E^{\top}) = -4 \sinh(2s) iF, \\ Q_{31} &= \left( Z \left( 1 - \frac{A}{D} \right) \right)^{\top} = E \frac{-2itF}{D} = \frac{t}{s+t} \delta^{\parallel} + t \frac{p \cosh(2s) - q \sinh(2s)}{2N} iF + t \frac{q \cosh(2s) - p \sinh(2s)}{2N} \delta^{\perp}, \\ &\equiv s_4 \delta^{\parallel} + \gamma_4 iF + \delta_4 \delta^{\perp}, \\ Q_{32} &= \left( EZ \frac{A}{D} \right)^{\top} = E^{\top} \frac{A}{D} = \frac{s}{s+t} \delta^{\parallel} + \frac{p(\sinh(2s) + t)}{2N} iF + \frac{p \cosh(2s) + t \sinh(2s)}{2N} \delta^{\perp}, \\ &\equiv s_3 \delta^{\parallel} + \gamma_3 iF + \delta_3 \delta^{\perp}, \\ S &= Z = \left( E - A \frac{A}{D} \right)^{\top} = \delta^{\parallel} + \frac{\alpha}{4N} iF + \frac{\beta}{4N} \delta^{\perp} \equiv r_1 \delta^{\parallel} + \alpha_1 iF + \beta_1 \delta^{\perp}, \\ T &= (EZ)^{\top} = 1 + A^{\top} \frac{A}{D} = \delta^{\parallel} + \frac{2pq}{4N} iF + \frac{p^2 + q^2}{4N} \delta^{\perp} \equiv s_2 \delta^{\parallel} + \gamma_2 iF + \delta_2 \delta^{\perp}, \\ U &= \left( \frac{A}{D} \right)^{\top} = \frac{s}{s+t} \delta^{\parallel} + \frac{tp}{2N} iF + \frac{p + t \sinh(2s)}{2N} \delta^{\perp} \equiv r_2 \delta^{\parallel} + \alpha_2 iF + \beta_2 \delta^{\perp}, \\ V &= 1 - \frac{A}{D} = \frac{t}{s+t} \delta^{\parallel} + \frac{tp}{2N} iF + \frac{tq}{2N} \delta^{\perp} \equiv s_1 \delta^{\parallel} + \gamma_1 iF + \delta_1 \delta^{\perp}, \end{aligned} \quad (54)$$

where (38), (44) and (45) were used. Here we listed all the representations which describe other terms of the polarization tensor. The notations  $r_i$ ,  $\alpha_i$ ,  $\beta_i$  and  $\delta_i$  are introduced here for later use.

As for the dependence on  $\tilde{u}$  we made use of the fact that only the fourth component of  $\tilde{u}_{\mu}$  is nonzero.

In order to continue and, for instance, to find the necessary structures for integration by parts, we divide the contributions into 4 parts,

1.  $M^{1,1} + M^{1,2} + M^{2,1} + M^{2,2}$ ,
2.  $M^{1,3} + M^{2,3} + M^{3,1} + M^{3,2}$
3.  $M^{3,3} + M^{\text{gh}}$

and consider them individually in the following subsections.

### 3.1 Contribution from $M^{1,1} + M^{1,2} + M^{2,1} + M^{2,2}$

We start from  $M^{1,1}$ . First of all we note that the relation

$$- \left( \frac{\partial}{\partial s} - \frac{\partial}{\partial t} \right) \left( P_{\lambda\lambda} - 2 \frac{\tilde{u}_{\lambda} \tilde{u}_{\lambda'}}{(\tilde{u}p)} \right) = 2Z \frac{2iF}{D^{\top}} \quad (55)$$

holds which can be verified by differentiation of (38) and (45). It should be mentioned that the term  $-2 \frac{\tilde{u}_{\lambda} \tilde{u}_{\lambda'}}{(\tilde{u}p)}$  in the left hand side vanishes under differentiation. It was added by hindsight.

Eq.(55) allows us to represent the contribution of  $M^{1,1}$  to the polarization tensor (48) in the form (up to the sum over  $N$ )

$$\int ds dt \Theta_T(l^2, h^2 + 2iF) \left( - \left( \frac{\partial}{\partial s} - \frac{\partial}{\partial t} \right) \left( P - 2 \frac{\tilde{u}_{\lambda} \tilde{u}_{\lambda'}}{(\tilde{u}p)} \right) \right) \text{tr}E. \quad (56)$$

In this integral we temporarily change variables to  $\lambda$  and  $u$  according to  $s = \lambda u$ ,  $t = \lambda(1-u)$  and with  $(\frac{\partial}{\partial s} - \frac{\partial}{\partial t}) = \frac{1}{\lambda} \frac{\partial}{\partial u}$  we integrate the derivative with respect to  $u$  by parts,

$$\begin{aligned} &\int_0^{\infty} d\lambda \lambda \int_0^1 du \Theta_T(l^2, h^2 + 2iF) \left( -\frac{1}{\lambda} \frac{\partial}{\partial u} \left( P - 2 \frac{\tilde{u}_{\lambda} \tilde{u}_{\lambda'}}{(\tilde{u}p)} \right) \right) \text{tr}E \\ &= \int_0^{\infty} d\lambda \lambda \left[ -\Theta_T(l^2, h^2 + 2iF) \left( P - 2 \frac{\tilde{u}_{\lambda} \tilde{u}_{\lambda'}}{(\tilde{u}p)} \right), \text{tr}E \right] \Big|_{u=0}^1 \\ &\quad + \int ds dt \Theta_T(l^2, h^2 + 2iF) \left\{ \left( P - 2 \frac{\tilde{u}_{\lambda} \tilde{u}_{\lambda'}}{(\tilde{u}p)} \right) \left( \widetilde{(pPp)} - 2(\tilde{u}p) \right) \text{tr}E + 4 \sinh(2s) P \right\}, \end{aligned} \quad (57)$$

where

$$(pPp) = - \left( \frac{\partial}{\partial s} - \frac{\partial}{\partial t} \right) H - \frac{1}{2N} \left( \frac{\partial}{\partial s} - \frac{\partial}{\partial t} \right) N \quad (58)$$

follows from (22), (24) and (54) and

$$- \left( \frac{\partial}{\partial s} - \frac{\partial}{\partial t} \right) \Theta_T = \Theta_T \left( \widetilde{(pPp)} - 2(\tilde{u}p) \right) \quad (59)$$

from (34). We have to take into account that we differentiate a  $\Theta$  which depends on  $h^2 + 2iF$  so that we got in place of (58) in fact

$$\widetilde{(pPp)} \equiv (pPp) \Big|_{h^2 \rightarrow h^2 + 2iF}. \quad (60)$$

In such expressions we shall use the tilde as notation for this substitution in the following several times. Further we used  $trE = 2(1 + \cosh(2s))$ .

As a result from the integration by parts we get surface contributions which have the general form

$$M_{\text{surface}} = \int_0^\infty d\lambda \lambda \Theta_T(l^2, h^2 + 2iF) \sum_{i,j} M_{\text{sf}}^{i,j} \Big|_{u=0}^1, \quad (61)$$

The surface contribution from  $M^{1,1}$  is then

$$M_{\text{sf}}^{1,1} = - \left( P_{\lambda\lambda'} - 2 \frac{\tilde{u}_\lambda \tilde{u}_{\lambda'}}{(\tilde{u}p)} \right) trE. \quad (62)$$

Taking the contribution from the last line in (57) we represent up to the surface contribution  $M^{1,1}$  in the form

$$M^{1,1} = \left[ (Pp - 2\tilde{u})_\lambda (P^\top p - 2\tilde{u})_{\lambda'} - \left( P_{\lambda\lambda'} - 2 \frac{\tilde{u}_\lambda \tilde{u}_{\lambda'}}{(\tilde{u}p)} \right) \left( \widetilde{(pPp)} - 2(\tilde{u}p) \right) \right] trE + 4 \sinh(2s) \left( P_{\lambda\lambda'} - 2 \frac{\tilde{u}_\lambda \tilde{u}_{\lambda'}}{(\tilde{u}p)} \right). \quad (63)$$

In this way other terms could be transformed.

Thus we get the surface contribution

$$M_{\text{sf}}^{1,2} = -\Theta_T(l^2, h^2 + 2iF) R_{\lambda\lambda'}^\top \quad (64)$$

and then we represent

$$\begin{aligned} M^{1,2} + M^{2,1} &= (Pp - 2\tilde{u})_\lambda (Rp)_{\lambda'} + (R^\top p)_\lambda (P^\top p - 2\tilde{u})_{\lambda'} - \left( P_{\lambda\lambda'} - 2 \frac{\tilde{u}_\lambda \tilde{u}_{\lambda'}}{(\tilde{u}p)} \right) (\widetilde{pR^\top p}) \\ &\quad - R_{\lambda\lambda'}^\top \left( \widetilde{(pPp)} - 2(\tilde{u}p) \right) - 4 \sinh(2s) \left( P_{\lambda\lambda'} - 2 \frac{\tilde{u}_\lambda \tilde{u}_{\lambda'}}{(\tilde{u}p)} \right) + 8 \cosh(2s) iF_{\lambda\lambda'}. \end{aligned} \quad (65)$$

Finally we turn to  $M^{2,2}$ . Here we rewrite

$$(pSp) = \widetilde{(pSp)} + (S + S^\top) iF, \quad (pT^\top p) = \widetilde{(pT^\top p)} + (T + T^\top) iF \quad (66)$$

and represent  $M^{2,2}$  in the form

$$M^{2,2} = -4 \left[ (Sp)_\lambda (Tp)_{\lambda'} + (T^\top p)_\lambda (S^\top p)_{\lambda'} - S_{\lambda\lambda'} (\widetilde{pT^\top p}) - T_{\lambda\lambda'}^\top (\widetilde{pSp}) \right] - 8 \cosh(2s) iF. \quad (67)$$

The last line is the result of a number of cancellations.

We continue with the observation that the last lines in (63), (65) and (67) compensate each other so that we are left with the corresponding first lines. In this way we get from this subsection the following contribution to the form factors, which we denote by  $M_i^a$ :

$$\begin{aligned} M_1^a &= - \left( \frac{s-t}{s+t} \right)^2 2(1 + \cosh(2s)) & +8, \\ M_2^a &= \frac{(tp)^2 - (p/2 - t^2)^2}{N^2} 2(1 + \cosh(2s)) & -8 \sinh(2s) \frac{tp}{N} & +8 \cosh(2s), \\ M_3^a &= \frac{s-t}{s+t} \frac{t^2 - p/2}{N} 2(1 + \cosh(2s)) & + \frac{\beta + p^2 + q^2}{N}, \\ M_4^a &= - \frac{s-t}{s+t} \frac{tp}{N} 2(1 + ch) & +4 \sinh(2s) \frac{s-t}{s+t} & + \frac{\alpha - 2pq}{N} \\ (11) & & (12) + (21) & (22) \end{aligned} \quad (68)$$

where in the last line the origin of the contribution is indicated.

For the temperature induced contributions we get with  $\mu = 2 \frac{iN}{2(s+t)T}$

$$M_7^a = -2 \frac{iN}{2(s+t)T} \frac{r_3}{(up)} trE, \quad M_7^a = -2 \frac{iN}{2(s+t)T} \frac{\beta_3}{(up)} trE, \quad M_9^a = -M_{(*)}^a = 2 \frac{iN}{2(s+t)T} \alpha_3 trE. \quad (69)$$

### 3.2 Contribution from $M^{1,3} + M^{2,3} + M^{3,1} + M^{3,2}$

In such a way after length cumbersome calculation we obtain the contributions of the terms from  $M^{1,3} + M^{2,3} + M^{3,1} + M^{3,2}$ . We denote the contributions to the form factors originating from this part by  $M_i^b$ . These read

$$\begin{aligned}
M_2^b &= \frac{1}{2N} \left( -\cosh^2(2s) + (2 - 4t^2) \cosh(2s) - 12t \sinh(2s) \right), \\
M_3^b &= \frac{1}{2(s+t)N} \left( -2t^3 - 10st^2 - 2(t^2 + st + 2) \cosh(2s)t \right. \\
&\quad \left. - 8(s+t) \sinh(2s)t + 5t - (s+t) \cosh^2(2s) + s \right), \\
M_4^b &= \frac{1}{2(s+t)N} \left( 4t(t-s) - (s+t)(2t^2 + 1) \sinh(2s) \right. \\
&\quad \left. + \cosh(2s)(4(s-t)t + (s+t) \sinh(2s)) \right), \\
M_5^b &= \frac{1}{2N} \left( (\cosh(2s) - 1)(2t^2 + \cosh(2s) - 1) \right), \\
M_{6a}^b &= \frac{1}{2N} \left( (-2t^2 + \cosh(2s) - 1) \sinh(2s) \right), \\
M_{6b}^b &= \frac{1}{2N} \left( (-2t^2 + \cosh(2s) - 1) \sinh(2s) \right). \tag{70}
\end{aligned}$$

We observe that  $M_{6a}^b$  and  $M_{6b}^b$  are equal. As a consequence, the operators structures  $T_{\lambda\lambda'}^{(6a)}$  and  $T_{\lambda\lambda'}^{(6b)}$  come with the same form factors, hence these contributions collect into the structure  $T_{\lambda\lambda'}^{(6)}$ , Eq.(5).

Finally we collect the temperature induced part. Its form factors can be written in the form

$$\begin{aligned}
M_7^b &= \frac{iN}{2(s+t)T} \frac{1}{(up)} (-2r_1 + r_4 + 2s_4 + 2s_2 + r_3 - 2s_3), \\
M_8^b &= \frac{iN}{2(s+t)T} \frac{1}{(up)} (-2\beta_1 + \beta_4 + 2\delta_4 + 2\delta_2 + \beta_3 - 2\delta_3), \\
M_{10a}^b &= \frac{iN}{2(s+t)T} \frac{1}{(up)} (2r_1 + r_4 - 2s_4 - 2s_2 + r_3 + 2s_3), \\
M_{10b}^b &= \frac{iN}{2(s+t)T} \frac{1}{(up)} (2\beta_1 + \beta_4 - 2\delta_4 - 2\delta_2 + \beta_3 + 2\delta_3), \\
M_9^b &= \frac{iN}{2(s+t)T} (2\alpha_1 + \alpha_4 + 2\gamma_4 + 2\gamma_2 - \alpha_3 - 2\gamma_4), \\
M_{(*)}^b &= \frac{iN}{2(s+t)T} (2\alpha_4 + 2\alpha_3). \tag{71}
\end{aligned}$$

The parameters  $\alpha_i, \beta_i, \dots$  where introduced in Eq.(54). Some of them are equal that will be noted below.

### 3.3 Contribution from $M^{3,3} + M^{\text{gh}}$ and tadpoles

These contributions need a treatment to some extend different from the preceding two subsections and could be presented in the form

$$\Pi_{\lambda\lambda'}^{33+\text{gh}} = - \sum_N \int_0^\infty ds E_{\lambda\lambda'} \Theta_T(l^2, h^2) \Big|_{t=0}^{t=\infty} - \sum_N \int_0^\infty dt \delta_{\lambda\lambda'} \Theta_T(l^2, h^2) \Big|_{s=0}^{s=\infty}, \tag{72}$$

where the integration over  $t$  or  $s$  parameter is assumed and the corresponding limits are marked.

Now we collect the contributions resulting from the tadpole graphs given by Eq.(12) and the surface contributions which appeared in the preceding subsections.

The tadpole contributions can be calculated easily since they are special cases of the basic loop contribution for  $s = 0$  collapsing the line of the charged gluon and keeping the line of the neutral gluon and for  $t = 0$  which the lines interchanged. All other rules remain valid so that these contributions can be written down easily,

$$\begin{aligned}
\Pi^{\text{tadpol}} &= \sum_N \int dt \Theta_T(l^2, h^2) (-\delta_{\lambda\lambda'} + 4\delta_{\lambda\lambda}) \Big|_{s=0} + \sum_N \int ds \Theta_T(l^2, h^2) \times \\
&\quad \times \left( \text{tr} E \delta_{\lambda\lambda'} - 4 \sinh(2s) iF - \left( \delta_{\lambda\lambda'}^{\parallel} + iF \sinh(2s) + \delta_{\lambda\lambda'}^{\perp} \right) \right) \Big|_{t=0}. \tag{73}
\end{aligned}$$

Now we collect the surface terms. A part of them has the form (61),

$$M_{\text{surface}} = \sum_N \int_0^\infty d\lambda \Theta_T(l^2, h^2 + 2iF) M_{\text{sf}} \Big|_{u=0}^1 \tag{74}$$

with contributions to  $M_{sf}$  from Eqs.(62), (64),

$$M_{sf} = - \left( P_{\lambda\lambda'} - 2 \frac{\tilde{u}_\lambda \tilde{u}_{\lambda'}}{(\tilde{u}p)} \right) \text{tr}E - R_{\lambda\lambda'}^\top + 2Q_{31\lambda\lambda'}^\top - 2Q_{32\lambda\lambda'}^\top. \quad (75)$$

which can be rewritten in the form

$$\Pi^{\text{surface}} = \sum_N \int ds \Theta_T(l^2, h^2) M_{sf} \Big|_{t=0} - \sum_N \int dt \Theta_T(l^2, h^2) M_{sf} \Big|_{s=0}. \quad (76)$$

Now it can be checked that when adding (73) and (76) and doing the obvious simplification all contributions cancel except for that which are proportional to  $u_\lambda u_{\lambda'}$ , i.e., to  $T_{\lambda\lambda'}^D$ , Eq.(9). These collect into  $\Pi^D$  defined in Eq.(10),

$$\Pi^D = \sum_N \int ds \frac{iN}{2s} \Theta_T(l^2, h^2) (-4 + 2\text{tr}E) \Big|_{t=0} - \sum_N \int dt \frac{iN}{2t} \Theta_T(l^2, h^2) (4 - 2\text{tr}E) \Big|_{s=0}. \quad (77)$$

Now we need from (21) and (34)

$$\begin{aligned} \Theta_T \Big|_{s=0} &= \frac{1}{(4\pi)^2 t^2} \exp\left(-\frac{N^2}{4tT^2}\right), \\ \Theta_T \Big|_{t=0} &= \frac{s}{\sinh(s)} \frac{1}{(4\pi)^2 s^2} \exp\left(-\frac{N^2}{4sT^2}\right) \exp\left(\frac{iN}{T} p_4\right) \end{aligned} \quad (78)$$

and after renaming the integration variables we obtain for the remaining contributions

$$\begin{aligned} \Pi^D &= \sum_N \int_0^\infty \frac{d\lambda}{\lambda} \frac{iN}{2Tp_4} [-4\Theta_T \Big|_{s=0} + 4\Theta_T \Big|_{t=0}] \\ &= -\frac{4}{(4\pi)^2} \sum_N \int_0^\infty \frac{d\lambda}{\lambda^3} \frac{iN}{2Tp_4} \left(1 - \frac{\lambda \cosh(2\lambda)}{\sinh(\lambda)} e^{iNp_4/T}\right) \exp\left(-\frac{N^2}{4\lambda T^2}\right). \end{aligned} \quad (79)$$

The expression for  $\Pi^D$  can be a bit simplified by writing as a sum over  $N > 0$  (note the contribution from  $N = 0$  vanishes),

$$\Pi^D = -\frac{4}{(4\pi)^2} \sum_{N=1}^\infty \int_0^\infty \frac{d\lambda}{\lambda^3} \frac{\sin(Np_4/T)}{Tp_4/N} \frac{\lambda \cosh(2\lambda)}{\sinh(\lambda)} \exp\left(-\frac{N^2}{4\lambda T^2}\right). \quad (80)$$

It is obvious that for external momenta obeying  $p_4 = 2\pi lT$  ( $l$  integer) only the contribution from  $l = 0$  is nonzero and we arrive at the Debye mass,  $\Pi^D = -\delta_{l,0} m_D^2$ ,

$$m_D^2 = \frac{1}{4\pi^2} \sum_{N=1}^\infty \int_0^\infty \frac{d\lambda}{\lambda^2} \left(\frac{N}{T}\right)^2 \frac{\cosh(2\lambda)}{\sinh(\lambda)} \exp\left(-\frac{N^2}{4\lambda T^2}\right). \quad (81)$$

This expression coincides with the Debye mass of the neutral gluon, Eq.(123) in [10]

## 4 Conclusions

Here we collect the contributions which were calculated in the preceding subsections. The form factors appearing in the decomposition (10) of the polarization tensor read

$$\Pi^i(l^2, h^2 + 2iF) = \sum_N \int_0^\infty ds \int_0^\infty dt \Theta_T(l^2, h^2 + 2iF) M_i \quad (82)$$

with

$$\begin{aligned}
M_1 &= \frac{4(s+t)^2 - 2(s-t)^2 \cosh(2s)}{(s+t)^2} \\
M_2 &= \frac{1}{N} (-2t^2 + 4 \sinh(2s)t + 2 \cosh^2(2s) + \cosh(2s) (4t^2 + 2 \sinh(2s)t - 3) + 1) \\
M_3 &= \frac{1}{4(s+t)N} (2(s+5t) \cosh^2(2s) + 4t (t^2 + 5st - 2) \cosh(2s) + 2(s+t) (2t^2 + 8 \sinh(2s)t - 1)) \\
M_4 &= \frac{1}{2(s+t)N} (4(s-t)t \cosh^2(2s) + (4(s-t)t + (s-7t) \sinh(2s)) \cosh(2s) \\
&\quad + 8t(t-s) + (-2t^3 + 14st^2 + 7t - s) \sinh(2s)) \\
M_5 &= \frac{1}{2N} ((\cosh(2s) - 1) (2t^2 + \cosh(2s) - 1)), \\
M_6 &= \frac{1}{2N} ((-2t^2 + \cosh(2s) - 1) \sinh(2s)),
\end{aligned} \tag{83}$$

with  $N$  given by Eq.(24).

The new temperature induced contributions from adding (69) and (71) read

$$\begin{aligned}
M_7 &= \frac{iN}{2(s+t)Tp_4} \frac{4(s-t) \cosh(2s)}{s+t}, \\
M_8 &= \frac{iN}{2(s+t)Tp_4} \frac{4 \cosh^2(2s) - 4(2t^2 + 1) \cosh(2s)}{2N}, \\
M_9 &= \frac{iN}{2(s+t)T} \frac{t \cosh^2(2s) + (t + \sinh(2s)) \cosh(2s) - 2t + (2t^2 - 1) \sinh(2s)}{N}.
\end{aligned} \tag{84}$$

In derivation of these expressions we have taken into consideration Eq.(54) and accounted for the relations  $\alpha_4 = \alpha_3, \beta_4 = \beta_3$ .

Furthermore it holds  $M_{10a} = M_{10b} = 0$  and  $M_{(*)} = -M_9$ . Here a comment is in order. The vanishing of  $M_{10a}$  and  $M_{10b}$  is the result of the calculations done here in one-loop order. At the moment it is not known whether there is some symmetry behind and whether this persists in higher loops. Similar remarks apply to the relation between  $M_9$  and  $M_{(*)}$ . As a result, these two form factors contribute proportional to the tensor structure

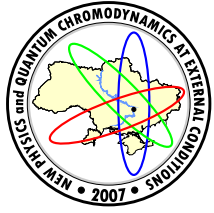
$$T_{\lambda\lambda'}^9 - T_{\lambda\lambda'}^{(*)} = u_\lambda i d_{\lambda'} - i d_\lambda u_{\lambda'} + i F(up) - \frac{u_\lambda u_{\lambda'}}{(up)}. \tag{85}$$

Finally we mention the contribution from the Debye mass, Eqs.(81), which by means of  $\Pi^D = \delta_{l,0} m_D^2$ , contributes to  $\Pi_{\lambda\lambda'}$ , (10).

These expressions can be used in different applications. For example, it is of interest to calculate the spectrum of gluon modes propagating in the deconfinement phase. The derived structure of the polarization tensor is necessary in resummation of series of diagrams under the background considered.

## References

- [1] P.Cea, L.Cosmai. Phys. Rev. **D 60**, 094506 (1999)
- [2] P.Cea, L.Cosmai. JHEP **0302**, 031 (2003); **0508** 079 (2005)
- [3] N. O. Agasian. Phys. Lett. **B562**, 257 (2003)
- [4] V. I. Demchik, V. V. Skalozub. The spontaneous generation of magnetic fields at high temperature in  $SU(2)$ -gluodynamics on a lattice hep-lat/0601035
- [5] A. O. Starinets, A. V. Vshivtsev, V. Ch. Zukovskii. Phys. Lett. **B 322**, 403 (1994)
- [6] V. V. Skalozub, M. Bordag. Nucl. Phys. **B576**, 430 (2000)
- [7] V. V. Skalozub, A. V. Strelchenko. Eur. Phys. J. **C33**, 105 (2004)
- [8] M. Bordag, V. V. Skalozub. Eur. Phys. J. **C45**, 159 (2006)
- [9] M. Bordag, Yu. O.Grebnyuk and V. V. Skalozub. Theor.and Math. Phys. **148(1)**, 910 (2006)
- [10] M. Bordag, V. V. Skalozub. Phys. Rev. **D75**, 125003 (2007)
- [11] J. S. Schwinger. Phys. Rev. **D7**, 1696 (1973)



## DECONFINEMENT PHASE TRANSITION IN 3D $U(1)$ LATTICE GAUGE THEORY

O. Borisenko<sup>a</sup>

N.N. Bogolyubov Institute for Theoretical Physics, Kiev, Ukraine

A review of compact three-dimensional  $U(1)$  gauge theory on asymmetric lattice is presented. A special attention is paid to the finite-temperature properties of the model, in particular to the deconfinement phase transition. We discuss how the phase transition exhibits itself in the behaviour of correlation functions, describe the universality class of the model and its relation to the two-dimensional  $XY$  model as well as the problems which remain to be solved. Then, correlation functions of the Polyakov loops and the 't Hooft operator are computed perturbatively at high temperatures. Performing dimensional reduction the effective two-dimensional model is obtained which describes vortex–anti-vortex dynamics in the high-temperature regime. We explore the effective model to study in details the critical behaviour. Under standard assumptions we compute critical indices and compare them with those of the two-dimensional  $XY$  model.

### 1 Overview of the results and problems

All studies of compact three-dimensional ( $3d$ )  $U(1)$  LGT without dynamical matter fields can be grouped into the following three categories: 1)  $3d$   $U(1)$  LGT at zero temperature; 2)  $3d$   $U(1)$  LGT on anisotropic lattice; 3)  $3d$   $U(1)$  LGT at finite temperature. Main motivation of these studies is two-fold. Firstly, at zero temperature the theory has a nonvanishing mass gap and a string tension at arbitrarily small coupling constant. This is a feature expected from  $4d$  QCD. Secondly, at finite temperature the theory undergoes a deconfinement phase transition. The corresponding phenomenon takes place in  $4d$  QCD as well. It thus appears that  $3d$   $U(1)$  gauge theory constitutes one of the simplest model with continuous gauge symmetry which possesses the same fundamental properties as QCD (at least, its pure gauge sector). Therefore, it is very important to understand in great details mechanism which underlies permanent confinement and deconfinement phase transition on the example of simpler three-dimensional abelian model.

#### 1.1 Theory at zero temperature

It seems, it was Polyakov who initiated investigations of compact  $U(1)$  model proving permanent confinement in this model [1]. To be precise, using dilute monopole gas and semiclassical approximations Polyakov has shown that the string tension  $\sigma(j)$  of the fundamental Wilson loop and the mass gap  $m$  behave at small coupling as

$$a^2\sigma(j=1) = \frac{8}{\sqrt{2\pi^2\beta}} \exp\left[-\frac{1}{2}\pi^2\beta G_0\right], \quad (1)$$

$$am = \sqrt{8\pi^2\beta} \exp\left[-\frac{1}{2}\pi^2\beta G_0\right]. \quad (2)$$

Here,  $\beta = 1/(g^2a)$  is dimensionless coupling constant and  $G_0 \approx 0.5054$  is zero-distance Green function. Polyakov's arguments have been extended to lattice formulation in [3] with the help of the dual representation of the  $U(1)$  model. Much more thorough calculations of the string tension have been accomplished in [3, 4]. A rigorous proof of permanent confinement was given in [5]. The proof uses the Villain formulation of  $U(1)$  LGT. It was shown that the semiclassical expression (1) is just lower bound on the string tension. Extension of Polyakov's semiclassical analysis to Wilson loops in higher representations ( $j \geq 2$ ) was performed in [1] with the result

$$\sigma(j) \sim j \sigma(j=1). \quad (3)$$

A very detailed investigation of a lattice version of the Polyakov saddle-point equation was done in [7]. Polyakov's scaling for the string tension (1) was verified in various Monte-Carlo (MC) simulations [7, 8] both in the Wilson and in the Villain formulations. In general, the scaling was confirmed though authors of [7] found essential difference between Wilson and Villain model which can be indicative that the true asymptotic region has

e-mail: <sup>a</sup>oleg@bitp.kiev.ua

not been reached. More recent MC simulations [9] also confirm asymptotic formula (1) but the amplitude of the exponentially small factor appears to be five times bigger than the semiclassical approximation predicts. MC computations which use dual formulation of  $U(1)$  LGT have been performed in [10]. In particular, a doubly charged Wilson loop, i.e. the Wilson loop in the representation  $j = 2$  has been computed in the dual simulations and the result has been reported which supports analytical formula (3). The flux-tubes generated by static sources were studied numerically both in the dual [10] and in the standard MC simulations [11]. Some physical quantities like the expectation value of the plaquette, various glueball masses have been computed in [9, 12].

Some important unsolved problems can be shortly summarized as follows.

1) Monopole dynamics. The role of monopoles in the long distance physics, in particular in producing the string tension was studied in [13] using cooling method. There is however neither analytical nor MC computations of such quantities like monopole density, percolation properties of monopole clusters, etc. But MC computations of various monopole properties have been done at finite temperature (see below).

2) Wilson loop in different representations  $j$ . In [14] Polyakov has argued that the string tension for even  $j$  should vanish. In contrast, paper [1] claims that the string tension in arbitrary representation is proportional to  $j$  times the string tension for the fundamental representation (3). Simulation of the dual model confirm this claim. However, earlier simulations of Ref.[11] support quadratic dependence of the form  $\sigma(j) \sim j^2 \sigma(j=1)$  rather than formula (3). Moreover, as can be seen from bounds of [5] (formula 8.3 of the first paper) string tension should be proportional to  $j^2$ .

3) Asymptotics of string tension and MC. All available MC results support the exponentially small behaviour of both the string tension and the mass gap. However, the amplitude at the exponential factor, as is seen in simulations is five times bigger than the theory predicts [9]. Thus, the theoretical question - how to account for this difference - is still open. Authors of [9] suppose that quantum corrections can improve the situation. Indeed, quantum corrections to the saddle-point solution by Polyakov have not been computed so far. Another possible reason for the disagreement could be the fact that only monopoles with lowest numbers  $0, \pm 1$  have been taken into account.

## 1.2 Theory at finite temperature

First investigations of  $U(1)$  LGT at finite temperature have been performed by Polyakov [15] and Susskind [16]. Their analysis, done for strong coupled Hamiltonian version of  $4d$  model, showed the possibility of the deconfinement phase transition at high temperatures. Three-dimensional case was studied by Parga using Lagrangian formulation of the theory [17]. The picture emerging from this study can be described as follows. At high temperatures the system becomes effectively two-dimensional, in particular the monopoles of the original  $U(1)$  gauge theory become vortices of the  $2d$  system. The partition function turns out to coincide (in the leading order of the high-temperature expansion) with the  $2d$   $XY$  model in the Villain representation. The effective coupling of the  $XY$  model reads

$$\beta_{\text{eff}} = 1/(g^2 \beta), \quad (4)$$

while the effective activity of the vortices is

$$y(\beta) = \exp \left[ -\frac{\pi^2}{2\beta_{\text{eff}}} \left( 1 + \frac{\beta^2}{3} \right) \right], \quad (5)$$

where  $\beta$  is the inverse temperature and  $g^2$  is coupling constant with dimension  $a^{-1}$ . The  $XY$  model is known to have the Berezinskii-Kosterlitz-Thouless (BKT) phase transition of the infinite order [18–20] which occurs for the Villain model at (a rigorous proof of the BKT phase transition existence was done in [21])

$$\beta_{\text{eff}} \approx 2/\pi. \quad (6)$$

According to the Svetitsky-Yaffe conjecture the finite-temperature phase transition in the  $3d$   $U(1)$  LGT should belong to the universality class of the  $2d$   $XY$  model [22]. This means, firstly that the global  $U(1)$  symmetry cannot be broken spontaneously because of the Mermin-Wagner theorem [23] and, consequently the absence of the local order parameter. Secondly, the correlation function of the Polyakov loops (which become spins of the  $XY$  model) decreases with the power law implying logarithmic potential between heavy electrons

$$P_1(R) \propto R^{-\eta(T)}, \quad (7)$$

where the  $R \gg 1$  is the distance between test charges (the definition of the Polyakov loop correlation  $P_j(R)$  is given in the Section 2). The critical index  $\eta(T)$  is known from the renormalization-group analysis of Ref.[20] and equals  $\eta(T_c) = 1/4$  at the critical point of the BKT transition. Therefore, it should be the same in the finite-temperature  $U(1)$  model if the Svetitsky-Yaffe conjecture holds in this case.

The first numerical check of these predictions was performed on the lattices  $N_s^2 \times N_t$  with  $N_s = 16, 32$  and  $N_t = 4, 6, 8$  in [24]. Though authors of [24] confirm the expected BKT nature of the phase transition, the reported critical index is almost three times of that predicted for the  $XY$  model,  $\eta \approx 0.78$ .

Quite an extensive numerical study of the monopole-anti-monopole dynamics both in the confinement and in the deconfinement phases have been accomplished in [25] on the lattice  $32^3 \times 8$ . In particular, such quantities like the monopole density, the second and the fourth Binder cumulants of the total number of monopoles and anti-monopoles have been computed as well as the temporal and the spatial string tensions.

The major remaining problems are the following.

- Monte-Carlo simulations. It seems to be beyond any doubts that the formula (1) correctly predicts the scaling of the string tension. Of course, the amplitude can be given incorrectly by the semiclassical approximation, and this is observed in all MC simulations. However, in finite-temperature simulations of Ref.[24] even the scaling was not reached. The problem can be in the finite-size effects. Neither Ref.[24] nor Ref.[25] addresses the problem of the finite-size scaling (FSS). The BKT phase transition is rather peculiar phenomenon. In particular, it is rather hard to investigate it numerically because of the logarithmic corrections. In a review by R.Kenna [26] a summary of recent numerical results on the critical indices and critical temperature of the  $XY$  model is presented. From this review it becomes transparent that in order to reliably describe all critical properties of the model one should at least use the FSS technics and/or simulate the model on large thermodynamic lattices, i.e.  $L \gg \xi$  ( $\xi$  is the correlation length). None of these have been accomplished in the simulations of 3d  $U(1)$  LGT at finite temperature so far.
- Universality problem. The phase transition in 3d  $U(1)$  LGT is of the BKT type. However, the results of [24] do not support the expected universality of the critical behaviour. In the continuum theory the problem was only addressed qualitatively. Thus, the problem remains open.
- Monopole dynamics in the vicinity of the phase transition. Despite thorough investigations of monopoles in [25], a number of issues is still to be solved. There is no any attempt in the literature to compute the 't Hooft loop expectation value. Certainly, such computations would provide an interesting insight into the monopole properties near the phase transition point. Percolation properties of the monopole clusters below and above the critical point have not been studied as well.

In what follows we concentrate on the studying of the universality problem. In the next section we introduce our conventions and give definition of the compact version of  $U(1)$  LGT together with some expectation values. Investigation of the model at limiting values of anisotropic couplings is presented in the Section 3. In this limit the BKT critical behaviour is clearly seen. In the Section 4 we derive the effective monopole action for the Villain version of 3d  $U(1)$  LGT at finite temperature in the presence of the Wilson (Polyakov) and/or 't Hooft loops. This is accomplished with the aid of the dimensional reduction of the model. The perturbative calculations of the Polyakov loop correlations at high temperatures are the subject of the Section 5. The Section 6 is devoted to the investigation of the effective monopole action at high temperatures. Here we give an analytical predictions for the critical indices of the theory. A summary of our results is presented in the Section 8. Asymptotic properties of the lattice Green function at finite temperatures are given in the appendix.

## 2 Lattice conventions and definition of the model

We work on a 3d lattice  $\Lambda = L^2 \times N_t$  with spatial extension  $L$  and temporal extension  $N_t$ .  $\vec{x} = (x_0, x_1, x_2)$ , where  $x_0 \in [0, N_t - 1]$  and  $x_1, x_2 \in [0, L - 1]$  denote the sites of the lattice and  $e_n$ ,  $n = 0, 1, 2$  denotes a unit vector in the  $n$ -th direction. Periodic boundary conditions (BC) on gauge fields are imposed in all directions. Notations  $p_t$  ( $p_s$ ) stay for the temporal (spatial) plaquettes,  $l_t$  ( $l_s$ ) for the temporal (spatial) links. In three dimensions temporal plaquettes are dual to spatial links while spatial plaquettes are dual to temporal links. In what follows we keep notations of the original lattice also for the dual lattice.

Introduce anisotropic dimensionless couplings in a standard way as

$$\beta_t = \frac{1}{g^2 a_t}, \quad \beta_s = \frac{\xi}{g^2 a_s} = \beta_t \xi^2, \quad (8)$$

where  $a_t$  ( $a_s$ ) is lattice spacing in the time (space) direction and  $\xi$  is a ratio of lattice spacings

$$\xi = \frac{a_t}{a_s}. \quad (9)$$

$g^2$  is a continuum coupling constant with dimension  $a^{-1}$ .

One should distinguish three different limits which can be obtained from the formulation of the theory on an anisotropic lattice

1. Euclidean limit is constructed as

$$\xi \rightarrow 1, \quad N_t = L, \quad L \rightarrow \infty. \quad (10)$$

2. Hamiltonian limit is constructed as

$$\xi \rightarrow 0, \quad N_t, L \rightarrow \infty. \quad (11)$$

3. Finite-temperature limit is constructed as

$$\xi \rightarrow 0, \quad N_t, L \rightarrow \infty, \quad a_t N_t = \beta, \quad (12)$$

where  $\beta = 1/T$  is the inverse temperature.

3d  $U(1)$  gauge theory on the anisotropic lattice is defined through its partition function as

$$Z \equiv Z(\Lambda; \beta_s, \beta_t) = \int_0^{2\pi} \prod_l \frac{d\omega_l}{2\pi} \exp S[\omega], \quad (13)$$

where  $S$  is the Wilson action

$$S[\omega] = \beta_s \sum_{p_s} \cos \omega(p_s) + \beta_t \sum_{p_t} \cos \omega(p_t) \quad (14)$$

and the plaquette angles  $\omega(p)$  are defined in a standard way.

In the following we shall also need the plaquette and dual formulations of the model (13). The plaquette formulation on the dual lattice can be easily obtained from the corresponding formulation on the isotropic lattice [27, 28] and takes the form

$$Z = \int_0^{2\pi} \prod_l \frac{d\omega_l}{2\pi} \exp \left[ \beta_s \sum_{l_t} \cos \omega(l_t) + \beta_t \sum_{l_s} \cos \omega(l_s) \right] \prod_x J(x), \quad (15)$$

where  $J(x)$  is the periodic delta-function which expresses the lattice Bianchi identity

$$J(x) = \sum_{r=-\infty}^{\infty} e^{ir\omega_x}, \quad \omega_x = \sum_n [\omega_n(x) - \omega_n(x - e_n)]. \quad (16)$$

Integration over plaquette (dual link) variables leads to the corresponding dual representation of the anisotropic model

$$Z = \sum_{r(x)=-\infty}^{\infty} \prod_x \prod_{n=0}^2 I_{r(x)-r(x+e_n)}(\beta_n), \quad (17)$$

where the product over  $x$  runs over all sites of the dual lattice,  $I_r(z)$  is the modified Bessel function and we introduced notations

$$\beta_n = \begin{cases} \beta_s, & n = 0 \\ \beta_t, & n = 1, 2. \end{cases} \quad (18)$$

The Villain formulation of 3D  $U(1)$  gauge theory on the anisotropic lattice can be deduced from last formulae. In particular, the dual formulation reads

$$Z = \sum_{r(x)=-\infty}^{\infty} \exp \left[ - \sum_x \sum_{n=0}^2 \frac{1}{2\beta_n} (r(x) - r(x + e_n))^2 \right]. \quad (19)$$

Clearly, the representations (15)-(19) can be viewed as the dimensional continuations of the link and dual representations of the 2d  $XY$  model [29–31].

Now we introduce some expectation values.

1. Wilson loop in representation  $j$

$$W_j(C) = \left\langle \exp \left[ ij \sum_{l \in C} \omega(l) \right] \right\rangle \quad (20)$$

can be written in the dual formulation as a ratio of partition functions

$$W_j(C) = \frac{Z_j}{Z_0}, \quad (21)$$

where  $Z_0 = Z$  and

$$Z_j = \sum_{r(x)=-\infty}^{\infty} \prod_x \prod_{n=0}^2 I_{r(x)-r(x+e_n)+\eta_n(x)}(\beta_n). \quad (22)$$

Here we have introduced sources  $\eta_n(x) = \eta(l)$  as

$$\eta(l) = \begin{cases} j, & l \in S_d, l = (x, n) \\ -j, & l \in S_d, l = (x - e_n, n) \\ 0, & \text{otherwise} \end{cases} \quad (23)$$

where  $S_d$  - surface dual to any surface  $S$  for which the contour  $C$  serves as a boundary.

2. Formulae (21)-(23) remain valid for the correlation of the Polyakov loops

$$P_j(R) = \left\langle \exp \left[ ij \sum_{x_0=0}^{N_t-1} (\omega_0(x) - \omega_0(R)) \right] \right\rangle \quad (24)$$

if  $S_d$  is a surface enclosed between two Polyakov loops.

3. The standard 't Hooft operator which measures a free energy of the monopole-antimonopole pair is given in the dual formulation by the following expectation value

$$T(x, y) = D_\pi(x, y) = \left\langle (-1)^{r(x)-r(y)} \right\rangle. \quad (25)$$

### 3 Limiting values of anisotropic couplings

We start by examining the limiting values of the anisotropic couplings.

**1. The limit  $\beta_t = 0$ .** This is the strong coupling limit. As follows from (8) it can be realized as the limit  $g^2 \rightarrow \infty$  such that  $g^2 a_t \rightarrow \infty$  but  $g^2 a_s$  remains bounded. This is the simplest limit because here the model reduces to a product of non-interacting two-dimensional gauge models. The solution of 2d gauge models is well known. For  $U(1)$  LGT we thus get

$$Z(\beta_t = 0, \beta_s) = \left[ \sum_{r=-\infty}^{\infty} I_r^{L^2}(\beta_s) \right]^{N_t}. \quad (26)$$

The model is in the confined phase at all values of  $\beta_s$ . The temporal Wilson loop, the Polyakov loop and all the correlations of the Polyakov loops are vanishing in the limit  $\beta_t = 0$ . The spatial Wilson loop in the thermodynamic limit behaves as

$$W_j(C) = \exp[-\alpha S], \quad \alpha = \ln \frac{I_0(\beta_s)}{I_j(\beta_s)}. \quad (27)$$

where  $S$  is the area of the loop  $C$ .

**2. The limit  $\beta_s = 0$ .** As follows from (8) this limit can be realized as the limit  $\xi \rightarrow 0$  such that  $g^2 a_t$  is non-vanishing. This can be considered as the finite-temperature limit. This is a non-trivial limit which cannot be solved exactly but in which the  $U(1)$  model reduces to the  $XY$ -like model. Indeed, from (17), and taking into account that  $I_r(0) = \delta_{r,0}$  one gets in the dual formulation

$$Z(\beta_t, \beta_s = 0) = \sum_{r(x)=-\infty}^{\infty} \prod_x \prod_{n=1}^2 I_{r(x)-r(x+e_n)}^{N_t}(\beta_t). \quad (28)$$

One can prove that the last formula on the original lattice is equivalent to

$$Z(\beta_t, \beta_s = 0) = \int_0^{2\pi} \prod_x \frac{d\omega_x}{2\pi} \prod_{x,n} \left[ \sum_{r=-\infty}^{\infty} I_r^{N_t}(\beta_t) \exp[i r(\omega_x - \omega_{x+e_n})] \right]. \quad (29)$$

Here,  $e^{ir\omega_x}$  is the Polyakov loop in the representation  $r$ .

For  $N_t = 1$  using the formula  $\sum_r I_r(x) e^{ir\omega} = e^{x \cos \omega}$  one finds

$$Z(\beta_t, \beta_s = 0, N_t = 1) = \int_0^{2\pi} \prod_x \frac{d\omega_x}{2\pi} \exp \left[ \beta_t \sum_{x,n} \cos(\omega_x - \omega_{x+e_n}) \right] \quad (30)$$

which is the partition function of the  $XY$  model. The formula (28) gives, for  $N_t = 1$ , the dual representation of the  $XY$  model. Thus, in this case the dynamics of the system is governed by the  $XY$  model with the inverse temperature  $\beta_t$ . For  $N_t \geq 2$  the model (28), (29) is of the  $XY$ -type, i.e. it describes interaction between nearest neighbours spins (Polyakov loops) and possesses the global  $U(1)$  symmetry. There is a little doubts that the critical behaviour for all  $N_t$  is the same as that of the  $XY$  model. Indeed, consider two different limits.

**2-A. Strong coupling limit**  $\beta_t \ll 1$ . In the leading order one can easily find from (29) up to irrelevant constant

$$Z(\beta_t \ll 1, \beta_s = 0) = \int_0^{2\pi} \prod_x \frac{d\omega_x}{2\pi} \exp \left[ h(\beta_t) \sum_{x,n} \cos(\omega_x - \omega_{x+e_n}) \right] \quad (31)$$

which is again the  $XY$  model with the coupling  $h$  given by

$$h(\beta_t) = 2 \left[ \frac{I_1 \beta_t}{I_0(\beta_t)} \right]^{N_t}.$$

The Polyakov loop and the spatial Wilson loop vanish while the correlations of the Polyakov loops are given by to the leading order

$$P_j(R) = \exp[-\alpha N_t R], \quad (32)$$

where the string tension  $\alpha$  coincides with (27) in the leading order.

**2-B. Weak coupling limit**  $\beta_t \gg 1$ , e.g.  $a_t \rightarrow 0$ ,  $g^2$  is fixed or vice-versa. Substituting asymptotics of the Bessel functions

$$I_r(x) \sim \exp \left[ -\frac{1}{2x} r^2 \right], \quad x \rightarrow \infty$$

into (28) we obtain for the partition function up to irrelevant constant

$$Z(\beta_t \gg 1, \beta_s = 0) = \sum_{r(x)=-\infty}^{\infty} \exp \left[ -\frac{\tilde{\beta}}{2} \sum_x \sum_{n=1}^2 (r(x) - r(x+e_n))^2 \right]. \quad (33)$$

This is nothing but the Villain version of the  $XY$  model in the dual formulation with an effective coupling  $\tilde{\beta}$  given by

$$\tilde{\beta} = N_t / \beta_t = g^2 / T. \quad (34)$$

This shows that the region  $\beta_s = 0$ ,  $\beta_t \gg 1$  is described by the  $XY$  model, presumably up to non-universal corrections.

#### 4 3d $U(1)$ model at finite temperature in the Villain formulation

Here we calculate the effective monopole action at finite temperatures and in the presence of sources using the Villain version of the theory given by Eq.(19). To introduce sources for both the Wilson and for the 't Hooft loops it is adventagous to start from the plaquette representation (15). The Villain approximation reduces then to the Tailor expansion of the cosine functions in the action and to keeping only the first two terms. Introducing sources both for the plaquette variables  $\eta(l)$  and for the auxiliary field  $s(x)$  one gets after some rearrangements of the sums up to a constant

$$Z_{\eta s} \equiv Z(\Lambda; \beta_t, \beta_s; \eta, s) = \sum_{r(x)=-\infty}^{\infty} \int_0^{2\pi} \prod_l \frac{d\omega_l}{2\pi} \exp \left[ -\frac{1}{2} \sum_{x,n} \beta_n \omega_n^2(x) \right] \times \exp \left[ i \sum_{x,n} \omega_n(x) (r(x) - r(x+e_n) + \eta_n(x)) + i \sum_x s(x) r(x) \right], \quad (35)$$

where  $\beta_n$  are defined in (18). Using the Poisson summation formula one can perform all Gaussian integrations. Lengthy but simple computations lead to a result which we present in the following form

$$Z_{\eta s} = Z_{\text{sw}}(\eta, s) Z_{\text{mon}}(\eta, s). \quad (36)$$

The spin-wave contribution is given by

$$Z_{\text{sw}}(\eta, s) = \exp \left[ -\frac{1}{4} \eta(l) G_{ll'} \eta(l') - \frac{1}{4} s(x) G_{xx'} s(x') - \frac{i}{2} s(x) D_l(x) \eta(l) \right], \quad (37)$$

where here and below the sums over all repeating indices are understood. The monopole contribution reads

$$Z_{\text{mon}}(\eta, s) = \sum_{m(x)=-\infty}^{\infty} \exp \left[ -\pi^2 \sum_{x,x'} m(x) G_{xx'} m(x') - \pi \sum_x h(x) m(x) \right]. \quad (38)$$

The sources  $h(x)$  are the following combination

$$h(x) = G_{xx'} s(x') + i\eta(l) D_l(x). \quad (39)$$

The link Green functions  $D_l(x)$  and  $G_{ll'}$  are given by

$$D_l(x) = \beta_n^{-1} (G_{xy} - G_{x,y+e_n}), \quad l = (y, n), \quad (40)$$

$$G_{ll'} = 2\beta_n^{-1} \delta_{ll'} - \beta_n^{-1} \beta_{n'}^{-1} (G_{xx'} - G_{x+e_n, x'} - G_{x, x'+e_n} + G_{x+e_n, x'+e_n}). \quad (41)$$

The Green function  $G_x$  on the anisotropic lattice can be written as

$$G_x = \frac{1}{L^2} \sum_{k_n=0}^{L-1} \frac{1}{N_t} \sum_{k_0=0}^{N_t-1} \frac{\exp \left[ \frac{2\pi i}{L} \sum_{n=1}^2 k_n x_n + \frac{2\pi i}{N_t} k_0 x_0 \right]}{f(k)}, \quad k_0 + k_1 + k_2 \neq 0, \quad (42)$$

where

$$f(k) = \frac{1}{\beta_s} \left( 1 - \cos \frac{2\pi k_0}{N_t} \right) + \frac{1}{\beta_t} \sum_{n=1}^2 \left( 1 - \cos \frac{2\pi k_n}{L} \right). \quad (43)$$

The expression (36) allows one to present any expectation value of the Wilson (Polyakov) and/or the 't Hooft loop in the form

$$O_{\eta s} = Z_{\text{sw}}(\eta, s) \frac{Z_{\text{mon}}(\eta, s)}{Z_{\text{mon}}(0, 0)}. \quad (44)$$

Sources  $\eta(l)$  can be taken as in (23) dependently on the Wilson and/or the Polyakov loop. Sources  $s(x)$  can be deduced from (25) dependently on the form of the string  $\mathcal{L}_{xy}$  for the monopole-anti-monopole pair.

Interactions appearing in (37) have transparent interpretation. The spin waves induce interaction  $\eta G\eta$  between elementary fluxes generated by the Wilson or the Polyakov loop (first term in (37)), the Coulomb interaction  $sGs$  between test magnetic charges (second term in (37)) and the interaction  $sD\eta$  between elementary fluxes and the magnetic charges (last term in (37)).

Effective monopole action

$$S_{\text{mon}} = -\pi^2 \sum_{x,x'} m(x) G_{xx'} m(x') - \pi \sum_x h(x) m(x) \quad (45)$$

describes the standard Coulomb interaction  $mGm$  between dynamical monopoles, the interaction  $mGs$  between dynamical monopoles and the test magnetic charges which is also of the Coulomb type and the interaction  $mD\eta$  between monopoles and elementary fluxes.

## 5 Perturbative calculation of the Polyakov loop correlator at high temperatures

Perturbative calculations for abelian models are especially simple in the plaquette formulation (15). The perturbation theory on isotropic lattice in the plaquette formulation has been developed in [28]. In that paper, a calculation of the first two perturbative coefficients of the Wilson loop can be found. An extension of those calculations to the anisotropic lattice is straightforward. Both for the temporal Wilson loop and for the Polyakov loop we write the result in the form

$$P_j(C) = 1 - g^2 C_1 + g^4 C_2 + \mathcal{O}(g^6) \quad (46)$$

$$\approx \exp \left[ -\frac{1}{4} \eta(l) G_{ll'} \eta(l') - \frac{1}{16} \eta(l) Q_{ll'} \eta(l') \right], \quad (47)$$

where

$$g^2 C_1 = \frac{1}{4} \eta(l) G_{ll'} \eta(l'), \quad (48)$$

$$g^4 C_2 = \frac{g^4}{2} C_1^2 - \frac{1}{16} \eta(l) Q_{ll'} \eta(l'), \quad (49)$$

$$Q_{ll'} = \sum_b \beta_n G_{bb} G_{lb} G_{bl'} \quad (50)$$

and the sum over  $b$  runs over all links of the (dual) lattice. For example, the first order coefficient of the Wilson loop of the size  $R \times T$  with  $R \gg 1, T \gg 1$  on the anisotropic lattice can be easily obtained from (48)

$$C_1 = \frac{j^2}{2\pi} [(a_s R) \ln T + (a_t T) \ln R] \quad (51)$$

what coincides with the result of [33] for  $j = 1$  on isotropic lattice.

These formulae are to be compared with the perturbative expansion of the two-point correlation function of the  $2d$   $XY$  model. If  $g^2$  is a dimensionless coupling constant of the  $XY$  model then the perturbative expansion takes the form [31]

$$\Gamma_{XY}(x, y) = 1 - \frac{g^2}{2} D(x - y) + \frac{g^4}{8} D(x - y) [D(x - y) - 1] + \mathcal{O}(g^6). \quad (52)$$

This result coincides with that quoted in the literature for  $O(2)$  model [32]. Taking asymptotics of the  $D$ -function  $D(x) \asymp (1/\pi) \ln |x|$  one can show that the  $\beta$ -function is vanishing in the weak coupling region of the  $XY$  model [32].

Now we analyze the weak coupling expansion (46) of the Polyakov loop at finite temperatures. Using the definition of the link Green function (41) and choosing appropriate sources described in (23), (24) one obtains after lengthy calculations

$$C_1 = \frac{1}{2} j^2 \beta D(R), \quad (53)$$

$$C_2 = \frac{1}{8} j^4 \beta^2 D^2(R) - \frac{1}{4} j^2 a_t \beta D(R) (1 - \beta_t^{-1} D_{n_1}), \quad (54)$$

where  $D(R) = G(0) - G(R)$  is the two-dimensional Green function appearing in (52) and  $D_{n_1} = G_0 - G_{n_1}$ . At high temperatures  $\beta_t^{-1} D_{n_1} \approx (2N_t)^{-1}$ . Substituting last formulae into (47) one can extract the potential between test charges

$$V_j(R) = -\frac{1}{\beta} \ln P_j(R) = \frac{1}{2} g^2 j^2 \left[ 1 + \frac{1}{2\beta_t} (1 - \beta_t^{-1} D_{n_1}) \right] D(R). \quad (55)$$

Comparing (52) with (53) and (54) one sees that the perturbative coefficients of the Polyakov loop behave qualitatively and quantitatively similar to those of the two-point correlation function of the  $2d$   $XY$  model.

## 6 The BKT-phase transition and critical indices

In this section we study the effective monopole theory (38). Our main goal is to compute critical indices  $\eta$  and  $\nu$  of the model which are defined as follows. At  $\beta \geq \beta_c$  the correlation function of the Polyakov loops decreases with the power law. This defines first critical index

$$P_1(R) \asymp R^{-\eta(T)}, \quad \eta(T_c) = 1/4. \quad (56)$$

For  $\beta < \beta_c$ ,  $t = \beta_c/\beta - 1$  one has

$$P_1(R) \asymp \exp[-R/\xi(t)], \quad \xi \sim \exp(bt^{-\nu}), \quad \nu = 1/2. \quad (57)$$

The values  $1/4$  and  $1/2$  are predictions of the BKT-theory for the  $XY$  model.

The strategy developed in the context of the  $XY$  model and described in many reviews and books can be easily adopted for effective monopole theory (38). In the leading order  $\tau/\beta \ll 1$  effective  $2d$  vortex model takes the form at zero sources,  $x = (x_1, x_2)$

$$Z_{\text{vor}} = \sum_{m(x)=-\infty}^{\infty} \delta \left[ \sum_x m(x) \right] \exp \left[ -\frac{\pi^2}{g^2 \beta} \sum_{x,x'} m(x) G_{xx'} m(x') - \kappa_0 \sum_x m^2(x) - \kappa_1 m(x) \Delta_{xx'} m(x') \right], \quad (58)$$

$$\kappa_0 = \kappa \frac{\pi^2 \beta}{6g^2 a_s^2}, \quad \kappa_1 = \kappa \frac{\pi^2 \beta^3}{180g^2 a_s^4}. \quad (59)$$

This vortex model can be exactly mapped onto the model of the sine-Gordon type

$$Z_{\text{vor}} = \int \prod_x d\alpha_x \exp \left[ - \sum_{x,x'} \alpha_x B_{xx'} \alpha_{x'} + y \sum_x \cos \alpha_x \right], \quad (60)$$

where

$$B_{xx'} = \frac{g^2 \beta}{4\pi} \Delta_{xx'} + \kappa \frac{g^2 \beta^5}{720 a_s^4} \Delta_{xy} \Delta_{yy'} \Delta_{y'x'}$$

and  $\Delta_{xy}$  is the lattice Laplace operator. Effective fugacity of the  $XY$  model reads

$$y = 2 \exp \left[ -\frac{\gamma \pi^2}{g^2 \beta} + \kappa \frac{\pi^2 \beta}{6g^2 a_s^2} \right].$$

The sine-Gordon model can be analyzed by the conventional RG methods [19, 20] where terms proportional to  $\kappa$  are treated perturbatively. We skip these well-known calculations which predict the  $XY$  critical indices  $\eta(T_c) = 1/4$  and  $\nu = 1/2$  also for our effective monopole theory.

## 7 Summary

Let us make the brief summary of main results.

At zero temperature 3d  $U(1)$  compact gauge theory exhibits permanent confinement at all values of coupling constant. At finite temperature a deconfinement phase transition takes place to a phase where the potential between test charges grows logarithmically. This is seen, e.g. from the behaviour of the correlation function of the Polyakov loops which have been computed perturbatively at high temperature. In the limit  $\beta_s = 0$  this is the BKT phase transition which belongs to the  $XY$  model universality class. At large values of  $\beta_s = 0$  we have computed effective static model for monopoles and studied it at high temperature. Assuming validity of the conventional RG methods we have obtained analytical predictions for the critical indices of the model. Our result implies that these indices coincide with those of the  $XY$  model at all values of couplings. Nevertheless, since this result relies on certain approximation the numerical check is very desirable. Such MC simulations are now in progress.

## Appendix. Green functions on anisotropic lattice

Here we derive high- and low-temperature asymptotic expansions of the Green function given by the Eq.(42). Performing summation over  $k_0$  one finds in the finite-temperature limit (12) [17]

$$G_x = \frac{1}{2g^2 a_s L^2} \sum_{k_n=0}^{L-1} \frac{\exp \left[ \frac{2\pi i}{L} \sum_{n=1}^2 k_n x_n \right]}{q(k)} \frac{\cosh \frac{\beta q}{a_s} \left( 1 - \frac{2x_0}{N_t} \right)}{\sinh \frac{\beta q}{a_s}}. \quad (61)$$

Here  $k_1 + k_2 \neq 0$  and  $q = (\sum_{n=1}^2 \sin^2 \pi k_n / L)^{1/2}$ . In the thermodynamic  $L \rightarrow \infty$  and continuum  $a_s \rightarrow 0$  limits one obtains the following expression after integration over momenta  $k_n$

$$G_x \equiv G(R, \tau) = \frac{2}{\pi g^2 \beta} \sum_{k=1}^{\infty} \cos \frac{2\pi}{\beta} k \tau K_0 \left( \frac{2\pi}{\beta} k R \right), \quad (62)$$

where

$$\tau = a_t x_0, \quad R = a_s (x_1^2 + x_2^2)^{1/2} \quad (63)$$

are the physical length and  $K_0(z)$  is the McDonald function.

The asymptotics can be easily derived from the last equations. In the high-temperature limit,  $\beta \rightarrow 0$ , we find

$$G_x = \frac{1}{g^2 \beta} G_x^{2d} + \frac{\beta}{g^2 a_s^2} B_2(\tau/\beta) \delta_{x,0} + \frac{\beta^3}{6g^2 a_s^4} B_4(\tau/\beta) \Delta_x + \mathcal{O}(\beta^5), \quad (64)$$

where  $G_x^{2d}$  is the Green function of the 2d model

$$G_x^{2d} = \frac{1}{L^2} \sum_{k_n=0}^{L-1} \frac{\exp \left[ \frac{2\pi i}{L} \sum_{n=1}^2 k_n x_n \right]}{2 - \sum_{n=1}^2 \cos \frac{2\pi}{L} k_n}, \quad k_1 + k_2 \neq 0, \quad (65)$$

$\Delta_x$  is the Laplace operator

$$\Delta_x = \sum_{n=1}^2 \left[ \delta_{x,0} - \frac{1}{2} (\delta_{x+e_n,0} + \delta_{x-e_n,0}) \right] \quad (66)$$

and  $B_n(z)$  are the Bernoulli polynomials

$$B_2(z) = \frac{1}{6} - z + z^2, \quad B_4(z) = -\frac{1}{30} + z^2 - 2z^3 + z^4. \quad (67)$$

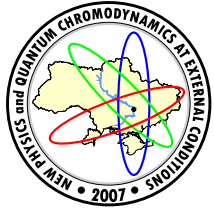
The low-temperature,  $\beta \rightarrow \infty$ , asymptotics is easily obtained from (61)

$$G_x = G_x^{3d} + \frac{1}{2g^2 a_s L^2} \sum_{k_n=0}^{L-1} \frac{\exp\left[\frac{2\pi i}{L} \sum_{n=1}^2 k_n x_n\right]}{q(k)} \sum_{r=\pm 1} \exp\left[-\frac{2q\beta}{a_s} \left|\frac{\tau}{\beta} + r\right|\right]. \quad (68)$$

Here,  $G_x^{3d}$  is the Green function of 3d theory on the anisotropic lattice (42) and which has to be computed in the Hamiltonian limit (11).

## References

- [1] A. Polyakov, Nucl.Phys. **B120**, 429 (1977).
- [2] T. Banks, J. Kogut, R. Myerson, Nucl.Phys. **B121**, 493 (1977).
- [3] S. Ben-Menaem, Phys.Rev. **D20**, 1923 (1979).
- [4] J. Ambjorn, A. Hye, S. Otto, Nucl.Phys. **B210**, 347 (1982).
- [5] M. Göpfert, G. Mack, Commun.Math.Phys. **81**, 97 (1981); **82**, 545 (1982).
- [6] J. Ambjorn, J. Greensite, JHEP **9805**, 004 (1998).
- [7] A. Duncan, R. Mawhinney, Phys.Rev. **D43**, 554 (1991).
- [8] A. Irbäck, C. Peterson, Phys.Rev. **D36**, 3804 (1987).
- [9] M. Loan, M. Brunner, C. Sloggett, C. Hamer, Phys.Rev. **D68**, 034504 (2003).
- [10] M. Zach, M. Faber, P. Skala, Nucl.Phys. **B529**, 505 (1998).
- [11] H. Trottier, R. Woloshyn, Phys.Rev. **D48**, 2290 (1993).
- [12] C. Hamer, J. Oitmaa, Zheng Weihong, Phys.Rev. **D45**, 4652 (1992); C. Hamer, Zheng Weihong, Phys.Rev. **D48**, 4435 (1993); C. Hamer, K. Wang, P. Price, Phys.Rev. **D50**, 4693 (1994).
- [13] H. Trottier, R. Woloshyn, Phys.Rev. **D48**, 4450 (1993).
- [14] A. Polyakov, *Gauge Fields and Strings* (Harwood Academic Publishers, 1987).
- [15] A. Polyakov, Phys.Lett. **B72**, 477 (1978).
- [16] L. Susskind, Phys.Rev. **D20**, 2610 (1979).
- [17] N. Parga, Phys.Lett. **B107**, 442 (1981).
- [18] V. Berezinskii, Sov.Phys. JETP **32**, 493 (1971).
- [19] J. Kosterlitz, D. Thouless, J.Phys. **C6**, 1181 (1973).
- [20] J. Kosterlitz, J.Phys. **C7**, 1046 (1974).
- [21] J. Fröhlich, T. Spencer, Commun.Math.Phys. **81**, 527 (1981).
- [22] B. Svetitsky, L. Yaffe, Nucl.Phys. **B210**, 423 (1982).
- [23] N. Mermin, H. Wagner, Phys.Rev.Lett. **22**, 1133 (1966); R. Dobrushin, S. Shlosman, Commun.Math.Phys. **42**, 31 (1975); C. Pfister, Commun.Math.Phys. **79**, 181 (1981).
- [24] P. Coddington, A. Hey, A. Middleton, J. Townsend, Phys.Lett. **B175**, 64 (1986).
- [25] M. Chernodub, E. Ilgenfritz, A. Schiller, Phys.Rev. **D64**, 054507 (2001).
- [26] R. Kenna, cond-mat/0512356.
- [27] G. Batrouni, Nucl.Phys. **B208**, 467 (1982).
- [28] O. Borisenko, S. Voloshin, M. Faber, hep-lat/0508003.
- [29] R. Savit, Phys.Rev.Lett. **39**, 55 (1977); Rev.Mod.Phys. **52**, 453 (1980).
- [30] G. Batrouni, M.B. Halpern, Phys.Rev. **D30**, 1775 (1984).
- [31] O. Borisenko, V. Kushnir, A. Velytsky, Phys.Rev. **D62**, 025013 (2000).
- [32] S. Elitzur, Nucl.Phys. **B212**, 501 (1983).
- [33] V.F. Müller, W. Rühl, Ann.Phys. **133**, 240 (1981).



## TOPOLOGY, CENTER VORTICES, CONFINEMENT AND CHIRAL SYMMETRY BREAKING IN SU(2) LATTICE QCD

Manfried Faber, Gerald Jordan and Roman Höllwieser

Atominstutut der Österreichischen Universitäten,  
 Vienna University of Technology,  
 Wien, Austria

### 1 Introduction

The fact that lattice QCD is able to describe confinement and chiral symmetry breaking is known since a long time. Actually, one of the pioneering papers of Mike Creutz [1] was already showing that the potential between static quarks and antiquarks is asymptotically linear rising with the distance. The corresponding constant force, the string tension, is incredible high, around 1 GeV/fm. The origin of this strong force should be found in the properties of the QCD vacuum. This is highly non-trivial, filled with quantum fluctuations and topological excitations which dominate the behaviour of the QCD vacuum at long distance scales. On the other hand the color electric field between quarks and antiquarks has regular flux lines and does not like to enter the stochastically fluctuating QCD vacuum. Therefore, it is energetically favourable to compress the electric flux-lines to a small tunnel between quark and antiquark. The distribution of these colour magnetic flux was nicely shown in lattice calculations [2]. Despite intensive efforts over three decades there is no derivation of confinement from first principles nor is there a generally accepted explanation. Candidates for topological excitations responsible for confinement were mainly instantons, abelian monopoles and vortices. Instantons live on a length scale of around 0.2 fm and can therefore contribute only little to the large distance force between heavy quarks [3].

By a transformation to the dual degrees of freedom one can show analytically that confinement in U(1) lattice gauge theory is due to magnetic monopoles. Kronfeld, Schierholz, and Wiese [4] devised a method for non-abelian gauge theories to detect monopoles by abelian gauge fixing and abelian projection. The property that an abelian component of the colour field can explain the full string tension was shown by [5] and was dubbed Abelian dominance. The monopole confinement mechanism leads to a very nice picture, the dual superconductor model of confinement, where magnetic monopoles and antimonopoles form a solenoidal current around the electric flux tube between quark and antiquark. But in ref. [6] we could show that the hypothesis of Abelian dominance in the maximal Abelian gauge, which was known to work for Wilson loops in the fundamental representation, fails for Wilson loops in higher group representations. Such a problem does not appear in the center vortex picture of confinement.

Center vortices are closed magnetic flux lines which carry flux corresponding to the center of the gauge group. The vortex model was first proposed by 't Hooft [7], Mack and Petkova [8] and [9]. Due to lack of an identification method for vortices, almost no numerical investigations were done for 25 years. Maximal center gauge and center projection gave us means to identify vortices[10] and led to new investigations using the vortex model. The central idea was to filter out the important infrared degrees of freedom responsible for confinement and then to simplify the field configurations by projection. Other identification methods for vortices were proposed, Laplacian center gauge by de Forcrand and coworkers [11, 12], a method by Langfeld it et al. [13] which combines Laplacian center gauge and direct maximal center gauge, and direct Laplacian center gauge [14]. All of the center gauges yield qualitatively similar results. The most important achievements are

- **Center dominance.** The vortices in the projected Z(2) gauge theory, the so called projected or P-vortices reproduce a good deal of the string tension of the full Yang-Mills theory, see Fig. 1 [14]. A removal of the P-vortices from the lattice configuration results in a loss of the confining properties [14] as depicted in Fig. 2.
- **Precocious linearity.** The projected potential is already linear at two lattice spacings [14], see Fig. 3.
- **P-vortices locate thick center vortices.** Vortex limited Wilson loops  $W_n$  are expectation values of Wilson loops in the subensemble of those configurations where the minimal area of the loop is pierced by precisely  $n$  P-vortices. As shown in Fig. 4 for large loop area  $W_n$  approaches the limit  $(-1)^n W_n$ .

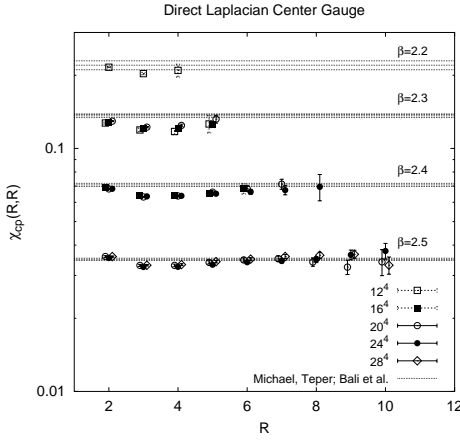


**Figure 1.** Center-projected Creutz ratios at  $\beta = 2.2 - 2.5$  obtained after direct Laplacian center gauge fixing. Horizontal bands indicate the asymptotic string tensions on the unprojected lattice, with the corresponding errorbars [14].

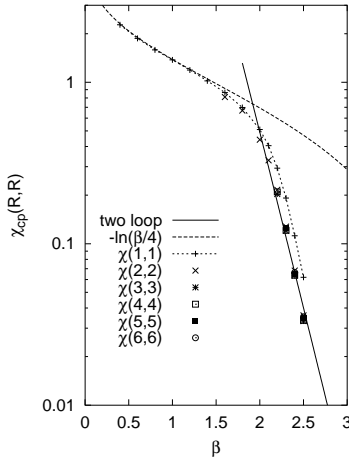


**Figure 3.** Creutz ratios from center-projected lattice configurations, in the direct Laplacian center gauge.[14]

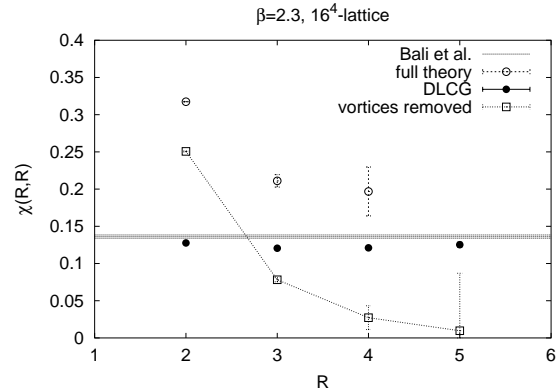


**Figure 2.** Creutz ratios on the modified lattice, with vortices removed, at  $\beta = 2.3$ . For comparison, we also display the unprojected Creutz ratios (open circles), the center projected Creutz ratios (solid circles), and the asymptotic string tension (horizontal band) [14].

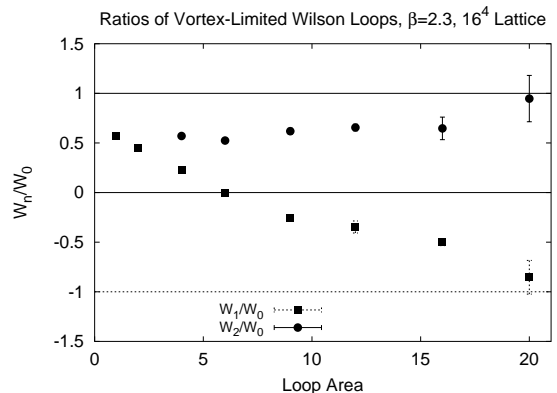


**Figure 4.**  $W_n/W_0$  ratios at  $\beta = 2.3$ .[14]

- **Scaling of vortex density.** This was first observed by Langfeld *et al.* [15] and can also be seen in Fig. 3.
- **Finite temperature.** The P-vortex density across the deconfinement phase transition was first carried out by Langfeld *et al.* [16] and Chernodub *et al.* [17]. At zero temperature vortices are unoriebtale surfaces and percolate through the lattice [18]. At finite temperature P-vortices exist also in the deconfined phase. They form cylindric objects which extend in time direction, see Fig. 5. This explains the area law for space-like Wilson loops and the perimeter law for time-like Wilson loops.
- **Casimir scaling.** The asymptotic string tension depends on N-ality of the color charge only, so that for  $SU(2)$   $\sigma_j = \sigma_{1/2}$  for  $j$  half-integer  $\sigma_j = 0$  for  $j$  integer there is still an intermediate range of distances where Casimir scaling applies (at least approximately), i.e. for  $SU(2)$   $\sigma_j = \frac{1}{2}j(j+1)$ . We could show by a very simple ansatz [19] that for charge distances comparable to the thickness of these vortices the proportionality of the string tensions to the eigenvalue of the quadratic Casimir operator is very natural in a thick vortex model (Fig. 6). For distances large compared to the vortex thickness the string tension reduces to that of the thin vortex model.
- **Topological charge.** The vortex world-surfaces allow to determine the topological charge of configurations. This was first discussed in the continuum by Cornwall [35, 36], Engelhardt and Reinhardt [37] and then on the lattice in ref. [38]. The topological charge arises at lattice sites at which the tangent vectors

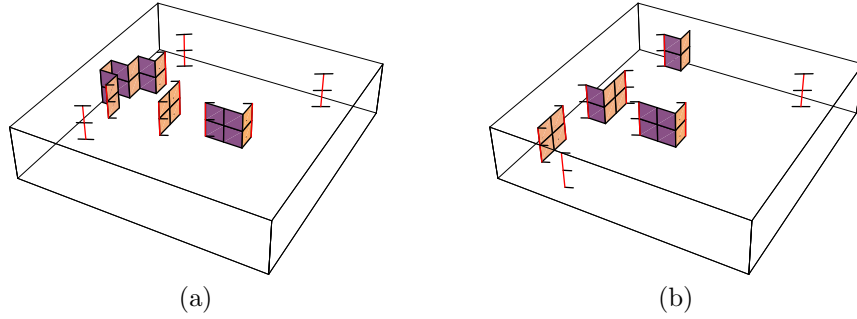


**Figure 5.** Dual P-plaquettes in a typical field configuration at  $\beta = 2.6$ , on a  $2 \cdot 12^3$ -lattice. Two successive z-slices for the x-y-t-subspace are shown. The amputated lines leaving the left figure towards right arrive in the right figure from the left.[18]

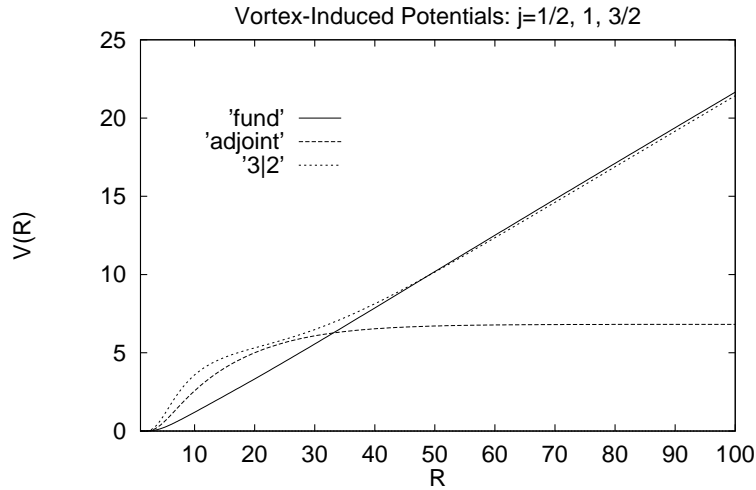


**Figure 6.** Interquark potential  $V(R)$  induced by center vortices, according to the thick vortex model discussed in the text, for quark charges in the  $j = \frac{1}{2}, 1, \frac{3}{2}$  representations.[19]

to the vortex surface span all four space-time directions. Such sites are either self-intersections points or writhing points, see Fig. 7.

- **Relation to monopole confinement.** Vortices carry colour magnetic flux, after Abelian projection this flux appears as a monopole-antimonopole chain, as indicated schematically in Fig. 8 and discussed in ref. [19].
- **Vortices and matter fields.** Matter fields lead to a breaking of the gluon string. The interesting question how matter fields influence vortices was first studied in the SU(2)-Higgs model in the continuum in refs. [20, 21] and then on the lattice in [22–24].

## 2 Vortices and chiral symmetry breaking

Concerning chiral symmetry breaking a remarkable result was found by Forcrand and d'Elia[35], removing vortices from lattice configurations leads to restoration of chiral symmetry.

That smooth vortex configurations give rise to zero-modes of the Dirac operator was shown first in analytical calculations by the Tbingen group [26]. The zero-modes of the Dirac operator tend to peak at the intersections as shown in Fig. 10. These plots show the probability density of the zero-mode in a background of two pairs of intersecting vortex sheets.

Using the chirally improved Dirac operator Gattringer and the Tbingen group[27, 28] have investigated the influence of center vortices on the properties of the Dirac spectrum. They have shown, see Fig. 11, that the removal of center vortices eliminates the zero-modes and near-zero modes of the Dirac operator implying via the Banks-Casher relation the restoration of chiral symmetry.

It was not understood why the spectra of the center projected configuration, the left diagram in Fig. 11, has developed a large gap indicating chirally symmetric field configurations. This is a very interesting result. It is up to now the only case where confinement does not lead to chiral symmetry breaking.

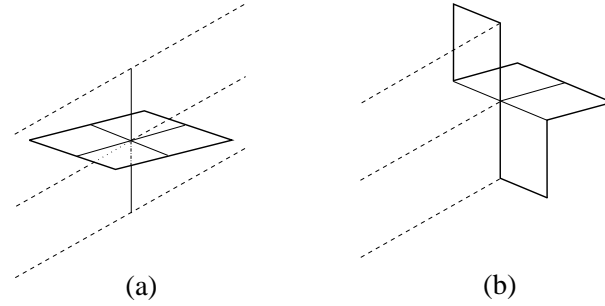


**Figure 7.** Intersection points (a) and writhing points (b) which contribute to the topological charge of a P-vortex surface. The full lines are space-like and the dashed lines time-like.

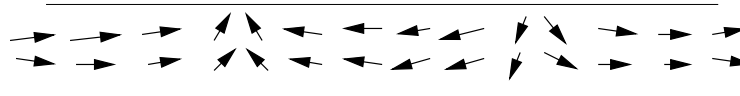


**Figure 8.** Vortex field strength after maximal abelian gauge fixing. Vortex strength is mainly in the horizontal  $\pm s_3$  direction.

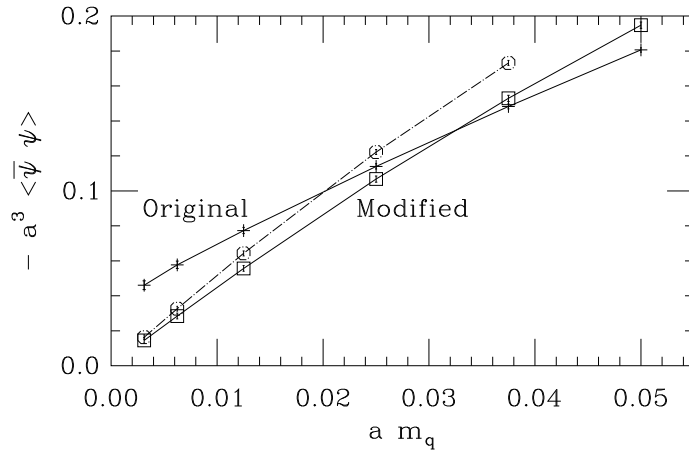


**Figure 9.** Chiral condensate in quenched lattice configurations before (“Original”) and after (“Modified”) vortex removal. From de Forcrand and D’Elia, ref.[35].

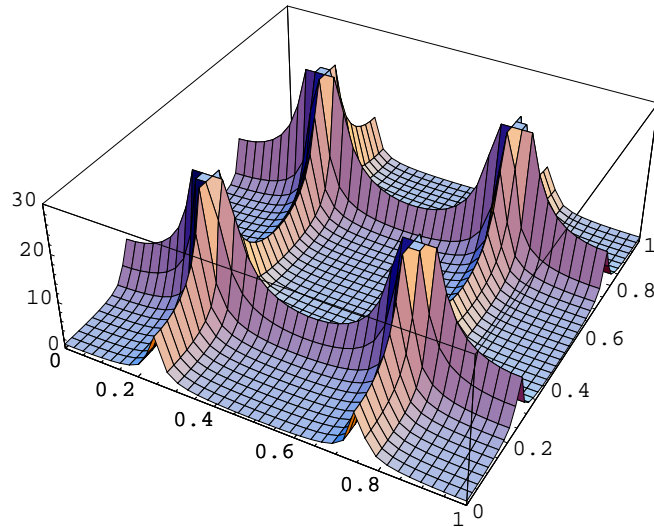


**Figure 10.** Probability density of the zero-mode in the background of four intersecting vortex sheets is shown in the two-dimensional subspace defined by the intersection points.[26]

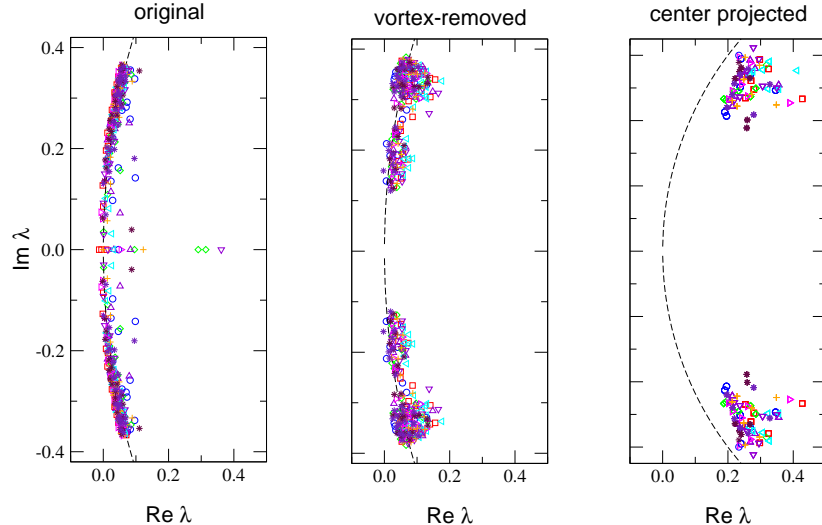


**Figure 11.** The 50 smallest Dirac eigenvalues from 10 different configurations are shown in the complex plane. The spectrum for the original ensemble (lhs. plot) are compared to the spectrum for vortex-removed configurations (rhs. plot) and the spectrum of center-projected configurations.[28]

### 3 Dirac operator and exact chiral symmetry

The chiral condensate

$$\bar{\psi}\psi = \bar{\psi}_l\psi_r + \bar{\psi}_r\psi_l \quad (1)$$

is the order parameter which indicates whether chiral symmetry is present or broken. In the chiral symmetric phase the phase transformations between right and left-handed quarks are independent and average  $\bar{\psi}\psi$  to zero. In the chirally broken phase transformations of left handed quarks lead to phase changes of right handed quarks and result in  $\bar{\psi}\psi \neq 0$ . Lattice calculations indicate that a transition from the confined to the quark-gluon plasma phase is associated with a transition from the chirally broken to the chiral symmetric phase. This indicates that both phenomena, confinement and dynamical chiral symmetry breaking may have the same origin. Due to the strong indications that vortices explain confinement it is very important to investigate the relation of vortices to chiral symmetry breaking.

The discretisation of fermions in lattice QCD is a hard problem. The reason for this difficulty lies in the celebrated no-go theorem of Nielsen and Ninomiya. It states that it is impossible to fulfill at the same time the conditions: no doublers, locality, translational invariance and reality of the bilinear fermion action. The theorem comes from topological arguments and implies that formulating fermions on a space-time lattice one of these requirements has to be given up.

The Nielsen-Ninomiya theorem requires

$$\{D, \gamma_5\} = 0 \quad (2)$$

to make the fermion action invariant under the usual continuum chiral rotations

$$\psi' = [1 + ie^a T^a \gamma_5] \psi, \quad \bar{\psi}' = \bar{\psi} [1 + ie^a T^a \gamma_5] \quad (3)$$

$T^a$  acts here in flavour space, where the Dirac operator  $D$  is proportional to unity. An interesting way around this dilemma was discovered by Ginsparg and Wilson in 1982[29]. The Ginsparg-Wilson operators obeys

$$\{D, \gamma_5\} = 2aD\gamma_5D, \quad (4)$$

the famous Ginsparg-Wilson relation, where  $a$  is the lattice constant. In the continuum limit  $a \rightarrow 0$ , this reduces to the usual chiral symmetry, so that actual physics is not affected. It was further shown that the Ginsparg-Wilson relation implies an exact symmetry of the fermion action[30], which may be regarded as a lattice form of an infinitesimal chiral rotation. Thus the Ginsparg-Wilson relation offers an exact chiral symmetry. The price to pay is that such operators are not ultralocal and therefore computationally very demanding.

The Overlap-Dirac operator [31, 32] is a solution of the Ginsparg-Wilson relation and hence a realisation of chiral symmetry on the lattice

$$D_{ov} = 1/2 [1 + \gamma_5 \epsilon(H_L^+)] \quad (5)$$

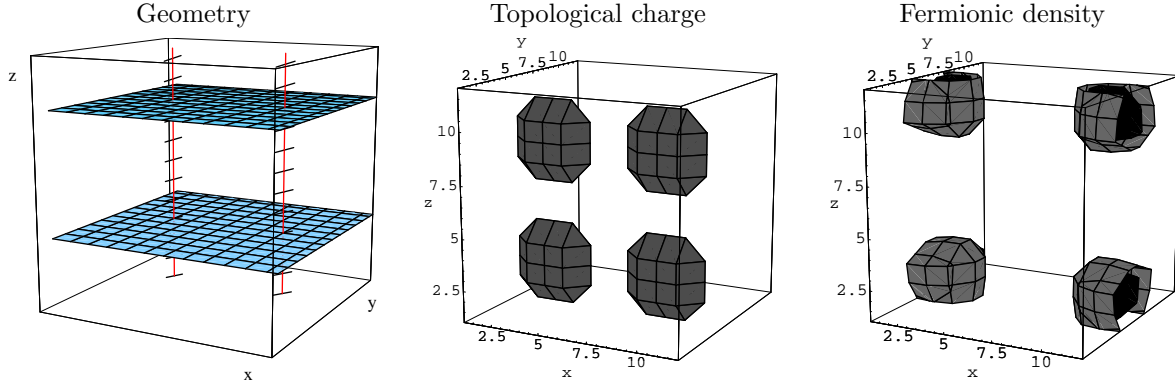


**Figure 12.** Two orthogonal pairs of plane vortices intersecting in four points

where  $\epsilon$  is the matrix sign function

$$\epsilon(H) = H/\sqrt{H^2} \quad (6)$$

and

$$H_L^+ = \gamma_5 D_w(-\mu_0) \quad (7)$$

$D_w$  is the usual lattice Wilson Dirac operator with  $r = 1$

$$(D_w)_{x,y}(\mu) = -\frac{1}{2} \sum_{\mu} [(1 + \gamma_{\mu}) U_{\mu}(x) \delta_{x+\hat{\mu},y} + (1 - \gamma_{\mu}) U_{\mu}^{\dagger}(x - \hat{\mu}) \delta_{x-\hat{\mu},y} - (\mu + 4) 2 \delta_{x,y}] \quad (8)$$

The chirally improved fermions which were developed by Gatringer and Lang[33, 34] give an approximate solution of the Ginsparg-Wilson relation. The Dirac spectra shown in Fig. 11 were produced with chirally improved fermions. It is an interesting question whether the above mentioned failure to get chiral symmetry breaking from configing P-vortex configurations is a consequence of the approximation in the solution of the Ginsparg-Wilson relation or whether it is related to some missing properties of the projected vortices.

### 3.1 Atiyah-Singer index theorem and exact zero-modes

As mentioned above, the vortex world-surfaces allow to determine the topological charge [35–38]. By the Atiyah-Singer index theorem the topological index, the topological charge, is related to the analytical index, the number of exact zero-modes.

$$\text{ind } D[A] = n_- - n_+ = Q[A] \quad (9)$$

with  $n_-, n_+$  number of left-/right-handed zeromodes. The axial anomaly

$$\gamma_{\mu} j_{\mu}^5 = -\frac{N_f}{16\pi^2} \text{Tr}(F_{\mu\nu} \tilde{F}_{\mu\nu}) \quad (10)$$

on the other hand gives upon integration again the topological charge.

$$Q := \int d^4x \gamma_{\mu} j_{\mu}^5 \quad (11)$$

We localise the eigenvectors  $\vec{v}$  for the zero-modes. Appropriate observables concerning the localisation are the scalar density

$$\rho(x) = \sum_{c,d} |\vec{v}(x)_{cd}|^2, \quad (12)$$

where the summation indices  $c$  and  $d$  refer to color und Dirac indices and further the chiral densities  $\rho_+(x)$  and  $\rho_-(x)$

$$\rho_{\pm}(x) = \sum_{c,d} \vec{v}(x)_{cd}^* \frac{1 - \gamma_5^{c,d'}}{2} \vec{v}(x)_{cd}^2 \quad (13)$$

For plane vortices the number of intersection points and the Atiyah-Singer index theorem lead to the correct topological charge.

Besides plain vortices which are usually of abelian nature it is interesting to study non-abelian vortices which may have a spherical geometry. We distinguish between an orientable and a non-orientable spherical vortex.

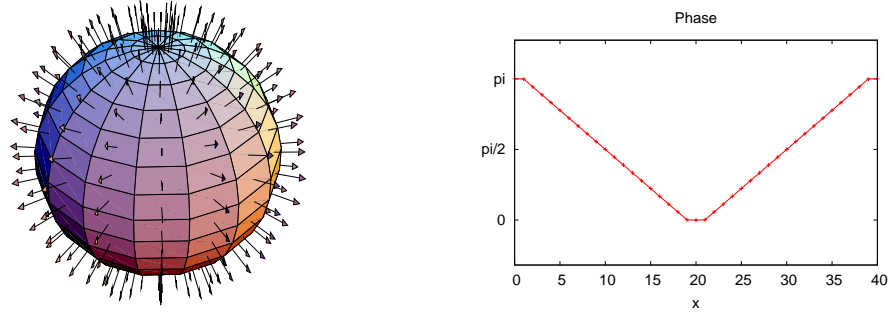


**Figure 13.** Thick Spherical SU(2)-vortex (hedgehog, non-orientable) and change of its link phase ( $\alpha_-$ )

1. The non-orientable spherical vortex of radius  $R$  and thickness  $\Delta$  is constructed with the following links:

$$U_\mu(x^\nu) = \begin{cases} \exp(i\alpha(r)\vec{n} \cdot \vec{\sigma}) & t = 1, \mu = 4 \\ \mathbf{1} & \text{else} \end{cases} \quad (14)$$

$$\vec{n} = \vec{r}/r, \vec{r} = (x, y, z), \quad (15)$$

where the function  $\alpha$  is either one from  $\alpha_+, \alpha_-$ , which are defined as

$$\alpha_+(r) = \begin{cases} \pi & r < R - \frac{\Delta}{2} \\ \frac{\pi}{2} \left(1 - \frac{r-R}{\Delta/2}\right) & R - \frac{\Delta}{2} < r < R + \frac{\Delta}{2}, \\ 0 & R + \frac{\Delta}{2} < r \end{cases} \quad \alpha_-(r) = \begin{cases} 0 & r < R - \frac{\Delta}{2} \\ \frac{\pi}{2} \left(1 + \frac{r-R}{\Delta/2}\right) & R - \frac{\Delta}{2} < r < R + \frac{\Delta}{2} \\ \pi & R + \frac{\Delta}{2} < r \end{cases} \quad (16)$$

This means that all links are equal to  $\mathbf{1}$  except for the  $t$ -links in a single time-slice at fixed  $t = 1$ . The phase changes from 0 to  $\pi$  from inside to outside (or inverse). The graphs of  $\alpha_\pm(r)$  for our largest lattice  $40^3 \times 2$  is shown in the right diagrams of fig. 16. In our computations,  $R$  is set to half the lattice size, and  $\Delta$  is chosen such that only 3 links along any direction are equal to  $+1$  and  $-1$ , respectively. The colour vector  $\vec{n}$  changes according to the spatial direction (see fig. 13).

2. The orientable vortex is constructed in a similar way:

$$U_\mu(x^\nu) = \begin{cases} \exp(i\alpha(r)|n_k| \sigma_k) & t = 1, \mu = 4 \\ \mathbf{1} & \text{else} \end{cases} \quad (17)$$

$$|n_k| = |x_k|/r, \vec{r} = (x, y, z). \quad (18)$$

Due to the absolute value of the coordinates which enter the definition, the orientable vortex is symmetric in  $x, y$  and  $z$ , in distinction to the non-orientable vortex.

The distinction non-/orientable refers to the orientation of the vortex surface assigned by abelian projection. While the orientable vortex has a global orientation, the non-orientable vortex consists of 2 patches of opposite orientation separated by a closed monopole worldline. The position of this worldline which can be determined in maximal abelian gauge depends on the  $U(1)$  subgroup which is chosen for the gauge and the projection. In fig. 14 the loops corresponding to the  $\sigma_1, \sigma_2$  and  $\sigma_3$  subgroups are depicted.

The fundamental difference between an orientable and a non-orientable vortex can be understood by considering the vector field  $\vec{n}$ , which parametrizes the direction of the links in colour space (see fig. 14). The orientation of a point in abelian projection is obtained by taking the sign of the  $z$ -component of the local  $\vec{n}$ -vector. Prior to that, one can however perform a gauge transformation in order to align all vectors along the positive or negative  $z$ -direction. For a non-orientable vortex, this is not possible by a continuous transformation.

For a spherical vortex alone, the topological charge measured on the unsmoothed links is vanishing, since only the  $U_{t\alpha}, \alpha = x, y, z$  plaquettes are non-zero, which gives a zero

$$Q \sim \epsilon_{\mu\nu\rho\sigma} U_{\mu\nu} U_{\rho\sigma} \quad (19)$$

This is independent of the lattice constant and thus holds also in the continuum limit. For the orientable vortex, the topological charge after cooling and the overlap index are also equal to 0, in keeping with the continuum expectation.

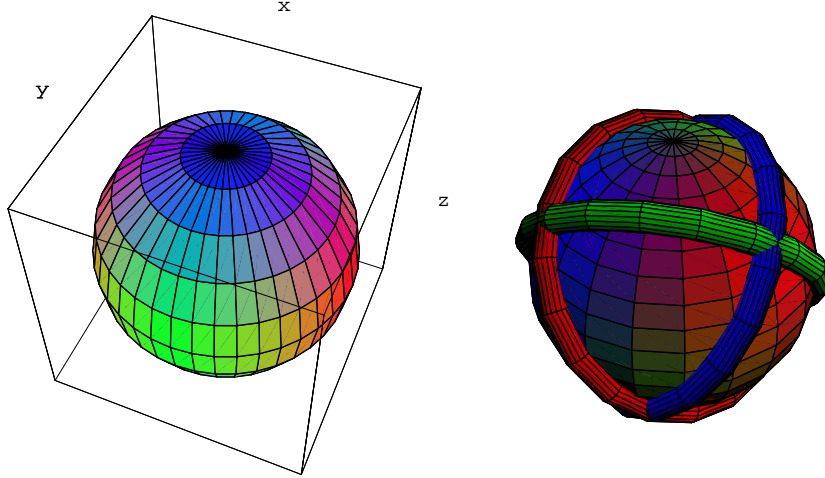


**Figure 14.** Non-orientable vortex surface (l) leads to monopole lines after abelian projection (r)

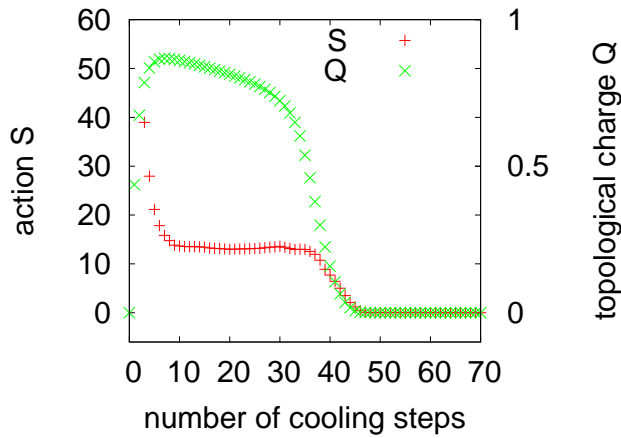


**Figure 15.** First, during cooling topological charge rises to  $\pm 1$  for  $\alpha_{\pm}$  while the action  $S$  reaches a (non-zero) plateau

However, we find a discrepancy in the case of the non-orientable sphere vortex. First, during cooling the topological charge rises near to  $\pm 1$  for  $\alpha_{\pm}$  (fig. 15).

Further, the index of the overlap operator is also non-zero,  $\text{ind}D = \pm 1$  for  $\alpha_{\pm}$ . Details are given in the table below:

type	$n_+$	$n_-$	$\text{ind}D = n_- - n_+$
non-orientable, $\alpha_-$	3	4	1
non-orientable, $\alpha_+$	1	0	-1
orientable, $\alpha_{\pm}$	0	0	0

The scalar density of the fermionic zeromodes is shown in fig. 16, along with the phase of the links. It appears that the fermions avoid regions with large link angles, or better, large Polyakov lines (which is a gauge-invariant quantity).

The non-orientable vortex also gives extra contributions to the index when it is combined with other vortices, possibly including intersection points which produce “real” topological charge.

More generally, the following empirical rule can be formulated: a non-orientable sphere vortex contributes to cooled topological charge and Dirac operator index with an integer given by the “winding number” of the links. To compute this “winding number”, the  $t$ -links are seen as a map not from  $\mathbf{T}^4$ , but from the compactified time-slice  $t = 1$ , in which the sphere is located, to  $\text{SU}(2)$ . The time-slice can be compactified to  $S^3$  because the links outside the sphere are all equal to  $+1$ .

The discrepancy between overlap index and continuum topological charge is not due to the coarse discretization. We have used lattice sizes with  $N_t = 2$  and  $N_s$  ranging from 8 to 40 in steps of 4.

The reason for the seeming contradiction is the singular nature of the continuum gauge field corresponding to a spherical vortex. This singularity invalidates the usual derivation of the index theorem.

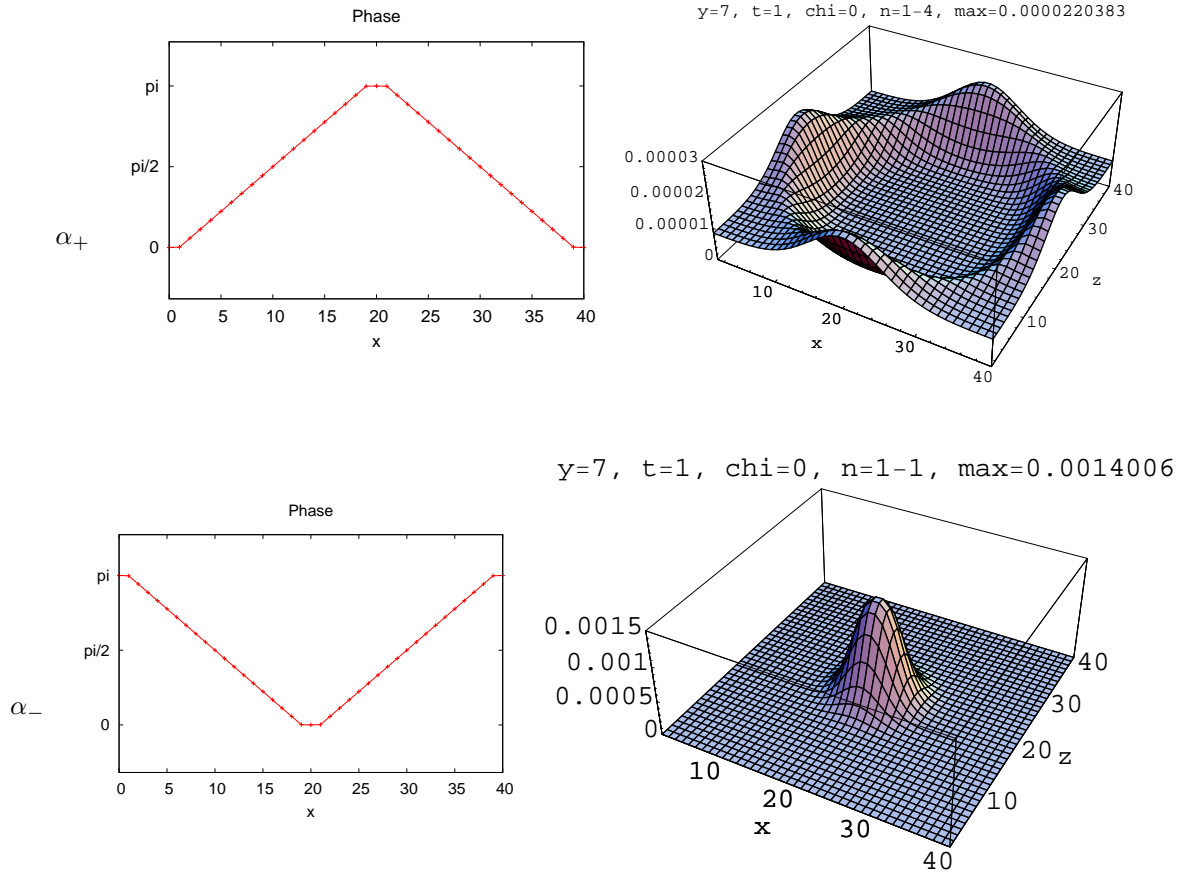


**Figure 16.**  $\alpha_+$ - resp.  $\alpha_-$ -link phase-diagrams with corresponding scalar density of the fermionic zero modes.

### 3.2 Investigation of near-zero modes of the Dirac operator

It is an interesting question whether the failure to explain the chiral condensate from center projected configurations is caused by the approximation which is due to the chirally improved fermions or whether pure P-vortices miss some important information concerning chiral symmetry breaking. This can be compared to the determination of the topological charge, where orientation information of the vortices is important for the determination of the topological charge. First we will again use the overlap Dirac operator which is obeying the Ginsparg-Wilson relation. Therefore the eigenvalues lie on the Ginsparg-Wilson circle, a circle with radius 1/2 and center (1/2, 0) in complex plane. Some results of these eigenvalues are shown in fig. 17.

The results for overlap fermions agree with those for chirally improved fermions [27, 28]. However we find a different behaviour for staggered fermions. The Dirac operator for massless staggered fermions  $\chi$  reads:

$$D_{sf} = \frac{1}{2a} \sum_{\mu} \eta(x, \mu) P(x, \mu) \quad (20)$$

with  $P(x, \mu) = [U(x, \mu)\chi(x + a_{\mu}) - U^{\dagger}(x - a_{\mu}, \mu)\chi(x - a_{\mu})]$ .

$\eta(x, \mu) = (-1)^{\sum_{\nu < \mu} x_{\nu}}$  are the staggered fermion phases. Its eigenvalues are imaginary and an example for a spectrum is shown in fig. 18.

We don't see any gap in center projected and vortex removed configurations in contradiction to overlap and chirally improved fermions. The gaps reappear again for vortex removed configurations if we use antiperiodic boundary conditions (see fig. 19).

## 4 Conclusion

To conclude we summarize the main facts of Center Vortex investigations:

- Confining Disorder  $\equiv$  Center Disorder, caused by center vortices.
- P-vortices locate center vortices  $W_n/W_0 = (-1)^n$

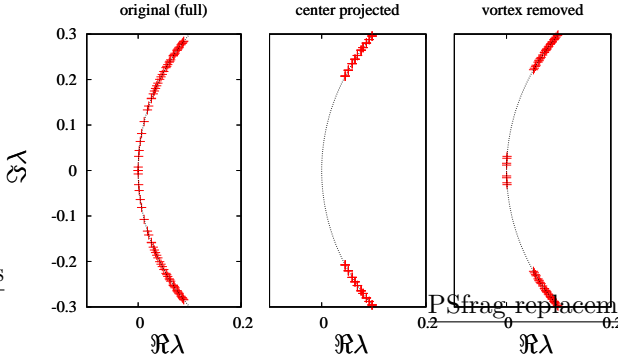


**Figure 17.** Eigenvalues of the Overlap Dirac operator

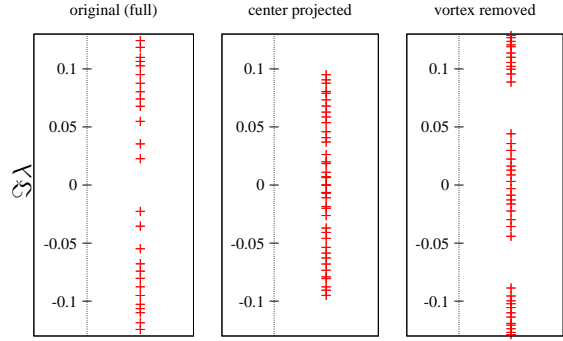


**Figure 18.** Eigenvalues of the Staggered Fermion operator

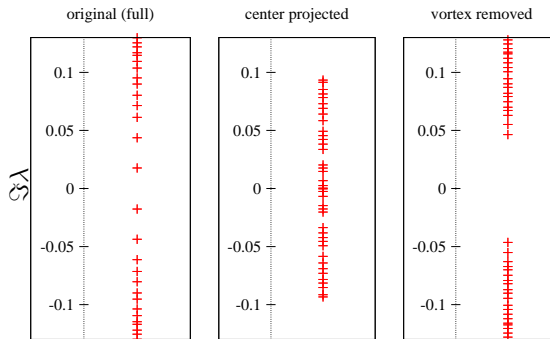


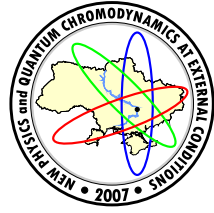
**Figure 19.** Eigenvalues of the Staggered Fermion operator for antiperiodic boundary conditions

- Center Dominance: The projected string tension is close to the asymptotic string tension  $\sigma$  of full Monte-Carlo configurations  $\chi_{cp}(R, R) \approx \sigma$  ( $R \geq 2$ )
- Vortex density shows asymptotic scaling.
- Upon abelian projection, center vortices appear as chains of monopoles and antimonopoles.
- In the deconfined phase, vortices are static. They are composed of space-space plaquettes. They are orientable and have the topology of a torus.  
(Polyakov loop behaviour)
- In the confined phase P-vortices are unorientable.
- Pontryagin index from vortex intersection and writhing points
- Topological susceptibility mainly from writhing points
- Vortex removal restores chiral symmetry
- Index theorem fulfilled for U(1) vortices
- Index theorem puzzeling for SU(2) vortices
- Discrepancy between staggered and overlap fermions for P-vortices

## References

- [1] M.Creutz, Phys.Rev. **D21**, 2308 (1980).
- [2] G.S.Bali, K.Schilling, C.Schlichter, Phys.Rev. **D51**, 5165 (1995).
- [3] T.A.DeGrand, A.Hasenfratz, T.G.Kovacs, Nucl.Phys.Proc.Suppl. **63**, 528 (1998).
- [4] A.S.Kronfeld, G.Schierholz, U.J.Wiese, Nucl.Phys. **B293**, 461 (1987).
- [5] T.Suzuki I.Yotsuyanagi, Phys.Rev. **D42**, 4257 (1990).
- [6] L.Del Debbio, M.Faber, J.Greensite, and S.Olejnik, Phys.Rev. **D53**, 5891 (1996).

- [7] G.'t Hooft, Nucl.Phys. **B138**, 1 (1978).
- [8] G.Mack, V.B.Petkova, Ann.Phys. **123**, 442 (1979).
- [9] J.M.Cornwall, Nucl.Phys. **B157**, 392 (1979).
- [10] L.Del Debbio, M.Faber, J.Greensite, and S.Olejnik, Phys.Rev. **D55**, 2298 (1997).
- [11] C.Alexandrou, P.de Forcrand, M.D'Elia, Nucl.Phys. **A663**, 1031 (2000).
- [12] P.de Forcrand, M.Pepe, Nucl.Phys. **B598**, 557 (2001).
- [13] K.Langfeld, H.Reinhardt, A.Schäfke, Phys.Lett. **B504**, 338 (2001).
- [14] M.Faber, J.Greensite, S.Olejnik, JHEP **11**, 053 (2001).
- [15] K.Langfeld, H.Reinhardt, O.Tennert, Phys.Lett. **B419**, 317 (1998).
- [16] K.Langfeld, O.Tennert, M.Engelhardt, H.Reinhardt, Phys.Lett. **B452**, 301 (1999).
- [17] M.N.Chernodub, M.I.Polikarpov, A.I.Veselov, M.A.Zubkov, Nucl.Phys.Proc.Suppl. **73**, 575 (1999).
- [18] R.Bertle, M.Faber, J.Greensite, S.Olejnik, JHEP **03**, 019 (1999).
- [19] M.Faber, J.Greensite, S.Olejnik, Phys.Rev. **D57**, 2603 (1998).
- [20] G.Mack, H.Meyer, Nucl.Phys. **B200**, 249 (1982).
- [21] H.Meyer, Nucl.Phys. **B235**, 115 (1984).
- [22] R.Bertle, M.Faber, in *Quark Confinement and the Hadron Spectrum V*, (ed. N.Brambilla and G.M.Prosperi, World Scientific, Singapore, 2003), pp. 3-12 [hep-lat/0212027].
- [23] K.Langfeld, hep-lat/0212032.
- [24] R.Bertle, M.Faber, J.Greensite, S.Olejnik, Phys.Rev. **D69**, 014007 (2004).
- [25] P.de Forcrand, M.D'Elia, Phys.Rev.Lett. **82**, 4582 (1999).
- [26] H.Reinhardt, O.Schroeder, T.Tok, V.C.Zhukovsky, Phys.Rev. **D66**, 085004 (2002).
- [27] S.Solbrig *et. al.*, PoS LAT2005, 301 (2005) [hep-lat/0509052].
- [28] J.Gattnar *et. al.*, Nucl.Phys. **B716**, 105 (2005).
- [29] P.H.Ginsparg, K.G.Wilson, Phys.Rev. **D25**, 2649 (1982).
- [30] M.Lüscher, Phys.Lett. **B428**, 342 (1998).
- [31] H.Neuberger, Phys.Rev. **D57**, 5417 (1998).
- [32] H.Neuberger, Phys.Lett. **B427**, 353 (1998).
- [33] C.Gattringer, Phys.Rev. **D63**, 114501 (2001).
- [34] C.Gattringer, I.Hip, C.B.Lang, Nucl.Phys. **B597**, 451 (2001).
- [35] J.M.Cornwall, Phys.Rev. **D58**, 105028 (1998).
- [36] J.M.Cornwall, Phys.Rev. **D61**, 085012 (2000).
- [37] M.Engelhardt, H.Reinhardt, Nucl.Phys. **B585**, 591 (2000).
- [38] R.Bertle, M.Engelhardt, M.Faber, Phys.Rev. **D64**, 074504 (2001).



## CONFINEMENT ENCODED IN LANDAU GAUGE GLUON AND GHOST PROPAGATORS

E.-M. Ilgenfritz<sup>a</sup>

Humboldt-Universität, Institut für Physik, Berlin, Germany

An introduction is given into current lattice investigations of the non-perturbative gluon and ghost propagators, in the light of the Gribov-Zwanziger and Kugo-Ojima scenarios of confinement, in the context of results obtained from the non-perturbative Dyson-Schwinger approach in the continuum and in connection with the vortex mechanism of confinement.

### 1 Introduction

In lattice gauge field theory, confinement of quarks is numerically proven although the dynamical origin is still under debate [1]. An exponential area law holds for Wilson loops in the fundamental representation. What about gluon confinement? Wilson loops with (static) adjoint charges do not decay with an area law, but gluons are confined, too. This talk is an introduction to alternative confinement ideas [2–4] and presents a report on combined efforts by continuum and lattice theorists to understand how they might be realized in Nature.

The infrared behavior of gluon, ghost and quark propagators is the focus of a field-theoretic approach [5] to confinement. Green's functions carry all information about the structure of a theory. These propagators, in distinction to hadron propagators, are gauge-variant. This is the origin of difficulties related to the *Gribov ambiguity* which shows up at different places. The first, pioneering study [6] of the gluon propagator in Landau gauge (on lattices as small as  $4^3 \times 8$ ) dates back to 1987. Gluon and ghost propagators became topics of stronger interest in the middle of the 90-s. A first review about this activity was given in [7].

To establish a relation between confinement and the gluon and ghost propagators one mostly concentrates on the infrared momentum range. Is this range, where the asymptotic behavior sets in,  $O(100)$  or  $O(10)$  MeV or smaller? In order to probe small momenta, one needs to control the infinite-volume limit. This makes the problem difficult on the lattice, even with present day lattice sizes and computers. The following are the signatures of confinement from this point of view:

- The gluon propagator should vanish in the limit  $q \rightarrow 0$  [8, 9]. The gluon dressing function  $Z(q^2)$ , defined through

$$D_{\mu\nu}^{ab}(q) = \delta^{ab} \left( \delta_{\mu\nu} - \frac{q_\mu q_\nu}{q^2} \right) \frac{Z(q^2)}{q^2}, \quad (1)$$

should behave in the infrared as  $Z(q^2) \propto (q^2)^{\kappa_D}$  with  $\kappa_D > 1$ .

- The ghost propagator ought to be more singular at  $q \rightarrow 0$  than a free scalar one [3, 10]. This is the *horizon condition*. The ghost dressing function, defined through

$$G^{ab}(q) = \delta^{ab} \frac{J(q^2)}{q^2}, \quad (2)$$

should behave in the infrared as  $J(q^2) \propto (q^2)^{\kappa_G}$  with  $\kappa_G < 0$ .

- Positivity of the spectral function is expected [3] to be violated for the gluon propagator, meaning that the weight function  $\rho(m^2)$  in the Källen-Lehmann representation

$$D(q^2) = \int_0^\infty \frac{dm^2 \rho(m^2)}{q^2 + m^2} , \quad D(t, \vec{q} = 0) = \int_0^\infty dm^2 \rho(m^2) e^{-mt} \quad (3)$$

would no longer be  $\rho(m^2) \geq 0$  for all  $m^2$ .

- The Kugo-Ojima (KO) confinement criterion [4] is formulated in terms of the ghost propagator  $G_{xy}^{ab} = \langle c_x^a \bar{c}_y^b \rangle$ . One defines  $u^{ab}(q^2)$  by

$$\int d^4x e^{iq(x-y)} \langle (D_\mu^{ac} c^e)_x (f^{bcd} A_\nu^d \bar{c}^c)_y \rangle = \left( \delta_{\mu\nu} - \frac{q_\mu q_\nu}{q^2} \right) u^{ab}(q^2) \quad (4)$$

and requires that  $u^{ab}(q^2) \rightarrow -\delta^{ab}$  in the limit  $q^2 \rightarrow 0$ . This guarantees the absence of colored asymptotic states. The criterion was derived from the so-called quartet mechanism within the BRST quantization of Yang-Mills theory.

The practical request from the side of hadron physics has stimulated non-perturbative studies in the continuum of the gluon and ghost propagator that have started ten years ago [5, 8, 9]. The authors were seeking for solutions of the hierarchy of Dyson-Schwinger equations (DSE) (coupled for both propagators) adopting some truncations. In this approach infinite volume presents no problem. More recently one has learned how to solve the DSE in a compactified space, on the 4-torus [11, 12]. The lessons from DSE, for infinite and compactified space, provide a framework to discuss the status of the lattice calculations. It helps to orient oneself on the “long march” to the infinite-volume limit.

The particular value of *lattice calculations* at first consists in their ability to *control* the assumptions and truncations made in the DSE approach. At second and even more interesting as I find, they are possible to assess the importance of special confining field excitations (monopoles and vortices, dyons and calorons) and/or external conditions on the functional form of the propagators. At third, from the beginning of the lattice studies it was clear that the Gribov ambiguity would present a hard problem.

Thus, it is left to the *lattice studies* to elucidate the open theoretical problems how to deal with it. If the lattice discretization *is the definition* of QCD in the non-perturbative regime, different prescriptions how to take into account the Gribov problem could lead to different versions of QCD requiring verification.

The vanishing (divergence) of the gluon (ghost) propagators can be traced back to the restriction inside the so-called *Gribov region*  $\Omega$  of the gauge field representants  $A_\mu$  (transverse gauge copies) that are contributing to the path integral. This is the region where the Faddeev-Popov operator  $\mathcal{M}$  is positive. The problem are more than one of such copies. In the infinite-volume limit the tendency emerges that the most important configurations concentrate at the boundary, the Gribov horizon, such that small non-trivial eigenvalues of  $\mathcal{M}$  accumulate close to zero with a finite density. This is the *Gribov-Zwanziger confinement scenario* [3]. The infrared exponents  $\kappa_D = 2\kappa \approx 1.2$  and  $\kappa_G = -\kappa \approx -0.595$  (constrained to  $1/2 < \kappa < 1$  [13]) have been obtained both by the DSE approach [13, 14] and by stochastic quantization [15, 16]. A consequence of the interrelation between both infrared exponents is an infrared fix-point of the strong coupling,  $\alpha_s(0) = 8.915/N_c$ .

The positivity violation was noticed very soon [6, 17, 18] in lattice simulations, when the “local mass”  $m_{eff}(t) = -d \log D(t, \vec{q} = 0)/dt > 0$  was found to *increase* with increasing  $t$ . For a physical particle in the asymptotic Hilbert space, the effective mass  $m_{eff}(t)$  approaches the actual mass from above.

## 2 The lattice framework

Lattice gauge theory is formulated in a way that circumvents the choice of a gauge. Apart from our task (to calculate Green’s functions) there are many other contexts in which fixing the gauge is necessary or useful. Gauge-fixing usually becomes a very time-consuming part of such calculations and deserves particular attention. The procedure of such a calculation is as follows: An ensemble of gauge configurations  $\{U\}$  is generated with one’s favorite action using the Monte Carlo (MC) method, either without (“quenched”) or with the back-reaction of (“dynamical”) quarks through the fermion determinant taken into account. In the quenched approximation one has just a gluonic inverse “bare coupling”  $\beta$ , and the lattice spacing  $a$  is a function of it,  $a(\beta)$ , that can be defined by putting the string tension  $\sigma = a^{-2} \sigma_L(\beta)$  equal to some physical value. Up to a global scale, the renormalization of the gluon propagator (matching the propagators measured at different  $\beta$ ) is an independent way to define the running lattice scale  $a(\beta)$ .

The vector potential needs to be extracted from the basic transporters (“links”) as

$$\mathcal{A}_{x+\hat{\mu}/2, \mu} = (U_{x\mu} - U_{x,\mu}^\dagger)_{\text{traceless}} / (2iag).$$

In order to implement the gauge in question, every gauge configuration  $\{U\}$  has to be gauge-transformed  $U_{x,\mu} \rightarrow U_{x,\mu}^g = g_x U_{x,\mu} g_{x+\hat{\mu}}^\dagger$  by a suitable  $\{g\}$ .

For example, for the Landau gauge an extremization

$$F_U[g] = \frac{1}{N_c} \sum_{x,\mu} \text{Re} \text{Tr} g_x U_{x,\mu} g_{x+\mu}^\dagger \rightarrow \text{Max} \quad (5)$$

with respect to  $\{g\}$  solves the problem. A *local maximum* is found when

$$(\partial_\mu \mathcal{A}_\mu^g)_x = \sum_\mu \left( \mathcal{A}_{x+\hat{\mu}/2, \mu}^g - \mathcal{A}_{x-\hat{\mu}/2, \mu}^g \right) = 0 \quad (6)$$

(the transversality condition) is satisfied with high precision. This defines the recommended stopping criterion for the various iterative gauge-fixing methods. Having found a local maximum  $\{g\}$ , for any infinitesimal  $\tilde{g}$ , one has  $F_{U^g}[\tilde{g}] < F_{U^g}[1]$ . For the absolute maximum  $\{g\}$ , this should hold for all  $\tilde{g}$ . Thus, the gauge-fixing problem has been put into the form of a disordered spin system. The search for the (classical) ground state of a spin glass is known to be a *non-polynomially hard* problem.

If extracting physics would depend on the ability to find the absolute maximum one had to stop here. In this case the measure is said to be restricted to the so-called *fundamental modular region*  $\Lambda$ . It is possible, however, to go a bit further and to investigate the convergence of gauge-variant observables with an increasing number  $n_{\text{copy}}$  of Gribov copies. A sequence of replica ensembles labelled by  $n_{\text{copy}}$  is recursively created (with  $n_{\text{copy}} = 0$  denoting to the original MC ensemble). Each time one steps from  $n_{\text{copy}} \rightarrow n_{\text{copy}} + 1$ , for each MC configuration a new gauge-fixing attempt is made starting from a random gauge transformation. If a better representant of the original MC configuration is found, it replaces the “previously best” copy, such that the  $n_{\text{copy}}$ -th ensemble is an ensemble of “currently best” copies after  $n_{\text{copy}}$  attempts.

On the other side, Zwanziger [19] gave arguments that in the infinite-volume limit an average over all gauge-fixed copies in the Gribov region would be the physically correct prescription. This would make the search for ever better copies obsolete, and it would be just a question of statistics how many gauge copies of one MC configuration are evaluated.

In any case, for the present lattice sizes it is important to assess the gauge copy dependence of the propagators. Following the “best copy vs. first copy” strategy, one sees that the dependence is stronger at small momenta and becomes indeed weaker with increasing volume.

In order to do the maximization, methods like overrelaxation (OR), Fourier accelerated gauge-fixing (FA) and simulated annealing (SA) are practically in use. The latter [20] is a quasi-equilibrium MC process with a probability distribution  $\propto \exp(F_U[g]/T)$ . Annealing means that the temperature is guided from  $T_{\text{max}}$  down to  $T_{\text{min}}$ . The idea is that OR following the SA (until the transversality is satisfied) finds the finally gauge-fixed copy with only few iterations within one basin of attraction. Therefore, improvement of the gauge-fixing is not mainly aiming to accelerate the relaxation but to increase the yield of “good” gauge-fixed copies, as close as possible to the best copy. Given this objective, SA strategies become superior on large lattices [21] also in terms of computing time.

The gluon propagator is defined immediately in momentum space by correlating Fourier transforms  $\tilde{\mathcal{A}}^g$  of the  $\mathcal{A}^g$  field,

$$D_{\mu\nu}^{ab}(q) = \langle \tilde{\mathcal{A}}_\mu^a(k) \tilde{\mathcal{A}}_\nu^b(-k) \rangle, \quad (7)$$

where the finite lattice Fourier transform is calculated for integers  $k_\mu \in (-L_\mu/2, L_\mu/2]$ . The momentum vector  $q_\mu(k_\mu) = (2/a) \sin(\pi k_\mu/L_\mu)$  is associated to them. If the gluon propagator is to be calculated for many momenta, use of fast Fourier transformation is necessary.

The ghost field is not a *c*-number field in the memory, such that the ghost propagator, similar to a quark propagator, must be obtained by inversion of the Faddeev-Popov operator

$$\mathcal{M}_{xy}^{ab}(U) = \sum_\mu (A_{x,\mu}^{ab}(U) \delta_{xy} - B_{x,\mu}^{ab}(U) \delta_{x+\hat{\mu},y} - C_{x,\mu}^{ab}(U) \delta_{x-\hat{\mu},y}), \quad (8)$$

with  $\mathcal{M}_{xy}^{ab} \rightarrow -\delta^{ab} \Delta_{xy}$  for  $U_{x,\mu} \rightarrow 1$ . The matrices  $A$ ,  $B$  and  $C$  are defined in terms of (gauge fixed) links as

$$\begin{aligned} A_{x,\mu}^{ab} &= \text{Re Tr} [T^a T^b (U_{x,\mu} + U_{x-\hat{\mu},\mu})] , \\ B_{x,\mu}^{ab} &= 2 \text{Re Tr} [T^b T^a U_{x,\mu}] \\ C_{x,\mu}^{ab} &= 2 \text{Re Tr} [T^a T^b U_{x-\hat{\mu},\mu}] . \end{aligned} \quad (9)$$

In momentum space the propagator is obtained by inverting  $\mathcal{M}$  on a plane wave source (for  $k \neq (0, 0, 0, 0)$ )

$$\sum_{b,y} \mathcal{M}_{xy}^{ab} \phi_y^{b(c)} = \psi_x^{a(c)} = \delta^{ac} e^{2\pi i k \cdot x}, \quad (10)$$

giving

$$G^{ab}(q) = \frac{1}{V(N_c^2 - 1)} \sum_c \sum_x \psi_x^{a(c)*} \phi_x^{b(c)}. \quad (11)$$

For the inversion the conjugate gradient algorithm is used. For preconditioning one uses the simple (not the covariant!) Laplacian.

If one defines the strong coupling  $\alpha_s$  through the ghost-gluon vertex, then, knowing the (renormalized) dressing functions  $Z_R$  and  $J_R$  and assuming for the vertex renormalization constant  $Z_1(q^2) \approx 1$ , one obtains [22] in the MOM-scheme the running coupling as follows

$$\alpha_R(p^2) = \alpha_R(\mu^2) Z_R(p^2, \mu^2) [J_R(p^2, \mu^2)]^2. \quad (12)$$

### 3 Some lattice results

The lattice calculations should give an answer to the following questions:

- Do the propagators show the infrared behavior proposed by DSE?
- What is the infrared limit of the MOM-scheme coupling  $\alpha_s(q^2)$ ?
- What is the impact of Gribov copies on the propagators?
- How fast is the infinite-volume limit reached?
- Which propagators are modified by “unquenching”?
- How are the other confinement criteria fulfilled?
- How do Faddeev-Popov eigenvalues and eigenmodes behave?
- Is the ghost propagator in the infrared dominated by the lowest eigenmodes of  $\mathcal{M}$ ?

Finally, one might ask:

- Are there modified gauge-fixing conditions, equivalent to the common ones in the infinite-volume limit, that are advantageous for convergence to the infinite volume limit and/or less vulnerable to discretization effects?

I will present some answers in the following. Our studies have included quenched  $SU(3)$  QCD on lattices from  $12^4$  to  $72^4$  generated with Wilson gauge action at  $\beta = 5.7, 5.8, 6.0$  and  $6.2$ . The full QCD configurations kindly provided by the QCDSF collaboration are  $16^3 \times 32$  and  $24^3 \times 48$  lattices created with Wilson gauge action at  $\beta = 5.29$  and  $5.25$  and  $N_f = 2$  clover-improved Wilson fermions of varying mass ( $\kappa = 0.135 \dots 0.13575$ ). The last question of an improved gauge-fixing was recently investigated in quenched  $SU(2)$  gauge theory [23] where the consequences of enlarging the set of admissible gauge transformations by global  $Z(N)$  flips (proposed in [24]) were further examined.

In Fig. 1a we show the gluon dressing function for quenched QCD [25, 26]. Characteristic is the intermediate bump of the dressing function. The exact form of the dressing function is *not described* by the DSE, which pretend to describe only the infrared and ultraviolet behavior. In particular the bump is underestimated. Fig. 2a shows that this enhancement becomes partly (30 %) depressed by the back-reaction of dynamical quarks [27]. The same is observed for dynamical configurations of the MILC collaboration in [28]. In view of the difficulties to determine the infrared exponent  $\kappa_D$  (see below) it is premature to speak about the dynamical-quark effect on  $\kappa_D$ . Since the main effect is not in the infrared behavior, the change could be considered irrelevant for the confinement problem. Indeed, breakdown of *gluon confinement* is not realistic in the real world with dynamical quarks. In contrast to that, it is known that dynamical quarks indeed change the confinement property of static quarks (“string breaking” [29]). In the quenched  $SU(2)$  theory the so-called “infrared bump” (sitting, however in fact at 1 GeV !) is entirely the result of the presence of P-vortices as confining agents seen in Maximal Center Gauge (MCG) and projection. The enhancement By the same operation confinement [30], topological charges and chiral symmetry breaking [31] are destroyed. A natural conjecture is that dynamical quarks to some extent suppress P-vortices. This hypothesis deserves closer investigation. That the opposite effect of unquenching is observed for the density of monopoles [32] can be explained that there is an “inert” component of monopoles [30] not related to P-vortices.

Fig. 1b presents the ghost dressing function [25, 26] for the quenched theory. The behavior in the infrared is opposite to the gluon dressing function and not incompatible with being divergent. In Fig. 2b one sees that unquenching [27] has no dramatic effect on the ghost propagator, except for the smallest momenta accessible, where also a splitting according to the quark masses (see the legend) becomes visible.

The infrared increase of the ghost structure function in the quenched theory is obvious, but the fitting of an infrared exponent does not give the expected  $\kappa$ . For  $SU(2)$  gauge theory it is known [34] that the removal of P-vortices leads to a global change of the ghost dressing function  $J(q^2)$  which becomes almost constant. One can say that the global (not only infrared) behavior of the ghost dressing function is the closest relative to the confinement of quarks. Since vortex removal also removes all non-perturbative attributes [35] (percolating monopole trajectories, string tension, chiral condensate and the topological charge [31], it is very likely that the original divergence of the ghost propagator like  $1/(q^2)^{1+\kappa}$  is mainly a result of the topological structure leading to an enhanced density of low-lying eigenvalues of  $\mathcal{M}$  as demonstrated for MC [36] and model configurations [37]. We have found, however, that the direct correspondence between the ghost propagator at lowest momenta and the lowest-lying Faddeev-Popov eigenmodes is rather weak [38]. The effect of dynamical quarks is not as strong as vortex removal, but it might be caused indirectly via the gradual suppression (or pairing) of topological

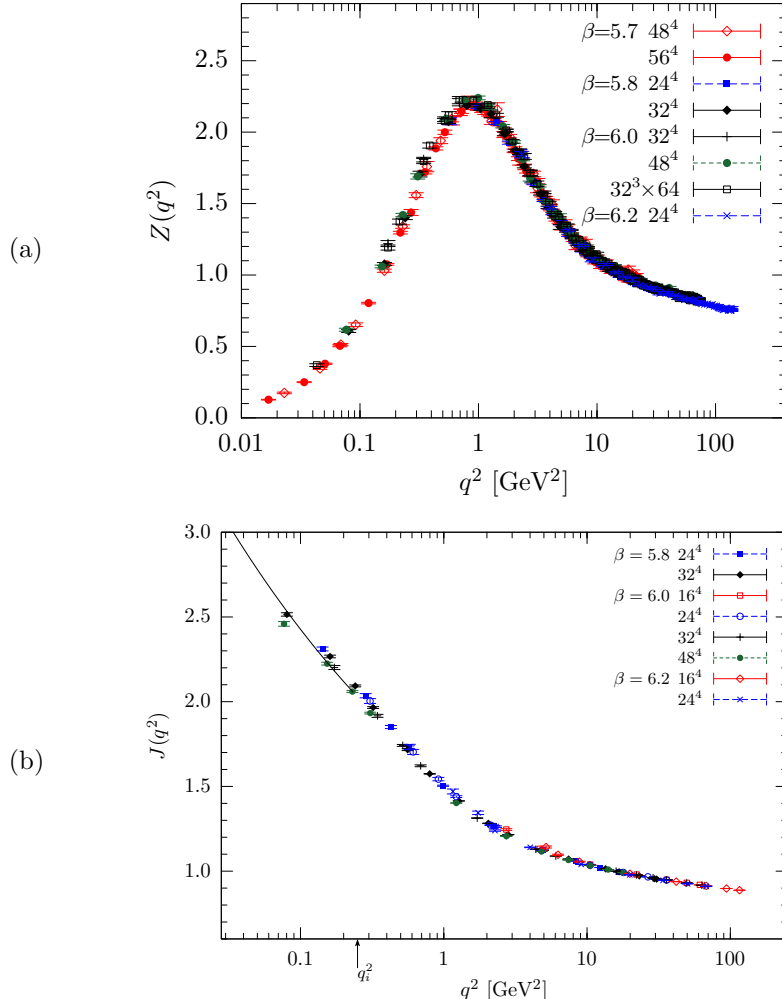


**Figure 1.** The gluon dressing function (a) and the ghost dressing function (b) for quenched QCD. Data from various lattice sizes and  $\beta$ -values are seen matching on one curve. The little  $q_i^2$  marks a momentum range  $q^2 < q_i^2$  where a power fit for  $\kappa$  has been attempted. Both propagators give a  $\kappa \approx 0.2$ .

objects by light sea quarks, too. The quark mass dependence of the effect might be related to the stronger string breaking induced by lighter sea quarks.

Our data suggest that both in the quenched and the dynamical case there are apparently no finite-volume effects on the ghost propagator. This will be made more precise later.

Figs. 1 and 2 for the gluon propagator come from a study where the Gribov ambiguity was ignored. Only one gauge-fixed copy (“first copy”) was evaluated. I should remark that this procedure is equivalent to the prescription of averaging over all gauge-fixed copies within the Gribov region (justified in [19]) for a given MC configuration.

In order to demonstrate that the propagators are all vulnerable to the Gribov ambiguity, but to a different extent, in Fig. 3 we present (for smaller lattices) the effect of the Gribov ambiguity on the gluon and ghost propagator (for the quenched case) [25, 26]. In the subpanels (a) and (b) the ratio of the dressing functions calculated in two different ensembles is shown. The “fc” ensemble is the ensemble of (arbitrary) first gauge-fixed copies for each MC configuration, “bc” is the ensemble of the best copies after  $n_c = 20$  to 30 gauge-fixing attempts. In the case of the gluon propagator in Fig. 3a we see a relatively broad band of “Gribov noise” that does not show a distinct momentum or volume tendency. On the other side, for the ghost dressing function in Fig. 3b a relatively sharp effect of overestimation for the first copy is seen that becomes stronger towards smaller momenta. The effect is slightly suppressed with increasing physical volume (see the data points for the lowest  $\beta = 5.8$ ), an observation that can be an early hint towards the weakening of the Gribov copy effect at very large volumes. For smaller lattices, however, the ghost propagator will be overestimated at the smallest momenta if there is no systematical search for better Gribov copies, i.e. if one averages over Gribov copies.

There are not enough data yet in the region of small enough momenta to get stable fits of the infrared exponents. If one attempts this,  $\kappa$  is found too small. In order to anticipate whether the gluon propagator finally may turn to zero in the limit  $q^2 \rightarrow 0$ , one looks at the propagator instead of the dressing function. Fig.

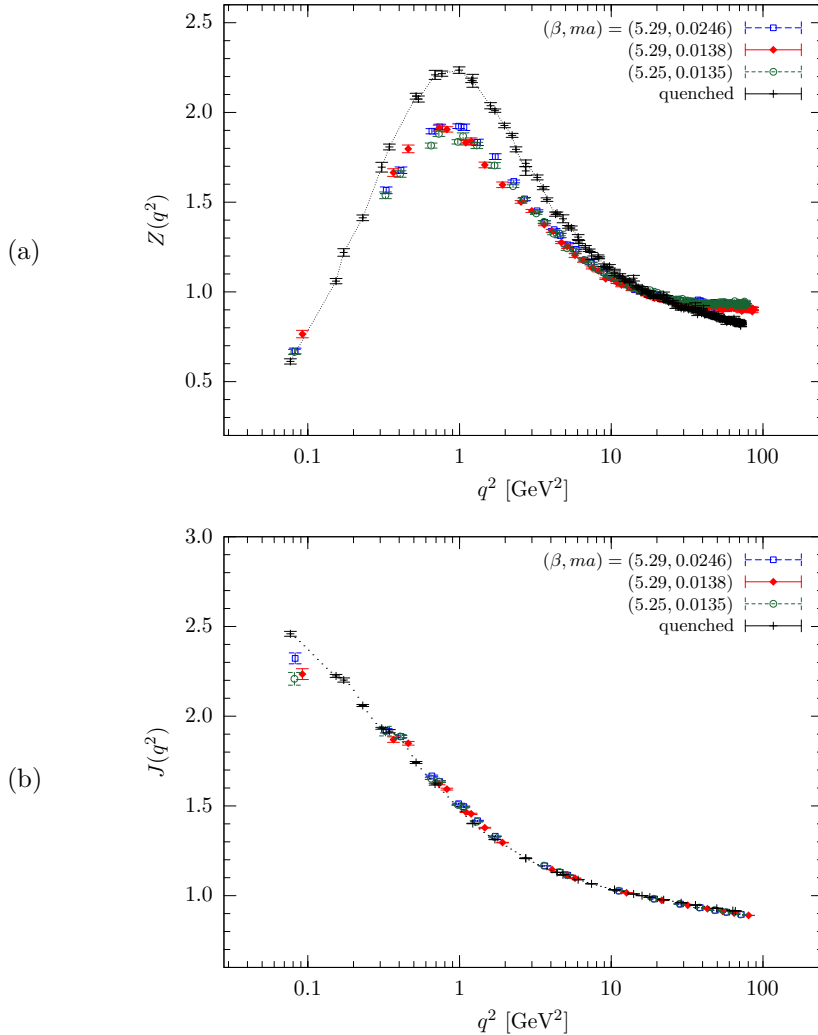


**Figure 2.** The effect of dynamical quarks (a) on the gluon propagator that becomes depressed in the intermediate momentum range around  $O(1$  GeV) ; (b) on the ghost propagator that becomes depressed only in the infrared region.

4 shows data for the gluon and the ghost propagator on a  $64^4$  lattice at  $\beta = 5.7$  obtained at the MVS-15000BM of the Joint Supercomputer Center (JSCC) Moscow. The gluon propagator in Fig. 4a shows at least a kind of plateau. The leftmost data point represents the gluon propagator at zero momentum,  $D(0)$ . The decreasing tendency of  $D(0)$  with the lattice volume (not shown here) suggests that the propagator function  $D(p)$  also cannot be taken as the infinite-volume limit. More recent data (on a lattice  $80^4$ ) presented at Lattice 2007 [39] indicate that the plateau extends to  $|q|$  below 100 MeV. The ghost propagator in Fig. 4b (shown in a log-log-plot) suggests already something close to a power law, but the corresponding  $\kappa$  comes also too small compared with the preferred  $\kappa = 0.595$ .

That means that the now accessible momentum range is probably still pre-asymptotic. DSE results anticipating the approach to the infinite-volume limit indicate how far lattice calculations are from seeing the asymptotic behavior. The DSE have been formulated and solved on a finite torus [11, 12], and an interesting pattern of finite-volume deviations for the calculated propagators has been found and compared with our lattice data (see Figs. 5a and 5b taken from [12]).

For the gluon propagator the approach to the infinite-volume curve is from above, with an enormous overshooting towards the lowest momentum for any given lattice volume (see Fig. 5a). For the ghost propagator the approach is from below and less dramatic. This is shown in Fig. 5b. The insufficient slope  $\kappa$  in the log-log-plot of the ghost propagator in Fig. 4b is well explained by this type of finite volume effect.

Fig. 6a shows the DSE result for the running coupling with the volume dependence induced by the volume dependence of the gluon and ghost propagators. This makes clear that it is illusory to see the running coupling approaching the infrared fix-point before lattices reach a linear size  $L = O(15$  fm). We have checked [26, 41] on the lattice the assumed  $q^2$  independence of the ghost-ghost-gluon vertex renormalization constant, a tacit assumption in deriving Eq. (12). Fig. 7b shows the result of our calculation of the gluon and ghost dressing

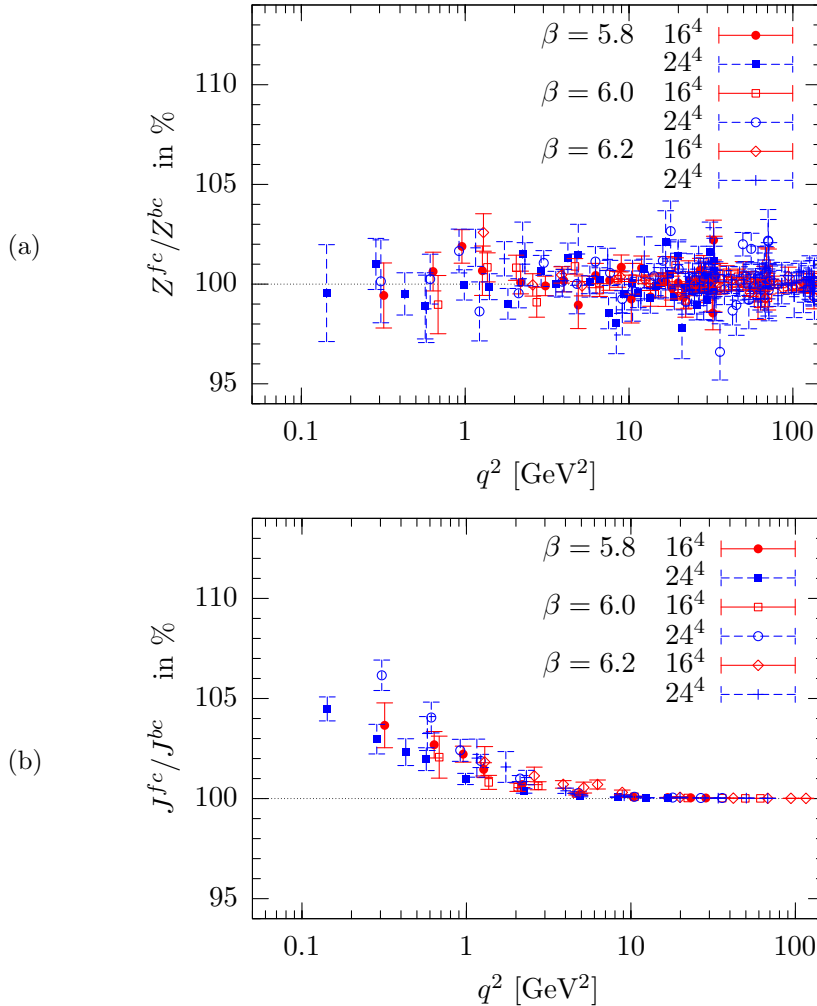


**Figure 3.** The ratio between first and best gauge copies used for calculating the dressing function (a) for the gluon propagator (“Gribov noise”), (b) for the ghost propagator where one sees a systematic Gribov copy effect becoming weaker with increasing physical volume.

functions, giving the running coupling [26]. The volume is just large enough to reveal the turn-over to an apparently decreasing behavior of coupling with  $q^2 \rightarrow 0$ . But this has nothing to do with the true asymptotic behavior. In the light of this observation, the optimism of *having seen* already the approach to the fix-point [42] seems to be premature.

The violation of positivity and the very slow approach to the KO confinement criterion have been presented at Lattice 2006 [40]. Recently, the Adelaide group [28] has discussed violation of positivity together with scaling and the effect of dynamical quarks in much more detail for lattice ensembles provided by the MILC collaboration.

#### 4 Summary

Various effects on the gluon and ghost propagators have already been studied for quenched QCD, and the effect of dynamical quarks and Gribov copies has been added by our investigations. The infrared exponents characteristic for the way how “ghosts manage to confine gluons” are still elusive. The infrared asymptotic region in momenta (volumes) is not yet reached. There are three extrapolations needed before lattice QCD can be applied to the real world: (a) to take the continuum limit, (b) to control the chiral limit and to extrapolate to the physical pion mass and (c) to take the infinite-volume limit. The latter is probed by the infrared behavior of gluon and ghost propagators, and it turns out that the approach is extremely slow. Discretization effects also show up in the data, but can be easily tamed by suitable momentum cuts. The effects of the vortex mechanism of quark confinement and of dynamical quarks on the form of the propagators are very interesting and worth to be microscopically understood.

*Acknowledgements.* To the organizers of the School-Seminar, in particular to Vladimir Skalozub, I am very grateful for inviting me and sponsoring my participation. I enjoyed the inspiring meeting and the interesting place. I wish to thank my co-authors A. Sternbeck, M. Müller-Preussker, I. Bogolubsky, V. Bornyakov,

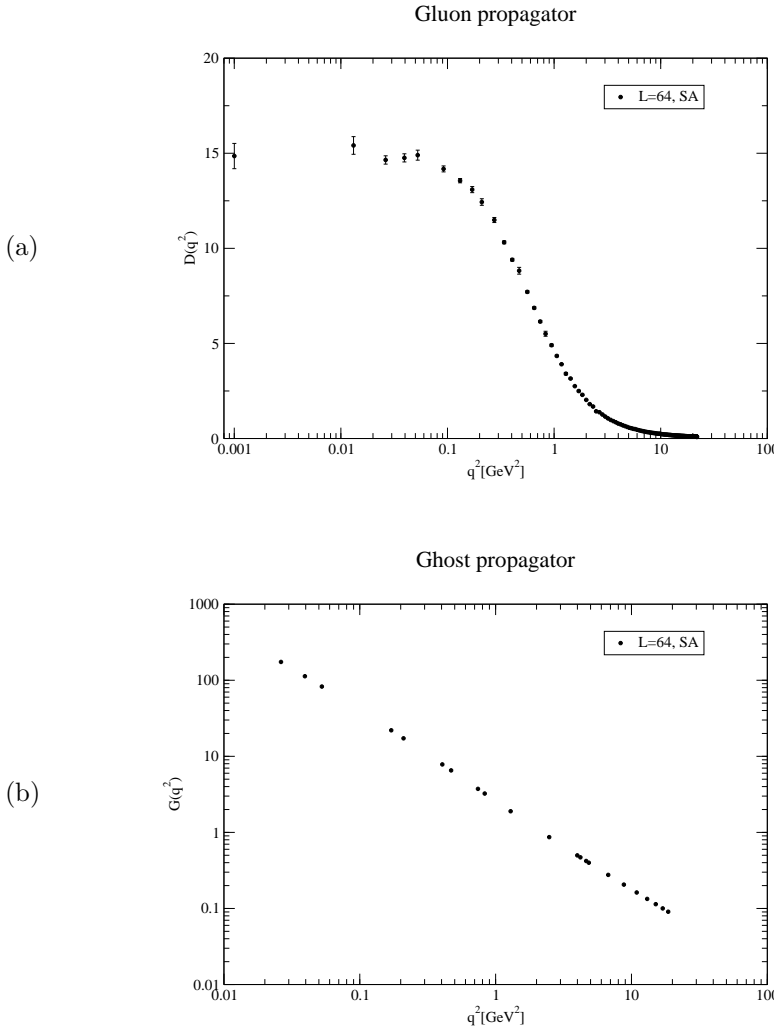


**Figure 4.** (a) The gluon propagator, (b) the ghost propagator, measured on the  $64^4$  lattice at  $\beta = 5.7$ . Notice that the leftmost data point of the gluon propagator actually refers to zero momentum,  $D(0)$ . So far there is no indication that  $D(p) \rightarrow 0$  for  $p \rightarrow 0$ .

G. Burgio, B. Martemyanov, V. Mitrjushkin, A. Schiller and A. Voigt for discussions on the ideas reported here. Thanks go to the HLRN regional computing center Berlin/Hannover and to the Joint Supercomputer Center (JSCC) Moscow for the computing resources. The support by DFG for my work, presently via the Forschergruppe FOR465, is highly appreciated.

## References

- [1] R. Alkofer and J. Greensite, J.Phys. **G34**, S3 (2007) [arXiv:hep-ph/0610365].
- [2] V. N. Gribov, Nucl.Phys. **B139**, 1 (1978).
- [3] D. Zwanziger, Nucl.Phys. **B378**, 525 (1992); Nucl.Phys. **B364**, 127 (1991); Nucl.Phys. **B412**, 657 (1994).
- [4] T. Kugo and I. Ojima, Prog.Theor.Phys.Suppl. **66**, 1 (1979); T. Kugo, arXiv:hep-th/9511033.
- [5] R. Alkofer and L. von Smekal, Phys.Rept. **353**, 281 (2001) [arXiv:hep-ph/0007355].
- [6] J. E. Mandula and M. Ogilvie, Phys.Lett. **185**, 127 (1987).
- [7] J. E. Mandula, Phys.Rept. **315**, 273 (1999) [arXiv:hep-lat/9907020].
- [8] L. von Smekal, R. Alkofer and A. Hauck, Phys.Rev.Lett. **78**, 3591 (1997) [arXiv:hep-ph/9705242].
- [9] L. von Smekal, A. Hauck and R. Alkofer, Ann.Phys. **267**, 1 (1998) [arXiv:hep-ph/9707327].
- [10] H. Suman and K. Schilling, Phys.Lett. **B373**, 314 (1996) [arXiv:hep-lat/9512003].
- [11] C. S. Fischer, B. Grüter and R. Alkofer, Ann.Phys. **321**, 1918 (2006) [arXiv:hep-ph/0506053].
- [12] C. S. Fischer *et al.*, arXiv:hep-ph/0701050 [Ann. of Phys., in print].
- [13] C. Lerche and L. von Smekal, Phys.Rev. **D65**, 125006 (2002) [arXiv:hep-ph/0202194].

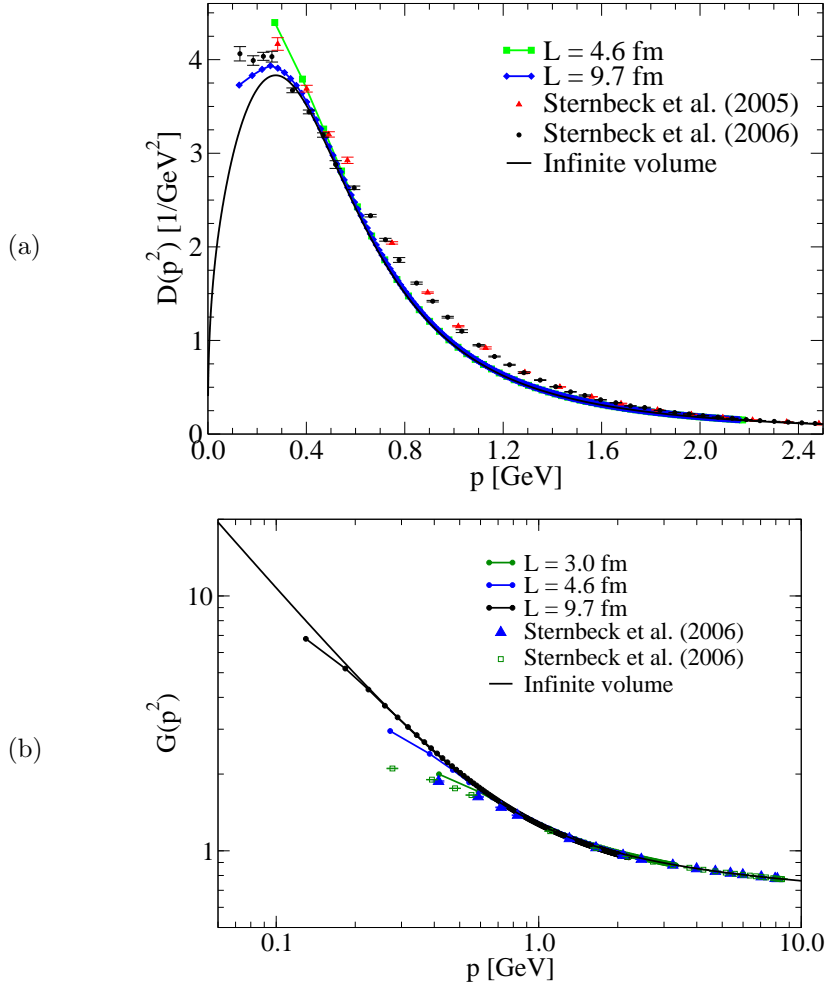


**Figure 5.** The propagators from DSE for a few volumes and for infinite volume shown together with our lattice data of [25, 40], (a) for the gluon propagator, where the lattice data, being tangents to the infinite-volume curve, are strongly deviating upward; (b) for the ghost propagator, where the lattice data, being tangents to the infinite-volume curve, are deviating downward with a pre-asymptotic slope. (Figures taken from [12])

- [14] P. Watson and R. Alkofer, Phys.Rev.Lett. **86**, 5239 (2001) [arXiv:hep-ph/0102332].
- [15] D. Zwanziger, Phys.Rev. **D65**, 094039 (2002) [arXiv:hep-th/0109224].
- [16] D. Zwanziger, Phys.Rev. **D67**, 105001 (2003) [arXiv:hep-th/0206053].
- [17] C. W. Bernard, C. Parrinello and A. Soni, Nucl.Phys.Proc.Suppl. **30**, 535 (1993) [arXiv:hep-lat/9211020].
- [18] P. Marenzoni *et al.*, Phys.Lett. **B318**, 511 (1993).
- [19] D. Zwanziger, Phys.Rev. **D69**, 016002 (2004) [arXiv:hep-ph/0303028].
- [20] G. S. Bali *et al.*, Phys.Rev. **D54**, 2863 (1996) [arXiv:hep-lat/9603012].
- [21] E.-M. Ilgenfritz, M. Müller-Preussker and P. Schemel, to be published (2007).
- [22] J. C. Taylor, Nucl.Phys. **B33**, 436 (1971).
- [23] I. L. Bogolubsky, V. G. Bornyakov, G. Burgio, E.-M. Ilgenfritz, M. Müller-Preussker and V. K. Mitrjushkin, arXiv:0707.3611 [hep-lat].
- [24] I. L. Bogolubsky *et al.*, Phys.Rev. **D74**, 034503 (2006) [arXiv:hep-lat/0511056].
- [25] A. Sternbeck *et al.*, Phys.Rev. **D72**, 014507 (2005) [arXiv:hep-lat/0506007].
- [26] A. Sternbeck *et al.*, Nucl.Phys.Proc.Suppl. **153**, 185 (2006) [arXiv:hep-lat/0511053].
- [27] E.-M. Ilgenfritz *et al.*, in *Sense of Beauty in Physics*, ed. by M. D'Elia *et al.*, Pisa 2006, p. 359 [arXiv:hep-lat/0601027].
- [28] P. O. Bowman *et al.*, arXiv:hep-lat/0703022.
- [29] G. S. Bali *et al.*, Nucl.Phys.Proc.Suppl. **153**, 9 (2006) [arXiv:hep-lat/0512018].
- [30] P. Y. Boyko *et al.*, Nucl.Phys. **B756**, 71 (2006) [arXiv:hep-lat/0607003].
- [31] V. G. Bornyakov *et al.*, arXiv:0708.3335 [hep-lat].
- [32] V. G. Bornyakov *et al.*, Phys.Rev. **D70**, 074511 (2004) [arXiv:hep-lat/0310011].

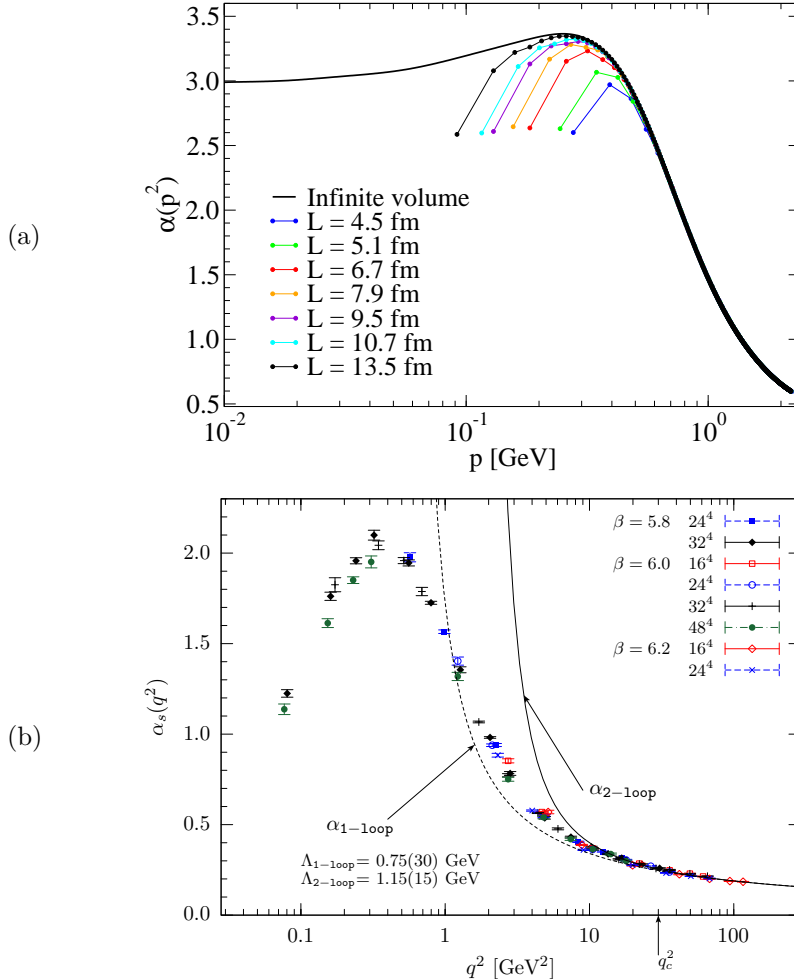
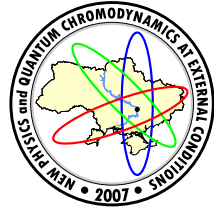


**Figure 6.** The MOM-scheme running coupling constant  $\alpha_s(q^2)$ : (a) from the DSE approach for different box sizes compared with the infinite volume limit (taken from [12]), (b) from our quenched lattice calculations. The little  $q_c^2$  indicates the end of a fit range  $q^2 > q_c^2$  where the 1- and 2-loop running coupling has been fitted. Notice the weak volume dependence on the right of the peak and the beginning splitting on the left of the peak between the largest volumes.

- [33] K. Langfeld, H. Reinhardt and J. Gattner, Nucl.Phys. **B621**, 131 (2002) [arXiv:hep-ph/0107141].
- [34] J. Gattner, K. Langfeld and H. Reinhardt, Phys.Rev.Lett. **93**, 061601 (2004) [arXiv:hep-lat/0403011].
- [35] P. de Forcrand and M. D'Elia, Phys.Rev.Lett. **82**, 4582 (1999) [arXiv:hep-lat/9901020].
- [36] J. Greensite, S. Olejnik and D. Zwanziger, JHEP **05**, 070 (2005) [arXiv:hep-lat/0407032].
- [37] A. Maas, Nucl.Phys. **A790**, 566 (2007) [arXiv:hep-th/0610011].
- [38] A. Sternbeck, E.-M. Ilgenfritz and M. Müller-Preussker, Phys.Rev. **D73**, 014502 (2006) [arXiv:hep-lat/0510109].
- [39] I. L. Bogolubsky *et al.*, poster presented at Lattice 2007.
- [40] A. Sternbeck *et al.*, PoS **LAT2006**, 076 (2006) [arXiv:hep-lat/0610053].
- [41] E.-M. Ilgenfritz *et al.*, Braz.J.Phys. **37**, 193 (2007) [arXiv:hep-lat/0609043].
- [42] J. C. R. Bloch *et al.*, Nucl.Phys. **B687**, 76 (2004) [arXiv:hep-lat/0312036].



## K–MESON PRODUCTION IN ELECTRON-POSITRON ANNIHILATION

A. Yu. Korchin<sup>a</sup>, S. A. Ivashyn<sup>b</sup>

National Science Center “Kharkov Institute of Physics and Technology”,  
Kharkov, Ukraine

A model for electromagnetic form factors of the charged and neutral on-shell  $K$ –mesons is developed. The formalism is based on Lagrangian of Chiral Perturbation Theory which includes vector mesons. Presented terms describe even- as well as odd-intrinsic-parity interactions up to  $\mathcal{O}(p^4)$ . The kaon form factor, calculated without parameters fine tuning, is compared to experiment for space-like and time-like photon momentum. The status of the muon anomalous magnetic moment (AMM) is reviewed and contribution of the two-kaon channels to AMM is calculated.

### 1 Introduction

$K$ –mesons (or kaons) are the particles with quantum numbers  $I (J^P) = \frac{1}{2} (0^-)$  and nonzero “strangeness”, which have lead to discovery of many interesting phenomena due to weak interactions, such as strangeness oscillation,  $K^0$  regeneration,  $CP$  violation. These particles have the following basic properties [1].

Quark composition of mass eigenstates reads :

$$\begin{aligned} K^+ &= u\bar{s}, & K^0 &= d\bar{s} & (\text{strangeness} = +1), \\ K^- &= \bar{K}^+ = \bar{u}s, & \bar{K}^0 &= \bar{d}s & (\text{strangeness} = -1). \end{aligned}$$

These particles are created in strong-interaction processes.

Time of life is defined and measured for the states participating in weak decays

$$\begin{aligned} K^\pm : \tau &= 1.2 \times 10^{-8} \text{ s}, \\ K_S = (1 + |\varepsilon|^2)^{-1/2}(K_1 + \varepsilon K_2) : \tau &= 0.9 \times 10^{-10} \text{ s}, \quad \text{short-lived}, \\ K_L = (1 + |\varepsilon|^2)^{-1/2}(K_2 + \varepsilon K_1) : \tau &= 5.2 \times 10^{-8} \text{ s}, \quad \text{long-lived}, \end{aligned}$$

where  $CP$ -eigenstates are defined as

$$\begin{aligned} K_1 &= \frac{1}{\sqrt{2}}(K^0 + \bar{K}^0) : \quad CP\text{-even}, \\ K_2 &= \frac{1}{\sqrt{2}}(K^0 - \bar{K}^0) : \quad CP\text{-odd} \end{aligned}$$

and parameter  $\varepsilon \sim 10^{-3}$  describes small  $CP$  violation effects.

**Electromagnetic properties of  $K$ –mesons.** Experimental information on  $K$ –meson electromagnetic (EM) properties in the time-like region ( $q^2 \equiv s \geq 4m_K^2$ ) of photon momentum  $q$  comes from measurements of the cross section of electron-positron annihilation  $e^+e^- \rightarrow K\bar{K}$ :

$$\sigma(e^+e^- \rightarrow K\bar{K}) = \frac{\pi\alpha^2}{3q^2} \left(1 - \frac{4m_K^2}{q^2}\right)^{3/2} |F_K(q^2)|^2. \quad (1)$$

High precision measurements are performed by CMD-2 and SND Collaborations in Novosibirsk [2, 3], and KLOE Collaboration in Frascati (Italy) [4].

In the space-like region ( $q^2 \equiv s < 0$ ) the form factor is measured in:

- (i) kaon scattering on atomic electrons at relatively small momentum transfer  $-s < 0.16 \text{ GeV}^2$  (CERN, SPS [5]),
- (ii) electron-proton scattering with kaon-hyperon production ( $ep \rightarrow e\Lambda K^+$  and  $ep \rightarrow e\Sigma^0 K^+$ ) at large momentum transfer up to  $-s \sim 3 \text{ GeV}^2$  (currently are carried out at Jefferson Laboratory in USA [6]).

Main motivations of the present work are:

e-mail: <sup>a</sup>korchin@kipt.kharkov.ua, <sup>b</sup>ivashin.s@rambler.ru

© Korchin A.Yu., Ivashyn S.A., 2007.

1. Test of effective hadronic models such as
  - (i) Chiral Perturbation Theory (ChPT) – effective low-energy theory,
  - (ii) vector-meson dominance of electromagnetic interaction,
  - (iii) anomalous Lagrangians<sup>1</sup>.
2. Study of vector mesons ( $J^P = 1^-$ ):  $\rho(770)$ ,  $\omega(782)$ ,  $\phi(1020)$ , and their radial excitations  $\rho' = \rho(1450)$ ,  $\omega' = \omega(1420)$ ,  $\phi' = \phi(1680)$ , etc.
3. Calculation of hadronic contribution to the muon anomalous magnetic moment (AMM). Hadronic contribution is the main source of uncertainty in theoretical prediction for muon AMM. The existing discrepancy between theory and experiment may indicate new physics beyond the Standard Model, thus it is important to precisely calculate every allowed contribution in Standard Model.

**Kaon form factors.** The quark EM current is

$$j_{em}^\mu(x) = \frac{2}{3}\bar{u}(x)\gamma^\mu u(x) - \frac{1}{3}\bar{d}(x)\gamma^\mu d(x) - \frac{1}{3}\bar{s}(x)\gamma^\mu s(x). \quad (2)$$

The EM form factors (FF's) are defined in terms of this current

$$\langle K(p_1)\bar{K}(p_2)|j_{em}^\mu(x=0)|0\rangle \equiv (p_1 - p_2)^\mu F_K(q^2), \quad (3)$$

where  $q^2 = (p_1 + p_2)^2 \equiv s$ .

The form factors are analytic functions of  $q^2$  and describe both the time-like and space-like regions of photon momentum.

## 2 Formalism

**Meson interactions in ChPT.** At low energies, strong, electromagnetic and weak interactions are described by effective Lagrangian of Chiral Perturbation Theory (ChPT). The underlying theory of strong interactions – Quantum Chromodynamics (QCD) – has global chiral symmetry  $SU(3)_L \times SU(3)_R$ , if masses of the quarks are zero, and ChPT has this symmetry built in on the hadronic level.

The version of ChPT which includes explicit vector meson degrees of freedom (Ecker, Gasser, Pich and de Rafael [7, 8]) has an extended range of applicability. In this approach the vector mesons  $\rho, \omega, \phi, \dots$  are not considered as gauge bosons of chiral symmetry and are treated on equal footing with other mesons.

The chiral symmetric part of Lagrangian is

$$\begin{aligned} \mathcal{L}_{\text{ch-sym}} = & \frac{F_\pi^2}{4} \text{Tr}(D_\mu U D^\mu U^\dagger) + \frac{eF_V}{2\sqrt{2}} F^{\mu\nu} \text{Tr}(V_{\mu\nu}(uQu^\dagger + u^\dagger Qu)) \\ & + \frac{iG_V}{\sqrt{2}} \text{Tr}(V_{\mu\nu}u^\mu u^\nu) + \mathcal{L}_{V, \text{kin}} + [\text{axial-vector + scalar mesons}], \end{aligned} \quad (4)$$

where the nonlinear field representation for pseudoscalar mesons is

$$U \equiv \exp(i\sqrt{2}\Phi/F_\pi), \quad u = U^{1/2}, \quad u^\mu = iu^\dagger(D^\mu U)u^\dagger.$$

Here  $\Phi$  is octet of pseudoscalar mesons ( $J^P = 0^-$ ) – Nambu-Goldstone bosons of spontaneously broken chiral symmetry

$$\Phi = \begin{pmatrix} \pi^0/\sqrt{2} + \eta_8/\sqrt{6} & \pi^+ & K^+ \\ \pi^- & -\pi^0/\sqrt{2} + \eta_8/\sqrt{6} & K^0 \\ K^- & \bar{K}^0 & -2\eta_8/\sqrt{6} \end{pmatrix},$$

and  $F_\pi = 92.4$  MeV is constant of the weak pion decay  $\pi^+ \rightarrow \mu^+ \nu_\mu$ . The covariant derivative is defined as

$$D_\mu U \equiv \partial_\mu U + ieB_\mu[U, Q]$$

with quark charge matrix for flavor  $SU(3)_f$

$$Q \equiv \text{diag}\left(\frac{2}{3}, -\frac{1}{3}, -\frac{1}{3}\right),$$

$B^\mu$  – electromagnetic field,  $F^{\mu\nu} = \partial^\mu B^\nu - \partial^\nu B^\mu$ ,  $V_{\mu\nu}$  is nonet of vector mesons ( $J^{PC} = 1^{--}$ )

$$V_{\mu\nu} = \begin{pmatrix} \rho^0/\sqrt{2} + \omega_8/\sqrt{6} & \rho^+ & K^{*+} \\ \rho^- & -\rho^0/\sqrt{2} + \omega_8/\sqrt{6} & K^{*0} \\ K^{*-} & \bar{K}^{*0} & -2\omega_8/\sqrt{6} \end{pmatrix}_{\mu\nu} + \frac{(\omega_1)_{\mu\nu}}{\sqrt{3}},$$

<sup>1</sup>By “anomalous” we mean interactions which do not conserve intrinsic parity and thus do not conserve “normality” quantum number  $\mathcal{N}$ .

**Table 1.** Electromagnetic coupling constants for vector mesons  $V = \rho^0, \omega, \phi$ 

	$\rho^0$	$\omega$	$\phi$
$f_V = m_\rho/F_V, \text{ } SU(3):$	$f$	$3f$	$-3f/\sqrt{2}$
exper. $f_V$	$4.966 \pm 0.038$	$17.06 \pm 0.29$	$-13.38 \pm 0.21$

**Table 2.** Vector-meson coupling to two pseudoscalars in  $SU(3)_f$ 

	$\pi^+ \pi^-$	$K^+ K^-$	$K^0 \bar{K}^0$
$\rho^0$	$G_V$	$G_V/2$	$-G_V/2$
$\omega$	–	$G_V/2$	$G_V/2$
$\phi$	–	$-G_V/\sqrt{2}$	$-G_V/\sqrt{2}$

in the antisymmetric tensor representation of the vector fields.  $\mathcal{L}_{V, \text{kin}}$  is the kinetic term for vector mesons.

The chiral symmetry breaking part

$$\mathcal{L}_{\text{ch-sym.break}} = \frac{F_\pi^2}{4} \text{Tr}(\chi U^\dagger + \chi^\dagger U) \quad (5)$$

arises due to non-vanishing quark masses  $m_u = 1.5 - 4$  MeV,  $m_d = 4 - 8$  MeV,  $m_s = 80 - 130$  MeV in QCD and quark condensate

$$\langle 0 | \bar{q}q | 0 \rangle \approx (-240 \pm 10 \text{ MeV})^3 \text{ (at scale } \mu = 1 \text{ GeV)}$$

where the vacuum is assumed  $SU(3)_f$  symmetric, i.e.  $\langle 0 | \bar{q}q | 0 \rangle = \langle 0 | \bar{u}u | 0 \rangle = \langle 0 | \bar{d}d | 0 \rangle = \langle 0 | \bar{s}s | 0 \rangle$ .

The condensate value gives typical scale parameter in QCD

$$-\langle 0 | \bar{q}q | 0 \rangle^{1/3} \approx \Lambda_{QCD} = 200 - 300 \text{ MeV}$$

which rules the energy dependence of the running coupling constant

$$\alpha_s(Q) = \frac{2\pi}{(\frac{11}{3}N_c - \frac{2}{3}N_f) \ln(Q/\Lambda_{QCD})}, \quad (6)$$

where  $N_f$  ( $N_c$ ) is the number of “active” quark flavors (quark colors).

Pion and kaon masses squared are proportional to quark masses and the condensate value, and the quantity  $\chi$  is

$$\chi = -\frac{2}{F_\pi^2} \text{diag}(m_u, m_d, m_s) \langle 0 | \bar{q}q | 0 \rangle \stackrel{SU(2)_f}{=} \text{diag}(m_\pi^2, m_\pi^2, 2m_K^2 - m_\pi^2).$$

Expansion of Lagrangian in powers of meson momenta (or derivatives of meson fields) gives interactions with even number of pseudoscalar mesons

$$\begin{aligned} \mathcal{L}_{\gamma\Phi\Phi} &= ieB_\mu \text{Tr}(Q[\partial_\mu\Phi, \Phi]), \\ \mathcal{L}_{\gamma\gamma\Phi\Phi} &= -\frac{e^2}{2}B^\mu B_\mu \text{Tr}([\Phi, Q]^2), \\ \mathcal{L}_{\gamma V} &= e\frac{F_V}{\sqrt{2}}F^{\mu\nu}\text{Tr}(V_{\mu\nu}Q), \quad (\text{vector-meson dominance}) \\ \mathcal{L}_{V\Phi\Phi} &= i\frac{\sqrt{2}G_V}{F_\pi^2}\text{Tr}(V_{\mu\nu}\partial^\mu\Phi\partial^\nu\Phi). \end{aligned}$$

These interactions conserve “normality” quantum number

$$\mathcal{N} = \text{Parity} \times (-1)^{\text{spin}}.$$

The coupling constants  $F_V$  and  $G_V$  can be found from experimental widths of decays  $\Gamma(\rho \rightarrow e^+e^-)$  and  $\Gamma(\rho \rightarrow \pi\pi)$ , respectively. It will be further convenient to use other constants,  $g$  and  $f$ , related to  $F_V$  and  $G_V$ . Using the data from [1] we obtain

$$\begin{aligned} F_V &= 156.35 \text{ MeV}, & G_V &= 65.65 \text{ MeV}, \\ f \equiv \frac{m_\rho}{F_V} &= 4.966, & g \equiv \frac{G_V m_\rho}{F_\pi^2} &= 5.965. \end{aligned}$$

**Anomalous meson-meson and meson-photon interactions.** Interactions of this type are not described by Lagrangians (4) and (5). They are proportional to Levi-Chivita tensor  $\epsilon^{\mu\nu\alpha\beta}$ , couple odd number of pseudoscalar mesons and do not conserve “normality”  $\mathcal{N}$ .

Lagrangian of Wess, Zumino and Witten [9, 10] describes interactions of photons with pseudoscalar mesons

$$\mathcal{L}_{WZW} = \mathcal{L}_{WZW}^{(1)} + \mathcal{L}_{WZW}^{(2)}, \quad (7)$$

$$\begin{aligned} \mathcal{L}_{WZW}^{(1)} &= -\frac{eN_c}{48\pi^2} \epsilon^{\mu\nu\alpha\beta} B_\mu \text{Tr} \left( Q [(\partial_\nu U)(\partial_\alpha U^+)(\partial_\beta U)U^+ \right. \\ &\quad \left. - (\partial_\nu U^+)(\partial_\alpha U)(\partial_\beta U^+)U] \right), \\ \mathcal{L}_{WZW}^{(2)} &= \frac{ie^2 N_c}{24\pi^2} \epsilon^{\mu\nu\alpha\beta} (\partial_\mu B_\nu) B_\alpha \\ &\quad \times \text{Tr} \left( Q^2 (\partial_\beta U)U^+ + Q^2 U^+ (\partial_\beta U) \right. \\ &\quad \left. - \frac{1}{2} QUQ(\partial_\beta U^+) + \frac{1}{2} QU^+ Q(\partial_\beta U) \right). \end{aligned}$$

The lowest-order WZW interaction is

$$\mathcal{L}_{\gamma\Phi\Phi\Phi} = -\frac{i\sqrt{2}eN_c}{12\pi^2 F_\pi^3} \epsilon^{\mu\nu\alpha\beta} B_\mu \text{Tr} (Q \partial_\nu \Phi \partial_\alpha \Phi \partial_\beta \Phi), \quad (8)$$

$$\mathcal{L}_{\gamma\gamma\Phi} = -\frac{\sqrt{2}e^2 N_c}{8\pi^2 F_\pi} \epsilon^{\mu\nu\alpha\beta} \partial_\mu B_\nu \partial_\alpha B_\beta \text{Tr} (Q^2 \Phi). \quad (9)$$

The latter in particular describes well-known  $\pi^0\gamma\gamma$  interaction and  $\pi^0 \rightarrow \gamma\gamma$  decay

$$\mathcal{L}_{\pi^0\gamma\gamma} = -\frac{e^2 N_c}{24\pi^2 F_\pi} \epsilon^{\mu\nu\alpha\beta} \partial_\mu B_\nu \partial_\alpha B_\beta \pi^0.$$

ChPT also predicts anomalous interactions of vector mesons with pseudoscalar mesons [11]

$$\mathcal{L}_{VV\Phi} = -\frac{\sqrt{2}\sigma_V}{F_\pi} \epsilon^{\mu\nu\alpha\beta} \text{Tr} (\partial_\mu V_\nu \{\Phi, \partial_\alpha V_\beta\}), \quad (10)$$

$$\mathcal{L}_{V\gamma\Phi} = -\frac{4\sqrt{2}eh_V}{F_\pi} \epsilon^{\mu\nu\alpha\beta} \partial_\mu B_\nu \text{Tr} (V_\alpha \{\partial_\beta \Phi, Q\}), \quad (11)$$

$$\mathcal{L}_{V\Phi\Phi\Phi} = -\frac{2i\sqrt{2}\theta_V}{F_\pi^3} \epsilon^{\mu\nu\alpha\beta} \text{Tr} (V_\mu \partial_\nu \Phi \partial_\alpha \Phi \partial_\beta \Phi) \quad (12)$$

with free parameters  $\sigma_V, h_V, \theta_V$  (see Table 3).

An extension of WZW anomaly for vector and axial-vector mesons was suggested by Kaymakcalan, Rajeev, Schechter, Ko and Rudaz [12]

$$\begin{aligned} \mathcal{L}_{V\Phi\Phi\Phi} &= \frac{ig}{4\pi^2 F_\pi^3} \epsilon^{\mu\nu\alpha\beta} \text{Tr} (V_\mu \partial_\nu \Phi \partial_\alpha \Phi \partial_\beta \Phi), \\ \mathcal{L}_{VV\Phi} &= \frac{3g^2}{8\sqrt{2}\pi^2 F_\pi} \epsilon^{\mu\nu\alpha\beta} \text{Tr} (\partial_\mu V_\nu \partial_\alpha V_\beta \Phi) \end{aligned}$$

with  $g = 5.96$  taken from  $\rho \rightarrow \pi\pi$  decay and EM field is included by the substitution

$$V_\mu \rightarrow V_\mu + \frac{\sqrt{2}e}{g} Q B_\mu$$

As a result one obtains an effective  $V\gamma\Phi$  interaction

$$\mathcal{L}_{V\gamma\Phi} = -\frac{3eg}{4\pi^2 F_\pi} \epsilon^{\mu\nu\alpha\beta} \partial_\mu B_\nu \text{Tr} (Q V_\alpha \partial_\beta \Phi).$$

Now we calculate the kaon form factors which in the present model are

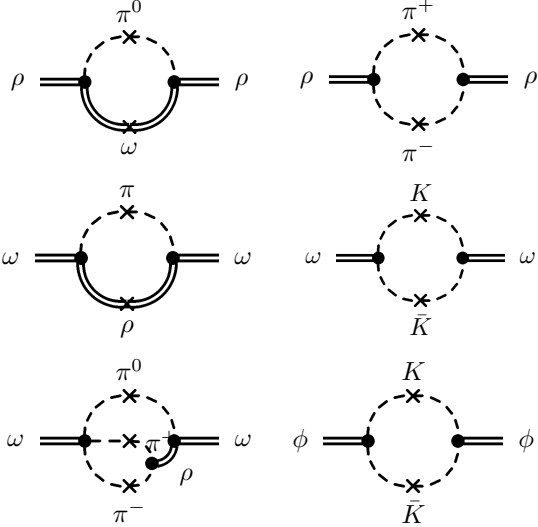
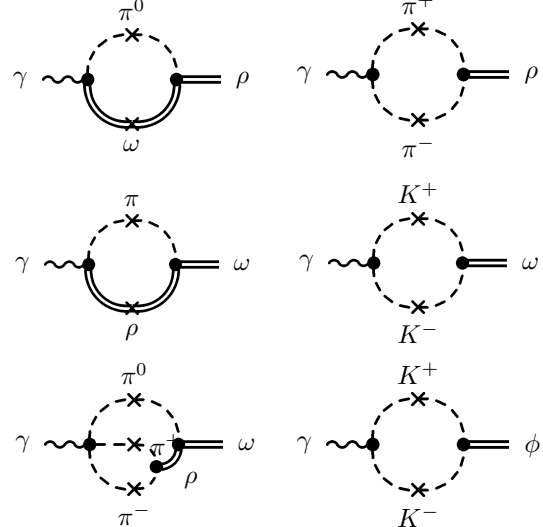
$$F_{K^+}(s) = 1 - \sum_{V=\rho,\omega,\phi} \frac{g_{VK^+K^-}}{f_V(s)} A_V(s), \quad (13)$$

$$F_{K^0}(s) = - \sum_{V=\rho,\omega,\phi} \frac{g_{VK^0\bar{K}^0}}{f_V(s)} A_V(s), \quad (14)$$

$$A_V(s) \equiv \frac{s}{s - m_V^2 - \Pi_V(s)},$$

**Table 3.** Values of parameters  $\sigma_V, h_V, \theta_V$  for vector mesons

Coupling constants	$h_V$	$\theta_V$	$\sigma_V$
“ideal” values [12]	$\frac{3g}{32\sqrt{2}\pi^2} = 0.040$	$\frac{g}{8\sqrt{2}\pi^2} = 0.054$	$\frac{3g^2}{32\pi^2} = 0.34$
fixed by experiment	0.039	0.0011	0.33
Nambu-Jona-Lasinio model [11]	0.040	0.053	0.33

**Figure 1.** Loops included in self-energy of vector mesons.**Figure 2.** Loop corrections for photon-vector-meson vertex

where  $\Pi_V(s)$  is self-energy operator of vector meson  $V = \rho, \omega, \phi$ .

The correct normalization conditions at  $q^2 = 0$

$$F_{K^+}(0) = 1, \quad F_{K^0}(0) = 0 \quad (15)$$

are fulfilled due to gauge invariance of the theory.

**Self-energy operators.** Dressed (“exact”, or full) propagator of vector particles includes self-energy operators  $\Pi_V(s)$  which account for intermediate states, such as  $\pi^+\pi^-$ ,  $\omega\pi^0$ ,  $K\bar{K}$ ,  $\omega\pi^0 \rightarrow \pi^0K^+K^-$  for  $\rho$  meson, etc. The dominant contributions are (see Fig. 1)

$$\begin{aligned} \Pi_\rho &= \Pi_{\rho(\pi^0\omega)\rho} + \Pi_{\rho(\pi\pi)\rho}, \\ \Pi_\omega &= \Pi_{\omega(\pi^0\rho)\omega} + \Pi_{\omega(KK)\omega} + 2\Pi_{\omega(3\pi,\pi\rho)\omega}, \\ \Pi_\phi &= \Pi_{\phi(KK)\phi}, \end{aligned}$$

Imaginary part of self-energy gives rise to energy-dependent widths of vector mesons

$$\Gamma_V(s) = -m_V^{-1} \operatorname{Im} \Pi_V(s)$$

One can find the imaginary parts of self-energy by applying the Cutkosky rules. To restrict fast growth of the partial widths with  $s$  we have to introduce a cut-off form factors (for details see [13]).

**Electromagnetic vertex modification.** Vertex corrections (see Fig. 2) are related to self-energy corrections, for example

$$\operatorname{Im} \Pi_{\gamma(\pi^0\omega)\rho}(s) = \frac{\sqrt{2}e h_V}{\sigma_V} \operatorname{Im} \Pi_{\rho(\pi^0\omega)\rho}(s). \quad (16)$$

Modified (or exact) EM vertex satisfies equation

$$\frac{1}{f_V(s)} = \frac{1}{f_V^{(0)}} - \frac{i}{e s} \sum_c \operatorname{Im} \Pi_{\gamma(c)V}(s) \quad (17)$$

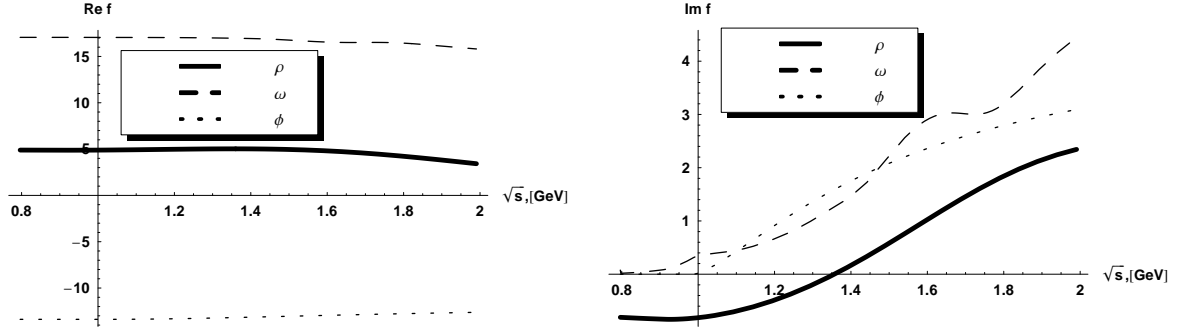


Figure 3. Real and imaginary parts of modified  $\gamma - V$  vertex.

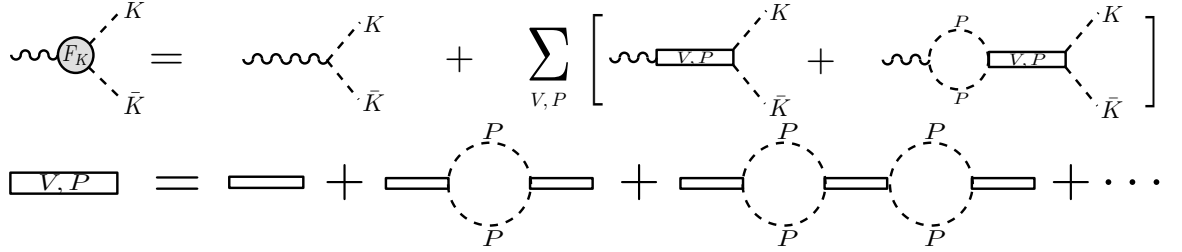


Figure 4. Electromagnetic form factor of  $K^+$  ( $K^-$ ).

and at  $s = m_V^2$  (on the mass shell) describe the leptonic decay widths of vector mesons

$$|f_V(s = m_V^2)|^2 = \frac{4}{3}\pi\alpha^2 \frac{m_V}{\Gamma(V \rightarrow e^+e^-)}.$$

This, together with information from “Particle Data Group” compilation [1] allows one to find the “bare” couplings

$$f_\rho^{(0)} = 5.026, \quad f_\omega^{(0)} = 17.060, \quad f_\phi^{(0)} = -13.382$$

and then obtain real and imaginary parts of the momentum-dependent couplings  $f_V(s)$  for arbitrary  $s$  (see Fig. 3).

Fig. 4 schematically illustrates the model for the form factors including self-energy and EM vertex loop corrections.

**Higher vector resonances.** Contribution from higher resonances  $\rho' = \rho(1450)$ ,  $\omega' = \omega(1420)$  and  $\phi' = \phi(1680)$  is

$$\Delta F_{K^+}(s) = - \sum_{V'=\rho',\omega',\phi'} \frac{g_{V'K^+K^-}}{f_{V'}(s)} A_{V'}(s), \quad (18)$$

$$\Delta F_{K^0}(s) = - \sum_{V'=\rho',\omega',\phi'} \frac{g_{V'K^0\bar{K}^0}}{f_{V'}(s)} A_{V'}(s). \quad (19)$$

We assume  $SU(3)_f$  for ratios of the strong and EM couplings for “primed” resonances

$$\begin{aligned} \frac{g_{\rho'K^+K^-}}{f_{\rho'}} : \frac{g_{\omega'K^+K^-}}{f_{\omega'}} : \frac{g_{\phi'K^+K^-}}{f_{\phi'}} &= \frac{1}{2} : \frac{1}{6} : \frac{1}{3}, \\ \frac{g_{\rho'K^0\bar{K}^0}}{f_{\rho'}} : \frac{g_{\omega'K^0\bar{K}^0}}{f_{\omega'}} : \frac{g_{\phi'K^0\bar{K}^0}}{f_{\phi'}} &= -\frac{1}{2} : \frac{1}{6} : \frac{1}{3} \end{aligned}$$

and use the known branching ratios from [1], then obtain

$$\begin{aligned} g_{\rho'K^+K^-}/f_{\rho'} &= -0.063, & g_{\omega'K^+K^-}/f_{\omega'} &= -0.021, \\ g_{\phi'K^+K^-}/f_{\phi'} &= -0.036. \end{aligned}$$

**High  $q^2$  behavior of form factors.** On the basis of quark counting rule in perturbative QCD (Lepage, Brodsky, Farrar and Jackson [14])

$$F_{K^+}(s) \rightarrow \frac{A}{s} \quad \text{at } s \rightarrow -\infty, \quad A = -16\pi F_\pi^2 \alpha_s(s). \quad (20)$$

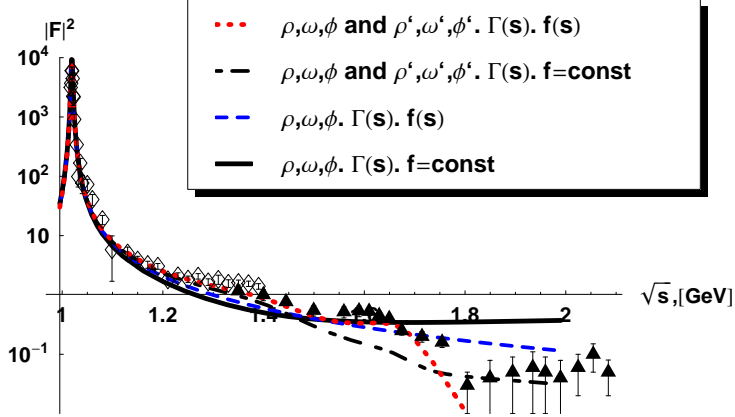


**Figure 5.** Charged kaon form factor in the time-like region  $s \geq 4m_{K^\pm}^2$ . Data: diamonds (open) are from [15], triangles – from [16].

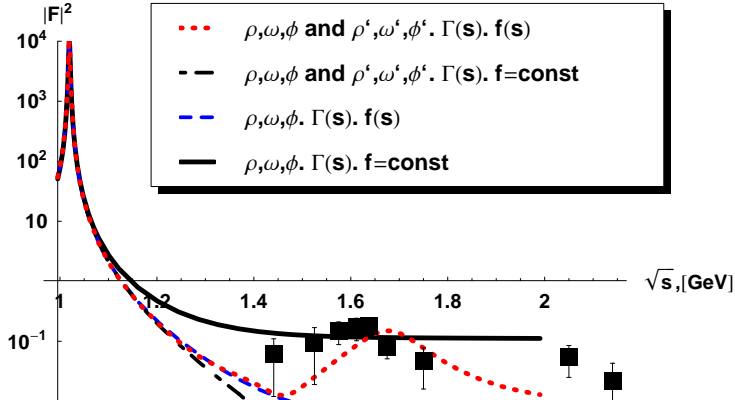


**Figure 6.** Neutral kaon form factor in the time-like region  $s \geq 4m_{K^0}^2$ . Data (boxes) are from [17].

In the present model we obtain at  $s \rightarrow -\infty$

$$\begin{aligned}
 F_{K^+}(s) &\rightarrow B + \frac{A'}{s}, \\
 B &= 1 - \sum_{V=\rho,\omega,\phi} \frac{g_{VK^+K^-}}{f_V} - \sum_{V'=\rho',\omega',\phi'} \frac{g_{V'K^+K^-}}{f_{V'}}, \\
 A' &= - \sum_{V=\rho,\omega,\phi} \frac{g_{VK^+K^-} - m_V^2}{f_V} - \sum_{V'=\rho',\omega',\phi'} \frac{g_{V'K^+K^-} - m_{V'}^2}{f_{V'}}.
 \end{aligned} \tag{21}$$

For the correct asymptotic behavior the constant  $B$  should be zero. Contribution from  $\rho, \omega, \phi$  with  $g_{VK^+K^-}/f_V$  taken from experiment does not lead to  $B = 0$ . If we add the higher resonances  $\rho', \omega', \phi'$  and choose negative relative sign of couplings  $g_{V'K^+K^-}/f_{V'}$  with respect to  $g_{VK^+K^-}/f_V$ , then  $B \approx 0$  and asymptotic behavior of the form factors is improved.

### 3 Comparison with experiment

In this section we present results for the charged and neutral kaons. Figs. 5 and 6 show FF in the time-like region, while Fig. 7 shows FF in the space-like region.

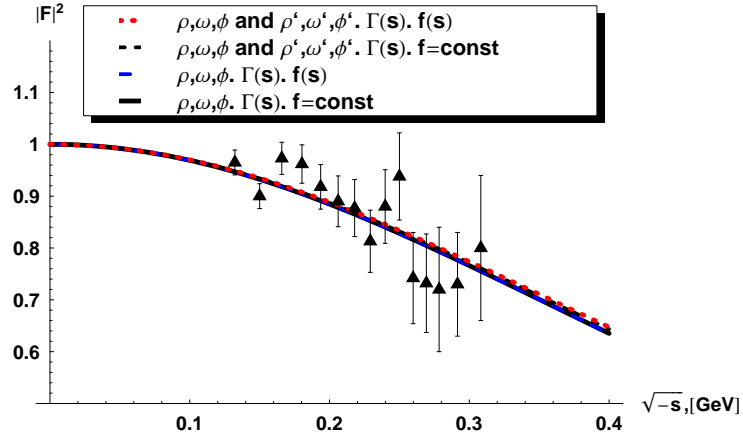


**Figure 7.** Charged kaon form factor in the space-like region  $s < 0$ . Data from NA7 Collaboration (CERN, SPS) [5].

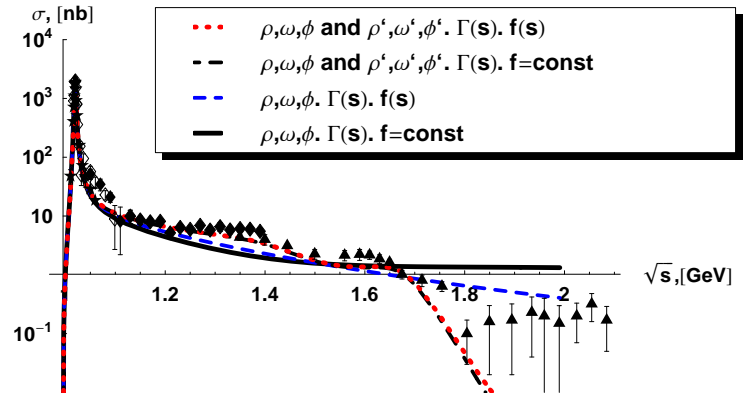


**Figure 8.** Total cross section of  $e^+e^-$  annihilation into charged kaons. Data: stars are from [18], diamonds (filled) – from [19], triangles – from [16], diamonds (open) – from [15].

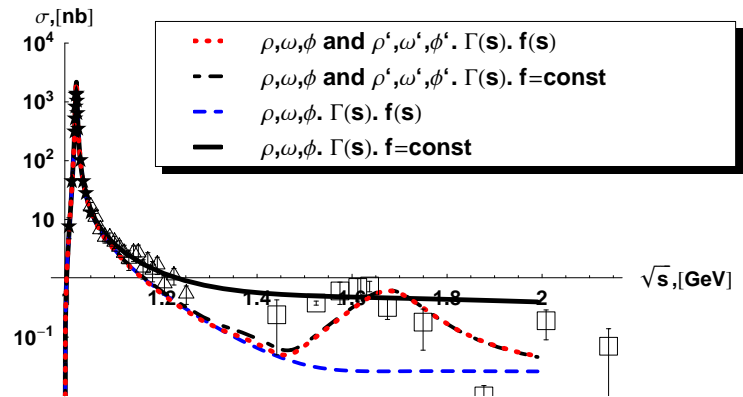


**Figure 9.** Total cross section of  $e^+e^-$  annihilation into neutral kaons. Data: stars are from [18], triangles (open) – from [2], boxes (open) – from [17].

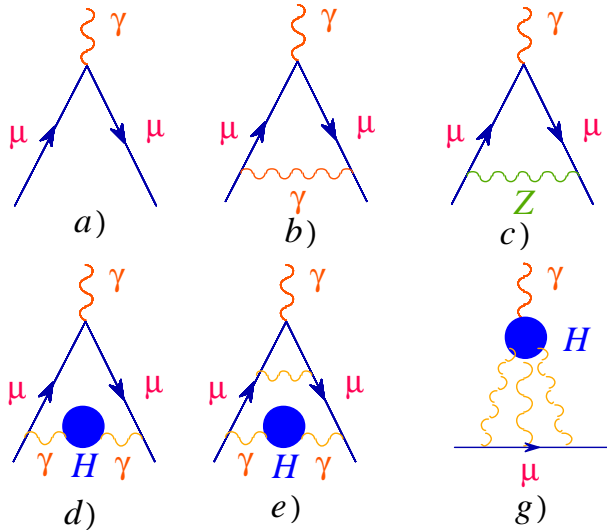
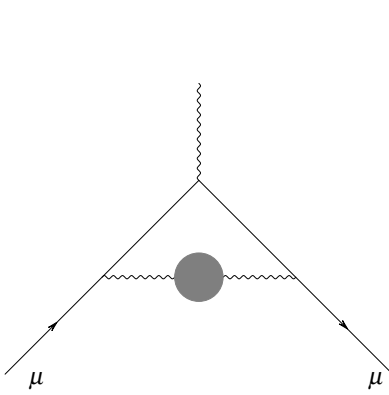


**Figure 10.** Hadronic contributions to muon AMM.

**Figure 11.** Typical diagrams contributing to muon AMM.

#### 4 $K\bar{K}$ production and anomalous magnetic moment of muon

If  $g_\mu$  is gyromagnetic ratio defined through the relation between magnetic moment and spin of the muon

$$\vec{M} = g_\mu \frac{e}{2m_\mu} \vec{s}, \quad (22)$$

and  $a_\mu \equiv g_\mu/2 - 1$  is a measure of AMM, then  $K\bar{K}$  contribution to  $a_\mu$  can be determined via the dispersion integral (Brodsky and de Rafael [20]) which follows from analyticity of the photon polarization operator:

$$a_\mu^{had, K\bar{K}} = \frac{\alpha^2}{3\pi^2} \int_{4m_K^2}^\infty W(s) R(s) \frac{ds}{s}, \quad (23)$$

$$W(s) = \int_0^1 \frac{x^2(1-x)}{x^2 + (1-x)s/m_\mu^2} dx,$$

where  $m_\mu$  is muon mass and  $R(s)$  is ratio of cross sections

$$R(s) = \frac{\sigma(e^+e^- \rightarrow K\bar{K})}{\sigma(e^+e^- \rightarrow \mu^+\mu^-)} = \frac{(1 - \frac{4m_K^2}{s})^{3/2}}{4(1 + 2\frac{m_\mu^2}{s})(1 - \frac{4m_\mu^2}{s})^{1/2}} |F_K(s)|^2.$$

The calculated values are presented in Table 4 together with the inaccuracy caused by uncertainty in the model parameters. The value  $(34.70 \pm 1.01) \times 10^{-10}$  is close (within 1.5%) to results from  $e^+e^-$  annihilation by CMD-2 and SND Collaborations in Novosibirsk [21].

Note that  $K\bar{K}$  channels contribute about 5% of the hadronic contributions to AMM (Fig. 10).

The total AMM in the Standard Model includes various contributions (see Fig. 11) and is equal to [22]

$$a_\mu^{theor} = a_\mu^{QED} + a_\mu^{weak} + a_\mu^\gamma \text{ by } \gamma + a_\mu^{had, LO} + a_\mu^{had, HO}, \quad (24)$$

where

$$a_\mu^{QED} = (11658471.81 \pm 1.45 \text{ loops} \pm 0.08_\alpha) \times 10^{-10},$$

$$a_\mu^{weak} = (15.4 \pm 0.1 \text{ had} \pm 0.2 \text{ Higgs, 3 loops}) \times 10^{-10},$$

$$a_\mu^\gamma \text{ by } \gamma = (8 \pm 4) \times 10^{-10},$$

$$a_\mu^{had, LO} = (690.9 \pm 3.9_{exp} + 1.9_{rad} + 0.7_{QCD}) \times 10^{-10},$$

$$a_\mu^{had, HO} = (-9.79 \pm 0.09_{exp} + 0.03_{rad}) \times 10^{-10}.$$

The difference between the most precise experimental value ( $g-2$  Collaboration, experiment E821, BNL, Brookhaven) and the theoretical value is (in units  $10^{-10}$ )

$$a_\mu^{exp} - a_\mu^{theor} = (11659208.0 \pm 6.3) - (11659176.3 \pm 6) = 31.7 \pm 8.7$$

**Table 4.** Contribution of  $K\bar{K}$ –channels to muon AMM  $a_\mu^{had, K\bar{K}}$ 

channel	$K^+K^-$	$K^0\bar{K}^0$	total $KK$
$a_\mu^{had, K\bar{K}}, 10^{-10}$	$19.06 \pm 0.57$	$15.64 \pm 0.44$	$34.70 \pm 1.01$

The discrepancy is only about  $3 \times 10^{-6}$  of the experimental value. Nevertheless it is more than 3 “standard deviations”  $\sigma$  and is therefore important. Whether this indicates new physics beyond the Standard Model remains to be studied further. There are other possible contributions which may add to the theoretical value, and from the experimental side there is a puzzling discrepancy between results from  $e^+e^- \rightarrow \pi^+\pi^-$  and  $\tau$ –decay  $\tau^- \rightarrow \pi^-\pi^0\nu_\tau$ .

New experiment E969 is scheduled at BNL [23] aiming to reduce experimental error in muon AMM from  $6.3 \times 10^{-10}$  to  $2.5 \times 10^{-10}$ .

## 5 Conclusions

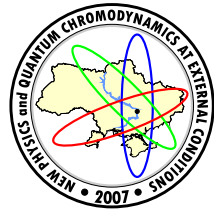
1. A model for electromagnetic form factors of the  $K$ –mesons in the time-like ( $s \geq 4m_K^2$ ) and space-like ( $s < 0$ ) regions of the photon momentum is developed up to  $\mathcal{O}(p^4)$  [13].
2. Agreement with experiments on  $e^+e^- \rightarrow K\bar{K}$  annihilation at  $\sqrt{s} = 1 - 1.75$  GeV is obtained without fitting parameters. Deviations from the data at  $\sqrt{s} > 2$  GeV are probably related to higher resonances  $\rho(1700)$  and  $\omega(1650)$ .
3. Form factor agrees with the data in the space-like region at  $-q^2 < 0.16$  GeV $^2$ . Results from Jefferson Laboratory at large momentum transfer  $-q^2 \sim 3$  GeV $^2$  [6] which are coming soon may help to test further the model.
4. Contribution of  $K\bar{K}$  channels to anomalous magnetic moment of the muon is found to be:

$$a_\mu^{had, K^+K^-} + a_\mu^{had, K^0\bar{K}^0} = (34.70 \pm 1.01) \times 10^{-10}$$

which agrees with  $e^+e^-$  annihilation results from Novosibirsk.

## References

- [1] W.-M. Yao *et al.* (Particle Data Group), *Review of Particle Physics*. J.Phys. **G33**, 1–1232 (2006), <http://pdg.lbl.gov>
- [2] R.R. Akhmetshin *et al.*, Phys.Lett. **B551**, 27 (2003) [hep-ex/0211004].
- [3] M.N. Achasov *et al.* [SND Collaboration], Preprint Budker INP-2005-35, Novosibirsk, 2005.
- [4] A. Aloisio *et al.* [KLOE Collaboration] Phys.Lett. **B606**, 12 (2005).
- [5] S.R. Amendolia *et al.* [NA7 Collaboration], Phys.Lett. **B178**, 435 (1986).
- [6] Jefferson Lab experiment E98-108, spokesperson P. Markowitz.
- [7] G. Ecker, J. Gasser, A. Pich and E. de Rafael, Nucl.Phys. **B321**, 311 (1989).
- [8] G. Ecker, J. Gasser, H. Leutwyler and A. Pich, Phys.Lett. **B223**, 425 (1989).
- [9] J. Wess and B. Zumino, Phys. Lett. **B 37**, 95 (1971).
- [10] E. Witten, Nucl.Phys. **B223**, 422 (1983).
- [11] J. Prades, Z.Phys. **C63** 491 (1994); Erratum, Eur.Phys.J. **C11**, 571 (1999).
- [12] O. Kaymakcalan, S. Rajeev and J. Schechter, Phys.Rev. **D30**, 594 (1984);  
P. Ko and S. Rudaz, Phys.Rev. **D50**, 6877 (1994).
- [13] S.A. Ivashyn and A.Yu. Korchin, Eur. Phys. J. **C 49**, 697 (2007).
- [14] G.R. Farrar and D.R. Jackson, Phys.Rev.Lett. **43**, 246 (1979); G.P. Lepage and S.J. Brodsky, Phys.Rev. **D22**, 2157 (1980).
- [15] P.M. Ivanov *et al.*, Phys.Lett. **B107**, 297 (1981).
- [16] D. Bisello *et al.* [DM2 Collaboration], Z.Phys. **C39**, 13 (1988).
- [17] F. Mane *et al.* [DM1 Collaboration], Phys.Lett. **B99**, 261 (1980).
- [18] M.N. Achasov *et al.* [SND Collaboration], Phys.Rev. **D63**, 072002 (2001) [hep-ex/0009036].
- [19] S.I. Dolinsky *et al.*, Phys.Rep. **202**, 99 (1991).
- [20] S.J. Brodsky and E. de Rafael, Phys.Rev. **168**, 1620 (1968).
- [21] M. Davier, S. Eidelman, A. Höcker and Z. Zhang, Eur.Phys.J. **C31**, 503 (2003).
- [22] M. Passera, hep-ph/0702027.
- [23] D.W. Hertzog, hep-ex/0611025.



## INDIRECT COLLIDER TESTS FOR LARGE EXTRA DIMENSIONS

A.A. Pankov<sup>a</sup>, A.V. Tsytrinov<sup>b</sup>

ICTP Affiliated Centre, Pavel Sukhoi Technical University, Gomel, Belarus

New physics signatures arising from different sources may be confused when first observed at future colliders. Thus it is important to examine how various scenarios may be differentiated given the availability of only limited information. Arkani-Hamed, Dimopoulos, and Dvali have proposed a model (ADD) of low-scale quantum gravity featuring large extra dimensions. In this model, the exchange of Kaluza-Klein towers of gravitons can manifest themselves through deviations of the observables from the Standard Model predictions. Here, we assess the expected “identification reach” on the ADD model of gravity in large compactified extra dimensions, against the compositeness-inspired four-fermion contact interaction. As basic observables we take the differential cross sections for fermion-pair production at a 0.5–1 TeV electron-positron linear collider with both beams longitudinally polarized. For the four-fermion contact interaction we assume a general linear combination of the individual models with definite chiralities, with arbitrary coupling constants. In this sense, the estimated identification reach on the ADD model can be considered as “model-independent”. In the analysis, we give estimates also for the expected “discovery reaches” on the various scenarios. We emphasize the substantial rôle of beams polarization in enhancing the sensitivity to the contactlike interactions under consideration.

### 1 Introduction

Numerous New Physics (NP) scenarios are described by local, contactlike, effective interactions between the Standard Model (SM) particles. This is the typical case of interactions mediated by exchanges of quanta that are constrained, by either conceptual or phenomenological considerations, to have a mass, we generically denote as  $\Lambda$ , in the multi-TeV range. These states may be beyond the kinematical reach of the collider and therefore could not appear as final products of the studied reactions. Accordingly, the existence of such nonstandard scenarios can be verified only through their *indirect* effects, represented by deviations of the measured observables from the SM predictions. The effective interaction framework leads to the expansion of the deviations caused by these novel interactions in powers of the corresponding small ratios  $E_{\text{C.M.}}/\Lambda \ll 1$ , multiplied by matrix elements of local operators between initial and final states. Generally, the dominance of the leading power is taken as a reasonable assumption.

Referring to experiments at planned high energy colliders and their sensitivity to NP, one can define for the individual contactlike effective interactions the expected *discovery reach*, as the maximum value of the relevant  $\Lambda$  for which deviations from the SM predictions can be detected within the foreseen experimental accuracy. This limit can be assessed by a comparison of theoretical deviations, functions of  $\Lambda$ , and expected experimental uncertainties by assuming that no such deviations are observed.

Conversely, one can envisage a situation where corrections to the SM predictions are observed, and found compatible with one of the effective interactions for a certain value of the relevant  $\Lambda$ . In this case, one should consider that, in principle, different contactlike interactions can cause similar corrections. Therefore, it should be desirable to attempt the identification of the source of the observed deviations among the various possible scenarios. To this purpose, one can define the expected *identification reach* on an individual contact interaction model, as the maximum value of the corresponding  $\Lambda$  for which not only it can cause observable deviations but, also, can be discriminated as the source of such corrections, were they observed, against the other effective interactions for any value of their characteristic  $\Lambda$ s. Obviously, the identification reach can only be smaller than the discovery reach.

Here, we consider as basic observables the differential cross sections for the fermion pair production processes

$$e^+ + e^- \rightarrow \bar{f} + f, \quad f = e, \mu, \tau, c, b, \quad (1)$$

at the International Linear Collider (ILC) with longitudinally polarized electron and positron beams [1]. This option is considered with great interest in the project for this collider, and its impact on the physics programme has been reviewed recently in Ref. [2].

e-mail: <sup>a</sup>pankov@ictp.it, <sup>b</sup>atsytrin@ictp.it

© Pankov A.A., Tsytrinov A.V., 2007.

As a significant example, we focus on the identification reach on the ADD model of gravity in large, compactified, extra spatial dimensions [3–5], with respect to the compositeness-inspired four-fermion contact interactions [6, 7]. Also, we insist on the rôle played by the longitudinal polarization of the  $e^+$  and  $e^-$  beams in enhancing the identification power of processes (1) on this scenario, at the planned ILC energies and luminosities.

## 2 Polarized differential observables

The expression of the polarized differential cross section for the process  $e^+e^- \rightarrow f\bar{f}$  with  $f \neq e, t$  and in approximation where  $m_f \ll \sqrt{s}$  can be expressed as [8]:

$$\frac{d\sigma(P^-, P^+)}{dz} = \frac{D}{4} \left[ (1 - P_{\text{eff}}) \left( \frac{d\sigma_{\text{LL}}}{dz} + \frac{d\sigma_{\text{LR}}}{dz} \right) + (1 + P_{\text{eff}}) \left( \frac{d\sigma_{\text{RR}}}{dz} + \frac{d\sigma_{\text{RL}}}{dz} \right) \right]. \quad (2)$$

In Eq. (2),  $z = \cos\theta$  with  $\theta$  the angle between initial and final fermions in the C.M. frame, and the subscripts L, R denote the respective helicities. Furthermore, with  $P^-$  and  $P^+$  denoting the degrees of longitudinal polarization of the  $e^-$  and  $e^+$  beams, respectively, one has

$$D = 1 - P^-P^+, \quad P_{\text{eff}} = \frac{P^- - P^+}{1 - P^-P^+}. \quad (3)$$

The SM amplitudes for these processes are determined by  $\gamma$  and  $Z$  exchanges in the  $s$ -channel.

The polarized differential cross section for the Bhabha process  $e^+e^- \rightarrow e^+e^-$ , where  $\gamma$  and  $Z$  can be exchanged also in the  $t$ -channel, can be conveniently written as [9–11]:

$$\frac{d\sigma(P^-, P^+)}{dz} = \frac{(1 + P^-)(1 - P^+)}{4} \frac{d\sigma_{\text{R}}}{dz} + \frac{(1 - P^-)(1 + P^+)}{4} \frac{d\sigma_{\text{L}}}{dz} + \frac{(1 + P^-)(1 + P^+)}{4} \frac{d\sigma_{\text{RL},t}}{dz} + \frac{(1 - P^-)(1 - P^+)}{4} \frac{d\sigma_{\text{LR},t}}{dz}, \quad (4)$$

with the decomposition

$$\frac{d\sigma_{\text{L}}}{dz} = \frac{d\sigma_{\text{LL}}}{dz} + \frac{d\sigma_{\text{LR},s}}{dz}, \quad \frac{d\sigma_{\text{R}}}{dz} = \frac{d\sigma_{\text{RR}}}{dz} + \frac{d\sigma_{\text{RL},s}}{dz}. \quad (5)$$

In Eqs. (4) and (5), the subscripts  $t$  and  $s$  denote helicity cross sections with SM  $\gamma$  and  $Z$  exchanges in the corresponding channels. In terms of helicity amplitudes:

$$\begin{aligned} \frac{d\sigma_{\text{LR},t}}{dz} &= \frac{d\sigma_{\text{RL},t}}{dz} = \frac{2\pi\alpha_{\text{e.m.}}^2 |G_{\text{LR},t}|^2}{s}, & \frac{d\sigma_{\text{LR},s}}{dz} &= \frac{d\sigma_{\text{RL},s}}{dz} = \frac{2\pi\alpha_{\text{e.m.}}^2 |G_{\text{LR},s}|^2}{s}, \\ \frac{d\sigma_{\text{LL}}}{dz} &= \frac{2\pi\alpha_{\text{e.m.}}^2 |G_{\text{LL},s} + G_{\text{LL},t}|^2}{s}, & \frac{d\sigma_{\text{RR}}}{dz} &= \frac{2\pi\alpha_{\text{e.m.}}^2 |G_{\text{RR},s} + G_{\text{RR},t}|^2}{s}. \end{aligned} \quad (6)$$

The polarized differential cross section (2) for the leptonic channels  $e^+e^- \rightarrow l^+l^-$  with  $l = \mu, \tau$  can be obtained directly from Eq. (4), basically by dropping the  $t$ -channel poles. The same is true, after some obvious adjustments, for the  $\bar{c}c$  and  $\bar{b}b$  final states.

According to the previous considerations the amplitudes  $G_{\alpha\beta,i}$ , with  $\alpha, \beta = \text{L, R}$  and  $i = s, t$ , are given by the sum of the SM  $\gamma, Z$  exchanges plus deviations representing the effect of the novel, contactlike, effective interactions:

$$\begin{aligned} G_{\text{LL},s} &= u \left[ \frac{1}{s} + \frac{g_{\text{L}}^2}{s - M_Z^2} + \Delta_{\text{LL},s} \right], & G_{\text{LL},t} &= u \left[ \frac{1}{t} + \frac{g_{\text{L}}^2}{t - M_Z^2} + \Delta_{\text{LL},t} \right], \\ G_{\text{RR},s} &= u \left[ \frac{1}{s} + \frac{g_{\text{R}}^2}{s - M_Z^2} + \Delta_{\text{RR},s} \right], & G_{\text{RR},t} &= u \left[ \frac{1}{t} + \frac{g_{\text{R}}^2}{t - M_Z^2} + \Delta_{\text{RR},t} \right], \\ G_{\text{LR},s} &= t \left[ \frac{1}{s} + \frac{g_{\text{R}} g_{\text{L}}}{s - M_Z^2} + \Delta_{\text{LR},s} \right], & G_{\text{LR},t} &= s \left[ \frac{1}{t} + \frac{g_{\text{R}} g_{\text{L}}}{t - M_Z^2} + \Delta_{\text{LR},t} \right]. \end{aligned} \quad (7)$$

Here  $u, t = -s(1 \pm z)/2$ ,  $g_{\text{R}} = \tan\theta_W$  and  $g_{\text{L}} = -\cot 2\theta_W$  with  $\theta_W$  the electroweak mixing angle. The deviations  $\Delta_{\alpha\beta,i}$  caused by the models of interest here have been tabulated in earlier references, see for example Refs. [10, 12, 13]. However, for convenience, we report their explicit expressions and briefly comment on their properties in the next section.

The contactlike nonstandard interactions considered in the sequel are listed below:

**a)** The ADD, compactified large extra dimensions, scenario [3–5], motivated by the gauge hierarchy problem. In this scenario, only gravity can propagate in the full multidimensional space. Correspondingly, a tower of graviton KK states with equally-spaced spectrum is exchanged in the ordinary four-dimensional space, and induces indirect corrections to the SM  $\gamma$  and  $Z$  exchanges. The relevant Feynman rules have been derived in Refs. [14, 15]. In the parameterization of Ref. [16], the exchange of such a KK tower is represented by the effective interaction:

$$\mathcal{L} = i \frac{4\lambda}{\Lambda_H^4} T^{\mu\nu} T_{\mu\nu}, \quad \lambda = \pm 1. \quad (8)$$

In Eq. (8),  $T_{\mu\nu}$  denotes the energy-momentum tensor of the SM particles and  $\Lambda_H$  is an ultraviolet cut-off on the summation over the KK spectrum, expected in the (multi) TeV range. The corresponding corrections to the SM amplitudes for Bhabha scattering, see Eq. (7), read:

$$\begin{aligned} \Delta_{\text{LL},s} = \Delta_{\text{RR},s} &= \frac{\lambda(u + 3s/4)}{\pi\alpha_{\text{e.m.}}\Lambda_H^4}, & \Delta_{\text{LL},t} = \Delta_{\text{RR},t} &= \frac{\lambda(u + 3t/4)}{\pi\alpha_{\text{e.m.}}\Lambda_H^4}, \\ \Delta_{\text{LR},s} &= -\frac{\lambda(t + 3s/4)}{\pi\alpha_{\text{e.m.}}\Lambda_H^4}, & \Delta_{\text{LR},t} &= -\frac{\lambda(s + 3t/4)}{\pi\alpha_{\text{e.m.}}\Lambda_H^4}. \end{aligned} \quad (9)$$

As observed in the previous section, the deviations for the other processes in Eq. (1) can easily be obtained from Eqs. (9). One can remark, also, that the effective interaction (8) has dimension-8, which explains the high negative power of the characteristic mass scale  $\Lambda_H$ .

**b)** The dimension-6 four-fermion contact interaction (CI) scenario [6, 7]. With  $\Lambda_{\alpha\beta}$  ( $\alpha, \beta = \text{L, R}$ ) the “compositeness” mass scales, and  $\delta_{ef} = 1$  (0) for  $f = e$  ( $f \neq e$ ):

$$\mathcal{L} = \frac{4\pi}{1 + \delta_{ef}} \sum_{\alpha, \beta} \frac{\eta_{\alpha\beta}}{\Lambda_{\alpha\beta}^2} (\bar{e}_\alpha \gamma_\mu e_\alpha) (\bar{f}_\beta \gamma^\mu f_\beta), \quad \eta_{\alpha\beta} = \pm 1, 0. \quad (10)$$

The induced deviations in Eq. (7) are:

$$\Delta_{\alpha\beta,s} = \Delta_{\alpha\beta,t} = \frac{1}{\alpha_{\text{e.m.}}} \frac{\eta_{\alpha\beta}}{\Lambda_{\alpha\beta}^2}. \quad (11)$$

Rather generally, this kind of effective interactions applies to the cases of very massive virtual exchanges, such as heavy  $Z$ 's, leptoquarks, etc.

Current experimental lower bounds on  $\Lambda$ s are mostly derived from nonobservation of deviations at LEP and Tevatron colliders. At the 95% C.L., they are:  $\Lambda_H > 1.3$  TeV [17] and, generically,  $\Lambda_{\alpha\beta} > 10 - 15$  TeV, depending on the processes measured and the type of analysis performed [18].

**c)** In models with  $\text{TeV}^{-1}$ -scale extra dimensions, the SM gauge bosons may propagate also in the additional dimensions, and the new, contact-like, effective interaction relevant to the processes of interest here is generated by the exchange of  $\gamma$  and  $Z$  KK excitations [19, 20]. For one additional dimension, and with  $M_C \gg M_{W,Z}$  the inverse of the compactification radius, for  $e^+e^- \rightarrow \bar{f}f$  it can be written as

$$\begin{aligned} \mathcal{L}^{\text{TeV}} &= -\frac{\pi^2}{3M_C^2} [Q_e Q_f (\bar{e} \gamma_\mu e)(\bar{f} \gamma^\mu f) \\ &+ (g_L^e \bar{e}_L \gamma_\mu e_L + g_R^e \bar{e}_R \gamma_\mu e_R)(g_L^f \bar{f}_L \gamma^\mu f_L + g_R^f \bar{f}_R \gamma^\mu f_R)]. \end{aligned} \quad (12)$$

The corresponding deviation can be written as

$$\Delta_{\alpha\beta,s} = \Delta_{\alpha\beta,t} = -(Q_e Q_f + g_\alpha^e g_\beta^f) \frac{\pi^2}{3M_C^2} \quad (13)$$

For the  $\text{TeV}^{-1}$ -scale extra dimension scenario the current limit, mostly determined by LEP data, is  $M_C > 6.8$  TeV [17].

It may be worth noticing that in cases **b)** and **c)**, Eqs. (11) and (13), the deviations are  $z$ -independent and the appropriate helicity cross sections have the same angular structure as in the case of the SM. Conversely, in case **a)**, Eq. (9), the deviations introduce extra  $z$ -dependencies in the angular distributions. It turns out that, as a consequence, the ADD model contribution to the integrated cross sections for the annihilation channels in Eq. (1) is quite small, due to the vanishing interference with the SM amplitudes after integration over the full angular range  $-1 \leq z \leq 1$ . This suppresses the possibility of identifying the ADD interaction effects in the total cross sections for these processes. In these cases, specifically defined integrated asymmetries with polarized initial beams may be expected to be more efficient contactlike interaction analyzers [8, 21]. In the next section we discuss the rôle of polarized angular differential distributions themselves, in selecting signatures of ADD effective interactions at ILC.

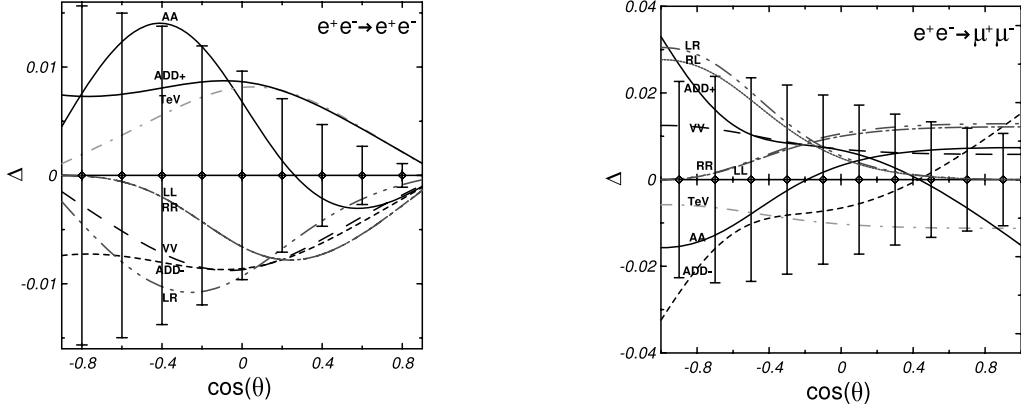


**Figure 1. Left panel:** relative deviations of the unpolarized Bhabha differential cross section from the SM prediction as a function of  $\cos \theta$  at  $\sqrt{s} = 0.5$  TeV for the CI models: AA ( $\Lambda_{\text{AA}}^+ = 48$  TeV), VV ( $\Lambda_{\text{VV}}^+ = 76$  TeV), LL ( $\Lambda_{\text{LL}}^+ = 37$  TeV), RR ( $\Lambda_{\text{RR}}^+ = 36$  TeV), LR ( $\Lambda_{\text{LR}}^+ = 60$  TeV); for the  $\text{TeV}^{-1}$  model ( $M_C = 12$  TeV) and the ADD $\pm$  models ( $\Lambda_H = 4$  TeV). The vertical bars represent the statistical uncertainty in each bin for  $\mathcal{L}_{\text{int}} = 100 \text{ fb}^{-1}$ . **Right panel:** same as in left panel but for  $e^+e^- \rightarrow \mu^+\mu^-$ , for the CI models: AA ( $\Lambda_{\text{AA}}^+ = 80$  TeV), VV ( $\Lambda_{\text{VV}}^+ = 90$  TeV), LL ( $\Lambda_{\text{LL}}^+ = 45$  TeV), RR ( $\Lambda_{\text{RR}}^+ = 42$  TeV), LR ( $\Lambda_{\text{LR}}^+ = 41$  TeV), RL ( $\Lambda_{\text{RL}}^+ = 43$  TeV); for the  $\text{TeV}^{-1}$  model ( $M_C = 17$  TeV) and the ADD $\pm$  models ( $\Lambda_H = 2.8$  TeV).

### 3 Discovery and identification reaches

We here briefly outline the derivation of the expected ‘‘discovery reaches’’ on the New Physics scenarios introduced in the previous section. The basic objects are the relative deviations of observables from the SM predictions due to the NP:

$$\Delta(\mathcal{O}) = \frac{\mathcal{O}(\text{SM} + \text{NP}) - \mathcal{O}(\text{SM})}{\mathcal{O}(\text{SM})}, \quad (14)$$

and, as anticipated, we concentrate on the polarized differential cross section,  $\mathcal{O} \equiv d\sigma/d\cos\theta$ . To get an illustration of the effects induced by the individual NP models, we show in Fig. 1 the angular behaviour of the relative deviations (14) for the two leptonic processes under consideration (with unpolarized beams), for c.m. energy  $\sqrt{s} = 0.5$  TeV and selected values of the relevant mass scale parameters close to their ‘‘discovery reaches’’ (unpolarized cross sections). The superscript ‘‘+’’ on the CI mass scales  $\Lambda_{\alpha\beta}^+$  denotes the choice  $\eta_{\alpha\beta} = 1$  in Eq. (10), while the notation ADD $\pm$  corresponds to  $\lambda = \pm 1$  in Eq. (8). Vertical bars represent the statistical uncertainty in each angular bin, for an integrated luminosity  $\mathcal{L}_{\text{int}} = 100 \text{ fb}^{-1}$ . The comparison of deviations with statistical uncertainties is an indicator of the sensitivity of an observable to the individual non-standard effective interaction models.

In this figure, the numerical value chosen for  $\Lambda_H$  is such that the interference of the graviton-exchange with the SM dominates the deviations of the differential cross sections, so that the ADD+ and ADD- models give corrections of the same size and opposite sign. Moreover, due to the chosen values  $\Lambda_{\text{LL}}^+ \simeq \Lambda_{\text{RR}}^+$ , the corresponding CI models generate almost equal deviations of the differential cross sections because, in the (dominant) interferences with the SM, numerically  $g_L^2 \simeq g_R^2$  [see Eq. (7)].

To derive the constraints on the models, one has to compare the theoretical deviations from the SM predictions, that are functions of  $\Lambda$ s, to the foreseen experimental uncertainties on the differential cross sections. To this purpose, taking the polarized angular distributions as basic observables for the analysis,  $\mathcal{O} = d\sigma(P^-, P^+)/dz$ , we introduce  $\chi^2$ :

$$\chi^2(\mathcal{O}) = \sum_{\{P^-, P^+\} \text{ bins}} \sum \left( \frac{\Delta(\mathcal{O})^{\text{bin}}}{\delta\mathcal{O}^{\text{bin}}} \right)^2. \quad (15)$$

Here, for the individual processes, the cross sections for the different initial polarization configurations are combined in the  $\chi^2$ , and  $\delta\mathcal{O}$  denotes the expected experimental relative uncertainty (statistical plus systematic one). As indicated in Eq. (15), we divide the angular range into bins. For Bhabha scattering, the cut angular range  $|\cos\theta| < 0.90$  is divided into ten equal-size bins. Similarly, for annihilation into muon, tau and quark pairs we consider the analogous binning of the cut angular range  $|\cos\theta| < 0.98$ .

For the Bhabha process, we combine the cross sections with the following initial electron and positron longitudinal polarizations:

$$(P^-, P^+) = (|P^-|, -|P^+|); \quad (-|P^-|, |P^+|); \quad (|P^-|, |P^+|); \quad (-|P^-|, -|P^+|).$$

For the ‘‘annihilation’’ processes in Eq. (1), with  $f \neq e, t$ , we limit to combining the  $(P^-, P^+) = (|P^-|, -|P^+|)$  and  $(-|P^-|, |P^+|)$  polarization configurations. Numerically, we take the ‘‘standard’’ envisaged values  $|P^-| = 0.8$  and  $|P^+| = 0.6$ .

Regarding the ILC energy and time-integrated luminosity, for simplicity we assume the latter to be equally distributed among the different polarization configurations defined above. The explicit numerical results will refer to C.M. energy  $\sqrt{s} = 0.5$  TeV with time-integrated luminosity  $\mathcal{L}_{\text{int}} = 100 \text{ fb}^{-1}$ , and to  $\sqrt{s} = 1$  TeV with  $\mathcal{L}_{\text{int}} = 1000 \text{ fb}^{-1}$ . The assumed reconstruction efficiencies, that determine the expected statistical uncertainties, are 100% for  $e^+e^-$  final pairs; 95% for final  $l^+l^-$  events ( $l = \mu, \tau$ ); 35% and 60% for  $c\bar{c}$  and  $b\bar{b}$ , respectively. The major systematic uncertainties are found to originate from uncertainties on beams polarizations and on the time-integrated luminosity: we assume  $\delta P^-/P^- = \delta P^+/P^+ = 0.2\%$  and  $\delta \mathcal{L}_{\text{int}}/\mathcal{L}_{\text{int}} = 0.5\%$ , respectively.

As theoretical inputs, for the SM amplitudes we use the effective Born approximation [22] with  $m_{\text{top}} = 175$  GeV and  $m_H = 120$  GeV. Concerning the  $\mathcal{O}(\alpha)$  QED corrections, the (numerically dominant) effects from initial-state radiation for Bhabha scattering and the annihilation processes in (1) are accounted for by a structure function approach including both hard and soft photon emission [23], and by a flux factor method [24], respectively. Effects of radiative flux return to the  $s$ -channel  $Z$  exchange are minimized by the cut  $\Delta \equiv E_\gamma/E_{\text{beam}} < 1 - M_Z^2/s$  on the radiated photon energy, with  $\Delta = 0.9$ . In this way, only interactions that occur close to the nominal collider energy are included in the analysis and, accordingly, the sensitivity to the manifestations of the searched for nonstandard physics can be optimized. By a calculation based on the ZFITTER code [25], other QED effects such as final-state and initial-final state emission are found, in processes  $e^+e^- \rightarrow l^+l^-$  and  $e^+e^- \rightarrow \bar{q}q$  ( $q = c, b$ ), to be numerically unimportant for the chosen kinematical cuts. Finally, correlations between the different polarized cross sections (but not between the individual angular bins) are taken into account in the derivation of the numerical results presented below.

The expected discovery reaches on the contactlike effective interactions are assessed by assuming a situation where no deviation from the SM predictions is observed within the experimental uncertainty. Accordingly, the corresponding upper limits on the accessible values of  $\Lambda$ s are determined by the condition  $\chi^2(\mathcal{O}) \leq \chi^2_{\text{CL}}$ , and we take  $\chi^2_{\text{CL}} = 3.84$  for a 95% C.L.

In Table 1, we present the numerical results from the processes listed in the caption, at an ILC with  $\sqrt{s} = 0.5$  TeV,  $\mathcal{L}_{\text{int}} = 100 \text{ fb}^{-1}$ , and with  $\sqrt{s} = 1$  TeV,  $\mathcal{L}_{\text{int}} = 1000 \text{ fb}^{-1}$ . Here,  $l^+l^-$  denotes the combination of  $\mu^+\mu^-$  and  $\tau^+\tau^-$  final states, and  $\mu-\tau$  universality has been assumed for the limits on the CI mass scales. In this table, only the results for positive interference between SM amplitudes and nonstandard contributions are reported, i.e., the cases  $\lambda = 1$  for the ADD model of Eq. (8) and  $\eta_{\alpha\beta} = 1$  for the CI models of Eq. (10). The sensitivity reach for negative interference turns out to be practically the same. Indeed, the angular dependence of the corrections to the SM predictions induced by NP is found to be almost symmetric under reversing the sign of the interference terms, see for example Ref. [10]. Therefore, the interference terms turn out to numerically dominate over the pure, quadratic, NP contributions.

The results in Table 1 clearly show the enhancement in sensitivity to the considered effective interactions allowed, for given C.M. energy and luminosity, by beams polarization. This effect is particularly substantial in the case of the CI models (10), for which the limits on the relevant  $\Lambda$ s are quite high compared to the current ones.

Continuing the previous  $\chi^2$ -based analysis, we now assume that deviations has been observed and are consistent with the ADD scenario (8) for some value of  $\Lambda_H$ . To assess the level at which the ADD model can be discriminated from the general CI model as the source of the deviations or, equivalently, to determine the ‘model-independent’ identification reach on the effective interaction (8), we introduce in analogy with Eq. (15) the relative deviations  $\tilde{\Delta}$  and the corresponding  $\tilde{\chi}^2$ :

$$\tilde{\Delta}(\mathcal{O}) = \frac{\mathcal{O}(\text{CI}) - \mathcal{O}(\text{ADD})}{\mathcal{O}(\text{ADD})}; \quad \tilde{\chi}^2(\mathcal{O}) = \sum_{\{P^-, P^+\} \text{ bins}} \sum \left( \frac{\tilde{\Delta}(\mathcal{O})^{\text{bin}}}{\tilde{\delta} \mathcal{O}^{\text{bin}}} \right)^2. \quad (16)$$

In Eq. (16),  $\tilde{\Delta}(\mathcal{O})$  depends on all  $\Lambda$ s, and somehow represents the ‘distance’ between the ADD and the CI model in the parameter space  $(\Lambda_H, \Lambda_{\alpha\beta})$ . Moreover,  $\tilde{\delta} \mathcal{O}^{\text{bin}}$  is the expected relative uncertainty referred to the cross sections that include the ADD model contributions: its statistical component is therefore determined from helicity amplitudes with the deviations (9) predicted for the given value of  $\Lambda_H$ . In turn, the CI contributions to the cross sections bring in the dependence of Eq. (16) on the parameters  $\Lambda_{\alpha\beta}$  of Eq. (11), now considered as *all* independent. Therefore, for each of processes (1),  $\tilde{\chi}^2$  is a function of  $\lambda/\Lambda_H^4$  and in general, simultaneously of the four CI couplings  $\eta_{\alpha\beta}/(\Lambda_{\alpha\beta}^{ef})^2$ .

In this situation we can determine *confusion regions* in the parameter space, where the CI model can be considered as consistent with the ADD model, in the sense that it can mimic the differential cross sections of the individual processes (1) determined by the latter one. At a given C.L., these confusion regions are determined by the condition

$$\tilde{\chi}^2 \leq \chi^2_{\text{CL}}. \quad (17)$$

**Table 1.** 95% C.L. discovery reaches (in TeV). Left and right entries in each column refer to the polarizations  $(|P^-|, |P^+|) = (0,0)$  and  $(0.8, 0.6)$ , respectively.

Model	Process			
	$e^+e^- \rightarrow e^+e^-$	$e^+e^- \rightarrow l^+l^-$	$e^+e^- \rightarrow b\bar{b}$	$e^+e^- \rightarrow \bar{c}c$
$\sqrt{s} = 0.5 \text{ TeV}, \mathcal{L}_{\text{int}} = 100 \text{ fb}^{-1}$				
$\Lambda_H$	4.1; 4.3	3.0; 3.2	3.0; 3.4	3.0; 3.2
$\Lambda_{VV}^{ef}$	76.2; 86.4	89.7; 99.4	76.1; 96.4	84.0; 94.1
$\Lambda_{AA}^{ef}$	47.4; 69.1	80.1; 88.9	76.7; 98.2	76.5; 85.9
$\Lambda_{LL}^{ef}$	37.3; 52.5	53.4; 68.3	63.6; 72.7	54.5; 66.1
$\Lambda_{RR}^{ef}$	36.0; 52.2	51.3; 68.3	42.5; 71.2	46.3; 66.8
$\Lambda_{LR}^{ef}$	59.3; 69.1	48.5; 62.8	51.3; 68.7	37.0; 57.7
$\Lambda_{RL}^{ef}$	$\Lambda_{RL}^{ee} = \Lambda_{LR}^{ee}$	48.7; 63.6	46.8; 60.1	52.2; 60.7
$\sqrt{s} = 1 \text{ TeV}, \mathcal{L}_{\text{int}} = 1000 \text{ fb}^{-1}$				
$\Lambda_H$	8.7; 9.4	6.7; 7.0	6.7; 7.5	6.7; 7.1
$\Lambda_{VV}^{ef}$	173.6; 205.1	218.8; 244.3	185.6; 238.2	206.2; 232.3
$\Lambda_{AA}^{ef}$	109.9; 166.1	194.7; 217.9	186.; 242.7	186.4; 210.8
$\Lambda_{LL}^{ef}$	83.7; 122.8	128.3; 165.5	154.5; 175.8	131.3; 159.6
$\Lambda_{RR}^{ef}$	80.5; 122.1	123.4; 166.1	103.5; 176.9	111.8; 164.1
$\Lambda_{LR}^{ef}$	136.6; 166.8	120.5; 156.6	124.9; 170.2	92.7; 144.6
$\Lambda_{RL}^{ef}$	$\Lambda_{RL}^{ee} = \Lambda_{LR}^{ee}$	120.8; 158.3	120.1; 151.9	129.6; 151.1

**Table 2.** 95% C.L. identification reach on the ADD model parameter  $\Lambda_H$  obtained from  $e^+e^- \rightarrow \bar{f}f$  at  $\sqrt{s} = 0.5$  (1) TeV and  $\mathcal{L}_{\text{int}} = 10^2$  ( $10^3$ )  $\text{fb}^{-1}$  with polarizations  $(|P^-|, |P^+|) = (0,0)$  and  $(0.8, 0.6)$ , respectively.

$\sqrt{s}$	Process			
	$e^+e^- \rightarrow e^+e^-$	$e^+e^- \rightarrow l^+l^-$	$e^+e^- \rightarrow b\bar{b}$	$e^+e^- \rightarrow \bar{c}c$
0.5 TeV	2.2; 2.9	2.3; 2.3	2.6; 2.9	2.3; 2.4
1.0 TeV	5.0; 6.4	4.9; 5.1	5.8; 6.2	5.1; 5.3

According to the number of independent CI couplings active in the different processes, for 95% C.L. we choose  $\chi_{\text{CL}}^2 = 7.82$  for Bhabha scattering and  $\chi_{\text{CL}}^2 = 9.49$  for lepton ( $\mu^+\mu^-, \tau^+\tau^-$ ) and quark ( $\bar{c}c, \bar{b}b$ ) pair production processes.

The simple  $\chi^2$  procedure outlined above is clearly ‘CI model-independent’, and we represent graphically some examples of the numerical results from Bhabha scattering at  $\sqrt{s} = 0.5 \text{ TeV}$  and  $\mathcal{L}_{\text{int}} = 100 \text{ fb}^{-1}$ . For this process, Eq. (17) defines a four-dimensional surface enclosing a volume in the  $(\lambda/\Lambda_H^4, \eta_{LL}/\Lambda_{LL}^2, \eta_{RR}/\Lambda_{RR}^2, \eta_{LR}/\Lambda_{LR}^2)$  parameter space. In Fig. 2, we show the planar surfaces that are obtained by projecting the 95% C.L. four-dimensional surface, hence the corresponding confusion region that results from the condition  $\tilde{\chi}^2 = \chi_{\text{CL}}^2$ , onto the two planes  $(\eta_{LL}/\Lambda_{LL}^2, \lambda/\Lambda_H^4)$  and  $(\eta_{LR}/\Lambda_{LR}^2, \lambda/\Lambda_H^4)$  (we limit our graphical examples to these pairs of parameters).

As suggested by Fig. 2, the contour of the confusion region turns out to identify a maximal value of  $|\lambda/\Lambda_H^4|$  (equivalently, a minimum value of  $\Lambda_H$ ), for which the CI scenario can be excluded at the 95 % C.L. for any value of  $\eta/\Lambda_{\alpha\beta}^2$ . This value,  $\Lambda_H^{\text{ID}}$ , is the identification reach on the ADD scenario, namely, for  $\Lambda_H < \Lambda_H^{\text{ID}}$  the CI scenario can be excluded as explanation of deviations from SM predictions attributed to the ADD interaction, and the latter can therefore be *identified*.

Fig. 2 shows the dramatic rôle of initial beams polarization in obtaining a restricted region of confusion in the parameter space or, in other words, in enhancing the identification sensitivity of the differential angular distributions to  $\Lambda_H^{\text{ID}}$ . Table 2 shows the numerical results for the foreseeable ‘model-independent’ identification reaches on  $\Lambda_H$ , for the two choices of C.M. energy and luminosity.

#### 4 Concluding remarks

We have presented a simple,  $\chi^2$ -based, estimate of the power for discovering and for distinguishing signatures of the spin-2 graviton exchange envisaged by the ADD model, that is foreseeable at the polarized ILC with  $\sqrt{s} = 0.5\text{--}1 \text{ TeV}$ . The basic observables in the analysis are the polarized differential cross sections for fermion-pair production processes. The compositeness-inspired four-fermion contact interaction, from which the ADD

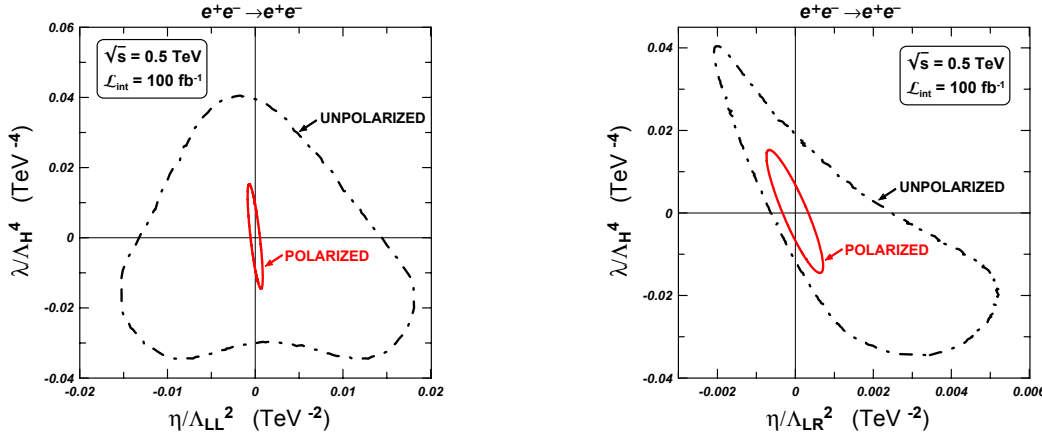


**Figure 2.** Two-dimensional projection of the 95% C.L. confusion region onto the planes  $(\eta_{LL}/\Lambda_{LL}^2, \lambda/\Lambda_H^4)$  (left panel) and  $(\eta_{LR}/\Lambda_{LR}^2, \lambda/\Lambda_H^4)$  (right panel) obtained from Bhabha scattering with unpolarized beams (dot-dashed curve) and with both beams polarized (solid curve).

model should be discriminated in case of observation of corrections to the SM predictions, has been assumed to be of the general form, i.e., a linear combination of the individual contact interaction operators with definite chiralities. The coefficients of such a combination have been taken into account simultaneously as independent, and potentially nonvanishing, constants.

The discovery reaches, as well as the identification reaches, are quite high compared to the current bounds, and depend on energy and luminosity as shown in Table 1 and in Table 2, respectively. In particular, Table 2 shows that, of the four considered  $e^+e^-$  processes, Bhabha scattering and  $\bar{b}b$  pair production definitely have the best identification sensitivity on the mass scale  $\Lambda_H$  characterizing the ADD model for gravity in ‘large’ compactified extra dimensions. The substantial rôle of beams polarization is exemplified by Fig. 2 (where the confusion region between the considered models is dramatically reduced), and by the discovery reaches on the models shown in Table 1.

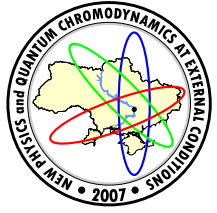
The enhancement of the estimated identification sensitivity on the ADD effective interaction is quite considerable: as exemplified by the entries of Table 2, in the polarized case the identification reach on  $\Lambda_H$  ranges from 2.9 TeV to 6.4 TeV, depending on energy, luminosity and degree of longitudinal polarization. Although unavoidably somewhat depressed by the penalty due to the general multi-parameter expression assumed for the CI scenario (that implies taking large values of the  $\chi^2_{\text{CL}}$ ), these ‘model-independent’ identification values of  $\Lambda_H$  are still much higher than the current limits. In fact, we find that they are only moderately lower (by some 10-20%) than the ‘model-dependent’ ones obtained in Ref. [10] by assuming only one nonzero CI coupling at a time. These nice features reflect in part the small values assumed for the relative uncertainties on electron and positron beams polarization in the previous section, and call for very high precision on polarimetry measurements at the ILC.

*Acknowledgements.* We would like to thank Prof. N. Paver for the enjoyable collaboration on the subject matter covered here.

## References

- [1] J. A. Aguilar-Saavedra *et al.* [ECFA/DESY LC Physics Working Group Collaboration], ‘‘TESLA Technical Design Report Part III: Physics at an  $e^+e^-$  Linear Collider,’’ DESY-01-011 [hep-ph/0106315];  
T. Abe *et al.* [American Linear Collider Working Group Collaboration], ‘‘Linear collider physics resource book for Snowmass 2001. 1: Introduction,’’ in *Proc. of the APS/DPF/DPB Summer Study on the Future of Particle Physics (Snowmass 2001)* ed. N. Graf, SLAC-R-570 [hep-ex/0106055].
- K. Abe *et al.* [ACFA Linear Collider Working Group Collaboration], hep-ph/0109166.
- [2] G. Moortgat-Pick *et al.*, hep-ph/0507011.
- [3] N. Arkani-Hamed, S. Dimopoulos and G. R. Dvali, Phys.Lett. **B429**, 263 (1998) [hep-ph/9803315].
- [4] N. Arkani-Hamed, S. Dimopoulos and G. R. Dvali, Phys.Rev. **D59**, 086004 (1999) [hep-ph/9807344].
- [5] I. Antoniadis, N. Arkani-Hamed, S. Dimopoulos and G. R. Dvali, Phys.Lett. **B436**, 257 (1998) [hep-ph/9804398].
- [6] E. Eichten, K. D. Lane and M. E. Peskin, Phys.Rev.Lett. **50**, 811 (1983).
- [7] R. Rückl, Phys.Lett. **B129**, 363 (1983).
- [8] A. A. Pankov and N. Paver, Phys.Rev. **D72**, 035012 (2005) [hep-ph/0501170].
- [9] A. A. Pankov and N. Paver, Eur.Phys.J. **C29**, 313 (2003) [hep-ph/0209058].

- [10] A. A. Pankov, N. Paver and A. V. Tsytrinov, Phys.Rev. **D73**, 115005 (2006).
- [11] A. A. Pankov, N. Paver and A. V. Tsytrinov, Phys.Rev. **D75**, 095004 (2007).
- [12] G. Pasztor and M. Perelstein, in *Proc. of the APS/DPF/DPB Summer Study on the Future of Particle Physics (Snowmass 2001)* ed. N. Graf [hep-ph/0111471].
- [13] S. Cullen, M. Perelstein and M. E. Peskin, Phys.Rev. **D62**, 055012 (2000) [hep-ph/0001166].
- [14] T. Han, J. D. Lykken and R. J. Zhang, Phys.Rev. **D59**, 105006 (1999) [hep-ph/9811350].
- [15] G. F. Giudice, R. Rattazzi and J. D. Wells, Nucl.Phys. **B544**, 3 (1999) [hep-ph/9811291].
- [16] J. L. Hewett, Phys.Rev.Lett. **82**, 4765 (1999) [hep-ph/9811356].
- [17] For a review see, e.g., K. Cheung, hep-ph/0409028.
- [18] W. M. Yao *et al.* [Particle Data Group], J.Phys. **G33**, 1 (2006).
- [19] K. M. Cheung and G. Landsberg, Phys.Rev. **D65**, 076003 (2002) [hep-ph/0110346].
- [20] T. G. Rizzo and J. D. Wells, Phys.Rev. **D 61**, 016007 (2000) [hep-ph/9906234].
- [21] P. Osland, A. A. Pankov and N. Paver, Phys.Rev. **D68**, 015007 (2003) [hep-ph/0304123].
- [22] M. Consoli, W. Hollik and F. Jegerlehner, CERN-TH-5527-89 *Presented at Workshop on Z Physics at LEP*; G. Altarelli, R. Casalbuoni, D. Dominici, F. Feruglio and R. Gatto, Nucl.Phys. **B342**, 15 (1990).
- [23] For reviews see, e.g., O. Nicrosini and L. Trentadue, in *Radiative Corrections for  $e^+e^-$  Collisions*, ed. J. H. Kühn 25 (Springer, Berlin, 1989), p. 25; in *QED Structure Functions, Ann Arbor, MI, 1989*, ed. G. Bonvicini, AIP Conf. Proc. No. 201 (AIP, New York, 1990), p. 12.
- [24] For a review see, e.g., W. Benakker and F. A Berends: *Proc. of the Workshop on Physics at LEP2*, CERN 96-01, vol. 1, p. 79 and references therein.
- [25] D. Y. Bardin, P. Christova, M. Jack, L. Kalinovskaya, A. Olchevski, S. Riemann and T. Riemann, Comput.Phys.Commun. **133**, 229 (2001) [hep-ph/9908433].



## CONFINEMENT ON THE LATTICE, NUMERICAL RESULTS AND THEORY

M. I. Polikarpov

Institute of Theoretical and Experimental Physics, Moscow, Russia

I give a short review of lattice study of confinement problem. The topics are: formation and breaking of the confining string, monopoles and vortices in Abelian and nonabelian gauge theories.

### 1 Introduction.

The numerical nonperturbative calculations in QCD become possible if we pass from continuous Minkovsky theory to discreet Euclidean lattice formulation. After the change of the time to the imaginary time,  $t \rightarrow i t$ , the partition function of a field theory become analogous to the statistical sum:

$$\mathcal{Z} = \int e^{iS_M[\varphi]} \mathcal{D}\varphi \rightarrow \int e^{-S_E[\varphi]} \mathcal{D}\varphi. \quad (1)$$

The similarity with the statistical physics become exact after the discretization of the space–time; we consider finite Euclidean space,  $0 < x, y, z, t \leq R$ , with periodic boundary conditions, the coordinates have discreet values. Thus we get the four-dimensional lattice with sites at the points  $s = (x_1, x_2, x_3, x_4)$ ,  $1 \leq x_k \leq L = R/a$ , where  $a$  is the lattice spacing and  $L$  is the size of the lattice<sup>1</sup>. After these changes the partition function of the theory is reduced to the finite-dimensional integral,

$$\mathcal{Z} = \int \prod_s d\varphi(s) e^{-S[\varphi]}, \quad (2)$$

which can be evaluated numerically using Monte-Carlo method. The continuum limit of the theory corresponds to the limits  $L \rightarrow \infty$ ,  $a \rightarrow 0$ , while numerical calculations are performed at finite values of  $L$  and  $a$ . The systematic errors corresponding to the finite volume and finite lattice spacing can be estimated using standard methods by varying  $L$  and  $a$ .

In lattice QCD the numerical integration is possible only over the gauge fields, integration over the quark (fermionic) fields can be performed analytically:

$$\int \mathcal{D}\psi \mathcal{D}\bar{\psi} e^{\bar{\psi} \hat{M} \psi} = \det \hat{M}. \quad (3)$$

Since matrix  $\hat{M}$  is the function of the gauge field,  $\hat{M} = \hat{M}(A_\mu)$ , after such integration the gauge action become effectively nonlocal:  $S(A_\mu) = S_{GF}(A_\mu) + \log \det \hat{M}(A_\mu)$ , here  $S_{GF}(A_\mu)$  is the lattice analogue of the gauge action  $\int \text{Tr} F_{\mu\nu}^2 d^4x$ .

Due to nonlocality of the gauge field action the calculations in lattice QCD with dynamical fermions are very time consuming and realistic spectrum of low lying hadrons can be obtained using only large-scale calculations on supercomputers. Only recently there appear calculations in QCD with two light and one massive (strange) quark. The hadron spectrum calculations in such lattice QCD, called (2+1)QCD, can be found in [1].

Calculations in lattice QCD with two light dynamical quarks are much more popular, in Section 2 we discuss some results of the DIK (DESY-ITEP-Kanazawa) collaboration, and when we refer to "full QCD" we mean  $N_f = 2$  lattice QCD with nonperturbatively improved Wilson fermions (review of the results of the DIK collaboration is given in [2]). SU(2) and SU(3) lattice gluodynamics is much simpler to study in computer simulations than QCD with dynamical quarks, but, as we show in Section 2, from these simple models we can get useful information about confining strings. In Section 3 we present two examples of confinement mechanisms in Abelian gauge models. In Section 4 we discuss monopoles and vortices in lattice gluodynamics as gauge field fluctuations responsible for confinement of color.

<sup>1</sup>For calculations at the finite temperature we consider asymmetric lattices  $L \times L \times L \times N_t$  ( $N_t < L$ ), and the temperature of the system is defined as  $T = (N_t a)^{-1}$ .

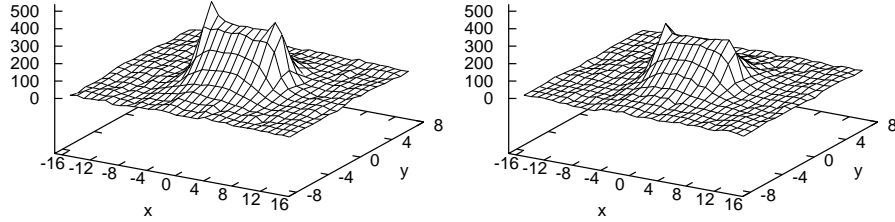


**Figure 1.** The action density  $\rho_A(s)r_0^4$  of the Abelian flux tube in full (left) and in quenched (right) QCD.

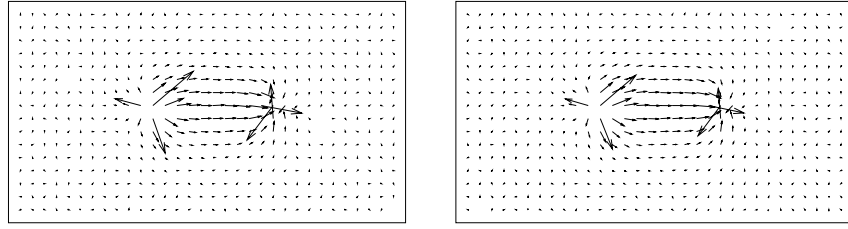


**Figure 2.** Distribution of the color electric field in full (left figure) and quenched (right figure) QCD.

## 2 Visualization of confining strings.

We can not strictly prove the confinement of color in nonabelian gauge theories, but we can clearly see the formation of gluonic cylinder-type object between quark and antiquark. This object called confining string was first time observed in SU(2) gluodynamics in ref. [3]. The material of this Section is based on papers of the DIK collaboration [2, 4, 5]. The difference between confining string in gluodynamics (quenched QCD) and in QCD with dynamical quarks is not very large as it is seen from Fig. 1, the definition of Abelian action density is given in [4],  $r_0$  is the parameter which defines the scale,  $r_0 \approx 0.5 \text{ fm}$ .

In Fig. 2 we show the color electric field in Abelian projection [4]. One can see only small differences between distributions obtained in full and in quenched QCD. Fig. 2 shows that the electric field is purely longitudinal in a region between the sources as we expect for the flux tube.

At zero temperature it is hard to observe the confining string breaking due to large statistical noise. At finite temperature below the phase transition we can observe the formation of the confining string in the static meson, and also the string breaking. The explanation is simple: the heavy quark potential  $V(r, T)$  is determined from the Polyakov loop correlator:

$$V(r, T) = -\frac{1}{L_t} \ln \langle L(\vec{s}) L^\dagger(\vec{s}') \rangle . \quad (4)$$

When  $r \rightarrow \infty$ ,

$$\langle L(\vec{s}) L^\dagger(\vec{s}') \rangle \longrightarrow |\langle L \rangle|^2 , \quad (5)$$

and  $|\langle L \rangle|^2 \neq 0$  even below  $T_c$ , since global  $Z_3$  is broken by fermions. From (4) and (5) it follows that  $V(r, T) \rightarrow \text{const.}$  when  $r \rightarrow \infty$ . This flattening of the potential at  $T < T_c$  is due to the creation of a quark-antiquark pair from the vacuum which screen the test sources. The flattening (which corresponds to string breaking) is clearly seen in Fig. 3 where the monopole part of the potential is shown. Below we demonstrate how the mesonic flux tube breaks when the  $Q - \bar{Q}$  distance  $R$  is increasing at a fixed temperature  $T$ . We measure profiles of the action density, the color-electric field and the monopole current at  $T/T_c = 0.94$  for various values of  $R/r_0$ . The static quark-antiquark pair is created by Abelian, monopole, and photon Polyakov loops. Fig. 4 shows the profiles of the action density. We show both the two-dimensional contour plot and the three-dimensional plot for various distances. In these plots the horizontal axis is directed along the line connecting the static sources. First two rows of this figure indicate that the flux tube persists for distances  $R/r_0 = 0.98, 1.71$  while for  $R/r_0 = 2.42$  it seems to disappear, leaving only lumps of the action density around the sources. The difference between left and central columns is that in the monopole part the data have much lower noise and two-peaks at locations of the quark and antiquark are less pronounced. In the photon part only two lumps around sources can be seen at all distances.

It is important to learn about the forces and the distribution of color electric flux in the  $3Q$  system, a particularly interesting question is whether a three-body force exists and the confining flux tube is of  $Y$ -shape, or whether the long-range potential is simply the sum of two-body potentials, resulting in a flux tube of  $\Delta$ -shape. Several lattice studies give evidence for a  $\Delta$ -type long-range potential [6, 7], while others show the existence of

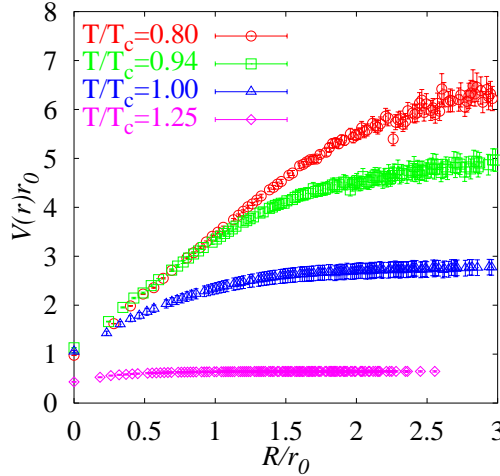


**Figure 3.** Static potential from monopole Polyakov loop correlators for  $\beta = 5.2$ .

a  $Y$ -type potential [8, 9]. The latter result is also being supported by the field correlators method [18]. The difference between a  $\Delta$  and  $Y$ -shape potentials is rather small and it is difficult to detect it numerically. The recent results [5] obtained by DIK collaboration show that the baryon flux tube in quenched lattice QCD and in full QCD has  $Y$ -shape. The example of the density of baryon flux in the full QCD is shown in Fig. 5. The pick in the center of three quark system support the  $Y$ -shape of the flux. To obtain this figure we used the baryon creation operator (the analogue of the Wilson loop which create the meson state):

$$W_{3Q} = \frac{1}{3!} \varepsilon_{ijk} \varepsilon_{i'j'k'} U^{ii'}(\mathcal{C}_1) U^{jj'}(\mathcal{C}_2) U^{kk'}(\mathcal{C}_3), \quad (6)$$

where  $U(\mathcal{C}) = \prod_{s, \mu \in \mathcal{C}} U_\mu(s)$  is the ordered product of link matrices, along the path  $\mathcal{C}$ , as shown in Fig. 6. As in case of the meson, if we separate the source quarks by sufficient distance the effect of baryon string breaking appears. It can be easily seen at finite temperature below the deconfinement temperature, see Fig. 7. In this figure we use the natural measure of the distance between three quarks for the baryon system,  $R_Y$ , which is the minimal  $Y$ -type distance between the three quarks, *i.e.* the sum of the distances from the three quarks to the Fermat point,

$$R_Y^2 = \frac{1}{2} \sum_{i>j} r_{ij}^2 + 2\sqrt{3}S_\Delta, \quad (7)$$

$r_{ij} = |\vec{s}_i - \vec{s}_j|$ ,  $S_\Delta$  is the area of the corresponding triangle. Eq.(7) defines  $R_Y$  when all angles in the three quarks triangle are less than  $2\pi/3$ . If one of the angles is equal or larger than  $2\pi/3$ , then  $R_Y = \sum_{i>j} r_{ij} - \max r_{ij}$ .

### 3 Confinement in Abelian theories

The theory of the confining QCD strings discussed in the previous Section is not very well developed. Really there are only models of confinement in nonabelian theories. Most of these models are based on two confining mechanisms well known in Abelian theories. These are magnetic monopole and magnetic vortex confining scenarios.

Magnetic monopole confining mechanism is very well known in compact electrodynamics [11]. It can be shown that the partition function of compact QED can be rewritten as the partition function of the dual Abelian Higgs (see e.g. [13]) model in the limit where the bare masses of the gauge and the Higgs bosons are infinite. The Higgs boson field corresponds to the topological defects of compact QED which are monopoles. Since monopoles are condensed in the strong coupling phase of 4D compact QED, confinement is due to the dual Meissner effect, monopole playing the role of the Cooper pairs and electrical charges are connected the by dual Abrikosov string, which lead to the linearly rising potential.

Confinement by random vortices is well known in  $Z(2)$  gauge theory. The topological objects in this theory are closed lines in 3D and closed surfaces in 4D. When surface spanned on the Wilson loop is intersected by vortex, the sign of Wilson loop is changed. The expectation value of the plaquette (the elementary Wilson loop) is  $(1 - p) \cdot (+1) - p \cdot (-1) = 1 - 2p$ , where  $p$  is the probability that some plaquette intersects with vortex. If vortices are random (not correlated at the small distances) then the expectation value of the Wilson loop is equal to the product of the expectation values of the plaquettes:  $\langle W \rangle = (1 - 2p)^S$ , where  $S$  is the number of plaquettes on the surface spanned on the Wilson loop, thus we get the area law  $\langle W \rangle = e^{-\sigma S}$ ,  $\sigma = -\ln(1 - 2p)$ . In this simple derivation we do not specify the shape of the surface spanned on the loop, and the area  $S$  is

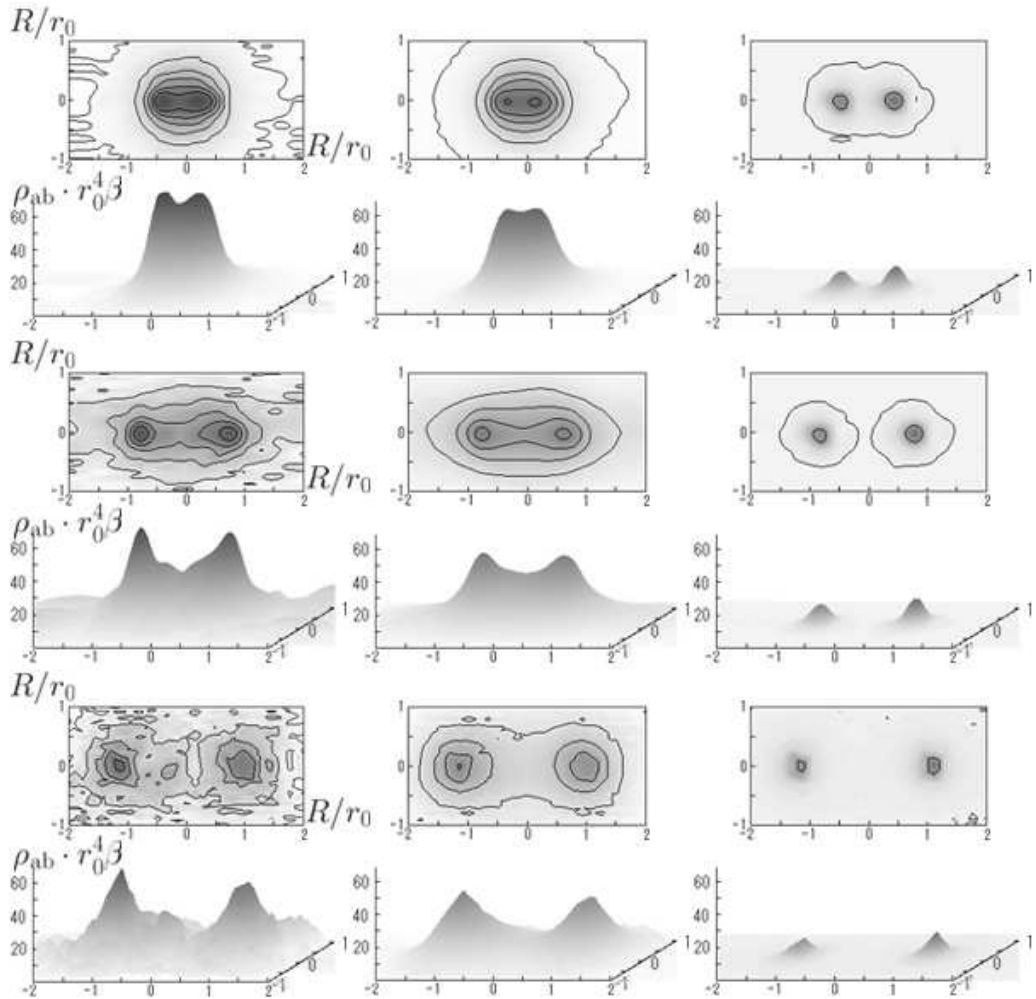


**Figure 4.** The profile of the action density of the mesonic system at  $T/T_c = 0.94$ . The sources are made of Abelian (left), monopole (center) and photon (right) Polyakov loops. The  $Q\bar{Q}$  distances are  $R/r_0 = 0.98$  (top), 1.71 (middle), 2.42 (bottom).

not definite. To resolve this uncertainty we have to note that the number of intersections of the vortex with surface spanned on the loop is odd or even independently on the shape of the surface. This follows from the closeness of the vortex. The next (less nontrivial) step is to show that in the leading order we have to consider the minimal surface spanned on the loop, that can be proven in the strong coupling expansion of the original  $Z(2)$  gauge theory. After these remarks vortex confinement mechanism become very close to confinement in the leading order of the strong coupling expansion in lattice gauge theories. Confinement in this case can be found as for Abelian as for nonabelian gauge groups, and the reason is trivial, it is due to completely uncorrelated gauge field distribution on the plaquettes.

These are basic known examples of confinement in gauge theories, as we see in the next Section in lattice gluodynamics we have the synthesis of monopole and vortex confinement.

#### 4 Confinement in nonabelian theories

Now we discuss a possible mechanism of the formation of the flux tube in lattice gluodynamics. Below we discuss confinement in  $SU(2)$  lattice gluodynamics, since main results were obtained in this theory. The first model of confinement which was carefully studied in lattice gauge theories was the monopole model [12], for review see [13]. This model explains the formation of the flux tube as the dual Meissner effect, the monopoles correspond to the Cooper pairs and flux tube is the dual analogue of the Abrikosov string. There are many numerical facts which confirm this confinement model. The next model of confinement well studied in lattice gauge theories is the center vortex confinement mechanism [15], for review see [1]. Recently it occurs that at least for  $SU(2)$  lattice gluodynamics these two models are interrelated: monopole trajectories (which are closed lines in 4D) belong to vortices (closed surfaces in 4D) [16]. Moreover there exist procedures of removing of monopoles [17] or vortices [18] from the vacuum. It occurs [19] that removing monopoles we remove vortices

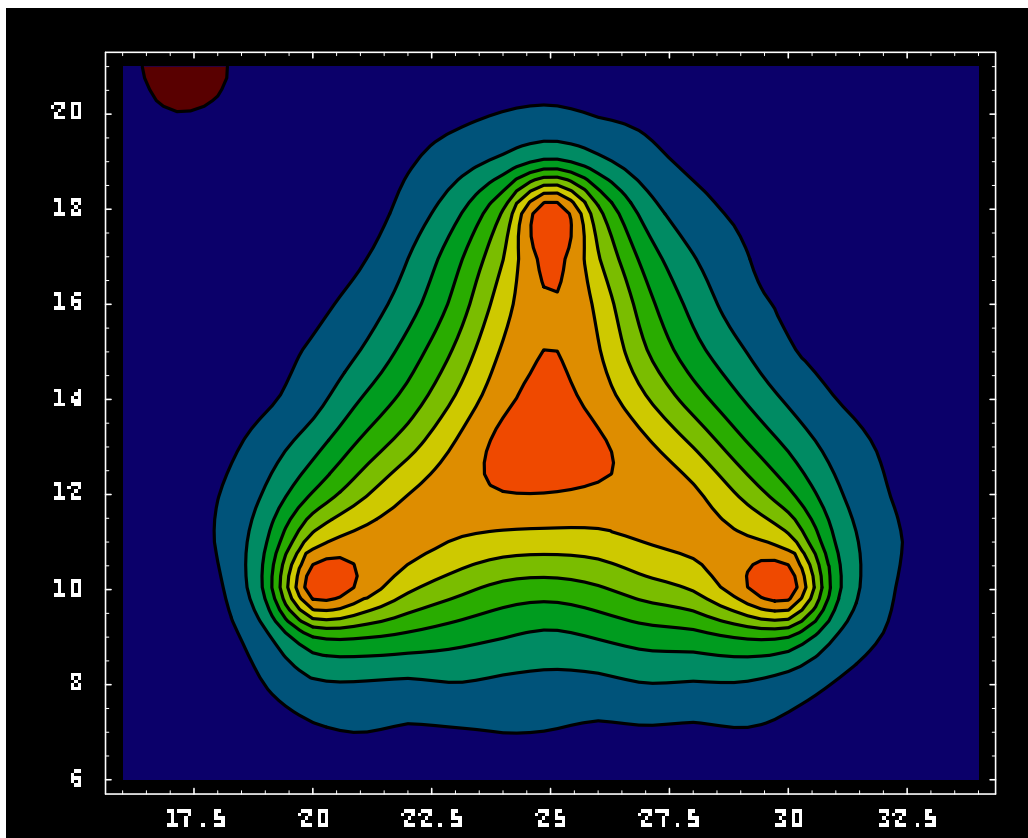
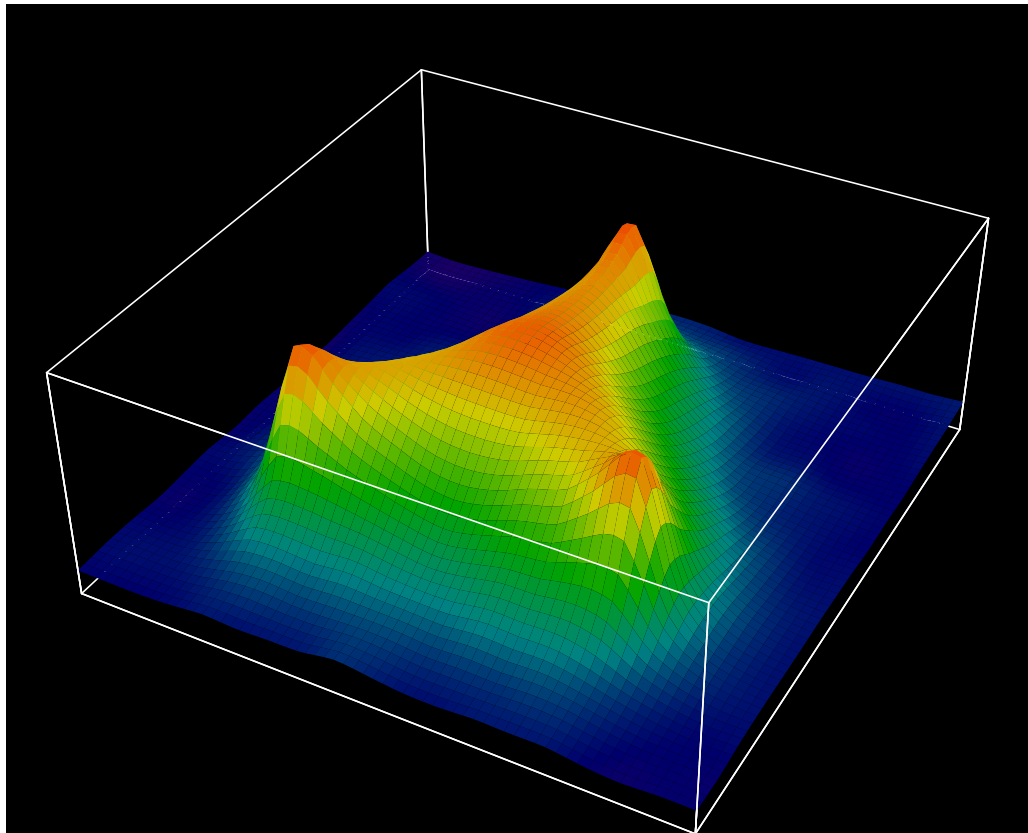


**Figure 5.** Abelian action density in  $3Q$  system in full QCD.

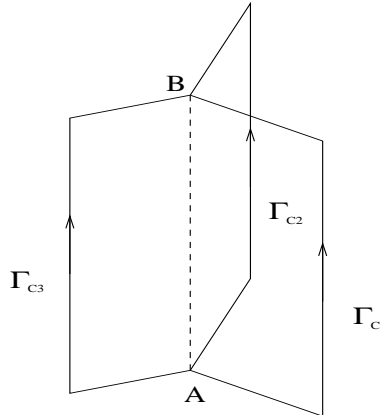


**Figure 6.** Three quark Wilson loop.

and removing vortices we remove monopoles. Moreover removing monopoles (or vortices) we loose confinement and chiral symmetry breaking<sup>2</sup> [18]. This is the most serious numerical indication that monopoles and vortices are responsible for confinement and chiral symmetry breaking.

The main criticism of the monopole and vortex confinement mechanism is the uncertainty in the gauge projection. To extract monopole currents from the gauge field configuration we have to choose  $SU(2) \rightarrow U(1)$  gauge projection and only in Maximal Abelian gauge we have clear indication that monopoles are responsible for infrared properties of the vacuum<sup>3</sup>. For center vortices, we have clear results only for direct and indirect central projections  $SU(2) \rightarrow Z(2)$ . Thus the results seem to be projection dependent. But now we have many facts showing that Maximal Abelian and Maximal center projections detect gauge invariant objects from the vacuum. Monopoles and vortices behave in these projections as “physical objects”. By “physical object” we mean some object which have scaling properties, that is the physical characteristics of the object depend on the lattice spacing<sup>4</sup> as predicted by renormalization group. In this case in the continuum limit such object is characterized by physical dimensional quantities. For example the length of the percolating monopole cluster is in physical units in the given four-dimensional volume [21]:

$$L_{mon} \approx 31 \frac{V_4}{fm^3}, \quad (8)$$

here  $V_4$  is the total lattice volume in  $fm$ . Similarly the area of the of central vortices is in physical units in the given lattice volume [23]:

$$A_{vort} \approx 24 \frac{V_4}{fm^2}. \quad (9)$$

The entropy of the extended objects (monopole trajectories and world sheets of vortices) is infinite in the continuum limit. To survive in the continuum limit the *nonabelian* action of such objects should also be infinite, since the quantity which should be finite is  $\{action - \ln(entropy)\}$ . At finite lattice spacing the action of percolating monopole cluster of length  $L_{perc}$  is [24]:

$$S_{mon} \approx 1.9 \frac{L_{perc}}{a}, \quad (10)$$

and the action of center vortex of the area  $A_{vort}$  is<sup>5</sup> [23]:

$$S_{vort} \approx 0.53 \frac{A_{vort}}{a^2}. \quad (11)$$

Thus it seems that the center gauges detect physical structures which we call Abelian monopoles and center vortices.

<sup>2</sup>We presented now a simplified picture, to be precise we have to consider percolating and not percolating clusters of monopoles and vortices. Only percolating clusters are responsible for the infrared properties of the QCD vacuum, also there exists some difference in the results of the removing of vortices for different gauge projections, for details see ref. [19].

<sup>3</sup>Recently there appears the claim [20] that monopoles are responsible for confinement without gauge fixing (in the random gauge).

<sup>4</sup>The lattice spacing  $a$  playing the role of ultraviolet cutoff:  $\Lambda_{UV} = 1/a$ .

<sup>5</sup> $S_{mon}$  and  $S_{vort}$  are excesses of the actions on the monopole trajectories and on world sheets of vortices over the average vacuum action  $S_{vac} = \langle \beta(1 - \frac{1}{2} \text{Tr } U_P) \rangle$ , which is also ultraviolet divergent,  $S_{vac} \propto \frac{1}{a^4}$

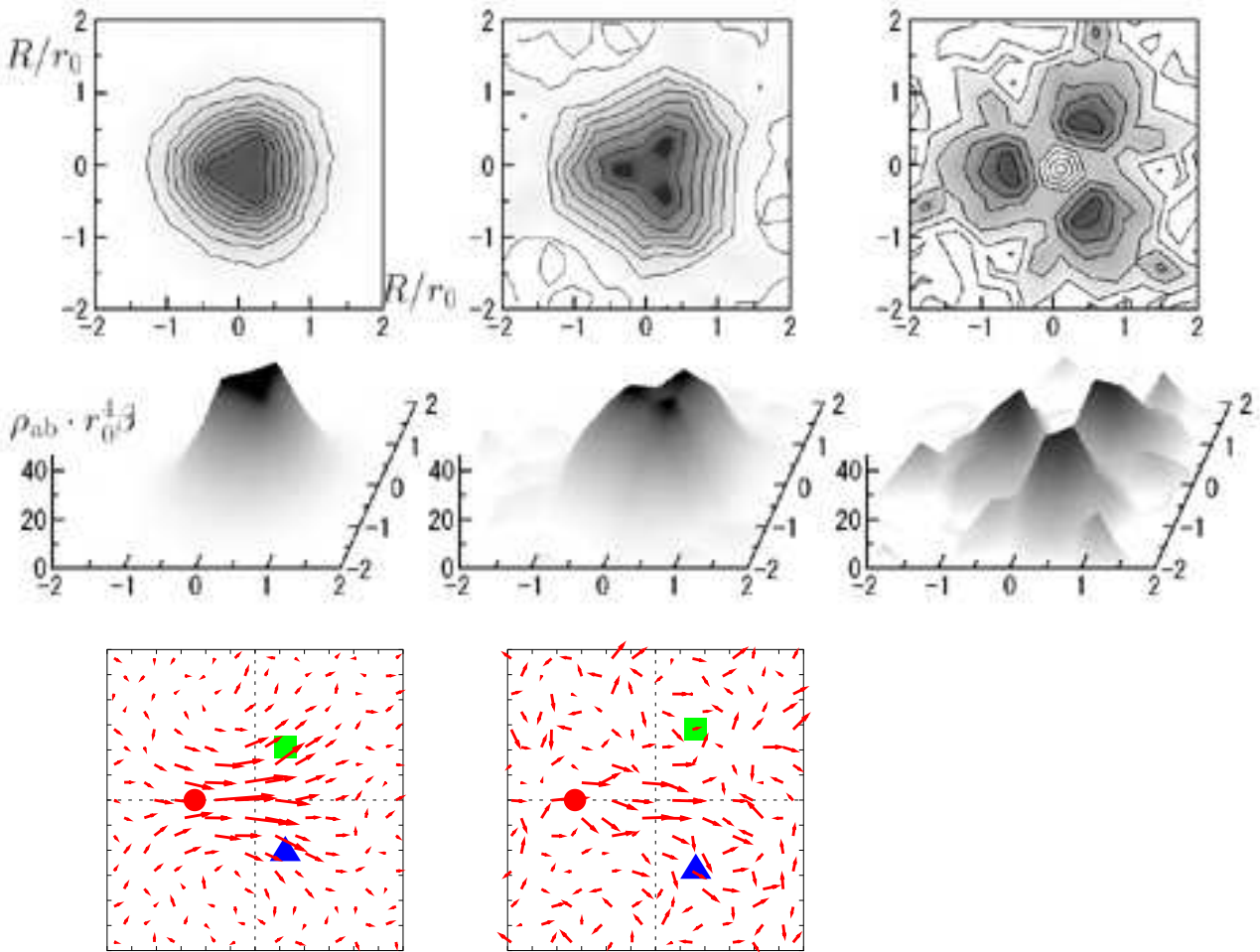


**Figure 7.** Abelian action density (up) and electric field (down) for the baryon system. Static quarks are created by monopole Polyakov line. Interquark distances are  $R_Y/r_0 = 2.08$  (left),  $2.77$  (center) and  $3.46$  (right), the temperature  $T = 0.82T_c$  ( $\kappa = 0.1330$ ). Electric field for  $R_Y/r_0 = 3.46$  is not shown, since it is completely random.

In addition to above mentioned features there are two important properties of center vortices. The first one is called “holography” [25]. If we minimize the number of negative links<sup>6</sup> by  $Z(2)$  gauge transformations then the gauge is fixed completely and vortices are boundaries of some 3-dimensional volumes. It occurs that these volumes scale in physical units:

$$V_3 \approx 2.1 \frac{V_4}{fm}. \quad (12)$$

If we calculate the expectation value of the Wilson loop then corresponding loop  $\mathcal{C}$  intersects  $V_3$  volumes by points in 4D space. The distance between these points of intersections is approximately  $2\text{ fm}$ . If we kill confinement removing negative links we change gauge fields in these points of intersections, thus all information about confinement is encoded in three-dimensional volumes  $V_3$ . That compression of information about four-dimensional confinement into three-dimensional volumes is called holography.

The next property is the existence of long range correlations along the vortex. First it was found that the direction of the monopole current lying on the vortex have a very long range correlation [22], the probability to have the same direction of the current at the distance  $l$  (measured along the monopole trajectory) fall off exponentially,  $\propto \exp\{-\mu la\}$ ,  $\mu \approx 260\text{ Mev}$ . This number should be compared with the lightest glueball mass for  $SU(2)$  gluodynamics,  $M_{0++} = 1.65 \pm 0.05\text{ Gev}$  [26]). The complimentary measurement was done in ref. [27] where the correlation of the action densities was measured for the points which are separated by only one lattice spacing in four-dimensional space but no less than 6 spacings along the vortex ( $d_4 < 2$ ,  $d_2 \geq 6$ ). For comparison the correlation between neighboring vortex plaquettes ( $d_4 < 2$ ,  $d_2 < 2$ ) was also measured. The measured

<sup>6</sup>By negative link we mean link with negative trace:  $\text{Tr } U_l < 0$ .

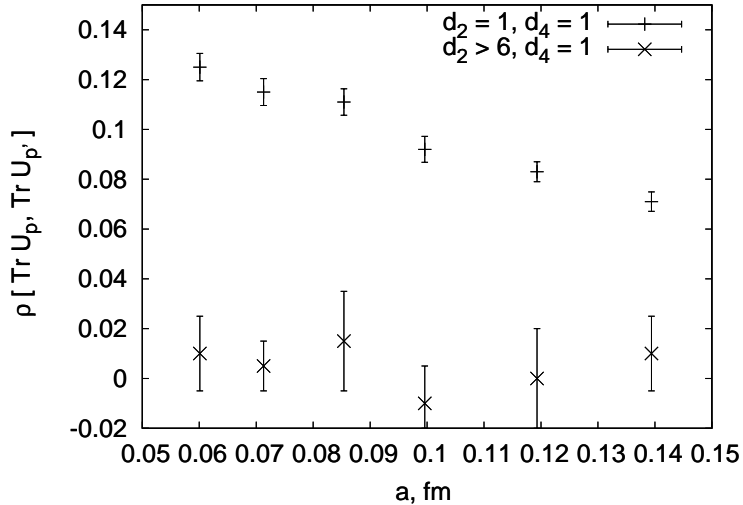


**Figure 8.** Correlation between neighboring plaquettes with  $d_4 = 1$ ,  $d_2 \geq 6$  and  $d_4 = 1$ ,  $d_2 < 2$

quantity was:

$$\rho[\text{Tr } U_p, \text{Tr } U_{p'}] = \frac{\langle \text{Tr } U_p \text{ Tr } U_{p'} \rangle - \langle \text{Tr } U_p \rangle^2}{\langle (\text{Tr } U_p)^2 \rangle - \langle \text{Tr } U_p \rangle^2} \quad (13)$$

which is plotted on Fig. 8. It can be seen that the correlation in four-dimensional space is notably smaller than along the surface of the vortex, this fact can be indication that some two-dimensional fields (monopoles) propagate along the vortex. The detailed discussion of such picture is given in ref. [27].

## 5 Conclusions

Calculations in lattice QCD and in lattice gluodynamics show that objects like monopoles and vortices are physical objects which are important for description of nonperturbative effects. For the description of the chiral symmetry breaking and topological properties of the vacuum some low-dimensional multifractal structures are important [28]. Thus we have serious indications that extended low-dimensional objects play important role in the dynamics of nonperturbative field theory (see detailed discussion of these questions in reviews [29]).

*Acknowledgements.* I am very grateful to my collaborators V.G. Bornyakov, P.Yu. Boyko, M.N. Chernodub, A.N. Gradoboev, H. Ichie, E.-M. Ilgenfritz, S. Kitahara, Y. Koma, A.V. Kovalenko, Y.Y. Mori, S.M. Morozov, M. Müller-Preussker, Y. Nakamura, D. Pleiter, G. Schierholz, D. Sigaev, A.A. Slavnov, T. Streuer, H. Stuben, T. Suzuki, P.V. Uvarov, A.I. Veselov and V.I. Zakharov for numerous fruitful discussions. The work was partially supported by grants RFBR-DFG 06-02-04010 and DFG-RFBR 436 RUS 113/739/2, RFBR 06-02-16309, 05-02-16306, 05-02-17642 and 04-02-16079, and by the EU Integrated Infrastructure Initiative Hadron Physics (I3HP) under contract RII3-CT-2004-506078.

## References

- [1] S. Aoki, AIP Conf.Proc. **892**, 1-7 (2007); \*Ponta Delgada 2006, Quark confinement and the hadron spectrum\* 1-7, hep-lat/0611021;  
NPLQCD Collaboration (Silas R. Beane *et al.*), hep-lat/0612026.
- [2] Y. Mori *et al.*, Nucl.Phys. **A 721**, 930 (2003);  
V. G. Bornyakov, M. I. Polikarpov, M. N. Chernodub, T. Suzuki and G. Schierholz, Phys.Usp. **47**, 17 (2004) [Usp.Fiz.Nauk **47**, 19 (2004)].
- [3] G.S. Bali, Ch. Schlichter and K. Schilling, Phys.Rev. **D51**, 5165 (1995).
- [4] V. Bornyakov, H. Ichie, S. Kitahara, Y. Koma, Y. Mori, Y. Nakamura, M. Polikarpov, G. Schierholz, T. Streuer, H. Stuben, T. Suzuki, Nucl.Phys.Proc.Suppl. **106**, 634 (2002);  
V. Bornyakov, Y. Nakamura, M. Chernodub, Y. Koma, Y. Mori, M. Polikarpov, G. Schierholz, A. Slavnov, H. Stuben, T. Suzuki, P. Uvarov and A. Veselov, preprint DESY-02-135, Sep 2002, Nucl.Phys.Proc.Suppl. **119**, 703 (2003); \*Cambridge 2002, Lattice\* 703-708, hep-lat/0209157;  
V. Bornyakov *et al.*, DIK-collaboration, preprint ITEP-LAT-2002-23, KANAZAWA-02-32, Dec 2002, Nucl.Phys.Proc.Suppl. **119**, 712 (2003); \*Cambridge 2002, Lattice\* 712-714, hep-lat/0212023;  
V. Bornyakov, M. Chernodub, Y. Koma, Y. Mori, Y. Nakamura, M. Polikarpov, G. Schierholz, D. Sigaev,

A. Slavnov, H. Stuben, T. Suzuki, P. Uvarov and A. Veselov, preprint ITEP-LAT-2002-31, KANAZAWA-02-40, Jan 2003, \*Gargnano 2002, Quark confinement and the hadron spectrum\* 294-296; hep-lat/0301002; V. G. Bornyakov *et al.* [DIK Collaboration], Phys. Rev. **D 70**, 074511 (2004); V. G. Bornyakov *et al.*, Prog.Theor.Phys. **112**, 307 (2004); V. G. Bornyakov, M. I. Polikarpov, M. N. Chernodub, T. Suzuki and Y. Nakamura *et al.*, AIP Conf.Proc.756, 242-244 (2005), Nucl.Phys.Proc.Suppl. **140**, 535 (2005), also in \*Villasimius 2004, Quark confinement and the hadron spectrum\* 242-244, also in \*Batavia 2004, Lattice field theory\* 535-537; hep-lat/0409153.

[5] H. Ichie, V. Bornyakov, T. Streuer and G. Schierholz Nucl.Phys.Proc.Suppl. **B119**, 751 (2003) [hep-lat/0212024]; H. Ichie, V. Bornyakov, T. Streuer and G. Schierholz, to appear in Nucl.Phys. **A721**, 899 (2003); V. G. Bornyakov *et al.* [DIK Collaboration], Phys.Rev. **D 70**, 054506 (2004).

[6] G.S. Bali, Phys.Rep. **343**, 1 (2001).

[7] C. Alexandrou, Ph. de Forcrand and A. Tsapalis, Phys.Rev. **D65**, 054503 (2002).

[8] T.T. Takahashi, H. Suganuma, Y. Nemoto and H. Matsufuru, Phys.Rev. **D65**, 114509 (2002); T.T. Takahashi, H. Matsufuru, Y. Nemoto and H. Suganuma, Phys.Rev.Lett. **86**, 18 (2001).

[9] C. Alexandrou, Ph. de Forcrand and O. Jahn, Nucl.Phys.Proc.Suppl. **119**, 667 (2003).

[10] D.S. Kuzmenko and Yu.A. Simonov, Phys.Lett. **B494**, 81 (2000); D.S. Kuzmenko and Yu.A. Simonov, Phys.Atom.Nucl. **67**, 543 (2004) [Yad.Fiz. **67**, 561 (2004)].

[11] A.M. Polyakov, Phys.Lett. **59B**, 82 (1975).

[12] H. Shiba and T. Suzuki, Phys.Lett. **B 333**, 461 (1994).

[13] M. N. Chernodub and M. I. Polikarpov, “Abelian projections and monopoles”, in *Confinement, duality, and nonperturbative aspects of QCD*, Ed. by P. van Baal, Plenum Press, p. 387.

[14] J. Greensite, Prog.Part.Nucl.Phys. **51**, 1 (2003).

[15] L. Del Debbio, M. Faber, J. Greensite, and S. Olejnik, Phys.Rev. **D55**, 2298 (1997).

[16] J. Ambjorn, J. Giedt, and J. Greensite, JHEP **0002**, 033 (2000);  
A. V. Kovalenko, M. I. Polikarpov, S. N. Syritsyn, and V. I. Zakharov, Nucl.Phys.Proc.Suppl. **129**, 665 (2004);  
A. V. Kovalenko, M. I. Polikarpov, S. N. Syritsyn, and V. I. Zakharov, Phys.Rev. **D71**, 054511 (2005).

[17] O. Miyamura, Phys.Lett. **B353**, 91 (1995);  
S. Sasaki and O. Miyamura, Nucl.Phys.Proc.Suppl. **63**, 507 (1998), Phys.Lett. **B443**, 331 (1998), Phys.Rev. **D59**, 094507 (1999).

[18] P. de Forcrand and M. D’Elia, Phys.Rev.Lett. **82**, 4582 (1999).

[19] P.Yu. Boyko, V.G. Bornyakov, E.-M. Ilgenfritz, A.V. Kovalenko, B.V. Martemyanov, M. Muller-Preussker, M.I. Polikarpov, A.I. Veselov, Nucl.Phys **B756**, 71 (2006).

[20] T. Suzuki, K. Ishiguro, Y. Koma, T. Sekido, arXiv:0706.4366.

[21] V. Bornyakov and M. Müller-Preussker, Nucl.Phys.Proc.Suppl. **106**, 646 (2002) [hep-lat/0110209].

[22] P.Yu. Boyko, M.I. Polikarpov, V.I. Zakharov, Nucl.Phys. **B672**, 222 (2003).

[23] A.V. Kovalenko, M.I. Polikarpov, S.N. Syritsyn, V.I. Zakharov, Phys.Rev. **D71**, 054511 (2005).

[24] V.G. Bornyakov, M.N. Chernodub, F.V. Gubarev, M.I. Polikarpov, T. Suzuki, A.I. Veselov, V. I. Zakharov, Phys.Lett. **B537**, 291 (2002).

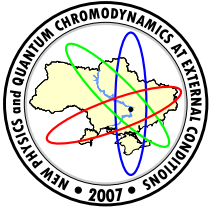
[25] A.V. Kovalenko, M.I. Polikarpov, S.N. Syritsyn, V.I. Zakharov, Phys.Lett. **B613**, 52 (2005).

[26] M. J. Teper, hep-th/9812187.

[27] P.V. Buividovich, M.I. Polikarpov, arXiv:0705.3745; accepted for publication in Nucl.Phys.B.

[28] I. Horvath, S.J. Dong, T. Drape, N. Isgur , F.X. Lee, K.F. Liu, J. McCune, H.B. Thacker , J.B. Zhang, Phys.Rev. **D66**, 034501 (2002) [hep-lat/0201008]; I. Horvath *et al.*, Phys.Rev. **D68**, 114505 (2003); I. Horvath, S. J. Dong, T. Draper, F. X. Lee, K. F. Liu, H. B. Thacker and J. B. Zhang, Phys.Rev. **D67**, 011501 (2003);  
C. Aubin *et al.* [MILC Collaboration], hep-lat/0410024;  
F.V. Gubarev, S.M. Morozov, M.I. Polikarpov and V.I. Zakharov, JETP Lett. **82**, 343 (2005) [Pisma Zh.Eksp.Teor.Fiz. **82**, 381 (2005)];  
E.-M. Ilgenfritz, K. Koller, Y. Koma, G. Schierholz, T. Streuer, V. Weinberg, arXiv:0705.0018.

[29] V.I. Zakharov, AIP Conf.Proc **756**, 182 (2005) [hep-ph/0501011];  
V.I. Zakharov, hep-ph/0612342.



## INTERFEROMETRY ANALYSIS AND INITIAL CONDITIONS IN A+A COLLISIONS

Yu.M. Sinyukov, Iu. Karpenko, A.V. Nazarenko

Bogolyubov Institute for Theoretical Physics, Kiev, Ukraine

The behavior of the interferometry radii in central A+A collisions at different energies and also for different nuclei or impact parameters indicates the initial transverse flows at very early stage of the matter evolution. Development of such flows at pre-thermal partonic stage is considered.

### 1 Introduction

The first results of the femtoscopy, or HBT analysis at RHIC experiments [1] (as it was first announced by the STAR Collaboration) have revealed unexpected results - the so-called RHIC HBT puzzle [2]. The puzzle implies, firstly, that the absolute values of the interferometry radii/volume in central Au+Au collisions do not change essentially at RHIC as compared to the SPS energies for Pb+Pb collisions despite much higher multiplicities. It was in contrast with, expected at that time, possibility of the proportionality law between the interferometry volumes and multiplicities. At the same time there is an approximate proportionality between interferometry volume and different initial volumes which can be associated, e.g., with number of participants (nucleons of nuclei) in the collision process and, thus, with the multiplicity. Secondly, the ratio of outward to sideward transverse radii is opposite to what was expected in standard hydrodynamic and hadronic cascade pictures. The ratio measured by STAR and PHENIX collaborations at RHIC BNL is close to unity in a wide momentum region. At the first sight these observations are in a contradiction with an existence of quark-gluon plasma and mixed phase as it implies a long time pion radiation which usually results in the large ratio of outward to sideward transversal radii. As a result, now the phenomenological parameterizations, like the blast wave model just ignore the emission from the surface of expanding system despite the fact that it should last at least about the extracted life-time of the fireball: 10-12 fm/c.

These notes represent the possible explanation of the peculiarities of the observed behaviors of the interferometry radii based on an analysis of the temporal evolution of observables [3, 4]. As a result, one can conclude that initial flows in pre-thermal partonic matter, which precede hydrodynamical expansion, should develop in the system. We discuss the possible scenario of the pre-thermal evolution of partonic matter and estimate the collective velocities at this early stage of the processes of ultrarelativistic A+A collisions.

### 2 Analysis and treatment of experimental data

As it was shown in Ref.[3] the phase-space density of thermal pions *totally averaged* over freeze-out hypersurface  $\sigma$  and over momenta except the longitudinal one (rapidity is fixed, e.g.,  $y = 0$ ),  $\langle f \rangle$ , is an approximate integral of motion.

The conservation of the APSD allows one to study the hadronization stage of the matter evolution based on the possibility to define the APSD of thermal pions at the final stage of the matter evolution through the integral (over momentum) representation of this value through the observed spectra and interferometry volumes [3]. The results for the APSD at mid-rapidity for pions at the AGS, SPS, RHIC demonstrate a plateau at low SPS energies that indicates, apparently, a transformation of an excess of initial energy to non-hadronic forms of matter, a saturation of the APSD at RHIC energies can be treated as an existence of the limiting Hagedorn temperature of hadronic matter, or maximal temperature of deconfinement [4].

Let us use these results for an analysis of the behavior of the pion interferometry volumes  $V_{int}$ . If one consider them at small transverse momenta, then they can be represented approximately through the APSD as the following:

$$V_{int} \simeq C \frac{dN/dy}{\langle f \rangle T_{eff}^3} \quad (1)$$

It is easy to see then that at any *fixed* energy  $\sqrt{s_{NN}}$  the  $V_{int}$  is nearly constant in time since the values  $dN/dy$ , APSD  $\langle f \rangle$  and effective temperature  $T_{eff}$  in r.h.s. of Eq. (1) are approximately conserved for the

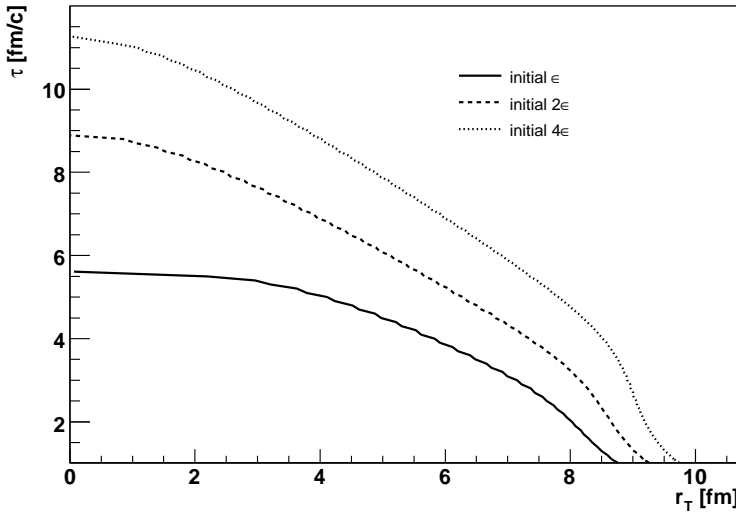


**Figure 1.** The typical freeze-out hypersurfaces with the *fixed* f.o. energy density presented in  $\tau - r$  plane for Bjorken-like azimuthally symmetric hydrodynamic expansion with equation of state  $P = \epsilon/3$  and zero initial transverse flow. The curves correspond to the different initial energy densities  $\epsilon_i(\tau_i, y, r) = \epsilon_0(\tau_i, y, r), 2\epsilon_0(\tau_i, y, r), 4\epsilon_0(\tau_i, y, r)$  distributed in  $r$ -plane according to the Woods-Saxon formula. The initial proper time is  $\tau_i = 1$  fm/c.

thermal pions during the chemically frozen hydro-evolution. As the result, the HBT microscope at diverse energies “measures” the radii that are similar to the sizes of colliding nuclei. It explains the experimental observations that at the same collision energy, the  $V_{int}$  depends strongly on the sizes of colliding nuclei and on the impact parameters in non-central collisions [5].

The RHIC experiments show clearly that there is no proportionality law between  $V_{int}$  and  $dN^\pi/dy$ : the later value grows with energy significantly faster than  $V_{int}$ . This fact is the main component of the HBT puzzle. According to Eq. (1), a proportionality between  $V_{int}$  and the particle numbers  $dN/dy$  may be destroyed by a factor  $\langle f \rangle T_{eff}^3$ . So, if the APSD and  $V_{int}$  only slightly grow with energy, mostly an increase of  $T_{eff}^3$  could compensate a growth of  $dN/dy$  in Eq. (1). One can see that it is the case: for example, the ratio of cube of effective temperatures of negative pions at  $\sqrt{s_{NN}} = 200$  GeV (RHIC) to one at 40 AGeV (CERN SPS) gives approximately 2, while the ratio of correspondent mid-rapidity densities is approximately equal to 3. It can be only in the case of an increase of the pion transverse flows in A+A collisions with energy. If the intensity of flows grows, it leads to a reduction of the corresponding homogeneity lengths which contribute to the interferometry radii. This effect can almost compensate a contribution to observed interferometry volumes of the geometrical system sizes that grow with energy. The question is then: why does the intensity of flow grow? It is clear that an increase of collision energy  $\sqrt{s}$  results in a rise of initial energy density  $\epsilon$  and hence of (maximal) initial pressure  $p_{max}$ . At the same time the initial transverse acceleration  $a = \text{grad}(p)/\epsilon \propto p_{max}/\epsilon$  does not change. Thus, one can conclude that there could be the two reasons for an increase of transverse pion flows with collision energy. First one is obvious, it is an increase of the time of hydro-evolution that the system needs to reach the same (or less) freeze-out energy density or temperature at higher initial density (see Fig. 1)

However, apparently, relativistic hydrodynamic picture overestimate the increase of the longitudinal interferometry radii, that is associated with life-time of the system, as compare to the experimental data.

The another reason for an increase of the observed transverse flows is the presence of the initial transverse velocity which may develop at the pre-thermal partonic stage and obviously has an influence on the time of evolution and intensity of transverse flow at freeze-out. Moreover, what is essentially important, this factor has the direct connection to the second component of HBT puzzle: the unexpectedly small ratio of outward to sideward interferometry radii. In relativistic hydrodynamics or realistic hydro-inspired parametrization the freeze-out hypersurface should be enclosed, so the protractive surface emission of pions (hadrons) from fairly cold periphery of the expanding system take place. Normally, it should lead to large  $R_{out}$  to  $R_{side}$  ratio, however, as demonstrated in Ref. [6], it is possible, nevertheless, to describe the data successfully, including  $R_{out}$  to  $R_{side}$  ratio, if there are positive  $r - t$  correlations between the radial  $r$  coordinates and times  $t$  of surface emission of the particles. The term associated with these correlations gives the negative contribution to  $R_{out}$  interferometry radius and so compensates the positive contribution to it from long time surface emission.

The only fit with positive  $r - t$  correlations, as it presented in Fig.2, results in good description of the the spectra pions, kaons and protons and pion interferometry data, including  $R_{side}$  and  $R_{out}$ . All details are presented in Ref.[6].

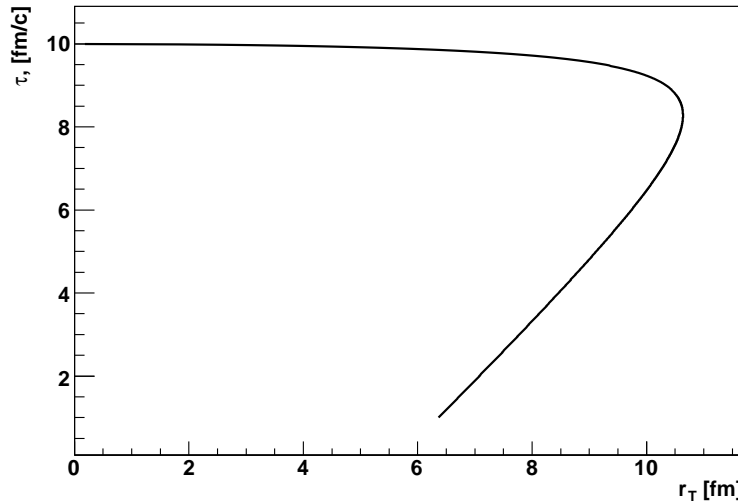


**Figure 2.** The dynamical realization of the freeze-out with positive  $r - \tau$  correlations at constant energy density [7] based on the (3+1)D exact analytical solutions of relativistic hydrodynamics [8] with intensive initial transverse flows

One of the most important observation is that the  $r - t$  correlation at the freeze-out hypersurface, according to equations of relativistic hydrodynamics, can be predominantly positive only if the system has at initial moment a developed transverse flow. The typical situation presented in Fig.1 and Fig.2. The former figure corresponds to an absence of the initial transverse flow, the second describe intensive blast-like expansion into vacuum that starts at early stage of the evolution, say, at  $\tau=1$  fm/c. In the first case the negative  $r - t$  correlations between the surface emission points takes place, and it leads to a positive contribution to  $R_{out}$  in addition to big positive contribution associated with protracted surface emission. In the second case the latter positive term is compensated by the positive  $r - t$  correlation term. It leads to experimentally observed  $R_{out}$  to  $R_{side}$  ratio *in presence* of protracted surface emission.

### 3 Pre-thermal partonic stage : The free-streaming approximation

A problem of formation of the initial transverse velocity at pre-thermal partonic stage leads inevitably to the complex matter of the initial stage in ultrarelativistic A+A collisions and the problem of thermalization. In these notes we will not discuss in details this very complicated topic just keeping in mind quite simple physical picture and apply it phenomenologically.

Let us imagine a box (with size  $L$ ) that have the ideally reflecting walls and contains the standing (electromagnetic) waves inside. Then collide the two such boxes with the energy that allows to crush them completely. Standing waves then will be destroyed due to a stochastisation that is accompanied by the crashing *processes* [9]. In other words, strong correlations between phases of traveling “backward” and “forward” waves, with discrete momenta, say,  $2\pi/L$  and  $-2\pi/L$ , caused by ideal reflections from the opposite walls, will vanish and instead the random phases  $\exp(\alpha_{p_i})$  will appear:

$$\sin \frac{2\pi x}{L} = \frac{1}{2} \left( \exp \frac{i2\pi x_T}{L} - \exp \frac{-i2\pi x_T}{L} \right) \Rightarrow \sum \rho_{p_i} e^{\alpha_{p_i}} e^{ip_i x_T}.$$

In the case of very weak field we will see then, say, two incoherent photons traveling, for instance, in transversal plane in opposite directions.

Let us provide an analogy now with high energy nucleus-nucleus collisions by imaging them as the collisions of the two “boxes” (containing many “small boxes” – nucleons). Due to the non-commutativity of the gluon number operator with the operator of Lorenz boost, there is a huge number of coherent partons in the fast moving box – this state probably can be represent within the Color Glass Condensate (CGC) approach [10]. Correspondingly, after collision there will be not just two gluons but the classical color field (because of large occupation number) expanding into vacuum. When occupation number reduces, one can see the picture of the expanding system of incoherent partons. It may call “partonic explosion” when many hidden degrees of freedom, associated with incoherent partons and carried significant transverse momentum, are liberated almost suddenly. An estimate of the thermalization time for this system is a rather complicated problem and we just mention about it later. It seems that partons interact weakly enough and instability mechanism [11] works not

so fast, as necessary to reach very small time of momentum symmetrization (thermalization?), less then 1 fm/c, required by hydrodynamics models to describe elliptic flows.

Let us simplify the problem again and consider now the developing of transverse velocity at pre-thermal partonic stage in an approximation of free streaming for this weakly interacting particles.

We start from the simple non-relativistic example. Let us put the initial momentum distribution of particles with mass  $m$  to be spherically symmetric Gaussian with the width corresponding to thermal Boltzmann distribution with uniform temperature  $T_0$ , no flows:  $\mathbf{u}(t=0, \mathbf{r}) = 0$ , and also spherically symmetric Gaussian profile (with radius  $R_0$ ) for particle density. Let the particles just to free stream. Then according to [3] the collective velocities, which can be defined at any time  $t$  according to Eckart:

$$u^i = \int \frac{d^3 p}{m^4} p^i f(t, \mathbf{x}; p)$$

are

$$\mathbf{u}(t, \mathbf{r}) = \mathbf{r} \frac{t T_0}{m R_0^2 + T_0 t^2}.$$

As one can see the collective velocities in free streaming system grow with decrease of particle mass, grow with initial parameter  $T_0$  for  $m \neq 0$ , and are independent of the initial “temperature” at  $m = 0$ . Qualitatively, the same happens for relativistic partonic gas.

Let us consider relativistic partonic picture with the initial momentum distribution at Björken proper time  $\tau=1$  fm/c corresponds to “transverse momentum” Fourier components in the color field in the CGC picture found in Ref.[12]. Suppose that after collision the similar transverse spectrum will appear for incoherent partons. As for the longitudinal ones we will use the local 3D isotropic quasi-thermal distribution as it was proposed in Ref.[13] based on the Schwinger mechanism of the partonic production: the partons created by a pulse of the strong chromo-electric field during collision process are distributed (locally) quite isotropically since the limited in time action of the field. Let us use the boost-invariant approximation in mid-rapidity and the Woods-Saxon initial profile for energy density in transverse plane. Then the partonic distribution function at the initial proper time  $\tau = \tau_0$  is:

$$f_0 = \frac{1}{\exp \frac{m_T}{T} \cosh \theta - 1} \frac{1}{\exp \frac{1}{\delta} (r_T - R) + 1}, \quad (2)$$

where  $\theta$  is the difference between particle and fluid rapidities. The main parameters of the distribution is agreed with Refs.[12, 13]:  $T = 0.465 \Lambda_s$ ,  $\delta = 0.67$  fm,  $\Lambda_s = 1.3$  GeV,  $\tau_0 = 1$  fm/c,  $R = 7.3$  fm, partonic mass is taken to be equal to  $m = m_0 = 0.0358 \Lambda_s$ . The evolution of this function is defined by the equation for free streaming,

$$p^\mu \frac{\partial f}{\partial x^\mu} = 0. \quad (3)$$

The solution of this equation describes the distribution function at any hypersurface  $\tau = \text{const}$  by the use of the following substitution in the arguments of the function  $f_0$  related to the initial proper time  $\tau_0=1$  fm/c:

$$\mathbf{r}_T \rightarrow \mathbf{r}_T - \frac{\mathbf{p}_T}{m_T} \left( \tau \cosh \theta - \sqrt{\tau_0^2 + \tau^2 \sinh^2 \theta} \right), \quad (4)$$

$$\theta \rightarrow \text{arcsinh} \left( \frac{\tau}{\tau_0} \sinh \theta \right). \quad (5)$$

In what follows we will consider the properties of such a free-streaming expansion of boost-invariant and cylindrically symmetric finite system into vacuum as a first approximation and discuss the possible whole picture of the early pre-thermal stage.

#### 4 Collective velocities and local anisotropy in partonic system

Let us study the free-streaming stage of the evolution, supposing, as it was argued above, that incoherent partonic system arise at the time of order of 1 fm/c as a locally isotropic boost-invariant and weakly interacting gas. Then gas will free stream into vacuum. The process itself will lead to a local anisotropy which we will study in this section. The increase of the anisotropy may be compensated by the process of turbulency (instability) and gradual thermalization associated with Balescu-Lenard term for QCD fields.

The analysis of the local anisotropy of the distribution function can be done in the two ways. The first one deals with a study of distribution function properties, while the second one deals the difference between spatial components of the energy-momentum tensor in local rest frames. In both cases, we are forced to consider the distribution and the energy-momentum tensor in a co-moving reference frame determined by collective velocity. Here we will apply both Eckart and Landau-Lifshitz definitions of the collective velocities  $\mathbf{v}(\mathbf{x})$  related to fairly small elements associated with point  $(x^\mu)$ .

The connection between the global and local rest frame moving with 3-velocity  $\mathbf{v} = (v^i)$ , is Lorentz transformation defined by matrix of the form:

$$(\Lambda^\mu{}_\nu) = \left( \begin{array}{c|c} \gamma & v^i \gamma \\ \hline v^j \gamma & \delta^{ij} + v^i v^j (\gamma - 1) / \mathbf{v}^2 \end{array} \right), \quad (6)$$

where  $\gamma = 1/\sqrt{1 - v^2}$  is a Lorentz factor;  $v \equiv |\mathbf{v}|$ .

Making use this matrix, the contravariant vector and tensor transformations read

$$a^\mu = \Lambda^\mu{}_\nu a_*^\nu, \quad a^{\mu\nu} = \Lambda^\mu{}_\lambda a_*^{\lambda\sigma} \Lambda^\nu{}_\sigma, \quad (7)$$

where  $a_*^\mu$  and  $a_*^{\mu\nu}$  denote these quantities in co-moving reference frame.

Therefore the 3-vector  $\mathbf{p}$  is transformed as follows

$$\mathbf{p} = \mathbf{p}_* + \frac{\mathbf{v}}{v^2} \frac{(\mathbf{v}\mathbf{p}_*)(1 - \sqrt{1 - v^2}) + v^2 E_*}{\sqrt{1 - v^2}}, \quad (8)$$

where  $E_* = \sqrt{m^2 + \mathbf{p}_*^2}$ .

It is possible to examine anisotropy of momentum distribution in different co-moving reference frames associated with different spacial points, where 3-momentum  $\mathbf{p}_*$  determines  $\mathbf{p}$  in accordance with Eq. (8).

The local anisotropy reveals itself also in structure of the energy-momentum tensor, which in pseudo-Cartesian coordinates reads

$$T^{\mu\nu}(x) = \int p^\mu p^\nu f(x, p) p_T dp_T dy d\phi, \quad (9)$$

where the Lorentz-invariant integration measure  $d^3p/E$  in Cartesian variables is already re-written in Björken variables:  $(p^\mu) = (m_T \cosh y, p_T \cos \phi, p_T \sin \phi, m_T \sinh y)$ .

To find  $T^{\mu\nu}$  in central rapidity slice, we numerically calculate energy-momentum tensor (9) at longitudinal coordinate  $z = 0$  ( $\eta = 0$ ), when  $\tau = t$ . Due to the symmetry properties of distribution, one finds  $T^{tz} = T^{xz} = T^{yz} = 0$ . Let  $\psi$  be the angular direction relative to the radial axis  $x$ . Note that  $T^{xy} = 0$  at  $\psi = n\pi/2$ ,  $n = 0, \pm 1, \pm 2, \dots$ . Fixing  $\psi = 0$ , the non-vanishing components of the energy-momentum tensor are

$$(T^{\mu\nu}) = \begin{pmatrix} T^{tt} & T^{tx} & 0 & 0 \\ T^{tx} & T^{xx} & 0 & 0 \\ 0 & 0 & T^{yy} & 0 \\ 0 & 0 & 0 & T^{zz} \end{pmatrix}. \quad (10)$$

It is understandable that the direction of collective velocities  $\mathbf{v}$  in the global (origin) reference frame at  $z = 0$  should coincide with vector  $\mathbf{r}_T$  and therefore  $\mathbf{v} = (v \cos \psi, v \sin \psi, 0)$ .

The tensor  $T_*^{\mu\nu}$  in the co-moving reference frame, associated with local velocity  $\mathbf{v}$ , is defined from (10) by use of the matrix  $\Lambda_\mu{}^\nu$  inverse to (6). (Actually, matrix  $\Lambda_\mu{}^\nu$  is derived from (6) by replacement  $v^i \rightarrow -v^i$ .) In the case of a boost, the components of the energy-momentum tensor in two reference frames are related by

$$T_*^{\mu\nu} = \Lambda_\lambda{}^\mu T^{\lambda\sigma} \Lambda_\sigma{}^\nu. \quad (11)$$

#### 4.1 Eckart Frame

Now we are concentrated on the collective velocity computation. In this subsection we deal with 4-velocity defined by Eckart:

$$u_E^\mu = \frac{N^\mu}{\sqrt{N_\nu N^\nu}}, \quad (12)$$

where

$$N^\mu = \int p^\mu f(x, p) p_T dp_T dy d\phi$$

is the particle flux.

The collective 3-velocity is simply given by  $\mathbf{v}_E = \mathbf{u}_0^E / u_0^E$ . The dependence of transverse velocity  $v_E = \sqrt{v_x^2 + v_y^2}$  on  $r_T$  at  $\eta = 0$  is demonstrated in Fig. 3.

Having got numerically the values of collective velocity, one can re-write the distribution function at the fixed point of space-time in Eckart co-moving reference frame by means of Lorentz transformation (8). At  $\tau = \tau_0 = 1$  fm/c, the distribution is isotropic, as must be according to initial conditions. Increasing  $\tau$ , the distribution becomes more and more anisotropic that is reflected on the collective velocity development.

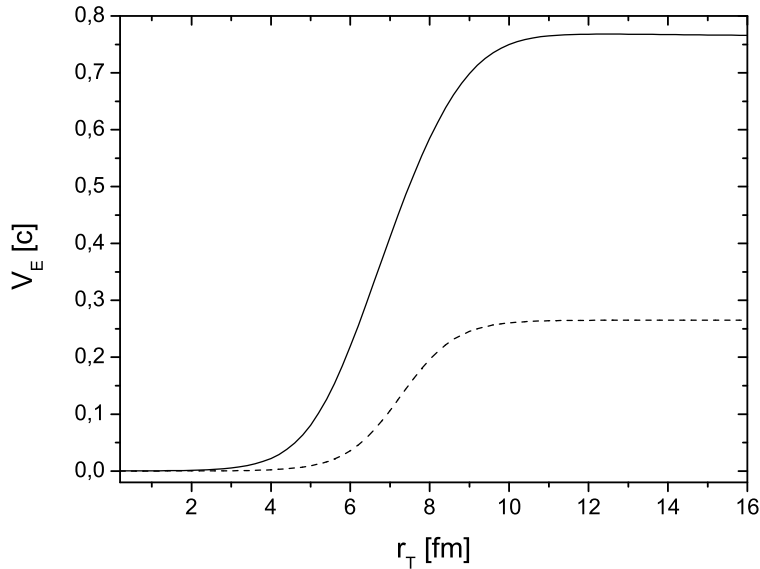


**Figure 3.** The Eckart collective transverse velocity in weakly interacting partonic system in the approximation of free streaming. The initial state at 1 fm/c is supposed to be quasi-thermal and corresponds to the distribution (2). Dashed curve correspond to  $\tau=1.5$  fm/c, solid line – 3 fm/c.

Another possibility to observe the anisotropy in the given system is to compare the components of energy-momentum tensor in a given co-moving reference frame, which is introduced by means of formula (11). The result of numerical calculations is shown in Fig. 4. Abbreviation “Arb. units” means that the distribution function is not normalized.

We find  $T_*^{xx} = T_*^{yy} = T_*^{zz}$  at  $\tau = \tau_0 = 1$  fm/c, that also confirms the isotropy at the initial moment. Changing  $\tau$ , the value of  $T_*^{zz}$  turns out essentially less than  $T_*^{xx}$  and  $T_*^{yy}$ , which also differ.

Remark that, putting  $v = v_E$  in Eq. (11), it is impossible to cancel  $T_*^{tx}$  in whole region of values of  $r_T$ . Further, we will demonstrate that the requirement  $T_*^{tx} = 0$  corresponds to definition of Landau-Lifshitz frame.

#### 4.2 Landau-Lifshitz Frame

The Landau-Lifshitz definition of collective velocity can be formulated as

$$u_L^\mu = \frac{T^{\mu\nu} u_\nu^L}{u_L^\lambda T_{\lambda\sigma} u_\nu^\sigma}. \quad (13)$$

In general, this expression is equation with respect to  $u_L^\mu$ , which should be solved numerically. However, in our case of cylindrical symmetry, when the free streaming is going on along  $r_T$ -axis, the collective velocity can be found explicitly.

Substituting the expression for  $T_*^{\mu\nu}$ , the components of the collective 4-velocity in co-moving reference frame are

$$(u_{*L}^\mu) = (1, 0, 0, 0) = \left(1, \frac{T_*^{tx}}{T_*^{tt}}, 0, 0\right). \quad (14)$$

It means that  $T_*^{tx} = 0$  and then one can get from Eq. (11) the expression for velocity in the global reference frame:

$$v_L = \frac{T^{tt} + T^{xx}}{2T^{tx}} \left(1 - \sqrt{1 - \frac{4(T^{tx})^2}{(T^{tt} + T^{xx})^2}}\right). \quad (15)$$

The behavior of  $v_L$  is shown in Fig. 5. The velocity  $v_L$  also vanishes at  $\tau = \tau_0$ . Although  $v_L$  is close to  $v_E$  (see Fig. 3) they are not completely coincided since the system is not in locally equilibrated state.

In the case of  $v = v_L$  (see (11)), the anisotropy of energy-momentum tensor is demonstrated in Fig. 6 and it is qualitatively the same as in the Eckart case presented in Fig. 4.

#### 4.3 Analysis of Weak Anisotropy

As one can see from Figs. 4, 6 the diagonal spatial components of the energy-momentum tensor of partonic system, even if they were equal at the initial formation time [13], are splitting during free-streaming expansion so that  $T_*^{yy}(x) > T_*^{xx}(x) > T_*^{zz}(x)$ . Thus the components of  $T_*^{\mu\nu}(x)$  associated with directions of non-zero

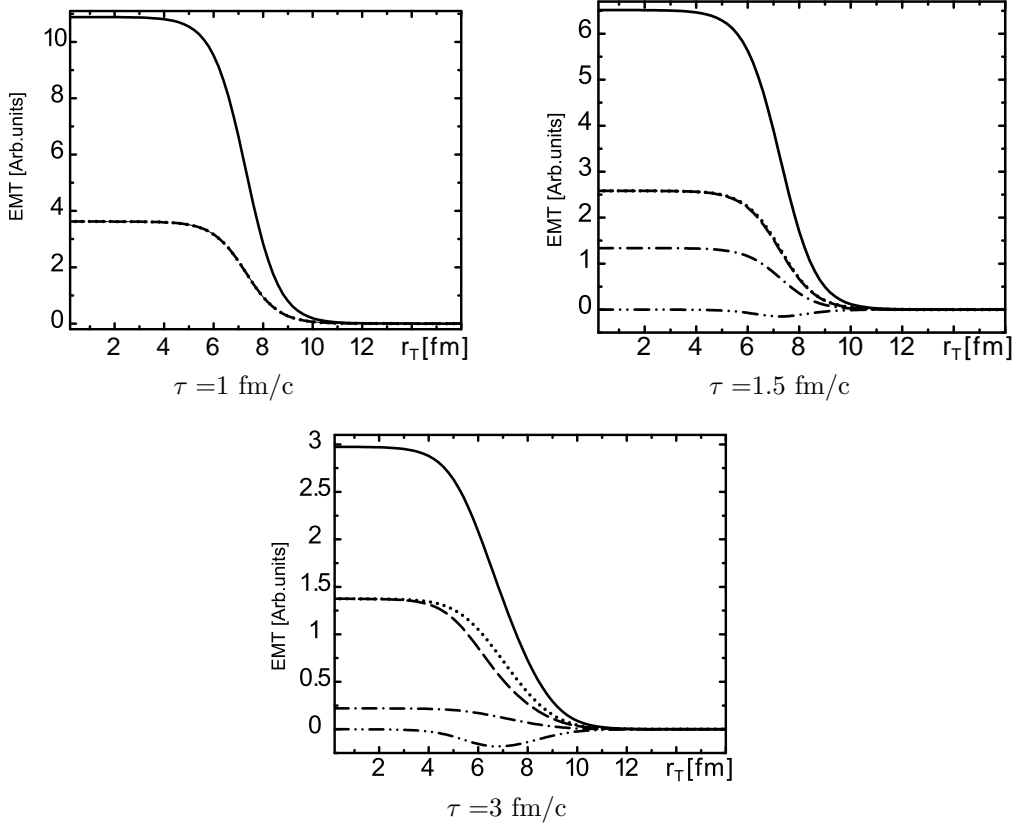


**Figure 4.** The components of the energy-momentum tensor,  $T_*^{tt}$  (solid),  $T_*^{xx}$  (dashed),  $T_*^{yy}$  (dotted),  $T_*^{zz}$  (dot-dashed),  $T_*^{tx}$  (dot-dot-dashed), at  $\tau = 1, 1.5, 3$  fm/c and  $\psi = 0$ . Eckart co-moving frame.

collective velocities (initial and developed) become suppressed as compare with other ones. Correspondingly, the particle distribution function gradually loses the local momentum isotropy during the expansion. Let us parameterize this anisotropy as depending on  $\tau = t$  and  $r_T$  at fixed  $z = 0$ .

It is useful to analyze the case of weak anisotropy and relate our result to other models. For this aim we represent distribution function (2), (4), (5) in the form  $f = F \cdot W$  where

$$F(a) = \frac{1}{\exp \frac{a}{T} - 1}, \quad W(b) = \frac{1}{\exp \frac{b - R}{\delta} + 1}. \quad (16)$$

Fixing  $z = 0$ ,  $\psi = 0$ , the arguments of these functions are presented as

$$\begin{aligned} a^2 &= E^2 + \xi p_z^2, \\ b^2 &= r_T^2 - 2 \frac{r_T p_x}{m^2 + \mathbf{p}_T^2} \tau_0 (\sqrt{1 + \xi} E - a) + \frac{\mathbf{p}_T^2}{(m^2 + \mathbf{p}_T^2)^2} \tau_0^2 (\sqrt{1 + \xi} E - a)^2, \end{aligned} \quad (17)$$

where we have introduced the parameter of anisotropy  $\xi(\tau) = \tau^2/\tau_0^2 - 1$  and  $E = \sqrt{m^2 + \mathbf{p}^2}$ . Note that the same dependence of  $\xi$  on the proper time has already pointed out in Ref.[14] to account for longitudinally boost invariant expansion in partonic system.

Let us write distribution function  $f$  in the linear approximation in  $\xi$ . The form of such a distribution is

$$f \approx f_{\text{iso}} + \frac{\xi(\tau)}{2} \left\{ W(r_T) \frac{dF(E)}{dE} \frac{p_z^2}{E} - F(E) \frac{dW(r_T)}{dr_T} \frac{p^x E \tau_0}{m^2 + \mathbf{p}_T^2} \left( 1 - \frac{p_z^2}{E^2} \right) \right\}, \quad (18)$$

where  $f_{\text{iso}} \equiv F(E)W(r_T)$  is the initial isotropic distribution function in the global reference frame.

We see that the first term in the brackets  $\{\}$  corresponds to momentum anisotropy due to initial momentum inhomogeneity, while the second one is related to the initial inhomogeneity in coordinate space.

Since the axial symmetry we can put  $\psi = 0$ , and the transition to the co-moving frame associated with some point  $(x, y = 0, z = 0)$  is determined in the simple way:

$$p^x = \frac{p_*^x + v E_*}{\sqrt{1 - v^2}}, \quad E = \frac{E_* + v p_*^x}{\sqrt{1 - v^2}}, \quad p^y = p_*^y, \quad p^z = p_*^z, \quad (19)$$

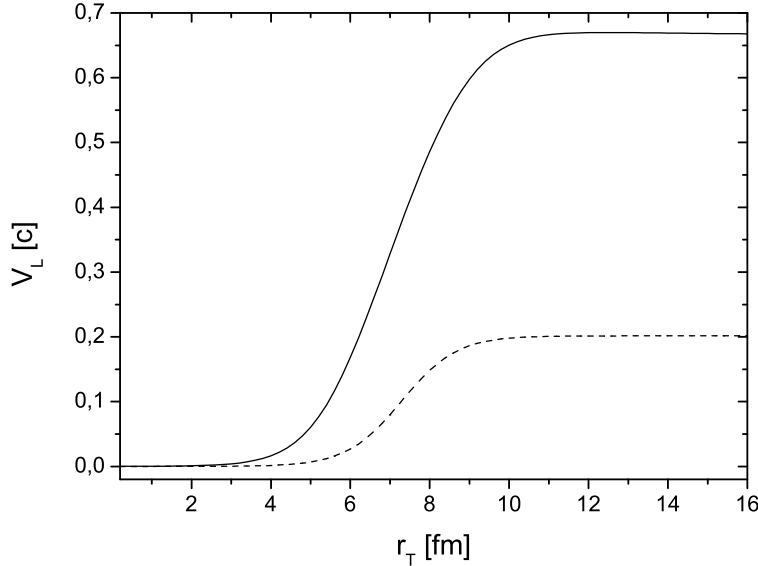


**Figure 5.** The Landau-Lifshitz collective transverse velocity in weakly interacting partonic system in the approximation of free streaming. The initial state at 1 fm/c is supposed to be quasi-thermal and corresponds to the distribution (2). Dashed curve correspond to  $\tau=1.5$  fm/c, solid line – 3 fm/c.

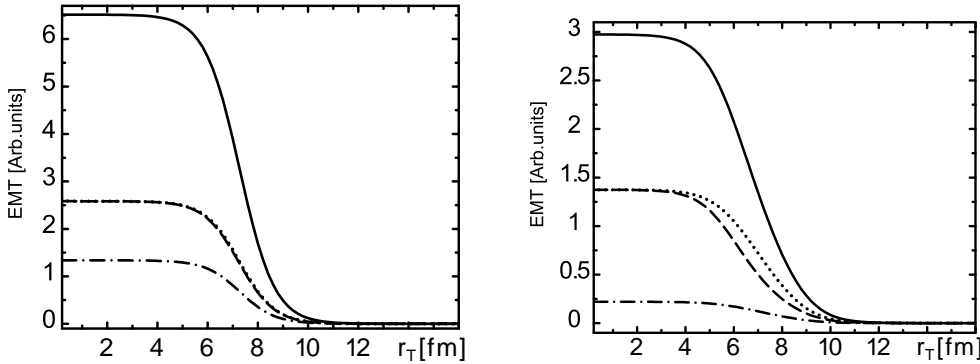


**Figure 6.** The components of the energy-momentum tensor,  $T_*^{tt}$  (solid),  $T_*^{xx}$  (dashed),  $T_*^{yy}$  (dotted),  $T_*^{zz}$  (dot-dashed), at  $\tau=1.5, 3$  fm/c (from left to right) and  $\psi=0$ . Landau-Lifshitz co-moving frame.

where  $E_* = \sqrt{m^2 + \mathbf{p}_*^2}$ .

Limiting ourselves by the linear approximation in the parameters of anisotropy, when  $v$  is also supposed to be small and discarding the term of order  $v\xi$ , we find

$$f_* \approx f_{\text{iso}}^* - W(r_T) \frac{dF(E_*)}{dE_*} p_*^x v + \frac{\xi(\tau)}{2} \left\{ W(r_T) \frac{dF(E_*)}{dE_*} \frac{(p_*^z)^2}{E_*} - F(E_*) \frac{dW(r_T)}{dr_T} \frac{p_*^x E_* \tau_0}{m^2 + (\mathbf{p}_T^*)^2} \left[ 1 - \left( \frac{p_*^z}{E_*} \right)^2 \right] \right\}, \quad (20)$$

where  $f_{\text{iso}}^* \equiv F(E_*)W(r_T)$  is the isotropic distribution function in co-moving reference frame.

The radial collective velocity  $v$  is actually a dependent parameter. Following the Eckart definition,

$$v_E = \int p^x f(x, p) \frac{d^3 p}{E} \Big/ \int f(x, p) d^3 p, \quad (21)$$

(where we put  $\psi=0$  again, and then the collective velocity direction coincides with  $x$ -axis), we get in linear approximation

$$v_E \approx \xi(\tau) \frac{\lambda_0}{\int f_{\text{iso}} d^3 p}, \quad (22)$$

where

$$\lambda_n = -\frac{\tau_0}{2} \int \frac{p_x^2 E^n F(E)}{m^2 + \mathbf{p}_T^2} \left(1 - \frac{p_z^2}{E^2}\right) \frac{dW(r_T)}{dr_T} d^3 p. \quad (23)$$

Similar computations can be also performed to obtain the form of Landau-Lifshitz collective velocity in the linear approximation in  $\xi$ . The result looks like

$$v_L \approx \xi(\tau) \frac{\lambda_1}{T_{tt}^{\text{iso}} + T_{xx}^{\text{iso}}}, \quad (24)$$

where  $T_{tt}^{\text{iso}}$  and  $T_{xx}^{\text{iso}}$  are the energy-momentum tensor components found on the basis of the isotropic distribution function  $f_{\text{iso}} \equiv F(E)W(r_T)$  in the global reference frame.

Now let us compare our results with the parametrization proposed by P. Romatschke with collaborators in Ref.[15]. It was assumed there that the anisotropic distribution function  $h(\mathbf{p})$  is independent on space-time coordinates and constructed from an (arbitrary) isotropic distribution function by the rescaling of one direction in momentum space,

$$h(\mathbf{p}) = h_{\text{iso}}(\sqrt{\mathbf{p}^2 + \xi(\mathbf{p})^2}), \quad (25)$$

where  $\mathbf{n}$  is the direction of anisotropy,  $\xi > -1$  is a constant parameter reflecting the strength of anisotropy. We omit here the normalization constant  $N(\xi)$  which was used in Ref.[15] as not relevant to our problem since the particle number conservation during the evolution from initially isotropic state is guaranteed by Eq. (3).

Expanding the distribution  $h(\mathbf{p})$ , in the linear approximation in  $\xi$  one can write that

$$h(\mathbf{p}) \approx h_{\text{iso}}(p) + \xi \frac{dh_{\text{iso}}(p)}{dp} \frac{(\mathbf{n}\mathbf{p})^2}{2p}. \quad (26)$$

It is easy to see that the expression (18) for central slice  $z = 0, v_z = 0$  is reduced to the last formula (26) at  $\xi = \tau^2/\tau_0^2 - 1$  and anisotropy vector  $\mathbf{n}$  directed along  $z$ -axis in the particular case supposed in Ref.[15], namely, spatially homogeneous distribution,  $W(r_T) \equiv \text{const}$ , and massless particles,  $E = |\mathbf{p}_*| \equiv p$ .

In our inhomogeneous case, we can present linearized form (20) for distribution function in local rest frame associated with some point  $(x, y = 0, z = 0)$  as the following

$$f_*(\tau, \mathbf{x}, \mathbf{p}_*) \approx f_{\text{iso}}^*(\mathbf{x}, |\mathbf{p}_*|) + \xi(\tau) g(\mathbf{x}, \mathbf{p}_*). \quad (27)$$

## 5 Problem of the evolution at pre-thermal stage

As it was demonstrated in [14, 15] the *ansatz* (25), is useful for analytical studies of dispersion law and isotropisation driven by instabilities. The latter can be caused by momentum anisotropy in a system of ultrarelativistic electro- or color- charged particles. The expression (27) also can be utilized for this aim. However, in our case, when initial partonic system is supposed to be formed in pseudo-thermal state due to Schwinger production in the pulse of chromoelectric field, the problem is to estimate whether this state, first, preserve its (local) isotropy due to instability/turbulency mechanism and, then, if it transforms into true thermal state due to the interactions. As we see in previous Section, the anisotropy caused by a free expansion of the finite system into vacuum can be characterized in linear approximation by one parameter  $\xi$ , which is a function of proper time  $\tau$ . One can estimate the possible rate of anisotropy growth at the following

$$R(\tau) \equiv \frac{1}{f^*(\tau)} \frac{df^*(\tau)}{d\tau} \simeq \frac{2\tau}{\tau_0^2} \frac{g^*}{f_{\text{iso}}^*}. \quad (28)$$

Approximate equality is written down for the case  $\tau/\tau_0 - 1 \ll 1$ .

In order to maintain the initial isotropization of the partonic system during the evolution, it is obvious that the rate  $R(\tau)$  should be smaller than  $1/\tau_{\text{iso}}$ , where  $\tau_{\text{iso}}$  is a characteristic, or relaxation time of isotropization driven by instability. This time  $\tau_{\text{iso}}$  is planning to be estimated in forthcoming work, as well as rate of thermalisation due to color interaction described by Balescu-Lenard term in the kinetic equation.

In previous section we analize the developing of collective transverse flows in the finite non-thermal partonic system in the first free-streaming approximation. The results are presented in Figs. 3, 5. Unlike discussed in a Sec. 3 the specific non-relativistic case, where the initial isotropy in local rest frames of the distribution function is preserved during the further evolution, the ultra-relativistic evolution is not locally equilibrated, the distribution function and energy-momentum tensor become anisotropic in the local rest frames, and thus the development of the transverse velocities is not associated with hydrodynamics of ultrarelativistic gas. Nevertheless, as we demonstrate in Fig. 7, such a development of transverse velocities can be approximated by the hydrodynamic expansion with abnormal hard EoS:  $P = 0.45\epsilon$  (“normal” upper limit  $P = \epsilon/3$  has ultrarelativistic gas).

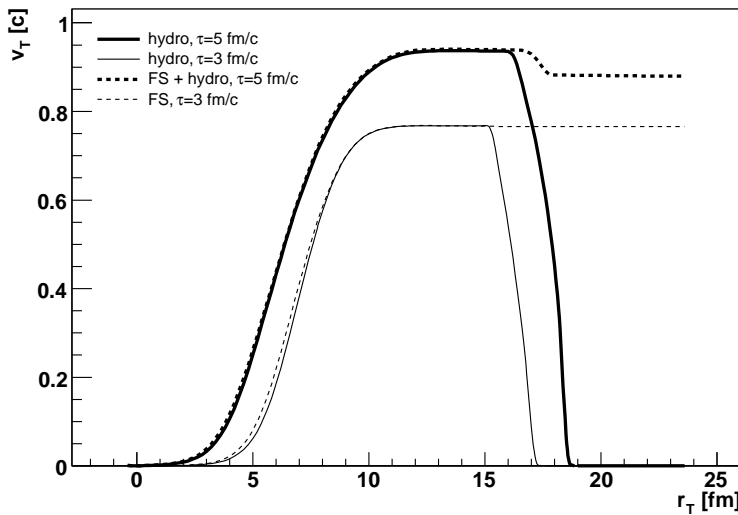


**Figure 7.** The simulation of the transverse collective velocities (according to Ekkart  $\approx$  Landau-Lifshitz) of the quasi-free and almost massless partons within ideal hydrodynamics with the same initial conditions as for partonic system. The velocity is good approximated by such a hydro-evolution with extra-hard EoS  $P = 0.45\epsilon$ . Dashed curve corresponds to a weakly interacting partonic system at  $\tau=3$  fm/c and 5 fm/c, solid line - to hydro-evolution at corresponding proper times.

Therefore, it might be that a short thermalization time is not necessary for development of the observed radial flows. They can be developed, and even more effectively, at the pre-thermal or pseudo-thermal stage. The natural objection against such a scenario might mean the problem of not radial but the elliptic flows. They need earlier thermalization in order to the initial geometrical asymmetry in transverse plane transforms more effectively into momentum asymmetry. The pre-thermal transverse flows can smear out the asymmetry in momenta coming from the asymmetry in pressure gradients.

The solution of the problem could be an account for the residual – after the exclusion of the non-participants – a transversely directed angular momentum which the system of participants has just after collision due to a shift of the center of masses of colliding nuclei in reaction plane, that is associated with impact parameter [16]. Then, as it is shown in Ref.[17], the corresponding tilt in the major axis of longitudinal expansion gives positive contribution to the asymmetry of the particle momenta in transverse to beam plane, or in  $v_2$  coefficient. The account for an interplay between the initial pre-thermal transverse velocity and the angular momentum which the system of participants obtains in non-central collisions can open the new way in an understanding of the problem of matter evolution in nucleus-nucleus collisions.

## 6 Conclusions

The approximate conservation of the pion averaged phase-space density (APSD) in A+A collisions during the hadronic stage of the evolution allows one to explain proportionality between interferometry volume and different initial volumes, e.g., in non-central collisions, and also explain the relative independence of the interferometry volumes on energy in central Au+Au and Pb+Pb collisions by an increase of transverse flows with energy. The hydrodynamic picture with initially non-zero transverse flow can help in description of the latter effect.

The another component of the RHIC HBT puzzle - the relatively small ratio of outward to sideward interferometry radii at protracted surface emission also needs in intensive initial transverse flows for its explanation. The reason is that predominantly positive space-time ( $r - t$ ) correlations for emission points, which reduce the outward radius, can be realized only in hydrodynamic picture with strong enough transverse flow at initial moment.

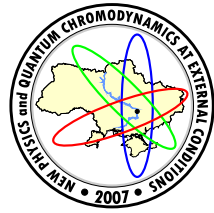
We demonstrate here that the intensive transverse flows can be developed at the very early pre-thermal partonic stage when many hidden degrees of freedom, associated with incoherent partons, are liberated. It is shown that the development of the transverse velocities at pre-thermal partonic stage can be approximated by the hydrodynamic expansion with abnormal hard equation of state. The interplay of those flows and angular momenta, which the system get in non-central collisions, could lead to new scenario of the matter evolution and help to describe the experimental data in central and non-central A+A collisions.

*Acknowledgements.* Yu.S. would like to thanks very much to Tetsufumi Hirano who give possibility to use the hydrodynamic code to clarify some features of relativistic evolution.

The research carried out within the scope of the ERG (GDRE): Heavy ions at ultrarelativistic energies – a European Research Group comprising IN2P3/CNRS, EMN, Universite de Nantes, Warsaw University of Technology, JINR Dubna, ITEP Moscow and Bogolyubov Institute for Theoretical Physics NAS of Ukraine.

## References

- [1] C. Adler *et al.* [STAR Collaboration], Phys. Rev. Lett. **87**, 082301 (2001); K. Adcox *et al.* [PHENIX Collaboration], Phys. Rev. Lett. **88**, 192302 (2002); S. Kniege *et al.* [NA49 Collaboration], J. Phys. **G30**, S1073 (2004).
- [2] U. Heinz, P.F. Kolb, hep-ph/0204061; U. Heinz, Nucl.Phys. **A721**, 30 (2003); S. Pratt, Nucl. Phys. **A715**, 389c (2003); S. Soff, S. Bass, D. Hardtke, S. Panitkin, Nucl. Phys. **A715**, 801c (2003).
- [3] S.V. Akkelin, Yu.M. Sinyukov, Phys. Rev. **C70**, 064901 (2004).
- [4] S.V. Akkelin, Yu.M. Sinyukov, Phys.Rev. **C73**, 034908 (2006); Nucl. Phys. **A774**, 674 (2006).
- [5] H. Appelshauser, J. Phys. **G30**, S935 (2004).
- [6] M.S. Borysova, Yu.M. Sinyukov, S.V. Akkelin, B. Erazmus, Iu.A. Karpenko, Phys.Rev. **C73**, 024903 (2006).
- [7] Iu.A Karpenko, Master Thesis, National University of Kiev, 2006.
- [8] Yu.M. Sinyukov, Iu.A. Karpenko, Acta Phys. Hung. **A25/1**, 141 (2006).
- [9] S. Mashkevich, private communication.
- [10] L. McLerran and R. Venugopalan, Phys. Rev. **D49**, 2233, 3352 (1994); **D50**, 2225 (1994); **D53**, 458 (1996); **D59**, 09400 (1999).
- [11] St. Mrowczynski, Phys. Rev. **D39**, 1940 (1989).
- [12] A. Krasnitz, Y. Nara, and R. Venugopalan, Nucl. Phys. **A727**, 427 (2003); hep-ph/0305112(2003).
- [13] D. Kharzeev, E. Levin, and K. Tuchin, hep-ph/0602063.
- [14] P. Romatschke and A. Rebhan, Phys. Rev. Lett. **97**, 252301 (2006); hep-ph/0605064.
- [15] P. Romatschke and M. Strickland, Phys. Rev. **D70**, 116006 (2004) [hep-ph/0406188]; P. Romatschke and M. Strickland, Phys. Rev. **D68**, 036004 (2003) [hep-ph/0304092]; P. Romatschke, Ph.D. Dissertation, hep-ph/0312152.
- [16] Yu.M. Sinyukov, Act. Phys. Polon. **B37**, 3343 (2006).
- [17] T. Csörgő, S.V. Akkelin, Y. Hama, B. Lukacs and Yu.M. Sinyukov, Phys. Rev. **C67**, 034904 (2003).



## SEARCH FOR EFFECTS BEYOND THE STANDARD MODEL IN PHOTON SCATTERINGS AND IN NONMINIMAL GAUGE THEORIES ON LINEAR COLLIDERS OF NEW GENERATION

T. V. Shishkina<sup>a</sup>

Belarusian State University, Minsk, Belarus

The main possibilities of investigation of leptons and bosons production in interaction of polarized photons are considered. The usage of  $\gamma\gamma \rightarrow f\bar{f} [+ \gamma]$  reactions for the luminosity measurement on linear photon collider is analyzed. The achievable precision of the luminosity measuring is considered and calculated. The first-order QED correction to  $\gamma\gamma \rightarrow l\bar{l}$  scattering is analyzed. All possible polarization states of interacting particles are investigated. For the detection of deviations from SM predictions at linear  $\gamma\gamma$  colliders with centre of mass energies running to 1 TeV the influence of three possible anomalous couplings on the cross sections of  $W^+W^-$  productions has been investigated. The significant discrimination between various anomalous contributions is discovered. The main contribution of high order electroweak effects is considered.

### 1 Introduction

The Standard Model (SM) has possibility to describe all experimental data up to now with typical precision around one per mil. Nevertheless the Model is not the final theory valid up to very high scales and at linear collider that can run at centre of mass energies around 1 TeV one can hope to see finally deviations in precision measurements occur typically for two reasons.

If the new physics occurs in loop diagrams their effect is usually suppressed by a loop factor  $\alpha/4\pi$  and very high precision is required to see it. If the new physics is already on the Born level but at very high masses the effects are suppressed by propagator factor  $s/(s - m_{NP}^2 - im_{NP}\Gamma)$  so that is important to work at the highest possible energies.

Linear lepton colliders will provide the opportunity to investigate photon collisions at energies and luminosities close to these in  $e^+e^-$  collisions [1].

The possibility to transform the future linear  $e^+e^-$ -colliders into the  $\gamma\gamma$  and  $e\gamma$ -colliders with approximately the same energies and luminosities was shown. The basic  $e^+e^-$ -colliders can be transformed into the  $e\gamma$ - or  $\gamma\gamma$ -colliders. The intense  $\gamma$ -beams for photon colliders are suggested to be obtained by Compton scattering of laser lights which is focused on electrons beams of basic  $e^+e^-$ -accelerators.

The electron and photon linear colliders of next generation will attack unexplored higher energy region where new behaviour can turn up. In this area the photon colliders have a number of advantages.

- The first of the above advantages is connected with the better signal/background ratio at both  $e^+e^-$ - and  $e\gamma/\gamma\gamma$ -colliders in comparison with hadron ones.
- The production cross sections at photon colliders are usually larger than those at electron colliders.
- The photon colliders permit to investigate both of the problems of new physics and those ones of "classical" hadron physics and QCD.

Compare of above mentioned electron and photon colliders.

1. In the scheme considered the maximal photon energy is slightly less than electron energy  $E$ .

To increase the maximal photon energy one can use the laser with the largest frequency. It seems also useful to do photon spectrum more monochromatic. However with such energy growth the new phenomenon takes place which destroy the obtained photon beams. The high energy photons disappear from the beam due to their collisions with laser ones producing  $e^+e^-$ -pairs.

2. The  $e\gamma$  and  $\gamma\gamma$  luminosities can be the same as basic  $e^+e^-$  luminosity or even larger (for instance for  $\gamma\gamma$  collisions).

3. It seems to be an important advantage of the electron beams that they are the monochromatic ones. It isn't correct.

Really the production of the heavy particles in electron colliders can be represented as two-step process. At the first step an electron emits photons (it is standard bremsstrahlung – initial state radiation). After that the

electrons with the lower energies collide and produce the heavy particles. Secondly, the electron spectrum is smoothed due to bremsstrahlung. This spectrum varies during bunch collision.

4. The photon spectrum is nonmonochromatic. Its effective form depends on the conditions of the conversion. Besides the collisions of electron with a few laser photons simultaneously result in high energy tail of spectrum (nonlinear QED effect). On the other hand due to angular spread of photons the effective form of their spectrum varies with the distance between conversion and collision points.

5. Only with using of detailed data on momenta of particles observed one can restore the real energy dependencies of cross sections. The determination of cross section averaged over the above wide spectra seems to be useful for very preliminary estimations only.

At the colliders discussed the data processing should be performed with equation of the form:

$$\int \frac{\partial^2 L(E_1, E_2)}{\partial E_1 \partial E_2} \cdot \sigma(W^2)|_{W^2=4E_1 E_2} \cdot dE_1 dE_2. \quad (1)$$

Therefore the special measurements of the spectral luminosity  $dL(E_1, E_2)$  (i. e. the distribution of luminosity in  $W$  and in the rapidity of produced system) are necessary. The preliminary estimations shows that one could use for this aim the Bhabha scattering for electron colliders, the Bethe-Heitler  $e\gamma \rightarrow e\mu^+\mu^-$  processes for  $e\gamma$  -colliders,  $\gamma\gamma \rightarrow \mu^+\mu^-\mu^+\mu^-$  process for  $\gamma\gamma$  -colliders.

6. In the  $e^+e^-$  -colliders the region of small angles closed for the observations. The small angle region will be open for investigation at  $\gamma\gamma$  and  $\gamma e$ - colliders.

7. The degree of photon polarization correlates with its energy. The polarization of hard photons can be calculated: the special measurements for soft tail are needed. The same problem for electrons is due to the variation of their polarizations induced by bremsstrahlung.

8. In the  $e^+e^-$  -collisions in the most cases the states  $J = 1$  are produced. Therefore, the  $e^+e^-$  -colliders are suitable for investigation of neutral vector bosons.

At the  $\gamma\gamma$  -colliders all the partial waves are produced. The set physical processes which can be investigated at the  $\gamma\gamma$  -colliders is richer than that in the  $e^+e^-$ -colliders.

9. The production cross section at  $\gamma\gamma$  collisions are usually larger than those ones at  $e^+e^-$ -collisions and they are decreased slowly with the energy. It is the source of the additive advantage of  $\gamma\gamma$  colliders because the detailed investigation of many reactions and particles is preferable for above the threshold.

10. There is no need in the positron beams for the  $\gamma e$  and  $\gamma\gamma$  colliders. It is sufficient to have as a base the  $e^-e^-$  collider only.

So it is exclusively important task to use possibilities of  $\gamma\gamma$ -colliders to realize the experiments of the next generation.

If a light Higgs exists one of the main tasks of a photon collider will be the measurement of the partial width  $\Gamma(H \rightarrow \gamma\gamma)$ . Not to be limited by the error from luminosity determination the luminosity of the collider at the energy of the Higgs mass has to be known with a precision of around 1%.

To produce scalar Higgses the total angular momentum of the two photons has to be  $J=0$ . In this case the cross section  $\gamma\gamma \rightarrow l^+l^-$  is suppressed by factor  $m_l^2/s$  and thus not usable for luminosity determination.

In the SM the couplings of the gauge bosons and fermions are constrained by the requirements of gauge symmetry. In the electroweak sector this leads to trilinear and quartic interactions between the gauge bosons with completely specified couplings.

The trilinear and quartic gauge boson couplings probe different aspects of the weak interactions. The trilinear couplings directly test the non-Abelian gauge structure, and possible deviations from the SM forms have been extensively studied. In contrast, the quartic couplings can be regarded as a more direct way of consideration of electroweak symmetry breaking or, more generally, on new physics which couples to electroweak bosons.

In this respect it is quite possible that the quartic couplings deviate from their SM values while the triple gauge vertices do not. For example, if the mechanism for electroweak symmetry breaking doesn't reveal itself through the discovery of new particles such as the Higgs boson, supersymmetric particles or technipions it is possible that anomalous quartic couplings could provide the first evidence of new physics in this sector of electroweak theory.

The production of several vector bosons is the best place to search directly for any anomalous behaviour of triple and quartic couplings.

By using of transforming a linear  $e^+e^-$  collider in a  $\gamma\gamma$  collider, one can obtain very energetic photons from an electron or positron beams. Such machines as ILC which will reach a center of mass energy  $\sim 1000\text{GeV}$  with high luminosity ( $\sim 10^{33}\text{cm}^{-2}\text{s}^{-1}$ ) will be able to study multiple vector boson production with high statistics.

For obvious kinematic reasons, processes where at least one of the gauge bosons is a photon have the largest cross sections.

So the photon linear colliders have the great physical potential [2] (Higgs and SUSY particles searching, study of anomalous gauge boson couplings and hadronic structure of photons etc.). Performing of this set of

investigations requires a fine measurement of the luminosity of photon beams. For this purpose some of the well-known and precisely calculated reactions (see, for example,  $\gamma\gamma \rightarrow 2f, 4f$  [3–8]) are traditionally used.

It was shown that it is convenient to use the events of  $\gamma\gamma \rightarrow l^+l^-$  process for measuring the luminosity of the  $J = 2$ -beams ( $J$  is the total angular momentum of initial photon couple). Here  $l$  is the unpolarized light lepton ( $e$  or  $\mu$ ). It is the dominating QED process on  $J=2$  beams and its events are easily detected.

The difficulties appear in the calibration of photon beams of similar helicity (the total helicity of  $\gamma\gamma$ -system  $J=0$ ) since the small magnitude of cross sections of the most QED processes. For example, the leading term of cross section of  $\gamma\gamma \rightarrow l\bar{l}$  scattering on  $J=0$ -beams is of order  $\alpha/\pi$  ( $\approx 0.002$ ).

The exclusive reaction  $\gamma\gamma \rightarrow l^+l^-\gamma$  provides the unique opportunity to measure the luminosity of  $J=0$  beams on a linear photon collider.

One of the main purposes of the linear photon collider is the  $s$ -channel of the Higgs boson production at energies about  $\sqrt{s} = 120\text{GeV}$ . That is the reason of using this value of c.m.s. energy in our analysis.

## 2 Two lepton production with photon in $\gamma\gamma$ -collisions

The two various helicity configuration of the  $\gamma\gamma$ -system leads to the different spectra of final particles and requires the two mechanisms of beam calibration. We have analyzed [3] the behaviour of the  $\gamma\gamma \rightarrow l^+l^-\gamma$  reaction on beams with various helicities as a function of the parameters of detectors, and performed the detail comparison of cross section on  $\gamma^+\gamma^+$ - ( $J=0$ ) and  $\gamma^+\gamma^-$ -beams ( $J=2$ ). Since experimental beams are partially polarized the ratio of cross sections of  $\gamma\gamma \rightarrow l^+l^-\gamma$  scattering on  $J=0$  to  $J=2$ -beams should be high for the effective luminosity measurement. We have outlined the conditions that greatly restrict the observation of the process on  $J=2$  beams, remaining the  $J=0$  cross section almost unchanged.

Finally we estimate the precision of luminosity measurement.

Consider the process

$$\gamma(p_1, \lambda_1) + \gamma(p_2, \lambda_2) \rightarrow f(p_1', e_1') + \bar{f}(p_2', e_2') + \gamma(p_3, \lambda_3), \quad (2)$$

where  $\lambda_i$  and  $e_i'$  are the photon and the fermion helicities.

We denote the c.m.s. energy squared by  $s = (p_1 + p_2)^2 = 2p_1 \cdot p_2$ , the final-state photon energy by  $w$ . For the differential cross section the normalized final-state photon energy (c.m.s. is used)  $x = w/\sqrt{s}$  is introduced. The differential cross section  $d\sigma/dx$  appears to be the energy spectrum of final-state photons.

The matrix elements are obtained using two methods: the massless helicity amplitudes [9] for the fast estimations and the exact covariant analysis [10, 11] including finite fermion mass. Since final-state polarizations will not be measured we have summarized over all final particles helicities. The integration over the phase space of final particles is performed numerically using the Monte-Carlo method [12].

The calculations have been performed for various experimental restrictions on the parameters of final particles. Events are not detected if energies and angles are below the corresponding threshold values. The considering restrictions on the phase-space of final particles (the cuts) are denotes as follows:

- Minimum final-state photon energy:  $\omega_{cut}$ ,
- Minimum fermions energy:  $E_{f,cut}$ ,
- Minimum angle between any final and any initial particles (polar angle cut):  $\Theta_{cut}$ ,
- Minimum angle between any pair of final particles:  $\varphi_{cut}$ .

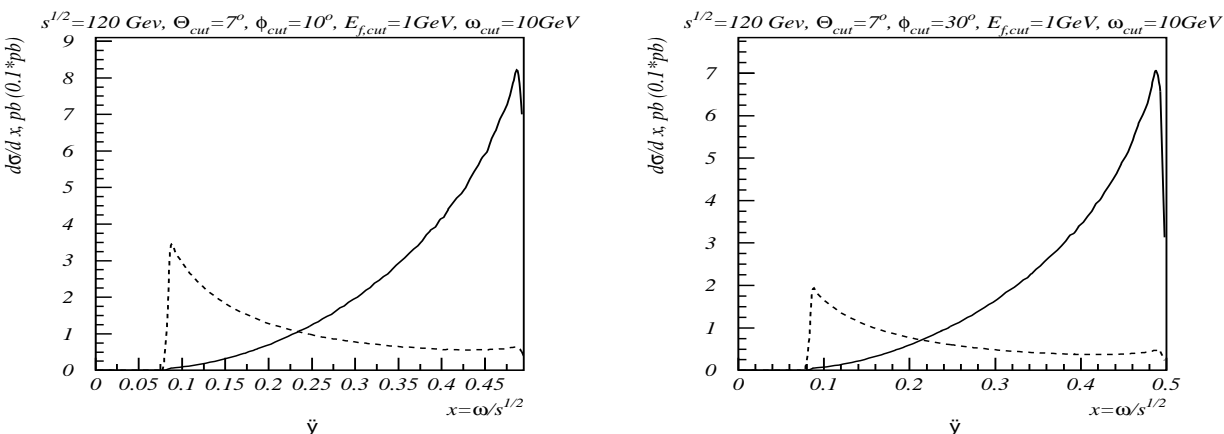


**Figure 1.** Final-state photon energy spectrum for  $J=0$  (solid) and  $(J=2)*0.1$  (dotted) at  $\sqrt{s} = 120\text{GeV}$  and cuts:  $\Theta_{min} = 7^\circ$ ,  $\varphi_{min} = 10^\circ$  (left) and  $\Theta_{min} = 30^\circ$ ,  $\varphi_{min} = 30^\circ$  (right),  $E_{f,min} = 1\text{GeV}$ ,  $\omega_{min} = 10\text{GeV}$ .

Consider the energy spectrum of final photons. In Fig. 1 the spectra for  $J=0$  and ( $J=2$ ) are presented (the ( $J=2$ )-cross section is scaled on factor 0.1 for the convenience). The differential cross section  $d\sigma/dx$  on  $J=2$  beams decreases while one on  $J=0$  beams raises with increasing of the final-state photon energy. This leads to the conclusion that if one increases the threshold on  $w$ , the process on  $J=2$  beams will be greatly restricted, but the rate of  $J=0$  events remains almost unchanged.

The ratio of events on  $J=0$  and  $J=2$  beams strongly depends on the experimental cuts. We obtained the region (the configuration of cuts) where the processes on the both  $J=0$  and  $J=2$  beams have the cross sections close by each other. That is the region of small polar angle cut, high collinear angle cut as well as high minimal energy of final-state photons. At these parameters the total cross sections of  $\gamma\gamma \rightarrow f\bar{f}\gamma$  in experiments using  $\gamma^+\gamma^+$ - and  $\gamma^+\gamma^-$  beams appear to be the same order of magnitude.

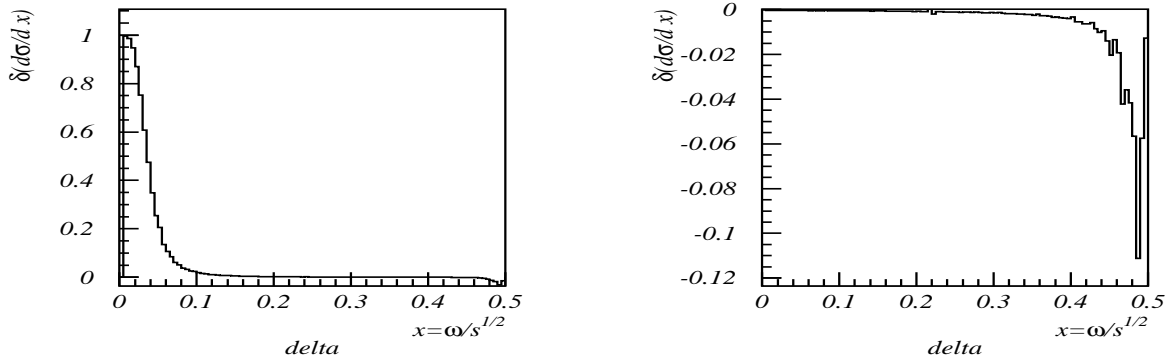


**Figure 2.** The relative mass contribution to energy spectra of final photon for  $J=0$  (left) and  $J=2$  (right) beams ( $w_{cut}=1GeV$ ,  $\mathcal{E}_{cut}=1GeV$ ,  $\Theta_{cut}=7^\circ$ ,  $\varphi_{cut}=3^\circ$ ).

The mass contribution is small in the great part of phase space of final particles. The most significant contribution is for the  $J=0$  energy spectra (see Fig. 2). The high value of the contribution corresponds to regions where the differential cross section is minimal. The mass contribution to the total cross section is below the 1% level at any realistic set of cuts. It means that the helicity amplitudes is a good approach for study the  $\gamma\gamma \rightarrow l^+l^-\gamma$  process.

### 3 Luminosity measurement of $J=0$ beams.

For analysis the precision of luminosity measurement [3] that can be achieved using the reaction  $\gamma\gamma \rightarrow f\bar{f}\gamma$ , the most interest are offered by the two kinds of measurement. The first one is the measuring of beams luminosity with the wide energy spectrum. The second one is the same measurement for the narrow band around the energy of Higgs boson production.

We use for consideration the following parameters:

1. luminosity

$$\begin{aligned} \mathcal{L}(\sqrt{s'} > 0.8\sqrt{s'_{\max}}) &= 5.3 \cdot 10^{33} cm^{-2}s^{-1}, \\ \mathcal{L}(m_H \pm 1GeV) &= 3.8 \cdot 10^{32} cm^{-2}s^{-1}; \end{aligned}$$

2. polarization  $\mathcal{P} \approx 90\%$ .

Our calculations allow to choose the set of cuts with the high  $J=0$  cross section and high ratio  $\sigma_{J=0}/\sigma_{J=2}$ :  $w_{cut}=20GeV$ ,  $E_{f,cut}=5GeV$ ,  $\Theta_{cut}=6^\circ$ ,  $\varphi_{cut}=30^\circ$ . For these cuts the total cross sections have the following values:

$$\begin{aligned} \sigma(J=0) &= 0.82 pb, \\ \sigma(J=2) &= 1.89 pb. \end{aligned}$$

So for the precision of luminosity measurement in a 2 years run ( $2 \cdot 10^7$ s) one can obtain:

$$\begin{aligned} \frac{\Delta\mathcal{L}}{\mathcal{L}} \left( \sqrt{s'} > 0.8\sqrt{s'_{\max}} \right) &= 0.35\%, \\ \frac{\Delta\mathcal{L}}{\mathcal{L}} (m_H \pm 1GeV) &= 1.3\%. \end{aligned}$$

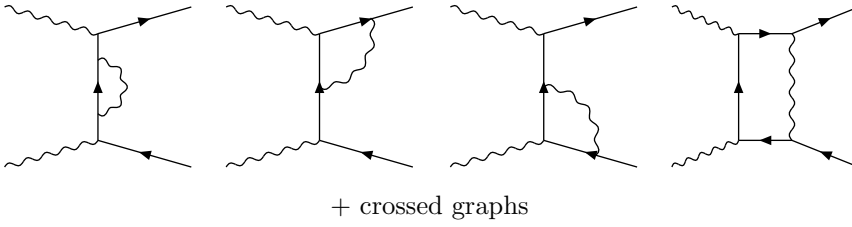


**Figure 3.** QED loop corrections.

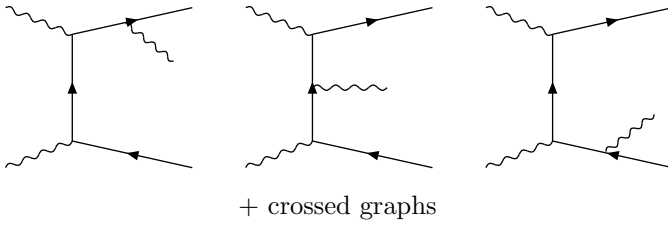


**Figure 4.** Real photon emission diagrams.

#### 4 Lepton-antilepton production in high energy polarized photons interaction

The luminosity measurement at  $J=2$  beams will be performed using the reaction  $\gamma\gamma \rightarrow l^+l^-$ . It has the great cross section that provides the number of events enough for the 0.1% precision of luminosity determination.

The main task is to calculate the cross section with maximal precision. For realization of this purpose we have calculated the complete one-loop QED radiative corrections to cross section of  $\gamma\gamma \rightarrow l^+l^-$  process including the hard photon bremsstrahlung.

The major feature of  $\gamma\gamma \rightarrow f\bar{f}$  process is the small value of cross section if the total angular momentum of  $\gamma\gamma$ -beams equals zero.

We analyze both the angular spectra and the invariant distributions of final particles. The angular spectrum of final leptons is calculated in form  $d\sigma/d\cos\Theta(p_l, p_\gamma)$ . It is more convenient to use Lorentz-invariant results for the experimental reasons. Therefore we analyze the process  $\gamma\gamma \rightarrow f\bar{f}[\gamma]$  including  $O(\alpha)$ -corrections using the method of covariant calculations [10, 11]. The invariant differential cross section is calculated in the form  $d\sigma/d(p_l - p_\gamma)^2$  and can be used in the arbitrary experimental configuration.

The cross section of process 2 to be calculated is

$$d\sigma = \frac{1}{2s} \left| M_{fi}^{\lambda_1, \lambda_2, e_1', e_2', [\lambda_k]} \right|^2 \cdot d\phi,$$

where

$$\int Ad\phi_{2[3]} = \frac{1}{(2\pi)^2} \cdot \frac{d^3 p'_1}{2\mathcal{E}'_1} \cdot \frac{d^3 p'_2}{2\mathcal{E}'_2} \left[ \frac{d^3 k}{(2\pi)^3 2\omega} \right] \cdot \delta(p_1 + p_2 - p'_1 - p'_2[-k]).$$

The matrix elements are obtained using the method of helicity amplitudes [9]:

$$\left| M_2^{+-+-} \right|^2 = 4e^4 \frac{u}{t} = 4e^4 \frac{1 + \cos\Theta_{2,2'}}{1 - \cos\Theta_{2,2'}} = 4e^4 \frac{s+t}{-t}, \quad (3)$$

$$\left| M_2^{+-++} \right|^2 = 4e^4 \frac{t}{u} = 4e^4 \frac{1 - \cos\Theta_{2,2'}}{1 + \cos\Theta_{2,2'}} = 4e^4 \frac{-t}{s+t}. \quad (4)$$

The set of invariants

$$\begin{aligned} s &= (p_1 + p_2)^2, & t &= (p_2' - p_2)^2, & u &= (p_2' - p_1)^2, & y &= -t/s, \\ v &= 2p_1 \cdot k, & \nu &= 2p_2 \cdot k, & z &= 2p_1 \cdot k, & z' &= 2p_2 \cdot k \end{aligned}$$

are introduced.

It is essential feature of this process that  $M_2^{++xx}$  and  $M_2^{--xx}$  amplitudes at the Born approximation have the order  $(m^2/s)^2$  and are negligible at high energies.

The integration over  $d\phi$  for the  $\gamma\gamma \rightarrow l^+l^-$  process is performed as follows:

$$\int A d\phi_2 = \frac{1}{8\pi s} \int A dt_{(2)} \simeq \frac{1}{16\pi} \int A d\cos\Theta_{2,2'}. \quad (5)$$

The QED loop corrections are represented by diagrams on Fig. 4. We can factorize them upon the Born cross section as follows:

$$d\sigma^{+-xx} = d\sigma_{(2)}^{+-xx} \cdot \frac{\alpha}{2\pi} \cdot \delta_V^{+-xx}, \quad (6)$$

$$\begin{aligned} \delta_V^{+-+-} = & 2 \ln \frac{s}{\lambda^2} \left( 1 - \ln \frac{s}{m^2} \right) + \ln^2 \frac{s}{m^2} + \ln \frac{s}{m^2} + \ln^2 \frac{-u}{s} + \\ & + \frac{s^2}{u^2} \ln^2 \frac{-t}{s} + \left( 1 - \frac{2s}{u} \right) \ln \frac{-t}{s} + \frac{4\pi^2}{3} - 3; \end{aligned} \quad (7)$$

$$\begin{aligned} \delta_V^{--+-} = & 2 \ln \frac{s}{\lambda^2} \left( 1 - \ln \frac{s}{m^2} \right) + \ln^2 \frac{s}{m^2} + \ln \frac{s}{m^2} + \ln^2 \frac{-t}{s} + \\ & + \frac{s^2}{t^2} \ln^2 \frac{-u}{s} + \left( 1 - \frac{2s}{t} \right) \ln \frac{-u}{s} + \frac{4\pi^2}{3} - 3. \end{aligned} \quad (8)$$

Here we have introduced the finite photon mass  $\lambda$  to remove the infrared divergence.

The real photon emission for this process is a pure QED reaction. It is indistinguishable from the  $\gamma\gamma \rightarrow l^+l^-$  process in the infrared (IR) limit and it's singularities cancel ones caused by loop corrections.

The integration over  $d\phi$  leads to (in non-covariant expressions the c.m.s. system is used) [10, 11]

$$\int A d\phi_3 = \frac{1}{24\pi^3} \int \mathcal{J}(A) dv dy = \frac{1}{44\pi^3 s} \int \mathcal{J}(A) \psi_v dv d\cos\Theta_{2,2'}, \quad (9)$$

here

$$\mathcal{J}(A) = \frac{1}{\pi} \int \frac{d^3 k}{\omega} A \delta(Q^2 - m^2 - 2Q_0\omega) \Theta(Q_0 - \omega), \quad (10)$$

$$Q = p_1 + p_2 - p_2'.$$

Using the method of helicity amplitudes [9], one can calculate

$$|M^{+-++}|^2 = e^6 \frac{4 p_1' \cdot p_2' (p_2' \cdot p_2)^2}{p_1' \cdot k \ p_2' \cdot k \ p_1' \cdot p_1 \ p_2' \cdot p_1}, \quad (11)$$

The other non-vanishing amplitudes are obtained from  $|M^{+-++}|$  by using C, P, Bose and crossing (between final and initial particles) symmetries:

$$\begin{aligned} d\sigma^{-\lambda_1, -\lambda_2, -e_1', -e_2', -\lambda_3} &= d\sigma^{\lambda_1, \lambda_2, e_1', e_2', \lambda_3}, \quad (P) \\ d\sigma^{+-+-} &= d\sigma^{+-++} \Big|_{1 \leftrightarrow 2}, \quad (P + \text{Bose}) \\ d\sigma^{+-+-} &= d\sigma^{+-++} \Big|_{1' \leftrightarrow 2'}, \quad (C) \\ d\sigma^{+-+-} &= d\sigma^{+-++} \Big|_{\substack{1 \leftrightarrow 2 \\ 1' \leftrightarrow 2'}}, \quad (CP + \text{Bose}) \\ d\sigma^{+++-} &= d\sigma^{+++-} \Big|_{\substack{3 \leftrightarrow 2 \\ 1' \leftrightarrow 2'}}, \quad (C + \text{crossing}) \\ d\sigma^{+++-} &= d\sigma^{+++-} \Big|_{1' \leftrightarrow 2'}. \quad (C) \end{aligned}$$

The last couple of substitutions leads to the non-divergent leading term of  $\gamma^+ - \gamma^+$  scattering.

It is convenient to perform the integration over the phase-space of the final particles numerically. But the Monte-Carlo methods of numerical analysis [12] require to eliminate all the divergences in the integration expressions.

The "forward-backward" divergences can be deleted by imposing cuts on the scattering angle (in calculation of  $d\sigma/d\cos\Theta$ ) or on the  $(p_i \cdot p_f)$ -invariants (for  $d\sigma/dy$ ). Another singularities should be extracted as a single

expression  $|M|_{sub}^2$ . After this term has been subtracted the matrix element doesn't contain divergences and can be integrated numerically. The singular term  $|M|_{sub}^2$  should be integrated analytically.

The infrared behaviour of helicity amplitudes can be found by covariant expanding (11) of matrix elements into a series around pole  $\omega_{\gamma real} \rightarrow 0$ :

$$\begin{aligned} |M^{+-+ -}|_{IR}^2 &= 16e^6 \frac{s}{v\nu} \frac{u}{t} \left( 1 - \frac{\nu}{s} - \frac{v}{s} \right) + 8e^6 \frac{s}{v\nu} \frac{(v-z)u + (\nu-z)t}{t^2}, \\ |M^{+-+ +}|_{IR}^2 &= 16e^6 \frac{s}{v\nu} \frac{t}{u} \left( 1 - \frac{\nu}{s} - \frac{v}{s} \right) - 8e^6 \frac{s}{v\nu} \frac{(v-z)u + (\nu-z)t}{u^2}. \end{aligned} \quad (12)$$

The first term of each expression has the usual IR-singularity and the rest one is divergent in the massless limit.

The divergences caused by  $p_f \cdot k \rightarrow 0$  can be extracted [11] using the method of peaking approximation:

$$\begin{aligned} |M^{+-+ -}|_{peak}^2 &= 8e^6 \frac{s}{v\nu} \frac{u}{t} \left( 1 - \frac{\nu}{s} + \frac{\nu^2}{s^2} - \frac{v}{s} + \frac{v^2}{s^2} \right), \\ |M^{+-+ +}|_{peak}^2 &= 8e^6 \frac{s}{v\nu} \frac{t}{u} \left( 1 - \frac{\nu}{s} + \frac{\nu^2}{s^2} - \frac{v}{s} + \frac{v^2}{s^2} \right). \end{aligned} \quad (13)$$

Each formula of eqs. (12) and (13) can be combined into the united expression:

$$\begin{aligned} |M^{+-+ -}|_{sub}^2 &= 8e^6 \frac{s}{v\nu} \left( \frac{u}{t} \left( 1 - \frac{\nu}{s} + \frac{\nu^2}{s^2} - \frac{v}{s} + \frac{v^2}{s^2} \right) + \frac{tu' - ut'}{t^2} \right), \\ |M^{+-+ +}|_{sub}^2 &= 8e^6 \frac{s}{v\nu} \left( \frac{t}{u} \left( 1 - \frac{\nu}{s} + \frac{\nu^2}{s^2} - \frac{v}{s} + \frac{v^2}{s^2} \right) - \frac{tu' - ut'}{u^2} \right). \end{aligned} \quad (14)$$

This directly leads to eqs. (12) in the IR-limit. And it differs from (13) on the term that vanishes in the peaking limits due to

$$(v-z)u + (\nu-z)t = (tu' - ut') \xrightarrow{peak} 0. \quad (15)$$

The analytical integration of (14) over the phase-space is performed according to (9). The second term in (14) is only a IR-divergent one. To simplify further calculations we introduce arbitrary value  $\bar{v}$  as an upper bound for it's integration (and subtraction). Neither numerical no analytical part of the result does not depend on  $\bar{v}$  if it is chosen in the region  $m^2 \ll \bar{v} \ll s$  (or  $m^2 \ll \bar{v} \ll (s+t)$  in case of  $y$ -dependent differential cross-section).

The IR-divergences can be factorized upon matrix element in a covariant path as follows

$$M^\lambda = e M^{Born} \left( \frac{p_1' \mu}{p_1' \cdot k} - \frac{p_2' \mu}{p_2' \cdot k} \right) \epsilon_k^\mu, \quad (16)$$

that after squaring gives

$$|M^\lambda|^2 = 4e^2 |M^{Born}|^2 \left( \frac{s'}{v\nu} - \frac{m^2}{v^2} - \frac{m^2}{\nu^2} \right). \quad (17)$$

The  $m^2$ -dependent terms form (17) do not appear in helicity amplitude expressions since setting mass to zero but they should be included in calculations for proper cancelation of divergences.

The result of analitical integration over the phase space of final photon for the "soft" and "collinear" parts of bremsstrahlung is

$$\delta_R^\Theta = 2 \ln \frac{s}{\lambda^2} \left( \ln \frac{s}{m^2} - 1 \right) - \ln^2 \frac{s}{m^2} - \ln \frac{s}{m^2} - \frac{4\pi^2}{3} + \frac{13}{2}. \quad (18)$$

Combining loop correction expressions (7, 8) and the bremsstrahlung contribution (18) one can obtain

$$\delta_R^\Theta + \delta_V^{+-+ -} = \ln^2(1-y) + \frac{1}{(1-y)^2} \ln^2 y + \left( 1 + \frac{2}{1-y} \right) \ln y + \frac{7}{2}, \quad (19)$$

$$\delta_R^\Theta + \delta_V^{+-+ +} = \ln^2(y) + \frac{1}{y^2} \ln^2(1-y) + \left( 1 + \frac{2}{y} \right) \ln(1-y) + \frac{7}{2}. \quad (20)$$

Here  $y$  is the function of angle between initial and final particles:

$$y = \frac{1}{2} (1 - \cos \Theta_{2,2'}). \quad$$

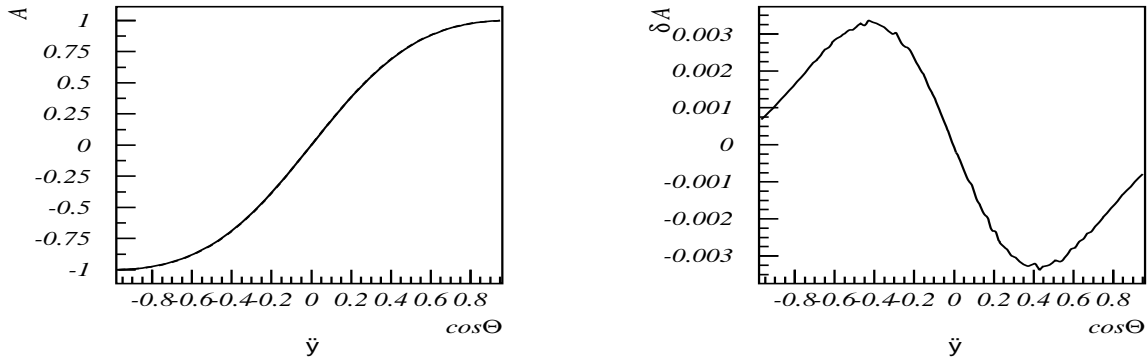


Figure 5. Angular-dependent polarization asymmetry and QED correction contribution  $\delta(A) = A_{tot} - A_{Born}$ .

The integration results for the invariant-dependent spectra are so complicated that can't be outlined here. The final state polarization can scarcely be measured at experiment. That is the reason for summarizing over the helicities of all final particles.

We present here plots for polarization asymmetries and  $\mathcal{O}(\alpha)$ -correction to it (see Figs. 5, 6). The graphs are composed for c.m.s. energy  $\sqrt{s}=120\text{ GeV}$  (the energy of supposed resonant Higgs boson production [13]).

The major feature of  $\gamma\gamma \rightarrow l^+l^-$  process is the small value of cross section if the total angular momentum of  $\gamma\gamma$ -beams equals zero. This polarization selectivity can be useful at the experiment.

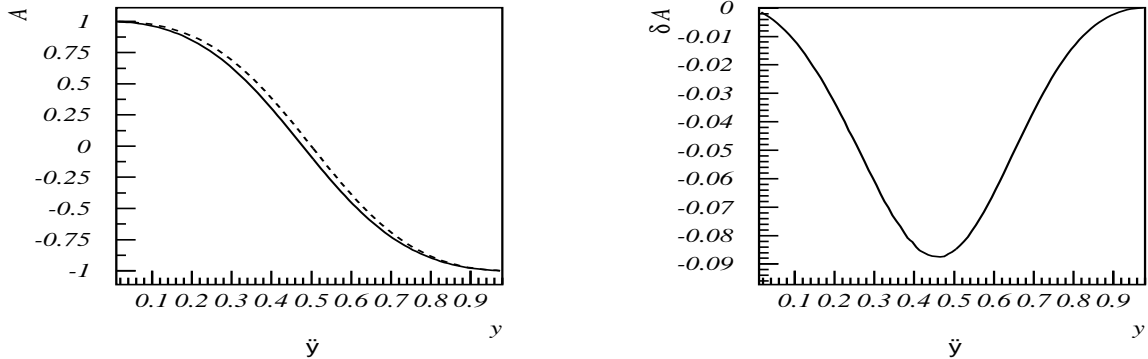


Figure 6. Polarization asymmetry and QED correction contribution  $\delta(A) = A_{tot} - A_{Born}$ .

For the measurement the luminosity of  $J=2$  beams one will use the events of  $\gamma\gamma \rightarrow l^+l^-$  process. The precision of measurement the luminosity of  $J=2$  beams that can be achieved using  $\gamma\gamma \rightarrow l^+l^-$  process can be calculated in the same way that one for  $J=0$  beams. We introduce the  $\omega_{max}$  parameter for the maximal energy of bremsstrahlung photon that will still result the detection of single exclusive  $\gamma\gamma \rightarrow l^+l^-$  event. For the supposed detector parameters ( $\omega_{max}=1\text{ GeV}$ ,  $E_{f,cut}=1\text{ GeV}$ ,  $\Theta_{cut}=7^\circ$ ) one can obtain:

$$\frac{\Delta\mathcal{L}}{\mathcal{L}} \left( \sqrt{s'} > 0.8\sqrt{s'_{max}} \right) = 0.04\%, \quad \frac{\Delta\mathcal{L}}{\mathcal{L}} (m_H \pm 1\text{ GeV}) = 0.1\%.$$

The achieved precision is sufficient for the huge variety of experiments at the photon collider.

## 5 Boson production in $\gamma\gamma$ -collisions

Future high-energy linear  $e^+e^-$  colliders in  $\gamma e$  and  $\gamma\gamma$  mode could be a very useful instrument to explore mechanism of symmetry breaking in electroweak interaction using self couplings test of the  $W$  and  $Z$  bosons in non-minimal gauge models.  $WW$ -production would be provided mainly by  $\gamma\gamma$ -scattering [14]. The Born cross section  $\sigma(\gamma\gamma \rightarrow W^+W^-)$  is about 110pb at 1 TeV on unpolarized  $\gamma$ -beams. Corresponding cross section of  $WW$ -production on electron colliders is an order of magnitude smaller and amounts to 10pb. One needs to consider a reaction  $\gamma\gamma \rightarrow W^+W^-Z$  since its cross section becomes about 5%-10% of the cross section  $WW$ -production at energies  $\sqrt{s} \geq 500$  GeV. The anomalous three-linear [15]  $\gamma WW$  and  $ZWW$  and quartic [16]

$\gamma\gamma WW$ ,  $\gamma ZWW$ ,  $ZZWW$  etc. couplings induce deviations of the lowest-order cross section from the Standard Model.

In order to evaluate contributions of anomalous couplings a cross section of  $\gamma\gamma \rightarrow W^+W^-$  must be calculated with a high precision and extracted from experimental data. Therefore one needs to calculate the main contribution of high order electroweak effects: one-loop correction, real photon and  $Z$  emission.

Lagrangian of three-boson ( $WW\gamma$  and  $WWZ$ ) interaction in the most general form can be presented as

$$\begin{aligned} L_{WWV} = & -g_{WWV}i[g_1^V(W_{\mu\nu}^+W^\mu V^\nu - W_\mu^+V_\nu W^{\mu\nu}) + k_V W_\mu^+W^\nu V^{\mu\nu} + \\ & + i\lambda_V/m_W^2 W_{\lambda\mu}^+W^\mu V^{\nu\lambda} - g_4^V W_\mu^+W^\nu(\partial^\mu V^\nu + \partial^\nu V^\mu) + \\ & + g_5^V \epsilon^{\mu\nu\rho\sigma} (W_\mu^+ \overleftrightarrow{\partial}_\rho W_\nu) V_\sigma + ik_V W_\mu^+W_\nu \tilde{V}^{\mu\nu} + i\tilde{\lambda}_V/m_W^2 W_{\lambda\mu}^+W_\nu^\mu V^{\nu\lambda}]. \end{aligned} \quad (21)$$

Here  $V_\mu$  is the photon or  $Z$ -boson field (correspondingly,  $V = \gamma$  or  $V = Z$ ),  $W_\mu - W^-$ -boson field,

$$W_{\mu\nu} = \partial_\mu W_\nu - \partial_\nu W_\mu, \quad V_{\mu\nu} = \partial_\mu V_\nu - \partial_\nu V_\mu, \quad (22)$$

$\tilde{V}_{\mu\nu} = \frac{1}{2}\epsilon_{\mu\nu\rho\sigma}V^{\rho\sigma}$  and  $A \overleftrightarrow{\partial}_\mu B = A(\partial_\mu B) - (\partial_\mu A)B$ . The parameter of interaction  $g_{WWV}$  are fixed as follows:

$$g_{WW\gamma} = e, \quad g_{WWZ} = e \cos \theta_W. \quad (23)$$

In case of  $WW\gamma$ -interaction the first term corresponds to the minimal interaction (in case of  $g_1^\gamma = 1$ ). The parameters of the second and third terms are connected with magnetic momentum and quadrupole electric one of  $W$ -boson correspondingly as

$$\mu_W = \frac{e}{2m_W}(1 + k_\gamma + \lambda_\gamma), \quad Q_W = \frac{e}{m_W^2}(\lambda_\gamma - k_\gamma). \quad (24)$$

The last two operators parameters are connected with electric dipole moment  $d_W$  as well as quadrupole magnetic moment  $\tilde{Q}_W$ :

$$d_W = \frac{e}{2m_W}(\tilde{k}_\gamma + \tilde{\lambda}_\gamma), \quad \tilde{Q}_W = \frac{e}{m_W^2}(\tilde{\lambda}_\gamma - \tilde{k}_\gamma). \quad (25)$$

In frame of the SM  $WW\gamma$ - and  $WWZ$ -vertices are determined by gauge group  $SU(2) \otimes U(1)$ . In the lowest order of perturbative theory only  $C$ - and  $T$ -invariant corrections exist (in this case  $k_V = 1$ ,  $\lambda_V = 0$ ). However electroweak radiative corrections (loop diagrams with heavy charged fermions) can give significant contribution in  $k_V$  and  $\lambda_V$  as well as  $C$ - and  $T$ -violate interaction.

There are four-boson vertices giving additional independent information about gauge structure of electroweak interaction. The corresponding cross sections give contribution in cross section of boson production in  $e\gamma$ - and  $\gamma\gamma$ -scattering.

If we will consider only the interactions which conserve  $P$ - and  $C$ -symmetry, Lagrangian four-boson interaction includes two 6-dimension operators

$$L_Q^{(6)} = -\frac{\pi\alpha}{4m_W^2} \left[ a_0 F_{\alpha\beta} F^{\alpha\beta} (\vec{W}_\mu \cdot \vec{W}^\mu) + a_c F_{\alpha\mu} F^{\alpha\nu} (\vec{W}^\mu \cdot \vec{W}_\nu) \right], \quad (26)$$

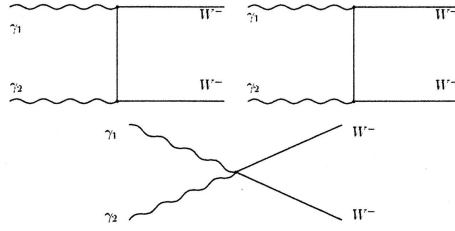
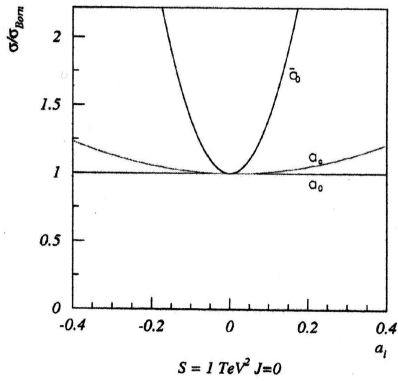
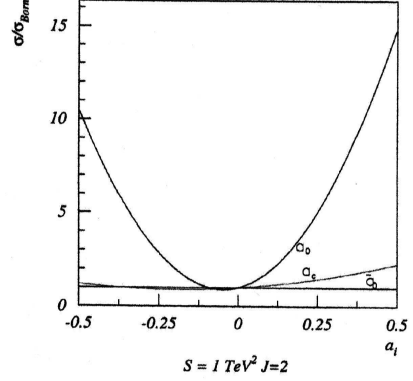
where  $F_{\alpha\beta}$  – tensor of electromagnetic field,  $\vec{W}_\mu$  represent  $W$ -triplet,  $a_0$  and  $a_c$  – anomalous constants. The first term corresponds to neutral scalar exchange. One-loop corrections due to charged heavy fermions give contributions with four-boson vertices to the both terms of the Lagrangian (26).

Charged scalars give contribution proportional to  $a_0$  only.

Since cross section of photoboson production rises to constant value and cross section of electron-positron interaction decreases with energy growth as reverse proportional dependence  $s^{-1}$  when central mass is equal to 500 GeV, the photoproduction of boson cross section is an order bigger than  $e^+e^-$  interaction cross section and is the most important source of information about anomalous boson couplings.

We have considered the anomalous quartic boson vertices. For this purpose the following 6-dimensional  $SU(2)_C$  Lagrangian [16, 17] have been chosen:

$$\begin{aligned} L_0 &= -\frac{e^2}{16\Lambda^2} a_0 F^{\mu\nu} F_{\mu\nu} \vec{W}^\alpha \cdot \vec{W}_\alpha, \\ L_c &= -\frac{e^2}{16\Lambda^2} a_c F^{\mu\alpha} F_{\mu\beta} \vec{W}^\beta \cdot \vec{W}_\alpha, \\ \tilde{L}_0 &= -\frac{e^2}{16\Lambda^2} \tilde{a}_0 F^{\mu\alpha} \tilde{F}_{\mu\beta} \vec{W}^\beta \cdot \vec{W}_\alpha. \end{aligned} \quad (27)$$

Figure 7. The Feynman diagrams for  $W^+W^-$ -productionFigure 8. Dependencies of the ratio  $\sigma/\sigma_{SM}$  on the various couplingsFigure 9. Dependencies of the ratio  $\sigma/\sigma_{SM}$  on the various couplings

where the triplet gauge boson  $\vec{W}_\mu$  and the field-strength tensors

$$F_{\mu\nu} = \partial_\mu A_\nu - \partial_\nu A_\mu, \quad W_{\mu\nu}^i = \partial_\mu W_\nu^i - \partial_\nu W_\mu^i, \quad \tilde{F}_{\mu\nu} = \frac{1}{2} \epsilon_{\mu\nu\rho\sigma} F^{\rho\sigma}$$

are introduced. As one can see the operators  $L_0$  and  $L_c$  are  $C$ -,  $P$ - and  $CP$ -invariant.  $\tilde{L}_0$  is the  $P$ - and  $CP$ -violating operator.

We start from the explicit expression for the amplitude of the process  $\gamma\gamma \rightarrow W^+W^-$

$$M = G_\nu \epsilon_\mu(k_1) \epsilon_\nu(k_2) \epsilon_\alpha(p_+) \epsilon_\beta(p_-) M_T^{\mu\nu\alpha\beta}, \quad (28)$$

where

$$M_T^{\mu\nu\alpha\beta} = \sum_{i=1}^3 M_i^{\mu\nu\alpha\beta}, \quad (29)$$

$k_1, k_2, p_+, p_-$  are four-momenta for the  $\gamma, \gamma, W^+, W^-$  and  $\epsilon_\mu(k_1), \epsilon_\nu(k_2), \epsilon_\alpha(p_+), \epsilon_\beta(p_-)$  their polarizations respectively,

$$G_\nu = e^3 \cot \theta_W.$$

Total cross section of  $\gamma\gamma$ -boson production can be presented as

$$\sigma = \frac{1}{2s} \sum_{\lambda_1 \lambda_2 \lambda_3 \lambda_4} \int |M_{\lambda_1 \lambda_2 \lambda_3 \lambda_4}|^2 d\Gamma, \quad (30)$$

where  $M_{\lambda_1 \lambda_2 \lambda_3 \lambda_4}$  have been defined by eq. (29),  $d\Gamma$  is phase space element of the bosons. The dependence of total cross section  $\sigma(W^+W^-)$  on anomalous parameters was investigated at the following experimental conditions:

- The center-of-mass energy of  $\gamma\gamma(\sqrt{s})$  in  $\gamma\gamma \rightarrow W^+W^-$  is fixed at 1 TeV;
- Photon luminosity  $L$  is supposed to be  $100 \text{ fb}^{-1}/\text{year}$ ;
- In ILC experiments for  $\gamma\gamma$ -scattering polarization states of the photon beams will be fixed by  $J = 0$  or  $J = 2$  states;
- In addition it is assumed that the final  $W$ -bosons will be detected with certain polarization states; and the results are presented in Figs. 8–13.

It is evident that minima of the curves are close to the Standard Model point  $a_i = 0$  since the interference between anomalous and standard part of cross section is very small. Through the region of  $a_i$  is small (about 0.05) the cross section with anomalous constants may reach values of  $1.6\sigma$ . Taking into account a luminosity of photons and beams energy statistical error will be equal to 0.05 %. Therefore for precision analysis of

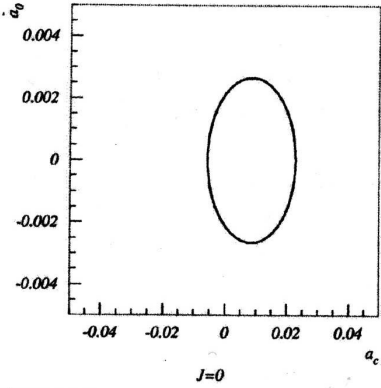


**Figure 10.** Contour plots on  $(a_c, \tilde{a}_0)$  for  $1\delta$  at  $J = 0$  photon beams

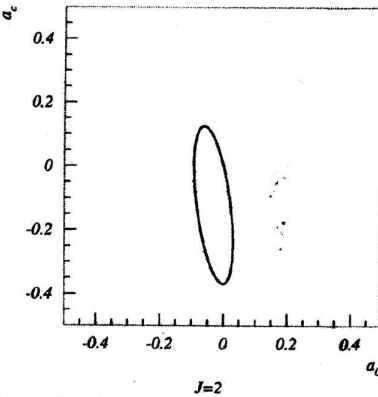


**Figure 11.** Contour plots on  $(a_0, a_c)$  for  $1\delta$  at  $J = 2$  photon beams

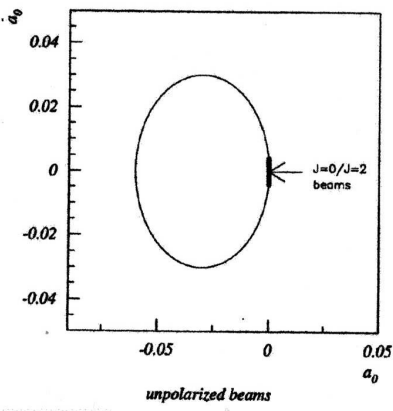


**Figure 12.** Contour plots on  $(a_0, \tilde{a}_0)$  for  $1\delta$

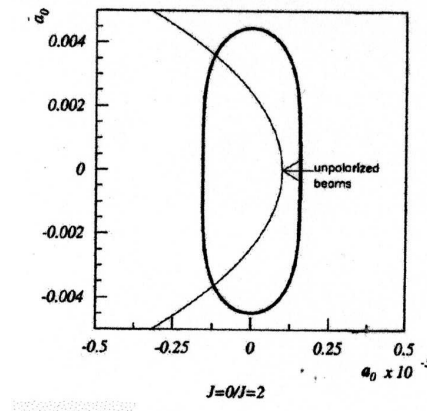


**Figure 13.** Contour plots on  $(a_0, \tilde{a}_0)$  for  $1\delta$

experimental data it is important to calculate radiative corrections. We calculate  $\mathcal{O}(\alpha)$  radiative correction giving maximal contribution to cross section value. It includes real photon emission as well as a set of one-loop diagrams (see. Fig. 14–15). Since of ILC-beams energy exceeds the threshold of three boson production this process must be considered as radiative effect too:

$$d\sigma(\gamma\gamma \rightarrow W^+W^-) = d\sigma^{\text{Born}}(\gamma\gamma \rightarrow W^+W^-) + \frac{1}{s} \Re(M^{\text{Born}} M^{1\text{-loop}*}) d\Gamma^{(2)} + d\sigma^{\text{soft}}(\gamma\gamma \rightarrow W^+W^-\gamma) + d\sigma^{\text{hard}}(\gamma\gamma \rightarrow W^+W^-\gamma) + d\sigma^Z(\gamma\gamma \rightarrow W^+W^-Z). \quad (31)$$

Here  $d\sigma^{\text{soft}}(\gamma\gamma \rightarrow W^+W^-\gamma) = d\sigma^{\text{Born}}(\gamma\gamma \rightarrow W^+W^-)R^{\text{soft}}(\omega)$ , where  $\omega$  is soft photon energy cutoff,

$$R^{\text{soft}} = \frac{2\alpha}{\pi} \left\{ \left[ -1 + \frac{1}{\beta} \left( 1 - \frac{2m_W^2}{s} \right) \ln \frac{1+\beta}{1-\beta} \right] \times \left[ \ln 2\omega + \frac{1}{n-4} - \ln \left( 2\sqrt{\pi} + \frac{C}{2} \right) \right] + \frac{1}{2\beta} \ln \frac{1+\beta}{1-\beta} + \frac{1}{2\beta} \left( 1 - \frac{2m_W^2}{s} \right) \left( \text{Spence} \frac{-2\beta}{1-\beta} - \text{Spence} \frac{2\beta}{1-\beta} \right) \right\}. \quad (32)$$

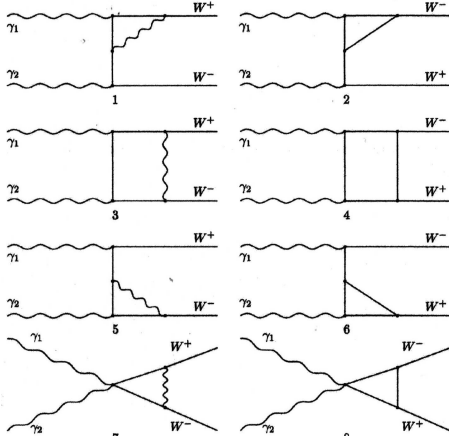
with  $\beta = \sqrt{1 - 4m_W^2/s}$ . The differential cross section of hard photon emission is given by

$$d\sigma^{\text{hard}}(\gamma\gamma \rightarrow W^+W^-\gamma) = d\sigma(\gamma\gamma \rightarrow W^+W^-\gamma) - d\sigma^{\text{soft}}(\gamma\gamma \rightarrow W^+W^-\gamma) \quad (33)$$

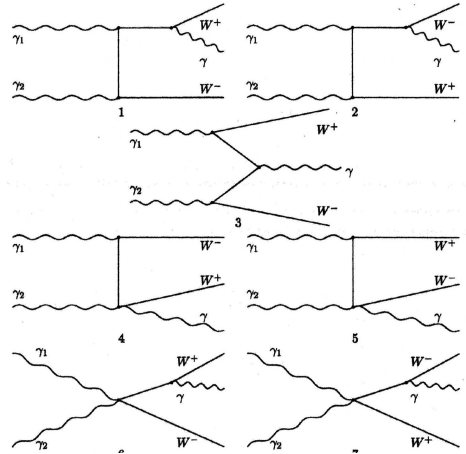
and can not be factorized.  $d\sigma^{\text{soft}}$  and  $d\sigma^{\text{hard}}$  are independent from infrared divergence and from cutoff parameter.

Fig. 16 demonstrates the considered radiative correction has significant magnitude and its calculation increases the precision of anomalous couplings measurement.

It must be noted that consideration of  $W^+W^-\gamma$ ,  $ZZ\gamma$ ,  $Z\gamma\gamma$  processes in electron-positron annihilation gives additional information about  $a_0$  and  $a_e$ , but the precision is two orders worse [18]. But  $e^+e^-$  beams open possibility to measure four-boson connections [18]–[20] such as  $W^+W^-W^+W^-$ ,  $W^+W^-ZZ$ ,  $ZZZZ$ -production



**Figure 14.** The Feynman diagrams of one-loop amplitudes of the  $\gamma\gamma \rightarrow W^+W^-$



**Figure 15.** The Feynman diagrams of  $\gamma\gamma \rightarrow W^+W^-$  accompanied real photon emission

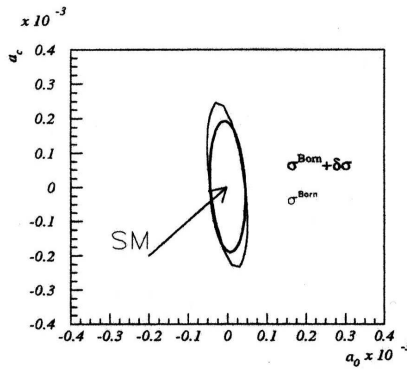


**Figure 16.** Contour plots on  $(a_0, a_c)$  for  $+2\delta$  deviations of  $\sigma(W^+W^-)$

that it's impossible for  $\gamma\gamma$ -physics. Corresponding four-boson anomalous weak interaction are presented by the Lagrangian with two four-dimension operators:

$$L_Q^{(a)} = \frac{1}{4}g_w^2 \left[ g_o \left( \vec{W}_\mu \cdot \vec{W}^\mu \right)^2 + g_c \left( \vec{W}_\mu \cdot \vec{W}^\nu \right) \left( \vec{W}^\mu \cdot \vec{W}_\nu \right) \right]. \quad (34)$$

Here the first operator describes the exchange of neutral scalar particle with very high mass, but the second one corresponds to triplet of massive scalar particles. If four neutral boson vertex ( $ZZZZ$ ) is absent (e.g.  $g_0 = g_c$ ), interaction can be realized by massive vector boson exchange.

Using  $e\gamma$  modes of two-boson production,  $W^+W^-e$ ,  $Z\gamma e$ ,  $ZZe$ ,  $W^-\gamma\nu$ ,  $W^-Z\nu$ , one can consider additional four-boson vertex  $WWZ\gamma$  [21]:

$$L_n^{(6)} = i \frac{\pi\alpha}{m_V^2} a_n \vec{W}_\alpha \left( \vec{W}_\nu \cdot \vec{W}_\mu^\alpha \right) \vec{F}^{\mu\nu}. \quad (35)$$

This Lagrangian conserves  $U(1)_{EM}$ ,  $C$ -,  $P$ - and  $SU(2)_C$ -symmetry, but violates  $SU(2)_L \otimes U(1)_Y$  symmetry.

From all above mentioned processes the most sensitive reactions for  $a_0$  and  $a_e$  investigation are  $ZZe$  and  $WW\gamma$ -production. The bounds of these constants magnitudes are one order better than in  $e^+e^-$ -process, but about 5 times worse than in  $\gamma\gamma$ -mode. The vertices  $\gamma\gamma\gamma Z$  and  $4\gamma$  are absent on tree level. One-loop contribution contain both fermion loops and  $W$ -boson loops. The last ones give contribution to be measured on photon collider [22].

## 6 Conclusion

We have analyzed the possible usage of  $\gamma\gamma \rightarrow f\bar{f}\gamma$  reaction for the luminosity measurement at  $J=0$  beams on linear photon collider. The achievable precision of the luminosity measuring is considered and calculated. The optimal conditions for that measurement are found (for the high magnitude of  $J=0$  cross section and small  $J=2$  background). The first-order QED correction to  $\gamma\gamma \rightarrow l\bar{l}$  cross section is calculated and analyzed at  $J=2$ -beams.

The considered process gives the excellent opportunity for luminosity measurements with substantial accuracy.

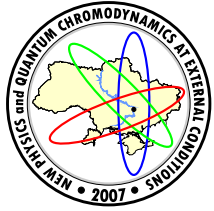
The investigation of the sensitivity of process of  $\gamma\gamma \rightarrow W^+W^-$  and  $\gamma\gamma \rightarrow W^+W^-Z$  to genuine anomalous quartic couplings  $a_0$ ,  $a_c$  and  $\tilde{a}_0$  was performed at center-of-mass energy  $\sqrt{s} = 1 \text{ TeV}$ . It was discovered that two-boson production has great sensitivity to anomalous constants  $a_c$  and  $a_0$  but process  $\gamma\gamma \rightarrow W^+W^-Z$  is more suitable for study of  $\tilde{a}_0$ .

The fact that the minimum of the curves are close to the SM point  $a_i = 0$  demonstrates the small value of the anomalous and the standard part interference. The first-order radiative correction to cross section  $\sigma(\gamma\gamma \rightarrow W^+W^-)$  has significant magnitude and its calculation increases the precision of the  $a_0$  and  $a_c$  measurement.

The theoretical analysis demonstrates that investigation of four-boson anomalous weak interaction in frame of four-dimension anomalous Lagrangian of  $\gamma\gamma$  scattering as well as in frame of  $e\gamma$  modes of two-boson production have great importance for reconstruction gauge group of electroweak interaction beyond the Standard theory of electroweak interaction.

## References

- [1] I.F.Ginzburg, G.L.Kotkin, V.G.Serbo and V.I.Telnov, Nucl.Instr.Meth. **205**, 47 (1983);  
I.F.Ginzburg, G.L.Kotkin, S.L.Panfil, V.G.Serbo and V.I.Telnov, Nucl.Instr.Meth. **219**, 5 (1984).
- [2] E.A.Kuraev, M.V.Galynskii, M.I.Levchuk, Phys.Part.Nucl. **31**, 76 (2000), Fiz.Elem.ChastAtom.Yadra **31**, 155 (2000);  
V.Telnov, Nucl.Instr.Meth. **A494**, 35 (2002), hep-ex/0207093.
- [3] T.V.Shishkina and V.V.Makarenko, hep-ph/0212409;  
V.Makarenko, K.Mönig, T.Shishkina, Eur.Phys.J. **C30**, d01, 011 (2003), LC-PHSM-2003-016, hep-ph/0306135;  
V.V.Makarenko and T.V.Shishkina, hep-ph/0310104.
- [4] V.V.Makarenko and T.V.Shishkina, Proceedings of 8th International School-Seminar On The Actual Problems Of Microwold Physics, Gomel (2003).
- [5] A.Denner and S.Dittmaier, Eur.Phys.J. **C9**, 425 (1999), hep-ph/9812411.
- [6] M.Moretti, Nucl.Phys. **B484**, 3 (1997), hep-ph/9604303;  
M.Moretti, hep-ph/9606225.
- [7] C.Carimalo, W.da Silva, F.Kapusta, Nucl.Phys.Proc.Suppl. **82**, 391 (2000), hep-ph/9909339.
- [8] T.Shishkina and I.Sotsky, hep-ph/0312208.
- [9] P.de Causmaecker *et al.*, Nucl.Phys. **B206**, 53 (1982);  
F.A.Berends *et al.*, Nucl.Phys. **B206**, 61 (1982).
- [10] D.Yu.Bardin and N.M.Shumeiko, Nucl.Phys. **B127**, 242 (1977).
- [11] T.V.Kukhto(Shishkina), N.M.Shumeiko, S.I.Timoshin, J. Phys. G: Nucl.Phys. **13**, 725 (1987).
- [12] S.Weinzierl, NIKHEF-00-012, hep-ph/0006269.
- [13] D.L.Borden and D.A.Bauer, D.O.Caldwell, Phys.Rev. **D48**, 4018 (1993);  
J.F.Gunion and H.E.Haber, Phys.Rev. **D48**, 5109 (1993).
- [14] K.Hagiwara *et al.*, Nucl.Phys. **B282**, 253, (1987).
- [15] G.Belander *et al.*, Eur.Phys.J. **C283**, 376 (2006); hep-ph/9908254.
- [16] I.Marfin and T.Shishkina, Nonlin.Phen. in Compl.Syst. **8**, 4 150 (2005); Elem.Part. and Field **69**, 4 710 (2006).
- [17] A.Denner *et al.*, Eur.Phys.J. **C20**, 201 (2001); hep-ph/0104057.
- [18] G.Belander and F.Boundjema, Phys.Lett. **B288**, 201 (1992).
- [19] V.Barger, T.Han, R.J.N.Phillips, Phys.Rev. **D39**, 146 (1989).
- [20] C.Grosse-Knetter and D.Schidknecht, Phys.Lett. **B302**, 309 (1993).
- [21] O.J.P.Eboli, H.C.Gonzalez-Garcia, S.F.Novaes, Nucl.Phys. **B411**, 381 (1994).
- [22] G.Jikia and A.Thahbladze, Phys.Lett. **B332**, 441 (1994); Phys.Lett. **B223**, 453 (1994).



## COHERENT EFFECTS IN RADIATION AT COLLISIONS OF SHORT BUNCHES OF HIGH ENERGY PARTICLES

N. F. Shul'ga,<sup>a</sup>, D. N. Tyutyunnik<sup>b</sup>

National Science Center “Kharkov Institute of Physics and Technology”,  
 Kharkov, Ukraine

Conditions for the coherent effect in radiation at collision of relativistic electron with a bunch of relativistic particles are analysed. The factors leaded to the destruction of this effect are considered. It is shown, that the transversal distances responsible for this process are greater than the coherent length of the radiation process. The reason of this is concluded in long-distant type of an electron interaction with the bunch.

### 1 Introduction

The coherent effect in radiation at collision of relativistic electron with a short and narrow bunch of relativistic particles is possible. The spectral density of radiation is proportional in this case to the square of particles number in the bunch [1–5]. In proposed paper conditions for arising of this effect and factors leaded to it's destruction are discussed. The main attention was paid to the analysis of longitudinal and transversal distances, which are important for this process.

### 2 Radiation by relativistic electron in the field of falling bunch of relativistic particles

Consider the radiation process in the region of low frequencies of radiated waves, arising at collision of relativistic electron with the falling bunch of relativistic particles. Consideration will be given in the frame of classical radiation theory. The applicability of this approach in the considered problem was given in [5].

In classical electrodynamics spectral and angular radiation density is determined by the electron trajectory  $\vec{r}(t)$  in an external field [6]

$$\frac{dE}{d\omega d\Omega} = \frac{e^2}{4\pi^2} \left| \vec{k} \times \vec{I} \right|^2, \quad \vec{I} = i \int_{-\infty}^{\infty} dt e^{i(\omega t - \vec{k}\vec{r}(t))} \frac{d}{dt} \frac{\vec{v}(t)}{\omega - \vec{k}\vec{v}(t)}, \quad (1)$$

where  $\vec{v}(t)$  is the velocity vector of an electron,  $\omega$  and  $\vec{k}$  are the frequency and wave vector of an emitted wave,  $\omega = |\vec{k}|$ ,  $d\Omega$  is the element of solid angle in the emission direction (we suppose that the speed of light is equal to unity).

The electron trajectory  $\vec{r}(t)$  in the field of incident bunch is determined by the equation of motion

$$\dot{\vec{v}} = \frac{e}{\varepsilon} \left[ \vec{E} + \vec{v} \times \vec{H} - \vec{v}(\vec{v} \cdot \vec{E}) \right], \quad (2)$$

where  $\varepsilon$  is the electron energy,  $\vec{E}$  and  $\vec{H}$  are, respectively, electric and magnetic fields of the moving particle bunch ( $\vec{E} = -\nabla\varphi - \partial\vec{A}/\partial t$ ,  $\vec{H} = \nabla \times \vec{A}$ ). The scalar  $\varphi$  and vector  $\vec{A}$  potentials of the bunch are determined by the expressions

$$\varphi = \sum_n \frac{Q}{[(z - z_n + v_p t)^2 + |\rho - \rho_n|^2 / \gamma_p^2]^{1/2}}, \quad \vec{A} = \vec{v}_p \varphi, \quad (3)$$

where  $Q$  is the charge of bunch particle,  $\gamma_p$  is the Lorentz factor of particles in the bunch,  $(z_n, \rho_n)$  are the coordinates of particles at  $t = 0$ ,  $z$  and  $\rho$  are the coordinates parallel and orthogonal to the initial electron velocity  $\vec{v}_0$  and  $\vec{v}_p$  is the velocity of incident particles ( $\vec{v}_p$  is assumed to be directed along the negative  $z$  semiaxis and identical for all particles in the bunch). Summation in Eqs. (2) takes over all bunch particles.

Characteristic scattering angles of relativistic electron in the field of bunch particles are small. Therefore the electron velocity can be written in the form

$$\vec{v}(t) = \vec{v}_0 \left( 1 - \frac{1}{2} \vec{v}_\perp^2 \right) + \vec{v}_\perp(t) \quad (4)$$

where  $\vec{v}_\perp(t)$  are the electron-velocity components orthogonal to the velocity  $\vec{v}_0$  of the incident electron,  $|v_\perp| \ll |v_0|$ . The electron is supposed to move along the axis of falling bunch.

Using the smallness of electrons scattering angles  $\vartheta \sim v_\perp/v_0$ , the Eq. (1) can be expanded on this angle. In the first-order of that approach the spectral density of radiation takes the form [6]

$$\frac{dE}{d\omega} = \frac{e^2}{2\pi} \omega \int_{\delta}^{\infty} \frac{dq}{q^2} \left[ 1 - 2\frac{\delta}{q} \left( 1 - \frac{\delta}{q} \right) \right] \left| \vec{W}(q) \right|^2 , \quad (5)$$

where  $\vec{W}(q)$  is the Fourier transformation of orthogonal component of an electron acceleration,

$$\vec{W}(q) = \int_{-\infty}^{\infty} dt e^{iqt} \dot{\vec{v}}_\perp(t), \quad (6)$$

$\delta = \omega/(2\gamma^2)$ ,  $q = \omega - \vec{k} \vec{v}_0$  and  $q \geq \delta$ .

The expression (4) holds, if the condition  $\gamma\vartheta \ll 1$  is fulfilled. This corresponds to the dipole approximation in the classical radiation theory [6].

It is necessary to know the transverse electron-velocity component  $\vec{v}_\perp(t)$  for determination of  $\vec{W}(q)$ . In view of the relation  $\vec{v} \times (\nabla \times \vec{A}) = -\nabla\varphi - \vec{v}_p(\vec{v} \cdot \nabla)\varphi$ , it is easy to check, that Eq. (2) for  $\vec{v}_\perp(t)$  can be written, to the terms of the order of  $\gamma^{-2}$  and  $v_\perp^2/v^2$  in the form

$$\frac{d}{dt} \vec{v}_\perp = -\frac{2e}{\varepsilon} \frac{\partial \varphi}{\partial \vec{\rho}}. \quad (7)$$

Substituting (2) and (1) into (7), we have

$$\vec{W}(q) = -\frac{2eQ}{\varepsilon} \frac{\partial}{\partial \vec{\rho}(t)} \sum_n \int_{-\infty}^{\infty} dt e^{iqt} \frac{1}{[(z(t) - z_n + \nu_p t)^2 + |\vec{\rho}(t) - \vec{\rho}_n|/\gamma_p^2]^{1/2}}.$$

The electron trajectory in the field of particles bunch is close to rectilinear. Therefore the solution of Eq. (1) can be obtained as an expansion by the potential  $\varphi$ . In the first order of such expansion  $\vec{r}(t) \approx \vec{v}_0 t + \vec{\rho}$  and for  $\vec{W}(q)$  we get the next expression

$$\vec{W}(q) = -\frac{2eQ}{\varepsilon} \frac{\partial}{\partial \vec{\rho}} \sum_n \int_{-\infty}^{\infty} dt e^{iqt} \frac{1}{[(\nu_0 t - z_n + \nu_p t)^2 + |\vec{\rho} - \vec{\rho}_n|/\gamma_p^2]^{1/2}}. \quad (8)$$

Carrying out the substitution  $t \rightarrow t + z_n/(2\nu_p)$  in this expression, we receive the next expression for (7):

$$\vec{W}(q) = -\frac{2eQ}{\varepsilon} \frac{\partial}{\partial \vec{\rho}} \sum_n \exp\left(i \frac{qz_n}{2\nu_p}\right) \int_{-\infty}^{\infty} dt e^{iqt} \frac{1}{[(2\nu_p t)^2 + |\vec{\rho} - \vec{\rho}_n|/\gamma_p^2]^{1/2}}. \quad (9)$$

After integrating by  $t$ , we can find that

$$\vec{W}(q) = -\frac{eQq}{\varepsilon\gamma} \sum_n \exp\left(i \frac{qz_n}{2\nu_p}\right) \frac{\vec{\rho} - \vec{\rho}_n}{|\vec{\rho} - \vec{\rho}_n|} K_1\left(\frac{q}{2\nu_p} \frac{|\vec{\rho} - \vec{\rho}_n|}{\gamma_p}\right), \quad (10)$$

where  $K_1(x)$  is the McDonald first-order function.

If the condition  $\rho \gg \rho_n$  is hold, the Eq. (2) takes the form

$$\vec{W}(q) = -\frac{eQq}{\varepsilon\gamma} \frac{\vec{\rho}}{\rho} K_1\left(\frac{q}{2\nu_p} \frac{\rho}{\gamma_p}\right) \sum_n \exp\left(i \frac{qz_n}{2\nu_p}\right). \quad (11)$$

### 3 Coherent effect in radiation

The main contribution in the integral in (4) gives the values  $q \sim \delta$ . If the condition  $\delta\Delta t \ll 1$  is hold, then we have

$$\vec{W} \approx v_0 \vec{\vartheta}_N, \quad (12)$$

where  $\Delta t$  is the time interval, when the bunch field has an influence on the particle and  $\vec{\vartheta}_N$  is the full scattering angle of electron on  $N$  particles of the bunch,

$$\vec{\vartheta}_N = \frac{2eQ}{\varepsilon} \sum_n \frac{\vec{\rho} - \vec{\rho}_n}{|\vec{\rho} - \vec{\rho}_n|^2}. \quad (13)$$

In this case

$$\frac{dE}{d\omega} = \frac{2e^2}{3\pi} \gamma^2 \vartheta_N^2. \quad (14)$$

For distances  $\rho \gg \rho_n$  we have  $\vec{\vartheta}_N = N \frac{2eQ}{\varepsilon\rho} \frac{\vec{\rho}}{\rho}$  and therefore

$$\frac{dE}{d\omega} = N^2 \frac{8e^4 Q^2}{3\pi m^2 \rho^2}. \quad (15)$$

Thus if the conditions  $\delta\Delta t \ll 1$  and  $\gamma\vartheta \ll 1$  are hold the coherent effect in radiation takes place, for which  $E' \sim N^2$ .

Let us consider now applicability conditions of (10).

If  $\rho \rightarrow 0$  holds the value  $E'$  has a fast increasing. However this increasing is limited by two applicability conditions of this formula. First condition is connected with the dispersion of particle positions in the orthogonal plane. Supposing that this dispersion is Gaussian, we can get the next expression for  $\langle |\vartheta_N| \rangle$  [7]:

$$\langle |\vartheta_N| \rangle = \frac{2NeQ}{\varepsilon\rho} \left[ 1 - \exp\left(-\frac{\rho^2}{\bar{u}^2}\right) \right], \quad (16)$$

where  $\bar{u}^2$  is the average square of particle shift relative to the bunch axis.

If  $\rho \rightarrow 0$  holds the angle value  $\langle |\vartheta_N| \rangle \rightarrow 0$ . The maximum of this value has been reached at  $\rho \sim \sqrt{\bar{u}^2}$ . Therefore if  $\rho \gg \sqrt{\bar{u}^2}$  holds the spectral density  $E'$  is defined by the formula (10), whereas if  $\rho \rightarrow 0$  holds, then  $E' \rightarrow 0$ .

This result is true if the condition  $\gamma \langle |\vartheta_N| \rangle \ll 1$  is hold. But if this condition is violated in the maximum of Eq. (11), i.e. at  $\rho \sim \sqrt{\bar{u}^2}$ , then we must to account the effect, connected with the nondipolarity of radiation. The account of this effect can be simply taken if the condition

$$\frac{\delta^{-1}}{1 + \gamma^2 \vartheta_N^2} \gg \Delta t \quad (17)$$

holds. Really, if this condition holds the exponential factor in (1) can be replaced by the unity and therefore

$$\vec{I} = i \left( \frac{\vec{v}'}{\omega - \vec{k}\vec{v}'} - \frac{\vec{v}_0}{\omega - \vec{k}\vec{v}_0} \right), \quad (18)$$

where  $\vec{v}'$  is the final vectors of the electron velocity. In this case for the spectral density of radiation we have [6]

$$\frac{dE_N}{d\omega} = \frac{2e^2}{\pi} \left[ \frac{2\xi^2 + 1}{\xi\sqrt{\xi^2 + 1}} \ln(\xi + \sqrt{\xi^2 + 1}) - 1 \right], \quad (19)$$

where  $\xi = \xi_N = \gamma\vartheta_N/2$  is the nondipolarity parameter. If the condition  $\xi_N \ll 1$  is hold, the expression (16) is transformed into the corresponding result of dipole approximation (8). But for the case when  $\xi_N \gg 1$ , we have

$$\frac{dE_N}{d\omega} = \frac{4e^2}{\pi} \ln 2\xi_N = \frac{4e^2}{\pi} \ln \left( N \frac{2eQ}{m\rho} \right). \quad (20)$$

Thus, the account of nondipolarity effect in radiation at  $\xi_N \gg 1$  leads to the suppression of coherent radiation – square dependence of  $E'$  is replaced by the weak logarithmic dependence with the increasing of  $N$  in this case. This means that the increasing of particles number in the bunch doesn't have an influence at radiation, if the condition  $\xi_N > 1$  holds. This effect of suppression of coherent radiation is an analog of the suppression effect in radiation by relativistic particles in a thin layer of matter [8].

Thus, the coherent effect in this problem takes place up to the values of  $N$  and  $\rho$ , which are defined by the relation

$$N \frac{2e^2}{m\rho} \sim 1. \quad (21)$$

If  $N \sim 10^{10}$ , then the coherent effect in radiation is destroyed for a particles, that has an impact parameter  $\rho \leq 10^{-2}$  cm.

#### 4 Efficiency of radiation

Above mentioned formulas are related to the electron radiation for given impact parameter  $\rho$ . Let us consider now peculiarities of radiation for the electron flow. If the distribution of particles in the initial electron flow has Gaussian form on impact parameters  $\rho$ , the average spectral density of radiation has the following form

$$\left\langle \frac{dE}{d\omega} \right\rangle = \frac{1}{\pi \bar{\Delta}^2} \int d^2 \rho \exp(-\rho^2/\bar{\Delta}^2) \frac{dE}{d\omega}, \quad (22)$$

where  $\bar{\Delta}^2$  is the mean square displacement of electrons relative to  $z$ -axis.

The formula (8) determines the radiation by homogeneous flow of electrons if  $\bar{\Delta}^2 \rightarrow \infty$ . The mean spectral density of radiation is connected for this case with the efficiency of radiation  $dK/d\omega$  by the following relation:

$$\left\langle \frac{dE}{d\omega} \right\rangle = \frac{1}{S} \frac{dK}{d\omega}, \quad (23)$$

where  $S$  is the orthogonal cross-section for the particles flow and

$$\frac{dK}{d\omega} = \int d^2 \rho \frac{dE(\vec{\rho})}{d\omega}. \quad (24)$$

Let us determine typical values of  $\rho$  which gives the main contribution for efficiency of radiation. Taking into account that the particle potential in the bunch is a long-distance potential, the special interest will be connected with the analysis of large  $\rho$  values contribution.

At  $\delta\Delta t \ll 1$  for large  $\rho$  values ( $\rho \gg \rho_n$ ) the underintegration function (12) is determined by relation (10). Using this expression for the spectral density  $dE/d\omega$  in (12) we found that the integral on  $\rho$  in (12) is divergent for both low and large values of impact parameters. Let us consider factors which remove these divergences.

This divergence is removed for low values of  $\rho$  by taking into account the distribution of bunch particles on impact parameter. We have according (11) for this case  $\rho_{\min} \sim \sqrt{\bar{u}^2}$ . But for  $\sqrt{\bar{u}^2} \rightarrow 0$  the value  $\rho_{\min}$  will be determined from validity condition of dipole approximation (7). So

$$\rho_{\min} \sim \max \left\{ \frac{\sqrt{\bar{u}^2}}{2Ne^2/m} \right\}. \quad (25)$$

Let us consider now the range of large  $\rho$  values.

The formula (10) for spectral density of radiation is valid if the coherent length  $l_c \sim \delta^{-1}$  is larger than the longitudinal size of the bunch

$$\delta^{-1} \gg L/2. \quad (26)$$

Except, it is needed that the condition

$$\rho \ll 2\gamma l_c \quad (27)$$

was fulfilled for  $q \sim \delta$ .

For the region  $\rho \gg 2\gamma l_c$  according to (5) and (10) we have the exponential decreasing for  $d/d\omega$ . So the main contribution for efficiency of radiation is determined by the region of impact parameters

$$\rho \leq \rho_{\max} \sim 2\gamma l_c. \quad (28)$$

Let us mark that these values of  $\rho_{\max}$  are in  $\gamma$  times more than the coherence length  $l_c$ . It is well known that  $\rho_{\max} \sim l_c$  for the rest charge. The additional term  $\gamma$  in (28) is caused by relativistic compression of Coulomb field of bunch particles.

The reason for changing of radiation character at  $\rho > \rho_{\max}$  relative to  $\rho < \rho_{\max}$  is in following. At  $l_c \gg l_{scat}$ , where  $l_{scat}$  is the length where we have the scattering, for  $\rho < \gamma l_c$  the scattering is on the distances of bunch length  $l_{scat} \sim L/2$ . The exponent  $\exp[iqz_n/(2v)]$  in (9) for this case is possible to change by unity and the same changing is possible to do for the exponential factor in underintegral expression. As a result we obtained the formula (8) for  $\vec{W}(q)$ . The electron is received the angle  $\vec{\vartheta}_N$  for this case at the distance of  $l_{scat} \sim L/2$ .

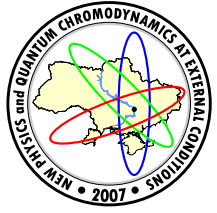
For  $\rho > \gamma l_c$  the exponential factor  $\exp[iqz_n/(2v)]$  in (9) is also possible to change by unity. But it is not possible to do such changing for the exponential factor  $\exp(iqt)$  in (9). The scattering angle of the particle is received for this case on the length  $l_{scat} \sim l_c$ . The condition  $l_{scat} \ll l_c$  is destroyed and consequently the formula (10) is not valid.

#### 5 Conclusions

The coherent effect in radiation is possible at collision of relativistic electron with a short and narrow bunch of relativistic particles. This effect takes place if the coherent radiation length  $l_c$  is large with respect to the longitudinal bunch length  $L$  and if the validity condition for dipole of radiation is fulfilled. The orthogonal distances, for which this effect holds, has the macroscopic size  $\rho_{\max} \sim \gamma l_c$ . This value  $\rho_{\max}$  is much more than the bunch length  $L$  and the coherent radiation length  $l_c$ . Such large values  $\rho_{\max}$  are caused with the long-distance Coulomb potential of relativistic particles of bunch.

## References

- [1] I.F. Ginzburg, G.L. Kotkin, S.I. Polityko, V.G. Serbo, Sov.J.Nucl.Phys **55**, 1847 (1992); **55**, 1855 (1992).
- [2] I.F. Ginzburg, G.L. Kotkin, S.I. Polityko and V.G. Serbo, Z.Phys **60**, 737 (1993).
- [3] S.I. Kotkin and V.G. Serbo, Phys.Rev. **E51**, 2493 (1995).
- [4] M.Bassetti, J.Bosser, M.Gygi-Henney, A.Hoffmann, E.Keil and R. Coisson, IEEE Trans.Nucl.Sci. NS **30**, 2182 (1983).
- [5] N.F. Shul'ga, D.N. Tyutyunnik, JETP Lett. **78**, 700 (2003).
- [6] A.I. Akhiezer and N.F. Shul'ga, *High-Energy Electrodynamics in Matter*, Gordon and Breach Pub., Amsterdam, 1996.
- [7] N.F. Shul'ga, D.N. Tyutyunnik, On coherent radiation and scattering at collisions of relativistic electrons with short and long bunches of relativistic particles, Proc. of *SPIE*, v.5974, 147 (2005).
- [8] N.F. Shul'ga, S.P. Fomin, JETP **86**, 32 (1998).



## NEW (VIRTUAL) PHYSICS IN THE ERA OF THE LHC

M.I. Vysotsky<sup>b</sup>

Institute of Theoretical and Experimental Physics, Moscow, Russia

A simple extension of the Standard Model demonstrates that New Physics non-reachable through direct production at LHC can induce up to 10% corrections to the Standard Model value of parameter  $\varepsilon_K$  and to the frequencies of  $B_d - \bar{B}_d$  and  $B_s - \bar{B}_s$  oscillations.

Let us imagine the worst scenario: the only new particle found at the LHC will be the Higgs boson of the Standard Model (SM). A natural question arises: is it possible to find traces of New Physics in low energy observables without observing the production of new particles at LHC? Another facet of this question: What changes of the unitarity triangle can be produced by such particles? This is the problem we will focus on.

In order to influence the quark weak currents the new particles should be strongly interacting. The natural example would be the fourth quark-lepton family: the fourth generation quarks deform unitarity triangle into unitarity quadrangle. However since the sequential fourth generation gets masses through Higgs mechanism, its quarks cannot be heavier than 1 TeV: so, they will be directly produced at LHC. That is why the heavy particles we are looking for should get their masses from a different source. So their contributions to low energy observables decouple, being suppressed as  $(\eta/M)^2$ , where  $\eta = 246$  GeV is the Higgs boson neutral component expectation value and  $M$  characterizes new particles masses,  $M \geq 5$  TeV in order to avoid their production at LHC. These 1% corrections are too small to be detected taken into account relatively low accuracy of theoretical formulas. Nevertheless we manage to find a model where corrections are enhanced and can be detected.

Let us study the extension of SM by  $SU(2)_L$  singlet heavy Dirac quark  $Q$  with electric charge +2/3 which mixes with the top quark. Recently the constraints from the  $B \rightarrow X_s \gamma$  branching ratio and electroweak precision observables in this model have been studied [1]. Authors of [1] are interested in manifestations of rather light  $Q$  with mass just above Tevatron bound. As a consequence  $Q$  mixes strongly with the top quark in their model. So our model with much heavier  $Q$  which mixes weakly with top (see below) can be considered as complementary to [1].

The model is described by the following lagrangian:

$$\mathcal{L} = \mathcal{L}_{SM} - M \bar{Q}' Q' + \left[ \mu_R \bar{Q}'_L t'_R + \frac{\mu_L}{\eta/\sqrt{2}} H^+ \bar{Q}'_R \begin{pmatrix} t' \\ b' \end{pmatrix}_L + c.c. \right], \quad (1)$$

where  $\mathcal{L}_{SM}$  is the SM lagrangian,  $M$ ,  $\mu_R$  and  $\mu_L$  are the parameters with the dimension of mass. The term proportional to  $M$  contains Dirac mass of the field  $Q'$  which is primed since it is not a state with a definite mass due to mixing with  $t$ -quark. The term proportional to  $\mu_R$  describes the mixing of two  $SU(2)_L$  singlets:  $Q'_L$  and  $t'_R$ , the latter being the right component of  $t$ -quark field in the Standard Model (in the absence of terms in square brackets). Finally, the term proportional to  $\mu_L$  describes mixing of a weak isodoublet with  $Q'$ . An upper component of this isodoublet is the left component of the field  $t'$  which would be  $t$ -quark without the terms in square brackets:

$$t'_L = U_{t't''}^L t''_L + U_{t'c'}^L c'_L + U_{t'u'}^L u'_L, \quad (2)$$

where  $t''$ ,  $c'$  and  $u'$  are the primary fields of SM lagrangian, while  $U_{ik}^L$  are the matrix elements of matrix  $U^L$  which transforms the primary fields  $c'_L$  and  $u'_L$  to the left-handed components of the mass eigenstates  $c$  and  $u$  and field  $t''_L$  to the field  $t'_L$  which would be the left-handed component of the top quark in the case  $\mu_L = \mu_R = 0$ . We do not mix  $Q$ -quark with  $u$ - and  $c$ - quarks in order to avoid FCNC which may induce too large  $D^0 - \bar{D}^0$  oscillations.

One can easily see that the lower component of the isodoublet is the combination of the down quark fields with definite masses rotated by CKM matrix  $V$ :

$$b'_L = V_{tb} b_L + V_{ts} s_L + V_{td} d_L. \quad (3)$$

In order to find the states with definite masses which result from  $t'-Q'$  mixing, the following matrix should

e-mail: <sup>a</sup>vysotsky@itep.ru

© Vysotsky M.I., 2007.

be diagonalized:

$$(\overline{t'_L t'_R Q'_L Q'_R}) \begin{pmatrix} 0 & m_t & 0 & \mu_L \\ m_t & 0 & \mu_R & 0 \\ 0 & \mu_R & 0 & -M \\ \mu_L & 0 & -M & 0 \end{pmatrix} \begin{pmatrix} t'_L \\ t'_R \\ Q'_L \\ Q'_R \end{pmatrix} , \quad (4)$$

where  $m_t$  is the mass of  $t$ -quark in SM. For the squares of masses of the eigenstates we get:

$$2(\lambda^2)_{t,Q} = M^2 + \mu_R^2 + \mu_L^2 + m_t^2 \mp \sqrt{(M^2 + \mu_R^2 + \mu_L^2 + m_t^2)^2 - 4M^2 m_t^2 - 4\mu_L^2 \mu_R^2 + 8m_t \mu_R \mu_L M} , \quad (5)$$

and the eigenstates look like (in what follows we put  $m_t = 0$ <sup>1</sup>):

$$t = t'_L + (1 - \frac{\lambda_t^2}{\mu_L^2}) \frac{\mu_R \mu_L}{\lambda_t M} t'_R + \frac{\mu_L}{M} (1 - \frac{\lambda_t^2}{\mu_L^2}) Q'_L + \frac{\lambda_t}{\mu_L} Q'_R , \quad (6)$$

$$\lambda_t = \frac{\mu_R \mu_L}{M} \left( 1 - \frac{\mu_R^2 + \mu_L^2}{2M^2} \right) + O(\frac{1}{M^5}) , \quad (7)$$

$$Q = Q'_R + (-\frac{\lambda_Q}{M} + \frac{\mu_L^2}{\lambda_Q M}) Q'_L + \frac{\mu_L}{\lambda_Q} t'_L + \frac{\mu_R}{M} \left( \frac{\mu_L^2}{\lambda_Q^2} - 1 \right) t'_R , \quad (8)$$

$$\lambda_Q = -M + O\left(\frac{1}{M}\right) , \quad (9)$$

the normalization factors of the quark fields which should be taken into account when calculating Feynman diagrams are omitted.

Now we are ready to discuss the flavor changing quark transitions.

$\bar{t}_R(b_L, d_L, s_L)H^+$  transition vertex originates in our model from  $Q_R$  admixture in the  $t$ -quark wave function:

$$\begin{aligned} & \frac{\mu_L}{\eta/\sqrt{2}} \frac{\lambda_t/\mu_L}{\sqrt{\frac{\mu_L^2 \mu_R^2}{\lambda_t^2 M^2} \left( 1 - \frac{\lambda_t^2}{\mu_L^2} \right)^2 + \frac{\lambda_t^2}{\mu_L^2}}} \bar{t}_R b'_L H^+ = \\ & = \frac{\lambda_t}{\eta/\sqrt{2}} \frac{1}{\sqrt{1 + (\frac{\mu_L}{M})^2 \left( 1 - \frac{\lambda_t^2}{\mu_L^2} \right)^2}} \bar{t}_R b'_L H^+ , \end{aligned} \quad (10)$$

that is why up to the corrections  $\sim (\mu_L/M)^2$  the box diagrams for  $B_{d,s} - \bar{B}_{d,s}$ ,  $K^0 - \bar{K}^0$  transitions with the intermediate  $t$ -quarks are the same as in SM<sup>2</sup>.

How large can the term  $(\mu_L/M)^2$  be? According to Eq.(1)  $\mu_L$  cannot be larger than 500 GeV: in the opposite case we will be out of the perturbation theory domain and no calculations can be trusted. That is why trying to have the largest possible deviations from SM we will take  $\mu_L = 500$  GeV in what follows. The smallest value of  $M$  which will prevent the production of  $Q$ -quarks at LHC is about 5 TeV, and we will use it in order to maximize deviations from SM (consequently  $\mu_R = m_t M / \mu_L \approx 1.7$  TeV). At one loop level  $Q$ -quark contributes to  $Z \rightarrow b\bar{b}$  decay. The analysis of the experimental data made in [1] lead to  $\mu_L/M \leq 0.4$ , and we are on the safe side. The constraint from  $B \rightarrow X_s \gamma$  decay is even weaker. The box with two intermediate  $t$ -quarks is equal to that in SM with  $(\mu_L/M)^2 \approx 1\%$  accuracy. Theoretical uncertainties in matrix elements calculations do not allow to detect 1% deviation from SM results.

Our model generates extra contributions to  $\Delta F = 2$  four-fermion operators due to the boxes with intermediate  $Q$ -quarks. The boxes with  $H^+$  exchanges generate leading contributions in the limit  $m_t, M \gg M_W$ . The box with one  $t$ -quark substituted by  $Q$  gives coefficient  $\sim G_F^2 m_t^2 (\mu_L/M)^2 \ln(M/m_t)^2$ : once more the correction is damped by the factor  $(\mu_L/M)^2 \approx 1\%$  relative to the SM contribution.

The largest correction comes from the box with two intermediate  $Q$ -quarks:

$$\left( \frac{|\mu_L|}{\eta/\sqrt{2}} \right)^4 \frac{1}{M^2} (\bar{b}_L \gamma_\mu d_L)(\bar{b}_L \gamma_\mu d_L) , \quad (11)$$

<sup>1</sup>We did it in order to simplify the formulas a bit; however this can be suggested as an explanation of heaviness of top:  $t$ -quark massless in SM gets all its mass due to mixing with heavy  $Q$ .

<sup>2</sup>Since  $H^+$  is the longitudinal  $W^+$ -boson polarization its interaction is the same as that of  $W^+$  and the square root in the denominator from  $(t_R, Q_R)$  proper normalization equals that for  $(t_L, Q_L)$  component.

where as an example we present the operator responsible for  $B_d - \bar{B}_d$  oscillations. In this way we get:

$$\frac{\text{box}(QQ)}{\text{box}(tt)} \approx \frac{\mu_L^4}{m_t^2 M^2} \approx 10\% . \quad (12)$$

The explicit formula which takes into account  $(tt)$  and  $(QQ)$  boxes can be easily obtained from that of SM [2]:

$$\begin{aligned} \Delta m_{B_d} &= \frac{G_F^2 B_{B_d} f_{B_d}^2}{6\pi^2} m_B \left[ m_t^2 I\left(\frac{m_t^2}{M_W^2}\right) + M^2 \left(\frac{|\mu_L|}{M}\right)^4 I\left(\frac{M^2}{M_W^2}\right) \right] \eta_B |V_{td}|^2, \\ I(\xi) &= \left\{ \frac{\xi^2 - 11\xi + 4}{4(\xi - 1)^2} - \frac{3\xi^2 \ln \xi}{2(1 - \xi)^3} \right\}, \\ I(0) &= 1; \quad I\left(\frac{m_t^2}{M_W^2}\right) \approx 0.55; \quad I(\infty) = 0.25. \end{aligned} \quad (13)$$

In conclusion we have found a simple extension of SM with one additional heavy quark  $Q$ ,  $M_Q \approx 5$  TeV (non-reachable by direct production at LHC), in which the corrections to CP violating factor  $\varepsilon$  in  $K - \bar{K}$  transitions and the values of  $\Delta m_{B_d}$  and  $\Delta m_{B_s}$  are universal and can reach 10%. We demonstrate that even with no new particles found at LHC one cannot claim that the Unitarity Triangle is universal and unambiguously extractable from different observables with the accuracy better than 10%. In our case the triangle determined by angles found from CP-asymmetries in B-decays and by one side ( $V_{cb}^* V_{cd}$ ) has the value of side ( $V_{tb}^* V_{td}$ ) which, being substituted into the SM expression for  $\Delta m_{B_d}$ , produces the number smaller than the one extracted from the measurement of the  $B_d - \bar{B}_d$  oscillation frequency by  $\approx 10\%$ . However, to detect this discrepancy one needs to have an accuracy in the value of the product  $f_{B_d}^2 B_{B_d}$  better than 10% (the present day accuracy is about 2 times worse [3]).

Heavy quark  $Q$  will lead to extra radiative corrections to electroweak observables ( $M_W$ ,  $M_Z$ ,  $\Gamma_Z$  ...). In this way the central value of the higgs mass which is extracted from the fit will be shifted. We plan to make necessary calculations in the nearest future.

In recent paper [4] the contribution to  $\Delta m_{B_{d,s}}$  due to singlet heavy fermion with electric charge  $+2/3$  has been studied. The analyzed model is motivated by a Little Higgs scenario. In this scenario our factor  $\mu_L$  is substituted by  $x_L \eta$ , where  $0 \leq x_L \leq 1$  [5]. That is why even for  $x_L = 1$  correction to  $\Delta m_{B_{d,s}}$  is damped by the factor  $2^4 = 16$  compared to our value.

This talk is based on the paper [6] which originates as the answer to A. Golutvin's question.

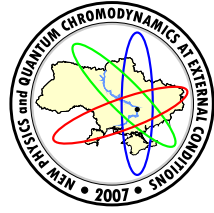
*Acknowledgements.* I am grateful to V. Novikov and A. Rozanov for interesting discussions.

I am very grateful to the Conference organizers and in particular to Vladimir Skalozub for their hospitality. This work was partly supported by grants RFBR 05-02-17203, 07-02-00021 and HSh-2603.2006.2.

## References

- [1] J. Alwall, R. Frederix, J.-M. Gerard, A. Giannanco, M. Herquet, S. Kalinin, E. Kou, V. Lemaitre, F. Maltoni, hep-ph/0607115 (2006).
- [2] M.I. Vysotsky, Yad. Fiz. **31**, 1535 (1980); Sov. J. Nucl. Phys. **31**, 797 (1980);  
T. Inami, C.S. Lim, Prog. Theor. Phys. **65**, 297 (1981).
- [3] Review of Particle Properties, W.-M. Yao et al., J. Phys. G **33**, 1 (2006).
- [4] M. Blanke, A.J. Buras, hep-ph/0610037 (2006).
- [5] Tao Han, Heather E. Logan, Bob McElrath, Lian-Tao Wang, Phys. Rev. D **67**, 095004 (2003).
- [6] M.I. Vysotsky, Phys. Lett. B **644**, 352 (2007).

## **Section Talks**



## ANNIHILATION MECHANISM OF DILEPTON PRODUCTION IN RELATIVISTIC HEAVY-ION COLLISIONS: GRANULAR FIREBALL

D.V. Anchishkin<sup>a</sup>

Bogolyubov Institute for Theoretical Physics, Kiev, Ukraine

We study the  $\pi^+\pi^-$  and  $q\bar{q}$  annihilation mechanisms of dilepton production during relativistic nuclear collisions. We focus on the modifications caused by the granular structure of the fireball rather than by medium modification of the  $\rho$ -meson spectral density. The main ingredient emerging in our approach is a form-factor of the multi-pion (multi-quark) system which reflects the granular structure. Replacing the usual delta-function the form-factor plays the role of distribution which, in some sense, “connects” the total 4-momenta of the annihilating and outgoing particles. We obtained that the form-factor of the multi-pion (multi-quark) system causes broadening of the rate which is most pronounced for small invariant masses, in particular, we obtain a growth of the rate for the invariant masses below two masses of the annihilating particles.

### 1 Introduction

Recent theoretical analysis of the correlation data made in Refs. [1, 2] gives a striking evidences of the clusterization of a fireball created in relativistic nuclear collisions. Investigating the correlation data which were presented by PHENIX [3, 4], STAR [5–7] and CERES [8] collaborations the authors of [1, 2] found that the number of all particles belonging to a single cluster is estimated as  $N_{\text{cl}} \sim 6 - 15$ .

On the other hand, the analysis of the Bose-Einstein correlations made on the basis of the RHIC data (see [11] and references therein) results in conclusion that the space-time size of the emission region reveals very weak dependence on the energy of the colliding nuclei. The experimental pion HBT measurements at RHIC gave the ratio of the radii  $R_{\text{out}}/R_{\text{side}} \approx 1$  which came in contradiction with theoretical expectations. The phenomenon was named as the “RHIC puzzle” [9, 10]. These findings give a solid evidence of a spatial (in this case) clusterization or *granulation* [12] of the fireball created in relativistic heavy-ion collisions.

We would like to point out above conclusions are in full agreement with our assumption of the granular structure of the short lived many-particle system (fireball) created in relativistic nuclear collisions [13]. Our model was proposed in [13] and further developed in [14, 15]. We exploited it in order to evaluate a lepton pair production in heavy-ion collisions. As an example the pion-pion and quark-quark annihilations were considered as a source of the lepton pairs. The main idea of the model is the following: due to strong screening effects in a dense many-particle system with very short life time the wave functions of two sample particles are overlapped when the particles are not far from one another. First of all this concerns the particles which are created during collision. Of course the wave functions of the created particles evolve with time but it interests us just during time span which precedes freeze-out. For instance, two particles can annihilate one another when they are just “under” freeze-out hyper-surface. By definition of the freeze-out pions or quarks cannot annihilate after freeze-out. Overlapping of the wave functions of two sample particles is in correspondence with existence of the Bose-Einstein correlations. Indeed, if one constructs a symmetrized two-particle wave function from two single-particle states and there is no overlapping of these states, then a second symmetrized term equals zero and there is no Bose-Einstein correlation at all. Hence, an existence of the Bose-Einstein correlations exhibits the overlapping of these two single-particle quantum states. If two particles start to “see one another” after freeze out, then, the distances between them are of order  $10 - 20$  fm and bigger what corresponds to relative momentum  $q_{\text{rel}} \sim 20 - 10$  MeV/c and smaller. This region of momenta is so small that it is beyond the experimental possibilities. In correspondence to STAR data [6, 7] the size of the emitted source is estimated as  $4 - 6$  fm depending on the transverse total momentum of the pion pair. This means that two pions which are separated by the mean distance  $r \approx 6$  fm can give contribution to the correlation function. The contribution from other pairs which are separated by the bigger distances decreases in accordance to the Gaussian dependence. Actually, this data gives us the mean size of the fireball granular which is achieved on the freeze-out hyper-surface. Meanwhile, every granular (cluster) starting from the creation evolves with time together with the fireball. It turns out that an experiment detects just the final stage of the granular evolution, hence we indicate experimentally just the maximum size of every small subsystem or a size of the particular granular where the

e-mail: <sup>a</sup>anch@bitp.kiev.ua

© Anchishkin D.V., 2007.

wave functions of the particles are overlapped. In order to take into account all stages of the granular evolution in our consideration we investigate the granulars which size is in the range from 1 fm to 10 fm.

So, we concentrate on the modifications which are due rather to intramedium pion and quark states, than on the discussion of a modification of the  $\rho$ -meson spectral density. In accordance with our suggestions, the main features of a pion wave function follow from the fact that pions live a finite time in the system where they can take part in the annihilation reaction. As a consequence, the off-shell effects give an appreciable contribution to the features of the annihilation process specifically in the region of low invariant masses. Moreover, if pions are the entities of a local subsystem, then the spatial structure of the pion states is far from a plane-wave one and this also gives the essential contribution to the features of the dilepton spectrum.

The main objective in studying strongly interacting matter, which is formed during relativistic heavy ion collisions, is identification of the quark-gluon plasma. Lepton pairs and photons created during relativistic nucleus-nucleus collision do not interact with the highly excited nuclear matter, they leave the reaction zone without further rescattering. That is why, the dileptons ( $e^+e^-$  and  $\mu^+\mu^-$  pairs) observed in high-energy heavy ion collisions carry undistorted information on the dense early stage of the reaction as well as on its dynamics. The enhancement with an invariant mass of  $200 \div 800$  MeV observed by the CERES collaboration [1, 2] in the production of dileptons has received a considerable attention (for the review, see Ref. [3]). It was found that a large part of the observed enhancement is due to the medium effects (see Refs. [4, 5] and references therein). Meanwhile, pion annihilation is the main source of dileptons which come from the hadron matter [6, 7] (see also [23]). That is why, the proper analysis of the dilepton spectra obtained experimentally gives important data which probe the pion dynamics in the dense nuclear matter. The purpose of the present paper is to look once more on the  $\pi^+\pi^-$  and  $q\bar{q}$  annihilation mechanisms of dilepton production from the hadron and quark-gluon plasmas by accounting the the granular structure of the fireball.

## 2 Annihilation of particles in finite space-time volume

To carry out the outlined program, we assume that the pion liquid formed after the equilibration exists in a finite volume (granular), and the confinement of pions to this volume is a direct consequence of the presence of the dense hadron environment which prevents the escape of pions during some mean lifetime  $\tau$ . The same can be assumed concerning a hot system of quarks which are confined to a quark-gluon droplet. So, we assume the system of pions (quarks) produced in high-energy heavy-ion collisions is effectively bounded in a finite volume.

We sketch a possible geometry in Fig. 1. A small circle of radius  $R$  represents the subsystem of pions which is in the local equilibrium and moves with collective velocity  $\mathbf{v}$ .

The pion (quark) wave functions  $\phi_\lambda(x)$ , where  $\lambda$  is a quantum number, satisfy the proper boundary conditions and belong to the complete set of functions. For instance, the stationary wave functions may be taken as the solutions of the Klein-Gordon equation  $(\nabla^2 + k^2)\phi_\lambda(\mathbf{x}) = 0$ , where  $k^2 = E^2 - m^2$ , which satisfy the Dirichlet boundary condition on the surface  $S$ :  $\phi_\lambda(\mathbf{x})|_S = 0$ . For the box boundary, we get  $\phi_{\mathbf{k}}(\mathbf{x}) = \sqrt{8/V} \prod_{i=1}^3 \theta(L_i - x_i) \theta(x_i) \sin(k_i x_i)$ , where  $V = L_1 L_2 L_3$  is the box volume,  $\lambda \equiv \mathbf{k} = (k_1, k_2, k_3)$ , and components of the quasi-momentum run through the discrete set  $k_i = \pi n_i / L_i$  with  $n_i = 1, 2, 3, \dots$ . For the spherical geometry, the normalized solutions are written as  $\phi_{klm}(\mathbf{r}) = \theta(R - r) (2/r)^{1/2} J_{l+1/2}(kr) Y_{lm}(\vartheta, \alpha) / R J_{l+3/2}(kR)$ , where  $\lambda = (k, l, m)$ . Next, the field operators  $\hat{\varphi}(x)$  corresponding to the pion field should be expanded in terms of these eigenfunctions, i.e.

$$\hat{\varphi}(x) = \int \frac{d^3 k}{(2\pi)^3 2\omega_{\mathbf{k}}} [a(\mathbf{k})\phi_{\mathbf{k}}(x) + b^+(\mathbf{k})\phi_{\mathbf{k}}^*(x)], \quad (1)$$

where  $a(\mathbf{k})$  and  $b(\mathbf{k})$  are the annihilation operators of positive and negative pions, respectively. On the other hand, the states corresponding to confined particles can be written in a common way as  $\phi_{\mathbf{k}}(\mathbf{x}) = \sqrt{\rho(\mathbf{x})/V} \Phi_{\mathbf{k}}(\mathbf{x})$ , where, for instance,  $\sqrt{\rho(\mathbf{x})} = \prod_{i=1}^3 [\theta(L_i - x_i)\theta(x_i)]$  for a box and  $\sqrt{\rho(\mathbf{x})} = \theta(R - r)$  for a sphere, respectively. The function  $\rho(\mathbf{x})$  represents the information about the geometry of a reaction region or cuts out the volume where the pions (quarks) can annihilate. Hence, for the evaluation of  $S$ -matrix elements wave functions  $\phi_{\mathbf{k}}(x)$  should be taken as the pion *in*-states once annihilating pions belong to finite system. The amplitude of the pion-pion annihilation to a lepton pair in the first non-vanishing approximation is calculated via the chain  $\pi^+\pi^- \rightarrow \rho \rightarrow \gamma^* \rightarrow l\bar{l}$ , where the  $\rho$ -meson appears as an intermediate state in accordance with the vector meson dominance. The matrix element of the reaction is  $\langle \text{out} | S | \text{in} \rangle = - \int d^4 x_1 d^4 x_2 \langle \mathbf{p}_+, \mathbf{p}_- | T [H_I^\pi(x_1) H_I^l(x_2)] | \mathbf{k}_1, \mathbf{k}_2 \rangle$ , where  $H_I^\pi(x) = -e j_\mu^\pi(x) A^\mu(x)$  and  $H_I^l(x) = -e j_\mu^l(x) A^\mu(x)$ . It is remarkable that the pion density  $\rho(\mathbf{x})$  appears as a factor of the pion current. Indeed,

$$j_\mu^\pi(x) = -i \hat{\varphi}(x) \overleftrightarrow{\partial}_\mu \hat{\varphi}^+(x) = \frac{\rho(\mathbf{x})}{V} \left[ -i \hat{\Phi}(x) \overleftrightarrow{\partial}_\mu \hat{\Phi}^+(x) \right], \quad (2)$$

where the field operator  $\hat{\Phi}(x)$  is defined in the same way as that in (1) with the functions  $\phi_{\mathbf{k}}(\mathbf{x})$  replaced by  $\Phi_{\mathbf{k}}(\mathbf{x})$ . Because of this factorization, after the integration over the vertex  $x$  the density  $\rho(\mathbf{x})$  automatically

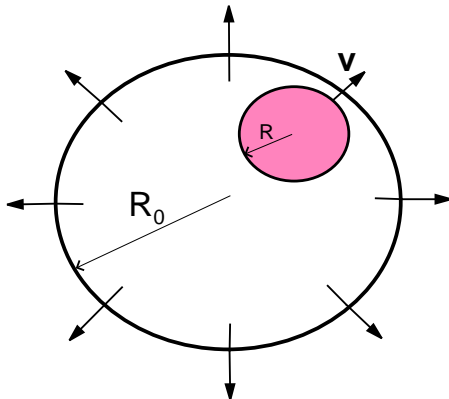


**Figure 1.** Sketch of an expanding fireball. The small circle of radius  $R$  represents the subsystem of pions which is in a local equilibrium state and moves with the collective velocity  $\mathbf{v}$ .

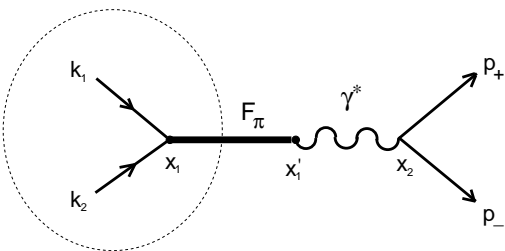


**Figure 2.** The first-order nonvanishing Feynman graph of the lepton pair creation in the process  $\pi^+ \pi^- \rightarrow \rho \rightarrow \gamma^* \rightarrow l \bar{l}$ . The circle which surrounds the vertex  $x_1$  sketches the finite space-time region of the pion-pion interactions.

cuts out the volume, where the  $\pi^+ \pi^-$  annihilation reaction is running. At the same time, this means that the density  $\rho(\mathbf{x})$  determines the volume of quantum coherence, i.e. just the particles from this spatial domain are capable to annihilate one with another and make contribution to the amplitude of the reaction. To obtain the overall rate, it is necessary then to sum up the rates from every coherent domain of the fireball.

For the sake of simplicity one can assume that the pion states can be approximately represented as  $\phi_{\mathbf{k}}(x) = \sqrt{\rho(x)/V} e^{-ik \cdot x}$  ( $\rho(x)$  is the 4-density of pions in the volume  $V$  where pions are in a local thermodynamic equilibrium). In essence, this approximation considers just one mode of the wave function  $\Phi_{\mathbf{k}}(\mathbf{x})$  and reflects the qualitative features of the pion states in a real hadron plasma. In the frame of this approximation a simple calculation immediately shows that the  $S$ -matrix element is proportional to the Fourier-transformed pion density  $\rho(x)$ , i.e.  $\langle \text{out} | S | \text{in} \rangle \propto \rho(k_1 + k_2 - p_+ - p_-)$ , where  $k_1$  and  $k_2$  are the 4-quasi-momenta of the initial pion states and  $p_+$  and  $p_-$  are the 4-momenta of the outgoing leptons. This means that the form-factor of the pion source  $\rho(k)$  stands here in place of the delta function which appears in the standard calculations, i.e.  $(2\pi)^4 \delta^4(K - P) \rightarrow \rho(K - P)$ , where  $K = k_1 + k_2$  and  $P = p_+ + p_-$  are the total (quasi-) momenta of pion and lepton pairs, respectively. An immediate consequence of this is a breaking down of the energy-momentum conservation in the  $s$ -channel of the reaction, which means that the total momentum  $K$  of the pion pair is no longer equal exactly to the total momentum  $P$  of the lepton pair. The physical interpretation of this fact is rather obvious: the effect of the hadron environment on the pion subsystem which prevents the escape of pions from the fireball can be regarded during the time span  $\tau$  as the influence of an external nonstationary field. The latter, as known, breaks down the energy-momentum conservation. From now, the squared form-factor  $|\rho(K - P)|^2$  of the pion system plays the role of a distribution which in some sense "connects" in  $s$ -channel the annihilating and outgoing particles instead of  $\delta$ -function. Indeed, the number  $N^{(\rho)}$  of produced lepton pairs from a finite pion system related to an element of the dilepton momentum space, reads

$$\left\langle \frac{dN^{(\rho)}}{d^4 P} \right\rangle = \int d^4 K |\rho(K - P)|^2 \left\langle \frac{dN}{d^4 K d^4 P} \right\rangle, \quad (3)$$

where

$$\left\langle \frac{dN}{d^4 K d^4 P} \right\rangle = \int \frac{d^3 k_1}{(2\pi)^3 2E_1} \frac{d^3 k_2}{(2\pi)^3 2E_2} \delta^4(k_1 + k_2 - K) f_{\text{BE}}(E_1) f_{\text{BE}}(E_2) \quad (4)$$

$$\times \int \frac{d^3 p_+}{(2\pi)^3 2E_+} \frac{d^3 p_-}{(2\pi)^3 2E_-} \delta^4(p_+ + p_- - P) |A_0(k_1, k_2; p_+, p_-)|^2. \quad (5)$$

Here,  $E_i = \sqrt{m_i^2 + \mathbf{k}_i^2}$ ,  $i = 1, 2$  for pions and  $E_i = \sqrt{m_l^2 + \mathbf{p}_i^2}$ ,  $i = +, -$  for leptons, respectively. To obtain Eq.(9), we represent the amplitude of the reaction (see Fig. 2) as

$$\langle \text{out} | S^{(2)} | \text{in} \rangle = \rho(k_1 + k_2 - p_+ - p_-) A_0(k_1, k_2; p_+, p_-). \quad (6)$$

Note that not only the form-factor  $\rho(K - P)$  contains information about the pion system. The amplitude  $A_0$  carries also new important features, which are related to the violation of the energy-momentum conservation in the  $s$ -channel. The latter is a consequence of the medium effects through a partial confinement of the pion

states inside fireball what results in the breaking of the translation invariance. Indeed, the pion-pion c.m.s. moves with the velocity  $\mathbf{v}_K = \mathbf{K}/K_0$ , whereas the lepton-pair c.m.s. moves with the velocity  $\mathbf{v}_P = \mathbf{P}/P_0$ . Hence, these two center-of-mass systems are "disconnected" now, that is why any quantity should be Lorentz-transformed when transferred from one c.m.s. to another. Reflection of this is the appearance of the correction factor  $\left[1 + \frac{1}{3} \left(\frac{(P \cdot K)^2}{P^2 K^2} - 1\right)\right]$  in the formula for the dilepton production rate (for details see [13, 14]).

By the broken brackets in Eq.(9), we denote the thermal averaging over the pion quasi-momentum space. Actually, we assume a *local thermal equilibrium* in the multi-hadron (-pion) system. Hence, the Green's function,  $D^<(x_1, x_2) = \langle \hat{\Phi}^+(x_2) \hat{\Phi}(x_1) \rangle$ , which appears after thermal averaging, can be represented as

$$D^<(x_1, x_2) = \int \frac{d^4 k}{(2\pi)^4} e^{-ik \cdot x} A(k) f_{\text{BE}}(k, X), \quad (7)$$

where  $X = (x_1 + x_2)/2$ ,  $x = x_1 - x_2$ , and

$$f_{\text{BE}}(k, X) = \frac{1}{e^{\beta(X)[k \cdot u(X) - \mu(X)]} - 1}, \quad (8)$$

is the Bose-Einstein distribution function, which depends on space-time variables,  $X = (X^0, \mathbf{X})$ ,  $\beta$  is the inverse temperature,  $u(X)$  is the hydrodynamical velocity and  $\mu$  is the chemical potential. For the ideal gas (infinite life time of the system) the spectral function  $A(k^0, \mathbf{k})$  indicates that all states are on the mass-shell:  $A(k) = 2\pi\delta(k^2 - m_\pi^2)\theta(k^0)$ . In the interacting system the spectral function reflects a collision broadening of the states which includes as well a global decay of the system if collisions in the system exist during finite time span. For instance, the fireball, which is nothing else as a system of strongly interacting particles, lives until its decay, i.e. starting from the creation till the freeze-out, after which there are no strong interactions between particles at all. In our further consideration we will take into account just a global decay of the multi-pion (multi-quark) system. Assuming a proper model of the spectral function,  $A(k)$ , which responsible in the present approach for finite life time of the system, we incorporate it together with the spatial density  $\rho(\mathbf{x})$  to the global system form-factor  $\rho(x)$ .

Concerning the physical meaning of Eq. (9), we note that one can regard it as the averaging of the random quantity  $\langle \frac{dN}{d^4 K d^4 P} \rangle$  with the help of the distribution function  $|\rho(K - P)|^2$  centered around the value  $P$ , which is fixed by experimental measurement. In this sense, the hadron medium holding pions in a local spatial region for some time, which is expressed as the local pion distribution  $\rho(x)$ , plays the role of an environment randomizing the pion source. This randomization is a purely quantum one in contrast to the thermal randomization of the multi-pion system which is already included to the quantity  $\langle \frac{dN}{d^4 K d^4 P} \rangle$ .

### 3 Dilepton emission rates

In order to transform the distribution of the number of created lepton pairs over the dilepton momentum space to the distribution over invariant masses, one has to perform additional integration using  $\langle dN^{(\rho)}/d^4 P \rangle$  from (9), i.e.  $\left\langle \frac{dN^{(\rho)}}{dM^2} \right\rangle = \int \frac{d^3 P}{2P_0} \left\langle \frac{dN^{(\rho)}}{d^4 P} \right\rangle$ , where  $P_0 = \sqrt{M^2 + \mathbf{P}^2}$ . This results in:

$$\begin{aligned} \left\langle \frac{dN^{(\rho)}}{dM^2} \right\rangle &= \frac{\alpha^2}{3(2\pi)^8} \left(1 - \frac{4m_e^2}{M^2}\right)^{1/2} \left(1 + \frac{2m_e^2}{M^2}\right) |F_\pi(M^2)|^2 \int \frac{d^3 P}{2P_0} \int d^4 K \frac{K^2}{M^2} \\ &\times |\rho(K - P)|^2 e^{-\beta K_0} \left(1 - \frac{4m_\pi^2}{K^2}\right)^{3/2} \left[1 + \frac{1}{3} \left(\frac{(P \cdot K)^2}{M^2 K^2} - 1\right)\right], \end{aligned} \quad (9)$$

where we take the Boltzmann distribution  $f_{\text{BE}}(E) \approx \exp(-\beta E)$ . Note, that during integration with respect to a 4-momentum  $K$  one should keep the invariant mass of a pion pair,  $M_\pi = \sqrt{K^2}$ , not less than two pion masses. On the other hand, possible finite values of the distribution  $\left\langle \frac{dN^{(\rho)}}{dM^2} \right\rangle$  below the two-pion mass threshold can occur just due to the presence of the pion system form-factor  $\rho(K - P)$ . The factor in the square brackets on the r.h.s. of (4) is a correction which is due to the Lorentz transformation of the quantity  $(\mathbf{k}_1 - \mathbf{k}_2)^2$  from the dilepton c.m.s. to the pion-pion c.m.s. This factor gives a remarkable contribution to the dilepton spectrum for invariant masses below the two-pion mass value. Its influence is especially pronounced for  $e^+e^-$  production as was shown in [13, 14].

In Eq.(4) the  $\rho$ -meson form-factor,  $F_\pi(M^2)$ , is a vacuum one. Actually, there are two ways to take into account effects of the hadron medium: first, one can account for distortion of the pion states caused by dense environment; second, one can look for  $\rho$ -meson polarization effects during its passing through the hadron environment. In the present paper we choose the first way of accounting for the medium effects (see also [24]). Just to elucidate as much as possible the consequences of the contraction of the pion states in the hadron medium and to prevent a double counting we take the vacuum  $\rho$ -meson form-factor.

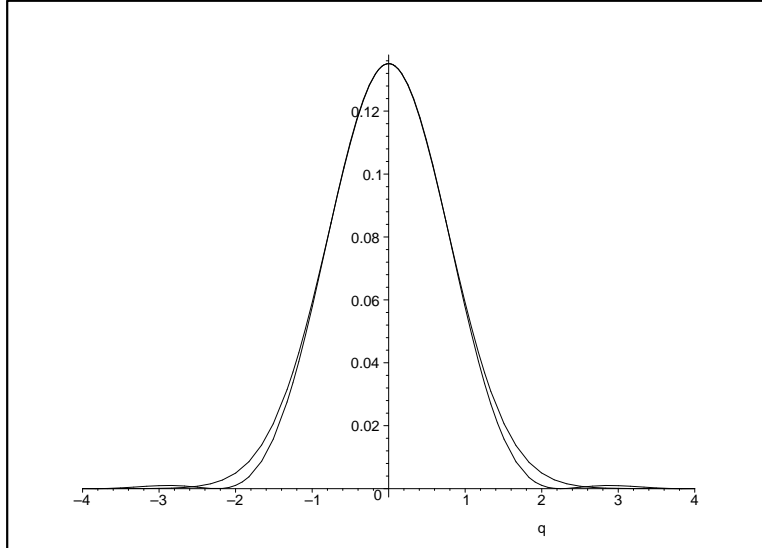


**Figure 3.** Comparison of the Gaussian and  $\theta$ -function form-factors  $|\rho(\mathbf{q})|^2/V$ .

For particular evaluations we take as a model of the pion system the Gaussian distribution of the particles in space and the Gaussian decay of the system (this form-factor succeeded in HBT interferometry):

$$\rho(x) = \exp\left(\frac{x^2 - 2(u \cdot x)^2}{2R^2}\right), \quad (10)$$

where  $u$  is the hydrodynamical (collective) velocity of the element of the total system which is in a local thermodynamic equilibrium;  $R$  is the spatial radius of the element. In the rest frame of the element the form-factor looks like:  $\rho_0(t, \mathbf{r}) = \exp[-(t^2 + \mathbf{r}^2)/2R^2]$ . To get a proper interpretation in terms of the mean life time of the system element,  $\tau$ , one needs to make a scale transformation during integration over the time variable:  $\int_{-\infty}^{\infty} dt \rho_0(t, \mathbf{r}) F(t, \mathbf{r}) = \int_{-\infty}^{\infty} dt \exp(-t^2/2\tau^2 - \mathbf{r}^2/2R^2) F_0(t, \mathbf{r})$ , where  $F_0(t, \mathbf{r}) = \frac{R}{\tau} F(\frac{R}{\tau}t, \mathbf{r})$ .

Meanwhile, it can be another choice of the pion source function. Indeed, one can choose, for instance, a geometry with sharp boundaries which are determined by the  $\theta$ -function. To show that the final answer is not sensitive to the form of the cutting function we compare two form-factors (normalized to the unit volume) which correspond to the Gaussian distribution  $\rho(\mathbf{r}) = \exp(-\mathbf{r}^2/2R^2)$  and to the  $\theta$ -function distribution  $\rho(\mathbf{r}) = \theta(R - |\mathbf{r}|)$  (see Fig. 3). Only a slight difference between these form-factors is seen and, therefore, the choice of pion source distribution does not affect much the dilepton production rate.

We evaluate the rate in the rapidity window,  $y_{\min} \leq y \leq y_{\max}$ , which corresponds to CERES experimental conditions [1, 2]

$$\frac{dR}{dM dy} = 2\pi M \frac{1}{\Delta y} \int_{y_{\min}}^{y_{\max}} dy \int_{P_{\perp \min}}^{\infty} dP_{\perp} P_{\perp} \frac{dN}{d^4x d^4P},$$

where  $\tanh y = P^3/P^0$ ,  $P_{\perp}^2 = (P^1)^2 + (P^2)^2$ . The results of evaluation of the production rates  $dR_{e^+e^-}^{(\rho)}/dM dy$  and  $dR_{\mu^+\mu^-}^{(\rho)}/dM dy$  for electron-positron and muon-muon pairs, respectively, in pion-pion annihilation are depicted in Figs. 4,5. Note, the calculations are carried out in the frame of the element of the system where particles are in a local thermal equilibrium. Different curves correspond to the different "spatial sizes"  $R$  and different "lifetimes"  $\tau$  (for particular values of these parameters see Figs. 4,5) of a hot pion system at the temperature  $T = 180$  MeV.

For comparison, we present in Figs. 6,7 the results of evaluation of the rate  $dR_{e^+e^-}^{(\rho)}/dM dy$  of electron-positron pair production in quark-antiquark annihilation

in a hot QGP drop,  $T = 180$  MeV. The evaluation was carried out in the frame of the quark drop under the same assumptions as for pion-pion annihilation. As in the previous case, an increase in the rate with decrease in the invariant mass up to two electron masses is seen. This real threshold is close to the total mass of annihilating quarks  $M = 2m_q \approx 10$  MeV/c<sup>2</sup>.

#### 4 Conclusions

From two-particle and many-particle correlation experiments (see Introduction) we conclude that the fireball created in relativistic nuclear collisions has a granular structure. We parameterize the size of a particular granular (a small subsystem of the fireball) by the Gaussian radius  $R$  and the lifetime  $\tau$ , which accounts for

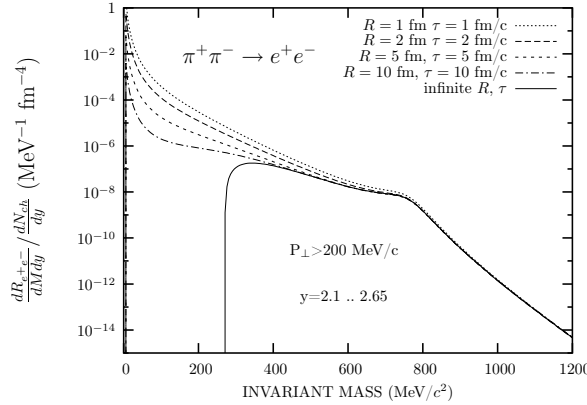


**Figure 4.** Rates of electron-positron productions in pion-pion annihilation in a small finite system,  $T = 180$  MeV.

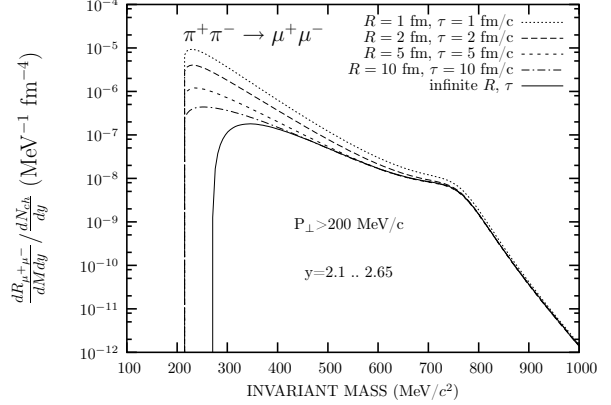


**Figure 5.** Rates of muon-muon productions in pion-pion annihilation in a small finite system,  $T = 180$  MeV.

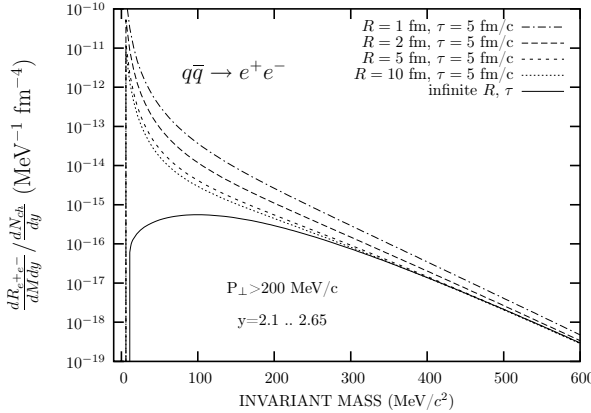


**Figure 6.** Electron-positron production rates in quark-antiquark annihilation in a hot QGP drop.

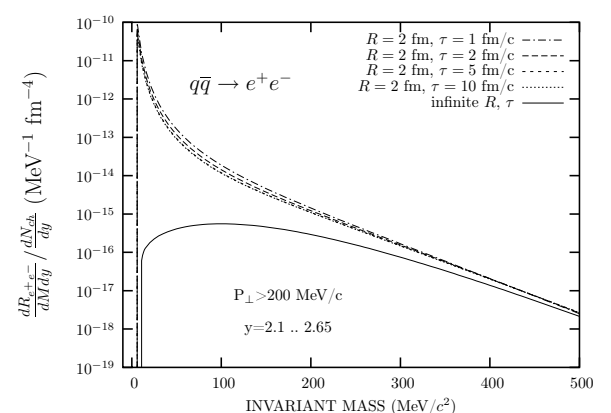


**Figure 7.** Electron-positron production rates in quark-antiquark annihilation in a hot QGP drop.

a time span from creation of the granular till freeze-out times. We notice that the production rate in a finite small system differs from the rate in an infinite pion gas where pion *in*-states can be taken as plane waves. The deviation bigger when the parameters  $R$  and  $\tau$  are smaller. Of course, this is a reflection of the uncertainty principle which is realized by the presence of the distribution (form-factor)  $|\rho(K - P)|^2$  as the integrand factor in (9). Basically, the presence of the form-factor of the multi-pion system results in a broadening of the rate for small invariant masses  $M \leq 800$  MeV/c $^2$  which is wider at the smaller parameters  $R$  and  $\tau$ . This seems natural because the quantum fluctuations of the momentum are more pronounced in smaller systems. We emphasize as well that the behavior of the curves in Figs. 4,5 which correspond to a finite system has a similar to the CERES data tendency [1, 2].

The same behavior of the rate is seen for a hot quark drop (see Figures 6,7): small parameters  $R$  and  $\tau$  in the region of small invariant masses  $M \leq 500$  MeV/c $^2$ , as compared to the rate for infinite parameters  $R = \infty$ ,  $\tau = \infty$ , give a rise of quantum fluctuations which are evidently bigger for a smaller size of the QGP drop.

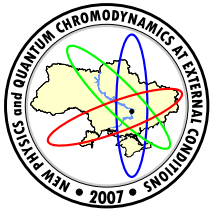
Note, the enhancement of the dilepton production rate for the low invariant mass region is much more sensitive to the variation in the spatial size of a many-particle (pion, quark) system than to the variation in the system lifetime (see Fig. 7) [15].

*Acknowledgment.* The author would like to express his gratitude to V. Khryapa, R. Naryshkin and V. Ruuskanen for fruitful collaboration.

## References

- [1] W.Broniowski, B.Hiller, W.Florkowski and P.Bozek, Phys.Lett. **B635**, 290 (2006) [nucl-th/0510033].
- [2] W.Broniowski, P.Bozek, W.Florkowski, B.Hiller, nucl-th/0611069 [Proceedings of Science (CFRNC2006) 020].
- [3] K.Adcox *et al.* [PHENIX Collaboration], Phys.Rev. **C66**, 024901 (2002) [nucl-ex/0203015].
- [4] S.S.Adler *et al.* [PHENIX Collaboration], Phys.Rev.Lett. **93**, 092301 (2004) [nucl-ex/0310005].

- [5] J.Adams *et al.* [STAR Collaboration], Phys.Rev. **C71**, 064906 (2005) [nucl-ex/0308033].
- [6] J.Adams *et al.* [STAR Collaboration], Phys.Rev. **C72**, 044902 (2005) [nucl-ex/0504031].
- [7] J.Adams *et al.* [STAR Collaboration], Phys.Rev. **C71**, 044906 (2005) [nucl-ex/0411036].
- [8] H.Appelshauser *et al.*, Nucl.Phys. **A752**, 394 (2005).
- [9] U.A.Wiedemann and U.Heinz, Phys.Rept. **319**, 145 (1999).
- [10] R.M.Weiner, Phys.Rept. **327**, 249 (2000).
- [11] E.Frodermann, U.Heinz, M.A.Lisa, Phys.Rev. **C73**, 044908 (2006) [nucl-th/0602023].
- [12] Wei-Ning Zhang, Cheuk-Yin Wong, hep-ph/0702120.
- [13] D.Anchishkin, V.Khryapa, and V.Ruuskanen, hep-ph/0210346.
- [14] D.Anchishkin, V.Khryapa, R.Naryshkin, V.Ruuskanen, Ukrainian Journal of Physics **49**, 1039 (2004).
- [15] D.Anchishkin, R.Naryshkin, Mod.Phys.Lett. **A20**, 2047 (2005) [nucl-th/0407042].
- [16] G.Agakichiev *et al.*, Phys.Rev.Lett. **75**, 1272 (1995).
- [17] G.Agakichiev *et al.*, Phys.Lett. **B422**, 405 (1998).
- [18] C.Gale and K.L.Haglin, hep-ph/0306098.
- [19] W. Cassing and E.L. Bratkovskaya, Phys.Rept. **308**, 65 (1999).
- [20] R.Rapp and J.Wambach, Adv.Nucl.Phys. **25**, 1 (2000) [hep-ph/9909229].
- [21] V.Koch and C.Song, Phys.Rev. **C54**, 1903 (1996).
- [22] K.Haglin, Phys.Rev. **C53**, R2606 (1996).
- [23] G.Agakichiev *et al.*, Eur.Phys.J. **C41**, 475 (2005) [nucl-ex/0506002].
- [24] H. van Hees, J.Knoll, Nucl.Phys. **A683**, 369 (2000) [hep-ph/0007070].



## THE ROLE OF SURFACE TENSION FOR THE EQUATION OF STATE OF QUARK-GLUON BAGS

K. A. Bugaev

Bogolyubov Institute for Theoretical Physics, Kiev, Ukraine

The temperature and chemical potential dependent surface tension of bags is introduced into the gas of quark-gluon bags model. The suggested model is solved analytically. It resolves a long standing problem of a unified description of the first and second order phase transition with the cross-over. Such an approach is necessary to model the complicated properties of quark-gluon plasma and hadronic matter from the first principles of statistical mechanics. In addition to the deconfinement phase transition, we found that at the curve of a zero surface tension coefficient there must exist the surface induced phase transition of the 2<sup>nd</sup> or higher order, which separates the pure quark gluon plasma (QGP) from the cross-over states. Thus, the present model predicts that the critical endpoint of quantum chromodynamics is the tricritical endpoint.

### 1 Introduction

The strongly interacting matter properties studied in relativistic nuclear collisions has reached the stage when the predictions of the lattice quantum chromodynamics (QCD) can be checked experimentally on the existing data and future measurements at BNL RHIC, CERN SPS, and GSI FAIR. However, a comparison of the theoretical results with the experimental data is not straightforward because during the collision process the matter can have several phase transformations which are difficult to model. The latter reason stimulated the development of a wide range of phenomenological models of the strongly interacting matter equation of state which are used in dynamical simulations.

One of these models, the gas of bags model (GBM) [1–3], itself contains two well-known models of deconfined and confined phases: the bag model of QGP [5] and the hadron gas model [6]. Hence there were hopes [7] that an exact analytical solution of the GBM found in [2] could be helpful in understanding the properties of strongly interacting matter. However, this solution does not allow one to introduce the critical end point of the strongly interacting matter phase diagram. Also, a complicated construction of the line, along which the phase transition order gradually increases, suggested in [7], does look too artificial. Therefore, the present GBM formulation lacks an important physical input and is interesting only as a toy example which can be solved analytically. However, there are the great demands [8–10] for the phenomenological models, which can correctly describe the properties of the end point of the 1<sup>st</sup> order deconfinement phase transition (PT) to QGP.

In statistical mechanics there are several exactly solvable cluster models with the 1<sup>st</sup> order PT which describe the critical point properties very well. These models are built on the assumptions that the difference of the bulk part (or the volume dependent part) of free energy of two phases disappears at phase equilibrium and that, in addition, the difference of the surface part (or the surface tension) of free energy vanishes at the critical point. The most famous of them is the Fisher droplet model (FDM) [12–14] which has been successfully used to analyze the condensation of a gaseous phase (droplets of all sizes) into a liquid. The FDM has been applied to many different systems [13, 14].

The other well established statistical model, the statistical multifragmentation model (SMM) [15–17], was recently solved analytically both for infinite [18, 20] and for finite [21, 22] volumes of the system. In the SMM the surface tension temperature dependence differs from that one of the FDM, but it was shown [20] that the value of Fisher exponent  $\tau_{SMM} = 1.825 \pm 0.025$ , which contradicts to the FDM value  $\tau_{FDM} \approx 2.16$ , but is consistent with ISiS Collaboration data [23] and EOS Collaboration data [24].

From the structure of these models, it follows that the GMB can be drastically improved by the inclusion of such a vitally important element as the surface tension of the quark-gluon bags. The obtained model is called the QGBST model. Its detailed discussion and the full list of related references can be found in [11, 25, 26].

The great success of the SMM initiated the studies of the surface partitions of large clusters within the Hills and Dales Model [27, 28] and led to a discovery of the origin of the temperature independent surface entropy similar to the FDM. It was proven that the surface tension coefficient of large clusters consisting of the discrete constituents should linearly depend on the temperature of the system [27] and must vanish at the critical endpoint. Thus, the Hills and Dales Model [27, 28] is our main guide in formulating the QGBST model.

However, for definiteness we assume a certain dependence of the surface tension coefficient on temperature and baryonic chemical potential, and concentrate on the impact of surface tension of the quark-gluon bags on the properties of the deconfinement phase diagram and the QCD critical endpoint.

Here we will show that the existence of a cross-over at low values of the baryonic chemical potential along with the 1<sup>st</sup> order deconfinement PT at high baryonic chemical potentials leads to the existence of an additional PT of the 2<sup>nd</sup> or higher order along the curve where the surface tension coefficient vanishes [25]. Thus, it turns out that the QGBST model predicts the existence of the tricritical rather than critical endpoint.

The work is organized as follows. Sect. 2 contains the formulation of the QGBST model and analyze all possible singularities of its isobaric partition for vanishing baryonic densities. This analysis is generalized to non-zero baryonic densities in Sect. 3. Sect. 4 is devoted to the analysis of the surface tension induced PT which exists above the deconfinement PT. The conclusions and research perspectives are summarized in Sect. 5.

## 2 The Role of Surface Tension

I begin with the isobaric partition:

$$\hat{Z}(s, T) \equiv \int_0^\infty dV \exp(-sV) Z(V, T) = \frac{1}{[s - F(s, T)]} \quad (1)$$

where the function  $F(s, T)$  is defined as follows

$$F(s, T) \equiv F_H(s, T) + F_Q(s, T) = \sum_{j=1}^n g_j e^{-v_j s} \phi(T, m_j) + u(T) \int_{V_0}^\infty dv \frac{\exp[-v(s - s_Q(T))]}{v^\tau}. \quad (2)$$

At the moment the particular choice of function  $F_Q(s, T)$  in (2) is not important. The key point of my treatment is that it should have the form of Eq. (2) which has a singularity at  $s = s_Q^*$  because for  $s < s_Q$  the integral over the bag volume  $v$  diverges at its upper limit. As will be shown below the isobaric partition (1) has two kind of singularities: the simple pole  $s = s_H^*$  and the essential singularity  $s = s_Q$ . The rightmost singularity defines the phase in which matter exists, whereas a PT occurs when two singularities coincide [2, 18, 25]. All singularities are defined by the equation

$$s^* = F(s^*, T), \quad (3)$$

Note that the exponential in (2) is nothing else, but a difference of the bulk free energy of a bag of volume  $v$ , i.e.  $-Tsv$ , which is under external pressure  $Ts$ , and the bulk free energy of the same bag filled with QGP, i.e.  $-Ts_Qv$ . At phase equilibrium this difference of the bulk free energies vanishes. Despite all positive features, Eq. (2) lacks the surface part of free energy of bags, which will be called a surface energy hereafter. In addition to the difference of the bulk free energies the realistic statistical models which demonstrated their validity, the FDM [12] and SMM [15], have the contribution of the surface energy which plays an important role in defining the phase diagram structure [18, 22]. Therefore, I modify Eq. (2) by introducing the surface energy of the bags in a general fashion [20]:

$$F_Q(s, T) = u(T) \int_{V_0}^\infty dv \frac{\exp[(s_Q(T) - s)v - \sigma(T)v^\kappa]}{v^\tau}, \quad (4)$$

where the ratio of the temperature dependent surface tension coefficient to  $T$  (the reduced surface tension coefficient hereafter) which has the form  $\sigma(T) = \frac{\sigma_o}{T} \cdot [(T_{cep} - T)/T_{cep}]^{2k+1}$  ( $k = 0, 1, 2, \dots$ ). Here  $\sigma_o > 0$  can be a smooth function of the temperature, but for simplicity I fix it to be a constant. For  $k = 0$  the two terms in the surface (free) energy of a  $v$ -volume bag have a simple interpretation [12]: thus, the surface energy of such a bag is  $\sigma_0 v^\kappa$ , whereas the free energy, which comes from the surface entropy  $\sigma_o T_{cep}^{-1} v^\kappa$ , is  $-T\sigma_o T_{cep}^{-1} v^\kappa$ . Note that the surface entropy of a  $v$ -volume bag counts its degeneracy factor or the number of ways to make such a bag with all possible surfaces. This interpretation can be extended to  $k > 0$  on the basis of the Hills and Dales Model [27, 28].

In choosing such a simple surface energy parameterization we follow the original Fisher idea [12] which allows one to account for the surface energy by considering some mean bag of volume  $v$  and surface  $v^\kappa$ . The consideration of the general mass-volume-surface bag spectrum is reserved for the future investigation. The power  $\kappa < 1$  which describes the bag's effective surface is a constant which, in principle, can differ from the typical FDM and SMM value 2/3. This is so because near the deconfinement PT region QGP has low density and, hence, like in the low density nuclear matter [35], the non-spherical bags (spaghetti-like or lasagna-like [35]) can be favorable (see a [25] and references therein). A similar idea of "polymerization" of gluonic quasiparticles was introduced recently [36].

The second essential difference with the FDM and SMM surface tension parameterization is that we do not require the vanishing of  $\sigma(T)$  above the CEP. As will be shown later, this is the most important assumption

which, in contrast to the GBM, allows one to naturally describe the cross-over from hadron gas to QGP. Note that negative value of the reduced surface tension coefficient  $\sigma(T)$  above the CEP does not mean anything wrong. As we discussed above, the surface tension coefficient consists of energy and entropy parts which have opposite signs [12, 27, 28]. Therefore,  $\sigma(T) < 0$  does not mean that the surface energy changes the sign, but it rather means that the surface entropy, i.e. the logarithm of the degeneracy of bags of a fixed volume, simply exceeds their surface energy. In other words, the number of non-spherical bags of a fixed volume becomes so large that the Boltzmann exponent, which accounts for the energy "costs" of these bags, cannot suppress them anymore.

Finally, the third essential difference with the FDM and SMM is that we assume that the surface tension in the QGBST model happens at some line in  $\mu_B - T$  plane, i.e.  $T_{cep} = T_{cep}(\mu_B)$ . However, in the subsequent sections we will consider  $T_{cep} = \text{const}$  for simplicity, and in Sect. V we will discuss the necessary modifications of the model with  $T_{cep} = T_{cep}(\mu_B)$ .

The surface energy should, perhaps, be introduced into a discrete part of the mass-volume spectrum  $F_H$ , but a successful fitting of the particle yield ratios [6] with the experimentally determined hadronic spectrum  $F_H$  does not indicate such a necessity.

In principle, besides the bulk and surface parts of free energy, the spectrum (4) could include the curvature part as well, which may be important for small hadronic bubbles or for cosmological PT. We stress, however, that the curvature term has not been seen in such well established models like the FDM, the SMM and many other systems [13, 14]. A special analysis of the free energy of 2- and 3-dimesional Ising clusters, using the Complement method [37], did not find any traces of the curvature term (see a detailed discussion in Ref. [25]).

According to the general theorem [2] the analysis of PT existence of the GCP is now reduced to the analysis of the rightmost singularity of the isobaric partition (1). Depending on the sign of the reduced surface tension coefficient, there are three possibilities.

**(I)** The first possibility corresponds to  $\sigma(T) > 0$ . Its treatment is very similar to the GBM choice (2) with  $\tau > 2$  [2]. In this case at low temperatures the QGP pressure  $Ts_Q(T)$  is negative and, therefore, the rightmost singularity is a simple pole of the isobaric partition  $s^* = s_H(T) = F(s_H(T), T) > s_Q(T)$ , which is mainly defined by a discrete part of the mass-volume spectrum  $F_H(s, T)$ . The last inequality provides the convergence of the volume integral in (4) (see the left panel in Fig. 1). On the other hand at very high  $T$  the QGP pressure dominates and, hence, the rightmost singularity is the essential singularity of the isobaric partition  $s^* = s_Q(T)$ . The phase transition occurs, when the singularities coincide:

$$s_H(T_c) \equiv p_H(T_c)/T_c = s_Q(T_c) \equiv p_Q(T_c)/T_c, \quad (5)$$

which is nothing else, but the Gibbs criterion. The graphical solution of Eq. (3) for all these possibilities is shown in Fig. 1. Like in the GBM [2, 7], the necessary condition for the PT existence is the finiteness of  $F_Q(s_Q(T), T)$  at  $s = s_Q(T)$ . It can be shown that the sufficient conditions are the following inequalities:  $F_Q(s_Q(T), T) > s_Q(T)$  for low temperatures and  $F(s_Q(T), T) < s_Q(T)$  for  $T \rightarrow \infty$ . These conditions provide that at low  $T$  the rightmost singularity of the isobaric partition is a simple pole, whereas for hight  $T$  the essential singularity  $s_Q(T)$  becomes its rightmost one (see Fig. 1 and a detailed analysis of case  $\mu_B \neq 0$ ).

The PT order can be found from the  $T$ -derivatives of  $s_H(T)$ . Thus, differentiating (3) one finds

$$s'_H = \frac{G + u \mathcal{K}_{\tau-1}(\Delta, -\sigma) \cdot s'_Q}{1 + u \mathcal{K}_{\tau-1}(\Delta, -\sigma)}, \quad (6)$$

where the functions  $G$  and  $\mathcal{K}_{\tau-a}(\Delta, -\sigma)$  are defined as

$$G \equiv F'_H + \frac{u'}{u} F_Q + \frac{(T_{cep} - 2kT)\sigma(T)}{(T_{cep} - T)T} u \mathcal{K}_{\tau-\kappa}(\Delta, -\sigma), \quad (7)$$

$$\mathcal{K}_{\tau-a}(\Delta, -\sigma) \equiv \int_{V_o}^{\infty} dv \frac{\exp[-\Delta v - \sigma(T)v^{\kappa}]}{v^{\tau-a}}, \quad (8)$$

where  $\Delta \equiv s_H - s_Q$ .

Now it is easy to see that the transition is of the 1<sup>st</sup> order, i.e.  $s'_Q(T_c) > s'_H(T_c)$ , provided  $\sigma(T) > 0$  for any  $\tau$ . The 2<sup>nd</sup> or higher order phase transition takes place provided  $s'_Q(T_c) = s'_H(T_c)$  at  $T = T_c$ . The latter condition is satisfied when  $\mathcal{K}_{\tau-1}$  diverges to infinity at  $T \rightarrow (T_c - 0)$ , i.e. for  $T$  approaching  $T_c$  from below. Like for the GBM choice (2), such a situation can exist for  $\sigma(T_c) = 0$  and  $3/2 < \tau \leq 2$  [25]. Studying the higher  $T$ -derivatives of  $s_H(T)$  at  $T_c$ , one can find a mare general statement, but for our purpose it is not necessary.

**(II)** The second possibility,  $\sigma(T) \equiv 0$ , described in the preceding paragraph, does not give anything new compared to the GBM [2, 7]. If the PT exists, then the graphical picture of singularities is basically similar to the left panel of Fig. 1. The only difference is that, depending on the PT order, the derivatives of  $F(s, T)$  function with respect to  $s$  should diverge at  $s = s_Q(T_c)$ .

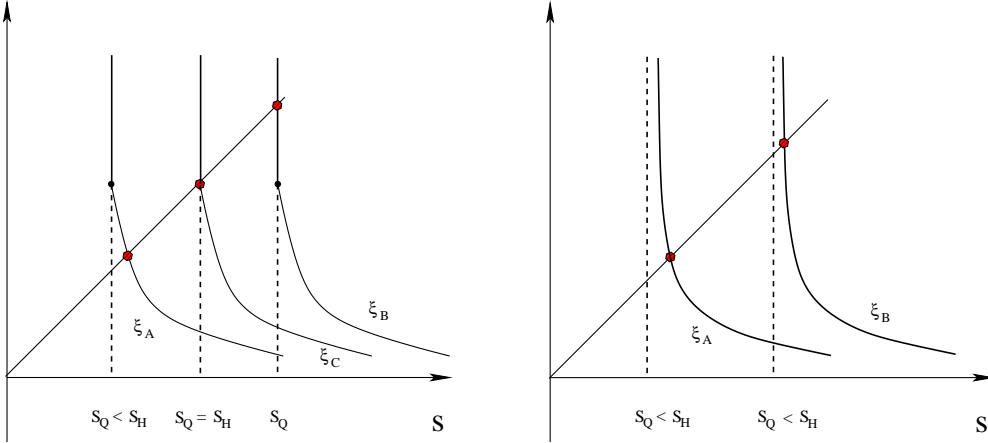


**Figure 1. Left panel.** Graphical solution of Eq. (3) which corresponds to a PT. The solution of Eq. (3) is shown by a filled hexagon. The function  $F(s, \xi)$  is shown by a solid curve for a few values of the parameter  $\xi$ . The function  $F(s, \xi)$  diverges for  $s < s_Q(\xi)$  (shown by dashed lines), but is finite at  $s = s_Q(\xi)$  (shown by black circle). At low values of the parameter  $\xi = \xi_A$ , which can be either  $T$  or  $\mu_B$ , the simple pole  $s_H$  is the rightmost singularity and it corresponds to hadronic phase. For  $\xi = \xi_B \gg \xi_A$  the rightmost singularity is an essential singularity  $s = s_Q(\xi_B)$ , which describes QGP. At intermediate value  $\xi = \xi_C$  both singularities coincide  $s_H(\xi_C) = s_Q(\xi_C)$  and this condition is a Gibbs criterion. **Right panel.** Graphical solution of Eq. (3) which corresponds to a cross-over. The notations are the same as in the left panel. Now the function  $F(s, \xi)$  diverges at  $s = s_Q(\xi)$  (shown by dashed lines). In this case the simple pole  $s_H$  is the rightmost singularity for any value of  $\xi$ .

**(III)** A principally new possibility exists for  $T > T_{cep}$ , where  $\sigma(T) < 0$ . In this case there exists a cross-over, if for  $T \leq T_{cep}$  the rightmost singularity is  $s_H(T)$ , which corresponds to the leftmost curve in the right panel of Fig. 1. Under the latter, its existence can be shown as follows. Let us solve the equation for singularities (3) graphically (see the right panel of Fig. 1). For  $\sigma(T) < 0$  the function  $F_Q(s, T)$  diverges at  $s = s_Q(T)$ . On the other hand, the partial derivatives  $\frac{\partial F_H(s, T)}{\partial s} < 0$  and  $\frac{\partial F_Q(s, T)}{\partial s} < 0$  are always negative. Therefore, the function  $F(s, T) \equiv F_H(s, T) + F_Q(s, T)$  is a monotonically decreasing function of  $s$ , which vanishes at  $s \rightarrow \infty$ . Since the left hand side of Eq. (3) is a monotonically increasing function of  $s$ , then there can exist a single intersection  $s^*$  of  $s$  and  $F(s, T)$  functions. Moreover, for finite  $s_Q(T)$  values this intersection can occur on the right hand side of the point  $s = s_Q(T)$ , i.e.  $s^* > s_Q(T)$  (see the right panel of Fig. 1). Thus, in this case the essential singularity  $s = s_Q(T)$  can become the rightmost one for infinite temperature only. In other words, the pressure of the pure QGP can be reached at infinite  $T$ , whereas for finite  $T$  the hadronic mass spectrum gives a non-zero contribution into all thermodynamic functions. Note that such a behavior is typical for the lattice QCD data at zero baryonic chemical potential [38].

It is clear that in terms of the present model a cross-over existence means a fast transition of energy or entropy density in a narrow  $T$  region from a dominance of the discrete mass-volume spectrum of light hadrons to a dominance of the continuous spectrum of heavy QGP bags. This is exactly the case for  $\sigma(T) < 0$  because in the right vicinity of the point  $s = s_Q(T)$  the function  $F(s, T)$  decreases very fast and then it gradually decreases as function of  $s$ -variable. Since,  $F_Q(s, T)$  changes fast from  $F(s, T) \sim F_Q(s, T) \sim s_Q(T)$  to  $F(s, T) \sim F_H(s, T) \sim s_H(T)$ , their  $s$ -derivatives should change fast as well. Now, recalling that the change from  $F(s, T) \sim F_Q(s, T)$  behavior to  $F(s, T) \sim F_H(s, T)$  in  $s$ -variable corresponds to the cooling of the system (see the right panel of Fig. 1), we conclude that that there exists a narrow region of temperatures, where the  $T$  derivative of system pressure, i.e. the entropy density, drops down from  $\frac{\partial p}{\partial T} \sim s_Q(T) + T \frac{ds_Q(T)}{dT}$  to  $\frac{\partial p}{\partial T} \sim s_H(T) + T \frac{ds_H(T)}{dT}$  very fast compared to other regions of  $T$ , if system cools. If, however, in the vicinity of  $T = T_{cep} - 0$  the rightmost singularity is  $s_Q(T)$ , then for  $T > T_{cep}$  the situation is different and the cross-over does not exist. A detailed analysis of this situation is given in Sect. 4.

Note also that all these nice properties would vanish, if the reduced surface tension coefficient is zero or positive above  $T_{cep}$ . This is one of the crucial points of the present model which puts forward certain doubts about the vanishing of the reduced surface tension coefficient in the FDM [12] and SMM [15]. These doubts are also supported by the first principle results obtained by the Hills and Dales Model [27, 28], because the surface entropy simply counts the degeneracy of a cluster of a fixed volume and it does not physically affect the surface energy of this cluster.

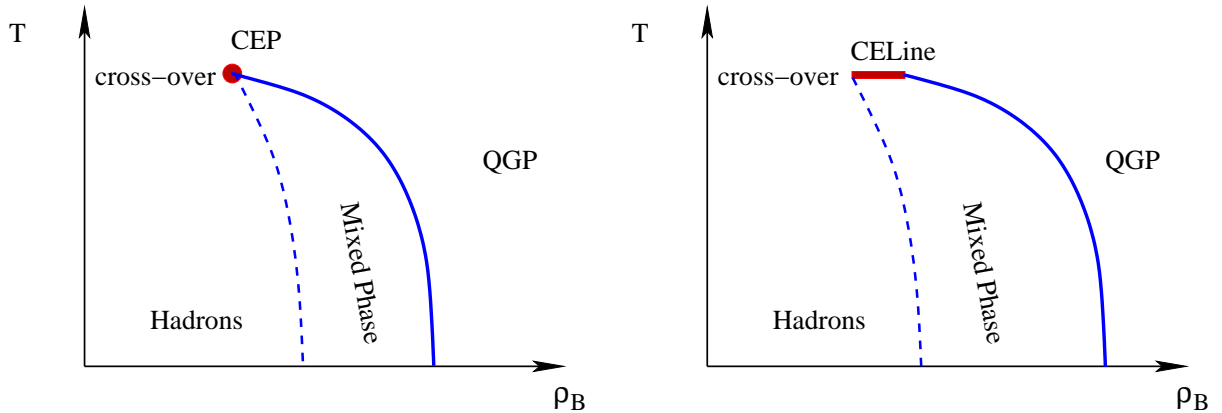


**Figure 2. Left panel.** A schematic picture of the deconfinement phase transition diagram in the plane of baryonic density  $\rho_B$  and  $T$  for the 2<sup>nd</sup> order PT at the critical endpoint (CEP), i.e. for  $\frac{3}{2} < \tau \leq 2$ . For the 3<sup>rd</sup> (or higher) order PT the boundary of the mixed and hadronic phases (dashed curve) should have the same slope as the boundary of the mixed phase and QGP (solid curve) at the CEP. **Right panel.** Same as in the left panel, but for  $\tau > 2$ . The critical endpoint in the  $\mu_B - T$  plane generates the critical end line (CELine) in the  $\rho_B - T$  plane shown by the thick horizontal line. This occurs because of the discontinuity of the partial derivatives of  $s_H$  and  $s_Q$  functions with respect to  $\mu_B$  and  $T$ .

### 3 Generalization to Non-Zero Baryonic Densities

The possibilities (I)-(III) discussed in the preceding section remain unchanged for non-zero baryonic numbers. The latter should be included into consideration to make our model more realistic. To keep the presentation simple, we do not account for strangeness. The inclusion of the baryonic charge of the quark-gluon bags does not change the two types of singularities of the isobaric partition (1) and the corresponding equation for them (3), but it leads to the following modifications of the  $F_H$  and  $F_Q$  functions:

$$F_H(s, T, \mu_B) = \sum_{j=1}^n g_j \exp\left(\frac{b_j \mu_B}{T} - v_j s\right) \phi(T, m_j), \quad (9)$$

$$F_Q(s, T, \mu_B) = u(T, \mu_B) \int_{V_0}^{\infty} dv \frac{\exp[(s_Q(T, \mu_B) - s)v - \sigma(T)v^\kappa]}{v^\tau}. \quad (10)$$

Here the baryonic chemical potential is denoted as  $\mu_B$ , the baryonic charge of the  $j$ -th hadron in the discrete part of the spectrum is  $b_j$ . The continuous part of the spectrum,  $F_Q$  can be obtained from some spectrum  $\rho(m, v, b)$  in the spirit of Ref. [26, 29], but this will lead us away from the main subject.

The QGP pressure  $p_Q = T s_Q(T, \mu_B)$  can be also chosen in several ways. Here we use the bag model pressure

$$p_Q = \frac{\pi^2}{90} T^4 \left[ \frac{95}{2} + \frac{10}{\pi^2} \left( \frac{\mu_B}{T} \right)^2 + \frac{5}{9\pi^4} \left( \frac{\mu_B}{T} \right)^4 \right] - B,$$

but the more complicated model pressures, even with the PT of other kind like the transition between the color superconducting QGP and the usual QGP, can be, in principle, used.

The sufficient conditions for a PT existence are

$$F([s_Q(T, \mu_B = 0) + 0], T, \mu_B = 0) > s_Q(T, \mu_B = 0), \quad (11)$$

$$F([s_Q(T, \mu_B) + 0], T, \mu_B) < s_Q(T, \mu_B), \quad \forall \mu_B > \mu_A. \quad (12)$$

The condition (11) provides that the simple pole singularity  $s^* = s_H(T, \mu_B = 0)$  is the rightmost one at vanishing  $\mu_B = 0$  and given  $T$ , whereas the condition (12) ensures that  $s^* = s_Q(T, \mu_B)$  is the rightmost singularity of the isobaric partition for all values of the baryonic chemical potential above some positive constant  $\mu_A$ . This can be seen in Fig. 1 for  $\mu_B$  being a variable. Since  $F(s, T, \mu_B)$ , where it exists, is a continuous function of its parameters, one concludes that, if the conditions (11) and (12), are fulfilled, then at some chemical potential  $\mu_B^c(T)$  the both singularities should be equal. Thus, one arrives at the Gibbs criterion (5), but for two variables

$$s_H[T, \mu_B^c(T)] = s_Q[T, \mu_B^c(T)]. \quad (13)$$

It is easy to see that the inequalities (11) and (12) are the sufficient conditions of a PT existence for more complicated functional dependencies of  $F_H(s, T, \mu_B)$  and  $F_Q(s, T, \mu_B)$  than the ones used here.

For our choice (9), (10) of  $F_H(s, T, \mu_B)$  and  $F_Q(s, T, \mu_B)$  functions the PT exists at  $T < T_{cep}$ , because the sufficient conditions (11) and (12) can be easily fulfilled by a proper choice of the bag constant  $B$  and the function  $u(T, \mu_B) > 0$  for the interval  $T \leq T_{up}$  with the constant  $T_{up} > T_{cep}$ . Clearly, this is the 1<sup>st</sup> order PT, since the surface tension is finite and it provides the convergence of the integrals (7) and (8) in the expression (6), where the usual  $T$ -derivatives should be now understood as the partial ones for  $\mu_B = \text{const}$ .

Assuming that the conditions (11), (12) are fulfilled by the correct choice of the model parameters  $B$  and  $u(T, \mu_B) > 0$ , one can see now that at  $T = T_{cep}$  there exists a PT as well, but its order is defined by the value of  $\tau$ . As was discussed in the preceding section for  $3/2 < \tau \leq 2$  there exists the 2<sup>nd</sup> order PT. For  $1 < \tau \leq 3/2$  there exist the PT of higher order, defined by the conditions formulated in [25]. This is a new possibility, which, to our best knowledge, does not contradict to any general physical principle (see the left panel in Fig. 2).

The case  $\tau > 2$  can be ruled out because there must exist the first order PT for  $T \geq T_{cep}$ , whereas for  $T < T_{cep}$  there exists the cross-over. Thus, the critical endpoint in  $T - \mu_B$  plane will correspond to the critical interval in the temperature-baryonic density plane. Since such a structure of the phase diagram in the variables temperature-density has, to our knowledge, never been observed, we conclude that the case  $\tau > 2$  is unrealistic (see the right panel in Fig. 2). Note that a similar phase diagram exists in the FDM with the only difference that the boundary of the mixed and liquid phases (the latter in the QGBST model corresponds to QGP) is moved to infinite particle density.

#### 4 Surface Tension Induced Phase Transition

Using our results for the case **(III)** of the preceding section, we conclude that above  $T_{cep}$  there is a cross-over, i.e. the QGP and hadrons coexist together up to the infinite values of  $T$  and/or  $\mu_B$ . Now, however, it is necessary to answer the question: How can the two different sets of singularities that exist on two sides of the line  $T = T_{cep}$  provide the continuity of the solution of Eq. (3)?

It is easy to answer this question for  $\mu_B < \mu_B^c(T_{cep})$  because in this case all partial  $T$  derivatives of  $s_H(T, \mu_B)$ , which is the rightmost singularity, exist and are finite at any point of the line  $T = T_{cep}$ . This can be seen from the fact that for the considered region of parameters  $s_H(T, \mu_B)$  is the rightmost singularity and, consequently,  $s_H(T, \mu_B) > s_Q(T, \mu_B)$ . The latter inequality provides the existence and finiteness of the volume integral in  $F_Q(s, T, \mu_B)$ . In combination with the power  $T$  dependence of the reduced surface tension coefficient  $\sigma(T)$  the same inequality provides the existence and finiteness of all its partial  $T$  derivatives of  $F_Q(s, T, \mu_B)$  regardless to the sign of  $\sigma(T)$ . Thus, using the Taylor expansion in powers of  $(T - T_{cep})$  at any point of the interval  $T = T_{cep}$  and  $\mu_B < \mu_B^c(T_{cep})$ , one can calculate  $s_H(T, \mu_B)$  for the values of  $T > T_{cep}$  which are inside the convergency radius of the Taylor expansion.

The other situation is for  $\mu_B \geq \mu_B^c(T_{cep})$  and  $T > T_{cep}$ , namely in this case above the deconfinement PT there must exist a weaker PT induced by the disappearance of the reduced surface tension coefficient. To demonstrate this we have solve Eq. (3) in the limit, when  $T$  approaches the curve  $T = T_{cep}$  from above, i.e. for  $T \rightarrow T_{cep} + 0$ , and study the behavior of  $T$  derivatives of the solution of Eq. (3)  $s^*$  for fixed values of  $\mu_B$ . For this purpose we have to evaluate the integrals  $\mathcal{K}_\tau(\Delta, \gamma^2)$  introduced in Eq. (8). Here the notations  $\Delta \equiv s^* - s_Q(T, \mu_B)$  and  $\gamma^2 \equiv -\sigma(T) > 0$  are introduced for convenience.

To avoid the unpleasant behavior for  $\tau \leq 2$  it is convenient to transform (8) further on by integrating by parts:

$$\mathcal{K}_\tau(\Delta, \gamma^2) \equiv g_\tau(V_0) - \frac{\Delta}{\tau - 1} \mathcal{K}_{\tau-1}(\Delta, \gamma^2) + \frac{\kappa \gamma^2}{\tau - 1} \mathcal{K}_{\tau-\kappa}(\Delta, \gamma^2), \quad (14)$$

where the regular function  $g_\tau(V_0)$  is defined as

$$g_\tau(V_0) \equiv \frac{1}{(\tau - 1)V_0^{\tau-1}} \exp[-\Delta V_0 + \gamma^2 V_0^\kappa]. \quad (15)$$

For  $\tau - a > 1$  one can change the variable of integration  $v \rightarrow z/\Delta$  and rewrite  $\mathcal{K}_{\tau-a}(\Delta, \gamma^2)$  as

$$\mathcal{K}_{\tau-a}(\Delta, \gamma^2) = \Delta^{\tau-a-1} \int_{V_0 \Delta}^{\infty} dz \frac{\exp[-z + \gamma^2 \Delta^{-\kappa} z^\kappa]}{z^{\tau-a}} \equiv \Delta^{\tau-a-1} \mathcal{K}_{\tau-a}(1, \gamma^2 \Delta^{-\kappa}). \quad (16)$$

This result shows that in the limit  $\gamma \rightarrow 0$ , when the rightmost singularity must approach  $s_Q(T, \mu_B)$  from above, i.e.  $\Delta \rightarrow 0^+$ , the function (16) behaves as  $\mathcal{K}_{\tau-a}(\Delta, \gamma^2) \sim \Delta^{\tau-a-1} + O(\Delta^{\tau-a})$ . This is so because for  $\gamma \rightarrow 0$  the ratio  $\gamma^2 \Delta^{-\kappa}$  cannot go to infinity, otherwise the function  $\mathcal{K}_{\tau-1}(1, \gamma^2 \Delta^{-\kappa})$ , which enters into the right hand side of (14), would diverge exponentially and this makes impossible an existence of the solution of Eq. (3) for  $T = T_{cep}$ . The analysis shows that for  $\gamma \rightarrow 0$  there exist two possibilities: either  $\nu \equiv \gamma^2 \Delta^{-\kappa} \rightarrow \text{const}$  or  $\nu \equiv \gamma^2 \Delta^{-\kappa} \rightarrow 0$ . The most straightforward way to analyze these possibilities for  $\gamma \rightarrow 0$  is to assume the following behavior

$$\Delta = A \gamma^\alpha + O(\gamma^{\alpha+1}), \quad \Rightarrow \quad \frac{\partial \Delta}{\partial T} = \frac{\partial \gamma}{\partial T} [A \alpha \gamma^{\alpha-1} + O(\gamma^\alpha)] \sim \frac{(2k+1)A \alpha \gamma^\alpha}{2(T - T_{cep})}, \quad (17)$$

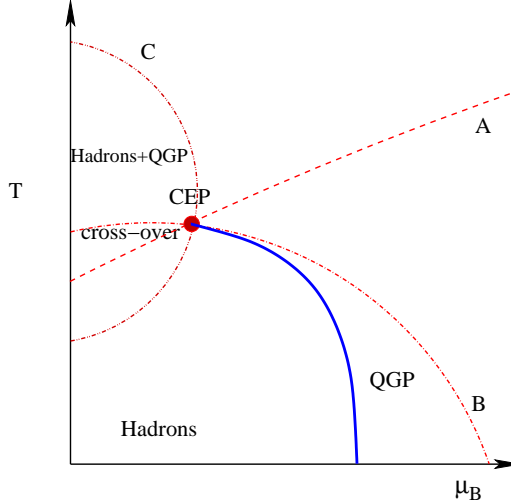


**Figure 3.** A schematic picture of the deconfinement phase transition diagram (full curve) in the plane of baryonic chemical potential  $\mu_B$  and  $T$  for the 2<sup>nd</sup> order PT at the tricritical endpoint (CEP). The model predicts an existence of the surface induced PT of the 2<sup>nd</sup> or higher order (depending on the model parameters). This PT starts at the CEP and goes to higher values of  $T$  and/or  $\mu_B$ . Here it is shown by the dashed curve CEP-A, if the phase diagram is endless, or by the dashed-dot curve CEP-B, if the phase diagram ends at  $T = 0$ , or by the dashed-double-dot curve CEP-C, if the phase diagram ends at  $\mu_B = 0$ . Below (above) each of A or B curves the reduced surface tension coefficient is positive (negative). For the curve C the surface tension coefficient is positive outside of it.

and find out the  $\alpha$  value by equating the  $T$  derivative of  $\Delta$  with the  $T$  derivative (6).

The analysis shows [25] that for  $\Delta^{2-\tau} \leq \gamma\gamma'\Delta^{1-\kappa}$  one finds

$$\gamma^{\alpha-2} \sim \Delta^{1-\kappa} \Rightarrow \alpha\kappa = 2 \quad \text{for } \tau \leq 1 + \frac{\kappa}{2k+1}. \quad (18)$$

Similarly, for  $\Delta^{2-\tau} \geq \gamma\gamma'\Delta^{1-\kappa}$  one obtains  $\gamma^{\alpha-1}\gamma' \sim \Delta^{2-\tau}$  and, consequently,

$$\alpha = \frac{2}{(\tau-1)(2k+1)} \quad \text{for } \tau \geq 1 + \frac{\kappa}{2k+1}. \quad (19)$$

Summarizing our results for  $\gamma \rightarrow 0$ , we can write the expression for the second derivative of  $\Delta$  as [25]:

$$\frac{\partial^2 \Delta}{\partial T^2} \sim \begin{cases} [(T - T_{cep})/T_{cep}]^{(2k+1)/\kappa-2}, & \tau \leq 1 + \kappa/(2k+1), \\ [(T - T_{cep})/T_{cep}]^{(3-2\tau)/(\tau-1)}, & \tau \geq 1 + \kappa/(2k+1). \end{cases} \quad (20)$$

The last result shows us that, depending on  $\kappa$  and  $k$  values, the second derivatives of  $s^*$  and  $s_Q(T, \mu_B)$  can differ from each other for  $3/2 < \tau < 2$  or can be equal for  $1 < \tau \leq 3/2$ . In other words, we found that at the line  $T = T_{cep}$  there exists the 2<sup>nd</sup> order PT for  $3/2 < \tau < 2$  and the higher order PT for  $1 < \tau \leq 3/2$ , which separates the pure QGP phase from the region of a cross-over, i.e. the mixed states of hadronic and QGP bags. Since it exists at the line of a zero surface tension, this PT will be called the *surface induced PT*. For instance, from (20) it follows that for  $k = 0$  and  $\kappa > \frac{1}{2}$  there is the 2<sup>nd</sup> order PT, whereas for  $k = 0$  and  $\kappa = 1/2$  or for  $k > 0$  and  $\kappa < 1$  there is the 3<sup>d</sup> order PT, and so on.

Since the analysis performed in the present section did not include any  $\mu_B$  derivatives of  $\Delta$ , it remains valid for the  $\mu_B$  dependence of the reduced surface tension coefficient, i.e. for  $T_{cep}(\mu_B)$ . Only it is necessary to make a few comments on a possible location of the *surface tension null line*  $T_{cep}(\mu_B)$ . In principle, such a null line can be located anywhere, if its location does not contradict to the sufficient conditions (11) and (12) of the 1<sup>st</sup> deconfinement PT existence. Thus, the surface tension null line must cross the deconfinement line in the  $\mu_B - T$  plane at a single point which is the tricritical endpoint  $(\mu_B^{cep}; T_{cep}(\mu_B^{cep}))$ , whereas for  $\mu_B > \mu_B^{cep}$  the null line should have higher temperature for the same  $\mu_B$  than the deconfinement one, i.e.  $T_{cep}(\mu_B) > T_c(\mu_B)$  (see Fig. 3). Clearly, there exist two distinct cases for the surface tension null line: either it is endless, or it ends at zero temperature or at other singularity, like the Color-Flavor-Locked phase. From the present lattice QCD data [38] it follows that the case C in Fig. 3 is the least possible.

To understand the meaning of the surface induced PT it is instructive to quantify the difference between phases by looking into the mean size of the bag:

$$\langle v \rangle \equiv -\frac{\partial \ln F(s, T, \mu_B)}{\partial s} \bigg|_{s=s^*-0}. \quad (21)$$

As was shown in hadronic phase phase  $\Delta > 0$  and, hence, it consists of the bags of finite mean volumes, whereas, by construction, the QGP phase is a single infinite bag. For the cross-over states  $\Delta > 0$  and, therefore, they are the bags of finite mean volumes, which gradually increase, if the rightmost singularity approaches  $s_Q(T, \mu_B)$ , i.e. at very large values  $T$  and/or  $\mu_B$ . Such a classification is useful to distinguish QCD phases of present model: it shows that hadronic and cross-over states are separated from the QGP phase by the 1<sup>st</sup> order deconfinement PT and by the 2<sup>nd</sup> or higher order PT, respectively.

## 5 Conclusions and Perspectives

Here we discussed an analytically solvable statistical model which simultaneously describes the 1<sup>st</sup> and 2<sup>nd</sup> order PTs with a cross-over. The approach is general and can be used for more complicated parameterizations of the hadronic mass-volume spectrum, if in the vicinity of the deconfinement PT region the discrete and continuous parts of this spectrum can be expressed in the form of Eqs. (9) and (10), respectively. Also the actual parameterization of the QGP pressure  $p = Ts_Q(T, \mu_B)$  was not used so far, which means that our result can be extended to more complicated functions, that can contain other phase transformations (chiral PT, or the PT to color superconducting phase) provided that the sufficient conditions (11) and (12) for the deconfinement PT existence are satisfied.

In this model the desired properties of the deconfinement phase diagram are achieved by accounting for the temperature dependent surface tension of the quark-gluon bags. As we showed, it is crucial for the cross-over existence that at  $T = T_{cep}$  the reduced surface tension coefficient vanishes and remains negative for temperatures above  $T_{cep}$ . Then the deconfinement  $\mu_B - T$  phase diagram has the 1<sup>st</sup> PT at  $\mu_B > \mu_B^c(T_{cep})$  for  $3/2 < \tau < 2$ , which degenerates into the 2<sup>nd</sup> order PT (or higher order PT for  $3/2 \geq \tau > 1$ ) at  $\mu_B = \mu_B^c(T_{cep})$ , and a cross-over for  $0 \leq \mu_B < \mu_B^c(T_{cep})$ . These two ingredients drastically change the critical properties of the GBM [2] and resolve the long standing problem of a unified description of the 1<sup>st</sup> and 2<sup>nd</sup> order PTs and a cross-over, which, despite all claims, was not resolved in Ref. [7]. In addition, we found that at the null line of the surface tension there must exist the surface induced PT of the 2<sup>nd</sup> or higher order, which separates the pure QGP from the mixed states of hadrons and QGP bags, that coexist above the cross-over region (see Fig. 3). Thus, the QGBST model predicts that the QCD critical endpoint is the tricritical endpoint. It would be interesting to verify this prediction with the help of the lattice QCD analysis. For this one will need to study the behavior of the bulk and surface contributions to the free energy of the QGP bags and/or the string connecting the static quark-antiquark pair.

Also in the QGBST model the pressure of the deconfined phase is generated by the infinite bag, whereas the discrete part of the mass-volume spectrum plays an auxiliary role even above the cross-over region. Therefore, there is no reason to believe that any quantitative changes of the properties of low lying hadronic states generated by the surrounding media (like the mass shift of the  $\omega$  and  $\rho$  mesons [39]) would be the robust signals of the deconfinement PT. On the other hand, the QGP bags created in the experiments have finite mass and volume and, hence, the strong discontinuities which are typical for the 1<sup>st</sup> order PT should be smeared out which would make them hardly distinguishable from the cross-over. Thus, to seriously discuss the signals of the 1<sup>st</sup> order deconfinement PT and/or the tricritical endpoint, one needs to solve the finite volume version of the QGBST model like it was done for the SMM [21] and the GBM [22]. This, however, is not sufficient because, in order to make any reliable prediction for experiments, the finite volume equation of state must be used in hydrodynamic equations which, unfortunately, are not suited for such a purpose. Thus, we are facing a necessity to return to the foundations of heavy ion phenomenology and to modify them according to the requirements of the experiments.

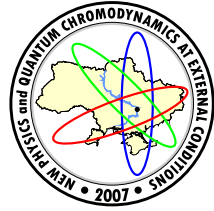
To apply the QGBST model to the experiments it is necessary to refine it: it seems that for the mixture of hadrons and QGP bags above the cross-over line it is necessary to include the relativistic treatment of hard core repulsion [40, 41] for lightest hadrons and to include into statistical description the medium dependent width of resonances and QGP bags, which can, in principle, change our understanding of the cross-over mechanism [42].

*Acknowledgments.* I am cordially thankful to the organizers of the seminar-workshop “New Physics and Quantum Chromodynamics at External Conditions” for a warm hospitality and the chance to visit my native city Dnipropetrovsk and discuss there the physics which is at the frontier line of research.

## References

- [1] R. Hagedorn and J. Rafelski, Phys.Lett. **B97**, 136 (1980).
- [2] M.I. Gorenstein, V.K. Petrov and G.M. Zinovjev, Phys.Lett. **B106**, 327 (1981).
- [3] J.I. Kapusta, Phys.Rev. **D23**, 2444 (1981).
- [4] A. Chodos *et. al.*, Phys.Rev. **D9**, 3471 (1974).
- [5] E.V. Shuryak, Phys.Rep. **61**, 71 (1980); J. Cleymans, R.V. Gavai, and E. Suhonen, Phys.Rep. **130**, 217 (1986).

- [6] see, for instance, J. Cleymans and H. Satz, Z.Phys. **C57**, 135 (1993); G.D. Yen, M.I. Gorenstein, W. Greiner, and S.N. Yang, Phys.Rev. **C56**, 2210 (1997); P. Braun-Munzinger, I. Heppe and J. Stachel, Phys.Lett. **B465**, 15 (1999); F. Becattini *et. al.*, Phys.Rev. **C69**, 024905 (2004).
- [7] M.I. Gorenstein, M. Ga  dzicki and W. Greiner, Phys.Rev. **C72**, 024909 (2005) and references therein.
- [8] for qualitative arguments see M. Stephanov, Acta Phys.Polon. **B35**, 2939 (2004).
- [9] Z. Fodor and S.D. Katz, JHEP **0203**, 014 (2002).
- [10] F. Karsch *et. al.*, Nucl.Phys.Proc.Suppl. **129**, 614 (2004).
- [11] L.G. Moretto, K.A. Bugaev, J.B. Elliott and L. Phair, LBNL preprint 59103 [nucl-th/0511180]
- [12] M. E. Fisher, Physics **3**, 255 (1967).
- [13] L. G. Moretto *et. al.*, Phys.Rep. **287**, 249 (1997).
- [14] for a review on Fisher scaling see J.B. Elliott, K.A. Bugaev, L.G. Moretto and L. Phair, nucl-ex/0608022 and references therein.
- [15] J.P. Bondorf *et al.*, Phys.Rep. **257**, 131 (1995).
- [16] S. Das Gupta and A.Z. Mekjian, Phys.Rev. **C57**, 1361 (1998)
- [17] S. Das Gupta, A. Majumder, S. Pratt, and A. Mekjian, nucl-th/9903007.
- [18] K.A. Bugaev, M.I. Gorenstein, I.N. Mishustin and W. Greiner, Phys.Rev. **C62**, 044320 (2000) [nucl-th/0007062].
- [19] K.A. Bugaev, M.I. Gorenstein, I.N. Mishustin and W. Greiner, Phys.Lett. **B498**, 144 (2001) [nucl-th/0103075].
- [20] P.T. Reuter and K.A. Bugaev, Phys.Lett. **B517**, 233 (2001).
- [21] K.A. Bugaev, Acta Phys.Polon. **B36**, 3083 (2005); nucl-th/0507028.
- [22] K.A. Bugaev, nucl-th/0511031 (to appear in Phys.Part.Nucl.Lett.)
- [23] L. Beaulieu *et al.*, Phys.Lett. **B463**, 159 (1999).
- [24] J.B. Elliott *et al.* [The EOS Collaboration], Phys.Rev. **C62**, 064603 (2000).
- [25] K.A. Bugaev, hep-ph/0703222 (will appear in Phys.Rev.C).
- [26] I. Zakout, C. Greiner, J. Schaffner-Bielich, Nucl.Phys. **A781**, 150 (2007).
- [27] K. A. Bugaev, L. Phair and J.B. Elliott, Phys.Rev. **E72**, 047106 (2005).
- [28] K.A. Bugaev and J.B. Elliott, Ukr.J.Phys. **52**, 301 (2007) [nucl-th/0501080].
- [29] M.I. Gorenstein, G.M. Zinovjev, V.K. Petrov, and V.P. Shelest Teor.Mat.Fiz. (Russ) **52**, 346 (1982).
- [30] R. Hagedorn, Nuovo Cimento Suppl. **3**, 147 (1965).
- [31] R. Hagedorn and J. Ranft, Suppl. Nuovo Cimento **6**, 169 (1968).
- [32] L.G. Moretto, K.A. Bugaev, J.B. Elliott and L. Phair, Europhys. Lett. **76**, 402 (2006).
- [33] K.A. Bugaev, J.B. Elliott, L.G. Moretto and L. Phair, LBNL preprint 57363 [hep-ph/0504011].
- [34] L.G. Moretto, K.A. Bugaev, J.B. Elliott and L. Phair, nucl-th/0601010.
- [35] D.G. Ravenhall, C.J. Pethick and J.R. Wilson, Phys.Rev.Lett. **50**, 2066 (1983).
- [36] J. Liao and E.V. Shuryak, Phys.Rev. **D73**, 014509 (2006) [hep-ph/0510110].
- [37] L.G. Moretto, K.A. Bugaev, J.B. Elliott, R. Ghetti, J. Helgesson and L. Phair, Phys.Rev.Lett. **94**, 202701 (2005).
- [38] F. Karsch and E. Laermann, in *Quark-Gluon Plasma 3*, edited by R.C. Hwa and X.-N. Wang (World Scientific, Singapore, 2004), p. 1 [hep-lat/0305025].
- [39] E. Shuryak, hep-ph/0504048.
- [40] K.A. Bugaev, M.I. Gorenstein, H. St  cker and W. Greiner, Phys.Lett. **B485**, 121 (2000); G. Zeeb, K.A. Bugaev, P.T. Reuter and H. St  cker, nucl-th/0209011.
- [41] K.A. Bugaev, nucl-th/0611102.
- [42] for a discussion and alternative cross-over mechanism see D.B. Blaschke and K.A. Bugaev, Fizika **B13**, 491 (2004); Phys.Part.Nucl.Lett. **2**, 305 (2005).



## THE SPONTANEOUS GENERATION OF MAGNETIC FIELD AT HIGH TEMPERATURE ON A LATTICE

V. I. Demchik<sup>a</sup>, V. V. Skalozub<sup>b</sup>

Dnipropetrovsk National University, Dnipropetrovsk, Ukraine

The spontaneous generation of the chromomagnetic field at high temperature is investigated in a lattice formulation of the  $SU(2)$ -gluodynamics. The procedure of studying this phenomenon is developed. The Monte Carlo simulations of the free energy on the lattices  $2 \times 8^3$ ,  $2 \times 16^3$  and  $4 \times 8^3$  at various temperatures are carried out. The creation of the field is indicated by means of the  $\chi^2$ -analysis of the data set accumulating 5–10 millions MC configurations. A comparison with the results of other approaches is done.

### 1 Introduction

Among interesting problems of modern cosmology the origin of large-scale magnetic fields is intensively attacked nowadays. Various mechanisms of the field generation at different stages of the universe evolution were proposed [1]. Basically they are grounded on the idea of Fermi, Chandrasekhar and Zel'dovich that to have the present day galaxy magnetic fields of order  $\sim 1\mu G$  correlated on a scale  $\sim 1\text{Mpc}$  seed magnetic fields must be present in the early universe. These fields had been frozen in a cosmic plasma and then amplified by some of the mechanisms of the field amplification. One of the ways to produce seed fields is a spontaneous vacuum magnetization at high temperature  $T$  [2–5]. Actually, this is an extension of the Savvidy model for the QCD vacuum [6], proposed already at  $T = 0$  and describing the creation of the Abelian chromomagnetic fields due to a vacuum polarization, in case of nonzero temperature. At zero temperature this field configuration is unstable because of the tachyonic mode in the gluon spectrum. At  $T \neq 0$ , the possibility of having strong temperature-dependent and stable magnetic fields was discovered [4]. The field stabilization is ensured by the temperature and field dependent gluon magnetic mass.

Another related field of interest is the deconfinement phase of QCD. As it was realized recently, this is not the gas of free quarks and gluons, but a complicate interacting system of them. This was discovered at RHIC experiments [7] and observed in either perturbative [4, 8] or nonperturbative [9] investigations of the vacuum state with magnetic fields at high temperature. In Refs. [4, 8] the spontaneous creation of the chromomagnetic fields of order  $gB \sim g^4 T^2$  was observed in  $SU(2)$ - and  $SU(3)$ -gluodynamics within the one-loop plus daisy resummation accounted for. In Ref. [9] the chromomagnetic condensate of same order was obtained in stochastic QCD vacuum model and method of dimensional reduction by comparison with lattice data. In Refs. [10] the response of the vacuum to the influence of strong external fields at different temperatures has been investigated and it was shown that the confinement is restored by increasing the strength of the applied field. These results stimulated the present investigation.

We are going to determine the spontaneous creation of magnetic fields in lattice simulations of  $SU(2)$ -gluodynamics. In contrast to the problems in the external field, in the case of interest the field strength is a dynamical variable which values at different temperatures have to be determined by means of the minimization of the free energy. This procedure is not a simple one as in continuum because the field strength on a lattice is quantized. To deal with this peculiarity, we consider magnetic fluxes on a lattice as the main objects to be investigated. The fluxes take continuous values, and therefore the minimization of the free energy in presence of magnetic field can be fulfilled in a usual way. These speculations serve as an explanation of the strategy of our calculations.

One of the methods to introduce a magnetic flux on a lattice is to use the twisted boundary conditions (t.b.c.) [11]. In this approach the flux is a continuous quantity. So, in what follows we consider the free energy  $F(\varphi)$  with the magnetic flux  $\varphi$  on a lattice in the  $SU(2)$ -gluodynamics and calculate its values at different temperatures by means of Monte Carlo (MC) simulations. We will show that the global minimum of  $F(\varphi)$  is located at some non-zero value  $\varphi_{min}$  dependent on the temperature. It means the spontaneous creation of the temperature-dependent magnetic fields in the deconfinement phase.

The paper is organized as follows. In sect. 2 some necessary information about the magnetic fluxes on a lattice is adduced. In sect. 3 the calculation details and the results are given. Section 4 is devoted to discussion.

e-mail: <sup>a</sup>vadimdi@yahoo.com, <sup>b</sup>skalozub@dsu.dp.ua

© Demchik V.I., Skalozub V.V., 2007.

## 2 Magnetic fields on a lattice

In perturbation theory, the value of the macroscopic (classical) magnetic field generated inside a system is determined by the minimization of the free energy functional. The interaction with the classical field is introduced by splitting the gauge field potential in two parts:  $A_\mu = \bar{A}_\mu + A_\mu^R$ , where  $A_\mu^R$  describes a radiation field and  $\bar{A}_\mu = (0, 0, Hx^1, 0)$  corresponds to the constant magnetic field directed along the third axis. However, on a lattice, the direct detection of the spontaneously generated field strength by straightforward analysis of the configurations, which are produced in the MC simulations, seems to be problematic. Therefore, it is reasonable to follow the approach used in the continuum field theory.

First, let us write down the free energy density,

$$F(\varphi) = -\log \frac{Z(\varphi)}{Z(0)}, \quad Z(\varphi) = \int [DU(\varphi)] \exp\{-S(U(\varphi))\}. \quad (1)$$

Here,  $Z(\varphi)$  and  $Z(0)$  are the partition function at finite and zero magnetic fluxes, respectively; the link variable  $U$  is the lattice analogue of the potential  $A_\mu$ .

The free energy density relates to the effective action as follows,

$$F(\varphi) = \bar{S}(\varphi) - \bar{S}(0), \quad (2)$$

where  $\bar{S}(\varphi)$  and  $\bar{S}(0)$  are the effective lattice actions with and without magnetic field, correspondingly.

To detect the spontaneous creation of the field it is necessary to show that the free energy density has the global minimum at a non-zero magnetic flux,  $\varphi_{min} \neq 0$ .

In what follows, we use the hypercubic lattice  $L_t \times L_s^3$  ( $L_t < L_s$ ) with the hypertorus geometry;  $L_t$  and  $L_s$  are the temporal and the spatial sizes of the lattice, respectively. In the limit of  $L_s \rightarrow \infty$  the temporal size  $L_t$  is related to physical temperature. The one-plaquette action of the  $SU(2)$  lattice gauge theory can be written as

$$S_W = \beta \sum_x \sum_{\mu > \nu} \left[ 1 - \frac{1}{2} \operatorname{Tr} U_{\mu\nu}(x) \right]; \quad (3)$$

$$U_{\mu\nu}(x) = U_\mu(x) U_\nu(x + a\hat{\mu}) U_\mu^\dagger(x + a\hat{\nu}) U_\nu^\dagger(x), \quad (4)$$

where  $\beta = 4/g^2$  is the lattice coupling constant,  $g$  is the bare coupling,  $U_\mu(x)$  is the link variable located on the link leaving the lattice site  $x$  in the  $\mu$  direction,  $U_{\mu\nu}(x)$  is the ordered product of the link variables.

The effective action  $\bar{S}$  in (2) is the Wilson action averaged over the Boltzmann configurations, produced in the MC simulations.

The lattice variable  $U_\mu(x)$  can be decomposed in terms of the unity,  $I$ , and Pauli,  $\sigma_j$ , matrices in the color space,

$$U_\mu(x) = I U_\mu^0(x) + i \sigma_j U_\mu^j(x) = \begin{pmatrix} U_\mu^0(x) + i U_\mu^3(x) & U_\mu^2(x) + i U_\mu^1(x) \\ -U_\mu^2(x) + i U_\mu^1(x) & U_\mu^0(x) - i U_\mu^3(x) \end{pmatrix}. \quad (5)$$

The four components  $U_\mu^j(x)$  are subjected to the normalization condition

$\sum_j U_\mu^j(x) U_\mu^j(x) = 1$ . Hence, only three components are independent.

Since the spontaneously generated magnetic field is to be the Abelian one, the Abelian parametrization of the lattice variables is used to introduce the magnetic field,

$$U_\mu(x) = \begin{pmatrix} \cos \phi_\mu(x) e^{i\theta_\mu(x)} & \sin \phi_\mu(x) e^{i\chi_\mu(x)} \\ -\sin \phi_\mu(x) e^{-i\chi_\mu(x)} & \cos \phi_\mu(x) e^{-i\theta_\mu(x)} \end{pmatrix}, \quad (6)$$

where the angular variables are changed in the following ranges  $\theta, \chi \in [-\pi; +\pi]$ ,  $\phi \in [0; \pi/2]$ .

The Abelian part of the lattice variables is represented by the diagonal components of the matrix and the condensate Abelian magnetic field influences the field  $\theta_\mu(x)$ , only.

The second important task is to incorporate the magnetic flux in this formalism. The most natural way was proposed by 't Hooft [11]. In his approach, the constant homogeneous external flux  $\varphi$  in the third spatial direction can be introduced by applying the following t.b.c.:

$$\begin{aligned} U_\mu(L_t, x_1, x_2, x_3) &\leftrightarrow U_\mu(0, x_1, x_2, x_3), & U_\mu(x_0, L_s, x_2, x_3) &\leftrightarrow U_\mu(x_0, 0, x_2, x_3), \\ U_\mu(x_0, x_1, L_s, x_3) &\leftrightarrow e^{i\varphi} U_\mu(x_0, x_1, 0, x_3), & U_\mu(x_0, x_1, x_2, L_s) &\leftrightarrow U_\mu(x_0, x_1, x_2, 0). \end{aligned} \quad (7)$$

It could be seen, the edge links in all directions are identified as usual periodic boundary conditions except for the links in the second spatial direction, for which the additional phase  $\varphi$  is added (Fig. 1). In the continuum

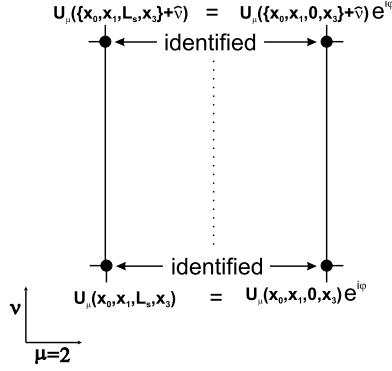


**Figure 1.** The plaquette presentation of the twisted boundary conditions.

limit, such t.b.c. settle the magnetic field with the potential  $A_\mu(x) = (0, 0, Hx^1, 0)$ . The magnetic flux  $\varphi$  is measured in angular units and can take a value from 0 to  $2\pi$ .

The lattice variables (in the Abelian parametrization) in the presence of the magnetic flux  $\varphi$  are

$$U_\mu(x) = \begin{pmatrix} \cos \phi_\mu(x) e^{i(\theta_\mu(x) + \varphi_\mu(x))} & \sin \phi_\mu(x) e^{i\chi_\mu(x)} \\ -\sin \phi_\mu(x) e^{-i\chi_\mu(x)} & \cos \phi_\mu(x) e^{-i(\theta_\mu(x) + \varphi_\mu(x))} \end{pmatrix}, \quad (8)$$

where  $\varphi_\mu(x) = \varphi$  for the edge links at  $x = (x_0, x_1, L_s, x_3)$  with  $\mu = 2$  and  $\varphi_\mu(x) = 0$  for other links.

The total flux through the plane spanned by the plaquettes  $p$ , which affects the edge links at  $x = (x_0, x_1, L_s, x_3)$  with  $\mu = 2$ , is

$$g\Phi = \sum_{p \in \text{plane}} (\theta_p + \varphi), \quad \theta_p = \theta_{\mu\nu}(x) = \theta_\mu(x) + \theta_\nu(x + a\hat{\mu}) - \theta_\mu(x + a\hat{\nu}) - \theta_\nu(x). \quad (9)$$

Eq. (9) is the lattice analogue of the flux in the continuum:

$$\Phi_c = \int_S d^2\sigma_{\mu\nu} F_{\mu\nu}. \quad (10)$$

In this approach the variable  $\varphi$  describes a flux through the whole lattice plane, not just through an elementary plaquette.

The t.b.c. for the components (8),

$$\begin{aligned} U_\mu^0(x) &= \cos(\theta_\mu(x) + \varphi_\mu(x)) \cos \phi_\mu(x), & U_\mu^1(x) &= \sin \phi_\mu(x) \cos \chi_\mu(x), \\ U_\mu^2(x) &= \sin \phi_\mu(x) \sin \chi_\mu(x), & U_\mu^3(x) &= \sin(\theta_\mu(x) + \varphi_\mu(x)) \cos \phi_\mu(x), \end{aligned} \quad (11)$$

read

$$U_\mu^0(x) \leftrightarrow \begin{cases} U_\mu^0(x) \cos \varphi - U_\mu^3(x) \sin \varphi & \text{for } x = \{x_0, x_1, L_s, x_3\}, \mu = 2, \\ U_\mu^0(x) & \text{for other links,} \end{cases} \quad (12)$$

$$U_\mu^3(x) \leftrightarrow \begin{cases} U_\mu^0(x) \sin \varphi + U_\mu^3(x) \cos \varphi & \text{for } x = \{x_0, x_1, L_s, x_3\}, \mu = 2, \\ U_\mu^3(x) & \text{for other links.} \end{cases} \quad (13)$$

The relations (12) and (13) have been implemented into the kernel of the MC procedure in order to produce the configurations with the magnetic flux  $\varphi$ . In this case the flux  $\varphi$  is accounted for in obtaining a Boltzmann ensemble at each MC iteration.

### 3 Description of simulations and data fits

The MC simulations are carried out by means of the heat bath method. The lattices  $2 \times 8^3$ ,  $2 \times 16^3$  and  $4 \times 8^3$  at  $\beta = 3.0, 5.0$  are considered. These values of the coupling constant correspond to the deconfinement phase and perturbative regime. To thermalize the system, 200-500 iterations are fulfilled. At each working iteration, the plaquette value (4) is averaged over the whole lattice leading to the Wilson action (3). Then the effective action is calculated by averaging over the 1000-5000 working iterations. By setting a set of magnetic fluxes  $\varphi$  in the MC simulations we obtain the corresponding set of values of the effective action. The value of the condensed magnetic flux  $\varphi_{min}$  is obtained as the result of the minimization of the free energy density (2).

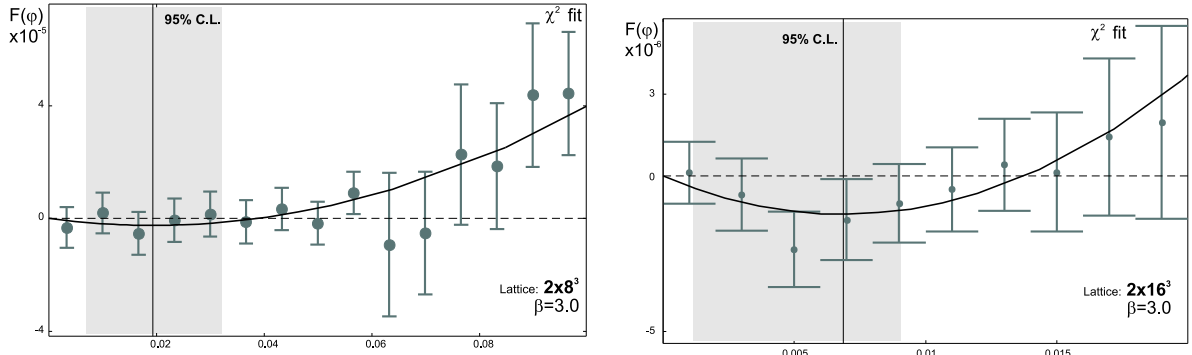


**Figure 2.**  $\chi^2$ -fit of the free energy density on lattice  $2 \times 8^3$  (left figure) and  $2 \times 16^3$  (right figure) for  $\beta = 3.0$  (grey regions describe the  $\varphi_{min} = 0.019^{+0.013}_{-0.012}$  and  $\varphi_{min} = 0.0069^{+0.0022}_{-0.0057}$ , at the 95% C.L., correspondingly).

The spontaneous generation of magnetic field is the effect of order  $\sim g^4$  [4]. The results of MC simulations show the comparably large dispersion. So, the large amount of the MC data is collected and the standard  $\chi^2$ -method for the analysis of data is applied to determine the effect. We consider the results of the MC simulations as observed “experimental data”.

The effective action depends smoothly on the flux  $\varphi$  in the region  $\varphi \sim 0$ . Therefore, the free energy density can be fitted by the quadratic function of the flux  $\varphi$ ,

$$F(\varphi) = F_{min} + b(\varphi - \varphi_{min})^2. \quad (14)$$

This choice is motivated also by the results obtained already in continuum field theory [13] where it was determined that free energy has a global minimum at  $\varphi \neq 0$ . The parametrization (14) is the most reasonable in this case. It is based on the effective action accounting for the one-loop plus daisy diagrams [13],

$$F(H) = \frac{H^2}{2} + \frac{11}{48} \frac{g^2}{\pi^2} H^2 \log \frac{T^2}{\mu^2} - \frac{1}{3} \frac{(gH)^{3/2} T}{\pi} - \frac{1}{12} \text{Tr} [\Pi_{00}(0)]^{3/2}, \quad (15)$$

having  $g^2$  and  $(g^2)^{3/2}$  orders in coupling constant. Here,  $H$  is field strength (flux  $\varphi \sim H$ ),  $T$  is the temperature,  $\mu$  is the normalization point,  $\Pi_{00}(0)$  is the zero-zero component of the gluon polarization operator calculated in the external field at the finite temperature and taken at zero momentum. The value of  $\beta = 3$ , which was used, corresponds to a deep perturbation regime. So, a comparison with perturbation results is reasonable. The systematic errors in fitting function (14) could come from not taking into account the high-order diagrams in (15). However, as it is well known [15], the lack of an expansion parameter at finite temperature starts from the three-loop diagram contributions that is of  $g^6$  order and could not remove an effect derived in  $g^2$  and  $g^3$  orders. As the finite-size effects are concerned, in the present investigation we just made calculations for two lattices  $2 \times 8^3$  and  $2 \times 16^3$  and have derived the same results for the  $\varphi_{min}$  (as it will be seen below). A more detailed investigation of this issue requires much more computer resources, which were limited.

There are 3 unknown parameters,  $F_{min}$ ,  $b$  and  $\varphi_{min}$  in Eq.(14). The parameter  $\varphi_{min}$  denotes the minimum position of the free energy, whereas the  $F_{min}$  and  $b$  are the free energy density at the minimum and the curvature of the free energy function, correspondingly.

The value  $\varphi_{min}$  is obtained as the result of the minimization of the  $\chi^2$ -function

$$\chi^2(F_{min}, b, \varphi_{min}) = \sum_i \frac{(F_{min} + b(\varphi_i - \varphi_{min})^2 - F(\varphi_i))^2}{D(F(\varphi_i))}, \quad (16)$$

where  $\varphi_i$  is the array of the set fluxes and  $D(F(\varphi_i))$  is the data dispersion. It can be obtained by collecting the data into the bins (as a function of flux),

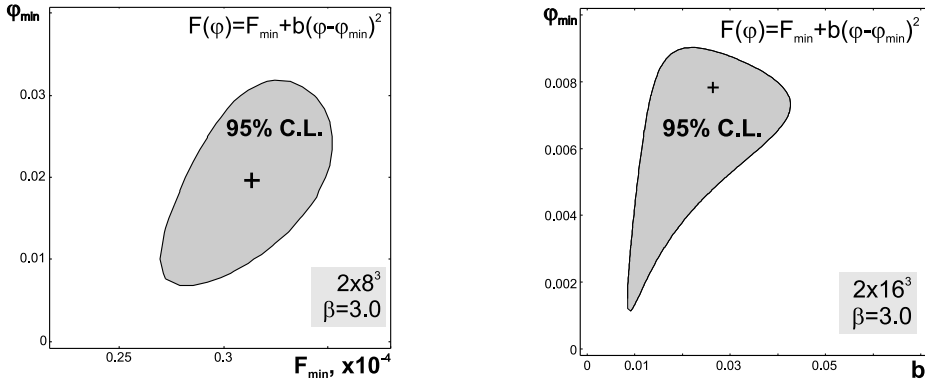
$$D(F(\varphi_i)) = \sum_{i \in bin} \frac{(F(\varphi_i) - \hat{F}_{bin})^2}{n_{bin} - 1}, \quad (17)$$

where  $n_{bin}$  is the number of points in the considered bin,  $\hat{F}_{bin}$  is the mean value of free energy density in the considered bin. As it is determined in the data analysis, the dispersion is independent of the magnetic flux values  $\varphi$ . The deviation of  $\varphi_{min}$  from zero indicates the presence of spontaneously generated field.

The fit results are given in the Table 1. As one can see,  $\varphi_{min}$  demonstrates the  $2\sigma$ -deviation from zero. The dependence of  $\varphi_{min}$  on the temperature is also in accordance with the results known in perturbation theory: the increase in temperature results in the increase of the field strength [4].

**Table 1.** The values of the generated fluxes  $\varphi_{min}$  for different lattices (at the 95% C.L.).

	$2 \times 8^3$	$2 \times 16^3$	$4 \times 8^3$
$\beta = 3.0$	$0.019^{+0.013}_{-0.012}$	$0.0069^{+0.0022}_{-0.0057}$	$0.005^{+0.005}_{-0.003}$
$\beta = 5.0$	$0.020^{+0.011}_{-0.010}$		

**Figure 3.** The 95% C.L. area for the parameters  $F_{min}$  and  $\varphi_{min}$ , determining the free energy density dependence on the flux  $\varphi_{min}$  on lattice  $2 \times 8^3$  for  $\beta = 3.0$  (left figure). The 95% C.L. area for the parameters  $F_{min}$  and  $b$ , determining the free energy density dependence on the flux  $\varphi_{min}$  on lattice  $2 \times 16^3$  for  $\beta = 3.0$  (right figure).

The fits for the lattices  $2 \times 8^3$  and  $2 \times 16^3$  at  $\beta = 3.0$  are shown in Fig. 2. The maximum-likelihood estimate of  $F(\varphi)$  by the whole data set is shown as the solid curve. In addition, all  $\varphi$  values are divided into 15 bins. The mean values and the 95% confidence intervals are presented as points for each bin. The first 9 bins contain about 600-2000 points per bin. The large number of points in the bins allow to find the free energy  $F$  with the accuracy which substantively exceeds the dispersion,  $\sqrt{D(F(\varphi_i))} \sim 10^{-4}$ . It makes possible to detect the effect of interest. As it is also seen, the maximum-likelihood estimate of  $F(\varphi)$  is in a good accordance with the bins pointed, because the solid line is located in the 95% confidence intervals of all bins.

The 95% C.L. area of the parameters  $F_{min}$  ( $b$  for the right figure) and  $\varphi_{min}$  is represented in Fig. 3. The black cross marks the position of the maximum-likelihood values of  $F_{min}$  ( $b$  for the right figure) and  $\varphi_{min}$ . It can be seen that the flux is positive determined. The 95% C.L. area becomes more symmetric with the center at the  $F_{min}$ ,  $b$  and  $\varphi_{min}$  when the statistics is increasing. This also confirms the results of the fitting.

#### 4 Discussion

The main conclusion from the results obtained is that the spontaneously created temperature-dependent chromomagnetic field is present in the deconfinement phase of QCD. This supports the results derived already in the continuum quantum field theory [4, 12] and in lattice data analysis [9].

Let us first discuss the stability of the magnetic field at high temperature. It was observed in Refs. [4, 12] that the stabilization happens due to the gluon magnetic mass calculated from the one-loop polarization operator in the field at temperature. This mass has the order  $m_{magn}^2 \sim g^2(gH)^{1/2}T \sim g^4T^2$  as it should be because the chromomagnetic field is of order  $(gH)^{1/2} \sim g^2T$  [4]. The stabilization is a nontrivial fact that, in principle, could be changed when the higher order Feynman diagrams to be accounted for. Now we see that the stabilization of the field really takes place.

Our approach based on the joining of calculation of the free energy functional and the consequent statistical analysis of its minimum positions at various temperatures and flux values. This overcomes the difficulties peculiar to the description of the field on a lattice. Here we mean that the field strength on a lattice is quantized and therefore a nontrivial tuning of the coupling constant, temperature and field strength values has to be done in order to determine the spontaneously created magnetic field.

We also would like to note that in the present paper the flux dependence on temperature remains not investigated in details. This is because of the small lattice size considered. That restricts the number of points permissible to study. However, at this stage we have determined the effect of interest as a whole. Even at the small lattice, one needs to take into consideration thousands points of free energy (that corresponds to

an analysis of 5-10 millions MC configurations for different lattices) to determine the flux value  $\varphi_{min}$  at the 95% C.L. In case of larger lattices this number and corresponding computer resources should be increased considerably. This problem is left for the future.

As we mentioned in Section 2, the finite-size effects have not been investigated in detail. However, these effects are important near the phase transition temperature. They make difficult to distinguish a first-order phase transition from a second-order one. In our case, the temperature is far from  $T_c$ . The fact that external field penetrates the Coulomb phase is well known [10, 16], so the only really new thing is that this field is spontaneously created. It was first observed in continuum [4], where the field strength of order  $g^4$  in coupling constant was established. Finite-size effects are not able to remove this result. The values  $\varphi_{min}$  obtained on the lattices  $2 \times 8^3$  and  $2 \times 16^3$  (see the Table 1) are in a good agreement with each other, within the statistical errors at 95% C.L.

One could speculate that the lattice sizes  $2 \times 8^3$  and  $2 \times 16^3$  are not sufficient. However, these lattice sizes were used in the Refs. [17]. The main aim of present paper is to show a possibility of spontaneous generation of chromomagnetic field at high temperature in lattice simulation, which was investigated already by perturbative methods [4, 8].

It is interesting to compare our results with that of in Ref. [10] where the response of the vacuum on the external field was investigated. These authors have observed in lattice simulations for the  $SU(2)$ - and  $SU(3)$ -gluodynamics that the external field is completely screened by the vacuum at low temperatures, as it should be in the confinement phase. With the temperature increase, the field penetrates into the vacuum and, moreover, increase in temperature results in existing more strong external fields in the vacuum. On the other hand, increase in the applied external field strength leads to the decreasing of the deconfinement temperature. These interesting properties are closely related to the studies in the present work. Actually, we have also investigated the vacuum properties as an external field problem when the field is described in terms of fluxes. This was the first step of the calculations. The next step was the statistical analysis of the minimum position of free energy, in order to determine the spontaneous creation of the field. In fact, at the first step we reproduced the results of Refs. [10] (in terms of fluxes).

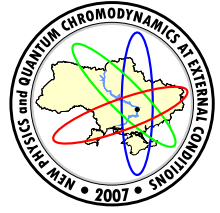
Note that the present investigations also correspond to the case of the early universe. They support our previous results on the magnetic field generation in the standard model [13] and in the minimal supersymmetric standard model [14]. As it was discussed by Pollock [5], the field generated by this mechanism at the Planck era might serve as a seed field to produce the present day magnetic fields in galaxies.

We would like to conclude with the note that the deconfinement phase of gauge theories is a very interesting object to study. The temperature dependent magnetic fields, which are present in this state, influence various processes that should be taken into consideration to have an adequate concept about them.

*Acknowledgement.* The authors would like to express sincere gratitude to Michael Ilgenfritz for his kind attention and help at each stage of the work. We also thank Alexey Gulov for numerous useful discussions. One of us (VD) is indebted for hospitality to ICTP (Trieste), where the final part of the work has been done.

## References

- [1] D.Grasso, H.Rubinstein, Phys. Rept. **348**, 163 (2001).
- [2] K.Enqvist, P.Olesen, Phys. Lett. B **329**, 195 (1994).
- [3] A.Starinets, A.Vshivtsev, V.Zhukovsky, Phys. Lett. B **322**, 403 (1994).
- [4] V.Skalozub, M.Bordag, Nucl. Phys. B **576**, 430 (2000).
- [5] M.Pollock, Int. J. Mod. Phys. D **12**, 1289 (2003).
- [6] G.Savvidy, Phys. Lett. B **71**, 133 (1977).
- [7] STAR Collaboration, J.Adams, et al., Nucl. Phys. A **757**, 102 (2005).
- [8] V.Skalozub, A.Strelchenko, Eur. Phys. J. C **40**, 121 (2005).
- [9] N.Agasian, Phys. Lett. B **562**, 257 (2003).
- [10] P.Cea, L.Cosmai, Phys. Rev. D **60**, 094506 (1999); P.Cea, L.Cosmai, JHEP **0508**, 079 (2005); P.Cea, L.Cosmai, hep-lat/0101017.
- [11] G.'t Hooft, Nucl. Phys. B **153**, 141 (1979).
- [12] V.Skalozub, A.Strelchenko, Eur. Phys. J. C **33**, 105 (2004).
- [13] V.Demchik, V.Skalozub, Eur. Phys. J. C **25**, 291 (2002).
- [14] V.Demchik, V.Skalozub, Eur. Phys. J. C **27**, 601 (2003).
- [15] A.Linde, Rept. Prog. Phys. **42**, 389 (1979).
- [16] M.Vettorazzo, Ph.de Forcrand, Nucl. Phys. B **686**, 85 (2004).
- [17] T.A.DeGrand, D.Toussaint, Phys. Rev. D **25**, 526 (1982); J.Engels, F.Karsch, H.Satz, Phys. Lett. B **101**, 89 (1981); J.Ambjorn, V.Mitrjushkin, V.Bornyakov, A.Zadorozhnyi, Phys. Lett. B **225**, 153 (1989); J.Fingberg, Urs M.Heller, V.K.Mitrjushkin, Nucl. Phys. B **435**, 311 (1995).



## THE GREEN FUNCTION OF NEUTRAL GLUONS IN COLOR MAGNETIC BACKGROUND FIELD AT FINITE TEMPERATURE

A. Ferludin, N. Khandoga, V. Skalozub<sup>a</sup>

Dnipropetrovsk National University, Dnipropetrovsk, Ukraine

In SU(2) gluodynamics, the structure of the exact Green function of neutral gluons in an Abelian homogeneous magnetic field at finite temperature is derived. It is expressed through 10 tensors, which form an algebra with respect to anticommutation operation, and corresponding form factors. The structure constants of the algebra are calculated. The spectrum of gluons is derived from the pole positions of this Green function for the form factors calculated in one-loop order. The high temperature limits for these form factors are computed. The spectra of different gluon states are obtained.

### 1 Introduction

Recent investigations of QCD at high temperature revealed an important role of colored magnetic fields. In particular, it has been elucidated in gluodynamics that color magnetic fields are spontaneously created at high temperature [1, 2, 6]. It is reasonable to suppose that the spontaneous generation of magnetic fields is also responsible for producing of seed magnetic fields in the early universe. From the analysis of the lattice simulations [4], and using the perturbative daisy resummations in the external field at high temperature [6] it was discovered that Abelian chromomagnetic fields of order  $gB \sim g^4 T^2$ , where  $g$  is a gauge coupling constant, are spontaneously created.

To investigate physics in this case one has to calculate the spectra of quarks and gluons in the background field and at finite temperature. As a first step, the operator structure of the gluon Green function and the spectra for this background should be calculated.

Let us divide the gauge field potential  $A_\mu^a(x)$  into the background Abelian homogeneous magnetic field  $B_\mu^a(x)$  and the quantum fluctuations  $Q_\mu^a(x)$ ,

$$A_\mu^a(x) = B_\mu^a(x) + Q_\mu^a(x). \quad (1)$$

The background field  $B_\mu^a(x)$  is directed along the third axis in both the color and the configuration spaces. Its vector potential is

$$B_\mu^a(x) = \delta^{a3} \delta_{\mu 2} x_1 B \quad (2)$$

and the corresponding field strength tensor equals to

$$F_{ij}^a = \delta^{a3} F_{ij} = \delta^{a3} B \epsilon^{3ij}, \quad (3)$$

where only the spatial components ( $i, j = 1, 2, 3$ ) are nonzero. In the field presence it is convenient to turn to the so-called “charged basis”  $W_\mu^\pm = (Q_\mu^1 \pm i Q_\mu^2)/\sqrt{2}$ ,  $Q_\mu = Q_\mu^3$ , with the interpretation of  $W_\mu^\pm$  as color charged fields (“charged” gluons) and  $Q_\mu$  as color neutral fields (“neutral” gluons). The neutral gluon has continuous momentum, whereas charged one forms the discrete Landau levels in the perpendicular with respect to the field direction. In Ref. [5] the gluon polarization tensor at zero temperature was derived. In Ref. [6] that has been done for the finite temperature case. In the present paper we investigate the properties of the exact neutral gluon Green function in the external field at zero and finite temperature.

We use the Feynman gauge where the propagator of neutral gluon in Euclidean’s metric with a momentum  $k_\mu$  is

$$D_{\mu\nu}^{(0)} = \frac{\delta_{\mu\nu}}{k^2}. \quad (4)$$

In a tree approximation, the spectrum can be determined from the pole position of  $D_{\mu\nu}^{(0)}$ , that is from the equation  $k^2 = 0$ . The aim of the present paper is to determine the gluon spectrum in the field  $B_\mu^a(x)$  derived from the pole position of the exact Green function. First we describe the tensor structure of the neutral gluon Green function at zero and finite temperature.

e-mail: <sup>a</sup>skalozub@dsu.dp.ua

## 2 The structure of the polarization tensor

The exact Green function  $D_{\mu\nu}$  of neutral gluons in the field  $B_\mu^a(x)$  is a function of two vectors formed from momentum components:  $h_\lambda = (k_1, k_2, 0, 0)$ ,  $l_\mu = (0, 0, k_3, k_4)$  and the field induction  $B$ . It is given by the operator Schwinger-Dyson equation

$$D = \frac{1}{(k^2 - \Pi)}, \quad (5)$$

where  $\Pi$  is the polarization tensor (PT).

As it was shown in Ref. [5], in a magnetic field the PT is not transversal. This means that the condition  $k_\mu \Pi_{\mu\nu} = 0$  does not hold. So, a weaker condition was used

$$k_\mu \Pi_{\mu\nu} k_\nu = 0. \quad (6)$$

In Ref. [6] the following tensor structure of the neutral gluon PT at finite temperature was derived

$$\Pi_{\mu\nu} = \sum_{i=1}^{10} \Pi^{(i)} T_{\mu\nu}^{(i)} \quad (7)$$

with

$$\begin{aligned} T_{\lambda\lambda'}^{(1)} &= l^2 \delta_{\lambda\lambda'}^{||} - l_\lambda l_{\lambda'}, & T_{\lambda\lambda'}^{(2)} &= h^2 \delta_{\lambda\lambda'}^\perp - h_\lambda h_{\lambda'} = d_\lambda d_{\lambda'}, \\ T_{\lambda\lambda'}^{(3)} &= h^2 \delta_{\lambda\lambda'}^{||} + l^2 \delta_{\lambda\lambda'}^\perp - l_\lambda h_{\lambda'} - h_\lambda l_{\lambda'}, & T_{\lambda\lambda'}^{(4)} &= h^2 \delta_{\lambda\lambda'}^{||} - l^2 \delta_{\lambda\lambda'}^\perp, \\ T_{\lambda\lambda'}^{(5)} &= i(l_\lambda d_{\lambda'} - d_\lambda l_{\lambda'}) + i l^2 F_{\lambda\lambda'}, & T_{\lambda\lambda'}^{(6)} &= i F_{\lambda\lambda'}, \end{aligned} \quad (8)$$

where we use the notation

$$\delta_{\lambda\lambda'}^{||} = \begin{pmatrix} 0 & 0 & 0 & 0 \\ 0 & 0 & 0 & 0 \\ 0 & 0 & 1 & 0 \\ 0 & 0 & 0 & 1 \end{pmatrix}, \quad \delta_{\lambda\lambda'}^\perp = \begin{pmatrix} 1 & 0 & 0 & 0 \\ 0 & 1 & 0 & 0 \\ 0 & 0 & 0 & 0 \\ 0 & 0 & 0 & 0 \end{pmatrix}, \quad F_{\lambda\lambda'} = \begin{pmatrix} 0 & 1 & 0 & 0 \\ -1 & 0 & 0 & 0 \\ 0 & 0 & 0 & 0 \\ 0 & 0 & 0 & 0 \end{pmatrix}, \\ l_\lambda = (0, 0, k_3, k_4), \quad h_\lambda = (k_1, k_2, 0, 0), \quad d_\lambda = (k_2, -k_1, 0, 0). \end{math>}(9)$$

The first four tensors  $T^{(i)}$  are transversal,  $k_\mu T_{\mu\nu} = 0$ , whereas the last two obey the Eq. (6), only. At finite temperature, we have to take into consideration the additional vector  $u = (0, 0, 0, 1)$  – the thermostat velocity. Using the vector  $u$  one can construct four additional tensors:

$$\begin{aligned} T_{\lambda\lambda'}^{(7)} &= (uk)(u_\lambda l_{\lambda'} + l_\lambda u_{\lambda'}) - \delta_{\lambda\lambda'}^{||}(uk)^2 - u_\lambda u_{\lambda'} l^2, & T_{\lambda\lambda'}^{(8)} &= (uk)(u_\lambda h_{\lambda'} + h_\lambda u_{\lambda'}) - \delta_{\lambda\lambda'}^\perp(uk)^2 - u_\lambda u_{\lambda'} h^2, \\ T_{\lambda\lambda'}^{(9)} &= i(u_\lambda d_{\lambda'} - d_\lambda u_{\lambda'}) + i F_{\lambda\lambda'}(uk), & T_{\lambda\lambda'}^{(10)} &= k^2 \delta_{\lambda\lambda'} - \frac{(k^2)^2 u_\lambda u_{\lambda'}}{(uk)^2}. \end{aligned} \quad (10)$$

Here the scalar product  $(uk) = k_4$  is the fourth component of the momentum. The tensors  $T^{(7)}$ ,  $T^{(8)}$ , and  $T^{(9)}$  are transversal, whereas  $T^{(10)}$  satisfies only the weaker condition (6).

It is possible to check that the set of tensors (8)–(10) together with the identity matrix  $T_{\mu\nu}^{(0)} = k^2(\delta_{\mu\nu}^{||} + \delta_{\mu\nu}^\perp)$  forms an algebra

$$\{T^{(i)}, T^{(j)}\} = 2C_k^{ij} T^{(k)}. \quad (11)$$

Its structure constants  $C_k^{ij}$  were calculated from explicit expressions for tensors  $T^{(i)}$ , where the indices run the values  $i, j = 0, 1, \dots, 10$ . This is assumed below. Due to completeness of the set of operators  $T^{(i)}$ , one can obtain  $D$  as a linear combination

$$D_{\mu\nu} = \sum_{i=0}^{10} D^{(i)} T_{\mu\nu}^{(i)}, \quad (12)$$

where  $D^{(i)}$  are some scalar functions of the form factors  $\Pi^{(j)}$ . They will be calculated in the next section.

## 3 The gluon Green function at finite temperature

First we notice that  $T^{(i)}$  are the functions of  $h_\mu = (k_1, k_2, 0, 0)$ ,  $l_\mu = (0, 0, k_3, k_4)$  and  $u_\mu = (0, 0, 0, 1)$ . The convolution of  $T^{(i)}$  and some linear combination of  $h_\mu$ ,  $l_\mu$  and  $u_\mu$  is again a linear combination of these vectors with other coefficients,  $(\alpha l_\mu + \beta h_\mu + \gamma u_\mu) T_{\mu\nu}^{(i)} = x l_\nu + y h_\nu + z u_\nu$ . Let us consider a tensor

$$P(\alpha, \beta, \gamma, x, y, z)_{\mu\nu} \equiv (\alpha l_\mu + \beta h_\mu + \gamma u_\mu)(x l_\nu + y h_\nu + z u_\nu) \quad (13)$$

and its convolution with  $D$ . From Eq. (12) we obtain

$$\begin{aligned} P(\alpha, \beta, \gamma, x, y, z)_{\mu\nu} D_{\mu\nu} &= (\alpha l_\mu + \beta h_\mu + \gamma u_\mu) D_{\mu\nu} (x l_\nu + y h_\nu + z u_\nu) = \\ &\sum_{i=0}^{10} D^{(i)} (\alpha l_\mu + \beta h_\mu + \gamma u_\mu) T_{\mu\nu}^{(i)} (x l_\nu + y h_\nu + z u_\nu). \end{aligned} \quad (14)$$

On the other hand, we can substitute  $(k^2 - \Pi)^{-1}$  for  $D_{\mu\nu}$  in Eq. (14) and get some functions which depend on the form factors  $\Pi^{(i)}$ ,

$$P(\alpha, \beta, \gamma, x, y, z)_{\mu\nu} \left[ \frac{1}{(k^2 - \Pi)} \right]_{\nu\mu} = \frac{1}{k^2} \sum_{t=0}^{\infty} \frac{1}{k^{2t}} [(\alpha l_\mu + \beta h_\mu + \gamma u_\mu) \Pi_{\mu\nu}^t] (x l_\nu + y h_\nu + z u_\nu). \quad (15)$$

Here we expressed the function of  $\Pi$  in the form of series to find

$$(\alpha l_\mu + \beta h_\mu + \gamma u_\mu) \Pi_{\mu\nu} = \alpha_1 l_\nu + \beta_1 h_\nu + \gamma_1 u_\nu. \quad (16)$$

In the operator form we get

$$A \begin{pmatrix} \alpha \\ \beta \\ \gamma \end{pmatrix} = \begin{pmatrix} \alpha_1 \\ \beta_1 \\ \gamma_1 \end{pmatrix}, \quad (17)$$

where  $A$  is a transformation matrix. Obviously that

$$(\alpha l_\mu + \beta h_\mu + \gamma u_\mu) \Pi_{\mu\nu}^t = \alpha_t l_\nu + \beta_t h_\nu + \gamma_t u_\nu, \quad (18)$$

where

$$(\alpha_t, \beta_t, \gamma_t)^T = A^t (\alpha, \beta, \gamma)^T. \quad (19)$$

So, if we have a function of  $\Pi$  we can replace it by  $A$ :

$$P(\alpha, \beta, \gamma, x, y, z)_{\mu\nu} \left[ \frac{1}{(k^2 - \Pi)} \right]_{\nu\mu} = (\alpha' l_\mu + \beta' h_\mu + \gamma' u_\mu) (x l_\mu + y h_\mu + z u_\mu), \quad (20)$$

where  $(\alpha', \beta', \gamma')^T = (k^2 - A)^{-1} (\alpha, \beta, \gamma)^T$ .

In our case, the matrix  $A$  has the following elements:

$$\begin{aligned} A_{11} &= h^2(\Pi^{(3)} + \Pi^{(5)}) + (uk)^2(\Pi^{(7)} - \Pi^{(8)}); \\ A_{12} &= -l^2\Pi^{(3)} + (uk)^2\Pi^{(8)}; \quad A_{13} = -h^2\Pi^{(8)}; \\ A_{21} &= -h^2\Pi^{(3)}; \quad A_{22} = l^2(\Pi^{(3)} - \Pi^{(5)}); \quad A_{23} = h^2\Pi^{(8)}; \\ A_{31} &= (uk)^2\Pi^{(1)}; \quad A_{32} = (uk)^2(\Pi^{(3)} + \Pi^{(8)}); \\ A_{33} &= l^2\Pi^{(1)} + h^2(\Pi^{(3)} + \Pi^{(5)}) + ((uk)^2 - h^2)\Pi^{(8)}. \end{aligned} \quad (21)$$

By specifying the values of coefficients  $\alpha, \beta, \gamma, x, y, z$  we can derive the factors  $D^{(i)}$ :

$$\begin{aligned} D^{(0)} &= \frac{B_{11} + B_{12} + B_{21} + B_{22}}{\psi k^2}, \\ D^{(1)} &= -\frac{\omega + (uk)^2\Pi^{(7)}\delta}{k^2 - l^2\Pi^{(1)} - h^2[\Pi^{(3)} + \Pi^{(5)}] + (uk)^2\Pi^{(7)}}, \\ D^{(2)} &= \frac{-k^2\Pi^{(2)} + h^2\Pi^{(2)}[\Pi^{(3)} + \Pi^{(5)}] + h^2\Pi^{(3)2} + (uk)^2\Pi^{(8)}[\Pi^{(2)} - \Pi^{(8)}]}{\psi [k^2 - h^2\Pi^{(2)} - l^2(\Pi^{(3)} - \Pi^{(5)}) + (uk)^2\Pi^{(8)}]}, \\ D^{(3)} &= -\frac{B_{12} + B_{32}}{\psi h^2[l^2 + (uk)^2]}, \\ D^{(5)} &= \frac{(uk)^2 - k^2}{\psi k^2 h^2[(uk)^2 - l^2]} \left[ B_{11} + B_{13} + B_{31} + \frac{h^2}{(uk)^2 - k^2} B_{32} \right], \\ D^{(7)} &= -\frac{\omega + (uk)^2\Pi^{(7)}\delta}{k^2 - l^2\Pi^{(1)} - h^2(\Pi^{(3)} + \Pi^{(5)}) + (uk)^2\Pi^{(7)}} - \delta, \\ D^{(8)} &= \frac{1}{\psi h^2[l^2 + (uk)^2]} \left[ B_{12} + \frac{l^2}{(uk)^2} B_{32} \right], \\ D^{(10)} &= \frac{B_{21} + B_{31} + B_{22} + B_{32} l^2/(uk)^2}{\psi k^4[1 - l^2/(uk)^2]}, \end{aligned} \quad (22)$$

where we denoted  $\psi = \det[k^2 - A]$ , and  $B_{ij}$  are the matrix elements of  $B = (k^2 - A)^{-1}\psi$ ,  $\delta = (B_{31} + B_{32})[l^2 - (uk)^2]^{-1}\psi^{-1}$ ,  $\omega = [k^2\Pi^{(1)}D_0 + h^2\Pi^{(1)}(D_3 + D_5) + h^2\Pi^{(3)}D_1]$ . Having calculated the factors in Eqs. (22) we derive the tensor structure of the exact neutral gluon Green function in the external magnetic field at finite temperature. Note that the coefficient  $\Pi^{(i)}$  are arbitrary functions of their arguments. In principle, they can be calculated in loop expansion or in a nonperturbative way.

To obtain the spectral equations for the neutral gluons we have to consider the pole positions of the Green function. There are three spectral equations, two of them are linear with respect to  $k^2$ , and one is the cubic equation in  $k^2$ :

$$k^2 - h^2\Pi^{(2)} - l^2(\Pi^{(3)} - \Pi^{(5)}) + (uk)^2\Pi^{(8)} = 0, \quad (23)$$

$$k^2 - l^2\Pi^{(1)} - h^2(\Pi^{(3)} + \Pi^{(5)}) + (uk)^2\Pi^{(7)} = 0, \quad \psi = 0. \quad (24)$$

The next step is to calculate the form factors  $\Pi^{(i)}$  in order to determine the spectra in a chosen approximation.

#### 4 Form factors in one-loop order

In Ref. [6] the form factors  $\Pi^{(i)}$  have been calculated as the two-parametric integrals of the form:

$$\Pi^{(i)}(k) = \sum_{N=-\infty}^{\infty} \int_0^{\infty} ds dt M^{(i)}(s, t) \Theta_T, \quad (25)$$

where the functions  $M^{(i)}(s, t)$  are

$$\begin{aligned} M^{(1)} &= 4 - 2 \left( \frac{\xi}{q} \right)^2 \cosh(2q), & M^{(2)} &= 4 \frac{1 - \cosh(q) \cosh(\xi)}{\sinh^2 q} - 2 + 8 \cosh(q) \cosh(\xi), \\ M^{(3)} &= -2 \cosh(2q) \frac{\xi \sinh \xi}{q \sinh q} - 2 + 6 \cosh(\xi) \cosh(q), \\ M^{(4)} &= -2 + 2 \cosh(q) \cosh(\xi), & M^{(5)} &= 2 \frac{\xi}{q} \left[ \sinh(2q) - \frac{\cosh q - \cosh \xi}{\sinh q} \right] - 6 \cosh(q) \sinh(\xi), \\ M_{(1)}^{(6)} &= 2 \left[ \frac{\xi}{q} \coth(q) (1 - 3 \sinh^2 q) + \sinh(\xi) \cosh(q) \right] l^2 \\ &+ 2 \left[ \frac{\sinh \xi}{\sinh q} \coth(q) (1 - 3 \sinh^2 q) + 2 \sinh(\xi) \cosh(q) \right] h^2, \\ M_{(2)}^{(6)} &= 2 \frac{iN}{qT} k_4 (\sinh(2q) - \coth q), \\ M^{(7)} &= -2 \frac{iN}{qT} \frac{1}{k_4} \frac{\xi}{q} \cosh(2q), & M^{(8)} &= \frac{iN}{qT} \frac{1}{k_4} \left[ -2 \frac{\sinh \xi}{\sinh q} - 4 \sinh(q) \sinh(\xi) \right], \\ M^{(9)} &= \frac{iN}{qT} 2 \left[ \frac{\cosh q - \cosh \xi}{\sinh q} - \sinh(2q) - 2 \sinh(q) \cosh(\xi) \right], & M^{(10)} &= 0, \end{aligned} \quad (26)$$

and  $\xi = s - t$ ,  $q = s + t$ . The symmetric form factors have to be multiplied by

$$\Theta_T^s = \frac{1}{2} \langle \Theta(s, t) \rangle \left[ \exp \left( \frac{ik_4 N}{qT} t \right) + \exp \left( \frac{ik_4 N}{qT} s \right) \right] \exp \left( -\frac{N^2 B}{4T^2 q} \right), \quad (27)$$

and the antisymmetric ones – by

$$\Theta_T^a = \frac{1}{2} \langle \Theta(s, t) \rangle \left[ \exp \left( \frac{ik_4 N}{qT} t \right) - \exp \left( \frac{ik_4 N}{qT} s \right) \right] \exp \left( -\frac{N^2 B}{4T^2 q} \right). \quad (28)$$

The function  $\langle \Theta \rangle$  equals to

$$\langle \Theta \rangle = \frac{1}{(4\pi)^2 (s+t) \sinh(s+t)} \exp \left[ -\frac{k}{B} \left( \delta^{\parallel} \frac{st}{s+t} + \delta^{\perp} \frac{ST}{S+T} \right) k \right], \quad (29)$$

where  $S \equiv \tanh s$  and  $T \equiv \tanh t$ .

In this paper we are interested in the spectrum at high temperature  $\sqrt{B}/T \ll 0$  in the limit of  $k_4 = 0$ ,  $\vec{k} \rightarrow 0$ . For this case we calculate the following asymptotic form for the form factors,

$$\Pi^{(n)}(k) = \frac{T}{\sqrt{B}(4\pi)^{3/2}} \left( a_n - \frac{k_3^2}{B} b_n - \frac{h^2}{B} c_n \right) - \theta_n. \quad (30)$$

**Table 1.** The coefficients  $a, b, c$  in Eq. (30)

n	$a_n$	$b_n$	$c_n$
1	$10.56832 - 0.59082i$	$1.85028 + 0.08862i$	$1.64935 + 0.29541i$
2	$-5.79894 - 7.08982i$	$-4.16625 + 3.54491i$	$-4.63238 - 1.77245i$
3	$1.04427 - 8.86227i$	$-4.16625 + 3.54491i$	$-2.84292 - 3.10179i$
4	0	0	0
5	$-4.21405 - 1.77245i$	$-1.60873 + 0.88622i$	$-1.58031 + 0.44311i$
6	0	0	0
7	$-1.40468 - 0.59082i$	$-0.10712 + 0.08862i$	$0.13310 + 0.29541i$
8	$1.71341 - 3.54491i$	$-1.90805 - 1.77245i$	$0.38174 - 1.77245i$
9	0	0	0

The corresponding coefficients  $a, b, c$  are shown in Table 1, and  $\theta$  are found to be

$$\theta_n = \frac{10}{3(4\pi)^2} \ln \frac{T^2}{B}, \quad n = 1, 2, 3; \quad \theta_n = 0, \quad n \neq 1, 2, 3. \quad (31)$$

The imaginary part is signaling the instability of the state because of the tachyonic mode presenting in the spectrum of charged gluons (see, for instance, Ref. [5]), and the real part is responsible for the screening of transversal gluon fields. It is important to note that at finite temperature all the states are unstable because of the Landau damping. So the ratio of the imaginary and the real parts,  $\rho$ , is an important parameter characterizing the stability of a state. If this ratio is less than 1, we consider corresponding state as a quasi-stable one. And in the opposite case this state is unstable. In other words, the tachyonic instability is not distinguishable from the usual instability of quasiparticles at finite temperature. As one can see from Table 1, for different form factors these ratios are different, smaller or larger than unit. This has an important role for resummation of perturbation series in order to improve the infrared behaviour of the corresponding state. In case of small  $\rho$  the form factor could not be resummed. For  $\rho > 1$  the form factor should be resummed.

In the same way we can calculate the form factors with the fourth momentum component  $k_4 = 2\pi n_k T$ ,  $n_k \neq 0$ . In this case we obtain the following results

$$\begin{aligned} \Pi^{(m)}(k) &= \frac{T}{(4\pi)^{3/2}} \left( \frac{1}{k_4} \tilde{a}_m - \frac{\vec{k}^2}{k_4^3} \tilde{c}_m + \frac{\sqrt{B}}{k_4^2} \tilde{b}_m \right) - \theta_m, \quad m = 1, 2, 3, 7, 8, \\ \Pi^{(5)}(k) &= \frac{T\sqrt{B}}{4\pi} \left[ (1+i) \frac{1}{k_4^2} - (1-i) \frac{B}{k_4^4} - \frac{1+i}{2} \frac{\vec{k}^2}{k_4^4} \right], \quad \Pi^{(4)}(k) = \Pi^{(6)}(k) = \Pi^{(9)}(k) = 0. \end{aligned} \quad (32)$$

For the coefficients  $\tilde{a}_m$ ,  $\tilde{b}_m$  and  $\tilde{c}_m$  the following expressions have been obtained:

$$\begin{aligned} \tilde{a}_1 = \tilde{a}_2 = \tilde{a}_3 &= 21.7315 + \frac{2}{(4\pi)^2} \frac{k_4}{T} \int_0^1 dx [1 + 4x(1-x)] \sum_{N \neq 0, -n_k} \left( \frac{2\pi T}{\sqrt{k_4^2 x(1-x) + (k_4 x + 2\pi N T)^2}} - \frac{1}{|N|} \right), \\ \tilde{a}_7 = \tilde{a}_8 &= -1.8906 + \frac{1}{4\pi} \frac{k_4}{T} \int_0^1 dx (1-2x) \sum_{N \neq 0, -n_k} \frac{k_4 x + 2\pi N T}{\sqrt{(k_4(1-x) + 2\pi N T)^2 + k_4^2 x(1-x)}}, \\ \tilde{b}_1 &= 1.0248 + 7.0898i, \quad \tilde{b}_2 = 20.2447 + 14.1796i, \quad \tilde{b}_3 = 11.6595 + 17.7245i, \quad \tilde{b}_7 = \tilde{b}_8 = 0; \\ \tilde{c}_1 = \tilde{c}_2 = \tilde{c}_3 &= 6.8873 + k_4^3 \sqrt{\pi} \sum_{N \neq 0, -n_k} \int_0^1 \frac{dx [1 + 4x(1-x)]}{[k_4^2 x(1-x) + (k_4 x + 2\pi N T)^2]^{3/2}}, \\ \tilde{c}_7 = \tilde{c}_8 &= 0.2708 + k_4^2 2\sqrt{\pi} \int_0^1 dx \sum_{N \neq 0, -n_k} \frac{(1-2x)x(1-x)(k_4 x + 2\pi N T)}{[(k_4(1-x) + 2\pi N T)^2 + k_4^2 x(1-x)]^{3/2}}. \end{aligned} \quad (33)$$

Function  $\theta_m$  is the same as in Eq. (31). Substituting  $B = 0$  in Eq. (32) we obtain the polarization tensor in the high temperature limit at zero field. In this case non-transversal form factor  $\Pi^{(5)}$  equals to zero, the form factors  $\Pi^{(1)}$ ,  $\Pi^{(2)}$ ,  $\Pi^{(3)}$  and  $\Pi^{(7)}$ ,  $\Pi^{(8)}$  become equal to each other. This is an expected result.

## 5 Conclusions

In the framework of SU(2) gluodynamics, we derived the tensor structure of the exact neutral gluon Green function in an Abelian homogeneous magnetic field at finite temperature. It is presented as the linear combination of ten tensors  $T^{(i)}$  introduced already in Ref. [6]. It was discovered that these tensors form an algebra with

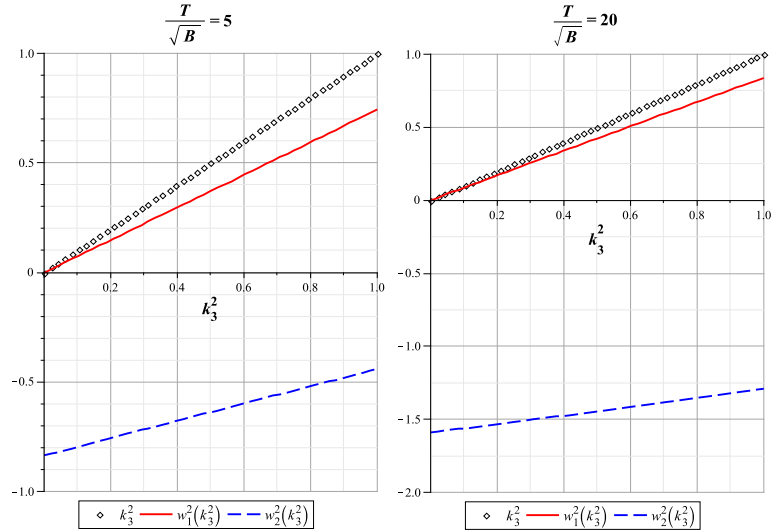
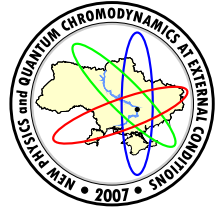


**Figure 1.** Dispersion relations for the transversal modes in case of motion along the field  $h^2 \rightarrow 0$ . Two cases are considered:  $T/\sqrt{B} = 5$  and  $T/\sqrt{B} = 20$ . Curves represent dependence between square of the gluon frequency  $w^2$  and square of the momentum  $\vec{k}^2 = k_3^2$ . Dot line is a trivial spectrum  $w^2 = k_3^2$ . Solid line is a first solution of the Eq. (24), dash line is the other.

respect to the operation of anticommutation, which structure constants have been calculated. To obtain the coefficients at the tensors in the Green function we have applied the method which can be useful in the more complicated case of SU(3) gluodynamics. For the one-loop form factors we obtain the explicit formulas in case of the motion along the field direction. The spectrum of gluons is derived from the pole position of the exact Green function with the one-loop form factors been accounted for. Spectral equations were obtained. In the case of  $T \neq 0$  the high temperature limit for the form factors was computed. It is found that in this approximation all the form factors contain imaginary parts. Therefore a resummation of perturbation series should be carry out in order to obtain a stable spectrum. That can be done on the base of solution of the Schwinger-Dyson equation where, to calculate the polarization tensor, as the neutral gluon propagator the derived Green function should be substituted.

## References

- [1] K. Enqvist and P. Olesen, Phys.Lett. **B329**, 195 (1994).
- [2] A.O. Starinets, A.S. Vshivtsev and V.Ch. Zhukovskii, Phys.Lett. **B322**, 287 (1994).
- [3] V. Skalozub and M. Bordag, Nucl.Phys. **B576**, 430 (2000).
- [4] N.O. Agasian, Phys.Lett. **B562**, 257 (2003).
- [5] M. Bordag, V. Skalozub, Eur.Phys.J. **C45**, 159 (2006).
- [6] M. Bordag, V. Skalozub, Phys.Rev. **D75**, 1250003 (2007).



## Z' SIGNALS FROM THE LEP2 DATA

A. V. Gulov<sup>a</sup>, V. V. Skalozub<sup>b</sup>

Dnipropetrovsk National University, Dnipropetrovsk, Ukraine

The LEP2 data on  $e^+e^- \rightarrow e^+e^-$ ,  $\mu^+\mu^-$ ,  $\tau^+\tau^-$  processes are fitted to estimate possible signals of the Abelian  $Z'$ -boson. In the many-parametric fits, four independent parameters must be fitted, if the derived already low-energy relations between the  $Z'$  couplings to the standard model fermions are taken into consideration. No signals are found for the complete LEP2 data set for these processes. In the fit of the backward bins, the hint at the  $1.25\sigma$  CL is detected. The  $Z'$  couplings to the vector and axial-vector lepton currents are constrained. The comparisons with the one-parameter fits are fulfilled.

### 1 Introduction

The standard model (SM) was precisely tested in LEP experiments, and all the parameters and particle masses were determined at the level of radiation corrections [1–3]. At the same time, these experiments afforded an opportunity for searching for signals of new heavy particles predicted by various models extending the SM. Although no new particles were discovered, a general belief is that the energy scale of new physics to be of order 1 TeV, that may serve as a guide for experiments at the LHC. In this situation, any information about new heavy particles obtained on the base of the present day data is desirable and important.

A lot of extended models includes the massive neutral vector particle associated with the extra  $U(1)$  subgroup of an underlying group. This particle is usually called the  $Z'$ -boson. Searching for  $Z'$ -boson as a virtual state in the either model-dependent or model-independent approaches is widely discussed in the literature (see for references [4]). In our papers [5–7] a new approach for the model-independent search for  $Z'$ -boson was proposed which, in contrast to other model-independent searches, gives a possibility to pick out uniquely this virtual state and determine its characteristics. Our consideration is based on two constituents: 1) The relations between the effective low-energy couplings derived from the renormalization group (RG) equation for fermion scattering amplitudes. We called them the RG relations. Due to these relations, a number of unknown  $Z'$  parameters entering the amplitudes of different scattering processes considerably decreases. 2) When these relations are accounted for, some kinematics properties of the amplitude become uniquely correlated with this virtual state and the  $Z'$  signals exhibit themselves.

In Refs. [5–7] the one-parametric observables were introduced and the signals of the  $Z'$  have been estimated at the  $1\sigma$  CL in the  $e^+e^- \rightarrow \mu^+\mu^-$  process, and at the  $2\sigma$  CL in the Bhabha process. The  $Z'$  mass was estimated to be 1–1.2 TeV. An increase in statistics could make these signals more pronounced and there is a good chance to discover this particle at the LHC.

Recently the final data of the LEP collaborations DELPHI and OPAL [2, 3] were published and new more precise estimates could be obtained. In the present paper we update the results of the one-parameter fit and perform the complete many-parametric fit of the LEP2 data to estimate a possible signal of the  $Z'$ -boson. Usually, in a many-parametric fit the uncertainty of the result increases drastically because of extra parameters. On the contrary, in our approach due to the RG relations between the low-energy couplings there are only 2–3 independent parameters for the LEP scattering processes. Therefore, we believe that an inevitable increase of confidence areas (CA) in the many-parametric space could be compensated by accounting for all the accessible experimental information. As it will be shown, the uncertainty of the many-parametric fit can be comparable with the uncertainty of the previous one-parametric fits in Refs. [6, 7]. In this approach the combined data fit for all lepton processes is also possible.

### 2 The Abelian $Z'$ boson at low energies

At low energies, the  $Z'$ -boson can manifest itself by means of the couplings to the SM fermions and scalars as a virtual intermediate state. Moreover, the  $Z$ -boson couplings are also modified due to a  $Z$ – $Z'$  mixing. In principle, arbitrary effective  $Z'$  interactions to the SM fields could be considered at low energies. However, the couplings of non-renormalizable types have to be suppressed by heavy mass scales because of decoupling. Therefore, significant signals beyond the SM can be inspired by the couplings of renormalizable types. Such

e-mail: <sup>a</sup>gulov@ff.dsu.dp.ua, <sup>b</sup>skalozub@dsu.dp.ua

© Gulov A.V., Skalozub V.V., 2007.

couplings can be derived by adding the new  $\tilde{U}(1)$ -terms to the electroweak covariant derivatives  $D^{\text{ew}}$  in the Lagrangian [4]

$$\mathcal{L} = \left| \left( D_\mu^{\text{ew}} - i \frac{\tilde{y}_\phi}{2} \tilde{Z}_\mu \right) \phi \right|^2 + i \sum_{f=f_L, f_R} \bar{f} \gamma^\mu \left( D_\mu^{\text{ew}} - i \frac{\tilde{y}_f}{2} \tilde{Z}_\mu \right) f, \quad (1)$$

where  $\phi$  is the SM scalar doublet;  $f_L, f_R$  are the SM left-handed fermion doublets and right-handed fermion singlets;  $\tilde{Z}_\mu$  denotes the  $\tilde{U}(1)$  symmetry eigenstate; and  $\tilde{y}_\phi, \tilde{y}_{f_L}$  and  $\tilde{y}_{f_R}$  mean the unknown couplings characterizing the model beyond the SM. Instead of the couplings to the left-handed and right-handed fermion states it is convenient to introduce the couplings to the axial-vector and vector currents:  $a_f = (\tilde{y}_{f_R} - \tilde{y}_{f_L})/2$ ,  $v_f = (\tilde{y}_{f_L} + \tilde{y}_{f_R})/2$ .

The spontaneous breaking of the electroweak symmetry leads to the  $Z$ - $Z'$  mixing. In case of the Abelian  $Z'$ -boson, the  $Z$ - $Z'$  mixing angle  $\theta_0$  is determined by the coupling  $\tilde{y}_\phi$  as follows [5]

$$\theta_0 = \frac{\sin \theta_W \cos \theta_W}{\sqrt{4\pi \alpha_{\text{em}}}} \frac{m_Z^2}{m_{Z'}^2} \tilde{y}_\phi + O\left(\frac{m_Z^4}{m_{Z'}^4}\right), \quad (2)$$

where  $\theta_W$  is the SM Weinberg angle, and  $\alpha_{\text{em}}$  is the electromagnetic fine structure constant. Although the mixing angle is a small quantity of order  $m_{Z'}^{-2}$ , it contributes to the  $Z$ -boson exchange amplitude and cannot be neglected at the LEP energies.

The Lagrangian (1) leads to the following interactions between the fermions and the  $Z$  and  $Z'$  mass eigenstates:

$$\begin{aligned} \mathcal{L}_{Z\bar{f}f} &= \frac{1}{2} i Z_\mu \bar{f} \gamma^\mu \left[ (v_{fZ}^{\text{SM}} + \gamma^5 a_{fZ}^{\text{SM}}) \cos \theta_0 + (v_f + \gamma^5 a_f) \sin \theta_0 \right] f, \\ \mathcal{L}_{Z'\bar{f}f} &= \frac{1}{2} i Z'_\mu \bar{f} \gamma^\mu \left[ (v_f + \gamma^5 a_f) \cos \theta_0 - (v_{fZ}^{\text{SM}} + \gamma^5 a_{fZ}^{\text{SM}}) \sin \theta_0 \right] f, \end{aligned} \quad (3)$$

where  $f$  is an arbitrary SM fermion state;  $v_{fZ}^{\text{SM}}, a_{fZ}^{\text{SM}}$  are the SM couplings of the  $Z$ -boson.

In a particular model the couplings  $v_f$  and  $a_f$  take some specific values. In case when the model is unknown, these parameters and the mixing angle remain potentially arbitrary numbers. However, this is not the case if one assumes that the underlying extended model is a renormalizable one. As it was shown in Ref. [5], some of them have to be correlated due to renormalizability. The corresponding relations are

$$v_f - a_f = v_{f^*} - a_{f^*}, \quad a_f = T_{3,f} \tilde{y}_\phi, \quad (4)$$

where  $f^*$  is the SU(2) partner of a fermion  $f$ , and  $T_{3,f}$  is the third component of the fermion isospin. They are motivated by the renormalization group equations at the  $Z'$  decoupling energies and also connected with the  $\tilde{U}(1)$  gauge symmetry of the Lagrangian. These relations cover all the popular models of the Abelian  $Z'$  boson allowing the model-independent searches for this particle.

The relations (2) incorporate the most common features of the Abelian  $Z'$ -boson. As it is seen, the axial-vector coupling is universal for all the fermion flavors. So, in what follows we will use the shorthand notation  $a = a_e = a_\mu = a_\tau$ . The axial-vector coupling determines also the coupling to the scalar doublet and, consequently, the mixing angle. As a result, the number of independent couplings is significantly reduced. Considering the leptonic processes  $e^+e^- \rightarrow \ell^+\ell^-$  ( $\ell = e, \mu, \tau$ ), one has to keep 4 unknown couplings:  $a, v_e, v_\mu$ , and  $v_\tau$ . Moreover, the RG relations serve to uniquely specify a kinematic domain of deviations from the SM predictions due to the virtual  $Z'$  boson. Thereof a unique definition of the  $Z'$  signal can be done.

In our analysis, as the SM values of the cross-sections we use the quantities calculated by the LEP2 collaborations [2, 3, 8, 9]. They account for either the one-loop radiative corrections or initial and final state radiation effects (together with the event selection rules, which are specific for each experiment). In our analysis the 2% theoretical error of the SM values is also added to the statistical and systematic ones.

The deviation from the SM is computed in the improved Born approximation. This approximation is sufficient for our analysis leading to the systematic error of the fit results less than 5-10 per cents. To convince ourselves that this is the case, we have altered the theoretical uncertainty of the deviations for 10-20 per cents, and the obtained results are not changed qualitatively.

The deviation from the SM of the differential cross-section for the process  $e^+e^- \rightarrow \ell^+\ell^-$  can be expressed through various quadratic combinations of couplings  $a, v_e, v_\mu, v_\tau$ . For the Bhabha process it reads

$$\frac{d\sigma}{dz} - \frac{d\sigma^{\text{SM}}}{dz} = f_1^{ee}(z) \frac{a^2}{m_{Z'}^2} + f_2^{ee}(z) \frac{v_e^2}{m_{Z'}^2} + f_3^{ee}(z) \frac{av_e}{m_{Z'}^2}, \quad (5)$$

where the factors are known functions of the center-of-mass energy and the cosine of the electron scattering angle  $z$ . The deviation of the cross-section for  $e^+e^- \rightarrow \mu^+\mu^-$  ( $\tau^+\tau^-$ ) processes has a similar form

$$\frac{d\sigma}{dz} - \frac{d\sigma^{\text{SM}}}{dz} = f_1^{\mu\mu}(z) \frac{a^2}{m_{Z'}^2} + f_2^{\mu\mu}(z) \frac{v_e v_\mu}{m_{Z'}^2} + f_3^{\mu\mu}(z) \frac{av_e}{m_{Z'}^2} + f_4^{\mu\mu}(z) \frac{av_\mu}{m_{Z'}^2}. \quad (6)$$

Since the  $Z'$  couplings enter the cross-section together with the inverse  $Z'$  mass, it is convenient to introduce the dimensionless couplings

$$\bar{a}_f = \frac{m_Z}{\sqrt{4\pi m_{Z'}}} a_f, \quad \bar{v}_f = \frac{m_Z}{\sqrt{4\pi m_{Z'}}} v_f, \quad (7)$$

which can be constrained by experiments.

Note again that the cross-sections in Eqs. (3)–(4) account for the relations (2) through the functions  $f_1(z)$ ,  $f_3(z)$ ,  $f_4(z)$ , since the coupling  $\tilde{y}_\phi$  (the mixing angle  $\theta_0$ ) is substituted by the axial coupling constant  $a$ . Usually, when a four-fermion effective Lagrangian is applied to describe physics beyond the SM, this dependence on the scalar field coupling is neglected at all. However, in our case, when we are interested in searching for signals of the  $Z'$ -boson on the base of the effective low-energy Lagrangian (1), these contributions to the cross-section are essential.

### 3 Many-parameter fits

As the basic observable to fit the LEP2 experiment data on the Bhabha process we propose the differential cross-section

$$\frac{d\sigma^{\text{Bhabha}}}{dz} - \frac{d\sigma^{\text{Bhabha, SM}}}{dz} \Big|_{z=z_i, \sqrt{s}=\sqrt{s_i}}, \quad (8)$$

where  $i$  runs over the bins at various center-of-mass energies  $\sqrt{s}$ . The final differential cross-sections measured by the ALEPH (130–183 GeV, [8]), DELPHI (189–207 GeV, [3]), L3 (183–189 GeV, [9]), and OPAL (130–207 GeV, [2]) collaborations are taken into consideration (299 bins).

As the observables for  $e^+e^- \rightarrow \mu^+\mu^-, \tau^+\tau^-$  processes, we consider the total cross-section and the forward-backward asymmetry

$$\sigma_T^{\ell^+\ell^-} - \sigma_T^{\ell^+\ell^-, \text{SM}}, \quad A_{FB}^{\ell^+\ell^-} - A_{FB}^{\ell^+\ell^-, \text{SM}} \Big|_{\sqrt{s}=\sqrt{s_i}}, \quad (9)$$

where  $i$  runs over 12 center-of-mass energies  $\sqrt{s}$  from 130 to 207 GeV. We consider the combined LEP2 data [1] for these observables (24 data entries for each process). These data are more precise as the corresponding differential cross-sections. Our analysis is based on the fact that the kinematics of  $s$ -channel processes is rather simple and the differential cross-section is effectively a two-parametric function of the scattering angle. The total cross-section and the forward-backward asymmetry incorporate complete information about the kinematics of the process and therefore are an adequate alternative for the differential cross-sections.

The data are analysed by means of the  $\chi^2$  fit. Denoting the observables (6)–(7) by  $\sigma_i$ , one can construct the  $\chi^2$ -function,

$$\chi^2(\bar{a}, \bar{v}_e, \bar{v}_\mu, \bar{v}_\tau) = \sum_i \left[ \frac{\sigma_i^{\text{ex}} - \sigma_i^{\text{th}}(\bar{a}, \bar{v}_e, \bar{v}_\mu, \bar{v}_\tau)}{\delta\sigma_i} \right]^2, \quad (10)$$

where  $\sigma^{\text{ex}}$  and  $\delta\sigma$  are the experimental values and the uncertainties of the observables, and  $\sigma^{\text{th}}$  are their theoretical expressions presented in Eqs. (3)–(4). The sum in Eq. (10) refers to either the data for one specific process or the combined data for several processes.

By minimizing the  $\chi^2$ -function, the maximal-likelihood estimate for the  $Z'$  couplings can be derived. The  $\chi^2$ -function is also used to plot the CA in the space of parameters  $\bar{a}$ ,  $\bar{v}_e$ ,  $\bar{v}_\mu$ , and  $\bar{v}_\tau$ . The CA corresponding to the probability  $\beta$  can be defined as [10]:

$$\chi^2 \leq \chi_{\text{CL}, \beta}^2(M), \quad (11)$$

where  $\chi_{\text{CL}, \beta}^2(M)$  is the  $\beta$ -level of the  $\chi^2$ -distribution with  $M$  d.o.f., and  $M$  is the number of linear-independent terms in the observables  $\sigma^{\text{th}}$ .

In the Bhabha process, the  $Z'$  effects are determined by 3 linear-independent contributions coming from  $\bar{a}^2$ ,  $\bar{v}_e^2$ , and  $\bar{a}\bar{v}_e$  ( $M = 3$ ). As for the  $e^+e^- \rightarrow \mu^+\mu^-, \tau^+\tau^-$  processes, the observables depend on 4 linear-independent terms for each process:  $\bar{a}^2, \bar{v}_e\bar{v}_\mu, \bar{v}_e\bar{a}, \bar{a}\bar{v}_\mu$  for  $e^+e^- \rightarrow \mu^+\mu^-$ ; and  $\bar{a}^2, \bar{v}_e\bar{v}_\tau, \bar{v}_e\bar{a}, \bar{a}\bar{v}_\tau$  for  $e^+e^- \rightarrow \tau^+\tau^-$  ( $M = 4$ ). Note that some terms in the observables for different processes are the same. Therefore, the number of  $\chi^2$  d.o.f. in the combined fits is less than the sum of d.o.f. for separate processes. Hence, the predictive power of the larger set of data is not drastically spoiled by the increased number of d.o.f. In fact, combining the data of the Bhabha and  $e^+e^- \rightarrow \mu^+\mu^- (\tau^+\tau^-)$  processes together we have to treat 5 linear-independent terms. The complete data set for all the lepton processes is ruled by 7 d.o.f. As a consequence, the combination of the data for all the lepton processes is possible.

The parametric space of couplings  $(\bar{a}, \bar{v}_e, \bar{v}_\mu, \bar{v}_\tau)$  is four-dimensional. However, for the Bhabha process it is reduced to the plane  $(\bar{a}, \bar{v}_e)$ , and to the three-dimensional volumes  $(\bar{a}, \bar{v}_e, \bar{v}_\mu)$ ,  $(\bar{a}, \bar{v}_e, \bar{v}_\tau)$  for the  $e^+e^- \rightarrow \mu^+\mu^-$  and  $e^+e^- \rightarrow \tau^+\tau^-$  processes, correspondingly. The predictive power of data is distributed not uniformly over the parameters. The parameters  $\bar{a}$  and  $\bar{v}_e$  are present in all the considered processes and appear to be

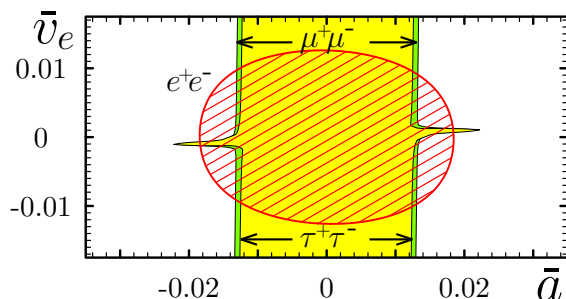


**Figure 1.** The 95% CL areas in the  $(\bar{a}, \bar{v}_e)$  plane for the Bhabha,  $e^+e^- \rightarrow \mu^+\mu^-$ , and  $e^+e^- \rightarrow \tau^+\tau^-$  processes.

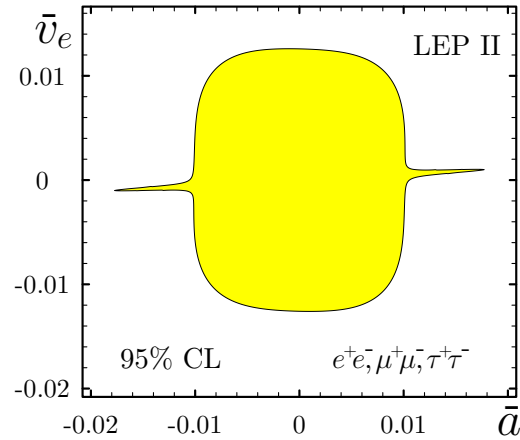


**Figure 2.** The projection of the 95% CL area onto the  $(\bar{a}, \bar{v}_e)$  plane for the combination of  $e^+e^- \rightarrow e^+e^-$ ,  $\mu^+\mu^-$ ,  $\tau^+\tau^-$  processes.

significantly constrained. The couplings  $\bar{v}_\mu$  or  $\bar{v}_\tau$  enter when the processes  $e^+e^- \rightarrow \mu^+\mu^-$  or  $e^+e^- \rightarrow \tau^+\tau^-$  are accounted for. So, in these processes, we also study the projection of the CA onto the plane  $(\bar{a}, \bar{v}_e)$ .

The origin of the parametric space,  $\bar{a} = \bar{v}_e = 0$ , corresponds to the absence of the  $Z'$  signal. This is the SM value of the observables. This point could occur inside or outside of the CA at a fixed CL. When it lays out of the CA, this means the distinct signal of the Abelian  $Z'$ . Then the signal probability can be defined as the probability that the data agree with the Abelian  $Z'$  boson existence and exclude the SM value. This probability corresponds to the most stringent CL (the largest  $\chi^2_{\text{CL}}$ ) at which the point  $\bar{a} = \bar{v}_e = 0$  is excluded. If the SM value is inside the CA, the  $Z'$  boson is indistinguishable from the SM. In this case, upper bounds on the  $Z'$  couplings can be determined.

The 95% CL areas in the  $(\bar{a}, \bar{v}_e)$  plane for the separate processes are plotted in Fig. 1. As it is seen, the Bhabha process constrains both the axial-vector and vector couplings. As for the  $e^+e^- \rightarrow \mu^+\mu^-, \tau^+\tau^-$  processes, the axial-vector coupling is significantly constrained, only. The CAs include the SM point at the meaningful CLs, so the experiment could not pick out clearly the  $Z'$  signal from the SM. An important conclusion from these plots is that the experiment significantly constrains only the couplings entering sign-definite terms in the cross-sections.

The combination of all the lepton processes is presented in Fig. 2. There is no visible signal beyond the SM. The couplings to the vector and axial-vector electron currents are constrained by the many-parameter fit as  $|\bar{v}_e| < 0.013$ ,  $|\bar{a}| < 0.019$  at the 95% CL. If the charge corresponding to the  $Z'$  interactions is assumed to be of order of the electromagnetic one, then the  $Z'$  mass should be greater than 0.67 TeV. For the charge of order of the SM  $SU(2)_L$  coupling constant  $m_{Z'} \geq 1.4$  TeV. One can see that the constraint is not too severe to exclude the  $Z'$  searches at the LHC.

Let us compare the obtained results with the one-parameter fits in Ref. [7]. Fitting the current data with the one-parameter observable, we find the updated values of the  $Z'$  coupling to the electron vector current together with their  $1\sigma$  uncertainties:

$$\begin{aligned}
 \text{ALEPH : } \bar{v}_e^2 &= -0.11 \pm 6.53 \times 10^{-4} \\
 \text{DELPHI : } \bar{v}_e^2 &= 1.60 \pm 1.46 \times 10^{-4} \\
 \text{L3 : } \bar{v}_e^2 &= 5.42 \pm 3.72 \times 10^{-4} \\
 \text{OPAL : } \bar{v}_e^2 &= 2.42 \pm 1.27 \times 10^{-4} \\
 \text{Combined : } \bar{v}_e^2 &= 2.24 \pm 0.92 \times 10^{-4}.
 \end{aligned}$$

As one can see, the most precise data of DELPHI and OPAL collaborations are resulted in the Abelian  $Z'$  hints at one and two standard deviation level, correspondingly. The combined value shows the  $2\sigma$  hint, which corresponds to  $0.006 \leq |\bar{v}_e| \leq 0.020$ .

On the other hand, our many-parameter fit constrains the  $Z'$  coupling to the electron vector current as  $|\bar{v}_e| \leq 0.013$  with no evident signal. Why does the one-parameter fit of the Bhabha process show the  $2\sigma$  CL hint whereas there is no signal in the two-parameter one? Our one-parameter observable accounts mainly for the backward bins. This is in accordance with the kinematic features of the process: the backward bins depend mainly on the vector coupling  $\bar{v}_e^2$ , whereas the contributions of other couplings are kinematically suppressed. Therefore, the difference of the results can be inspired by the data sets used. To check this, we perform the

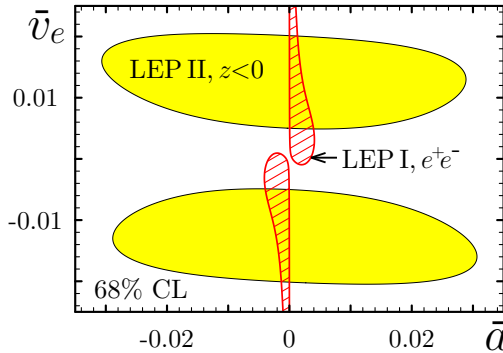


**Figure 3.** The 68% CL area in the  $(\bar{a}, \bar{v}_e)$  plane from the backward bins of the Bhabha process in the LEP2 experiments (the shaded area). The hatched area is the 68% CL area from the LEP 1 data on the Bhabha process.

many-parameter fit with the 113 backward bins ( $z \leq 0$ ), only. The  $\chi^2$  minimum,  $\chi^2_{\min} = 99.7$ , is found in the non-zero point  $|\bar{a}| = 0.00018$ ,  $\bar{v}_e = 0.015$ . This value of the  $Z'$  coupling  $\bar{v}_e$  is in an excellent agreement with the mean value obtained in the one-parameter fit. The 68% CA in the  $(\bar{a}, \bar{v}_e)$  plane is plotted in Fig. 3. There is a visible hint of the Abelian  $Z'$  boson. The zero point  $\bar{a} = \bar{v}_e = 0$  (the absence of the  $Z'$  boson) corresponds to  $\chi^2 = 104.2$ . It is covered by the CA with  $1.25\sigma$  CL. Thus, the backward bins show the  $1.25\sigma$  hint of the Abelian  $Z'$  boson in the many-parameter fit. So, the many-parameter fit is less precise than the analysis of the one-parameter observables.

From the analysis carried out we come to conclusion that, in principle, the LEP experiments were able to detect the  $Z'$ -boson signals if the statistics had been sufficient.

#### 4 Discussion

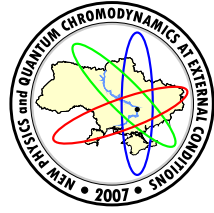
LEP collaborations have reported about a good agreement between the experimental data and the predictions of the SM [2, 3, 8, 9]. That means that the experiments have not shown any statistically significant deviations from its predictions. The analysis of the leptonic processes based on the same data set and the same SM values of cross-sections lead us to the conclusion that the existence of  $Z'$  boson with the mass of order 1-1.2 TeV is not excluded at the  $1-2\sigma$  CL. We observed that in the one-parameter fits in Refs.[6, 7] and in the many-parameter fit of the backward bins in the present investigation. The estimated  $Z'$  parameters derived by different methods are in a good agreement with each other. So, we conclude that there is a discrepancy which needs some explanations. We believe that the reason is in the RG relations playing a crucial role in our treating of experimental data. As it was showed, the RG relations have served to reduce a number of unknown parameters that gave a possibility to extract maximal information about the  $Z'$  signals from the experimental data set. If these relations are not taken into account (as this is the case in Refs.[2, 3, 8, 9]), no signals could be found. LEP collaborations performed also model-dependent fits concerning popular  $Z'$  models. These models suit the RG relations (2). So, it is interesting to compare their analysis with our results. In the experiments reported in Refs. [1-3, 8, 9] the low bound on the  $Z'$  mass was obtained. It varies from 400 GeV to 800 GeV at the 95% CL dependently on the specific model. These bounds allow the  $Z'$  boson with the mass of order 1 TeV that is in an agreement with our results. On the other hand, the possibility to select the  $Z'$  signals in specific scattering processes was not discussed in the papers mentioned.

As we have shown in Ref. [7], there is the  $2\sigma$  hint of the Abelian  $Z'$  boson in the one-parameter fit of LEP2 data for the Bhabha process. This result is reproduced also in the present paper by fitting the updated experimental data. In the present analysis, we applied the many-parameter fits of the leptonic processes for different sets of bins included. In particular, for the backward bins (responsible for the signal due to the kinematics of the process) the  $1.25\sigma$  hint of the particle is found. The fit of the complete set of bins constrains the  $Z'$  couplings to vector and axial-vector electron currents allowing the  $Z'$  boson with the mass of order 1 TeV. Thus, we have to conclude that the LEP2 data allow the existence of the quite light  $Z'$ -boson which has a chance to be discovered in the nearest future. We believe that the RG relations used in the present analysis will be also important in searches for the  $Z'$  boson at the LHC.

#### References

[1] The LEP Collaborations ALEPH, DELPHI, L3, OPAL, and the LEP Electroweak Working Group, arXiv:hep-ex/0511027.

- [2] G. Abbiendi *et al.* [OPAL Collaboration], Eur. Phys. J. C **33**, 173 (2004); Eur. Phys. J. C **6**, 1 (1999); K. Ackerstaff *et al.* [OPAL Collaboration], Eur. Phys. J. C **2**, 441 (1998).
- [3] J. Abdallah *et al.* [DELPHI Collaboration], Eur. Phys. J. C **45**, 589 (2006).
- [4] A. Leike, Phys. Rep. **317**, 143 (1999).
- [5] A. Gulov and V. Skalozub, Eur. Phys. J. C **17**, 685 (2000); Phys. Rev. D **61**, 055007 (2000).
- [6] V.I. Demchik, A.V. Gulov, V.V. Skalozub, and A.Yu. Tishchenko, Yadernaya Fizika 67, 1335 (2004) [Physics of Atomic Nuclei 67, 1312 (2004)].
- [7] A.V. Gulov and V.V. Skalozub, Phys. Rev. D **70**, 115010 (2004).
- [8] R. Barate *et al.* [ALEPH Collaboration], Eur. Phys. J. C **12**, 183 (2000).
- [9] M. Acciarri *et al.* [L3 Collaboration], Phys. Lett. B **479**, 101 (2000).
- [10] A. Gulov, V. Skalozub, hep-ph/0601183;  
W.T. Eadie, D. Dryard, F.E. James, M. Roos, B. Sadoulet, *Statistical methods in experimental physics*, (Amsterdam, North-Holland, 1971).



## MULTIPARTICLE PRODUCTION AT HIGH MULTIPLICITIES

E.S Kokoulin<sup>a</sup>, A. Kutow<sup>b</sup>  
 for **SVD-2 Collaboration**

JINR, Dubna, Russia

Theoretical and experimental studies of high multiplicity events are analyzed. Some interesting phenomena can be revealed at high multiplicities. Preliminary results of project *Thermalization* are reported.

### 1 Introduction

The multiparticle production (MP) study at high energies is one of the actual topics of high energy physics. The different theoretical approaches and the experimental programs are developed. The Quark-Gluon Matter search is the complicated problem of hadron and nucleus interactions [1]. We consider that our MP study at lower energies may be useful. The purpose of the "Thermalization" experiment [2] is to investigate the collective behavior of MP particles in proton and proton-nucleus interactions

$$p + p(A) \rightarrow n_{\pi\pi} + 2N \quad (1)$$

at the proton energy  $E_{lab} = 70$  GeV. We use modernized setup SVD-2 - Spectrometer with Vertex Detector (SVD). It was created to study of production and decay of charm particles, but had the basic components necessary for performance of the physical program of the *Thermalization* project.

At present multiplicity distributions (MD) at this energy is measured up to the number of charged particles  $n_{ch} = 18$  ([3]-[4]). In the region of high multiplicity (HM)  $n_{ch} > 20$  we expect [5]: formation of high density thermalized hadronic system, transition to pion condensate or cold QGP, increase of partial cross section  $\sigma(n)$  is expected in comparison with commonly accepted extrapolation, enhanced rate of direct soft photons. We will be continue to search for new phenomena: Bose-Einstein condensate (BEC), events with ring topology (Cherenkov gluon radiation). The available MP models and MC codes (PYTHIA) are distinguished considerably at the HM region. We also research hadronization mechanism and connected questions.

The review is organized as follows: sect. 2 presents a description of setup SVD-2, sect. 3 gives alignment results, sect. 4 informs about of new phenomena searching and our preliminary data of 2002 run. We summarize in sect. 5.

### 2 Experimental setup

#### 2.1 Setup schematic

The layout of the SVD installation at  $U - 70$  accelerator is shown on Figure 1. The basic requirements to the equipment consisted in the following:

- \* The study is carried out on the extracted beam of protons with energy 70 GeV and intensity  $\sim 10^7$  in a cycle of the accelerator.
- \* The liquid hydrogen target is used.
- \* Installation is capable to detect of events with HM of charged particles and  $\gamma$  quanta. Multiplicity of photons makes up to  $\leq 100$ . The lower energy threshold of the photon registration is 50 MeV.
- \* The HM trigger system is capable to select rare events with multiplicity  $n_{\pi} = 20 \div 30$ . The suppression factor of events with low multiplicity  $n_{\pi} < 20$  is  $10^4$ .
- \* The magnetic spectrometer has the momentum resolution  $\delta p/p \approx 1.5\%$  in the interval  $p = 0.3 \div 5.0$  GeV/c. At the beginning the experiment and subsequent data analysis the generator was developed. It is based on the assumption that in the HM region the particles in c.m.s. should have isotropic angular distribution and their energy distribution is Maxwell or Bose-Einstein type [5].

#### 2.2 Liquid hydrogen target

For a target accommodation in the design of installation there is a space along a beam only 7 cm. Design and manufacture of liquid hydrogen target is under a a complete JINR responsibility. The target has 7 cm thick and

e-mail: <sup>a</sup>kokoulin@sunse.jinr.ru, <sup>b</sup>kutov@dm.komisc.ru

© Kokoulin E.S., Kutow A., 2007.

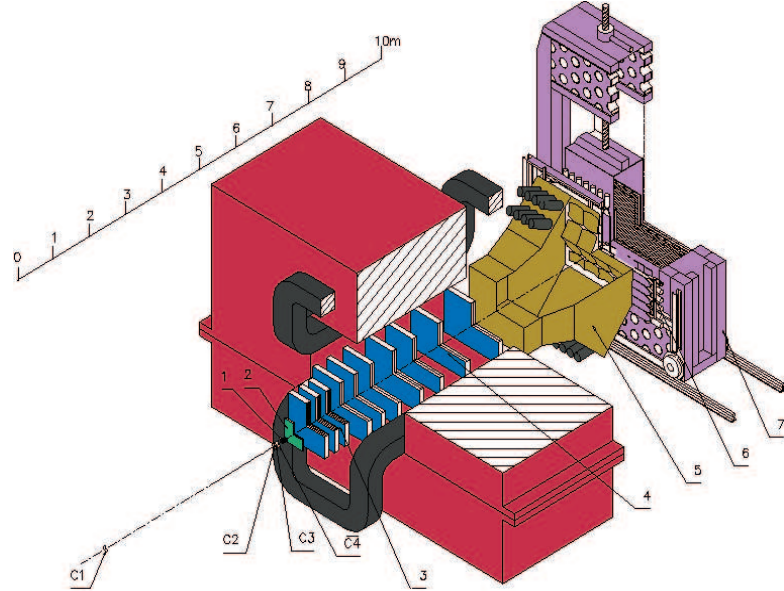


**Figure 1.** Schematic of the SVD installation at U-70.

3.5 cm in diameter vassal of liquid hydrogen. Thermostat is equipped with a thin ( $200 \mu\text{m}$ ) lavsan windows to suppress background scattering. Successful tests of a whole target system had indicated to advanced reduction of helium consumption in which resulting factor is expected in order of 1.5.

### 2.3 Straw tube chambers

Straw tube chamber system is a new addition of SVD setup. This detector has been designed in the department of V. Peshehonorov from LPP of JINR. It implements front end boards with preamplifiers produced in Minsk (NC PHEP BSU) and TDC modules produced in Protvino (IHEP) allowing to detect several pulses, consequently coming from the anode on each trigger signal. Typical plane dimension is  $70 \times 70 \text{ cm}^2$ . The total of channels is about 2400.

### 2.4 HM trigger

Our experiment owes to carry out at suppression of low multiplicity events by a trigger. It is urgent request for it. For this purpose the scintillation hodoscope or HM trigger was designed and manufactured. It suppresses interactions with track multiplicity below 20. Beyond this it is as so thin as not distorts an angular and momentum resolution of the setup to any kind fake signal. The scintillator counter array may operate at higher counting rate and more resistant to many kinds of noise.

### 2.5 Vertex detector

The vertex detector (VD) is necessary constituent of SVD setup because it allows to vertex position identify. Vertex front-end uses a integrated circuit called GASSIPLEX. As the GASSIPLEX is 16-channel design, only 1280 channels of detector may be placed on one board. For  $50 \mu\text{m}$  pitch detector the largest sensitive area dimension is 64 mm. To overcome this restriction the Collaboration had taken the decision to use integrated 128-channel circuits VIKING. JINR provides important technical support in this development. Now we had purchased a requisite consignment of these circuits and are installing in VD.

### 2.6 Magnetic spectrometer, Gamma-detector

The magnet MC-7A having length on the beam 3 m is used in spectrometer. Magnet field in the center is equal to 1.1 T at a current 4000 A. The detection system of the spectrometer includes 18 planes of proportional chambers (PC). The data analysis give the following characteristics of the spectrometer: average PC efficiency is 80%; coordinate accuracy on the reconstructed tracks is 1 mm; the momentum resolution on beam tracks ( $p=70 \text{ GeV}/c$ ) is 3 %; the momentum resolution on the secondary tracks is  $\sim 1 \%$ . Magnetic spectrometer electronics allows to register up to 1.5 thousand events per 1 accelerator cycle. Some of PC had been repaired, anode wires in beam region are covered with insulator to make them insensitive to beam particles. This modification improves efficiency of central part of chamber at high beam intensity  $10^7$  required for *Thermalization* project.

The gamma-detector consists of 1536 full absorption Cherenkov counters. Radiators from a lead glass have the size  $38 \times 38 \times 505 \text{ mm}^3$  and are connected with PMT-84-3. Total fiducial area of the detector is  $1.8 \times 1.2$

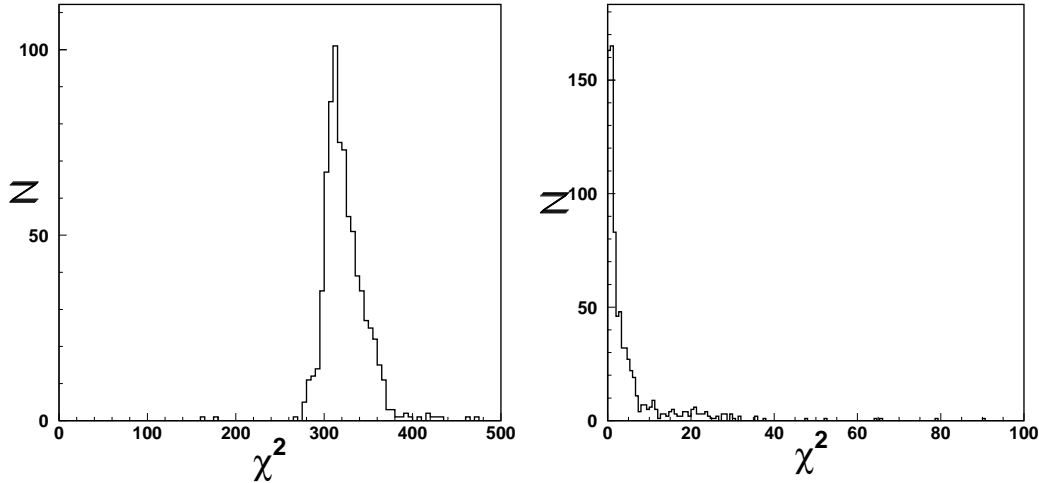


**Figure 2.**  $\chi^2/n_{df}$  for tracks: (left) before and (right) after alignment.

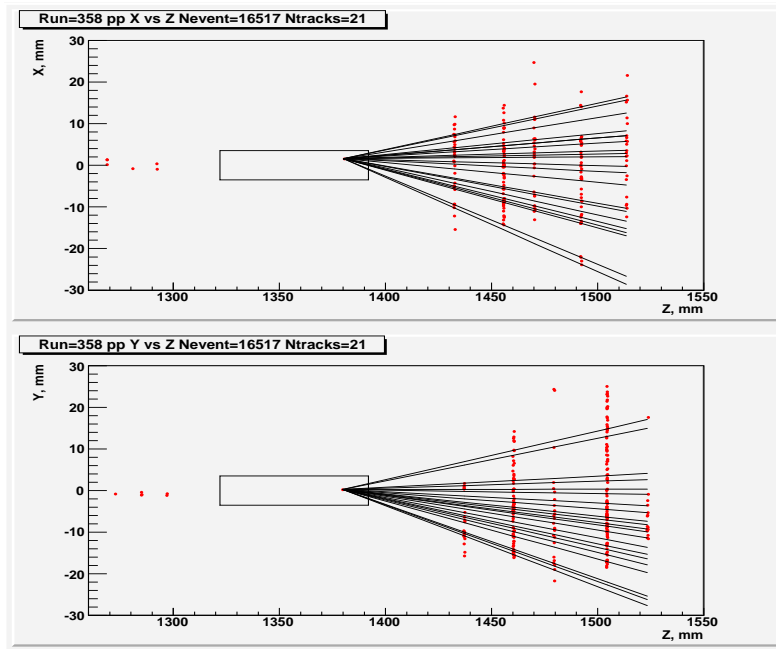


**Figure 3.** Event with multiplicity 21.

$m^2$ . The energy resolution on 15  $GeV$  electrons is 12%. Accuracy of the  $\gamma$  quantum coordinate reconstruction is  $\sim 2$   $mm$ . At run 2007 the gamma-detector calibration was carried out and gamma- quantum events were recorded.

### 3 Alignment

The importance task of any experiment is to provide reconstruction of charged particle tracks. Spatial characteristics and geometric position of detector modules can be differ from its design values. Possible reasons of detector misalignments are the limited accuracy of initial hardware, inaccuracies in placing of detectors and their internal dimensions. The alignment procedure intends to compensate such misalignment by a mathematical way. We use for alignment procedure more robust, efficient and high precision method based on the Linear Least Squares (LLS) [6].

At 2006 technical run we had obtained data on hydrogen target. We had picked out some events with good identification of 787 (single) space tracks on hits in vertex detector and carried out alignment. Histograms of  $\chi^2/n_{df}$  for local fits before and after alignment procedure are in Fig. 2. At present it is continued data processing and high multiplicity event searching. One of such events is shown on Fig. 3. Preliminary multiplicity distribution of charged particles was obtained based on VERTEX detector data. It is shown on Fig. 4.

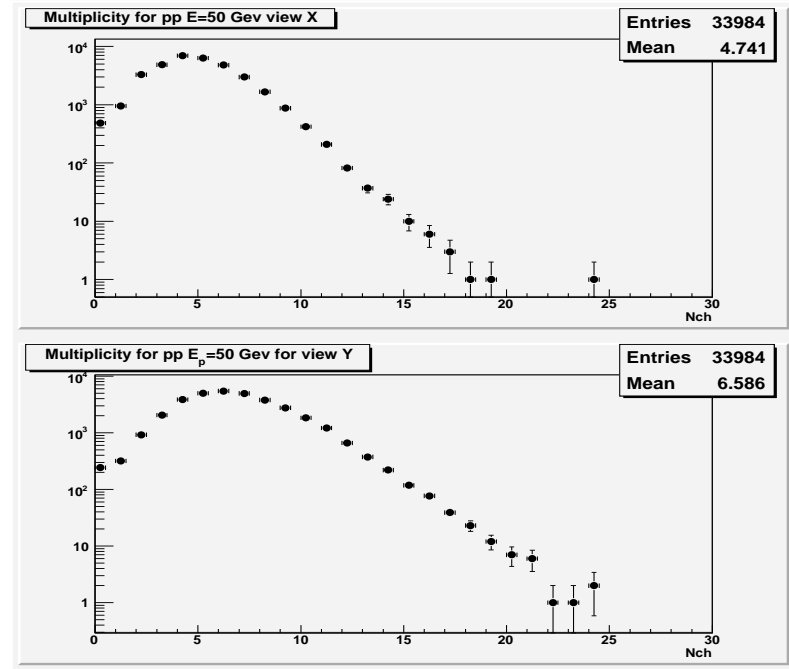


Figure 4. Preliminary MD in pp at HM region.

#### 4 Search for new phenomena

The HM region study is important, because MP models and Monte-Carlo generators are differed at high multiplicity ( $n > \bar{n}(s)$ ) very considerably. There are the theoretical predictions about manifestation such phenomena as Cherenkov-like (gluon) radiation [7], Bose-Einstein condensation (BEC) of pions [8, 9], excess of soft photon rate [10] and other collective phenomena. We like to reveal their in our findings.

For multiparticle dynamics insight and the MD description in hadron interactions we had proposed the Gluon Dominance model (GDM) [11]. In the framework of this model we research quark-gluon matter and hadronization stage detail by using MD of the charged and neutral particles and their moments [12]. GDM bases on the essentials of QCD and phenomenological scheme of hadronization. Our model studies had shown: valent quarks of initial protons are staying in leading particles (from 70 to 800 GeV/c and higher). MP is realized by gluons. We called them active ones.

Some of active gluons ( $\sim 50\%$ ) are staying inside quark-gluon system and do not fragment to hadrons. New formed hadrons catching up them, are excited and throw down excess of energy by soft photons (SP). We use the black body emission spectrum at the assumption that quark-gluon system or excited new formed hadrons set in almost equilibrium state during a short period. This assumption permits to estimate the line size of the SP emission region [13]. It is known that in this region hadronization is occurred.

Our model confirms the recombination mechanism of MP. We had obtained limitations on the number charged, neutral and total multiplicities in  $pp$  interactions at 70 GeV/c and higher. In project Thermalization we plan to verify these. There are many of experimental and theoretical results, which evidence of cluster nature of MP by significant short-range multiplicity correlations [14], the observed scaling of the dynamical fluctuations of mean transverse-momentum [15].

In GDM the evaporation of gluon sources may be realized by single gluons and also groups consisted from two or more fission gluons. The superposition of them explains the shoulder structure of MD at ISR and higher energies [11]. Our approach gives the possible interpretation of soft and semi-hard components [16].

We modified GDM by including of the intermediate quark topologies to explain the experimental differences between  $p\bar{p}$  and  $pp$  inelastic topological cross sections and second correlation moment behavior at few GeV/c [17]. The high multiplicity in this process originates from "4" or "6"-topologies. Our scheme of hadronization describes well MD for hadron interactions at 70 GeV and higher and could be used to study the central nuclear collisions at low and high energies.

The Cherenkov type radiation can be emitted in the projectile and target particles. This leads to two peaks of dense groups of particles (spikes) distribution in rapidity phase-space. At the same time the particle distribution at the azimuthal angle is uniform. Study of the spike center distribution [18] in central C-Cu collisions at 4.5 GeV/c/A (all charged particles) and Mg-Mg collisions at 4.3 GeV/c/A (only negative charged particles) were found to be in agreement with the hypothesis of mesonic Cherenkov radiation. For this goal it was used transformation of pseudorapidity spectra from  $\eta$  variable to  $\tilde{\eta}$  with the uniform spectrum. In each

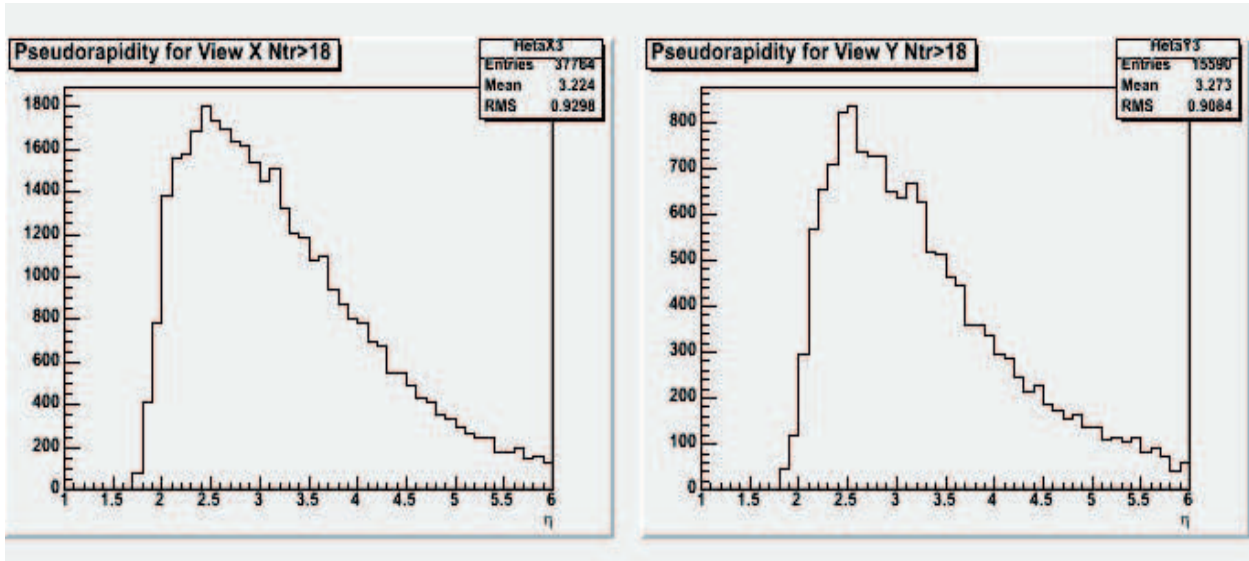


Figure 5. The pseudorapidity spectra in  $pPb$  at  $n > 18$ .

case the distance between peaks for these experiments is in agreement with Cherenkov radiation hypothesis, the charged-dependence was absent.

The ring-like substructures of secondary in  $^{208}Pb$  at 158 A GeV/c and  $^{197}Au$  at 11.6 GeV/c induced interactions with Ag(Br) nuclei in emulsion detector were investigated [19]. The good agreement was obtained with idea of Cherenkov radiation.

It must be emphasized that such events are rare, and represent at about 1% of full statistics. Therefore high luminosity and high multiplicity trigger of SVD setup agrees to collect enough statistics to study this phenomenon. The preliminary indications to the manifestation of the ring events are in Figure 12. This pseudorapidity spectra for  $pPb$ -interactions at high multiplicity ( $n > 18$ ) shows up such behavior.

As it was mentioned the Bose-Einstein condensation is very interesting phenomenon. The considerable efforts are necessary to confirm it experimentally. At HM events the plentiful number of pions (charged and neutral) are produced. All of them are bosons. When the multiplicity increase moments of them are approaching to zero. In the case of relativistic ideal Bose gas the pion number fluctuations may give a clear signal of approaching the BEC point [9]. When the temperature  $T$  decreases, the chemical potential increases and becomes equal to  $\mu_\pi = m_\pi$  at BEC temperature  $T = T_C$ . At this point the total number of particles takes up the lowest energy state.

M.I. Gorenstein and V.V. Begun had viewed the case of HM events in  $p + p$  interactions with beam energy of 70 GeV [9]. The volume of pion system was estimated as,  $V = E/\varepsilon(T, \mu_\pi)$ , and the number of pions was determined as,  $N_\pi = V\rho_\pi(T, \mu_\pi)$ . In the vicinity of the BEC point they revealed an abrupt and anomalous increase of the scaled variance of neutral and charged pion number fluctuations. Our experiment permits to experimental test of this phenomena. We are expected to take a lot of high multiplicity event statistics with reconstructed by gamma quantum neutral mesons and study scaled variance of neutral and charged pion number fluctuations,

## 5 Summary

We are continuing our work to making of program packets for data processing and new phenomena study at HM region.

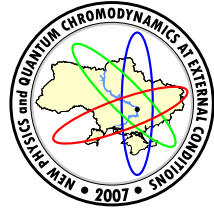
*Acknowledges.* Author E.K. is glad to thank the NPQCD-2007 Org. Committee for partial financial support and warm working atmosphere created.

These researches implemented into framework of project "Thermalization" is partially supported by RFBR grant 06 – 02 – 81010 – Bel-a.

## References

- [1] David d'Enterria. Quark-Gluon Matter. Submitted to: J.Phys. G: Nucl.Part.Phys. (nucl-ex/0611012).
- [2] V.V. Avdeichikov et al. Multiparticle production processes in  $p + p$  interaction with high multiplicity at  $E(p) = 70$  GeV. Proposal "Termalization". (In Russian) JINR-P1-2004-190, 45pp (2005).
- [3] V.V. Babintsev et al. IHEP preprint M-25, Protvino (1976).

- [4] M.Yu. Bogolyubsky et al. The methodic of film information handling in the experiment E-161. (In Russian) IHEP-INP-MSU-JINR E-161 Collaboration . IHEP-97-50, 9pp. (1997).
- [5] P.F. Ermolov et al. Proton-proton interaction with high multiplicity at energy of 70 GeV (proposal). *Phys.At.Nucl.*, **67** 107-113 (2004).
- [6] V.Blobel. Linear Least Squares Fits with a Large Number of Parameter. Version 0.999 - 17.10 2000. Institut fur experimentalphysik.Universitet Hamburg. 22pp. (2000).
- [7] A.V. Apanasenko et al. New interpretations of some 'anomalous' events in cosmic radiation. *Pisma Zh.Eksp.Teor. Fiz.* **30**, 157-161 (1979).
- I.M. Dremin. Ring-like events: Cerenkov gluons or Mach waves? *Nucl.Phys.* **A767**, 233-247 (2006).
- [8] J.Zimanyi, G.Fai and B.Jacobsson. Bose-Einstein condensation of pions in energetic heavy ion collisions? *Phys.Rev.Lett.* **43**, 1705-1707 (1979);  
I.N. Mishustin et al. Pion production and Bose enhancement effects in relativistic heavy ion collisions. *Phys.Lett.* **B276**, 403-408 (1992);  
R.Lednický et al. Multiboson effects in multiparticle production. *Phys.Rev.*, **C61**, 034901 (2000).
- [9] V.V. Begun and M.I.Gorenstein. Bose-Einstein condensation of pions in high multiplicity events. (hep-ph/0611043).
- [10] P.V.Chliapnikov et al. Observation of direct soft photon production in K+ p interactions at 70 GeV/c. *Phys. Let.*, **141B**, 276-287 (1984);  
S.Banerjee et al. Observation of direct soft photon production in pi- p interactions at 280-GeV/c. SO-PHIE/WA83 Collaboration. *Phys.Let.*, **B305**, 182-186 (1993);  
J.Antos et al. Soft photon production in 400-GeV/c p - Be collisions. *Z.Phys.*, **C59**, 547-554 (1993);  
J. Abdallah et al. Evidence for an excess of soft photons in hadronic decays of  $Z^0$ . DELPHI Collaboration. *Eur.Phys.J.* **C47**, 273-294 (2006).
- [11] E.S. Kokoulin and V.A.Nikitin. Study of multiparticle production by gluon dominance model. Proc. 17th ISHEPP, 319-326 (2005).JINR, Dubna;  
P.F. Ermolov et al. Study of multiparticle production by gluon dominance model. Part II. Proc. 17th ISHEPP, 327-336 (2005), JINR,Dubna.
- [12] E.S. Kokoulin. Gluon dominance model. *AIP Conf.Proc.* **828**, 81-86 (2006).
- [13] M.K. Volkov, E.S. Kokoulin and E.A.Kuraev. Excitation of Physical Vacuum. *Phys.Part.Nucl.Lett.* **1**, 235-239 (2004).
- [14] B. Alver. New PHOBOS results on event-by-event fluctuations. *AIP Conf.Proc.* **828**, 5-10 (2006).
- [15] W. Florkowski et al. Event-by-event fluctuations of transverse-momentum and multiparticle clusters in relativistic heavy-ion collisions. (nucl-th/0610035)
- [16] A. Giovannini and R. Ugocioni. Clan structure analysis and QCD parton showers in multiparticle dynamics: an intriguing dialog between theory and experiment. *Int.J.Mod.Phys.* **A20** 3897-4000 (2005).
- [17] J.G.Rushbrooke and B.R.Webber. High energy antiparticle-particle reaction differences and annihilations. *Phys. Rep.* **C44**, 1-92 (1978).
- [18] G.L. Gogiberidze, L.K. Gelovani and E.K. Sarkisian. Study of multiparticle spikes in central 4.5-A-GeV/c C-Cu collisions. *Phys.Lett.* **B430**, 368-374 (1998);  
G.L. Gogiberidze, L.K. Gelovani, E.K. Sarkisyan. On coherent particle production in central 4.3 A Gev/c Mg-Mg collisions. *Phys.Lett.* **B471**, 257-262 (1999);
- [19] S. Vokal, A. Kravcakova, S. Lehocka, G.I. Orlova. Azimuthal Structures of Produced Particles in Heavy Ion Interactions. Baldin Seminar on HEP Problems "Relativistic Nuclear Physics and Quantum Chromodynamics", JINR, Dubna, Russia, (2004).



## RELATIVISTIC WAVE EQUATION FOR ONE SPIN-1/2 AND ONE SPIN-0 PARTICLE

D. A. Kulikov<sup>a</sup>, R. S. Tutik<sup>b</sup>

Theoretical Physics Department  
Dnipropetrovsk National University, Dnipropetrovsk, Ukraine

A new approach to the two-body problem based on the extension of the  $SL(2, C)$  group to the  $Sp(4, C)$  one is developed. The wave equation with the Lorentz-scalar and Lorentz-vector potential interactions for the system of one spin-1/2 and one spin-0 particle with unequal masses is constructed.

### 1 Introduction

The relativistic two-body problem has numerous applications in particle and nuclear physics. Because the Bethe-Salpeter equation [1] is exceedingly difficult to solve, even numerically, different approaches to this problem have been developed. They include: reductions of the Bethe-Salpeter equation resulting in the quasipotential approach [2] and the Breit-type equations [3–5]; relativistic quantum mechanics with constraints [7, 8, 10] that uses a system of two coupled equations describing individual particles; the Barut method [9, 10] for deriving a single two-body wave equation from a field-theoretical action; Lorentz-invariant two-body wave equations having the Schrödinger-like [11] or Dirac-like [9] form.

In the last works the wave functions transform according to the more complicated representations than the one-particle wave functions that can be regarded as involving the extended Lorentz symmetry. The explicit extensions of the Lorentz group, including the symplectic [13] and the general complex [14] ones, have been studied, too.

Recently, the extension of the  $SL(2, C)$  group to the  $Sp(4, C)$  one has allowed us to formulate a new approach to the relativistic two-body problem [16]. The goal of the present work is to apply this technique for constructing the wave equation for the system composed of the spin-1/2 and spin-0 particles with unequal masses.

### 2 Symplectic space-time extension

The relativistic theory is usually formulated in the Minkowski space with the homogeneous Lorentz group  $SO(1, 3)$  as the local symmetry group. However, since the  $SO(1, 3)$  group is covered by the  $SL(2, C) \equiv Sp(2, C)$  group, the relativistic field theory can equivalently be formulated entirely within the framework of the  $Sp(2, C)$  Weyl spinors [16].

Recall that the symplectic  $Sp(2l, C)$  group is the group of  $2l \times 2l$  matrices with complex elements and determinant equal to one [17]. These matrices act on  $2l$ -component Weyl spinors and preserve an antisymmetric bilinear form which plays the role of "metrics" in the spinor space. For the  $Sp(4, C)$  group, we denote this form by  $\eta_{\alpha\beta} = -\eta_{\beta\alpha}$  ( $\alpha, \beta = 1, 2, 3, 4$ ). Then the  $Sp(4, C)$  Weyl spinors  $\varphi_\alpha$  with lower indices and their complex conjugates  $\bar{\varphi}_{\bar{\alpha}} = (\varphi_\alpha)^*$  are related to spinors with upper indices by transformations  $\varphi_\alpha = \eta_{\alpha\beta}\varphi^\beta$  and  $\bar{\varphi}_{\bar{\alpha}} = \eta_{\bar{\alpha}\bar{\beta}}\bar{\varphi}^{\bar{\beta}}$ .

Further, there exists one-to-one correspondence between  $Sp(2l, C)$  Hermitian spin-tensors of second rank and  $(2l)^2$ -component real vectors. In the case of the  $Sp(2, C)$  group, they are ordinary Minkowski four-vectors. For the case of  $Sp(4, C)$  group, we define the relationship between the Hermitian spin-tensor,  $P_{\alpha\bar{\alpha}}$ , and a real vector  $P_M$  by

$$P_{\alpha\bar{\alpha}} = \mu_{\alpha\bar{\alpha}}^M P_M, \quad P^M = \frac{1}{4} \tilde{\mu}^{M\bar{\alpha}\alpha} P_{\alpha\bar{\alpha}} \quad (1)$$

where  $\mu_{\alpha\bar{\alpha}}^M$  ( $M = 1 \div 16$ ) are matrices of the basis in the space of  $4 \times 4$  Hermitian matrices and tilde labels the transposed matrix with uppered spinor indices. In what follows, the spinor indices will be suppressed when possible.

To clarify the relationship between the discussed vector space and the Minkowski space  $\mathbb{R}^4$ , we represent 16 values of the vector index of  $P_M$  through  $4 \times 4$  combinations of two indices,  $M = (a, m)$ , with both  $a$  and  $m$

e-mail: <sup>a</sup>kulikov\_d\_a@yahoo.com, <sup>b</sup>tutik@ff.dsu.dp.ua

running from 0 to 3. Then the metrics of the discussed vector space is reduced to the factorized form

$$g^{MN} \equiv g^{(a,m)(b,n)} = \hat{h}^{ab} h^{mn} \quad (2)$$

where  $h^{mn} = \text{diag}(1, -1, -1, -1)$  is the usual Minkowski metrics and  $\hat{h}^{ab} = \text{diag}(1, 1, -1, 1)$  is caused by the group extension.

The factorization of the metrics means that the vector from  $\mathbb{R}^{16}$  may be decomposed into four Minkowski four-vectors. As a consequence, we can use these 16-component vectors or, equivalently,  $Sp(4, C)$  Hermitian spin-tensors to construct the wave equation for a few-body system.

### 3 Wave equation for a fermion-boson system

Let us consider a system consisted of one spin-1/2 and one spin-0 particle. With the total spin of the system being equal to 1/2, the wave equation must have the form of the Dirac-like equation in which the wave function is represented by a Dirac spinor or, in our case, by two  $Sp(4, C)$  Weyl spinors as

$$P_{\alpha\bar{\alpha}}\bar{\chi}^{\bar{\alpha}} = m\varphi_{\alpha}, \quad \tilde{P}^{\bar{\alpha}\alpha}\varphi_{\alpha} = m\bar{\chi}^{\bar{\alpha}} \quad (3)$$

where  $P_{\alpha\bar{\alpha}}$  is the  $Sp(4, C)$  momentum spin-tensor and  $m$  is a mass parameter. According to the splitting of the vector indices, we have

$$P = \mu^{(a,m)} P_{(a,m)} = \Sigma^0 \otimes \sigma^m w_m + \Sigma^1 \otimes \sigma^m p_m + \Sigma^2 \otimes \sigma^m r_m + \Sigma^3 \otimes \sigma^m q_m \quad (4)$$

where  $w_m, p_m, r_m, q_m$  are the Minkowski four-momenta and matrices  $\Sigma^a, \sigma^m$  may be expressed in terms of  $2 \times 2$  unit matrix  $I$  and the Pauli matrices  $\tau^i$ .

It has been shown [16] that the wave equation (3) describes the fermion-boson system with the equal mass constituents. Now we are going to generalize it to the case of the particles with unequal masses. For this purpose, let us replace the mass parameter in the right hand of Eq.(3) by a suitable matrix term which can be expressed as a combination of direct products of matrices. Though such term breaks the  $Sp(4, C)$  symmetry of the wave equation, but the Lorentz  $SO(1, 3) \subset Sp(4, C)$  symmetry is retained. It becomes obvious if the second matrix in the direct product is chosen as a unit matrix and the first one is written through the matrices  $\Sigma^a$ , like in Eq.(4). There are two equivalent possibilities, with the matrix  $\Sigma^a$  chosen as  $\Sigma^1 = \tau^1$  or  $\Sigma^3 = \tau^3$  ( $\Sigma^0 = I$  is the trivial choice), that result in the plus sign in the metrics  $\hat{h}^{ab}$  defined by Eq.(2). In view of this we replace the mass parameter as follows

$$m \rightarrow (m_1 + m_2)/2 + \tau^1 \otimes I(m_1 - m_2)/2, \quad (5)$$

so that the additional term vanishes if  $m_1 = m_2$ .

Thus, the wave equation for the fermion-boson system with unequal masses takes the form

$$P\bar{\chi} = (m_+ + \tau^1 \otimes Im_-)\varphi, \quad \tilde{P}\varphi = (m_+ + \tau^1 \otimes Im_-)\bar{\chi} \quad (6)$$

where  $m_{\pm} = (m_1 \pm m_2)/2$ .

Now, for elucidating the two-particle interpretation of the proposed equation, we consider the structure of the the  $Sp(4, C)$  momentum spin-tensor given by Eq.(4). It should be stressed that the description of the two-particle system requires only two four-momenta whereas the  $Sp(4, C)$  momentum spin-tensor corresponds to four four-momenta, collected in a 16-component vector. Therefore the number of the independent components of  $w_m, p_m, r_m$  and  $q_m$  must be decreased that can be implemented with subsidiary conditions.

In order to derive the subsidiary conditions we transform Eq.(6) to the form of the Klein-Gordon equation. By eliminating  $\bar{\chi}$  and using Eq.(4), we obtain

$$(w^2 + p^2 - r^2 + q^2 - \frac{2m_-}{m_+} wp - m_+^2 + m_-^2 + \sum_{A=1}^5 \gamma_A K^A)\varphi = 0 \quad (7)$$

where  $w^2 = (w^0)^2 - \mathbf{w}^2$ ,  $p^2 = (p^0)^2 - \mathbf{p}^2$  etc,  $\gamma_A$  are direct products of the Pauli matrices, and  $K^A$  are quadratic forms with respect to the four-momenta.

Because in this equation the non-diagonal terms  $\gamma_A K^A$  have no analog in the case of the ordinary Klein-Gordon equation, we put  $\gamma_A K^A = 0$  that yields

$$\begin{aligned} (m_+^2 - m_-^2)(wp - m_+ m_-) - m_+ m_- (r^2 - q^2) &= 0, \\ m_+ wq - m_- pq &= 0, \\ m_+ rp - m_- rw &= 0, \\ rq &= 0, \\ m_+ (r^m w^n - r^n w^m - \epsilon^{mnkl} p_k q_l) - m_- (r^m p^n - r^n p^m - \epsilon^{mnkl} w_k q_l) &= 0, \end{aligned} \quad (8)$$

with  $\epsilon^{mnkl}$  being the totally antisymmetric tensor ( $\epsilon^{0123} = +1$ ).

Thus, the imposed conditions and the Klein-Gordon-like equation set ten components of  $w_m$ ,  $p_m$ ,  $r_m$ ,  $q_m$  to be the independent ones. For the connection of these four-momenta with the four-momenta,  $p_{1m}$  and  $p_{2m}$ , of the constituent particles we assume

$$w_m = \frac{1}{2}(p_{1m} + p_{2m}), \quad p_m = \frac{1}{2}(p_{1m} - p_{2m}), \quad r_m = 0, \quad q_m = 0. \quad (9)$$

Then the only one condition from Eqs.(8) remains non-trivial that reads

$$(wp - m_+ m_-) \equiv (p_1^2 - p_2^2 - m_1^2 + m_2^2)/4 = 0. \quad (10)$$

This equality implies that the total spinor wave function does not depend on the relative time of the particles.

Further, the wave equation (6) and the condition (10) can be reduced to the one-particle Dirac and Klein-Gordon equations for the constituents of our system. Indeed, with decomposing the spinor wave functions into the projections

$$\varphi_{\pm} = \frac{1}{2}(1 \pm \tau^1 \otimes I)\varphi, \quad \bar{\chi}_{\pm} = \frac{1}{2}(1 \pm \tau^1 \otimes I)\bar{\chi} \quad (11)$$

which are two-component  $Sp(2, C)$  Weyl spinors as well, Eqs.(6) and (10) reduce to two uncoupled sets of equations

$$p_{1m}\sigma^m\bar{\chi}_+ = m_1\varphi_+, \quad p_{1m}\tilde{\sigma}^m\varphi_+ = m_1\bar{\chi}_+ \quad (12)$$

$$(p_2^2 - m_2^2)\varphi_+ = 0, \quad (p_2^2 - m_2^2)\bar{\chi}_+ = 0 \quad (13)$$

and

$$p_{2m}\sigma^m\bar{\chi}_- = m_2\varphi_-, \quad p_{2m}\tilde{\sigma}^m\varphi_- = m_2\bar{\chi}_-, \quad (14)$$

$$(p_1^2 - m_1^2)\varphi_- = 0, \quad (p_1^2 - m_1^2)\bar{\chi}_- = 0, \quad (15)$$

consisted of the free one-particle Dirac equations written in the Weyl spinor formalism [18] and the free Klein-Gordon equations.

Hence it appears that the wave equation (6) supplemented with the subsidiary conditions (8) describes two systems composed of the spin-1/2 and spin-0 particles. These systems differ from each other only in permutation of masses of the particles. As a next step, we must include the potential interaction in our equations.

#### 4 Inclusion of the potential interaction

A generally accepted receipt of introducing the interaction consists in the replacement of the four-momenta of the particles in the minimal manner by the generalized momenta ( $p_i^m \rightarrow \pi_i^m = p_i^m - A_i^m$ ,  $i=1,2$ ), so that each particle is in an external potential of the other. This kind of coupling is referred to as the Lorentz-vector interaction. Another possibility uses the mass-potential substitution,  $m_i \rightarrow m_i + S_i$ , that corresponds to the Lorentz-scalar interaction.

In our approach the masses and four-momenta of the particles are involved through the quantities  $w^m, p^m, m_+, m_-$ . For this reason, we introduce the Lorentz-vector and Lorentz-scalar interactions by the replacements

$$\begin{aligned} w^m &\rightarrow \omega^m = w^m - A^m, & m_+ &\rightarrow M_+ = m_+ + S_+, \\ p^m &\rightarrow \pi^m = p^m - B^m, & m_- &\rightarrow M_- = m_- + S_-. \end{aligned} \quad (16)$$

Here the involved potentials  $A^m, B^m, S_+, S_-$  may depend on the coordinates and momenta of the particles but the shape of these potentials is restricted. This restriction is caused by the requirement that the wave equation must be compatible with the subsidiary condition (10) written after the replacements (16) as

$$L \equiv \omega\pi + \pi\omega - M_+M_- - M_-M_+ = 0 \quad (17)$$

A sufficient condition for this compatibility is that the operator  $L$  of the subsidiary condition should commute with the operators in the wave equation:

$$[L, \omega_m] \approx 0, \quad [L, \pi_m] \approx 0, \quad [L, M_+] \approx 0, \quad [L, M_-] \approx 0 \quad (18)$$

where the weak equality sign means that the commutator may give an expression proportional to  $L$  itself which, on account of Eq.(17), equals to zero.

Because of the quantity  $wp$  appearing in Eqs.(16) and (17), we have  $[wp, x_m] \neq 0$  but  $[wp, x_{\perp m}] = 0$ , the conditions in Eqs.(18) require that the potentials depend on the relative coordinate  $x_m = x_{1m} - x_{2m}$  only through its transverse with respect to the total momentum part

$$x_{\perp}^m = (h^{mn} - w^m w^n / w^2) x_n \quad (19)$$

where the total momentum  $w_m$  is assumed to be a constant of motion.

The simplest solution to the compatibility condition (18) comes from the following ansatz

$$\omega\pi + \pi\omega = 2Cwp, \quad M_+M_- + M_-M_+ = 2Cm_+m_-, \quad (20)$$

where  $C = C(x_\perp^2)$  is an arbitrary function. Then the subsidiary condition (17) takes the form of Eq.(10), which describes the case without interaction, that brings at once to vanishing commutators.

Finally, let us derive an explicit form of the wave equation for the fermion-boson system with the potential interactions. With substituting the generalized momenta and the mass-potential terms (16) into Eqs. (4) and (6), we obtain

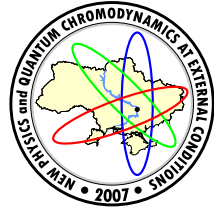
$$\begin{aligned} (I \otimes \sigma^m \omega_m + \tau^1 \otimes \sigma^m \pi_m) \bar{\chi} &= (M_+ + \tau^1 \otimes IM_-) \varphi, \\ (I \otimes \tilde{\sigma}^m \omega_m + \tau^1 \otimes \tilde{\sigma}^m \pi_m) \varphi &= (M_+ + \tau^1 \otimes IM_-) \bar{\chi}. \end{aligned} \quad (21)$$

Here the quantities  $\omega_m, \pi_m, M_+, M_-$  involve the interaction and satisfy the ansatz (20). Using this ansatz, we can introduce both the potential interaction described by the time-component of the Lorentz vector and the confinement potential included in the Lorentz-scalar term or in the spatial part of the Lorentz vector.

Thus, a new approach to the two-body problem based on the extension of the  $SL(2, C)$  group to the  $Sp(4, C)$  one has been developed. It permits us to construct the relativistic wave equation for the system consisted of spin-1/2 and spin-0 particles with unequal masses, involving the various forms of interaction.

## References

- [1] E.E. Salpeter, H.A. Bethe, Phys.Rev. **84**, 1232 (1951).
- [2] A.A. Logunov, A.N. Tavkhelidze, Nuovo Cim. **29**, 380 (1963).
- [3] G. Breit, Phys.Rev. **34**, 553 (1929).
- [4] J. Bijtebier, J. Broekaert, Nuovo Cim. **A105**, 625 (1992).
- [5] T. Tanaka, A. Suzuki, M. Kimura, Z.Phys. **A353**, 79 (1995).
- [6] H. Sazdjian, Phys.Rev. **D33**, 3401 (1986).
- [7] H.W. Crater, P. Van Alstine, Phys.Rev. **D36**, 3007 (1987).
- [8] H.W. Crater, C.-Y. Wong, P. Van Alstine, hep-ph/0603126.
- [9] A.O. Barut, S. Komy, Fortschr.Phys. **33**, 309 (1985).
- [10] W. Garczyński, M. Klimek, Acta Phys.Pol. **B20**, 755 (1989).
- [11] W.I. Fushchych, Lett. Nuovo Cim. **10**, 163 (1974).
- [12] M. Moshinsky, A.G. Nikitin, hep-ph/0502028.
- [13] Yu.F. Pirogov, Phys.Atom.Nucl. **66**, 136 (2003) [Yad.Fiz. **66**, 138 (2003)].
- [14] A.A. Bogush, V.M. Red'kov, hep-th/0607054.
- [15] D.A. Kulikov, R.S. Tutik, A.P. Yaroshenko, Phys.Lett. **B644**, 311 (2007) [hep-th/0701271].
- [16] R. Penrose, W. Rindler, *Spinors and Space-Time*, Vol.1 (Cambridge University Press, 1984).
- [17] H. Weyl, *The Classical Groups: Their Invariants and Representations* (Princeton University Press, 1946).
- [18] E.M. Lifshitz, L.P. Pitaevskii, V.I. Berestetskii, *Quantum Electrodynamics* (Pergamon, Oxford 1982).



## WAVE FUNCTIONS OF THE RELATIVISTIC THREE-BODY OSCILLATOR CONSTRUCTED WITH THE EXTENSION OF THE $SL(2, C)$ GROUP

D. A. Kulikov<sup>a</sup>, R. S. Tutik<sup>b</sup>, A.P. Yaroshenko

Theoretical Physics Department  
Dnipropetrovsk National University, Dnipropetrovsk, Ukraine

An approach based on the extension of the  $SL(2, C)$  group to the  $Sp(4, C)$  one is applied to the three-body problem. The relativistic wave equation for the three-body system with total spin 1/2 is constructed. For the system with oscillator interaction, involved through the linear in coordinates generalized momenta, a complete set of spatial wave functions is obtained.

### 1 Introduction

The harmonic oscillator occupies an important place in nuclear and particle physics. In hadron physics a relativistic equation for the symmetric quark model with harmonic interaction was proposed by Feynman, Kislinger and Ravndal [1] as far back as 1971. Since their work, the concept of relativistic oscillator has been used for describing the spectra of the both ordinary hadrons [2–4] and glueballs [5]. Of course, these models are purely phenomenological ones. But, through its covariant formulation, the relativistic oscillator is able to deal in a simple way with retardation effects, which are rather complicated in other approaches.

Up to now, different models of the relativistic two-body oscillators with spin-0 [6, 7] or spin-1/2 [8, 9] constituents, or with mixed spin-0-spin-1/2 content [10] have been offered. In contrast, for the three-body case, to the best of our knowledge there are only the models of the oscillators composed of the Klein-Gordon particles [11–13]. Generally, the three-body problems with fermions are approached by using the coupled one-particle wave equations [14] or the three-body versions of the Bethe-Salpeter equation [15].

Recently, a new approach to the relativistic two-body problem, based on the extension of the  $SL(2, C)$  group to the  $Sp(4, C)$  one, has been developed [16]. In the present work we intend to generalize this approach to the three-particle case and apply it to construct a model for the relativistic three-body oscillator with total spin 1/2.

The plan of the work is as follows. Section 2 is devoted to deriving the wave equation for a free three-body system with total spin 1/2 via the extension of the  $SL(2, C)$  group. In Section 3 we consider the three-body system with oscillator interaction involved through the generalized momenta linear in coordinates, in spirit of the Dirac-oscillator model [17]. We show that the wave equation for our system can be reduced to the equation describing two coupled three-dimensional harmonic oscillators with additional spin-orbit interaction. Finally, in Section 4, a complete set of spatial wave functions for this system is obtained.

### 2 Wave equation for a three-body system

We start with the symplectic symmetry which is laid in the basis of our construction of the relativistic equations in the Minkowski space. The homogeneous Lorentz group  $SO(1, 3)$  is covered by the  $SL(2, C) \equiv Sp(2, C)$  group. As a consequence, there exists one-to-one correspondence between the  $Sp(2, C)$  Hermitian spin-tensors of second rank and the Minkowski four-vectors. It means that the space-time position of a relativistic particle can be parametrized by the  $Sp(2, C)$  Hermitian spin-tensor.

In order to describe few-particle systems, we extend the  $Sp(2, C)$  group to the  $Sp(4, C)$  one. This is the minimal extension that preserves a non-degenerate antisymmetric bilinear form  $\eta_{\alpha\beta} = -\eta_{\beta\alpha}$  ( $\alpha, \beta = 1, 2, 3, 4$ ) in the spinor space.

In terms of the 4-component  $Sp(4, C)$  Weyl spinors  $\varphi_\alpha$  and  $\bar{\chi}^{\bar{\alpha}}$ , the Dirac-like equation takes the form

$$P_{\alpha\bar{\alpha}}\bar{\chi}^{\bar{\alpha}} = m\varphi_\alpha, \quad \tilde{P}^{\bar{\alpha}\alpha}\varphi_\alpha = m\bar{\chi}^{\bar{\alpha}} \quad (1)$$

where  $P_{\alpha\bar{\alpha}}$  is the  $Sp(4, C)$  momentum spin-tensor and  $m$  is a mass parameter. Because the wave functions are the spinors of first rank, the proposed wave equation can be adapted for the description of a three-body system with total spin equal to 1/2.

e-mail: <sup>a</sup>kulikov\_d\_a@yahoo.com, <sup>b</sup>tutik@ff.dsu.dp.ua

© Kulikov D.A., Tutik R.S., Yaroshenko A.P., 2007.

For construction of such an equation, let us at first consider the structure of the  $Sp(4, C)$  momentum spin-tensor. According to our previous analysis [16], this spin-tensor, with suppressed spinor indices, can be decomposed into four Minkowski four-momenta as

$$P = \Sigma^0 \otimes \sigma^m w_m + \Sigma^1 \otimes \sigma^m p_m + \Sigma^2 \otimes \sigma^m r_m + \Sigma^3 \otimes \sigma^m q_m \quad (2)$$

where  $w_m, p_m, r_m, q_m$  ( $m = 0, 1, 2, 3$ ) are the Minkowski four-momenta, and quantities  $\Sigma^a$  and  $\sigma^m$  are  $2 \times 2$  Hermitian matrices for which in following we use the matrix representation from Ref.[16].

It should be stressed that the description of the three-particle system requires one time-like and nine space-like variables whereas the  $Sp(4, C)$  momentum spin-tensor has sixteen components. In order to decrease the number of the independent components, we must supplement the wave equation with subsidiary conditions having the  $Sp(4, C)$ -invariant form.

For deriving these conditions, we transform Eq.(1) into the Klein-Gordon-like equation analogous to that of the three-boson model [13]. Upon eliminating  $\bar{\chi}^{\bar{\alpha}}$  and using Eq.(2), we obtain

$$(P\tilde{P} - m^2)\varphi \equiv (w^2 + p^2 - r^2 + q^2 - m^2 + \sum_{A=1}^5 \gamma_A K^A)\varphi = 0 \quad (3)$$

where  $w^2 = (w^0)^2 - \mathbf{w}^2$ ,  $p^2 = (p^0)^2 - \mathbf{p}^2$  etc,  $\gamma_A$  are direct products of the Pauli matrices, and  $K^A$  are quadratic forms with respect to the four-momenta.

Five quantities  $K^A$  are components of a complex vector that transforms according to the representation  $SO(5, C) \subset Sp(4, C)$ . For restoring the form of the Klein-Gordon equation, we put  $K^A = 0$  on the wave functions. This condition does indeed be invariant under transformations of the  $Sp(4, C)$  group, because if a vector equals to zero in one frame then it equals to zero also in all frames.

Being written in terms of the four-momenta, the imposed equality  $K^A = 0$  reads

$$\begin{aligned} wp &= 0, & wq &= 0, & rp &= 0, & rq &= 0, \\ r^m w^n - r^n w^m - \epsilon^{mnkl} p_k q_l &= 0 \end{aligned} \quad (4)$$

where  $\epsilon^{mnkl}$  is the totally antisymmetric tensor ( $\epsilon^{0123} = +1$ ).

Thus, the Klein-Gordon-like equation (3) with the conditions (4) set ten components of  $w_m, p_m, r_m, q_m$  to be the independent ones.

Now we introduce an explicit three-body interpretation. Let the above four-momenta be expressed through the four-momenta,  $p_1^m, p_2^m$  and  $p_3^m$ , of the constituent particles in the standard manner [18, 19] as

$$w^m = \frac{p_1^m + p_2^m + p_3^m}{\sqrt{3}}, \quad p^m = \frac{p_1^m - p_2^m}{\sqrt{2}}, \quad q^m = \sqrt{\frac{2}{3}} \left( \frac{p_1^m + p_2^m}{2} - p_3^m \right). \quad (5)$$

Since the considered three-body system is an isolated one, the total four-momentum  $w_m$  must be a constant of motion. Then for an arbitrary four-vector  $a_m$  we can introduce its transverse and longitudinal, with respect to  $w_m$ , parts

$$a_{\perp}^m = (h^{mn} - w^m w^n / w^2) a_n, \quad a_{\parallel}^m = (w^m w^n / w^2) a_n \quad (6)$$

where  $h^{mn} = \text{diag}(1, -1, -1, -1)$  is the Minkowski metrics.

With this notation, the subsidiary conditions (4) take the form

$$p_{\parallel}^m = 0, \quad q_{\parallel}^m = 0, \quad r_m = \frac{1}{w^2} \epsilon_{mnkl} w^n p^k q^l. \quad (7)$$

It is became evident that the first two equalities remove the relative time variables which correspond to  $p_{\parallel}^m$  and  $q_{\parallel}^m$ . The last equality says that the four-momentum  $r_m$  is also expressed through the four-momenta of the constituent particles. Thus, we conclude that the wave equation (1), based on the extension of the  $SL(2, C)$  group and supplemented with the subsidiary conditions (4), indeed describes the free three-particle system with the total spin 1/2.

### 3 The system with oscillator interaction

Now we intend to include the potential interaction in our description. This can be made by replacing the four-momenta of particles by the generalized momenta ( $p_i^m \rightarrow \pi_i^m = p_i^m - A_i^m$ ,  $i=1,2,3$ ), so that each particle is in an external potential of the others.

Because the generalized momenta do not, generally, commute with each other, the question on the compatibility of the subsidiary conditions among themselves arises. In the language of the Dirac's quantum mechanics with constraints, the subsidiary conditions (4) are the first-class constraints. Then a sufficient condition of their

compatibility implies that they must commute with each other and with the wave equation without producing second-class constraints.

Under this restriction, we can choose the simplest form of the generalized momenta with involving the linear in coordinates interaction

$$\begin{aligned}\pi_1^m &= p_1^m + \frac{\lambda}{\sqrt{3}}(x_{2\perp}^m - x_{3\perp}^m), & \pi_2^m &= p_2^m + \frac{\lambda}{\sqrt{3}}(x_{3\perp}^m - x_{1\perp}^m), \\ \pi_3^m &= p_3^m + \frac{\lambda}{\sqrt{3}}(x_{1\perp}^m - x_{2\perp}^m)\end{aligned}\quad (8)$$

where  $\lambda$  is a constant.

In terms of the relative momenta this means that

$$p^m \rightarrow \mathcal{P}^m = p^m + \lambda y_\perp^m, \quad q^m \rightarrow \mathcal{Q}^m = q^m - \lambda x_\perp^m \quad (9)$$

and the following commutation relations are valid

$$[p^m, x^n] = i h^{mn}, \quad [q^m, y^n] = i h^{mn} \quad (10)$$

where  $h^{mn}$  is the Minkowski metrics, and the relative coordinates are introduced as

$$x^m = \frac{x_1^m - x_2^m}{\sqrt{2}}, \quad y^m = \sqrt{\frac{2}{3}} \left( \frac{x_1^m + x_2^m}{2} - x_3^m \right). \quad (11)$$

Furthermore, with the generalized momenta (9) inserted, the subsidiary conditions (4) remain unaltered in the form and satisfy the compatibility requirement as before.

Now let us show that the included interaction is the oscillator one similar to the interaction in the model of the Dirac oscillator [17]. Remind that the Dirac oscillator is obtained from the one-particle Dirac Hamiltonian by the non-minimal substitution for the momentum,  $\mathbf{p} \rightarrow \mathbf{p} - im\omega\beta\mathbf{x}$ , where  $\omega$  is the oscillator frequency and  $\beta$  is the Dirac matrix. Inserting Eq.(9) into the  $Sp(4, C)$  momentum spin-tensor (2) and rearranging its terms, so that each relative momentum should be accompanied with the corresponding coordinate, we get

$$\begin{aligned}P &= \Sigma^0 \otimes \sigma^m w_m + \Sigma^1 \otimes \sigma^m (p_m + i\lambda\Sigma^2 \otimes I x_m) \\ &+ \Sigma^2 \otimes \sigma^m r_m + \Sigma^3 \otimes \sigma^m (q_m + i\lambda\Sigma^2 \otimes I y_m).\end{aligned}\quad (12)$$

It is seen that the expressions in parentheses in the last equation involve the Hermitian matrix times imaginary unit, similarly to the non-minimal substitution used in the Dirac oscillator model.

In order to obtain an explicit oscillator-type equation for our three-body system, we use the center-of-mass frame in which  $\mathbf{w} = 0$ . Then  $E = \sqrt{3}w^0$  is the total energy and the dynamics of the relative motion is described by the coordinates  $\mathbf{x}_\perp = \mathbf{x}$  and  $\mathbf{y}_\perp = \mathbf{y}$ . From Eq.(7) it follows that  $\mathcal{P}^0 = \mathcal{Q}^0 = r^0 = 0$ , and the wave equation (1) with the momentum spin-tensor (2), rewritten through the vectors of generalized relative momenta,  $\mathbf{P}$  and  $\mathbf{Q}$ , and the Pauli matrices  $\tau^i$ , becomes

$$\begin{aligned}\left( \frac{E}{\sqrt{3}} - \tau^1 \otimes \boldsymbol{\tau} \mathbf{P} - \tau^3 \otimes \boldsymbol{\tau} \mathbf{Q} + \frac{2\sqrt{3}\lambda}{E} \tau^2 \otimes \boldsymbol{\tau} \mathbf{M} \right) \bar{\chi} &= m\varphi \\ \left( \frac{E}{\sqrt{3}} + \tau^1 \otimes \boldsymbol{\tau} \mathbf{P} + \tau^3 \otimes \boldsymbol{\tau} \mathbf{Q} + \frac{2\sqrt{3}\lambda}{E} \tau^2 \otimes \boldsymbol{\tau} \mathbf{M} \right) \varphi &= m\bar{\chi}\end{aligned}\quad (13)$$

where

$$\mathbf{M} = \frac{1}{2\lambda} \mathbf{P} \times \mathbf{Q} \equiv \frac{1}{2\lambda} (\mathbf{p} + \lambda\mathbf{y}) \times (\mathbf{q} - \lambda\mathbf{x}). \quad (14)$$

It can be verified that, for this equation, the total angular momentum  $\mathbf{J} = \mathbf{x} \times \mathbf{p} + \mathbf{y} \times \mathbf{q} + \boldsymbol{\tau}/2$  is conserved. Moreover, the quantity

$$K = \tau^2 \otimes (\boldsymbol{\tau} \mathbf{M} + I), \quad (15)$$

playing the same role as the spin-orbit coupling operator in the one-particle Dirac equation, and the quantity  $\mathbf{N}$  given by

$$\mathbf{N} = -\frac{1}{2\lambda} (\mathbf{p} - \lambda\mathbf{y}) \times (\mathbf{q} + \lambda\mathbf{x}) \quad (16)$$

are conserved, too. The conservation of  $\mathbf{N}$  implies that the energy spectrum of the model possesses an "accidental" degeneracy.

At last, after substitution  $\psi = \varphi + \bar{\chi}$ , Eq.(13) is indeed transformed into the oscillator-type equation

$$[(\frac{E}{\sqrt{3}} + \frac{2\sqrt{3}\lambda K}{E})^2 - (m + \frac{2\sqrt{3}\lambda}{E}\tau^2 \otimes I)^2]\psi = \\ [\mathbf{p}^2 + \lambda^2\mathbf{x}^2 + \mathbf{q}^2 + \lambda^2\mathbf{y}^2 + \lambda(\mathbf{y}\mathbf{p} - \mathbf{x}\mathbf{q} + 2K + \tau^2 \otimes I)]\psi. \quad (17)$$

The derived equation describes two coupled three-dimensional harmonic oscillators with the additional spin-orbit interaction. The latter appears due to the quantity  $K$  having the product of the spin-1/2 Pauli matrix  $\tau$  and the orbital angular momentum incoming in the quantity  $\mathbf{M}$ .

#### 4 Spatial wave functions of the three-body oscillator

The next step is to derive the spatial wave functions for the obtained equations. Before proceeding further, let us make some comments. For the three-body problem, several sets of spatial basis functions are known such as the K-harmonics [18] and the harmonic-oscillator functions [19, ?]. However, the problem under consideration has a peculiarity. Namely, two oscillators entering Eq.(17) are the coupled ones. In view of this, we are going to construct a new set of basis functions that will be well-suited for the described system.

In what follows we consider only the spatial part of the wave functions. Upon excluding the spin-dependent terms from Eq.(17), we arrive at the quantity

$$\mathcal{O} = \mathbf{P}^2 + \mathbf{Q}^2 \equiv \mathbf{p}^2 + \lambda^2\mathbf{x}^2 + \mathbf{q}^2 + \lambda^2\mathbf{y}^2 + \lambda(\mathbf{y}\mathbf{p} - \mathbf{x}\mathbf{q}) \quad (18)$$

describing two coupled harmonic oscillators.

This quantity commutes with the orbital angular momentum  $\mathbf{L} = \mathbf{x} \times \mathbf{p} + \mathbf{y} \times \mathbf{q}$  which can be written as the sum of two parts

$$\mathbf{L} = \mathbf{M} + \mathbf{N} \quad (19)$$

where  $\mathbf{M}$  and  $\mathbf{N}$ , defined by Eq.(14) and Eq.(16), obey the usual commutation relations for angular momenta and commute with each other.

Moreover, the momenta  $\mathbf{M}$  and  $\mathbf{N}$  commute with  $\mathcal{O}$  separately. Hence, the spatial wave functions for our system can be expressed through the eigenstates of these two momenta determined by

$$\begin{aligned} \mathbf{M}^2\Phi &= M(M+1)\Phi, & M_3\Phi &= m\Phi, \\ \mathbf{N}^2\Phi &= N(N+1)\Phi, & N_3\Phi &= n\Phi. \end{aligned} \quad (20)$$

Further, it is convenient to use the lowering and raising operators

$$M_{\pm} = M_1 \pm iM_2, \quad N_{\pm} = N_1 \pm iN_2 \quad (21)$$

which do not change the representation defined by the pair of values  $M$  and  $N$ .

All solutions of the system (20), which we denote as  $\Phi_{Mm,Nn}$ , may be easily obtained if we find the state  $\Phi_{MM,NN}$  having the highest weight in the representation and, consequently, satisfying the equations

$$\begin{aligned} M_+\Phi_{MM,NN} &= 0, & N_+\Phi_{MM,NN} &= 0, \\ M_3\Phi_{MM,NN} &= M\Phi_{MM,NN}, & N_3\Phi_{MM,NN} &= N\Phi_{MM,NN}. \end{aligned} \quad (22)$$

The consideration can be simplified very much by introducing, as in the method of K-harmonics [18], two complex vectors

$$\mathbf{z} = (\mathbf{x} + i\mathbf{y})/\sqrt{2}, \quad \bar{\mathbf{z}} = (\mathbf{x} - i\mathbf{y})/\sqrt{2} \quad (23)$$

where bar means complex conjugation.

Now, if we pass from the cartesian components of  $\mathbf{z}$  and  $\bar{\mathbf{z}}$  to their combinations

$$u = (z_1 + iz_2)/\sqrt{2}, \quad v = (\bar{z}_1 + i\bar{z}_2)/\sqrt{2} \quad (24)$$

the explicit expressions for the operators in Eqs.(22) become

$$\begin{aligned} M_+ &= \frac{1}{\sqrt{2}\lambda} [(\lambda\bar{z}_3 - \partial_{z_3})(\lambda u + \partial_{\bar{u}}) - (\lambda v - \partial_{\bar{v}})(\lambda z_3 + \partial_{z_3})], \\ M_- &= \frac{1}{\sqrt{2}\lambda} [(\lambda z_3 + \partial_{z_3})(\lambda\bar{u} - \partial_u) - (\lambda\bar{v} + \partial_v)(\lambda\bar{z}_3 - \partial_{\bar{z}_3})], \\ M_3 &= \frac{1}{2\lambda} [(\lambda v - \partial_{\bar{v}})(\lambda\bar{v} + \partial_v) - (\lambda\bar{u} - \partial_u)(\lambda u + \partial_{\bar{u}})] \end{aligned} \quad (25)$$

whereas the expressions for  $N_{\pm}$  and  $N_3$  are obtained from these equations on replacing  $\lambda \rightarrow -\lambda$ .

After solving Eqs.(22), we get the state with the highest weight in the following form

$$\Phi_{MM,NN} = C_{MM,NN} \exp(-\lambda \mathbf{z} \bar{\mathbf{z}}) v^M u^N \quad (26)$$

where  $C_{MM,NN}$  is a normalization constant. The subsequent application of the lowering operators yields

$$\Phi_{Mm,Nn} = C_{Mm,Nn} (M_-)^{M-m} (N_-)^{N-n} \exp(-\lambda \mathbf{z} \bar{\mathbf{z}}) v^M u^N \quad (27)$$

which are the solutions for the system (20) and, hence, form a complete set of spatial basis functions for the three-body problem. Knowing the eigenstates of  $\mathbf{M}$  and  $\mathbf{N}$ , we can construct the eigenstates of the orbital angular momentum  $\mathbf{L} = \mathbf{M} + \mathbf{N}$  by using the conventional Clebsch-Gordan coefficients.

It should be pointed that for the states with  $N = 0$  the obtained expression essentially simplifies. Because for these states the orbital angular momentum has the definite value  $L = M$ , the spatial wave function (27) takes the form

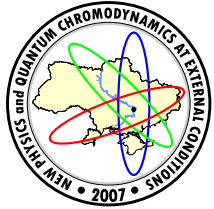
$$\Phi_{Lm,00} = A_{Lm} \exp(-\lambda \mathbf{z} \bar{\mathbf{z}}) \mathcal{Y}_{Lm}(\bar{\mathbf{z}}) \quad (28)$$

where  $A_{Lm}$  is a normalization constant and  $\mathcal{Y}_{Lm}(\bar{\mathbf{z}})$  is the solid harmonic. If we compare this result with the ground-state wave functions from the two-oscillator basis [19], the distinction will be in the dependence of the solid harmonic in Eq.(28) on the complex vector  $\bar{\mathbf{z}} = (\mathbf{x} - i\mathbf{y})/\sqrt{2}$  rather than on the relative coordinate  $\mathbf{x}$  or  $\mathbf{y}$ .

In conclusion, the approach, based on the extension of the  $SL(2, C)$  group to the  $Sp(4, C)$  one, has been applied to construct the relativistic wave equation for the three-body system with total spin 1/2. Upon inserting the linear in coordinates generalized momenta into this equation, the model for the relativistic three-body oscillator that represents two coupled three-dimensional harmonic oscillators with the additional spin-orbit interaction has been obtained. For this system, a complete set of spatial wave functions is derived. The discussion of the energy spectrum of the model will be published elsewhere.

## References

- [1] R.P. Feynman, M. Kislinger, F. Ravndal, Phys.Rev. **D3**, 2706 (1971).
- [2] A.N. Mitra, Phys.Rev. **D11**, 3270 (1975).
- [3] S. Ishida, T. Sonoda, Progr.Theor.Phys. **70**, 1323 (1983).
- [4] A. Bohm, M.E. Loewe, P. Magnollay, Phys.Rev. **D32**, 791 (1985).
- [5] F. Buisseret, C. Semay, Phys.Rev. **D73**, 114011 (2006).
- [6] Ph. Droz-Vincent, Annales Poincaré Phys.Theor. **27**, 407 (1977).
- [7] M.J. King, F. Rohrlich, Annals Phys. **130**, 350 (1980).
- [8] A. Del Sol Mesa, M. Moshinsky, J.Phys. **A27**, 4685 (1994).
- [9] M. Moshinsky, A.G. Nikitin, hep-ph/0502028.
- [10] H. Sazdjian, Phys.Rev. **D33**, 3435 (1986).
- [11] A. Maheshwari, Prog.Theor.Phys. **67**, 1278 (1982).
- [12] J. Bijtebier, Nuovo Cim. **A81**, 423 (1984).
- [13] Ph. Droz-Vincent, Phys.Rev. **A73**, 042101 (2006).
- [14] H. Sazdjian, Annals Phys. **190**, 52 (1989).
- [15] J. Bijtebier, J.Phys. **G26**, 871 (2000).
- [16] D.A. Kulikov, R.S. Tutik, A.P. Yaroshenko, Phys.Lett. **B644**, 311 (2007).
- [17] M. Moshinsky, A. Szczepaniak, J.Phys. **A22**, L817 (1989).
- [18] A.Yu. Simonov, Phys.Atom.Nucl. **3**, 461 (1966) [Yad.Fiz. **3**, 630 (1966)].
- [19] M. Moshinsky, Yu.F. Smirnov, *The Harmonic Oscillator in Modern Physics* (Hardwood Academic Publishers, 1996).
- [20] E. Chaćon, O. Castaños, A. Frank, J.Math.Phys. **25**, 1442 (1984).



## GLUON CONDENSATE BEHAVIOUR AT FILLING THE FERMI SPHERE UP

S.V. Molodtsov<sup>\*,‡</sup>, A.E. Dorokhov<sup>\*</sup>, G.M. Zinovjev<sup>‡</sup>

<sup>\*</sup>Joint Institute for Nuclear Research, Dubna, Russia

<sup>‡</sup>Institute of Theoretical and Experimental Physics, Moscow, Russia

<sup>‡</sup>N.N. Bogolyubov Institute for Theoretical Physics, National Academy of Sciences of Ukraine, Kiev, Ukraine

The impact of filling up the Fermi sphere with the quarks, which dynamically generated their masses on the instanton liquid at finite temperature and baryonic/quark number density, is investigated. It is demonstrated, in particular, that the boundary of chiral symmetry restoration phase transition is shifted to the larger (about 100 MeV more) value of quark chemical potential compared to the magnitude inherent in the Nambu-Jona-Lasinio model.

### 1 Introduction

Impressive results obtained in experimental study of ultrarelativistic ion collisions at RHIC (Brookhaven) and the experiments which are planned for the near future at ALICE LHC (CERN) [2] are standing in need of more accurate and precise theoretical predictions for possible signatures of new states of strongly interacting matter with fastly growing acuity. However, the theoretical advancement is much less appreciable especially in the latest years. For example, the predictions of various approaches for the behaviour of gluon condensate at finite  $T$  and non-zero values of baryonic/quark chemical potential  $\mu$  which is a key quantity for theoretical analysis are still inconsistent as before and at times simply conflicting. The possible changes appearing in the gluon sector at such conditions and usually described by varying the constants of multiquark interactions as the functions of  $T$  and  $\mu$  in the Nambu–Jona-Lasinio (NJL) model [2], need drawing almost inevitably the lattice numerical calculations of the gluon condensate [3] to be analysed. Practically to the same extent this remark is justified for the predictions of the chiral perturbation theory (CHPT) [4] and the QCD sum rules (SR) [5]. Both approaches have rather limited reliability for results of calculations around the critical parameter values. Actually, in Ref. [1] we have already tried to estimate the gluon condensate behaviour in hot and dense medium using the instanton liquid (IL) model [4, 8, 9] as an operative tool. In this case the screening impact of quarks filling the Fermi sphere up<sup>1</sup> on the gluon condensate has been calculated for the massless quarks.

In this paper we consider the influence of quarks with the finite masses on the gluon condensate. In the IL model the calculation of dynamical quark mass at zero temperature is grounded on making use the zero mode approximation [12]. However, even that calculation runs into rather serious technical difficulty (see also [13]) while interpreting the loop quark diagrams at the chemical potential values exceeding the magnitude of dynamical quark mass  $\mu \geq M_q$ . We are treating this point here based on the NJL model and are not interested in the asymptotic large values of  $\mu$  and  $T$  (see, for example, [14]) and omit an analysis of the colour superconducting phase as well as the discussion of the difficulty in stabilizing the instanton ensemble which is rather often resulted in the speculations about the ‘realistic’ structure of vacuum configurations.

### 2 Approximating the vacuum configurations at finite $T$ and $\mu$

Our purpose here is to find the practical and effective tool for evaluating the gluon condensate under extreme conditions. Obviously, such a task has been pending for rather long time and the prevailing number of scenarios to resolve it is grounded on the mean field approximation which supposes, actually, the simplified description of a system. It will be a guiding element of our approach while dealing with the instanton ensemble. For example, vacuum correlation function  $\langle A_\mu(x)A_\nu(y) \rangle$  of mean field description is transformed into the correlator which in the context of our approach leads to the mass generation for gluon field and, hence, to the colour screening factor.

As well known in the IL model at zero values of  $\mu$  and  $T$  the superposition of (anti-)instantons in the singular

<sup>1</sup>Following [10] we take this effect as the dominating one at high temperature though there exist the other interesting possibilities [11].

gauge

$$A_\mu^a(x; \gamma) = \frac{2}{g} \omega^{ab} \bar{\eta}_{b\mu\nu} a_\nu(y) , \quad a_\nu(y) = \frac{\rho^2}{y^2 + \rho^2} \frac{y_\nu}{y^2} , \quad y = x - z , \quad (1)$$

(where  $\mu, \nu = 1, 2, 3, 4$ ,  $\rho$  is a pseudo-particle size,  $\omega$  is a matrix of its colour orientation and  $z$  is its center coordinate) is considered as the ground vacuum field saturating the QCD generating functional (dealing with anti-instantons one has to change the't Hooft symbol  $\bar{\eta} \rightarrow \eta$ ). The QCD generating functional is evaluated to be as

$$Y = \sum_{N=1}^{\infty} \frac{1}{N!} \prod_{i=1}^N \int d\gamma_i d\omega_i d\rho_i e^{-\beta U_{int}(\gamma)} = \sum_{N=1}^{\infty} \frac{1}{N!} \prod_{i=1}^N \int d\gamma_i e^{-E(\gamma)} , \quad (2)$$

$$E(\gamma) = \beta U_{int}(\gamma) - \sum \ln d\omega_i d\rho_i , \quad \gamma = (z, \rho, \omega) ,$$

here

$$d\omega_i d\rho_i = \frac{1}{\rho^5} \tilde{\beta}^{2N_c} e^{-\beta(\rho)} \quad (3)$$

is the distribution function over the size of individual instanton (dilute instanton gas approximation) [4],  $d\gamma_i = d^4 z_i d\omega_i d\rho_i$  is the integration element,

$$\beta(\rho) = \frac{8\pi^2}{g^2} = -b \ln(C_{N_c}^{1/b} \Lambda \rho)$$

is the single instanton action ( $\Lambda = \Lambda_{\overline{MS}} = 0.92 \Lambda_{P.V.}$ ) with the constant  $C_{N_c}$  depending on the renormalization scheme

$$C_{N_c} \approx \frac{4.66 \exp(-1.68N_c)}{\pi^2 (N_c - 1)! (N_c - 2)!}$$

with another parameter  $b = (11 N_c - 2 N_f)/3$ . The auxiliary coefficients  $\tilde{\beta} = -b \ln(\Lambda \bar{\rho})$   $\beta$  in the exponent of Eq. (9) are fixed at the characteristic scale  $\bar{\rho}$  (pseudo-particle average size). Assuming the topologically neutral instanton liquid we do not differ the instantons and anti-instantons and  $N$  denotes (when used) the total number of pseudo-particles which occupy the volume  $V$ .

Taking into account the interaction of instantons with vacuum fluctuations is effectively presented by appearance of the screening factor in the distribution (2)

$$d(\rho) = \frac{1}{\rho^5} \tilde{\beta}^{2N_c} e^{-\beta(\rho) - \zeta \rho^2} , \quad (4)$$

where the magnitude of screening coefficient  $\zeta$  is dependent on the choice of superposition ansatz. For the pseudo-particles in the singular gauge the interaction term taken in the pair interaction approximation is [9]

$$\int d\omega_1 d\omega_2 dz_1 dz_2 U_{int}(\gamma_1, \gamma_2) = V \xi^2 \rho_1^2 \rho_2^2 ,$$

with the constant  $\xi^2 = \frac{27 \pi^2}{4} \frac{N_c}{N_c^2 - 1}$ . It is interesting to notice here that the configurations used in the valley method [15] result in the significantly smaller value (about one order) of coefficient  $\xi$  [16]. Besides, the screening factor can be steadily extracted from the lattice data as  $\lambda_A \sim 0.22$  fm [17] with the configuration cooling procedure. The corresponding configurations are reasonably well fitted by the instanton ensemble as was shown [18], although the analysis of optimal instanton configurations in the mean field approximation is worthy of special study and will be done in the separate paper [19].

The convexity property of exponential function allows us to estimate the partial contribution into the generating functional Eq. (9) at each value of  $N$  by the following approximating form

$$Y \geq Y_{approx} = Y_1 \exp(-\langle E - E_1 \rangle) , \quad (5)$$

which can be presented [9] as

$$Y_{approx} = e^{-X} , \quad X = N \left( \frac{\nu}{2} + 1 \right) [\ln(n/\Lambda^4) - 1] - N \ln \left[ C_{N_c} \tilde{\beta}^{2N_c} (\beta \xi^2 \nu)^{-\nu/2} \frac{\Gamma(\nu)}{2} \right] , \quad (6)$$

where  $n = N/V$ ,  $\nu = (b - 4)/2$ . Then the respective parameters of IL are defined by the maximum in  $n$  of generating functional with the interrelation of instanton average size and its density taken into account

$$\frac{\nu}{\rho^2} = \beta \xi^2 n \bar{\rho}^2 . \quad (7)$$

Now calculating the maximum of  $X$  in  $n$  we have to resolve the following equation

$$-\left(\frac{\nu}{2} + 1\right) \ln(n/\Lambda^4) + \ln \left[ C_{N_c} \tilde{\beta}^{2N_c} (\beta \xi^2 \nu)^{-\nu/2} \frac{\Gamma(\nu)}{2} \right] + n \frac{2N_c}{\tilde{\beta}} \frac{d\tilde{\beta}}{dn} - n \frac{\nu}{2\beta} \frac{d\beta}{dn} = 0. \quad (8)$$

Owing to the relation (5) we have

$$\frac{1}{\beta} \frac{d\beta}{d\bar{\rho}} + \frac{1}{n} \frac{dn}{d\bar{\rho}} + \frac{4}{\bar{\rho}} = 0.$$

From the other side  $\frac{d\beta}{d\bar{\rho}} = -\frac{b}{\bar{\rho}}$ ,  $\frac{d\tilde{\beta}}{d\bar{\rho}} = \frac{d\beta}{d\bar{\rho}}$ . Rewriting the derivative of  $\beta$  in the density as  $\frac{d\beta}{dn} = \frac{d\beta}{d\bar{\rho}} / \frac{dn}{d\bar{\rho}}$ , we come to the system of equations

$$\frac{d\beta}{dn} = \frac{1}{n} \frac{b \beta}{4\beta - b}, \quad \frac{d\tilde{\beta}}{dn} = \frac{d\beta}{dn}. \quad (9)$$

Finally resolving the system of transcendental equations we can determine the equilibrium IL parameters.

At the finite temperature the configuration saturating the generating functional is changed by the superposition of (anti-)colorons [20], [21] which are the periodical in the Euclidean 'time' (with the period of  $T^{-1}$ ) solutions of the Yang-Mills equations [5] i.e.

$$A_\mu^a(x, \gamma, T) = -\frac{1}{g} \omega^{ab} \bar{\eta}_{b\mu\nu} \partial_\nu \ln \Phi(x, T), \quad \Phi(x, T) = 1 + \frac{\pi \rho^2 T}{r} \frac{\sinh(2\pi rT)}{\cosh(2\pi rT) - \cos(2\pi \tau T)}. \quad (10)$$

Here  $r = |\mathbf{x} - \mathbf{z}|$  defines the distance from the coloron center  $z$  in three-dimensional space,  $\tau = x_4 - z_4$  is the 'time' interval. It can be easily seen that the solution is transformed into the (anti-)instanton one in the singular gauge at temperature going to zero. Clearly, the distribution function over the coloron size [10], [23] is also changed

$$d(\rho; \mu, T) = d(\rho) e^{-\eta^2(\mu, T)\rho^2}, \quad \eta^2(\mu, T) = 2\pi^2 \left[ \frac{N_c}{3} T^2 + \sum_{f=1}^{N_f} \Pi^f(\mu, T) \right]. \quad (11)$$

The first term of the screening factor describes the one-loop gluon contribution into the effective action and the second term generated by quark contribution in one-loop approximation can be exactly calculated and is free of the 'bad' singularities [24]. The 'time' component of polarization tensor generated by quark of fixed colour has the form

$$\Pi_{44}^f(k_4, \omega) = \frac{k^2}{\pi^2 \omega^2} \int_0^\infty \frac{dp}{\varepsilon_p} \frac{p^2}{n_p} \left[ 1 + \frac{4\varepsilon_p^2 - k^2}{8pk} \ln \frac{(k^2 + 2p\omega)^2 + 4\varepsilon_p^2 k_4^2}{(k^2 - 2p\omega)^2 + 4\varepsilon_p^2 k_4^2} - \frac{\varepsilon_p k_4}{p\omega} \arctan \frac{8p\omega \varepsilon_p k_4}{4\varepsilon_p^2 k_4^2 - 4p^2 \omega^2 + k^4} \right],$$

here  $\omega = |\mathbf{k}|$ ,  $k^2 = \omega^2 + k_4^2$ ,  $\varepsilon_p = (M_q^2 + \mathbf{p}^2)^{1/2}$  where  $M_q$  is the quark mass,  $n_p = n_p^- + n_p^+$ ,  $n_p^- = (e^{\frac{\varepsilon_p - \mu}{T}} + 1)^{-1}$ ,  $n_p^+ = (e^{\frac{\varepsilon_p + \mu}{T}} + 1)^{-1}$  ( $n_p^-$ ,  $n_p^+$  are the densities of anti-quarks and quarks, respectively). When summed up over all the components the polarization tensor can be presented in the following form

$$\Pi_{\mu\mu}^f(k_4, \omega) = \frac{2}{\pi^2} \int_0^\infty \frac{dp}{\varepsilon_p} \frac{p^2}{n_p} \left[ 1 + \frac{2M_q^2 - k^2}{8pk} \ln \frac{(k^2 + 2p\omega)^2 + 4\varepsilon_p^2 k_4^2}{(k^2 - 2p\omega)^2 + 4\varepsilon_p^2 k_4^2} \right]. \quad (12)$$

It is clear when the zero-component  $k_4 = 0$  the dominant contribution into the gluon mass at small values of  $\omega$  comes from the first term (a unit) and the space components are negligible. In particular, at  $\omega = 0$  it will be

$$\Pi^f(\mu, T) = \Pi_{44}^f(0, 0) = \frac{2}{\pi^2} \int_0^\infty \frac{dp}{\varepsilon_p} \frac{p^2}{n_p} . \quad (13)$$

Then at  $T = 0$  we have

$$\Pi^f(\mu, 0) = \left[ \frac{(\mu^2 - M_q^2)^{1/2} \mu}{\pi^2} - \frac{M_q^2}{\pi^2} \ln \frac{\mu + (\mu^2 - M_q^2)^{1/2}}{M_q} \right].$$

In order to calculate the IL equilibrium parameters as the functions of  $\mu$  and  $T$  one has to minimize the approximating functional (4) making the substitutions of (5) and (9) for

$$\frac{\nu}{\bar{\rho}^2} = \eta^2 + \beta \xi^2 n \bar{\rho}^2, \quad (14)$$

and

$$\frac{n}{\beta} \frac{d\beta}{dn} = \frac{b}{4\beta - b + \frac{2\eta^2 \bar{\rho}^2 \beta}{\nu - \eta^2 \bar{\rho}^2}} . \quad (15)$$

correspondingly.

### 3 Quark mass generation in stochastic field

It is anticipated that in the IL model the quarks are considered to 'live' (and to be influenced) in the stochastic (anti-)instanton ensemble which is defined by the following generating functional

$$Z = \int D[\psi] D[\bar{\psi}] \langle e^{\int dx \mathcal{L}_q} \rangle_A , \quad \mathcal{L}_q = \bar{\psi}(x) \left( i\hat{\partial}_x + \sum_{k=1}^N g\hat{A}(x; \gamma_k) \right) \psi(x) , \quad (16)$$

where the averaging over (anti-)instanton ensemble is implied. The consistency requirement for effective Lagrangian in the Hartree approximation results in the equation for the quark Green function [25] which reads as

$$M(p) = -\frac{N}{V} \frac{1}{N_c} \sum_{n=2}^{\infty} \int \prod_{k=1}^n \frac{dq_k}{(2\pi)^4} (2\pi)^4 \delta^4 \left( \sum_{i=1}^n q_i \right) \text{Tr} \left[ g \hat{A}(q_1) S(p - q_1) \dots g \hat{A}(q_n) \right] . \quad (17)$$

Being summed up the right hand side of Eq. (12) can be presented in the compact form as [26]

$$M(p) = \frac{1}{N_c V} \text{Tr} \sum_{i=1}^N \langle p | \left[ S - (g \hat{A}(q_i))^{-1} \right]^{-1} | p \rangle , \quad (18)$$

(in such a form the averaging over the pseudo-particle location  $z$  and calculation of colour trace is meant). Analyzing the solution in the form

$$S(p) = \frac{1}{\hat{p} - iM(p)} , \quad (19)$$

where  $M(p)$  denotes the quark mass, one can calculate the highest term of expansion in the IL density (presented by the zero quark mode  $\Phi(p)$  in the instanton field) as [26]

$$M(p) \sim n^{1/2} \frac{p^2 \Phi^2(p)}{\left[ \int \frac{dp}{(2\pi)^4} p^2 \Phi^4(p) \right]^{1/2}} .$$

At finite quark chemical potential the derivative  $i\hat{\partial}$  in Eq. (8) should be substituted for  $i\hat{\partial} - i\hat{\mu}$  where  $\hat{\mu} = \mu\gamma_4$ . Then quark Green function (11) develops the following form

$$S(p; \mu) = \frac{1}{\hat{p} + i\hat{\mu} - iM(p; \mu)} . \quad (20)$$

where

$$M(p; \mu) \sim n^{1/2} \frac{(p + i\mu)^2 \Phi^2(p; \mu)}{\left[ \int \frac{dp}{(2\pi)^4} (p + i\mu)^2 \Phi^2(p; \mu) \Phi^2(p; \mu) \right]^{1/2}} ,$$

and the overt expression of the zero mode could be found, for example, in [27]. With the chemical potential increasing and reaching the values of dynamical quark mass order ( $\mu \sim M_q$ ) the quark mass magnitude  $M(p; \mu)$  begins to increase as a power. The similar situation with the dynamical mass increase takes place for the approach in which the unperturbed quark Green function  $S_0$  is approximated by the zero modes [27], [28]<sup>2</sup>. Such a behaviour is non-physical and contradicts to the intuitive expectations. It seems, the situation could be improved by taking into account the non-zero mode contributions but very complicated analytical structure of the corresponding expressions makes this calculation practically hopeless. Thus, the question about the estimate of non-zero mode contribution is still vague (see, however, [29]). The proposition to treat poles as in Ref. [13] leads, unfortunately, to unphysically small values of the chemical potential of chiral symmetry restoration phase transition. It is interesting to notice here that the zero mode approximation is quite reliable even at the finite temperature if one confines oneself to work with the chemical potential values not larger than the dynamical quark mass  $\mu \sim 300$  MeV. The quark condensate estimates are quite suitable in this case even if one makes use simply non-coloron zero mode. These results put forward the task of searching the effective approximations

<sup>2</sup>Determining the saddle point parameter in this case one encounters the problem of calculating a loop integral in which the pole of Eq. (26) appears on the real axis. The treatment of that integral as a principle value gives its real part only which is not enough, of course. However, this problem is softened by the situation that the pole appearance on the real axis occurs in the local vicinity of transition point into the colour superconducting phase and, therefore, more precise definition of the saddle point parameter looks superfluous. However, the general problem of calculating the loop integrals is entirely hot and actual in the context of analyzing the chiral symmetry restoration. (Prof. T. Hatsuda has drawn our attention to this aspect of the problem and the authors are very grateful to him for that.)

for the equations of type (12). The significant progress in studying the systems of quarks at finite temperature and chemical potential has been reached in the framework of NJL approach. (Let us remember here that at finite temperature the integration over the fourth component in Eq. (8) should be performed in the interval from zero till  $T^{-1}$  and gluon fields obey the periodic boundary conditions whereas the fermion fields obey the anti-periodic ones.)

As it is difficult to handle (anti-)instanton ensemble directly we are going to retain some essential features of (anti-)instanton configuration contribution and approximate it with the simplest form. Actually, we suppose the existence of superposition of stochastic randomly oriented color gluon fields in the Euclidean space. These fields have the  $\delta$ -function form with their randomly distributed centers  $z$ , i.e.

$$A_\mu(x) = U^\dagger \tau^a U a_\mu^a (2\pi)^4 \delta^{(4)}(x - z), \quad A_\mu(p) = U^\dagger \tau^a U a_\mu^a (2\pi)^4 e^{ipz} = A_\mu e^{ipz}. \quad (21)$$

It is clear if one considers one-particle correlations only (just what is done for the pseudo-particle ensemble) the simplest non-trivial correlation function  $\langle \hat{A}(x_1) \hat{A}(x_2) \rangle_{z,U}$  will lead to the point-like interaction of quarks

$$\langle \hat{A}(x_1) \hat{A}(x_2) \rangle_{z,U} \sim \delta^{(4)}(x_1 - x_2)$$

which is specific for NJL. In further analysis we do not need to know the concrete form of stochastic factor  $\hat{A}$  and do not specify it here. Searching the solution of Eq. (12) in the form  $M(p) = M$  we introduce the auxiliary function  $\psi(q, p)$  the following way

$$\begin{aligned} M &= \frac{-i n}{N_c} \int \frac{dq}{(2\pi)^4} \text{Tr} \langle \hat{A}(q - p) \frac{1}{\hat{q} + i\hat{\mu} - iM} \psi(q, p) \rangle_{z,U}, \\ \psi(p, p') &= \hat{A}(p - p') + \int \frac{dq}{(2\pi)^4} \hat{A}(q - p) \frac{1}{\hat{q} + i\hat{\mu} - iM} \psi(q, p'), \end{aligned} \quad (22)$$

(of course, we imply non-zero quark chemical potential). Presenting the solution for  $\psi(q, p)$  in the form  $\psi(q, p) = \psi e^{i(q-p)z}$  we are able to obtain the following equation to determine the function  $\psi$  of our interest<sup>3</sup>

$$\psi = \hat{A} + \hat{A} \int \frac{dq}{(2\pi)^4} \frac{1}{\hat{q} + i\hat{\mu} - iM} \psi. \quad (23)$$

As in the NJL model Eq. (17) requires the regularization. Here we are using the conventional procedure of three-dimensional momentum regularization [2] which allows us to obtain

$$\begin{aligned} I &= \int \frac{dq}{(2\pi)^4} \frac{1}{\hat{q} + i\hat{\mu} - iM} = iC \gamma_4 + iDM, \quad C = -\frac{\theta(\mu - M)}{(2\pi)^2} \frac{(\mu^2 - M^2)^{3/2}}{3}, \\ D &= \begin{cases} \frac{1}{8\pi^2} \left[ \tilde{\Lambda} \sqrt{\tilde{\Lambda}^2 + M^2} - M^2 \ln \left| \frac{\tilde{\Lambda} + \sqrt{\tilde{\Lambda}^2 + M^2}}{M} \right| \right], & \mu \leq M \\ \frac{1}{8\pi^2} \left[ \tilde{\Lambda} \sqrt{\tilde{\Lambda}^2 + M^2} - \mu \sqrt{\mu^2 - M^2} - M^2 \ln \left| \frac{\tilde{\Lambda} + \sqrt{\tilde{\Lambda}^2 + M^2}}{\mu + \sqrt{\mu^2 - M^2}} \right| \right], & \mu > M \end{cases} \end{aligned}$$

$\tilde{\Lambda}$  denotes here the cut-off value of three dimensional momentum in the  $I$  integral. Finally, we have for the solution of Eq. (17) the following result

$$\psi = \frac{B + C^2 A^2}{B(1 + D^2 A^2 M^2)} (\hat{A} + iDA^2 M) + \frac{iC}{B(1 + D^2 A^2 M^2)} (\hat{A} + iDA^2 M) \gamma_4 (\hat{A} + iDA^2 M), \quad (24)$$

where  $B = 1 - 2iCA_4 - C^2 A^2 + D^2 A^2 M^2$ . Using this solution in Eq. (16), averaging over the colour orientation and holding the highest terms of the  $N_c$  expansion we come to the mass gap equation

$$M = 4n \frac{DA^2 M}{1 + D^2 A^2 M^2 - C^2 A^2}. \quad (25)$$

<sup>3</sup>Another utmost regime where the correlation length is supposed to be infinitely large  $\langle A(x)A(y) \rangle = A^2$  is also very interesting. It was analyzed in the Keldysh model [30] and the exact solution was found out. The complete summation of series for the quark Green function results in the expression as

$$S(p) = \frac{1}{(2\pi)^{1/2}} \int_{-\infty}^{\infty} dt e^{-\frac{t^2}{2}} \frac{1}{\hat{p} + \hat{\mu} - t A},$$

(it is given here in the Minkowski space). Apparently, it has no poles similar to the non-relativistic Green function as well as the 'analytical' model of confinement [31].

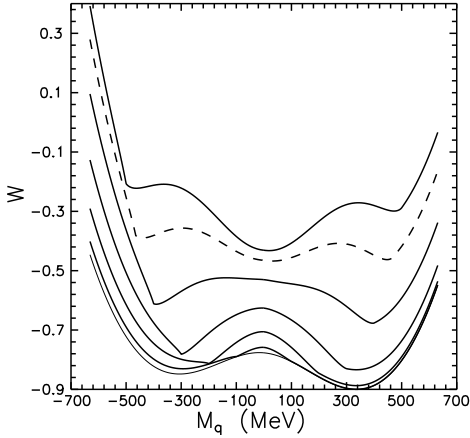


**Figure 1.** The effective potential  $W$  as the function of quark mass for different values of chemical potential  $\mu = 0$  (lower curve),  $\mu = 100$ ,  $\mu = 200$ ,  $\mu = 300$ ,  $\mu = 400$ ,  $\mu = 450$ ,  $\mu = 500$  MeV.

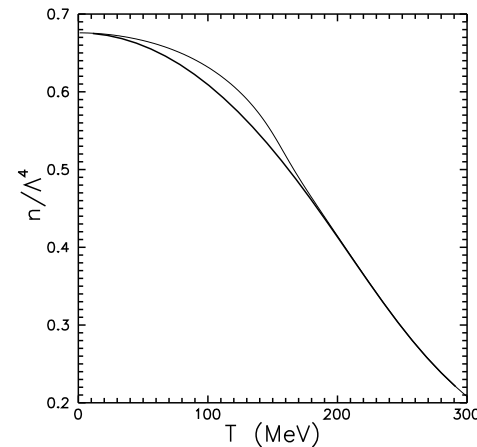


**Figure 2.** The IL density as the function of the temperature  $T$ . The lower curve corresponds to the calculation with massless quarks.

It enables to formulate the condition which signals the breakdown of chiral symmetry (the generation of quark mass) if such a constraint is obeyed

$$A^2 > \frac{1}{4n D - D^2 M^2 + C^2} . \quad (26)$$

If one neglects the contributions proportional to  $A^2$  in the denominator of Eq. (20) the gap equation of the NJL model with the coupling constant  $G$  of four-fermion interaction is exactly reproduced

$$G = 4n A^2 \frac{\tilde{\Lambda}^2}{8\pi^2} . \quad (27)$$

In order to receive the qualitative estimates it is worthwhile using the characteristic cutoff parameter of the NJL phenomenology  $\tilde{\Lambda} \sim 600$  MeV. In our estimates we rely on the constraints  $D^2 M^2 A^2 \ll 1$ ,  $C^2 A^2 \ll 1$  only. The estimate of  $A^2$  for instanton ensemble could be obtained from the corresponding correlation function [32]

$$\langle A(x-z) A(y-z) \rangle_{z,U} = F(x-y) .$$

Actually, we have  $F(0) = \frac{4\pi^2}{N_c^2 - 1} \rho^2$ , which means  $A_x^2 \sim \frac{1}{\rho^2}$  and then we receive for the Fourier component  $A_p^2 \sim \rho^6$ . Taking into account that  $\rho \sim \tilde{\Lambda}^{-1}$  and  $D \sim \tilde{\Lambda}^2$  (see Eq. (10)) we obtain  $D^2 A^2 M^2 \sim \frac{M^2}{\tilde{\Lambda}^2}$ . The standard parameter values of the NJL model provide us with the small magnitude of this factor and it could be neglected. Surely, it is a fairly serious argument in favour of using the developed approach.

#### 4 Approximation of NJL and IL model

Our above analysis demonstrates that approximating the instanton correlator with the delta- function form and using the regularized NJL model at the same time is the fully compatible procedure. Moreover, Eq. (22) provides us with the possibility to consider the interrelation of gluon and quark sectors. It relates the constant  $G$  and the IL parameters such as the IL density  $n$  and average potential  $A$  and  $G$  is related to the dynamical quark mass  $M = M(0)$  which defines the screening effect.

Let us now remind that the generating functional of the NJL model has the following form [2]

$$Z = e^{-\Omega},$$

$$\Omega = G_0 \sigma^2 - \frac{N_f N_c}{\pi^2} \int_0^{\tilde{\Lambda}} p^2 \varepsilon_p dp - \frac{N_f N_c}{\pi^2} T \int_0^{\tilde{\Lambda}} p^2 \left[ \ln \left( 1 + e^{-\frac{\varepsilon_p + \mu}{T}} \right) + \ln \left( 1 + e^{-\frac{\varepsilon_p - \mu}{T}} \right) \right] dp, \quad (28)$$

where  $\varepsilon_p = (M^2 + \mathbf{p}^2)^{1/2}$ ,  $M = m - 2G_0 \sigma$ ,  $m$  is the current quark mass and for the quark condensate we have

$$\langle \bar{\psi} \psi \rangle = -M \frac{N_c}{\pi^2} \int_0^{\tilde{\Lambda}} \frac{p^2}{\varepsilon_p} (1 - n_p^- - n_p^+) dp, \quad \sigma = N_f \langle \bar{\psi} \psi \rangle \quad (29)$$

The quark mass is defined by calculating the minimum of  $\Omega$  as the function of  $M$  (or quark condensate  $\sigma$ ) and the coupling constant  $G_0$  together with the cutoff parameter  $\tilde{\Lambda}$  is fixed phenomenologically (by fitting the

experimental data). We suppose to take this quantity as an estimate of quark determinant while quarks are in the stochastic field of (anti-)instantons and modify the determinant aiming to include the interrelation of quark and gluon sectors. In this way we use (instead of  $G$ ) in Eq. (23)  $G \rightarrow \frac{n}{n_0} G_0$  where  $n_0, G_0$  are the IL density and the constant of fourquark interaction at zero temperature and zero chemical potential. In full analogy with the IL model it is easy to understand the parameter  $\hat{A}$  should generate the factor of the  $\rho^3$  type and the substitution of the coupling constant for  $\frac{n\rho^6}{n_0\rho_0^6} G_0$  looks quite natural. On the other hand as the simplest option we could take the cutoff parameter in the quark sector  $\tilde{\Lambda}$  unchanging as the parameter  $\hat{A} \sim \tilde{\Lambda}^{-3}$ . Thus, for the quarks in stochastic instanton ensemble we should change  $\Omega$  in Eq. (23) for

$$\Omega = \frac{n}{n_0} G_0 \sigma^2 - \frac{N_f N_c}{\pi^2} \int_0^{\tilde{\Lambda}} p^2 \varepsilon_p dp - \frac{N_f N_c}{\pi^2} T \int_0^{\tilde{\Lambda}} p^2 \left[ \ln \left( 1 + e^{-\frac{\varepsilon_p + \mu}{T}} \right) + \ln \left( 1 + e^{-\frac{\varepsilon_p - \mu}{T}} \right) \right] dp. \quad (30)$$

Apparently, the vacuum parameters of the IL model and the NJL one should not change. In order to realize that one should make the corresponding subtractions just to retain the effect caused by the quarks filling the Fermi sphere up because the interrelation of vacuum (at zero  $T$  and  $\mu$ ) quark and gluon fields has been already discounted effectively in the running coupling constant and by tuning the NJL model parameters. The (anti-)instanton ensemble and quark field are described by the product of functionls  $Y_{approx}$  and  $Z$ . Therefore, for the effective potential we have

$$W = X + \Omega.$$

The equilibrium IL parameters are defined by the effective potential minimum on the IL density, i.e. by  $\frac{\partial W}{\partial n} = 0$ . However, as was declared the following subtraction

$$\frac{\partial X}{\partial n} + \frac{\partial \Omega}{\partial n} - \frac{\partial \Omega}{\partial n} |_{\mu=0, T=0} = 0. \quad (31)$$

should be done. Similar operation should be executed at determining the quark mass  $\frac{\partial W}{\partial M} = 0$ , i.e.

$$\frac{\partial X}{\partial \eta^2} \frac{\partial \eta^2}{\partial M} - \frac{\partial X}{\partial \eta^2} \frac{\partial \eta^2}{\partial M} |_{\mu=0, T=0} + \frac{\partial \Omega}{\partial M} = 0. \quad (32)$$

Two first terms of Eq. (36) are the result of the fact that the overt dependence on the quark mass in the contribution into the effective potential is available in the screening factor  $\eta^2$  only. Strictly speaking one should integrate till the momentum order of  $\tilde{\Lambda}$  in Eq. (13), too. However, such an amplification is superfluous as the detailed analysis shows. In practice, obviously, it is simpler not to resolve the transcendental equation (which has two branches, at least) but calculate simply the minimum of effective potential in  $M$ . It is easy to understand that for the concrete form of our quark effective potential  $\Omega$  the equation for determining the equilibrium IL parameters coincides with the vacuum one because the direct dependence on the IL density  $n$  is present in the first term of Eq. (30) only. Just because of that reason two last terms of Eq. (35) are canceled. The subtraction in the second equation of (36) should not be performed as  $\frac{\partial X}{\partial \eta^2} = -\frac{n\rho^2}{2}$  and the function  $\eta^2 = 0$  at  $\mu < M$ . Thus, the equilibrium IL parameters are defined by the same scheme as before [1] and minimum of the generating functional  $W$  in  $M$  fixes the dynamical quark mass.

Here we are using the following set of the NJL model parameters [2] (T. Hatsuda, T. Kunihiro). We take for the current mass of  $u$  and  $d$  quarks the same value  $m = 5.5$  MeV, for the cutoff parameter as  $\tilde{\Lambda} = 631$  MeV and for the ratio of the coupling constant to its critical value as  $\alpha = G_0/G_c = 1.33/N_f$ ,  $\left( G_c = \frac{\pi^2}{N_c \tilde{\Lambda}^2} \right)$ . Such a set of parameters results in the following values of the  $\pi$ -meson mass  $m_\pi = 139$  MeV and the constant of pion decay  $F_\pi = 93$  MeV.

The Fig. 1 shows the effective potential  $W$  as the quark mass function for the different values of chemical potential  $\mu$ . The lower curve corresponds to zero value of chemical potential and is in full coincidence with the respective curve of the NJL model. With the chemical potential increasing the process of filling up the Fermi sphere starts and it is easy to see that the effect of pseudo-particle field screening by the quarks of small masses occurs dominating (see Eq. (13) and the next one). The screening effect leads to diminishing the absolute value of gluon condensate and, hence, the effective potential of (anti-)instanton and quark system is increasing. It is distinctly visible in Fig. 1 in the region of small quark masses. With the quark mass increasing, the impact of the filling up process is amplified. Starting on some value of small quark mass the saturation regime manifest itself and the gluon condensate is suppressed. The plateau is formed and it is well seen in Fig. 1. At the larger values of chemical potential the chiral symmetry restoration starts and the corresponding curve is shown with the dashed curve in Fig. 1. More detailed analysis allows us to conclude the simplifications made do not deprecate the qualitative picture of screening.

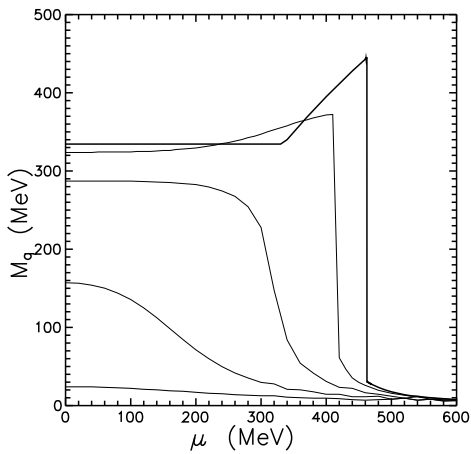


**Figure 3.** The dynamical quark mass as the function of chemical potential for different temperature values  $T = 0$  (upper line),  $T = 50$ ,  $T = 100$ ,  $T = 150$ ,  $T = 200$  MeV.

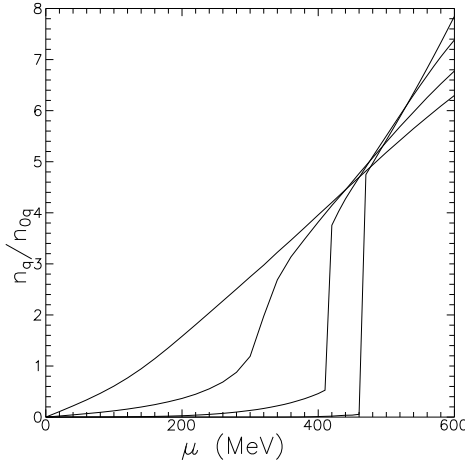
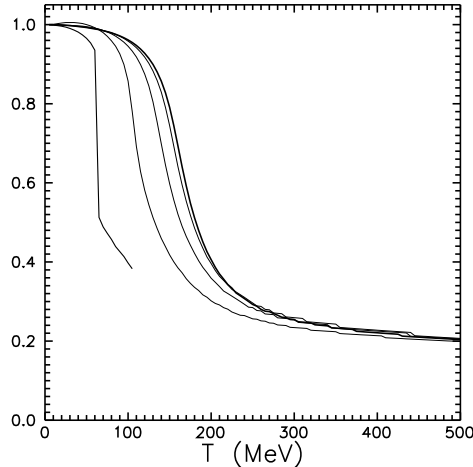


**Figure 4.** The quark matter density as the function of chemical potential. The last right curve corresponds to the zero temperature. The next left curve corresponds to the temperature 50 MeV, then 100 MeV, and eventually  $T=150$  MeV.  $n_{0q} = 0.062 \text{ fm}^{-3}$  is the normal density of quark matter calculated from the normal baryon matter density  $n_B = 0.45 \text{ fm}^{-3}$ .

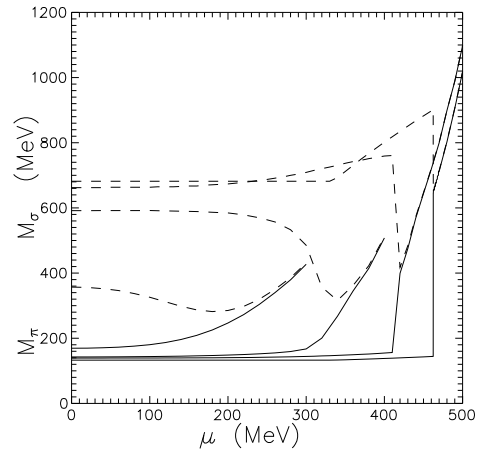
The IL density as the function of chemical potential at the various values of temperature (with the temperature increasing the IL density is decreasing) is plotted in the Fig. ???. The dashed curve which was obtained by us in [1] (the similar mechanism of screening was discussed also in [10], [20]) corresponds to the calculation with the massless quarks. The mechanism of forming the observable plateau is quite understandable. Until the chiral symmetry restoration does not take place the quarks are ineffective in the gluon field screening and the gluon condensate practically does not change.

Fig. 2 presents the dependence of IL density on the temperature. As it was expected the density is larger for the massive quarks than for the massless ones in the region of low temperature (below 200 MeV). This result agrees qualitatively with the observation done in [33]. Some lattice calculations support this scenario of screening. For example, in [34] it was proven that the Debye screening mass behaves as  $m_{el} \sim gT$  and depends on the quark flavours (see Eq. (7)). Exponential suppression of gluon field with increasing temperature was also found out in the lattice measurements of correlation functions dealing with the cooled configurations [35]. In fact, gazing into the detailed analysis of the problem under consideration we collected a lot of reasons to have the topological solution with the suppressed chromoelectrical component instead of the (anti-)coloron one to construct more realistic approach. In particular, it was noticed in [36] the coloron solution mainly does not fit the lattice data. However, we understand such global pretension (as a disproving conclusion) is rather naive because our result here shows the coloron solution is quite practical for estimating the screening effect.

Analyzing the quark sector we calculated the behaviour of dynamical quark mass as the function of chemical potential and plotted it in Fig. 3 for various values of temperature. The upper curve corresponds to zero temperature and the quark mass behaviour along this curve coincides with the NJL model up to the chemical potential value of  $\mu \sim 300$  MeV. With a further increase of  $\mu$  the quark mass increases. It is quite understandable qualitatively if one looks at Fig. 1. At the commencement of chemical potential increase the screening effect does not produce any noticeable impact on the minimum of effective potential  $W$ . In spite of effective potential increase in the region of small quark mass the threshold value of chemical potential should be reached at which the forming plateau begins to expel the effective potential minimum to the larger mass values. The size of region in which the quark mass increase takes place is comparable with the quark mass (order of 100 MeV) and is of interest, in particular, for investigating the equation of the state of strongly interacting matter. In the version of the NJL model with the parameter choice suggested by T. Hatsuda and T. Kunihiro [2] the chiral symmetry restoration occurs at quite low density (the order of normal nuclear matter density). In our approach the significant decrease of quark mass is shifted (drags on) to the region of large chemical potential values approximately 100 MeV larger, which agrees entirely with an intuitive expectation. Fig. 4 is devoted to analyzing the quark matter density as the function of chemical potential. It seems the shift of chiral symmetry restoration phase transition to the region of larger chemical potential values (order of 400 MeV), could generate an essential increase of quark matter density. However, Fig. 4 demonstrates the change in this interval is inessential (the increase of quark mass  $n_q \sim (\mu^2 - M^2)^{3/2}$  provides the compensation), and in actual fact we



**Figure 5.** The ratio of quark condensate value to its magnitude at zero temperature and zero chemical potential as the function of temperature at the various values of chemical potential  $\mu = 0$  (last right curve corresponds to the zero value of chemical potential),  $\mu = 110$ ,  $\mu = 200$ ,  $\mu = 300$ ,  $\mu = 400$  MeV (last left curve).



**Figure 6.** The masses of  $\pi$ - and  $\sigma$ -mesons as the functions of chemical potential at different values of temperature  $T = 0$ ,  $T = 50$ ,  $T = 100$ ,  $T = 150$  MeV. The dashed lines correspond to the  $\sigma$ -meson and the upper dashed line corresponds to the zero temperature. Last right solid line shows the  $\pi$ -meson mass behaviour at zero temperature.

have to deal with the same vacuum quarks as at  $\mu < 300$  MeV.

The quark condensate normalized to its value at zero temperature and zero chemical potential is depicted in Fig. 5 as the function of temperature for different values of chemical potential. The behaviours shown are in full agreement with the predictions of the other models. Finally, two last Figs give more information on the masses of  $\pi$ - and  $\sigma$ -mesons which are also calculated in the NJL model (see, for example, M.K. Volkov, A.E. Radzhabov [2]). The  $\pi$ -meson mass is given by

$$M_\pi^2 = g_{\pi qq}^2 \frac{m}{2GM} , \quad (33)$$

where  $g_{\pi qq}^2 = \frac{1}{4I_2}$  is the renormalized constant of meson field interaction including the following auxiliary integral

$$I_2 = \frac{N_c}{8\pi^2} \int_0^{\tilde{\Lambda}} \frac{p^2}{\varepsilon_p^3} (1 - n_p^- - n_p^+) dp .$$

The mass of  $\sigma$ -meson is defined by the mass of  $\pi$ -meson and dynamical quark mass as

$$M_\sigma^2 = M_\pi^2 + 4M^2 . \quad (34)$$

Pion decay constant which is a key element of model tuning is defined as  $F_\pi = \frac{M}{g_{\pi qq}}$ . Fig. 6 presents the masses of  $\pi$ - and  $\sigma$ -mesons as the functions of chemical potential for various values of temperature. The dashed curves correspond to  $\sigma$ -meson. The upper dashed line shows behaviour at zero temperature and the solid lower line corresponds to zero temperature behaviour of the  $\pi$ -meson mass. The interval in which the  $\sigma$ - and  $\pi$ -meson masses become identical defines the parameters (on the  $\mu$ - $T$  plot) corresponding to the chiral symmetry restoration. It is clear from Fig. 6 that such a restoration at zero temperature occurs around  $\mu \simeq 460$  MeV, at  $T = 50$  MeV around  $\mu \simeq 410$  MeV, at  $T = 100$  MeV around  $\mu \simeq 350$  MeV and at  $T = 150$  MeV around  $\mu \simeq 220$  MeV. Besides, this plot allows us to fix the line  $m_\sigma = 2m_\pi$  on which the strong decay channel of  $\sigma$ -meson is close. At low temperature ( $T < 100$  MeV) the  $\pi$ -meson mass undergoes a significant change in the region of chiral symmetry restoration only and the estimate that the line  $m_\sigma = 2m_\pi$  approximates chiral symmetry restoration curve ( $m_\sigma = m_\pi$ ) looks rather practical. At  $T = 100$  MeV the chemical potential for the line  $m_\sigma = 2m_\pi$  is about  $\mu \simeq 320$  MeV and at  $T = 150$  we have  $\mu \simeq 0$  MeV. The details of this line behaviour could be quite indicative for searching the mixed phase in relativistic heavy ion collisions [37].

## 5 Conclusion

In the present paper we investigated the effect of gluon condensate screening with the massive quarks filling up the Fermi sphere. We developed the approach based on the NJL model highlights which allows us to get informative qualitative estimates. In particular, we argue that one of the manifestations of filling up the

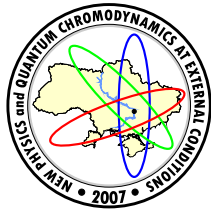
Fermi sphere could be an increase of the quark mass and, hence, the shift of chiral symmetry restoration phase transition to the larger values (about  $\simeq 100$  MeV) of quark chemical potential. Another instructive result obtained implies that the gluon condensate does not die out completely in the parameter region characteristic for this phase transition even at the most advantegeous regime of vacuum gluon field screening. The lattice measurements of the same quantity confirm such a conclusion allowing us to predict that gluon condensate are surviving even in the region of parameters essentially beyond the values admissible for our approximation.

*Acknowledgments.* The authors are very grateful to I.V. Anikin, M.K. Volkov, S.B. Gerasimov, P. Giubellino, G.V. Efimov, Yu.B. Ivanov, Yu.L. Kalinovsky, A.E. Kuraev, A.E. Radzhabov, V.V. Skokov, V.D. Toneev, V.L. Yudichev for numerous fruitful discussions. Financial support within the Grant INTAS 2004-398 is greatly acknowledged. We are grateful very much to organizers of the conference "NEW PHYSICS and QUANTUM CHROMODYNAMICS AT EXTERNAL CONDITIONS (2007)" in Dnipropetrovsk for kind hospitality.

## References

- [1] B. Müller, nucl-th/0508062.
- [2] M.K. Volkov, A.E. Radzhabov, *Uspekhi Fiz. Nauk* **176** (2006) 569; T. Hatsuda and T. Kunihiro, *Phys. Rep.* **247** (1994) 221; S.P. Klevansky, *Rev. Mod. Phys.* **64** (1992) 649.
- [3] C. Ratti, M.A. Thaler, and W. Weise, *Phys. Rev. D* **73** (2006) 014019.
- [4] J. Gasser and H. Leutwyler, *Phys. Lett. B* **184** (1987) 83; J.L. Goity and H. Leutwyler, *Phys. Lett. B* **228** (1989) 517; H. Leutwyler and A.V. Smilga, *Nucl. Phys. B* **342** (1990) 302.
- [5] V.L. Eletsky, *Phys. Lett. B* **245** (1990) 229; V.L. Eletsky and B.L. Ioffe, *Phys. Rev. D* **47** (1993) 3083; R.J. Furnstahl, T. Hatsuda, and Su H. Lee, *Phys. Rev. D* **42** (1990) 1744; C. Adami, T. Hatsuda, and I. Zahed, *Phys. Rev. D* **43** (1991) 921.
- [6] G.M. Zinovjev, S.V. Molodtsov, *Physics of Particles and Nuclei Letters*, **4** (2007) 25.
- [7] G.'t Hooft, *Phys. Rev. D* **14** (1976) 3432.
- [8] C.G. Callan, R. Dashen, and D.J. Gross, *Phys. Lett. B* **66** (1977) 375; C.G. Callan, R. Dashen, and D.J. Gross, *Phys. Rev. D* **17** (1978) 2717. A. Schäfer and E.V. Shuryak, *Rev. Mod. Phys.* **70** (1998) 323.
- [9] D.I. Diakonov and V.Yu. Petrov, *Nucl. Phys. B* **245** (1984) 259.
- [10] D.J. Gross, R.D. Pisarski, and L.G. Yaffe, *Rev. Mod. Phys.* **53** (1981) 43.
- [11] G. Ripka, *Nucl. Phys. A* **683** (2001) 463.
- [12] D.I. Diakonov and V.Yu. Petrov, in *Hadronic Matter under Extreme Conditions*, ed. by V. Shelest and G. Zinovjev (Naukova Dumka, Kiev, 1986) p. 192.
- [13] I. General, D. Gomez Dumm, and N.N. Scoccola, *Phys. Lett. B* **506** (2001) 267; D. Gomez Dumm and N.N. Scoccola, *Phys. Rev. B* **65** (2002) 074021.
- [14] D.T. Son, *Phys. Rev. D* **59** (1999) 094019.
- [15] I.I. Balitsky and A.V. Yung, *Phys. Lett. B* **168** (1986) 113.
- [16] I.I. Balitsky and A.V. Yung, *Nucl. Phys. B* **274** (1986) 475; A.V. Yung, *Nucl. Phys. B* **297** (1988) 47; A.V. Yung, *Nucl. Phys. B* **344** (1990) 73; J.J.J. Verbaarschot, *Nucl. Phys. B* **362** (1991) 33; D. Forster, *Phys. Lett. B* **66** (1977) 279.
- [17] A. Di Giacomo, E. Meggiolaro, and H. Panagopoulos, *Nucl. Phys. B* **483** (1997) 371; M. DÉlia, A. Di Giacomo and E. Meggiolaro, *Phys. Rev. D* **67** (2003) 114504.
- [18] A.E. Dorokhov, S.V. Esaibegyan, and S.V. Mikhailov, *Phys. Rev. D* **56** (1997) 4062; E.-M. Ilgenfritz, B.V. Martemyanov, S.V. Molodtsov, M. Müller-Preussker, and Yu.A. Simonov, *Phys. Rev. D* **58** (1998) 114508; E.-M. Ilgenfritz, B.V. Martemyanov, and M. Müller-Preussker, *Phys. Rev. D* **62** (2000) 096004.
- [19] S.V. Molodtsov, G.M. Zinovjev, hep-ph/0704.0141
- [20] D.I. Diakonov and A.D. Mirlin, *Phys. Lett. B* **203** (1988) 299.
- [21] M.A. Novak, J.J.M. Verbaarschot, and I. Zahed, *Nucl. Phys. B* **325** (1989) 581.
- [22] B.J. Harrington and H.K. Shepard, *Phys. Rev. D* **17** (1978) 2122.
- [23] C.A. Carvalho, *Nucl. Phys. B* **183** (1981) 182; A.A. Abrikosov (Jr), *Yad. Fiz.* **37** (1983) 772; V. Baluni, *Phys. Lett. B* **106** (1981) 491.
- [24] I.A. Akhiezer and S.V. Peletminsky, *JETP* **38** (1960) 1829.

- [25] Yu.A. Simonov, Phys. Lett. **B 412** (1997) 371.
- [26] P.V. Pobylitsa, Phys. Lett. **B 226** (1989) 387.
- [27] C.W. Carter and D.I. Diakonov Phys. Rev. **D 60** (1999) 016004.
- [28] S.V. Molodtsov and G.M. Zinovjev, Yad. Fiz. **66** (2003) 1000; ibid. **66** (2003) 1389; S.V. Molodtsov and G.M. Zinovjev, Mod. Phys. Lett. **A 18** (2003) 817.
- [29] A.G. Zubkov, O.V. Dubasov, and B.O. Kerbikov, Int. J. Mod. Phys. **A 14** (1999) 241.
- [30] L.V. Keldysh, Doctor thesis (FIAN, 1965);  
E.V. Kane, Phys. Rev. **131** (1963) 79;  
V.L. Bonch-Bruevich, Collection "Physics of Solid States", Moscow, VINITI Publ., 1965.
- [31] G.V. Efimov and S.N. Nedelko, Eur. Phys. J. **C 1** (1998) 343;  
A.C. Kolloniatis and S.N. Nedelko, Phys. Rev. **D 64** (2001) 114025
- [32] A.E. Dorokhov, N.I. Kochelev, S.V. Molodtsov, and G.M. Zinovjev Yad. Fiz. **70** (2007) 461.
- [33] M.-C. Chu and S. Schramm, Phys. Rev. **D 51** (1995) 4580;  
M.-C. Chu, S.M. Ouellette, S. Schramm, and R. Seki, Phys. Rev. **D 62** (2000) 094508.
- [34] O. Kaczmarek and F. Zantow, Phys. Rev. **D 71** (2005) 114510.
- [35] A. Di Giacomo, E. Meggiolaro, and H. Panagopoulos, Nucl. Phys. **B 483** (1997) 371.  
M. DÉlia, A. Di Giacomo and E. Meggiolaro, Phys. Rev. **D 67** (2003) 114504.
- [36] N.O. Agasian and S.M. Fedorov, JHEP **07** (2004) 007.
- [37] A.N. Sissakian, A.S. Sorin, M.K. Suleymanov, V.D. Toneev, and G.M. Zinovjev,  
nucl-ex/0601034.



## TOWARDS SCREENING OF COLOR FIELD IN INSTANTON LIQUID

S.V. Molodtsov<sup>\*</sup><sup>‡</sup>, G.M. Zinovjev<sup>‡</sup>

<sup>\*</sup>State Research Center, Institute of Theoretical and Experimental Physics, Moscow, Russia

<sup>‡</sup>Joint Institute for Nuclear Research, BLTP JINR, Dubna, Russia

<sup>‡</sup>Bogolyubov Institute for Theoretical Physics,  
National Academy of Sciences of Ukraine, Kiev, Ukraine

The effect of external colour field impact on the instanton liquid is studied. In the course of this study the corresponding effective Lagrangians are derived for both regimes of weak and strong external field and in long wave-length approximation. The example of Euclidean colour point-like source is analyzed in detail and the feedback of field on the instanton liquid is estimated as a function of source intensity.

### 1 Introduction

The declarations of discovering new state(s) of matter in relativistic heavy ion collisions at RHIC which are actively wandering in the papers nowadays are sometimes based on the results of different nature. From one side it is the striking result of direct experimental measurements of a strong suppression (comparing to  $pp$  and  $pA$  collisions) of particle production at high transverse momentum well-known as a jet quenching. And although the jet reconstruction in these experiments is a nontrivial task the (and accompanying) result(s) is(are) interpreted as a degradation of hard parton (initiating a jet) energy induced by medium (new thermalized matter) produced in collision long before hadronizing in the QCD vacuum. On the other hand the convincing success of phenomenological analysis of the other measurable characteristics based on the perfect liquid hydrodynamics results in the question about the sort of quark-gluon plasma (QGP) (if produced) and intimately related one about the origin of the QCD vacuum Ref.[1]. These investigations devoted to exploring collisions of ultrarelativistic heavy ions and aimed at producing quark-gluon plasma under laboratory conditions pose the interesting problem of studying the effect of intense gluon fields on the QCD physical vacuum. It is assumed that such fields can be generated in the collision process within a relatively macroscopic region and that they can be described in the semiclassical approximation. Currently available models of radiative gluon fields rely on various premises, but they do not provide an unambiguous and sound prediction for the intensity of the field (see, for example, [2]). These difficulties could have been sidestepped if the detailed structure of the physical vacuum had been known. The corresponding threshold value could then have been extracted on the basis of knowledge of characteristic vacuum-fluctuation fields. Unfortunately, we know at the present time only rather general features of the physical vacuum, such as gluon condensates, preliminary data on virtualities [3], and data from some lattice simulations [4]. In this situation, it only remains to estimate relevant effects on the basis of some plausible models of the QCD vacuum. The instanton liquid model seems to be of great value in this respect. The present study is devoted to describing the effects of the screening of an external color field precisely within this model. In general, this formulation of the problem may seem somewhat unexpected from the point of view of the model, since the additional components are introduced in an instanton liquid in order to describe the confining component and to remove simultaneously the problem of large-size instantons [5, 6].

In the case of a week external field, we adopt a diametrically opposite approach in a sense, assuming that it will play as if subordinate role. Nevertheless, the conclusions at which we are arrive will perfectly correspond to the phenomenology of strong interactions. An instanton liquid will be considered within the simplest approximation – a the stochastic ensemble of instantons in the singular gauge. The generating functional is estimated on the basis of the variational principle proposed in Ref.[7]. Comparative simplicity of the superposition ansatz and variational procedure allows us to analyze the effects almost analytically, but, in principle, our analysis is applicable to any other saturating configuration. Further, we proceed to estimate the effect of a strong external field on the instanton liquid. We consider the simplest model problem of an Euclidean pointlike color source in order to get an idea of the characteristic scale of the phenomenon.

## 2 External weak field in an instanton liquid

As a major configuration saturating the generating functional

$$Z = \int D[\mathcal{A}] e^{-S(\mathcal{A})} \quad (1)$$

where  $S(\mathcal{A})$  is a standard Yang-Mills action we take the approximate solution for the Yang-Mills equations in the form of the following superposition

$$\mathcal{A}_\mu^a(x) = B_\mu^a(x) + \sum_{i=1}^N A_\mu^a(x; \gamma_i), \quad (2)$$

here  $A_\mu^a$  implies the field of (anti-)instantons in the singular gauge

$$A_\mu^a(x) = \frac{2}{g} \omega^{ab} \bar{\eta}_{b\mu\nu} a_\nu(y), \quad a_\nu(y) = \frac{\rho^2}{y^2 + \rho^2} \frac{y_\nu}{y^2}, \quad y = x - z, \quad (3)$$

with the parameters  $\gamma_i = (\rho_i, z_i, \omega_i)$  describing the  $i$ -th instanton of the  $\rho$  size centered at the pseudo-particle coordinate  $z$ , with the matrix of colour orientation  $\omega$ , and  $g$  denotes the coupling constant of non-abelian field; for the anti-instanton the 't Hooft symbols should be changed according to  $\bar{\eta} \rightarrow \eta$ ; and  $B_\mu^a(x)$  is an external field. As was indicated in introduction, we are interested in quite a specific configuration generated in heavy-ion collisions rather than in an arbitrary external field. The localization of this field within a nuclear-size scale and its semiclassical character might be features peculiar to such configurations. An analogy with electrodynamics suggests that such fields can be approximately described by means of a multipole expansion. It is precisely this qualitative pattern that we will use here as a guideline.

The non-abelian strength tensor from external field and individual pseudo-particle is defined by

$$G_{\mu\nu}^a(\mathcal{A}) = \partial_\mu \mathcal{A}_\nu^a - \partial_\nu \mathcal{A}_\mu^a + g f^{abc} \mathcal{A}_\mu^b \mathcal{A}_\nu^c = G_{\mu\nu}^a(B) + G_{\mu\nu}^a(A) + G_{\mu\nu}^a(A, B) \quad (4)$$

with entirely anti-symmetric tensor  $f^{abc}$ , where the first two terms in the second relation correspond to standard strength tensors of non-abelian field. In particular,

$$G_{\mu\nu}^a(A) = -\frac{4}{g} \omega^{ak} \bar{\eta}_{k\alpha\beta} M_{\mu\alpha} M_{\nu\beta} \frac{\rho^2}{(y^2 + \rho^2)^2}, \quad (5)$$

where  $M_{\mu\nu} = \delta_{\mu\nu} - 2\hat{y}_\mu \hat{y}_\nu$ ,  $\hat{y}_\mu = y_\mu/|y|$ . The 'mixed' component of the instanton strength field looks like

$$G_{\mu\nu}^a(A, B) = g f^{abc} (B_\mu^b A_\nu^c - B_\nu^b A_\mu^c) = g f^{abc} \omega^{cd} \frac{2}{g} (B_\mu^b \bar{\eta}_{d\nu\alpha} - B_\nu^b \bar{\eta}_{d\mu\alpha}) a_\alpha(y). \quad (6)$$

Calculating now  $G^2$  we receive the partial contributions of external field and each separate pseudo-particle as

$$\begin{aligned} G_{\mu\nu}^a G_{\mu\nu}^a &= G_{\mu\nu}^a(B) G_{\mu\nu}^a(B) + G_{\mu\nu}^a(A) G_{\mu\nu}^a(A) + G_{\mu\nu}^a(A, B) G_{\mu\nu}^a(A, B) \\ &+ 2G_{\mu\nu}^a(B) G_{\mu\nu}^a(A) + 2G_{\mu\nu}^a(B) G_{\mu\nu}^a(A, B) + 2G_{\mu\nu}^a(A) G_{\mu\nu}^a(A, B). \end{aligned} \quad (7)$$

In order to keep the further steps as simple and transparent as possible we limit ourselves with the standard sum of partial contributions in the superposition ansatz action and hold the highest in IL density (precisely in packing fraction parameter  $n\rho^4$ ) one particle contributions

$$S(B, \gamma) = \int dx \frac{G_{\mu\nu}^a G_{\mu\nu}^a}{4} \simeq \sum_i \int dx \frac{G_{\mu\nu}^a(i) G_{\mu\nu}^a(i)}{4}. \quad (8)$$

The crossing terms of different pseudo-particles (which are proportional to the IL density squared) are neglected here because of very small packing fraction parameter characteristic to IL, i.e.  $n\rho^4 \sim 0.01$ . Thus, the regularized generating functional for the IL model takes the following form (for denotations see Ref.[7])

$$Y = \int D[B] \frac{1}{N!} \int \prod_{i=1}^N d\gamma_i e^{-S(B, \gamma)}. \quad (9)$$

First we consider the case of weak external field. We assume that the characteristic parameters of the instanton liquid, such as average pseudoparticle size  $\bar{\rho}$  and the IL density  $n$ , do not change, coinciding with their vacuum magnitudes. For the saturating configuration chosen here, these values of the pseudoparticle size is immaterial.

In order to avoid cumbersome expressions, we therefore assume that all pseudoparticles have the same size,  $\bar{\rho}$ . Those are fixed by some repulsive mechanism (see, however, the remark at the end of paper) for the particular choice of saturating configuration done above<sup>1</sup>. In calculating the generating functional (10), it therefore only remains to perform averaging over the pseudoparticle positions and color orientations.

In order to calculate the effective action, it is necessary to find the contribution of the fields of quantum fluctuation in the vicinity of the saturating configuration (1). By convention, this contribution can be written in terms of the running coupling constant as a function of the external field and characteristic pseudoparticle size,  $g(\rho, B)$ . With the aid of this quantity, one can correctly go over to the relevant scale. For the goals pursued in the present study, however, it is sufficient to use an approximate expression that is obtained upon the substitution  $g(\bar{\rho}, B) \rightarrow g(\bar{\rho})$ . Indeed, the fields at short distances (where according to our assumption, the external field is concentrated) are not singular by virtue of asymptotic freedom. Dangerous singularities may arise at long distances, but an ensemble of pseudoparticles controls the situation there. Thus, we will describe the external field less accurately (but we do not aim at reaching a high accuracy here) but will not miss dangerous singular contributions. It turns out that even this extremely simple estimate of generating functional at the saddle point leads to the emergence of an infrared singularity, and we now proceed to describe it.

Making use the cluster decomposition we obtain the corresponding average of exponential as

$$\langle \exp(-S) \rangle_{\omega z} = \exp \left( \sum_k \frac{(-1)^k}{k!} \langle \langle S^k \rangle \rangle_{\omega z} \right), \quad (10)$$

where  $\langle S_1 \rangle = \langle \langle S_1 \rangle \rangle$ ,  $\langle S_1 S_2 \rangle = \langle S_1 \rangle \langle S_2 \rangle + \langle \langle S_1 S_2 \rangle \rangle, \dots$ . The first cumulant is simply defined by the action averaged. Taking into account the direct form of field strength tensors (4) and (5) it is evident that the following terms will only be present in the partial contribution after averaging over colour orientation

$$\langle G_{\mu\nu}^a G_{\mu\nu}^a \rangle_{\omega} = G_{\mu\nu}^a(B) G_{\mu\nu}^a(B) + \langle G_{\mu\nu}^a(A) G_{\mu\nu}^a(A) \rangle_{\omega} + \langle G_{\mu\nu}^a(A, B) G_{\mu\nu}^a(A, B) \rangle_{\omega} + 2 \langle G_{\mu\nu}^a(A) G_{\mu\nu}^a(A, B) \rangle_{\omega}. \quad (11)$$

The colour averaging is performed by the help of equality

$$\langle \omega^{ak} \omega^{cd} \rangle = \frac{\delta^{ac} \delta^{kd}}{N_c^2 - 1}, \quad (12)$$

implying  $N_c$  as the number of colours. Averaging over the pseudo-particle positions results in the following integral

$$\int \frac{dz}{V} a_{\alpha}(y) a_{\gamma}(y) = \delta_{\alpha\gamma} \frac{1}{V} \frac{\pi^2}{4} \rho^2, \quad (13)$$

because the basic IL parameters, as we agreed, are unchanged. Handling the 'mixed' component average we have it in the form as reads (all the other terms disappear)

$$\langle G_{\mu\nu}^a(A, B) G_{\mu\nu}^a(A, B) \rangle_{\omega z} = \frac{18 \pi^2 \rho^2}{V} \frac{N_c}{N_c^2 - 1} B_{\mu}^b B_{\mu}^b, \quad (14)$$

Finally, collecting all appropriate terms we find the effective action for the external field in IL as

$$\langle \langle S \rangle \rangle_{\omega z} = \int dx \left( \frac{G(B) G(B)}{4} + \frac{m^2}{2} B^2 \right) + N \beta, \quad (15)$$

$$m^2 = 9\pi^2 n \rho^2 \frac{N_c}{N_c^2 - 1}, \quad (16)$$

here  $N$  is the full number of particles in volume  $V$  with  $n = N/V$  and a single pseudo-particle action  $\beta = 8\pi^2/g^2$ . The last term of Eq.(16) introduces the contribution of purely instanton component  $\langle G(A) G(A) \rangle_{\omega z}$ . The contribution of repulsive term which fixes the pseudo-particle size in IL is omitted in Eq.(16) so long as it is not a principal point in this context and adding it, leads to the insignificant correction to the last condensate term in Eq.(16). An amusing point is that the mass term of Eq.(17) has been well-known for rather long time and as a matter of fact fixing the pseudo-particle size in the variational procedure of Ref.[7] is provided just by this mechanism of mass generation. With the characteristic IL parameters ( $N_c = 3$  and number of flavours  $N_f = 2$ )  $n/\Lambda_{QCD}^4 = 1.2$ ,  $\bar{\rho}\Lambda_{QCD} = 0.27$ ,  $\beta = 18$ , see for example [32], the mass estimate is  $m \sim 440$  MeV for  $\bar{\rho} \sim 1$  GeV and  $\Lambda_{QCD}$  in the interval of 200 — 300 MeV. The screening properties of the repulsive interaction were highlighted in [7], and the value of  $m \sim 350$  MeV was presented there for the screening mass. The studies of Hütter [10], where the estimate  $m \sim 480$  MeV was obtained for the mass of the gluon in an instanton medium,

<sup>1</sup>In the literature three mechanisms for fixing ensemble of pseudoparticles are discussed: repulsive [7]; freezing of the coupling constant [8]; stabilization due to influence of confining vacuum component

is also worthy of note. One can see that all these estimates are rather close since, in all of the cases, the effect arises owing to the mixed term in the field strength (5). We also note that the compatibility conditions for the equations resulting from Eq.(16) is  $\partial_\mu B_\mu = 0$  which is satisfied by the pseudo-particle field Eq.(9) as well. There may arise the question of why pseudoparticles oriented at random in color space lead to screening — which component plays the role of a distribution function. In the present case (in non-Abelian theory), this is the exponential function featuring the Yang–Mills action functional. A nontrivial contribution originating from mixed term in the field strength (5) is generated in it. In the Abelian case, there are no such contributions by virtue of the superposition principle.

Turning now to the next term of cluster decomposition to calculate the effective Lagrangian corrections we conclude immediately that in the second cumulant

$$\frac{1}{2} \left\langle \left\langle \int dx_x \frac{G}{4} \int dx_2 \frac{G_2}{4} \right\rangle \right\rangle, \quad (17)$$

there are two nontrivial terms

$$\frac{1}{2} \left\langle \int dx_1 2 \frac{G_{\mu\nu}^a(B)G_{\mu\nu}^a(A)}{4} \int dx_2 2 \frac{G_{\alpha\beta}^b(B_2)G_{\alpha\beta}^b(A_2)}{4} \right\rangle, \quad (18)$$

$$\frac{1}{2} \left\langle \int dx_1 2 \frac{G_{\mu\nu}^a(A)G_{\mu\nu}^a(A, B)}{4} \int dx_2 2 \frac{G_{\alpha\beta}^b(A_2)G_{\alpha\beta}^b(A_2, B_2)}{4} \right\rangle, \quad (19)$$

here the index 2 underlines the fact that corresponding functions are dependent on  $x_2$ . The remaining terms originate from either the interference terms (and are cancelled by the contribution of the first cumulant squared) or lead to the contributions anharmonic in  $B$  which are not in our interest for this paper. It was analyzed for the first time in Ref.[11] that  $G(B)G(A)$  in (6) generates the dipole interaction. However, this interaction does not manifest itself in the first term of cluster decomposition if the averaging over the colour orientation is performed. It comes into focus starting on the second order of decomposing. In particular Eq.(10) can be presented in the following form

$$\begin{aligned} & \frac{1}{2} \left\langle \int dx_1 2 \frac{G_{\mu\nu}^a(B)G_{\mu\nu}^a(A)}{4} \int dx_2 2 \frac{G_{\alpha\beta}^b(B_2)G_{\alpha\beta}^b(A_2)}{4} \right\rangle_\omega = \\ & = \frac{1}{2} \frac{1}{N_c^2 - 1} \int dx_1 dx_2 \frac{G_{\mu\nu}^a(B)G_{\alpha\beta}^b(B_2)}{4} G_{\mu\nu}^a(A)G_{\alpha\beta}^b(A_2), \end{aligned} \quad (20)$$

if one exploits Eq.(4) and Eq.(12) keeping in mind that  $G_{\mu\nu}^a(A)G_{\alpha\beta}^b(A_2)$  is colour independent because of the identity  $\omega^{ab}\omega^{ac} = \delta^{bc}$ . Eq.(20) should be also averaged over the pseudo-particle positions which results in the correlation function for the instantons in singular gauge developing the following form obtained in Ref.[1]

$$\int \frac{dz}{V} G_{\mu\nu}^a(A)G_{\alpha\beta}^a(A_2) = \frac{1}{V} \frac{16}{g^2} (\delta_{\mu\alpha}\delta_{\nu\beta} - \delta_{\mu\beta}\delta_{\nu\alpha} + \varepsilon_{\mu\nu\alpha\beta}) I_s \left( \frac{\Delta}{\rho} \right), \quad (21)$$

where  $\Delta = |x_1 - x_2|$ , and for the anti-instanton the substitution  $\varepsilon \rightarrow -\varepsilon$  should be done. The analytical form of function  $I_s$  is not our priority here, however, it is shown in Fig.1. If the numbers of instantons and anti-instantons are balanced then the term proportional to the tensor  $\varepsilon$  disappears.

Now collecting the terms together we find the contribution of Eq.(10) in the IL approach as

$$\frac{16}{g^2} \frac{1}{N_c^2 - 1} n \int dx_1 dx_2 I_s \left( \frac{\Delta}{\rho} \right) G_{\mu\nu}^a(B)G_{\mu\nu}^a(B_2). \quad (22)$$

Clearly, it leads to an abatement of initial action and it is more convenient for analyzing to present the non-local factor of dielectrical susceptibility type in the Fourier components Ref.[11]

$$\int dk \left( 1 - \frac{16}{g^2} \frac{1}{N_c^2 - 1} n \tilde{I}_s(k\rho) \right) G_{\mu\nu}^a[B(k)]G_{\mu\nu}^a[B(-k)]. \quad (23)$$

Numerical estimate of  $\tilde{I}_s(k\rho)$  at the zero value of argument is  $\tilde{I}_s(0) \sim 6\rho^4$ , and at  $N_c = 3$ ,  $N_f = 2$  the correction coefficient can be estimated as

$$\kappa = \frac{16}{g^2} \frac{1}{N_c^2 - 1} n \tilde{I}_s(0) \sim 0.013. \quad (24)$$

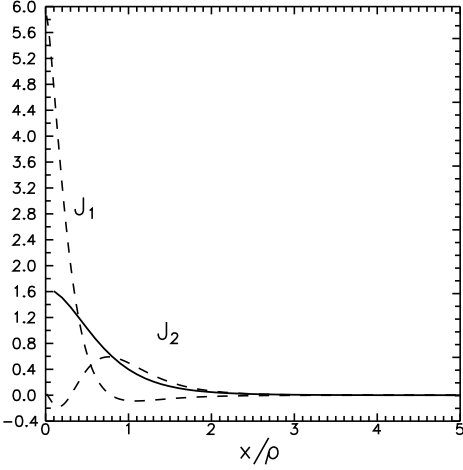


**Figure 1.** Correlation function  $I_s$  is given by solid line and the correlation functions  $J_1$  and  $J_2$  are given by the dashed lines.

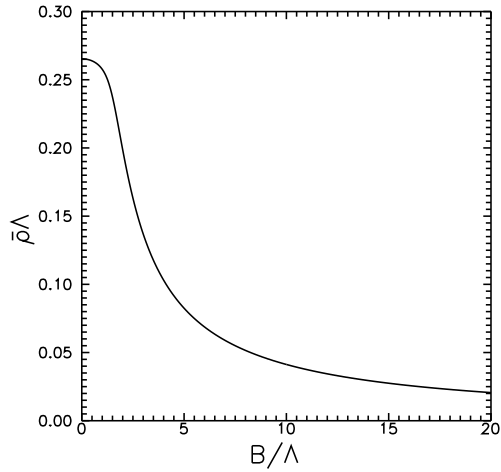


**Figure 2.** Pseudo-particle mean size as a function of applied external field.

Analyzing now the term Eq.(11) we present it as

$$\begin{aligned} & \frac{1}{2} \left\langle \int dx_1 2 \frac{G_{\mu\nu}^a(A) G_{\mu\nu}^a(A, B)}{4} \int dx_2 2 \frac{G_{\alpha\beta}^b(A_2) G_{\alpha\beta}^b(A_2, B_2)}{4} \right\rangle_\omega = \\ & = \frac{1}{2} \left\langle \int dx_1 dx_2 \omega^{ak} G_{\mu\nu}^k(A) f^{amn} \omega^{nl} (B_\mu^m \bar{\eta}_{l\nu\gamma} - B_\nu^m \bar{\eta}_{l\mu\gamma}) a_\gamma \times \right. \\ & \left. \times \omega^{bc} G_{\alpha\beta}^k(A_2) f^{bde} \omega^{ef} (B_{2\alpha}^d \bar{\eta}_{f\beta\delta} - B_{2\beta}^d \bar{\eta}_{f\alpha\delta}) a_{2\delta} \right\rangle_\omega. \end{aligned} \quad (25)$$

and imply the dependence of  $G$  on the colour matrix  $\omega$  might be given by the common factor (without introducing new symbol for  $G$ ). Formally, this term looks like the next one expanding in  $1/N_c$ , i.e.  $(\sim \omega^4)$ . However, using the identity for colour matrices  $f^{man} \omega^{ak} \omega^{nl} = \epsilon^{klg} \omega^{mg}$ , we have  $\langle f^{man} \omega^{ak} \omega^{nl} f^{dbe} \omega^{bc} \times \omega^{ef} \rangle = \delta^{md} (\delta^{kc} \delta^{lf} - \delta^{kf} \delta^{lc}) / (N_c^2 - 1)$ , and then Eq.(21) receives the following form

$$\begin{aligned} & \frac{1}{2} \left\langle \int dx_1 2 \frac{G_{\mu\nu}^a(A) G_{\mu\nu}^a(A, B)}{4} \int dx_2 2 \frac{G_{\alpha\beta}^b(A_2) G_{\alpha\beta}^b(A_2, B_2)}{4} \right\rangle_\omega = \\ & = 2 \frac{1}{N_c^2 - 1} \int dx_1 dx_2 [G_{\mu\nu}^k(A) G_{\alpha\beta}^k(A_2) \bar{\eta}_{l\nu\gamma} \bar{\eta}_{l\beta\delta} - G_{\mu\nu}^k(A) G_{\alpha\beta}^l(A_2) \bar{\eta}_{k\beta\delta} \bar{\eta}_{l\nu\gamma}] a_\gamma a_{2\delta} B_\mu^m B_{2\alpha}^m, \end{aligned} \quad (26)$$

The lower line here develops this form because of an asymmetric property of tensor  $G$ . Averaging over the pseudo-particle positions we may extract the correlation function in the following form

$$\begin{aligned} & \int \frac{dz}{V} [G_{\mu\nu}^k(A) G_{\alpha\beta}^k(A_2) \bar{\eta}_{l\nu\gamma} \bar{\eta}_{l\beta\delta} - G_{\mu\nu}^k(A) G_{\alpha\beta}^l(A_2) \bar{\eta}_{k\beta\delta} \bar{\eta}_{l\nu\gamma}] a_\gamma a_{2\delta} = \\ & = \frac{16}{g^2} \frac{1}{V} \left[ J_1 \left( \frac{\Delta}{\rho} \right) \delta_{\mu\alpha} + J_2 \left( \frac{\Delta}{\rho} \right) \hat{\Delta}_\mu \hat{\Delta}_\alpha \right], \end{aligned} \quad (27)$$

where  $\hat{\Delta} = x_2 - x_1 / |x_2 - x_1|$  is the unity vector.

The simple algebra allows us to calculate the functions

$$\begin{aligned} J_1 &= \int dy \frac{\rho^8 (16t^3 - 8t + 4pq + 6(p^2 + q^2)t - 12t^2pq)}{3(y^2 + \rho^2)^3(z^2 + \rho^2)^3 |y| |z|}, \\ J_2 &= \int dy \frac{4\rho^8 (4t^3 + 5t - 4pq - 6(p^2 + q^2)t + 12t^2pq)}{3(y^2 + \rho^2)^3(z^2 + \rho^2)^3 |y| |z|}, \end{aligned} \quad (28)$$

with  $z = y + \Delta$ ,  $t = \frac{(y \cdot z)}{|y| |z|}$ ,  $p = \frac{(y \cdot \Delta)}{|y| |\Delta|}$ ,  $q = \frac{(z \cdot \Delta)}{|z| |\Delta|}$ . Similarly to  $I_s$  we do not need their explicit forms here but one may estimate their behaviours looking at the dashed lines in Fig.1. Finally, the additional contribution to the mass term reads as

$$\frac{1}{N_c^2 - 1} \frac{32}{g^2} n \int dx_1 dx_2 \left[ J_1 \left( \frac{\Delta}{\rho} \right) \delta_{\mu\alpha} + J_2 \left( \frac{\Delta}{\rho} \right) \hat{\Delta}_\mu \hat{\Delta}_\alpha \right] B_\mu^a B_{2\alpha}^a, \quad (29)$$

and in the Fourier components as

$$\int dk \left[ \frac{m^2}{2} - \frac{32}{g^2} \frac{1}{N_c^2 - 1} n \left( \tilde{J}_1(k\rho) \delta_{\mu\alpha} + \tilde{J}_2(k\rho) \hat{k}_\mu \hat{k}_\alpha \right) \right] B_\mu^a(k) B_\alpha^a(-k). \quad (30)$$

Estimating numerically the nonlocal correction to the mass we find out that  $\tilde{J}_1(0) \sim -1.4 \rho^2$  unlikely above result. Then the mass term and corresponding correction in Eq.(22) come about at zero momentum  $9\pi^2 N_c$  and  $(-\frac{4\beta}{\pi^2} 1.4)$ , respectively. At the characteristic value  $\beta \sim 18$  it means the quantitative correction smallness or, globally, the corrections initiated by the second term of cumulant expansion are negligible at the contemporary values of basic IL parameters. There is another contribution to the effective Lagrangian which comes from the interaction of sources generating the external field with (anti-)instanton superposition

$$S_{int} = \sum_{i=1}^N \int dx j_\mu^a(x) A_\mu^a(x; \gamma_i).$$

Making use the cluster decomposition one expects the possibility to calculate corresponding small contributions (if the sources are treated in the quasiclassical approximation) which are given by the correlation functions of the form  $\langle A_\mu^a(x; \gamma) A_\nu^b(y; \gamma) \rangle_\gamma$  Ref.[11].

To conclude this section, we will consider, for the effective Lagrangian in (16) a somewhat different interpretation following which one can obtain the infrared singularity mentioned at the beginning of this section, see also Ref.[13]. Let us suppose that the quasi-classical field  $B$  is described in the infra-red momentum region by the initial Yang-Mills action without the term breaking down gauge symmetry as before. In particular, we consider the field of point-like Euclidean source of intensity  $e$  with only one non-zero  $n$ -th component

$$B_\mu^a(x) = (\mathbf{0}, \delta^{an} \varphi), \quad \varphi = \frac{e}{4\pi} \frac{1}{|\mathbf{x}|}.$$

Then  $B^2$  integrated over the 4-dimensional space gives

$$\int dx \left( \frac{e}{4\pi |\mathbf{x}|} \right)^2 = \frac{e^2}{4\pi} X_4 L,$$

where  $X_4$ ,  $L$  are some formal upper limits of corresponding integrals. In this approach the contribution of the first cumulant Eq.(16) could be written down as

$$\langle\langle S \rangle\rangle_{\omega z} = E X_4, \quad E = \frac{e^2}{4\pi} \frac{1}{r_0} + \sigma L + \beta n L^3, \quad (31)$$

with  $\sigma = \frac{9\pi}{8} \frac{N_c}{N_c^2 - 1} e^2 n \bar{\rho^2}$ . The first term in defining  $E$  comes from the Coulomb energy of point-like source and  $r_0$  represents a formal particle radius. The last term is originated by the gluon condensate and the previous term looks like negligibly small correction to the condensate term. However, this contribution linearly increasing with  $L$  is proportional to  $e^2$  and has different physical meaning as a term additional to the self-energy of source. In other words, it demonstrates an impossibility for the source with an open colour to be available in IL because the amplitude of such a state is very strongly suppressed ( $e^{-S}$ ) comparing to the condensate contribution if the screening effects are not taken into account. For the dipole in 'isosinglet' ( $s$ ) and 'isotriplet' ( $t$ ) states (i.e.  $N_c = 2$ ) we obtain

$$B_\mu^a(x) = (\mathbf{0}, \delta^{a3} \varphi), \quad \varphi = \frac{e}{4\pi} \left( \frac{1}{|\mathbf{x} - \mathbf{z}_1|} \mp \frac{1}{|\mathbf{x} - \mathbf{z}_2|} \right),$$

where  $\mathbf{z}_1$ ,  $\mathbf{z}_2$  are the dipole coordinates what leads to

$$\int dx B_s^2 = \frac{e^2}{4\pi} X_4 l, \quad \int dx B_t^2 = \frac{e^2}{4\pi} X_4 (4L - l),$$

with  $l = |\mathbf{z}_1 - \mathbf{z}_2|$  to be the distance separating sources. We have another confirmation of suppression effect for the states with open colour in IL, i.e. the energy of 'isosinglet' dipole state increases with  $l$  enlarging and the corresponding coefficient is  $\sigma \sim 0.6$  GeV/fm if we take  $e \sim g$ . In principle the same situation for arbitrary oriented in color space charges is valid, as comes from analysis of corresponding exact solution obtained in [14].

Thus, we are quite allowed to conclude the regime of weak external field in IL is described by effective Lagrangian Eq.(16) and basic IL parameters are within a well adapted interval. Moreover all the corrections originated by the second cumulant should be certainly neglected.

### 3 Long-wave approximation for a strong field

In the preceeding section, we have derived the effective action for a weak external field under the assumption that the parameters describing the state of the instanton liquid remain unchanged, but we did not formulate a corresponding criterion of weakness of the external field. In the case of a strong external field, the validity of the naive approximate solution to the Yang–Mills equations (1) is naturally questionable, since a substantial distortion of the pseudoparticle fields may be expected here. In order to estimate these effects, we have investigated in detail the behaviour of an (anti)instanton in the field of an Euclidean pointlike color source. The instanton-like configurations (9) having a variable size  $\rho \rightarrow R(x, z)$  and a variable color orientation  $\omega^{ab} \rightarrow \Omega^{ab}(x, z)$  were considered in [15]. The singular nature of the solution used in the instanton liquid model for the pseudoparticles makes it possible to apply the multipole expansions of deformation fields; that is,

$$\begin{aligned} R_{in}(x, z) &= \rho + c_\mu y_\mu + c_{\mu\nu} y_\mu y_\nu + \dots, & |y| \leq L, \\ R_{out}(x, z) &= \rho + d_\mu \frac{y_\mu}{y^2} + d_{\mu\nu} \frac{y_\mu}{y^2} \frac{y_\nu}{y^2} + \dots, & |y| > L, \end{aligned} \quad (32)$$

(the same concerns instanton orientation in color space  $\Omega(x, z)$ ). Here,  $L$  is a parameter that determines the radius of the sphere where the multipole expansion increasing with distance gives way to a decrasing one, in accordance with requirement that the deformations be regular. The coefficients  $c_\mu, c_{\mu\nu}, \dots$  and  $d_\mu, d_{\mu\nu}, \dots$  are functions of the external field and are determined by solving the corresponding variational problem. It can easily be seen that, at nonzero coefficients, the opposite parts of a pseudoparticle may have different sizes and different color orientations. In view of this, we reffered to these configurations as crumpled instantons. Investigations revealed that, in the problem being considered, there appears a characteristic scale that is on the same order of magnitude as the pseudoparticle size and at which deformations become significant, but repulsion effects remain dominant. In a rough approximation, we can discard deformations completely since the instanton liquid density decreases fast at short distances from the source, as well see below. We also note that the deformation fields are of interest in themselves because they make it possible to describe excited states of instanton liquid [16].

We are going to modify slightly the variational procedure of Ref.[7] to implement possibility of the changing IL parameters. We retain here the same designations to demonstrate precisely where the changes are introduced and imply  $S(B, \gamma)$  in Eq.(10) in the following form

$$S(B, \gamma) = - \sum \ln d(\rho_i) + \beta U_{int} + \sum U_{ext}(\gamma_i, B) + S(B). \quad (33)$$

The first term here describes one-instanton contributions with the following distribution function over the (anti-)instanton sizes

$$d(\rho) = C_{N_c} \Lambda_{QCD}^b \rho^{b-5} \tilde{\beta}^{2N_c}, \quad (34)$$

where  $b = \frac{11}{3}N_c - \frac{2}{3}N_f$ ,  $\tilde{\beta} = -b \ln(\Lambda_{QCD} \bar{\rho})$ ,  $\Lambda_{QCD} = \Lambda_{\overline{MS}} = 0.92\Lambda_{P.V.}$  with  $C_{N_c}$  dependent on renormalization scheme

$$C_{N_c} \approx \frac{4.66 \exp(-1.68N_c)}{\pi^2(N_c - 1)!(N_c - 2)!}.$$

The second term of Eq.(33) is responsible for providing pseudo-particles with repulsive interaction which fixes their sizes. The characteristic single instanton action is defined on the scale of average pseudo-particle size  $\beta = \beta(\bar{\rho})$  where  $\beta(\rho) = -\ln C_{N_c} - b \ln(\Lambda_{QCD} \rho)$ .

The partial pseudo-particle contributions grouped in the third term and we take only

$$U_{ext}(\gamma_i, B) = \int dx \frac{G_{\mu\nu}^a(A_i, B) G_{\mu\nu}^a(A_i, B)}{4},$$

because the other contributions at the standard IL parameters are small as we have seen. At last, the fourth term represents simply the Yang–Mills action of the  $B$  field

$$S(B) = \int dx \frac{G_{\mu\nu}^a(B) G_{\mu\nu}^a(B)}{4}.$$

The well-known property of exponential makes it possible to estimate the generating functional of Eq.(10) with the approximating functional as

$$Y \geq Y_1 \exp(-\langle S - S_1 \rangle), \quad (35)$$

where

$$Y_1 = \int D[B] \frac{1}{N!} \int \prod_{i=1}^N d\gamma_i e^{-S_1(B, \gamma) - S(B)}, \quad S_1(B, \gamma) = - \sum \ln \mu(\rho_i),$$

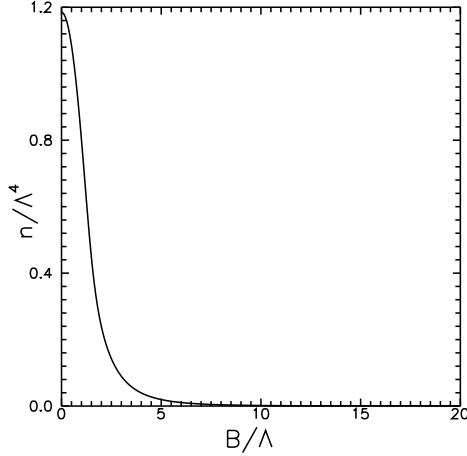


**Figure 3.** The IL density as a function of applied external field.

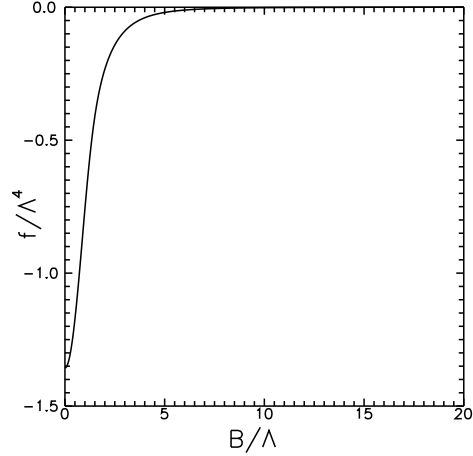


**Figure 4.** Free energy density as a function of external field  $B$ .

and  $\mu(\rho)$  is an effective one-particle distribution function which may be derived with the variational procedure. In our particular situation a mean value of corresponding difference is given by

$$\begin{aligned} \langle S - S_1 \rangle &= \frac{1}{Y_1 N!} \int \prod_{i=1}^N d\gamma_i [\beta U_{int} + U_{ext}(\gamma, B) - \sum \ln d(\rho_i) + \sum \ln \mu(\rho_i)] e^{\sum \ln \mu(\rho_i)} \\ &= \frac{N}{\mu_0} \int d\rho \mu(\rho) \ln \frac{\mu(\rho)}{d(\rho)} + \frac{\beta}{2} \frac{N^2}{V^2 \mu_0^2} \int d\gamma_1 d\gamma_2 U_{int}(\gamma_1, \gamma_2) \mu(\rho_1) \mu(\rho_2) + \int dx \frac{N}{V \mu_0} \int d\rho \mu(\rho) \rho^2 \zeta B^2 \\ &= \int dx n \left( \frac{1}{\mu_0} \int d\rho \mu(\rho) \ln \frac{\mu(\rho)}{d(\rho)} + \frac{\beta \xi^2}{2} n \left( \overline{\rho^2} \right)^2 + \zeta \overline{\rho^2} B^2 \right), \end{aligned} \quad (36)$$

with  $\zeta = \frac{9}{2} \frac{\pi^2}{N_c^2 - 1}$ ,  $\xi^2 = \frac{27}{4} \frac{N_c}{N_c^2 - 1} \pi^2$ ,  $\mu_0 = \int d\rho \mu(\rho)$ . Here we estimate the functional in the adiabatic (long wave-length) approximation. It means we consider the IL elements of some characteristic size (of the same order of magnitude as the mean distance between pseudo-particles) being equilibrated by the presence of some fixed field  $B$ . Then calculating the optimal configurations of pseudo-particles we found out the effective action in the mean field. Eq.(36) is given just in the form underlining that an integration is performed over liquid elements and the proper parameters describing their states could be dependent on the external field, i.e. could be the functions of coordinate  $x$ . Physical meaning of such a functional is quite transparent, it implies that each separate element of IL possesses a characteristic aptitude of screening external field assessed by  $U_{ext}$ .

Calculating the variation of  $\langle S - S_1 \rangle$  in  $\mu(\rho)$  we have

$$\mu(\rho) = C d(\rho) e^{-(n\beta\xi^2\overline{\rho^2} + \zeta B^2)\rho^2},$$

where  $C$  is an arbitrary constant and we fix it demanding the coincidence of its value when the external field is absent with its vacuum average. Then

$$\mu(\rho) = C_{N_c} \tilde{\beta}^{2N_c} \Lambda_{QCD}^b \rho^{b-5} e^{-(n\beta\xi^2\overline{\rho^2} + \zeta B^2)\rho^2}. \quad (37)$$

and making use the definition of an average as

$$\overline{\rho^2} = \frac{\int d\rho \rho^2 \mu(\rho)}{\mu_0},$$

we obtain the practical relation between mean pseudo-particle size and the IL density

$$(n \beta \xi^2 \overline{\rho^2} + \zeta B^2) \overline{\rho^2} \simeq \nu, \quad (38)$$

where  $\nu = (b - 4)/2$ . Apparently, it results in a well-known form of pseudo-particle size distribution

$$\mu(\rho) = C_{N_c} \tilde{\beta}^{2N_c} \Lambda_{QCD}^b \rho^{b-5} e^{-\nu \rho^2 / \overline{\rho^2}}. \quad (39)$$

Now Eq.(38) allows us to formulate the criterion we are interested in. It looks like  $\zeta B^2 \ll n \beta \xi^2 \overline{\rho^2}$  and for the IL parameters mentioned above it is  $B \ll 400$  MeV.

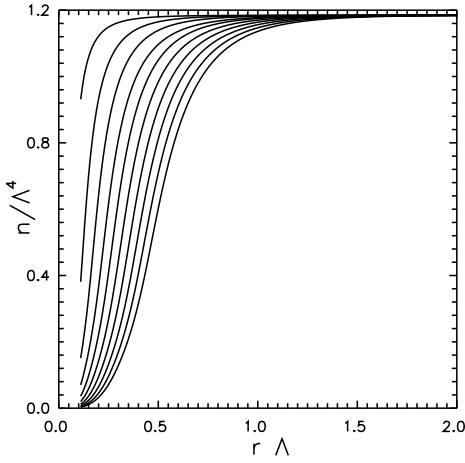


**Figure 5.** The IL density  $n/\Lambda^4$  as a function of  $r$  for different values of intensity. Extreme right hand side line corresponds to  $e/4\pi = 1$ . Going to the left corresponds to changing  $e/4\pi$  with a pace of 0.1 up to  $e/4\pi = 0.1$  what corresponds to extreme left hand side line.

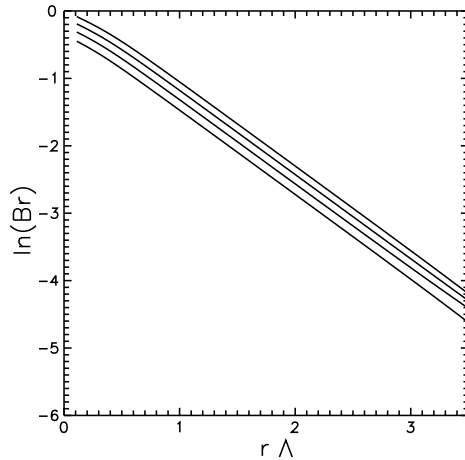


**Figure 6.**  $\ln(Br)$  as a function of  $r$  for four various solutions. The upper line corresponds to  $e/4\pi = 1$ . Going down the lines correspond to decreasing  $e/4\pi$  with spacing 0.1.

Dealing with Eq.(36) and Eq.(39) the generating functional estimate Eq.(35) may be presented as

$$Y \geq \int D[B] e^{-S(B)} e^{-F}, \quad (40)$$

$$F = \int dx n \left\{ \ln \frac{n}{\Lambda_{QCD}^4} - 1 - \frac{\nu}{2} + \frac{\zeta \bar{\rho}^2 B^2}{2} - \ln[\Gamma(\nu) C_{N_c} \tilde{\beta}^{2N_c}] - \nu \ln \frac{\bar{\rho}^2}{\nu} \right\}.$$

Making use of the relation Eq.(38) it is not difficult to find the maximum of functional Eq.(40) in the IL parameters at the fixed  $B$  value as a solution of transcendental equation  $(\frac{dF}{d\bar{\rho}} = 0)$ . As an information we give the simple expression of its derivative in  $n$

$$F'_n = \ln \frac{n}{\Lambda_{QCD}^4} + \frac{1}{4} \frac{n^2 \xi^4 \beta b (\bar{\rho}^2)^3}{2n\beta \xi^2 \bar{\rho}^2 \zeta B^2 - n \xi^2 \frac{b}{2} \bar{\rho}^2} - \ln[\Gamma(\nu) C_{N_c} \tilde{\beta}^{2N_c}] - 2N_c n \frac{\tilde{\beta}'_n}{\tilde{\beta}} - \nu \ln \frac{\bar{\rho}^2}{\nu}.$$

Fig.2 and Fig.3 demonstrate the solutions for  $\bar{\rho}$  and  $n$  at  $N_c = 3$  and  $N_f = 2$  as the functions of field  $B$ . Fig.4 shows the plot of free energy density  $f/\Lambda_{QCD}^4$  where  $F = \int dx f$  and convinces IL is steady as to an impact of external field. At strong external field the IL parameters are given by the following asymptotic formulae

$$\bar{\rho}^2 \simeq \frac{\nu}{\zeta B^2} \left( 1 - \frac{n \nu \beta \xi^2}{\zeta^2 B^4} \right), \quad n \simeq \frac{\Gamma(\nu) C_{N_c} \tilde{\beta}^{2N_c}}{(\zeta B^2)^\nu} \left( 1 + \frac{\Gamma(\nu) C_{N_c} \tilde{\beta}^{2N_c}}{(\zeta B^2)^\nu} \frac{N_c b \nu \beta \xi^2}{\zeta^2 B^4} \right).$$

This regime starts somewhere around  $B\Lambda_{QCD}^{-1} \sim 10$  at all the plots given.

Thus, the effective action for the  $B$  field is given by the following nonlinear functional

$$S_{eff} = \int dx \left( \frac{G_{\mu\nu}^a(B) G_{\mu\nu}^a(B)}{4} + f[B] \right). \quad (41)$$

This functional makes possible to calculate the external field as a function of  $x$  and IL parameters  $\bar{\rho}[B]$  and  $n[B]$ .

It is interesting to note that the variant of variational principle applied here makes it possible obtain self-consistent description of the instanton ensemble, with slightly deviated parameters in comparison with singular instanton profile, see Ref. [17].

#### 4 Charged sphere in an instanton liquid

To get any estimate of the IL feedback on the presence of external field could be very practical for instanton liquid model. If so let us try to extract such an estimate from very simple example. Now we will search the minimum of effective action resolving the following boundary value problem

$$\Delta_r B = \frac{df[B]}{dB}, \quad B|_{r=r_0} = p(e), \quad \nabla_r B|_{r=r_0} = -\frac{e}{4\pi} \frac{1}{r_0^2}.$$

The source intensity here is controlled by  $e$ , and parameter  $r_0$  sets a radius of colour ball which we take as  $\sim 0.1\bar{\rho}$  (albeit it is unessential) in order to avoid the difficulties in resolving the singular boundary value problem of Eq.(42). The solution could be accomplished numerically probing such values of potential  $p(e)$  which provide with the solution going to zero magnitude at large values of  $r$ .

The IL density as a function of  $r$  is plotted in Fig.5 for ten various quantities of intensity. The extreme right hand side line corresponds to  $e/4\pi = 1$  and the extreme left hand side corresponds to  $e/4\pi = 0.1$ . The same quantity of spacing corresponds to the lines running to the right with intensity increasing. As it was expected the solution has the Yukawa like behaviour which is well seen in Fig.6 where  $\ln(Br)$  is plotted as a function of  $r$  for four various values of intensity with the pace of 0.1 and  $e/4\pi = 1$  for the upper line. Fitting it with the linear function gives the estimate of screening radius which looks as follows

$$R_d \sim (1.24 \Lambda_{QCD})^{-1},$$

Amazingly, this results remains practically unchanged for the whole interval of the intensities from  $e/4\pi = 0.1$  to  $e/4\pi = 1$  and implies that such a parameter characterizes (at least in this interval of values) the screening properties of IL itself. In a context of the model it looks like rather soft scale for the screening radius and might be taken as another confirmation of adiabatic approximation relevance for the Coulomb external field.

Eventually let us comment on how it is essential that we are dealing with singular (anti-)instanton ensemble as a saturating configuration. Apparently, the screening properties of effective Lagrangian for external field  $B$  could be provided by any stochastic configuration of small characteristic size. The assumption of superposition ansatz validity occurs crucial to have all the leading contributions coming from the 'mixed' (repulsive) component of  $G(A, B)$  again. Another solution of the problem may appear, of course, in the quantum approach but this discussion is out of this paper scope. Studying the pseudo-particle behaviour while inside (anti-)instanton medium ( $n \neq 0$ ) one could explore the interrelation of two mechanisms (the repulsive interaction and freezing the coupling constant out Ref.[8]) of fixing instanton size.

## 5 Conclusion

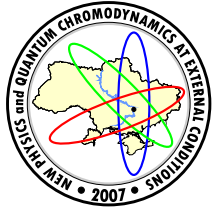
To summarize the foregoing, we will list the main results of our study. The effect of the screening of an external color field in an instanton liquid has been studied. For the case of a weak field and for the case of strong field in the long-wave approximation, we have derived the corresponding effective Lagrangians. It should be noted that, in the case of a strong field, there is a pronounced trend toward the restoration of gauge invariance. Thus, the Lagrangian in (41) demonstrates that it is possible to describe correctly the introduction of external sources at a qualitative level and to take effectively into account charge conservation [even within the simplest superposition form of an approximate solution to the Yang-Mills equations (1)], wherein precisely lies the physical meaning of gauge invariance. One encounters a similar situation in the case of superconductivity in Abelian theory (see, for example, [18]). We have derived a criterion that specifies the field strength above which the effect of the field on the instanton liquid may prove to be significant. For example of the model problem of an Euclidean charged color source, we have estimated the variations in the instanton liquid parameters versus the coupling constant. Also we have obtained an estimate for the Debye screening radius. We have indicated that the interplay of two mechanisms fixing the pseudoparticle size in an instanton liquid (repulsion and freezing of the coupling constant) is possible.

*Acknowledgements.* The paper was supported by INTAS-04-84-398, NATO PDD(CP)-NUKR980668. The authors are also indebted to Barbara Jacak and Tetsuo Hatsuda for stimulating discussions. We are grateful very much to organizers of the conference "NEW PHYSICS and QUANTUM CHROMODYNAMICS AT EXTERNAL CONDITIONS (2007)" in Dnipropetrovsk for kind hospitality.

## References

- [1] B. Jacak, Probing the Quark-Gluon Plasma, Lecture given at the NATO ARW, Crimea, May 2005;
- [2] B.G. Zakharov, JETP Lett. **80**, 67 (2004);  
N.N. Nikolaev, W. Schafer, B.G. Zakharov, and V.R. Zoller, hep-ph/0511285;  
Yu.V. Kovchegov, D.H. Rischke, Phys.Rev. **C56**, 1084 (1997);  
D.E. Kharzeev, Yu.V. Kovchegov, and E. Levin, Nucl.Phys. **A699**, 745 (2002);  
M. Gyulassy and L. McLerran, Nucl.Phys. **A750**, 30 (2005);  
R. Baier, Yu. L. Dokshitzer, D. Schiff, JHEP **09**, 033 (2001);  
A.V. Leonidov, Phys. Usp. **175**, 345 (2005).
- [3] A.E. Dorokhov, S.V. Esaibegyan, and S.V. Mikhailov, Phys.Rev. **D56**, 4062 (1997).
- [4] A. Di Giacomo, E. Meggiolaro, and H. Panagopoulos, Nucl.Phys. **B483**, 371 (1997).
- [5] A.E. Dorokhov, S.V. Esaibegyan, A.E. Maximov, and S.V. Mikhailov, Eur.Phys.J. **C13**, 331 (2000).
- [6] N.O. Agasian and S.M. Fedorov, JHEP **12**, 019 (2001).

- [7] D.I. Diakonov and V.Yu. Petrov, Nucl.Phys. **B245**, 259 (1984).
- [8] E.V. Shuryak, Phys.Rev. **D52**, 5370 (1995).
- [9] N.O. Agasian, S.M. Fedorov, Phys.Atom.Nucl. **67**, 376 (2004).
- [10] M. Hütter, hep-ph/9603280; M. Hütter, preprint LMU-Muenchen HEP 93/18 (1993).
- [11] C.G. Callan, R. Dashen, and D.J. Gross, Phys.Lett. **B66**, 375 (1977); Phys.Rev. **D17**, 2717 (1978).
- [12] E.-M. Ilgenfritz, B.V. Martemyanov, S.V. Molodtsov, M. Müller-Preussker, and Yu.A. Simonov, Phys.Rev. **D58**, 114508 (1998);  
A.E. Dorokhov, S.V. Esaibegyan, and S.V. Mikhailov, Phys.Rev. **D56**, 4062 (1997).
- [13] S.V. Molodtsov, G.M. Zinovjev, Physics of Particles and Nuclei Letters **2**, 331 (2005).
- [14] V.V. Goloviznin, S. V. Molodtsov, and A. M. Snigerev, Yad.Fiz. **56**, 123 (1993) [Phys.At.Nucl. **56**, 782 (1993)].
- [15] S.V. Molodtsov, G.M. Zinovjev, Theor.Math.Phys. **146**, 267 (2006) [hep-ph/0410395].
- [16] S.V. Molodtsov, A.M. Snigirev, and G.M. Zinovjev, Phys.Rev. **D60**, 056006 (1999); in *Lattice Fermions and Structure of the Vacuum*, ed. by V. Mitrjushkin and G. Schierholz (Kluwer Academic Publisher, Dordrecht, The Netherlands, 2000) p. 307; Yad.Fiz. **63**, 975 (2000) [Phys.At.Nucl. **63**, 903 (2000)].
- [17] S.V. Molodtsov and G.M. Zinovjev, hep-ph/0704.0141.
- [18] P.I. Arseev, N.K. Fedorov, and S.O. Loi'ko, Phys.Usp. **176**, 3 (2006).



## STRINGS AND QCD: PROBLEMS AND PERSPECTIVES

A.J. Nurmagambetov<sup>a</sup>

A.I. Akhiezer Institute for Theoretical Physics  
NSC “Kharkov Institute of Physics and Technology”, Kharkov, Ukraine

We review some cracks and gaps in the Stringy description of Strong interactions and the recent particular progress in their filling.

### 1 Introduction

Some years ago new physics got started with dual models of Strong interactions. Now it is referred to as String theory, a model of unification of the Fundamental Forces, early days of which was recently reviewed in [1]. Having the success as a Unified Theory, String theory was not so winning in hadronic physics. Nonetheless, some progress on this way was achieved last time, so String theory regaines control of this sector of Particle Physics stepwise. In this notes, prepared mostly for Particle (i.e. non-Stringy) Physics audience, we recall some of the old problems in the Stringy description of Strong interactions, reasons of neglecting the dual models in favor of Quantum Chromodynamics, what is wrong with QCD in the regimes where String theory works good and why it is reasonable to imagine on getting String theory back. We end up with reviewing the recent progress in phenomenological applications of Strings en route to realistic theory.

### 2 Different descriptions of hadronic physics

Hadronic physics can be divided into four regions of “phase space” which includes

1. Low energy limit;
2. Spectrum;
3. High energy limit, soft (with small scattering angles) processes;
4. High energy limit, hard (with large scattering angles) processes.

Depending on the standpoint in such a “phase space” one should take into account essentially different points of view on the description of hadrons. Low energy (in compare with a natural for QCD scale  $\Lambda_{QCD} \sim 300\text{MeV}$ ) limit is described by non-perturbative methods like QCD on lattices, instantons, as well as by some phenomenological models, examples of which are non-linear chiral sigma-models and non-relativistic quarks models. Perturbative QCD is handled with hard processes at high energy, and to lesser extent with soft processes. Regge theory is suited well for soft processes, describes the spectrum, and is consistent with low energy. Here we will mainly focus on the Regge approach.

Regge theory [2] describes the spectrum of hadrons and soft scattering amplitudes in terms of Regge trajectories  $\alpha(t)$  ( $t$  is the Mandelstam variable, the c.m.s. energy in the cross-channel). The spectrum consists of infinite number of states with spin  $J$ , and at mass  $M$

$$J = \alpha(M^2). \quad (1)$$

The soft scattering amplitudes go as

$$s^{\alpha(t)}, \quad (2)$$

where we have introduced another Mandelstam variable  $s$  (the c.m.s. energy in the direct-channel).

Experiments have verified that up to 10% amplitudes of hadrons inelastic scattering can be presented either as the sum of the direct channel resonances or as the sum of the Regge poles in the cross channel, see Fig.1 for four-point amplitudes. Such a feature of hadrons interactions was christened (global or Dolen-Horn-Schmid [3]) Duality. Applying Duality gives essentially better results of calculations in compare to summing up contributions of different channels required by QFT. It is worth mentioning that Duality is not exact, it is based on the “narrow

e-mail: <sup>a</sup>ajn@kipt.kharkov.ua

© Nurmagambetov A.J., 2007.

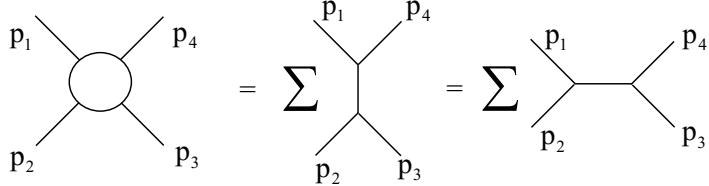


**Figure 1.** Duality of Strong interactions amplitudes.

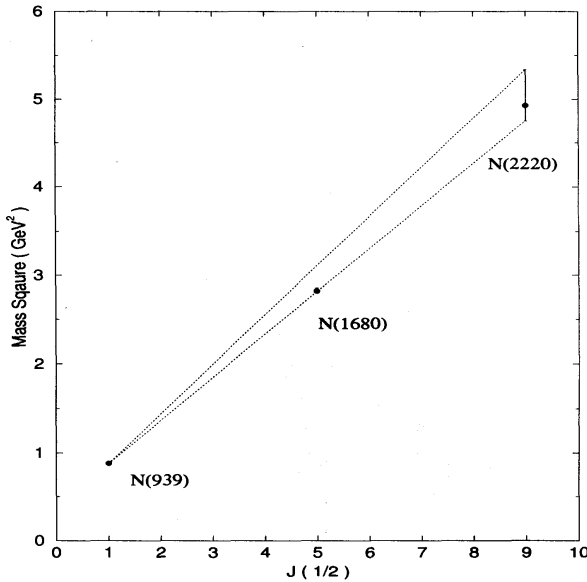


**Figure 2.** The Chew-Frautschi plot for the neutron Regge trajectory. Taken from Ref. [7].

resonances” approximation and does not take into account corrections to amplitudes coming from Unitarity of S-matrix [4].

The most striking confirmation of the Regge behavior (2) is the appearance of the known hadrons (up to spin as high as 4) on very linear trajectories

$$\alpha(t) = \alpha(0) + \alpha'(0) \cdot t, \quad (3)$$

with the Regge intercept  $\alpha(0)$  and the Regge slope  $\alpha'$ . This result is also not exact, it is known as the Chew-Frautschi conjecture [5] that allowed to divide hadrons into different w.r.t. Regge trajectories sets [6]. Then one may place all known hadrons and resonances at special plots as in Fig.2, where the Chew-Frautschi plot for neutron and corresponding baryonic resonances is given.

This example clearly demonstrates the relevance of an early proposal by Blankenbecler and Goldberger [8] that the nucleon is only the  $J = 1/2$  member of family which could also include higher  $J$  members. There are not “quarks” in the approach, any particles (stable/unstable) enter the theory on equal footing thus realizing “nuclear democracy”, and self-reproducing each other (“bootstrap” conjecture) [9, 10].

The Duality conjecture can be pushed forward with the requirement of local Duality. The latter is nicely described by the following duality-symmetric amplitude postulated by Veneziano [11]

$$A(s, t) = \frac{\Gamma(-\alpha(s))\Gamma(-\alpha(t))}{\Gamma(-\alpha(s) - \alpha(t))}, \quad (4)$$

$$\alpha(s) = \alpha(0) + \alpha'(0) \cdot s, \quad \alpha(t) = \alpha(0) + \alpha'(0) \cdot t.$$

Under the assumption that  $\text{Im } \alpha(s, t) = 0$ , and taking into account the asymptotic of Gamma-function, we get

$$A(s \rightarrow \infty, t \rightarrow 0) \sim s^{\alpha(t)}, \quad A(t \rightarrow \infty, s \rightarrow 0) \sim t^{\alpha(s)}. \quad (5)$$

On this account the spectrum is formed with equidistant resonances with masses

$$m_n^2 = \frac{(n - \alpha(0))}{\alpha'(0)}, \quad (6)$$

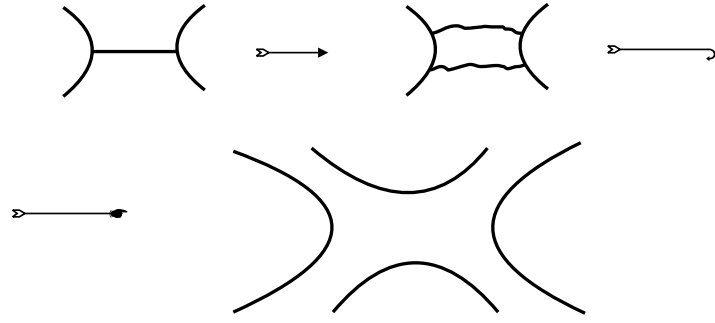


**Figure 3.** Reggeization of Feynman diagrams.

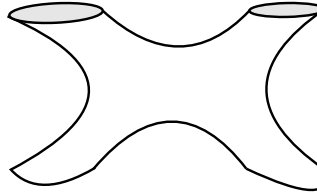


**Figure 4.** Reggeon exchange in closed string theory.

and such resonances may be treated as oscillations of a string. Hence properties of hadronic physics are encoded in the geometry of the string surface that appears after Reggeization of Feynman diagrams. This process is outlined in Fig.3. Duality can be recognized then as the topological equivalence of “rubber strips” in different channels.

There are general restrictions on a theory which have to be satisfied quite independently on a way of the theory formulation. One of them is the Froissart bound [12], which is a bound on the total cross section of s-channel at  $s \rightarrow \infty$ . Unitarity requires the following bound saturation

$$\sigma_{\text{total}} \sim \ln^2 \frac{s}{s_0}, \quad (7)$$

that corresponds to the amplitude

$$A_{\text{total}} \sim s \ln^2 \frac{s}{s_0}. \quad (8)$$

A single particle of spin  $J$  exchange amplitude behaves as  $A_J \sim s^J$  ( $s \rightarrow \infty$ ,  $t$  – fixed). Clearly, once  $J > 1$  we will get into trouble since the high spin single particle exchange violates the Froissart bound. This situation is improved in dual models (that is, in string theory), where we have a multiparticle with spin  $J = \alpha(M^2)$  exchange (Fig.4, Fig.5). It does not violate the Unitary bound iff  $\alpha(t) \leq 1$  at high energies in s-channel.

However, string theory predicts the soft scattering amplitudes at fixed angles (corresponding to the limit of  $s \rightarrow \infty$  with  $s/t$  fixed) to be

$$A_{\text{Veneziano}} \sim \exp(-\alpha' s f(\theta)), \quad (9)$$

with some function of the scattering angle  $f(\theta)$ . Meanwhile, experiments show a power law scattering

$$A_{\text{experimental}} \sim s^{2-\Delta/2}. \quad (10)$$

$\Delta$  in (10) is the number of external particles taking the part in the process, and the amplitude behavior (10) is successfully reproduced from QCD [13], [14].

There also are other obstacles coming from strings, e.g.: 1) The conformal anomaly that leads to very high ( $D=26$  for bosonic,  $D=10$  for fermionic strings) critical dimensions, in which the anomaly may be removed; 2)

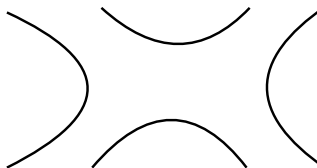


**Figure 5.** Pomeron exchange in open string theory.

Zero-mass gauge and spin-2 fields in the spectra of strings. They are hard to be associated with known hadronic resonances; 3) The tachyonic field as the ground state of bosonic strings.

All these and other facts remained little place for string theory as the theory of strong interactions, mainly favored QCD on this role.

QCD has been tested and confirmed with success in numerous high energy experiments. But QCD is not so much predictable for low energy physics, since it is non-perturbative there. Honestly speaking, confinement and mass generation still lack a satisfactory description. Another problem is to describe the interaction of high spin hadronic resonances in terms of QCD, when the Froissart bound should be presumably violated. Summing up, one may wonder about a compromise between string theory and QCD as a right way in the quest of more realistic theory.

### 3 Duality between strings and QCD

An apparent question then is how to make the happy marriage of strings and QCD? The concept of Duality helps to (at least particularly) answer the question.

Duality often means different things, but it commonly is the description of the same physics in terms of different concepts. For instance, we deal with particle-wave duality in QM, there is duality between Resonances and Regge poles, one may encounter strong-weak duality in statistical physics, Dirac monopole theory etc.

An early connection between  $SU(N)$  gauge theories in the  $N \rightarrow \infty$  limit and string theory was realized long ago by 'tHooft [15]. There is was drawn that the large  $N$  Yang-Mills (YM) theory Feynman diagrams are topologically the same as the planar diagrams of a string in flavor space of the model with a quark at the ends. But such an interpretation has nothing to do with space-time strings of the dual models.

More important result which relates superstring theory on  $AdS_5 \times S^5$  with  $\mathcal{N} = 4$  superconformal Yang-Mills  $SU(N)$  for large  $N$  theory was obtained by Maldacena [16]. This is known as AdS/CFT correspondence [17], [18]. Within the conjecture on AdS/CFT we have the exact duality between a four dimensional gauge theory and ten dimensional string theory compactifying on a five sphere  $S^5$ . After compactifying, the string modes propagate in the bulk of Anti-de-Sitter (AdS) five-dimensional space-time, while the dual gauge theory lives on the four dimensional time-like boundary of AdS space.

#### 3.1 A few words on AdS space and its boundary

Anti-de-Sitter space is a maximally-symmetric constant curvature space. It in particular means that the curvature tensor of AdS space obeys

$$R_{mnpq} = \frac{1}{R^2} (g_{mp}g_{nq} - g_{mq}g_{np}). \quad (11)$$

$R$  is a constant that characterize the size of AdS (the AdS radius).

As for Minkowski  $(d+1)$ -dimensional flat space with  $SO(1, d)$  isometry group of the metric

$$ds^2 = -dx_0^2 + \sum_{i=1}^d dx_i^2, \quad (12)$$

AdS space in  $(d+2)$ -dimensions has  $SO(2, d+1)$  isometry group corresponding to the following metric

$$ds^2 = -dx_0^2 - dx_{d+2}^2 + \sum_{i=1}^{d+1} dx_i^2. \quad (13)$$

The boundary-bulk relation between AdS and Minkowski space can be simply realized with their Euclidisation (see e.g. [19]). Minkowski space becomes  $d+1$ -dimensional Euclidean space which is isomorphic (through the stereographic projection) to the  $(d+1)$ -sphere, while AdS in  $(d+2)$  transforms into Minkowski space in  $(d+2)$  which is projected (like in the Poincare model) to the  $(d+2)$ -dimensional disk. Clearly, the  $d+1$ -sphere is the boundary of the  $(d+2)$ -disk. Getting back to usual (non-Euclidean) AdS and Minkowski space-times does not change the conclusion on the bulk-boundary relation.

#### 3.2 AdS/CFT correspondence on a nutshell

Let's now consider how Duality does the job. Our aim is to figure out a stringy way to describe D=4 YM. There is a spin-1 gauge field in the open string spectrum, hence we will use an open string. Open strings end on D(irichlet)-branes, thus  $U(1)$  gauge field is also confined on a D-brane. Taking a stack of  $N$  D-branes results in the enhancement of  $U(1)$  to  $U(N)$ . It happens due to open strings which end on different D-branes, Fig.6.

Since we are interested in a 4-dim. D-brane that corresponds to our visible world, the main candidate on this role is a D3-brane of (type IIB) superstring theory in D=10. Type IIB closed string theory with D3 branes is schematically described by the following effective action (see, for instance, [20] for details)

$$S_{\text{eff.}} = S_{\text{str. eff.}} + S_{\text{D3br. eff.}} + S_{\text{bulk-brane int.}} \quad (14)$$

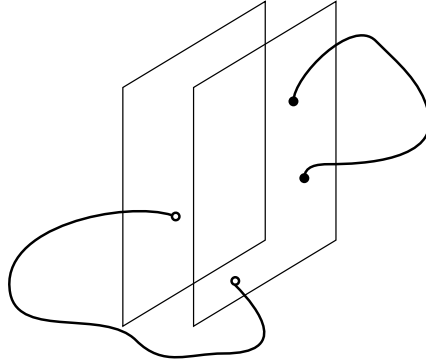


**Figure 6.** Interactions of D-branes via open strings.

The first term is the string theory effective action which in the low-energy limit is described by the type IIB supergravity action

$$S_{\text{IIB eff.}} = \frac{1}{k^2} \int \sqrt{-g} R + \dots \quad (15)$$

The D-dimensional gravitation coupling constant  $k$  is expressed through the string coupling constant  $g_s$  and the Regge slope  $\alpha'$  as  $k = g_s(\alpha')^{\frac{(D-2)}{4}}$ . In D=10 space-time  $k = g_s(\alpha')^2$  and once the string coupling constant becomes small, the effective action (15) gets transformed into the linearized action

$$S_{\text{IIB eff.}} \sim \int (\partial h)^2 + k(\partial^2 h)^2 h + \dots, \quad g_{mn} = \eta_{mn} + kh_{mn}. \quad (16)$$

Moreover, since the bulk-brane interaction term depends on  $k$ , the brane decouples from the bulk at  $k \rightarrow 0$ .

On the other hand the D3-brane is a solution to type IIB supergravity eqs. of motion [19], in particular with

$$ds^2 = f^{-1/2} \sum_{m,n=0}^3 dx^m \eta_{mn} dx^n + f^{1/2} (dr^2 + r^2 d\Omega_5^2), \quad (17)$$

$$f = 1 + \frac{R^4}{r^4}, \quad R^4 \sim g_s \alpha'^2 N.$$

On this side  $N$  is the magnetic charge of D3-branes counting via a 4th rank antisymmetric tensor gauge field  $A_4$

$$N = \int_{S^5} *F_5, \quad F_5 = dA_4 + \dots \quad (18)$$

The solution (17) is similar to that of the Black Hole type, with the horizon at  $r = 0$ . In the near horizon region  $r \ll R$  we get

$$ds^2 = \frac{r^2}{R^2} \sum_{m,n=0}^3 dx^m \eta_{mn} dx^n + R^2 \frac{dr^2}{r^2} + R^2 d\Omega_5^2. \quad (19)$$

The latter metric is the metric of  $AdS_5 \times S^5$ .

Since two open strings can form a closed string,  $g_{YM}^2 \sim g_s$ . We also have

$$g_{YM}^2 N \sim g_s N \sim \frac{R^4}{l_s^4} = \frac{R^4}{\alpha'^2}. \quad (20)$$

Once  $N$  is large and the string coupling constant is fixed and small we get the regime where the supergravity approximation is valid

$$\frac{R^4}{l_s^4} \gg 1. \quad (21)$$

On the other side, the regime with the small 'tHooft coupling constant corresponds to the perturbative Superconformal YM (SYM)

$$g_{YM}^2 N \sim g_s N \sim \frac{R^4}{l_s^4} \ll 1. \quad (22)$$

The common of two different sides is a D3-brane which in one regime describes the SYM theory, while in the other it corresponds to small fluctuations of supergravity fields over the AdS bulk metric. Hence we describe the same object in terms of different concepts. This is Duality.

Within the superconformal theory there is no room for massive particles, thus to construct the realistic QCD with massive quarks we have to break both SUSY and conformal invariance. It may be realized in many ways, most popular of which are

- Introducing a cut-off on the AdS geometry (see e.g. [21])

$$ds^2 = \frac{R^2}{z^2} \left( \sum_i dx_i^2 - dz^2 \right) + d\Omega_5^2, \quad (23)$$

$$0 \leq z \leq z_{\max}, \quad z_{\max} \sim \Lambda_{QCD}^{-1},$$

- Introducing a Black Hole which cuts-off AdS at the horizon [22]

$$ds^2 = \frac{R^2}{z^2} \left[ -f(z) dx_0^2 + dx_i^2 + f(z)^{-1} dz^2 \right] + d\Omega_5^2, \quad (24)$$

$$f(z) = 1 - z^4/z_T^4.$$

Such a cut-off is also equivalent to introducing the non-zero temperature  $T = (\pi z_T)^{-1}$ .

### 3.3 High energy QCD amplitudes from strings

Duality and String theory on AdS lead to a significant result [23]: the QCD high-energy amplitude power-law behaviour, eq. (10), is reproduced from the dual string theory. It comes in brief as follows. Consider the dual string on  $AdS_5 \times S^5$ , i.e. with the metric of D=10 space-time to be (19). Then, the gauge theory momentum is related to the string momentum as

$$p_{\text{YM}} = \frac{r}{R} P_{\text{str.}}. \quad (25)$$

Introducing the cut-off on AdS,  $r_{\min} \sim \Lambda R^2$  with the scale  $\Lambda$  to be of the lightest glueball mass, one relates the string tension to that of in the confining gauge theory

$$\sqrt{\alpha'} P_{\text{str.}} = \sqrt{\tilde{\alpha}'} p_{\text{YM}} \frac{r_{\min}}{r} \leq \sqrt{\tilde{\alpha}'} p_{\text{YM}}. \quad (26)$$

Hence a high energy process in gauge theory may involve all energy range processes on the string theory side.

Suppose that glueballs correspond to the closed string dilaton. We take  $\Phi = e^{ipx} \varphi(r, \Omega)$  and in the large  $N$  limit we get a very slow variation of the dilaton in the transverse to the AdS directions. Therefore, the amplitude of the gauge theory is that of the string theory integrated over transverse coordinates

$$A(p_{\text{YM}}) = \int dr d^5\Omega \sqrt{-g} A_{\text{str.}}(P_{\text{str.}}) \prod \varphi_i(r, \Omega). \quad (27)$$

We will also assume that the string scattering amplitude is dominated by the momenta at the string scale, i.e.  $r_{\text{scatt.}} \sim r_{\min}(\sqrt{\tilde{\alpha}'} p_{\text{YM}})$ . Then if  $\sqrt{\tilde{\alpha}'} p_{\text{YM}} \gg 1$ , that corresponds to the high-energy limit of gauge theory, the main contribution to the integral is at  $r_{\text{scatt.}} \gg r_{\min}$ ; and

$$\varphi(r, \Omega) \sim f(r/r_{\min}) F(\Omega) \sim (r/r_{\min})^{-\Delta} F(\Omega). \quad (28)$$

The latter relation comes from the superconformal side of AdS/CFT, since in the conformal theory a state  $f$  is completely defined by its conformal dimension  $\Delta$  (see [19] for details), and  $f \sim r^{-\Delta}$ . Though the considered case is non-conformal,  $f \sim r^{-\Delta}$  still applies for large  $r_{\text{scatt.}}$ .

Summing up the above we arrive at

$$A(p_{\text{YM}}) \sim \int dr r^3 \left[ \prod (r_{\min}/r)^\Delta \right] A_{\text{str.}}(p_{\text{YM}} R/r) \sim \left( \frac{\Lambda}{p_{\text{YM}}} \right)^{\Delta-4} \quad (29)$$

that is the same as in QCD result.

## 4 Resumé

The recent progress in the description of QCD within the AdS/CFT correspondence that was successful in

1. Realizing the hard scattering power law from string theory on AdS [23] (see also [24]);
2. Calculating the lightest glueball states masses [21, 25, 26];
3. Computing the spectrum of light hadrons [27];

4. Evaluating the amplitude of the single Pomeron exchange in a good agreement with the BFKL Pomeron on the QCD side [28]

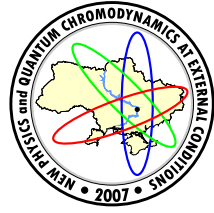
strongly suggests that many failures of string theory as a good model of physics of Strong interactions are due to not to having the wrong string theory, but to putting the right string theory on the wrong space-time background, i.e. on flat Minkowski space.

At the same time the development of String theory applications to hadronic physics is far from complete. Many problems have to be solved on this way; the longstanding Pomeron problem (see [28] for a review, and Refs therein) is among them, and clearly requires more sophisticated ideas than just AdS/CFT.

*Acknowledgements.* The author thanks Organizers and participants of NPQCD-2007 for a very creative atmosphere during the Conference. Special thanks to Volodya Skalozub for inviting me at NPQCD-2007, and to Igor Bandos for discussions of some points of the paper. Partial support under the INTAS Grant No 2005-2006-7928 is also acknowledged.

## References

- [1] P. Di Vecchia, arXiv:0704.0101[hep-th].
- [2] P.D.B.Collins, *An Introduction To Regge Theory And High-Energy Physics* (Cambridge, 1977), 445p.
- [3] R. Dolen, D. Horn and C. Schmid, Phys.Rev. **166**, 1768 (1968).
- [4] G. Veneziano, Phys.Rept. **9**, 199 (1974).
- [5] G.F. Chew and S.C. Frautschi, Phys.Rev.Lett. **7**, 394 (1961).
- [6] G.F. Chew and S.C. Frautschi, Phys.Rev.Lett. **8**, 41 (1962).
- [7] A. Tang and J.W. Norbury, hep-ph/0004078.
- [8] R. Blankenbecler and M.L. Goldberger, Phys.Rev. **126**, 766 (1962).
- [9] G.F. Chew, Science **161**, 762 (1968).
- [10] G.F. Chew, Phys.Today **23**, 23 (1970).
- [11] G. Veneziano, Nuovo Cim. **A57**, 190 (1968).
- [12] M. Froissart, Phys.Rev. **123**, 1053 (1961).
- [13] V.A. Matveev, R.M. Muradian, A.N. Tavkhelidze, Lett.Nuovo Cim. **7**, 719 (1973).
- [14] S.J. Brodsky and G.R. Farrar, Phys.Rev.Lett. **31**, 1153 (1973).
- [15] G. 't Hooft, Nucl.Phys. **B72**, 461 (1974).
- [16] J.M. Maldacena, Adv.Theor.Math.Phys. **2**, 231 (1998).
- [17] S.S. Gubser, I.R. Klebanov, A.M. Polyakov, Phys.Lett. **B428**, 105 (1998).
- [18] E. Witten, Adv.Theor.Math.Phys. **2**, 253 (1998).
- [19] O. Aharony, S.S. Gubser, J.M. Maldacena, H. Ooguri and Y. Oz, Phys.Rept. **323**, 183 (2000).
- [20] A.J. Nurmagambetov, Phys.Lett. **B436**, 289 (1998).
- [21] H. Boschi-Filho and N.R.F. Braga, hep-th/0604091.
- [22] E. Witten, Adv.Theor.Math.Phys. **2**, 505 (1998).
- [23] J. Polchinski and M.J. Strassler, Phys.Rev.Lett. **88**, 031601 (2002).
- [24] O. Andreev and W. Siegel, Phys.Rev. **D71**, 086001 (2005).
- [25] H. Boschi-Filho and N.R.F. Braga, Phys.Lett. **B525**, 164 (2002).
- [26] H. Boschi-Filho and N.R.F. Braga, Phys.Lett. **B560**, 232 (2003).
- [27] G.F. de Teramond and S.J. Brodsky, Phys.Rev.Lett. **94**, 201601 (2005).
- [28] R.C. Brower, J. Polchinski, M.J. Strassler and C.-I. Tan, hep-th/0603115.



## STUDY OF WEAK CHARGED CURRENT POLARIZED LEPTON-NUCLEON DEEP INELASTIC SCATTERING

S. N. Sevbitov<sup>a</sup>, T. V. Shishkina<sup>b</sup>

Belarusian State University, Minsk, Belarus

The processes of lepton-nucleon scattering, including ones with both polarized beams, at high energy provide relevant information about interaction and particles structure, allowing to analyze nucleon spin structure. As energy and experimental accuracy rise, necessity to improve Born cross sections and polarized asymmetries with higher order radiative corrections becomes substantial. In this report we stress on lowest order bremsstrahlung corrections treatment using helicity amplitudes method as applied to actual nowadays charged current lepton-nucleon deep inelastic processes, that allows to simplify matrix element calculation procedure. Real photon emission contribution is calculated by means of Lorentz-invariant formalism. Kinematical peculiarities on bremsstrahlung correction are discussed.

### 1 Introduction

The processes of deep inelastic lepton-nucleon scattering (DIS) are of interest at present and planned experiments, today with particular emphasis on both polarized beams interaction investigation, as it provides essential data on the internal structure of the nucleon spin. Special interest to charged current interaction is connected with the absence of large electromagnetic effects contribution to these processes. Some extensive reviews on nowadays and forthcoming experimental facilities on such processes can be found for instance in refs. [1, 2]. Asymmetries withdrew from phenomenological interaction parameters on certain experiments allow to extract detailed information on nucleon’s spin, concealed in polarized structure functions  $g_1$  and  $g_{2(5,6)}$  or individual quark contributions to nucleon’s spin. As expected, obtained information can be used to expand and to refine nucleon nature knowledge, to compare experimental data with other related experiments on nucleon structure (e.g. neutral current or pure electromagnetic DIS ones, which have been studied at a stretch of many years, see for instance refs. [3–5]) as well as with Standard Model predictions or perhaps to search deviations from it.

Processes in question have been investigated before mainly at Born approach, for instance in our previous papers (see in refs. [6, 7]) we realized Born level phenomenological analysis in comparison with quark-parton model approach, Born asymmetry analysis with stress on polarized structure functions extraction scheme. In this report we restrict oneself to detailed treatment of the bremsstrahlung correction calculation, as correct treatment with observed experimental data at high energies requires allowance for various radiative effects. Here to perform calculations we use the formalism of helicity amplitudes method offered firstly in ref. [8, 9] relevant for single and multiply bremsstrahlung processes. Using of such analytical method allows to practically avoid intermediate operations with traces of Dirac matrices products and undesirable calculations of cross-elements of  $S$ -matrix. This method of matrix element calculation mainly consists in special representation of 4-vectors of the photon polarization through expressions with bispinors, in using of special transformation rules likewise Chisholm identities and in treatment with  $\bar{u}_\mp(p)u_\pm(k)$  constructions as simple scalar function of  $p$  and  $k$  to cancellate unnecessary terms.

### 2 Radiative corrections

To calculate radiative corrections we employ quark-parton model, which allows to obtain reasonable quantitative predictions for nucleon and leptonic bremsstrahlung contributions. Feynman diagrams of processes in question

$$l(\bar{l}) + N \rightarrow \nu(\bar{\nu}) + X, \quad \nu(\bar{\nu}) + N \rightarrow l(\bar{l}) + X,$$

are presented in FIG.1 (one of the diagram in particular case vanishes, as neutrino contain no charge).

Let’s consider firstly the case of  $l_i = l$ ,  $l_f = \nu_l$ ,  $q_i$ ,  $q_f$ . To make use of helicity amplitudes method one should represent photon polarization vectors as following:

$$\hat{\varepsilon}^\pm = \hat{\varepsilon}_q^\pm = N_q \left[ \hat{q}'' \hat{q}' \hat{k} (1 \mp \gamma_5) - \hat{k} \hat{q}'' \hat{q}' (1 \pm \gamma_5) \right],$$

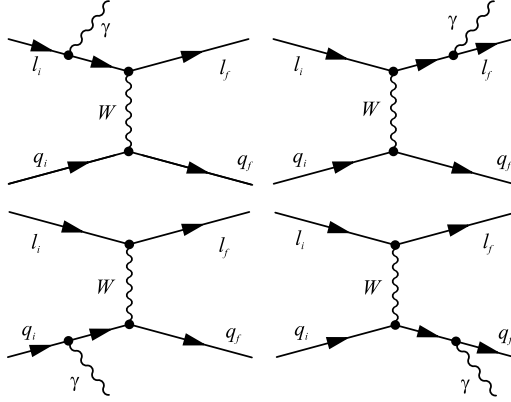


**Figure 1.** Photon bremsstrahlung diagrams for charged current lepton-nucleon DIS processes.

$$N_q = \left( 4\sqrt{-(q''q')(q''k)(q'k)} \right)^{-1}, \quad \varepsilon^\pm = 2N_q \left[ \hat{q}''\hat{q}'\hat{k}(1 \mp \gamma_5) - \hat{k}\hat{q}''\hat{q}'(1 \pm \gamma_5) \mp \varepsilon_{\nu\alpha\beta\gamma} q_\alpha'' q_\beta' k_\gamma \right],$$

where  $q', q'', p'_i, p''_f$  correspond to incoming  $l$  or outgoing  $\nu_l$  leptons and quarks  $q_i, q_f$  momenta,  $k$  is emitted photon momentum. This representation conserves common requirements  $\varepsilon^\pm \varepsilon^\pm = 0$ ,  $\varepsilon^\pm \varepsilon^{\pm*} = \varepsilon^\pm \varepsilon^{\mp*} = 1$ ,  $\varepsilon^\pm k = 0$ . Given form suitable for calculation of the leptonic bremsstrahlung term. For hadronic terms one should involve form, dependent on quark's momenta as following

$$\hat{\varepsilon}^\pm = \hat{\varepsilon}_p^\pm = e^{\pm i\varphi} N_p \left[ \hat{p}_f'' \hat{p}_i' \hat{k}(1 \mp \gamma_5) - \hat{k} \hat{p}_f'' \hat{p}_i'(1 \pm \gamma_5) \right] + \beta_\pm \hat{k}, \quad N_p = \left( 4\sqrt{-(p''_f p'_i)(p''_f k)(p'_i k)} \right)^{-1},$$

where

$$e^{\pm i\varphi} = (\varepsilon_q^\pm \varepsilon_p^\mp) = \frac{1}{4} Sp(\hat{\varepsilon}_q^\pm \hat{\varepsilon}_p^\mp) = N_p N_q Sp \left[ \hat{p}_f'' \hat{p}_i' \hat{k} \hat{q}'' \hat{q}' \hat{k}(1 \mp \gamma_5) \right].$$

Free parameter  $\beta$  can be omitted, as longitudinal component.

One can get the following expressions for matrix element using technique thoroughly described in ref. [9]

$$M_{-+-+} = -8 \frac{AN_p e^{+i\varphi} e_f}{\sqrt{2k^0 p'_{i0} p''_{f0}}} \bar{u}(q'') \hat{q}' u(p'_i) \bar{u}(p''_f) \hat{p}'_i u(q') D^W,$$

$$M_{----} = -8 \frac{A [N_q + N_p e^{-i\varphi} e_i]}{\sqrt{2k^0 p'_{i0} p''_{f0}}} \bar{u}(q'') \hat{p}''_f u(p'_i) \bar{u}(p''_f) \hat{q}'' u(q') D^W, \quad |A|^2 = \frac{e^2 G_F^2 M_W^4}{2} \frac{1}{4q_0'' q_0'}. \quad |A|^2 = \frac{e^2 G_F^2 M_W^4}{2} \frac{1}{4q_0'' q_0'}.$$

Here  $D^W$  –  $W$ -boson propagator, signs  $\pm$  refer to the particle helicity and photon polarization in the following order:  $l, \nu_l, \gamma, q_i, q_f; e_i$  and  $e_f$  – initial and final quark's charges.

The advantage of using helicity amplitudes method is that it allows to obtain squared matrix element directly without interference terms common in straightforward calculations. It is readily to show, that squared matrix element of the lepton-quark process  $lq_i \rightarrow \nu_l q_f$  with real photon emission have the following form

$$|M_{-+-+}|^2 + |M_{----}|^2 = \frac{4e^2 G_F^2}{q_0' q_0'' k_0 p'_{i0} p''_{f0}} \frac{M_W^4}{(Q^2 + M_W^2)^2} \times \left\{ \frac{1}{2} \frac{(p''_f q'')^2}{(p'_i k)(p''_f k)(q' k)(q'' k)} \left[ e_i(q' k)(q'' k) \left( \frac{q'}{q' k} - \frac{q''}{q'' k} \right) + (p'_i k)(p''_f k) \left( \frac{p'_i}{p''_i k} - \frac{p''_f}{p''_f k} \right) \right]^2 - \frac{e_f(q' q'')(p'_i q')^2}{(p'_i k)(p''_f k)} \right\}.$$

Similar formulas for other cases of electroweak lepton-quark scattering can be evolved using transformation rules

$$\begin{aligned} l\bar{q}_i \rightarrow \nu_l \bar{q}_f : \quad & p'_i \leftrightarrow p''_f, \quad e_i \leftrightarrow e_f \\ \bar{l}q_i \rightarrow \bar{\nu}_l q_f : \quad & q' \leftrightarrow q'', \\ \bar{l}\bar{q}_i \rightarrow \bar{\nu}_l \bar{q}_f : \quad & q' \leftrightarrow q'', \quad p'_i \leftrightarrow p''_f, \quad e_i \leftrightarrow e_f. \end{aligned}$$

We use here the following common notations for kinematical variables:

$$\begin{cases} Q_l = q' - q'', \quad Q_l^2 \approx -2q'q'', \\ Q_h = Q_l - k = p''_f - p'_i, \quad Q_h^2 \approx -2p'_i p''_f, \end{cases} \quad \begin{cases} X_i = -2p'_i q'', \\ S_i = -2p'_i q', \end{cases} \quad \begin{cases} u = -2p'_i k, \quad z_2 = -2q'' k, \\ v = -2p''_f k = u - Q_l^2 + Q_h^2, \\ z_1 = -2q' k = z_2 - Q_l^2 + Q_h^2, \end{cases}$$

where  $x_{h[l]} = -Q_{h[l]}^2/2p'Q_h$ ,  $y_{h[l]} = -2p'Q_{h[l]}/S$  – standard hadron and lepton scaling variables,  $p'$  and  $p''$  – nucleon and jet 4-momenta. To obtain cross sections or polarized asymmetry including radiative corrections one should switch from lepton-quark interaction to lepton-nucleon one integrating over quark momenta being carried in the nucleon, and over radiated photon momentum. If we suppose quark to possess momentum  $p'_i = x_{ih}p'$  with the probability of  $f(x_{ih})$ , the first integration over  $p'_i$  could be performed by means of the following substitutions:

$$f(x_{ih}) \rightarrow \frac{f(x_h)}{-2p'Q_h} = \frac{f(x_h)}{y_h S}, \quad S_i \rightarrow x_{ih}S \rightarrow x_h S = \frac{Q_h^2}{y_h},$$

$$X_i \rightarrow x_{ih}X \rightarrow x_h X = \frac{Q_h^2}{y_h} (1 - y_h) S, \quad u \rightarrow x_{ih}u \rightarrow x_h u, \quad v \rightarrow x_h u - Q_l^2 + Q_h^2,$$

keeping  $Q_h^2 = (Q_l - k)^2$ ,  $Q_l^2$ ,  $z_1$  and  $z_2$  unaltered. Here  $S = -(p' + q')^2$ .

To integrate over photon momentum one can use covariant method of integration described, for instance, in ref. [10, 11], permitting to integrate directly over Lorentz-invariant kinematical variables. Covariant calculation has advantage of missing of the sophisticated Monte-Carlo techniques but presence of the analytical integration as well as it can be carried out for various kinematical experimental configurations.

Firstly, let's imply the following suitable phase space transformation, allowing to derive from its general form the expression containing introduced before invariant variables:

$$\begin{aligned} d\Gamma = dM_h^2 \frac{d^3 p''}{2p_0''} \frac{d^3 q''}{2q_0''} \frac{d^3 k}{2k_0} \delta^{(4)}(Q_l - k - Q_h) &= dM_h^2 dQ_h^2 \frac{d^3 q''}{2q_0''} \frac{d^3 k}{2k_0} \delta[(Q_l - k)^2 + M_h^2] \delta[Q_h^2 - (p'' - p')^2] = \\ &= \frac{\pi S}{2} dy_l dQ_l^2 dy_h dQ_h^2 \frac{dz}{2\sqrt{R_z}}. \end{aligned}$$

Here  $R_z$  is the Gram determinant [12] of 4-vectors  $q'$ ,  $p'$ ,  $q''$ ,  $p''$

$$R_z = -\Delta_4(q', p', q'', p'') = - \begin{vmatrix} q'^2 & q'p' & q'q'' & q'p'' \\ p'q' & p'^2 & p'q'' & p'p'' \\ q''q' & q''p' & q''^2 & q''p'' \\ p''q' & p''p' & p''q'' & p''^2 \end{vmatrix},$$

which can be expressed as quadratic polynomial of  $z_1$  or  $z_2$  variables defined before

$$R_z = -Az^2 + 2Bz - C,$$

where the coefficients in the ultrarelativistic limit are

$$\begin{aligned} A_{1,2} &= y_l^2 S^2 + 4M^2 Q_l^2, \\ B_1 &= -2M^2 Q_l^2 (Q_l^2 - Q_h^2) + (y_l Q_h^2 - y_h Q_l^2) S^2 + \\ &+ (1 - y_l) S^2 Q_l^2 (y_l - y_h) - m^2 (2M^2 Q_h^2 + 2M^2 Q_l^2 - S^2 y_h y_l), \\ B_2 &= 2M^2 Q_l^2 (Q_l^2 - Q_h^2) + (1 - y_l) (y_l Q_h^2 - y_h Q_l^2) S^2 + \\ &+ S^2 Q_l^2 (y_l - y_h) - m^2 (2M^2 Q_h^2 + 2M^2 Q_l^2 - S^2 y_h y_l), \\ C_1 &= S^2 [Q_h^2 + (-1 + y_l - y_h) Q_l^2]^2 + 4m^2 Q_l^2 (y_l - y_h)^3 (1 - y_l), \\ C_2 &= S^2 [(1 - y_l) Q_h^2 - (1 - y_h) Q_l^2]^2 + 4m^2 Q_l^2 (y_l - y_h)^3 (1 - y_l)^{-1}. \end{aligned}$$

In presented above expression we simplified common phase space by means of auxiliary invariant variables  $z_1$  or  $z_2$ . Next one can employ the following integration scheme:

$$d\sigma \sim \int_{y_h \text{ min}}^{y_h \text{ max}} dy_h \int_{Q_h^2 \text{ min}}^{Q_h^2 \text{ max}} dQ_h^2 \int_{z_{\min}}^{z_{\max}} \frac{dz dy_l dQ_l^2}{y_h S \sqrt{R_z}} A,$$

or

$$\begin{aligned} d\sigma \sim \int_{y_l \text{ min}}^{y_l \text{ max}} dy_l \int_{Q_l^2 \text{ min}}^{Q_l^2 \text{ max}} dQ_l^2 \int_{z_{\min}}^{z_{\max}} \frac{dz dy_h dQ_h^2}{y_h S \sqrt{R_z}} A, \\ A = |M|^2 f_i(x_h, Q_h^2), \end{aligned}$$

and so on, dependently on desired final variables. Here matrix element  $|M|^2$  expressed in terms of  $Q_{l[h]}^2, y_{l[h]}$  and  $z_{1[2]}$  have the following form:

$$|M(S_i, X_i, Q_h, Q_l, z_{[1,2]})|^2 \sim \frac{e_f^2 S_i^2 Q_l^2}{2uv} + (z_2 - Q_l^2 - X_l)^2 \times \\ \times \frac{[Q_h^2 uv + (e_i^2 Q_l^2 z_1 z_2 - e_i Q_l^2 u(z_1 + z_2) + e_i Q_l^2 (u - v)(S_i z_2 - X_i z_1))]}{2uv z_1 z_2}$$

for  $l_i = l, l_f = \nu_l, q_i, q_f$  and

$$|M(S_i, X_i, Q_h, Q_l, z_{[1,2]})|^2 \sim \frac{Q_h^2 X_l^2}{2z_1 z_2} + \frac{e_f^2 Q_l^2 X_l^2}{2uv} + \frac{e_i^2 Q_l^2 (z_1 + Q_l^2 - S_i)^2}{2uv} + \\ + \frac{e_f X_l^2 [u Q_l^2 (z_1 + z_2) - (u - v)(S_i z_2 - X_i z_1)]}{2uv z_1 z_2}$$

for  $l_i = l, l_f = \nu_l, \bar{q}_i, \bar{q}_f$ .

Calculation of the integral over  $z$  can be carried out using simple table integrals of the form

$$I = \int_{z_{\min}}^{z_{\max}} \frac{z^n}{A(z - z_{\min})(z_{\max} - z)} dz, \quad n = -2 \dots 2.$$

To evaluate remaining integrals one should firstly use some parameterizations on quark distribution functions  $f_i(x_h, Q_h^2)$ , for instance QCD-based fits from ref. [13], and then choose final variables in which result cross-section or asymmetry will be expressed.

In order to calculate infrared contribution, one can apply the limits  $\lim_{k \rightarrow 0} (u - v) = 0$  and  $\lim_{k \rightarrow 0} (z_2 - z_1) = 0$  to presented above relations. When calculating this part requires using of some regularization method as being infrared divergent part, for instance by introducing virtual photon mass or applying dimensional regularization method. Here we didn't stress on soft photon emission contribution calculation, as virtual loop contribution and soft emission one, infrared divergent separately, compensate partly each other, remaining uncompensated part have minor influence on the asymmetries for processes in question as reduced factor.

Kinematical peculiarities and variables limits for these integrals are thoroughly described e.g. in ref. [12], here we give only kinematical relations, necessary for determination of the integration bounds. Imposed constrains on the physical region of invariants have the following form in terms of kinematical  $\lambda$ -functions (see [12])

$$\begin{aligned} \lambda(\lambda_S, \lambda_l, \lambda_q) &\leq 0, \quad \lambda(\lambda_q, \lambda_h, \lambda_k) \leq 0, \\ \lambda(\lambda_S, \lambda_\tau, \lambda_h) &\leq 0, \\ \lambda_k &= (y_l - y_h)^2 S^2, \quad \lambda_S = S^2 - 4m^2 M^2, \\ \lambda_l &= (1 - y_l)^2 S^2, \quad \lambda_q = y_l^2 S^2 + 4M^2 Q_l^2, \\ \lambda_h &= y_h^2 S^2 + 4M^2 Q_h^2, \quad \lambda_\tau = (1 - y_h)^2 S^2 - 4M^2 z_2, \\ \lambda(x, y, z) &= x^2 + y^2 + z^2 - 2xy - 2yz - 2xz. \end{aligned}$$

The boundary equations for this conditions can be expressed in the form of three equations

$$\begin{aligned} M^2(Q_l^2 - m^2)^2 + Q_l^2 y_l S^2 - m^2 S^2 y_l (1 - y_l) - Q_l^2 \lambda_S &= 0, \\ y_l^2 S^2 Q_h^2 + y_h^2 S^2 Q_l^2 - M^2 (Q_l^2 - Q_h^2)^2 - y_l y_h (Q_l^2 + Q_h^2) S^2 &= 0, \\ (2M^2 z_2^2 - 2m^2 M^2 + y_h S^2 + 2M^2 Q_h^2)^2 - \lambda_S \lambda_h &= 0, \end{aligned}$$

consequently.

One can obtain certain integration bounds for chosen final variables by combining these constraints with  $z_1^{\min, \max}$  and  $z_2^{\min, \max}$  emerging from the condition  $R_{z_{1,2}} \geq 0$ .

In ref. [6, 7] we numerically calculated hard real photon emission contribution with low photon energy cut parameter  $\varepsilon_{\text{cut}}$ , where unpolarized quark distribution functions from ref. [13] with polarized one from ref. [14] were used. In FIG.2 we cite comparison of the corrected polarized asymmetry

$$A_{\parallel} = \left( \frac{d^2 \sigma^{\uparrow\uparrow}}{dxdy} - \frac{d^2 \sigma^{\uparrow\downarrow}}{dxdy} \right) / \left( \frac{d^2 \sigma^{\uparrow\uparrow}}{dxdy} + \frac{d^2 \sigma^{\uparrow\downarrow}}{dxdy} \right),$$

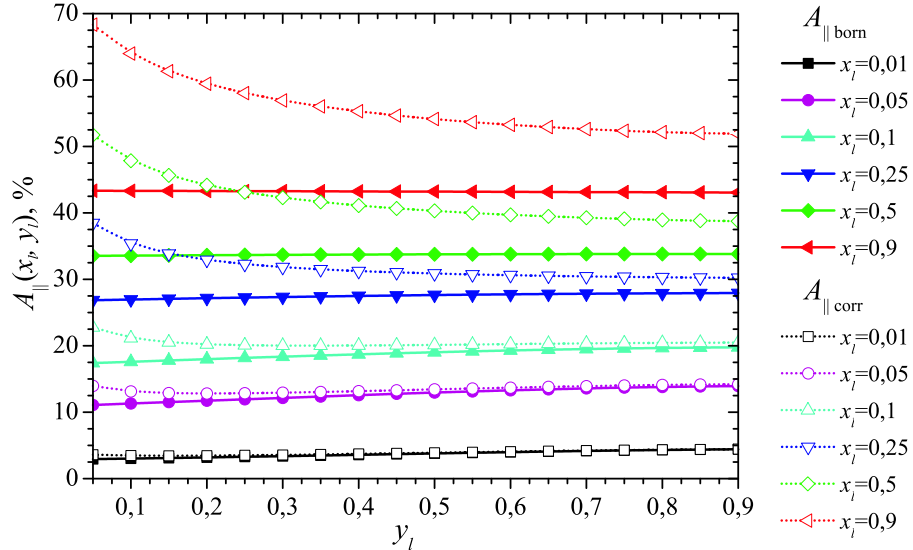


**Figure 2.** Born (solid line) and next to Born order (dotted line) longitudinal polarized asymmetry  $A_{\parallel}(x_l, y_l)$  for  $lN \rightarrow \nu_l X$  at  $E = 100$  GeV and  $\varepsilon_{\text{cut}} = 1$  MeV.

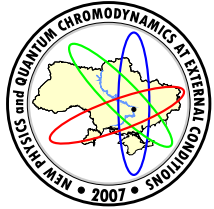
$d^2\sigma/dxdy$  – differential cross section,  $\uparrow$  ( $\downarrow$ ) corresponds to lepton helicity value  $-1(1)$ ,  $\uparrow$  ( $\downarrow$ ) for nucleon spin, parallel (antiparallel) to lepton momentum, with the Born one in lepton scaling variables  $x_l$  and  $y_l$ . Discussion of this result can be found in ref. [6, 7], here we only stress on significance of such contribution as it can be seen from Fig. 2.

As for multiply bremsstrahlung, such contributions can be obtained on the basis of single one by applying renormalization group equations, and will be treated hereafter.

In conclusion, real photon bremsstrahlung contribution calculated here affects significantly cross-sections and polarized asymmetries, so it's necessary to take into account such contribution, in that way it can be used for certain future experimental needs with the aim of precision DIS data extraction to improve accuracy of quark distribution functions as well as to detail nucleon's spin structure.

## References

- [1] J.Feltesse, A.Schäfer, Proc. of Workshop *Future Physics at HERA* (1996).
- [2] A.D.Roeck, T.Gehrman. Proc. of Workshop *Physics with Polarized Proto at HERA* (1997).
- [3] K.Abe *et al.* [E143 Collaboration], Phys.Rev. **D58**, 112003 (1998).
- [4] K.Abe *et al.* [E154 Collaboration], Phys.Rev.Lett. **79**, 1, 26 (1997).
- [5] K.Ackerstaff *et al.* [HERMES Collaboration], Phys.Lett. **B404**, 3, 383 (1997).
- [6] S.N.Sevbitov, T.V.Shishkina, Proc. NASB. (phys. and math. ser.) **4**, 72 (2006).
- [7] S.N.Sevbitov, T.V.Shishkina, Nonlin. Phen. in Compl. Syst. (in print).
- [8] P.de Causmaecker, R.Gastmans, W.Troost, T.T.Wu, Nucl.Phys. **B206**, 1, 53 (1982).
- [9] F.A.Berends, R.Kleiss, P.de Causmaecker *et al.*, Nucl.Phys. **B206**, 1, 61 (1982).
- [10] T.V.Kukhto(Shishkina), N.M.Shumeiko, Nucl.Phys. **B219**, 2, 412 (1983).
- [11] T.V.Shishkina, I.B.Marfin, *Scattering of polarized leptons on polarized nucleons: Phenomenology. Quark-parton model.* (BSU, Minsk, 2004).
- [12] E.Byckling, K.Kajantie, *Elementary particle kinematics.* (Mir, Moscow, 1975).
- [13] S.I.Alekhin, hep-ph/0508248.
- [14] E.Leader, A.V.Sidorov, D.B.Stamenov, Phys.Rev. **D73**, 034023 (2006).



## ELECTROWEAK PHASE TRANSITION IN A HYPERMAGNETIC FIELD

V. V. Skalozub<sup>a</sup>, V. I. Demchik<sup>b</sup>

Dnipropetrovsk National University, Dnipropetrovsk, Ukraine

The electroweak phase transition in a hypermagnetic field is analyzed within two approximations to the effective potential. One (weak field approximation to the Green functions) is recently applied in Ref. [1] where it was obtained that the external field makes the phase transition stronger first order. It is compared with other calculations which are based on the exact propagators and result in the phase transition which becomes weaker when the field strength is increased.

### 1 Introduction

Baryogenesis in the early universe is one of outstanding problems which is not solved, yet. Different scenarios are discussed in the literature. The most popular was proposed by Sakharov [2] 40 years ago. It requires as a necessary element a departure from thermal equilibrium. One of natural ways to produce that is the electroweak phase transition which must be strongly first order [3]. As it is known [4], in the standard model of elementary particles this transition is of first order for the Higgs boson masses  $m_H < 75 - 80$  GeV and becomes crossover or second order for heavier masses. So, for the realistic masses one has to consider some external conditions which are able to create the strong first-order phase transition. One of possibilities by analogy to superconductivity is an external magnetic field presence.

The electroweak phase transition in either external hypermagnetic field  $H_Y$  or external magnetic field  $H$  has been investigated in Refs. [5, 6] by means of different methods and in different approximations and different conclusions were obtained. In Refs. [5, 7] it was claimed that as in superconductivity the hypermagnetic field acts to increase the strength of the first order phase transition. On the contrary, in Refs. [6, 8] it was obtained that the phase transition becomes weaker when the additional terms omitted in the former papers were taken into consideration. A final conclusion within investigations carried out by analytic methods has been given in the survey [8] where, in particular, it was argued that due to the contributions of fermions, the electroweak phase transition in the standard model for the values of the mass  $m_H > 75$  GeV is crossover or second order. That is in correspondence with the results obtained in lattice simulations [9].

In recent paper by Sanchez, Ayala, Piccinelli [1] (SAP in what follows) the problem on the electroweak phase transition in a hypermagnetic field was investigated once else within a weak field approximation to the Green functions of charged particles. It has been concluded that the phase transition is of first order and becomes stronger if the external field is increased. The authors of this paper relate this obvious discrepancy with the results in Refs. [6, 8] with the approximation adopted in their approach. They consider the calculations in Refs. [6, 8] (BDS in what follows) as “strong external field approximation”. Because of the importance of the results mentioned the question on the cause of the discrepancies needs in a detailed analysis. That is the goal of the present paper. In fact, we will analyze not only the results obtained in different approximations to Green’s functions but also other peculiarities of calculations to make a reliable conclusion about the influence of the field on the electroweak phase transition.

### 2 The approach of SAP

The main goal announced in Ref. [1] is to investigate the influence of the ring diagram contributions on the electroweak phase transition in the hypermagnetic field. These terms play an important role because they give the first next-to-leading contributions to the effective potential at finite temperature having the order  $\lambda^{3/2}$  in coupling constant whereas the two-loop terms are of order  $\lambda^2$ , where  $\lambda$  stands for any coupling of the standard model: the weak isospin gauge coupling  $g^2$ , the hypercharge gauge coupling  $g_Y^2$ , the scalar field self-interaction  $\lambda$  [10, 11].

To analyze the results of the SAP paper, let us describe the approximations used therein. First of all we note that the contribution of fermion sector was restricted to the top quark only, the lepton part was omitted at all. Second that has been systematically applied was the so-called weak field approximation to the Green functions of charged fields. In practice that results in the replacement of the exact propagators of charged

e-mail: <sup>a</sup>skalozub@dsu.dp.ua, <sup>b</sup>vadimdi@yahoo.com

particles in the external hypermagnetic field by the truncated ones. The latter were obtained by the expansion of the former ones in a series in powers of  $g_Y H_Y$  up to the second order. These truncated functions were used in loop integrations. The authors claimed that this procedure corresponds to the relation  $g_Y H_Y \ll m^2 \ll T^2$  between the field strength, the typical mass in the problem and the temperature at the phase transition. Next, it was also assumed that the  $W$ -bosons do not interact with  $H_Y$  in the broken phase. As a result, to calculate the  $W$ -boson contributions to the effective potential the free-field propagator was substituted. As concerns the ring diagram parts, they also were calculated with the truncated propagators and moreover a number of next-to-leading terms have also been accounted for. As the authors noted themselves, just due to these parts of the effective potential (special type ring diagram contributions) the phase transition becomes a more strong first order as compared to the case when the effective potential takes into consideration the one-loop plus ring diagrams without the external field. In fact, this is the main conclusion. Its origin was not discussed in details therein.

### 3 The approach of BDS

In calculations carried out in Refs. [6, 8] the following assumptions and approximations were used: 1) The complete set of all the particles of the standard model – light and heavy fermions and bosons – was accounted for. 2) The exact propagators of charged particles in the external field  $H_Y$  were substituted into internal lines of the one-loop and ring diagrams. The reason for consideration of light fermions is that because at high temperatures in the field presence the effective potential contains the terms of the type  $\sim (g_Y H_Y)^2 \log(\pi T^2/m_f^2)$  which are nonperturbative. They are important for small fermion masses  $m_f^2 = m_D^2 + f^2 \phi^2$ , where  $m_D^2 = 1/3 g^2 T^2$  is the Debye temperature mass for fermion,  $f$  is the Yukawa coupling of the fermion to the scalar field  $\phi$ . 3) For different relations between the temperature, the field strength and the particle masses the different terms of the exact with respect to the external field effective potential are dominant. So, in the analysis of the phase transition numeric calculations were used. It was also observed that these results are in a qualitative agreement with that of obtained with the high temperature expansion of the derived effective potential. 4) The ring diagram contributions were calculated with exact propagators and the leading  $\sim T^2$  and the next-to-leading  $\sim (g_Y H_Y)^{1/2} T$  terms which obviously are also nonperturbative have been included. This point is very important and will be discussed in more detail below. 5) The contributions of the  $W$ -bosons in the broken phase is field-dependent. This is obvious and important for consistency of calculations. Really, the hypermagnetic field  $H_Y$  is generated by a current  $j_Y$  which in the broken phase is partially screened by the  $Z$ -field mass. But partially it contributes to other orthogonal combination which is massless and forms a familiar magnetic field  $H$ . Just this constituent of  $H_Y$  interacts with the  $W$ -bosons in the broken phase. This is a very important point because in the broken phase the  $W$ -boson spectrum in the field contains the mode  $\epsilon_{tach.}^2 = p_{||}^2 + m_W^2 - eH$  which may become unstable for  $eH > m_W^2$  [8]. Here  $p_{||}$  is the momentum component parallel to the external field direction. To treat this instability the ring diagrams of a special type must be accounted for also. Due to these terms the effective potential becomes real at high temperature and consistent. Thus, within the noted assumptions the calculations in Refs. [6, 8] have been carried out. The conclusion obtained was that due to the contribution of fermions in the field at finite temperature the phase transition becomes weaker not stronger as it is claimed in Ref. [5] and the SAP approach.

### 4 Comparison of SAP and BDS approaches

In this section we compare the explicit formulas for the effective potentials used in Ref. [1] and Refs. [6, 8]. First of all we note that because of the approximations used the results in the former paper actually correspond to the ones obtained in Ref. [5] in tree approximation, which actually has initiated the investigations and where the fermion contributions were neglected at all. In fact, we need to estimate and compare the role of two factors which are mainly the causes of the discrepancy in conclusion: 1) the influence of nonperturbative terms containing in the effective potential calculated with the exact propagators in BDS approach as compared to the truncated ones in SAP approach. 2) to compare in more detail the ring diagram contributions used in both approaches.

Remind once again that the role of fermions is crucial in the conclusions derived in BDS approach. One of the terms of the effective potential relevant is (see Eq.(58) in Ref. [8])

$$V^{(1)}(m_f, H_Y) = -\frac{\alpha_Y}{6\pi} \sum_f q_f^2 H_Y^2 \log\left(\frac{\pi T^2}{m_f^2}\right), \quad (1)$$

where  $m_f$  is a fermion mass at finite temperature,  $T$  – temperature,  $q_f$  – fermion charge in units of positron charge  $|e|$ ,  $\alpha_Y = g_Y^2/4\pi$ . Here we have substituted the asymptotic term of the effective potential in the limit of  $T \rightarrow \infty$ . At high temperatures light fermions give dominant contributions. On the other hand, this term is nonperturbative and therefore absent in Ref. [1].

Now, let us consider the contributions of ring diagrams. In the SAP approach, the contributions of either charged scalars or gauge bosons were included. They are of the form (Eqs. (57), (64) in Ref. [1])

$$V_{Higgs}^{(ring)} = - \sum_{i=1}^4 \frac{T}{12\pi} \left[ (m_i^2 + \Pi_1)^{3/2} - m_i^3 \right] + \sum_{i=1}^4 \frac{(g_Y H_Y)^2}{4\pi} \frac{\Pi_1}{48} \frac{T}{(m_i^2 + \Pi_1)^{3/2}}, \quad (2)$$

where  $i$  accounts for the charged scalars with the masses  $m_i$ ,

$$\Pi_1 = \frac{T^2}{4} \left( \frac{3}{4} g^2 + \frac{1}{4} g_Y^2 + 2\lambda + f^2 \right) \quad (3)$$

is the leading temperature contribution to the scalar field self-energies coming from the one-loop polarization tensor,  $g$ ,  $g_Y$ ,  $\lambda$ ,  $f$  are the coupling constants of the standard model. Similar term stands for the gauge boson contributions. For simplicity of comparison let us consider that in the restored phase. In this case the terms in the first line behave as  $\sim T^4$  and the ones in the second line are temperature independent  $\sim (g_Y H_Y)^2$ .

In BDS approach the corresponding part of the effective potential is given by the first line of Eq. (2) where one has to substitute  $\Pi_1$  by  $\Pi_\phi(0)$  from Ref. [8] Eq.(38):

$$\Pi_\phi(0) = \Pi_1 - 0.39 \frac{g_Y^2}{8\pi} (g_Y H_Y)^{1/2} T - \frac{g_Y^2}{2\pi^2} |q_f g_Y H_Y| \frac{m_f^2}{m_H^2}. \quad (4)$$

Here  $m_f$  and  $m_H$  are the fermion and Higgs boson masses and for comparison we have substituted only the top quark term  $m_f = m_t$ . We see again that the polarization tensor  $\Pi_\phi(0)$  contains the terms which could not be calculated by perturbation method. We present them in the high temperature limit for brevity. In the restored phase, this expression results in a number of temperature and field dependent terms in the effective potential which were missed in calculations with the truncated propagators. They are of the orders:  $\sim (g_Y H_Y)^{1/2} T^3$ ,  $\sim (g_Y H_Y) T^2$ ,  $\sim (g_Y H_Y)^{3/2} T$ . Other ones are inverse in temperature and could be neglected in given approximation. Thus, we come to the conclusion that if the truncated propagators were used the only one nonleading term  $\sim (g_Y H_Y)^2$  is taken into account in the ring diagram part that does not reproduce the properties of the exact with respect to the external field potential.

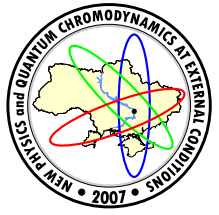
Next, the ring diagram part Eq. (2) possesses other shortcoming which needs a discussion. Remind that the ring contributions have the order  $\sim g_Y^3$  and are next-to-leading terms in coupling constant. This is seen from the first line of this equation as well as from Eq. (4). The two-loop diagram contributions have the order  $\sim g_Y^4$ . To obtain a correct estimate for the second line we note that the expansion parameters in the problem are  $(g_Y H_Y)/T^2$ ,  $m^2/T^2$ , and  $(g_Y H_Y)/m^2$ . By multiplying and dividing the terms of interest by  $T^4$  one finds their order  $\sim g_Y^{-1}$ . Formally, for small couplings, they give dominant contributions which are more essential than the one-loop ones. However, hence one has to conclude that this is inconsistent. The conclusions derived on this ground are not reliable.

Now let us compare the  $H_Y$  dependent terms in Eqs. (1) and (2) at high temperature in the restored phase. In this case  $\phi = m_i = 0$  and the factor standing under logarithm is  $3\pi/g_Y^2$  that is of order  $\sim 100$  for  $g_Y \sim 0.1$ . The value of logarithmic function is positive and not small. On the other hand, this contribution is of the type of the last one in Eq. (2) but having the opposite sign. That is important for the results obtained. But it was omitted in SAP paper.

As it follows from this and previous sections, the usage of the truncated propagators instead exact ones in not a good idea when the symmetry behavior in the external fields is investigated. The loop integration and the expansion in the field strength do not commute that results in different type effective potentials even in the weak field approximation. To convince ourselves in the correctness of our already obtained results, we have checked the calculations with the exact propagators and again came to the conclusion that due to the temperature and field dependent fermion part the increase in the field strength makes the phase transition weaker, not stronger. The accounting for the  $W$ -boson interaction in the broken phase plays an essential role. It influences the parameters of the first-order phase transition.

## References

- [1] A. Sanchez, A. Ayala, and G. Piccinelli, Phys.Rev. **D75**, 043004 (2007) [hep-th/0611337].
- [2] A. D. Sakharov, Pisma Zh.Eksp.Teor.Fiz. **5**, 32 (1967).
- [3] V. A. Rubakov and M. E. Shaposhnikov, Usp.Fiz.Nauk **166**, 493 (1996) [hep-ph/9603208].
- [4] K. Kajantie *et al.*, Nucl.Phys. **B544**, 357 (1999) [hep-lat/9809004].
- [5] M. Giovannini and M. E. Shaposhnikov, Phys.Rev. **D57**, 2186 (1998) [hep-ph/9710234].
- [6] V. Skalozub and M. Bordag, Int.J.Mod.Phys. **A15**, 349 (2000) [hep-ph/9904333].
- [7] P. Elm fors, K. Enqvist, and K. Kainulainen, Phys.Lett. **B440**, 269 (1998) [hep-ph/9806403].
- [8] V. Skalozub and V. Demchik, hep-th/9912071.
- [9] K. Kajantie *et al.*, Nucl.Phys. **B466**, 189 (1996) [hep-lat/9510020].
- [10] O. K. Kalashnikov, Fortschr.Phys. **32**, 525 (1984).
- [11] M. E. Carrington, Can.J.Phys. **71**, 227 (1993).



## ELECTRODYNAMICS OF CONTINUOUS MEDIA TAKING INTO ACCOUNT CORRELATIONS OF ELECTROMAGNETIC FIELD

A.I. Sokolovsky<sup>a</sup>, A.A. Stupka<sup>b</sup>

Dnipropetrovsk National University, Dnipropetrovsk, Ukraine

System of electromagnetic field and medium of nonrelativistic charged particles is considered. Investigation of statistical properties of electromagnetic field in the medium is conducted taking into account spatial correlations of the field on the basis of microscopic dynamics and the Bogolyubov method of reduced description of nonequilibrium processes. Equations for electromagnetic field in the medium are built and evolution of its correlations is investigated. The obtained results can be applied in various areas of theoretical physics.

### 1 Introduction

Description of electromagnetic (EM) processes in a medium is usually carried out only by Maxwell equations for average electric and magnetic fields  $E_n(x, t), B_n(x, t)$ , i.e. for condensate, using terminology of statistical physics. Description of the field besides of these parameters also by the normal and anomalous (in the presence of the condensate) distribution functions of photons corresponds to the study of kinetic stage of evolution of the EM field and is a natural generalization of the EM theory. The Fourier-transformed distribution functions give the binary correlation functions of the electric and magnetic fields. In our consideration subsystem of EM field is equal in rights with the subsystem of charged particles. Because of a macroscopic quantity and principle uncertainty of microscopic initial values of phase variables of particles and the EM field an investigation of the system should based on statistical mechanics even in the case of a classical theory. In this investigation EM field is considered as a random value and its complete description is given not only by average field but by all its correlation functions too.

Research of dynamics of correlations of the EM field began in statistical radiophysics on the basis of phenomenological Langevin methods. Significant contribution to the study of dynamics of correlations of the field was done in the quasilinear theory of plasma. However, this approach was based on phenomenological assumption about a randomness of phases of the field and degrees of freedom, which are described by correlations of the EM field, were not enough studied in it. Fundamental approach to description of statistical properties of the EM field in a medium was developed by Yu.L. Klimontovich, proceed from the hierarchy of equations for distribution functions of charged particles and transversal EM field obtained on the basis of microscopic dynamics. However, to truncate the hierarchy he used artificial procedures that can be applied only for some special cases. Last years investigations, in particular, conducted by Kharkiv school of statistical physics, showed universality of the N.N. Bogolyubov reduced description method (RDM) in theory on nonequilibrium processes. Nevertheless, in its study of kinetics of the transversal field in a hydrodynamic medium on the basis of the RDM equations for binary correlations of the field were not obtained, but the necessity of their accounting was discussed. Thus, in our work an actual problem is investigated, research of which will improve understanding of the course of electromagnetic processes in a medium, will give an example of consequent study of the fluctuation (correlation) phenomena.

The RDM was widely developed in works of the Kharkiv school of theoretical physics (S.V. Peletminsky and collaborators). Nonequilibrium states of the system are completely described by its statistical operator (SO)  $\rho(t)$ , which satisfies the quantum Liouville equation

$$\partial_t \rho(t) = -\frac{i}{\hbar} [\hat{H}, \rho(t)] \equiv \mathbf{L} \rho(t) \quad (1)$$

( $\hat{H}$  is the Hamilton operator,  $\mathbf{L}$  is the Liouville operator). According to the RDM in the presence in a system of several characteristic times its evolution passes through a series of stages. At each stage state of the system can be completely described by the relatively narrow set of parameters  $\text{Sp } \rho(t) \hat{\eta}_a$  (the reduced description parameters = RDP). For a stage at  $t \gg \tau_0$  SO of system depends on time only through the RDP  $\eta_a(t, \rho_0)$

$$\rho(t) \equiv e^{t \mathbf{L}} \rho_0 \xrightarrow[t \gg \tau_0]{} \rho(\eta(t, \rho_0)) \quad (\eta_a \equiv \text{Sp } \rho(\eta) \hat{\eta}_a), \quad (2)$$

e-mail: <sup>a</sup>alexsokolovsky@mail.ru, <sup>b</sup>antonstupka@mail.ru

© Sokolovsky A.I., Stupka A.A., 2007.

where SO  $\rho(\eta)$  does not depend on the initial SO of the system  $\rho_0$ . This relation expresses a general idea of the Bogolyubov functional hypothesis, which is basis of the RDM. Time  $\tau_0$  is duration of transition processes to the considered stage. Important tool of the RDM is the ergodic relation, which is the functional hypothesis taken in the leading order in a small parameters of the theory. In the case of small interaction in the system it can be written as follows

$$e^{\tau \mathbf{L}_0} \rho_0 \xrightarrow{\tau \gg \tau_0} e^{\tau \mathbf{L}_0} \rho^{(0)}(\eta^{(0)}(0, \rho_0)). \quad (3)$$

Ergodic relation can be used as a boundary condition to the Liouville equation (1) that allows to build a solvable in the perturbation theory integral equations for SO  $\rho(\eta)$  by a standard procedure. In our investigation perturbation theories in interaction and gradients were constructed.

## 2 Kinetics of the EM field in an equilibrium medium

Equations of motion for the EM field with average field and its correlations as the RDP have been obtained. Developed theory can be called the fluctuation electrodynamics (FED) in a equilibrium medium of the charged particles (or FED<sub>2</sub> in the case of account only binary correlations of the field). Equations of this theory give justified known results: theories of radiation transfer (for a weak nonuniform EM field), and the Vlasov theory with the self-consistent field (after an additional expansion in interaction). New motions of the correlation functions of the field are predicted. In nonrelativistic case a time equation for generating functional of the EM field is obtained.

In the Coulomb gauge and within the first order in interaction statistical operator of the system [1]

$$\rho(\eta) = \rho_q(\eta) w + \frac{i}{c\hbar} \int_0^\infty d\tau \int dx \left[ \hat{A}_n(x, \tau) \hat{j}_n(x, \tau), \rho_q(\eta) w \right] \quad (4)$$

is obtained. Here  $\hat{A}_n(x, t)$ ,  $\hat{j}_n(x, t)$  are vector potential of the transversal EM field and current in the Dirac picture

$$\begin{aligned} \hat{j}_n(x, t) &\equiv e^{t\mathbf{L}_0} \hat{j}_n(x), \quad \hat{A}_n(x, t) \equiv e^{t\mathbf{L}_0} \hat{A}_n(x) = \int dx' u_{nl}(x - x', t) \hat{B}_l(x') + \int dx' v(x - x', t) \hat{E}_n(x'); \\ u_{nl}(x) &\equiv i \int \frac{dk}{(2\pi)^3} \frac{\cos \omega_k t}{k} \tilde{k}_m \varepsilon_{nml} e^{ikx}, \quad v(x, t) \equiv - \int \frac{dk}{(2\pi)^3} \frac{\sin \omega_k t}{k} e^{ikx} \end{aligned} \quad (5)$$

( $\rho_q(\eta)$  is quasi-equilibrium SO of free EM field;  $\tilde{k}_n \equiv k_n/k$ ). The linear system of equations for the average field  $E_n(x, t)$ ,  $B_n(x, t)$

$$\partial_t \vec{E} = c \operatorname{rot} \vec{B} - 4\pi \vec{J}^{tr}, \quad \partial_t \vec{B} = -c \operatorname{rot} \vec{E}, \quad \operatorname{div} \vec{E} = 0, \quad \operatorname{div} \vec{B} = 0, \quad J_n^{tr}(x, t) = \operatorname{Sp} \rho(\eta(t)) \hat{J}_n^{tr}(x) \quad (6)$$

and its binary correlations

$$\begin{aligned} \partial_t (E_n^x E_l^{x'})_t &= c \operatorname{rot}_n (\vec{B}^x E_l^{x'})_t + c \operatorname{rot}'_l (E_n^x \vec{B}^{x'})_t - 4\pi \{ (J_n^{tr,x} E_l^{x'})_t + (E_n^x J_l^{tr,x'})_t \}, \\ \partial_t (E_n^x B_l^{x'})_t &= c \operatorname{rot}_n (\vec{B}^x B_l^{x'})_t - c \operatorname{rot}'_l (E_n^x \vec{B}^{x'})_t - 4\pi (J_n^{tr,x} B_l^{x'})_t, \\ \partial_t (B_n^x E_l^{x'})_t &= -c \operatorname{rot}_n (\vec{E}^x E_l^{x'})_t + c \operatorname{rot}'_l (B_n^x \vec{B}^{x'})_t - 4\pi (B_n^x J_l^{tr,x'})_t, \\ \partial_t (B_n^x B_l^{x'})_t &= -c \operatorname{rot}_n (\vec{E}^x B_l^{x'})_t - c \operatorname{rot}'_l (E_n^x \vec{B}^{x'})_t \end{aligned} \quad (7)$$

is received ( $(E_n^x E_l^{x'})_t \equiv \operatorname{Sp} \rho(t) \{ \hat{E}_n(x) \hat{E}_l(x') \} - 2E_n(x, t) E_l(x', t)$ , etc;  $\hat{J}_n(x)$  is gauge invariant current). Formulae (5) and (6) are equations of the fluctuation electrodynamics (i.e. equations of the FED<sub>2</sub>). Material equations for average transversal current  $J_n^{tr}(x, t)$  and current-field correlations are given by expressions

$$J_n^{tr}(x, t) = \int dx' M(x - x') E_n(x', t) + \int dx' N_{nl}(x - x') B_l(x', t); \quad (8)$$

$$(B_n^x J_l^{tr,x'})_t = \int dx'' \{ M(x' - x'') (B_n^x E_l^{x''})_t + N_{lm}(x' - x'') (B_n^x B_m^{x''})_t \} + S_{nl}(x - x'),$$

$$(J_n^{tr,x} B_l^{x'})_t = \int dx'' \{ M(x - x'') (E_n^{x''} B_l^{x'})_t + N_{lm}(x - x'') (B_m^{x''} B_l^{x'})_t \} + S_{nl}(x - x'),$$

$$(E_n^x J_l^{tr,x'})_t = \int dx'' \{ M(x' - x'') (E_n^x E_l^{x''})_t + N_{lm}(x' - x'') (E_n^x B_m^{x''})_t \} + T_{nl}(x - x'),$$

$$(J_n^{tr,x} E_l^{x'})_t = \int dx'' \{ M(x - x'') (E_n^{x''} E_l^{x'})_t + N_{lm}(x - x'') (B_m^{x''} E_l^{x'})_t \} + T_{nl}(x - x') \quad (9)$$

and confirm the Onsager principle. Microscopic expressions for kinetic coefficients  $M(x - x')$ ,  $N_{nl}(x - x')$  and free terms  $T_{nl}(x)$ ,  $S_{nl}(x)$  are found taking into account spatial dispersion:

$$M_k = \frac{\text{Im } G(k, \omega_k)}{\omega_k}, \quad N_{nl,k} = i\varepsilon_{nml} \tilde{k}_m \frac{\text{Re } G(k, \omega_k) - \chi}{\omega_k} \equiv i\varepsilon_{nml} k_m N_k; \quad (10)$$

$$S_{nl,k} = -8\pi T N_{nl,k}, \quad T_{nl,k} = -8\pi T \delta_{nl}^{tr} M_k \quad (11)$$

( $G(k, \omega)$  is transversal part of the current-current Green function;  $\delta_{nl}^{tr} \equiv \delta_{nl} - \tilde{k}_n \tilde{k}_l$ ). In stochastic approaches terms  $T_{nl}(x)$ ,  $S_{nl}(x)$  can be introduced as correlations of the Langevin forces. Values  $M_k$ ,  $N_k/c$  are conductivity and magnetic susceptibility of the system respectively. According equations (5), (7) dispersion relation for the transversal waves of the average EM field  $\omega = \pm \omega^{tr}(k) - i\delta^{tr}(k)$  is given by relations

$$\omega^{tr}(k) \equiv \sqrt{\omega_k^2 + \Omega^2 - 4\pi \text{Re } G(k, \omega_k) - \left( \frac{2\pi}{\omega_k} \text{Im } G(k, \omega_k) \right)^2}, \quad \delta^{tr}(k) \equiv -\frac{2\pi}{\omega_k} \text{Im } G(k, \omega_k), \quad (12)$$

which after additional expansion in interaction coincide with the results of other authors. For the first time concept of waves of binary correlations of the EM field is introduced and their dispersion relation is found

$$(E_n^k E_l^{k'}) : \delta(k, k') = \delta^{tr}(k) + \delta^{tr}(k'), \quad \omega(k, k') = \pm \omega^t(k) \pm \omega^t(k'). \quad (13)$$

The obtained by us equilibrium values of the correlations coincide with known ones.

For the EM field in equilibrium plasma kinetic equation for one-particle density matrix of photons  $n_{k\alpha, k'\alpha'}(t) \equiv \text{Sp } \rho(\eta(t)) c_{k\alpha}^+ c_{k'\alpha'}$  in the presence of the average field  $E_n(x, t)$ ,  $B_n(x, t)$  (we describe it by values  $\bar{c}_{k\alpha}(t) \equiv \text{Sp } \rho(\eta(t)) c_{k\alpha}$ ) is obtained [2]:

$$\partial_t n_{k\alpha, k'\alpha'} = i(\tilde{\omega}_k - \tilde{\omega}_{k'}) n_{k\alpha, k'\alpha'} - 2\pi (M_k + M_{k'}) \left( n_{k\alpha, k'\alpha'} - n_{k\alpha, k'\alpha'}^{eq} \right) + i(a_k \bar{c}_{-k\alpha} \bar{c}_{k'\alpha'} - c.c.) \quad (14)$$

( $a_k \equiv -2\pi(N_k + iM_k)$ ). Equation (26) is derived in the Coulomb gauge with an accuracy up to the second order in interaction and have to be considered together with the Maxwell equations (5), (7). In the framework of these equations frequencies of the EM waves  $\omega^{tr}(k)$ , decrement of their attenuation  $\delta^{tr}(k)$  and also renormalized photon frequencies  $\tilde{\omega}_k$  and relaxation time of the photon gas are found:

$$\tilde{\omega}_k = \omega_k - 2\pi c N_k, \quad n_{k\alpha, k'\alpha'}^{eq} = \frac{\delta_{k,k'} \delta_{\alpha,\alpha'}}{e^{\hbar\omega_k/T} - 1}, \quad \tau_{kk'} = 1/2\pi (M_k + M_{k'}). \quad (15)$$

In the case of nearly equal and large wave vectors, that corresponds to a weak nonuniform and fast changing EM field, dispersion relations for the waves of correlations coincide with the results described by (13). Consequently, theory of radiation transfer based on equation (26) is a special case of equations (6) for the correlation moments of the field.

We have studied nonrelativistic processes in the EM field interacting with classic equilibrium plasma too [3]. Consideration is performed in the Hamilton gauge within the second order in the field-plasma interaction. As RDP additional to standard ones (the average field  $E_n(x, t)$ ,  $B_n(x, t)$ ) binary correlations of the EM field are taken. Analogous to (5), (6) time equations for the mentioned RDP are obtained on the basis of the RDM. However, the medium is considered here only in the leading approximation i.e. as an ideal gas (the Maxwell plasma). The identity of the received Maxwell equations and results of the selfconsistent field approximation based on the Vlasov equation is proved after an additional expansion of the time dispersion with the help of formula

$$E_n(t - \tau) = \text{Sp } \rho(t - \tau) \hat{E}_n = \text{Sp } \rho(t) e^{-\tau \mathbf{L}} E_n \simeq \text{Sp } \rho(t) e^{-\tau \mathbf{L}_0} \hat{E}_n.$$

In this consideration contrary to the paper [1] the current has a longitudinal component and material equation is given by the formula

$$J_n(k, \omega) = \tilde{M}_{nl,k} E_l(k, \omega) + \tilde{N}_{nl,k} B_l(k, \omega) \quad (16)$$

with kinetic coefficients  $\tilde{M}_{nl,k}$ ,  $\tilde{N}_{nl,k}$ . Material equations for the current-field correlation functions have a similar to (10) form with replacement of  $M(x)$  by  $\tilde{M}_{nl}(x)$ . In the Maxwell plasma approximation is shown that equations for correlation moments correspond to the Onsager principle. For this case the known frequencies of the transversal EM waves are received  $\omega^{tr}(k) = \sqrt{c^2 k^2 + \Omega^2}$ , which do not attenuate for the Maxwell plasma. It is also shown that for small wave lengths, which are less than the Debye radius, the longitudinal EM waves do not exist  $\omega^l(k) = 0$  and this is explained by the effect of Cherenkov absorption. The equilibrium expressions for

the binary correlations of the field are obtained too, which coincide with ones calculated from the fluctuation-dissipation theorem. The waves of binary correlations are also considered with result similar to (13). The case of isotropic and homogeneous EM field is additionally analyzed, in which the average EM field is absent, and only transversal waves of binary correlations of the field with frequency  $2\omega^{tr}(k)$  are possible. It is necessary to emphasize that general consideration in paper [3] takes into account dynamics of the longitudinal EM field and can be applied not only for the Maxwell plasma.

The use of the Hamilton gauge in kinetics of the EM field gives an advantage connected with understanding of the vector potential of the field as its generalized coordinate. In this approach in the terms of the average field as RDP field kinetics in a quantum equilibrium medium is considered [4,5] and general expressions for the dispersion laws of the transversal and longitudinal EM waves are found. In the case of transversal waves results coincide with received in (12). It is shown that the Bogolyubov RDM can be used not only for obtaining of equations for RDP but also for calculation of an effective Hamilton operator of a subsystem. It was established that the effective Hamilton operator of the EM field in a equilibrium medium  $\hat{H}_{\text{ef}} = \sum_{k,\alpha} \hbar\omega_{\alpha}(k)(c_{k\alpha}^+ c_{k\alpha} + 1/2)$  describes quanta of waves of the average field. Studying of the EM field in a medium in the terms of quasiparticles is possible only for the case of a weak attenuation of the corresponding waves.

Next, in the Hamilton gauge equations of the FED for classical EM field in an equilibrium medium are built as a theory that describes nonequilibrium states of the field by the average field  $\xi_{\mu}(t) \equiv \xi_{in}(x, t) : E_n(x, t), B_n(x, t)$  and all its correlations  $g_{\mu_1 \dots \mu_s}(t)$  (or by all moments  $\eta_{\mu_1 \dots \mu_s}(t)$ ) [6]. With this purpose a classical perturbation theory for solution of the integral equation for the system SO is developed. The FED equations written in the terms of the generating functional of the field moments

$$F(\eta, u) = 1 + \sum_{s=1}^{\infty} \frac{1}{s!} \sum_{\mu_1 \dots \mu_s} u_{\mu_1} \dots u_{\mu_s} \eta_{\mu_1 \dots \mu_s}$$

$(\eta_{\mu} \equiv \xi_{\mu})$  have the form

$$\partial_t F(\eta(t), u) = F(\eta(t), u + \frac{\partial}{\partial \xi}) \sum_{\mu} u_{\mu} L_{\mu}(u, \xi) |_{\xi \rightarrow 0}, \quad L_{\mu}(u, \xi) \equiv i \sum_{\mu} c_{\mu\mu'} \xi_{\mu'} - 4\pi I_{\mu}(\xi + 4\pi T u), \quad (17)$$

where  $L_{\mu}(u = 0, \xi)$  it is the right hand side of equations for the average field in absence of correlations. Here  $I_{\mu}(\xi)$  is the average current, which is calculated with an accuracy up to the fourth order in EM interaction inclusive, that gives a material equation of the theory. It was established that dependence of electric current on correlations of the field is given by the formula  $I_{\mu}(\xi, g) = e^{[G(g, \partial/\partial \xi)]} I_{\mu}(\xi)$ , where  $G(g, u)$  is the generating functional of correlations. Function  $I_{\mu}(\xi, g)$  is nonlinear, local in time, but nonlocal in space taking into account spatial dispersion of material coefficients of the theory. A relation of the developed theory to description of the EM field by the average field and its binary correlations (i.e. to FED<sub>2</sub>) is discussed. It is shown that the equilibrium field is Gaussian (all its spatial correlations except of the binary ones  $(\xi_{\mu} \xi_{\mu'})$  are equal to zero) and  $(\xi_{\mu} \xi_{\mu'}) = 4\pi T \delta_{\mu\mu'}$ . Standard approach to solution of the obtained equation is discussed, in which nonlinear contributions to the current  $I_{\mu}(\xi)$  are considered as small values in accordance with their order in EM interaction. The current  $I_{\mu}(\xi)$  has been found up to the cubic terms in the field inclusive that allows on the basis of the obtained equations of the FED (17) to study problems of the nonlinear optics. In this consideration the Fourier transformed correlation function has dispersion  $\omega(k_1, \dots, k_n) = \sum_{i=1}^n \omega(k_i)$  i.e. is equivalent to product of the corresponding waves of the average EM field. Among subsequent applications of the FED equations theory of the Rayleigh scattering of the EM waves is considered.

### 3 Kinetics of the EM field in a hydrodynamic medium

A closed set of equations consisting of equations of hydrodynamics of a plasma medium and fluctuation electrodynamics taking into account binary correlations of the field (FED<sub>2</sub> in a hydrodynamic medium) has been built. New branches of oscillations in plasma are predicted that are related to effects of the correlations of the EM field. In particular, connected due to the EM interaction waves of transversal correlations of the field and medium densities are considered and their dispersion laws are found. Furthermore, an acoustic-optic effect for correlations of the field (i.e. an influence of sound waves on correlation of the EM field) is predicted. In homogeneous case for collisionless plasma oscillations of energies of subsystems of the field and plasma with double plasma frequency are found.

In the Hamilton gauge a new system of equations of electrodynamics in hydrodynamic medium is built that takes into account correlations of the field as new independent RDP [7,8]

$$\partial_t E_n = c \Delta_{nl} A_l - 4\pi J_n, \quad \partial_t A_n = -c E_n; \quad (18)$$

$$\begin{aligned} \partial_t (E_n^x E_l^{x'})_t &= c \Delta_{nm} (A_m^x E_l^{x'})_t + c \Delta'_{lm} (E_n^x A_m^{x'})_t - 4\pi \{(J_n^x E_l^{x'})_t + (E_n^x J_l^{x'})_t\}, \\ \partial_t (E_n^x A_l^{x'})_t &= c \Delta_{nm} (A_m^x A_l^{x'})_t - c (E_n^x E_l^{x'})_t - 4\pi (J_n^x A_l^{x'})_t, \end{aligned}$$

$$\begin{aligned}
\partial_t (A_n^x E_l^{x'})_t &= -c(E_n^x E_l^{x'})_t + c\Delta'_{lm}(A_n^x A_m^{x'})_t - 4\pi(A_n^x J_l^{x'})_t; \\
\partial_t (A_n^x A_l^{x'})_t &= -c(E_n^x A_l^{x'})_t - c(A_n^x E_l^{x'})_t, \\
\partial_t \pi_n &= -\frac{\partial t_{nl}}{\partial x_l} + \{\rho E_n + \frac{1}{c} e_{nlm} J_l B_m\} + \frac{1}{2}\{(\rho E_n)_t + \frac{1}{c} e_{nlm} (J_l B_m)_t\}, \\
\partial_t \sigma_a &= -\frac{\partial i_{an}}{\partial x_n}, \quad \partial_t \varepsilon = -\frac{\partial q_n}{\partial x_n} + J_n E_n + \frac{1}{2}(J_n E_n)_t
\end{aligned} \tag{19}$$

$((J_n B_l) \equiv (J_n^x B_l^x)$ , etc.;  $\Delta_{nl} \equiv \partial^2 / \partial x_n \partial x_l - \delta_{nl} \Delta$ ;  $\sigma_a, \pi_n, \varepsilon$  – densities of mass components, momentum, energy of the medium). For equations (10), (11) (FED<sub>2</sub> in a hydrodynamic medium) the corresponding system of material equations is obtained, which generalizes equations (7), (10) and contains new material equations for contributions of the field in hydrodynamic fluxes.

The waves of the average EM field and the waves of its binary correlations in an equilibrium medium were studied in the [1]. On the basis of the system of equations (10), (11) it is possible to study interaction of the mentioned waves with the sound waves in the medium. It leads to correction of dispersion laws of all waves in the system including effects of correlations of the field as new RDP. In the case of equilibrium medium obtained system of equations (10), (11) gives equations built in [3], where medium is considered as the Maxwell plasma, and equations (5), (6), where only dynamics of the transversal EM field is discussed. Among possible applications of equations (11) it is worth to mention construction of equations of radiation hydrodynamics. In the Hamilton gauge a homogeneous and isotropic system of plasma and EM field, described only by the correlations, is studied too [9]. An effect of the coupled oscillations of transversal correlations of the field and temperature of quasi-equilibrium medium with frequency that for the Maxwell plasma is approximately equal two plasma frequencies  $\omega \simeq 2\Omega$  is predicted. The obtained corresponding time equation for density of the medium energy has the form  $\partial_t \varepsilon(t) = \frac{1}{2V} \int d^3x (J_n^x E_n^x)_t$ . The predicted phenomenon is the most obvious correlation effect in this system. Besides, motion of a probe particle is studied in the mentioned EM field with the fixed wave vector. The effect of oscillations of its squared velocity is predicted with frequency of oscillations of correlations of the field  $\langle v^2 \rangle_t = \frac{(E_A)^{tr} \Omega^2}{2mc \omega^{tr}(k)} \sin 2\omega^{tr}(k)t$ .

Equations (10), (11) (the FED<sub>2</sub> in a hydrodynamic medium) obtained in the paper [7] are applied to the local equilibrium Maxwell plasma. For simplification correlations of the field are considered in a small radius limit. A closed system of equations for the Fourier components of deviations from the equilibrium of mass density, velocity and temperature of the plasma and correlations of the EM field is placed in the form [10]

$$\begin{aligned}
\partial_t \delta \sigma_k &= -ik_n \sigma \delta u_{nk}, \quad \partial_t \delta T_k = -ik_n w \delta u_{nk} + \frac{i}{2} \frac{\Omega^2}{qc} \delta (E_n Z_n)_k, \\
\partial_t \delta u_{nk} &= -ik_n (\alpha_\sigma \delta \sigma_k + \alpha_T \delta T_k) + i \frac{\Omega^2}{2c^2 r} \tilde{k}_n \{\delta (Z_l Z_l)_k - 8\pi \delta T_k\};
\end{aligned} \tag{20}$$

$$\partial_t \delta (E_n Z_l)_k = -ick \delta (Z_n Z_l)_t - i \frac{\Omega^2}{ck} \{\delta (Z_n Z_l)_k - 4\pi \delta_{nl}^{tr} \delta T_k\}, \quad \partial_t \delta (Z_n Z_l)_k = -ick \delta (E_n Z_l)_k \tag{21}$$

$(Z_{nk} \equiv \varepsilon_{nml} \tilde{k}_m B_{lk} = -ik A_{nk}^t, \alpha_\sigma \equiv T/m\sigma, \alpha_T \equiv 1/m, w \equiv 2T/3; q, r$  are constant parameters of the theory). On the basis of these equations interaction of transversal waves of correlations of the field (case of isotropic correlations) and sound waves is studied. Corrections to the dispersion laws of these waves due to EM interaction are found. An acoustic-optic effect for correlations of the field (an influence of sound waves on the waves of correlations) is predicted. In particular, the phenomenon of acoustic modulation of oscillations of correlations  $\omega = \sqrt{k_f^2 c^2 + \Omega^2} \pm k_s u$  is studied, which is similar to acoustic modulation of light by a sound wave. A new effect of oscillations of correlations with hydrodynamic frequencies  $\omega = k_s u, 2k_s u$  is predicted. In the Hamilton gauge a system of equations of FED<sub>2</sub> for the EM field in hydrodynamic nondissipative plasma with different velocities and temperatures of components is obtained too [11]. On the basis of these equations it is possible to study the influence of binary correlations of the EM field on processes in manycomponent plasma. In the case of coincided velocities and temperatures of the components the obtained equations give equations (10), (11) in the absence of dissipation. In the Hamilton gauge a system of equations FED<sub>2</sub> for a medium with one hydrodynamic and other equilibrium components is also derived [12]. Expressions for frequency and decrement of attenuation of longitudinal waves of the average EM field and its correlations of small radius are found. It is shown that only consequent account of dynamics of the system can give correct results

$$\begin{aligned}
\omega^l(k) &= \{\Omega - \xi^2/8\Omega + O(\lambda^3)\} + \{u^2/2\Omega - [8\theta(\psi(\theta + 8\pi\lambda_1) + \Delta) + \\
&+ 4(3\psi\theta + \Delta)\xi + 3u^2\xi^2]/16\Omega^3 + O(\lambda^3)\} k^2 + O(k^3)
\end{aligned} \tag{22}$$

$$\delta^l(k) = \{\xi/2 + O(\lambda^3)\} + \{-(\psi\theta + \Delta + u^2\xi)/2\Omega^2 + O(\lambda^3)\} k^2 + O(k^3) \tag{23}$$

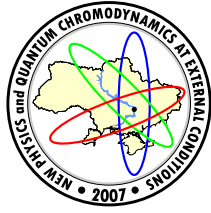
(here  $u$  is velocity of the sound;  $\theta, \xi, \Delta$  are kinetic coefficients of the theory,  $\lambda$  is small parameter of EM interactions).

#### 4 Conclusions

A nonrelativistic medium that consists of the charged and neutral particles was studied in the present research. Frequency of their collisions can be different in relation to time of observation, therefore cases of equilibrium, quasi-equilibrium and hydrodynamic medium were considered. The most nonequilibrium hydrodynamic states of the plasma medium is described in the consideration by mass densities, velocities and temperatures of the components. Frequency of EM interaction was estimated by us as the Langmuir one and considered as a value, which is much less than characteristic frequencies of motions in the medium. This allows to expand time dispersion everywhere in interaction and select spatial correlation functions of the EM field together with average field as the RDP. The most complete information about the system is contained in its statistical operator, which is a solution of the Liouville equation. This solution was obtained here in the terms of the mentioned RDP by the Bogolyubov reduced description method. Operators of the RDP satisfy the Peletminsky-Yatsenko condition and this simplifies the consideration. We use also a more general statistical operator of the leading order in small interaction. The system is studied at times, to which transition processes to the reduced description were finished, and there is a possibility to avoid using of the effective initial conditions. New nonrelativistic perturbation theories in EM interaction are developed that lead to the gauge invariant equations for the RDP. The performed analytical calculations lead to new contributions in equations of motion for RDP and generating functionals compared with stochastic theories. Wave solutions of the obtained equations have been studied. As a result description of the EM field in equilibrium medium by the Wigner distribution function of photons was elaborated. The coupled system of the hydrodynamic equations for plasma and equations for the average EM field and its binary spatial correlations was obtained too. Their wave solutions are found for the homogeneous and isotropic states of the system and in limit of small radius of correlations of the field. Extending of knowledge about the electromagnetic field by an investigation of properties of its correlations is the main result of the presented research.

#### References

- [1] A.I. Sokolovsky and A.A. Stupka, Visnyk of Dnipropetrovsk National University. Physics, Radio Electronics. **10**, 57 (2003) (in Ukrainian).
- [2] A.I. Sokolovsky and A.A. Stupka, The Journal of Kharkiv National University. Physical series. Nuclei, Particles, Fields. **642**, **3(25)**, 97 (2004) (in Ukrainian).
- [3] A.I. Sokolovsky and A.A. Stupka, Journal of Physical Studies. **10**, **1**, 12 (2006) (in Ukrainian).
- [4] A.I. Sokolovsky and A.A. Stupka, The Journal of Kharkiv National University. Physical series. Nuclei, Particles, Fields. **628**, **2(24)**, 87 (2004) (in Ukrainian).
- [5] A.I. Sokolovsky and A.A. Stupka, Problems of Atomic Science and Technology. **6(2)**, 268 (2001).
- [6] A.I. Sokolovsky and A.A. Stupka, Condensed Matter Physics. **8**, **4 (44)** 685 (2005).
- [7] A.I. Sokolovsky and A.A. Stupka, Ukrainian Mathematical Journal. **57**, **6**, 852 (2005).
- [8] A.I. Sokolovsky and A.A. Stupka, Visnyk of Dnipropetrovsk National University. Physics, Radio Electronics. **11(2)** 95 (2004) (in Ukrainian).
- [9] A.I. Sokolovsky and A.A. Stupka, The Journal of Kharkiv National University. Physical series. Nuclei, Particles, Fields. **721**, **1(29)** 61 (2006) (in Ukrainian).
- [10] A.I. Sokolovsky and A.A. Stupka, Proc. *11-th International Conference on Mathematical Methods of Electromagnetic Theory* (Kharkiv, 2006), 494.
- [11] A.I. Sokolovsky and A.A. Stupka, Proc. *10-th International Conference on Mathematical Methods of Electromagnetic Theory* (Dnipropetrovsk, 2004), 234.
- [12] A.I. Sokolovsky and A.A. Stupka, Proc. *13-th International Congress on Plasma Physics* (Kiev, 2006), 157.



## NONPERTURBATIVE CALCULATIONS IN QCD

I. L. Solovtsov<sup>a</sup>

International Center for Advanced Studies,  
P.Sukhoi Gomel State Technical University, Gomel, Belarus

A nonperturbative method based on variational perturbation theory in quantum chromodynamics is developed. A summation of threshold singularities and the nonperturbative character of the light quark masses are involved into consideration. The method is applied to find hadronic contributions to different physical quantities. It is shown that the approach allows us to describe well such objects as the hadronic contribution to the anomalous magnetic moment of the muon, the ratio of hadronic to leptonic tau-decay widths in the vector channel, the Adler function, the smeared function, and the hadronic contribution to the evolution of the fine structure constant.

### 1 Introduction

In comparing theoretical results with experimental data, it is important to connect measured quantities with “simplest” theoretical objects to check direct consequences of the theory without using model assumptions in an essential manner. Some single-argument functions which are directly connected with experimentally measured quantities can play the role of these objects. To compare theoretical results and experimental data one often uses the concept of quark-hadron duality, which establishes a bridge between quarks and gluons, a language of theoreticians, and real measurements with hadrons performed by experimentalists. The idea of quark-hadron duality was formulated in the paper by Poggio, Quinn, and Weinberg [1] as follows: Inclusive hadronic cross sections, once they are appropriately averaged over an energy interval, must approximately coincide with the corresponding quantities derived from the quark-gluon picture.

For many physical quantities and functions the corresponding interval of integration involves an infrared region and in this case nonperturbative effects may play an important role in their description. The following quantities and functions will be considered here:

- the ratio of hadronic to leptonic  $\tau$ -decay widths in the vector channel

$$R_\tau^V = R^{(0)} \int_0^{M_\tau^2} \frac{ds}{M_\tau^2} \left(1 - \frac{s}{M_\tau^2}\right)^2 \left(1 + \frac{2s}{M_\tau^2}\right) R(s); \quad (1)$$

- the “light” Adler function, which is constructed from  $\tau$ -decay data

$$D(Q^2) = -Q^2 \frac{d\Pi(-Q^2)}{dQ^2} = Q^2 \int_0^\infty ds \frac{R(s)}{(s + Q^2)^2}; \quad (2)$$

- the smeared  $R_\Delta$  function

$$R_\Delta(s) = \frac{\Delta}{\pi} \int_0^\infty ds' \frac{R(s')}{(s - s')^2 + \Delta^2}; \quad (3)$$

- the hadronic contribution to the anomalous magnetic moment of the muon (in the leading order in electromagnetic coupling constant)

$$a_\mu^{\text{had}} = \frac{1}{3} \left(\frac{\alpha}{\pi}\right)^2 \int_0^\infty \frac{ds}{s} K(s) R(s), \quad (4)$$

where  $K(s)$  is the vacuum polarization factor;

- and the strong interaction contribution to the running of the fine structure constant:

$$\Delta\alpha_{\text{had}}^{(5)}(M_Z^2) = -\frac{\alpha(0)}{3\pi} M_Z^2 \mathcal{P} \int_0^\infty \frac{ds}{s} \frac{R(s)}{s - M_Z^2}. \quad (5)$$

A common feature of all these quantities and functions is that they are defined through the function  $R(s)$ , the normalized hadronic cross-section, integrated with some other functions. By definition, all these quantities and functions include an infrared region as a part of the interval of integration and, therefore, they cannot be directly calculated within perturbative quantum chromodynamics.

The approach that we use here to describe the quantities and functions mentioned above is based on the nonperturbative expansion method [2–5]. In the case of QCD the method leads to a new small expansion parameter. Even going into the infrared region of small momenta where the running coupling becomes large and the standard perturbative expansion fails, the nonperturbative expansion parameter remains small and the approach holds valid. We formulate a model that also incorporates a summation of threshold singularities [6] and takes into account the nonperturbative character of the light quark masses [26].

## 2 Method

Here we formulate a method allowing us to derive nonperturbatively the Drell ratio  $R(s)$  within QCD. The approach based on a nonperturbative expansion method, variational perturbation theory, includes a summation of infinite number of threshold singularities and involves into analysis nonperturbative character of the quark masses.

### 2.1 Variational perturbation theory in QCD

The method on which we construct a description of the  $R$ -related quantities is variational perturbation theory (VPT). Within this approach, a quantity under consideration is represented in the form of the so-called floating or variational series. A certain variational procedure is combined with the possibility of calculating corrections to the principal contribution which allows the possibility of probing the validity of the leading contribution and the region of applicability of the results obtained. The VPT series is different from the conventional perturbative expansion and can be used to go beyond the weak-coupling regime. This allows one to deal with considerably lower energies than in the case of perturbation theory.

The new expansion parameter  $a$  is connected with the initial coupling constant  $g$  by the relation

$$\lambda = \frac{g^2}{(4\pi)^2} = \frac{\alpha_s}{4\pi} = \frac{1}{C} \frac{a^2}{(1-a)^3}, \quad (6)$$

where  $C$  is a positive constant. As follows from (6), for any value of the coupling constant  $g$ , the expansion parameter  $a$  obeys the inequality

$$0 \leq a < 1. \quad (7)$$

While remaining within the range of applicability of the  $a$ -expansion, one can deal with low-energy processes where  $\alpha_s$  is no longer small.

### Spacelike region

The positive parameter  $C$  plays the role of an auxiliary parameter of a variational type, which is associated with the use of a floating series. The original quantity, which is approximated by this expansion, does not depend on the parameter  $C$ ; however, any finite approximation depends on it due to the truncation of the series. Here we will fix this parameter using some further information, coming from the potential approach to meson spectroscopy. In the framework of this approach consider the following approximations to the renormalization group  $\beta$ -function, the functions  $\beta^{(3)}$  and  $\beta^{(5)}$ , which are obtained if one takes into consideration the terms  $O(a^3)$  and  $O(a^5)$  in the corresponding renormalization constant  $Z_\lambda$ . As has been shown in Ref. [3],  $C$  is determined by requiring that  $-\beta^{(k)}(\lambda)/\lambda$  tends to 1 for sufficiently large  $\lambda$ , which gives  $C_3 = 4.1$  and  $C_5 = 21.5$ . The increase of  $C_k$  with the order of the expansion is explained by the necessity to compensate for the higher order contributions. A similar phenomenon takes place also in zero- and one-dimensional models. The behavior of the functions  $-\beta^{(k)}(\lambda)/\lambda$  gives evidence for the convergence of the results, in accordance with the phenomenon of induced convergence.<sup>1</sup> The behavior of the  $\beta$ -function at large value of the coupling constant,  $-\beta^{(k)}(\lambda)/\lambda \simeq 1$ , corresponds to the infrared singularity of the running coupling:  $\alpha_s(Q^2) \sim Q^{-2}$  at small  $Q^2$ . In the potential quark model this  $Q^2$  behavior is associated with the linear growth of the quark-antiquark potential.

<sup>1</sup>It has been observed empirically [8, 9] that the results seem to converge if the variational parameter is chosen, in each order, according to some variational principle. This induced-convergence phenomenon is also discussed in [10].

The renormalization group  $\beta$ -function of the expansion parameter  $a$  is

$$\beta_a(a) = \mu^2 \frac{\partial a}{\partial \mu^2} = \frac{2\beta_0}{C} \frac{1}{F'(a)}, \quad (8)$$

where  $\beta_0 = 11 - 2f/3$  is the one-loop coefficient of the  $\beta$ -function in the usual perturbative expansion, and  $f$  is the number of active quarks, has a zero at  $a = 1$  that demonstrates the existence of the infrared fixed point of the expansion parameter and its freezing-like behavior in the infrared region. By finding the renormalization constants in the massless renormalization scheme with an accuracy  $O(a^3)$ , we find for the function  $F(a)$

$$F^{(3)}(a) = \frac{2}{a^2} - \frac{6}{a} - 48 \ln a - \frac{18}{11} \frac{1}{1-a} + \frac{624}{121} \ln(1-a) + \frac{5184}{121} \ln \left(1 + \frac{9}{2}a\right). \quad (9)$$

By solving the renormalization group equation (8) we find the momentum dependence of the running expansion parameter  $a(Q^2)$  as a solution of the following transcendental equation

$$\ln \frac{Q^2}{Q_0^2} = \frac{C}{2\beta_0} [F(a) - F(a_0)]. \quad (10)$$

For any values of  $Q^2$ , this equation has a unique solution  $a = a(Q^2)$  in the interval between 0 and 1.

By working at  $O(a^5)$  we obtain a more complicated result

$$F^{(5)}(a) = \frac{1}{5(5+3B)} \sum_{i=1}^3 x_i J(a, b_i) \quad (11)$$

with  $B = \beta_1/(2C\beta_0)$ , where the two-loop coefficient  $\beta_1 = 102 - 3f/3$ , and

$$\begin{aligned} J(a, b) = & -\frac{2}{a^2 b} - \frac{4}{a b^2} - \frac{12}{a b} - \frac{9}{(1-a)(1-b)} + \frac{4+12b+21b^2}{b^3} \ln a \\ & + \frac{30-21b}{(1-b)^2} \ln(1-a) - \frac{(2+b)^2}{b^3(1-b)^2} \ln(a-b) \end{aligned} \quad (12)$$

with

$$x_i = \frac{1}{(b_i - b_j)(b_i - b_k)}. \quad (13)$$

Here indices  $\{ijk\}$  are  $\{123\}$  and cyclic permutations. The values of  $b_i$  are the roots of the equation  $\psi(b_i) = 0$ , where the function  $\psi(a)$  is related to the  $\beta$ -function and is

$$\psi(a) = 1 + \frac{9}{2}a + 2(6+a)a^2 + 5(5+3B)a^3. \quad (14)$$

### Timelike region

The VPT approach allows one to perform the analytic continuation from the Euclidean to Minkowskian region self-consistently [11]. This situation is similar to the analytic approach in QCD [12, 13], where the connection space- and timelike regions can also be establish self-consistently [14, 15]. A problem of transition from the spacelike region, where the running coupling is initially defined by the renormalization group method, to the timelike region within perturbation theory has been discussed in [16–18].

Within the  $a$ -expansion method the timelike running coupling can be written as

$$\lambda_s^{(i)}(s) = \frac{1}{2\pi i} \frac{1}{2\beta_0} [\phi^{(i)}(a_+) - \phi^{(i)}(a_-)], \quad (15)$$

where  $a_{\pm}$  obey the equation

$$F(a_{\pm}) = F(a_0) + \frac{2\beta_0}{C} \left( \ln \frac{s}{Q_0^2} \pm i\pi \right). \quad (16)$$

At the level  $O(a^3)$ , the function  $\phi(a)$  has the form

$$\phi^{(3)}(a) = -4 \ln a - \frac{72}{11} \frac{1}{1-a} + \frac{318}{121} \ln(1-a) + \frac{256}{363} \ln \left(1 + \frac{9}{2}a\right). \quad (17)$$

Similarly, a more complicated expression for the  $O(a^5)$  level, we will use, can be derived.

## 2.2 Threshold singularities

In describing a charged particle-antiparticle system near threshold, it is well known from QED that the so-called Coulomb resummation factor plays an important role. This resummation, performed on the basis of the nonrelativistic Schrödinger equation with the Coulomb potential  $V(r) = -\alpha/r$ , leads to the Sommerfeld–Sakharov  $S$ -factor [19, 20]. In the threshold region one cannot truncate the perturbative series and the  $S$ -factor should be taken into account in its entirety. The  $S$ -factor appears in the parametrization of the imaginary part of the quark current correlator, which can be approximated by the Bethe–Salpeter amplitude of the two charged particles,  $\chi_{\text{BS}}(x=0)$  [21]. The nonrelativistic replacement of this amplitude by the wave function, which obeys the Schrödinger equation with the Coulomb potential, leads to the appearance of the resummation factor in the parametrization of the  $R(s)$ -function discussed above.

For a systematic relativistic analysis of quark-antiquark systems, it is essential from the very beginning to have a relativistic generalization of the  $S$ -factor. A new form for this relativistic factor in the case of QCD has been proposed in [6]

$$S(\chi) = \frac{X(\chi)}{1 - \exp[-X(\chi)]}, \quad X(\chi) = \frac{\pi \alpha}{\sinh \chi}, \quad (18)$$

where  $\chi$  is the rapidity which related to  $s$  by  $2m \cosh \chi = \sqrt{s}$ ,  $\alpha \rightarrow 4\alpha_s/3$  in QCD. The function  $X(\chi)$  can be expressed in terms of  $v = \sqrt{1 - 4m^2/s}$ :  $X(\chi) = \pi \alpha \sqrt{1 - v^2}/v$ . The relativistic resummation factor (18) reproduces both the expected nonrelativistic and ultrarelativistic limits and corresponds to a QCD-like Coulomb potential. Here we consider the vector channel for which a threshold resummation  $S$ -factor for the s-wave states is used. For the axial-vector channel the  $P$ -factor is required. The corresponding relativistic factor has recently been found in [27].

To incorporate the quark mass effects one usually uses the approximate expression proposed in [1, 22, 23] above the quark-antiquark threshold

$$\mathcal{R}(s) = T(v) [1 + g(v)r(s)], \quad (19)$$

where

$$T(v) = v \frac{3 - v^2}{2}, \quad g(v) = \frac{4\pi}{3} \left[ \frac{\pi}{2v} - \frac{3 + v}{4} \left( \frac{\pi}{2} - \frac{3}{4\pi} \right) \right], \quad v_f = \sqrt{1 - \frac{4m_f^2}{s}}. \quad (20)$$

The function  $g(v)$  is taken in the Schwinger approximation [24].

One cannot directly use the perturbative expression for  $r(s)$  in Eq. (19), which contains unphysical singularities, to calculate, for example, the Adler  $D$ -function. Instead, one can use the VPT representation for  $r(s)$ . Besides this replacement, one has to modify the expression (19) in such a way as to take into account summation of an arbitrary number of threshold singularities. Including the threshold resummation factor (18) leads to the following modification of the expression (19) (see [25] and [26]) for a particular quark flavor  $f$

$$\mathcal{R}_f(s) = [R_{0,f}(s) + R_{1,f}(s)] \Theta(s - 4m_f^2), \quad R_0(s) = T(v) S(\chi), \quad R_1(s) = T(v) \left[ r_{\text{vpt}}(s) g(v) - \frac{1}{2} X(\chi) \right]. \quad (21)$$

The usage of the resummation factor (18) reflects the assumption that the coupling is taken in the  $V$  renormalization scheme. To avoid double counting, the function  $R_1$  contains the subtraction of  $X(\chi)$ . The potential term corresponding to the  $R_0$  function gives the principal contribution to  $\mathcal{R}(s)$ , the correction  $R_1$  amounting to less than twenty percent for the whole energy interval [27].

## 2.3 Quark masses

The following considerations suggest the behavior of the mass function of the light quarks in the infrared region. A solution of the Schwinger–Dyson equations [28–31] demonstrates a fixed infrared behavior of the invariant charge and the quark mass function. The mass function of the light quarks at small momentum looks like a plateau with a height approximately equal to the constituent mass, then with increasing momentum the mass function rapidly decreases and approaches the small current mass.

This behavior can be understood by using the concept of the dynamical quark mass. This mass has an essentially nonperturbative nature. Its connection with the quark condensate has been established in [32]. By using an analysis based on the Schwinger–Dyson equations a similar relation has been found in [33]. It has been demonstrated in [34] that on the mass-shall one has a gauge-independent result for the dynamical mass

$$m^3 = -\frac{4}{3}\pi\alpha_s \langle 0|\bar{q}q|0\rangle. \quad (22)$$

A result obtained in [35] demonstrates the step-like behavior of the mass function. The height  $m$  of the plateau is given by the quark condensate (22). According to these results it is reasonable to assume that at small  $p^2$

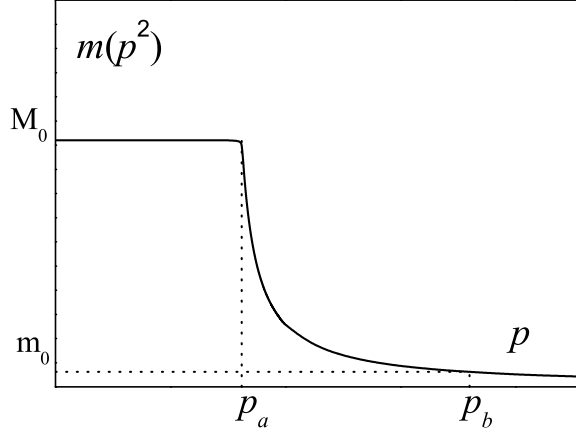


**Figure 1.** Effective quark mass.

**Table 1.**  $m_0^f$  and  $M_0^f$ .

$f$	$u$	$d$	$s$	$c$	$b$	$t$
$m_0^f$ (GeV)	0.004	0.007	0.130	1.35	4.4	174
$M_0^f$ (GeV)	0.260	0.260	0.450	1.35	4.4	174.0

the function  $m(p^2)$  is rather smooth (nearly constant). In the region  $p^2 > 1\text{--}2$  GeV the principal behavior of the function  $m(p^2)$  is defined by perturbation theory with the renormalization group improvement.

The following analysis was performed by using the model mass function  $m(p^2)$  that is shown in Fig. 1. We take the curve that connects the points  $p_a$  and  $p_b$  to have the form  $A^3/(p^2 - B^2)$ . The parameters  $m_0$  are taken from the known values of the running (current) masses at  $p_b = 2$  GeV. The quantities considered here are not too sensitive to the parameters of the heavy quarks and we take for  $c$ ,  $b$  and  $t$  quarks  $m^f(p^2) = m_0^f = M_0^f = \text{const}$ . The values of  $m_0^f$  at 2 GeV [36] and typical values of  $M_0^f$  are shown in Table 1.

### 3 Quantities and functions generated by $R(s)$

In this section we apply the model we have formulated to describe the physical quantities and functions connected with  $R(s)$ , described in the Introduction.

#### 3.1 Inclusive decay of the $\tau$ -lepton

The ratio of hadronic to leptonic  $\tau$ -decay widths in the vector channel is expressed by Eq. (20), where  $R^{(0)} = 3|V_{ud}|^2 S_{\text{EW}}/2$ ,  $|V_{ud}| = 0.9752 \pm 0.0007$  is the CKM matrix element,  $S_{\text{EW}} = 1.0194 \pm 0.0040$  is the electroweak factor, and  $M_\tau = 1776.99^{+0.29}_{-0.26}$  MeV is the mass of the  $\tau$ -lepton.[36] The experimental data obtained by the ALEPH and OPAL collaborations for this ratio is [1, 2, 38]:  $R_{\tau,V}^{\text{ALEPH}} = 1.775 \pm 0.017$ ,  $R_{\tau,V}^{\text{OPAL}} = 1.764 \pm 0.016$ .

In our analysis we use the nonstrange vector channel spectral function obtained by the ALEPH collaboration [1] and keep in all further calculations the value  $R_{\tau,V}^{\text{ALEPH}}$  as the normalization point. The range of estimates are obtained by varying the quark masses in the interval  $M_0^{u,d} = 260 \pm 10$  MeV (this band is fixed rather definitely by the  $D$ -function considered below) and  $M_0^{sL} = 450 \pm 100$  MeV.

#### 3.2 $D_V$ -function

The experimental information obtained by the ALEPH and OPAL collaborations allows us to construct the nonstrange vector channel “experimental”  $D$ -function. Within the analytic approach this function has been analyzed in [25]. Here we improve our method of constructing the “light”  $D$ -function by taking into account the global duality relation. We demonstrate that this Euclidean object is useful from the point of view of defining the effective masses of the light quarks.

In order to construct the Euclidean  $D$ -function (2) we use for  $R(s)$  the following expression

$$R(s) = R^{\text{expt}}(s) \theta(s_0 - s) + R^{\text{theor}}(s) \theta(s - s_0). \quad (23)$$

The continuum threshold  $s_0$  we find from the global duality relation [27]

$$\int_0^{s_0} ds R^{\text{expt}}(s) = \int_0^{s_0} ds R^{\text{theor}}(s). \quad (24)$$

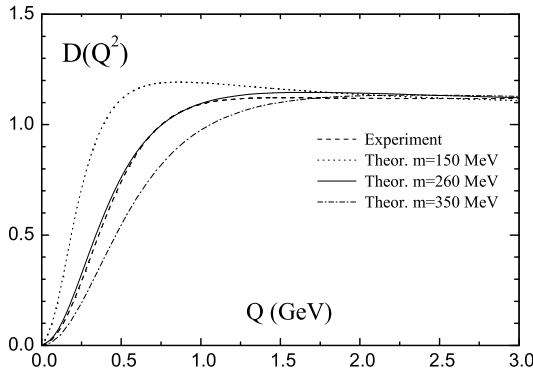


Figure 2.  $D$ -function for  $m = \text{const.}$

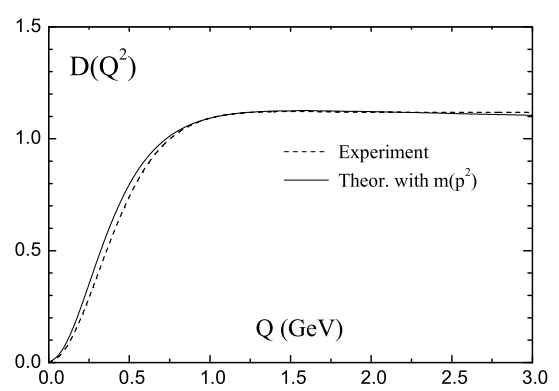


Figure 3.  $D$ -function for  $m = m(p^2)$ .

This gives  $s_0 \simeq 1.5$  GeV $^2$ . The value of  $s_0$  agrees with the results of papers [41–43]. A similar value of the continuum parameter is used in the QCD sum rules [28, 44]. Note, for some parameters there are two possible solutions of the duality condition (24). We exclude the second solution,  $s_0 \simeq 2.5$  GeV $^2$ , at this stage of the analysis due to the requirement of describing, in a self-consistent manner, different experimental data.

The low energy  $\tau$ -data in the nonstrange vector channel results in the curve for  $D(Q^2)$  in Fig. 2. In this figure we also plot three theoretical curves corresponding to masses of the light quarks of 150, 260 and 350 MeV. Fig. 2 demonstrates that the shape of the infrared tail of the  $D$ -function is quite sensitive to the value of the light quark masses. Note the experimental  $D$ -function turns out to be a smooth function without any trace of resonance structure. The  $D$ -function obtained in [46] from the data for electron-positron annihilation into hadrons also has a similar property.

The measured quantity  $R_\tau^V$  defined in Eq. (20) is less sensitive to  $m_u$  and  $m_d$  values than the infrared tail of the  $D_V$ -function. Varying the light quark masses over a wide range one finds  $R_\tau^V = 1.79$  for  $m_u = m_d = 150$  MeV and  $R_\tau^V = 1.66$  for 350 MeV. The values of masses  $m_u = m_d \simeq 260$  MeV agree with the experimental value  $R_\tau^V = 1.775 \pm 0.017$  [1]. The values of the light quark masses are close to the constituent quark masses and therefore incorporate nonperturbative effects. These values are consistent with other results in [47, 48] and [49] and with the analysis performed in [41, 50] and [51].

### 3.3 Smeared $R_\Delta$ -function

To compare experimental and theoretical results from the point of view of the quark-hadron duality, in Ref. [1] it was proposed to use the smeared function  $R_\Delta(s)$ . Instead of the Drell ratio  $R(s)$  defined in terms of the discontinuity of the correlation function  $\Pi(q^2)$  across the physical cut

$$R(s) = \frac{1}{2\pi i} [\Pi(s + i\epsilon) - \Pi(s - i\epsilon)], \quad (25)$$

the smeared function  $R_\Delta(s)$  is defined as

$$R_\Delta(s) = \frac{1}{2\pi i} [\Pi(s + i\Delta) - \Pi(s - i\Delta)], \quad (26)$$

with a finite value of  $\Delta$  to keep away from the cut. If  $\Delta$  is sufficiently large and both the experimental data and the theory prediction are smeared, it is possible to compare theory with experiment.

Equation (26) and the dispersion relation for the correlator  $\Pi(q^2)$  give the representation (3). Note that the smeared function  $R_\Delta(s)$  is defined both in the Minkowskian region of positive  $s$ , where a trace of resonances still remains for not too large  $\Delta$ , and in the Euclidean domain of negative argument  $s$ , where like the Adler function  $D(Q^2)$  the function  $R_\Delta(s)$  is smooth and monotone.

As with the Adler function we will construct the “light” experimental function  $R_\Delta(s)$ . For this purpose we match the experimental data taken with  $s < s_0$  to the theoretical result taken with  $s > s_0$  as in (25). The value  $s_0 \simeq 1.6$  GeV $^2$  is found from the duality relation (24).

For the charm region the value of  $\Delta$  is about 3 GeV $^2$ . An adequate choice in the case of the light smeared function is  $\Delta \simeq 0.5\text{--}1.0$  GeV $^2$ . In Figs. 4 and 5 the experimental and theoretical curves for  $\Delta = 0.5$  GeV $^2$ ,  $\Delta = 1.0$  GeV $^2$  and  $m = m(p^2)$  are shown. Let us emphasize that, for reasonable values of  $\Delta$ , in the spacelike region ( $s < 0$ ) there is a good agreement between data and theory starting from  $s = 0$ .

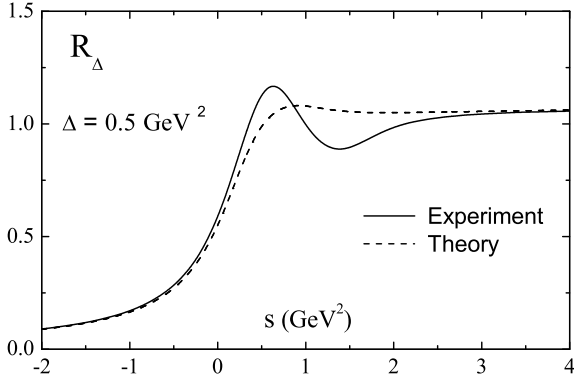


**Figure 4.** Smeared function for  $\Delta = 0.5 \text{ GeV}^2$ .

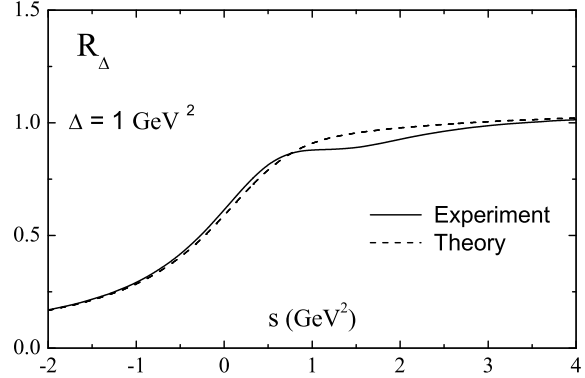


**Figure 5.** Smeared function for  $\Delta = 1.0 \text{ GeV}^2$ .

**Table 2.** Dependence of  $a_\mu^{\text{had}}$  on light quark masses.

		$a_\mu^{\text{had}} \times 10^{10}$			
$m_q$ (MeV)		LO		NNLO	
$q = u, d$	$q = s$	$m_q = \text{const}$	$m_q \neq \text{const}$	$m_q = \text{const}$	$m_q \neq \text{const}$
250	400	736	760	725	763
250	500	716	736	705	726
260	400	691	715	682	711
260	500	671	690	661	685

### 3.4 Hadronic contribution to $a_\mu$

The hadronic contribution to the anomalous magnetic moment of the muon in the leading order in the electromagnetic coupling constant is defined by (4), where  $\alpha^{-1} = \alpha(0)^{-1} = 137.035\,999\,11(46)$ , [36] and (see, for example, Ref. [24])

$$K(s) = \int_0^1 dx \frac{x^2(1-x)}{x^2 + (1-x)s/m_\mu^2}. \quad (27)$$

The muon mass is  $m_\mu = 105.7 \text{ MeV}$ .

The expression (4) can be rewritten in terms of the  $D$ -function

$$a_\mu^{\text{had}} = \frac{1}{3} \left( \frac{\alpha}{\pi} \right)^2 \frac{1}{2} \int_0^1 \frac{dx}{x} (1-x)(2-x) D \left( \frac{x^2}{1-x} m_\mu^2 \right). \quad (28)$$

It is should be emphasized that the expressions (4) and (28) are equivalent due to the analytic properties of the function  $\Pi(q^2)$ . If one uses a method that does not maintain the required properties of  $\Pi(q^2)$ , expressions (4) and (28) will no longer be equivalent and will imply different results (see Ref. [52] for details). This situation is similar to that which occurs in the analysis of inclusive  $\tau$ -decay, [53] where the initial integral, performed over an interval including a nonperturbative region, for which a perturbative QCD calculation is not valid, is transformed based on the analytic properties into a contour representation. Within VPT one is justified in doing this, and can use equally well either the expression (4) or the expression (28).

The value of  $a_\mu^{\text{had}}$  is not very sensitive to the values of the heavy quark masses, which we take as given in Table 1. The relative contributions of  $u$  and  $d$  quarks are about 72 and 19 %, respectively. The relative factor of 4 between  $u$  and  $d$  contributions is explained by the ratio of quark charges. The relative contribution of the  $s$ -quark to  $a_\mu^{\text{had}}$  is about 5–9 % for  $M_0^s = 400\text{--}500 \text{ MeV}$ . The contribution of the  $c$ -quark is about 2 %. Contributions of  $b$  and  $t$  quarks are very small.

There is a significant dependence on the mass parameters of the light quarks. This dependence we illustrate in Table 2. In our calculations we take into account the matching conditions at quark thresholds according to the procedure described in [15]. The mass parameters of  $u$  and  $d$  quarks are fixed rather well by the infrared tail of the light  $D$ -function and the value of  $R_\tau^V$ . If we take for the parameter  $M_0^{u,d}$  in the function  $m = m(p^2)$  the best fit value 260 MeV and vary  $M_0^s = 400\text{--}500 \text{ MeV}$ , we get

$$a_\mu^{\text{had}} = (702 \pm 16) \times 10^{-10}. \quad (29)$$

Note the method based on the analytic perturbation theory leads to very close result:  $a_\mu^{\text{had}} = (698 \pm 13) \times 10^{-10}$  [26].

Alternative “theoretical” values of  $a_\mu^{\text{had}}$  are extracted from  $e^+e^-$  annihilation and  $\tau$  decay data:  $(696.3 \pm 6.2_{\text{exp}} \pm 3.6_{\text{rad}}) \times 10^{-10}$  ( $e^+e^-$ -based), [54] which is  $1.9\sigma$  below the BNL experiment; [55]  $(711.0 \pm 5.0_{\text{exp}} \pm 0.8_{\text{rad}} \pm 2.8_{SU(2)}) \times 10^{-10}$  ( $\tau$ -based), [54] which is within  $0.7\sigma$  of experiment; and  $(693.4 \pm 5.3_{\text{exp}} \pm 3.5_{\text{rad}}) \times 10^{-10}$  ( $e^+e^-$ -based), [56]  $2.7\sigma$  below experiment. An even lower value  $(692.4 \pm 5.9_{\text{exp}} \pm 2.4_{\text{rad}}) \times 10^{-10}$  is given in [57]. The quantity  $a_\mu^{\text{had}}$  is rather sensitive to the light quark mass parameters, which are known only with large uncertainties. For this reason our estimations at this stage cannot give a preference to one or another of the above-mentioned fits to experimental data.

### 3.5 Hadronic contributions to $\Delta\alpha$

Consider the hadronic correction to the electromagnetic fine structure constant  $\alpha$  at the  $Z$ -boson scale. The evolution of the running electromagnetic coupling is described by

$$\alpha(s) = \frac{\alpha(0)}{1 - \Delta\alpha_{\text{lept}}(s) - \Delta\alpha_{\text{had}}^{(5)}(s) - \Delta\alpha_{\text{had}}^{\text{top}}(s)}. \quad (30)$$

The leptonic part  $\Delta\alpha_{\text{lept}}(s)$  is known to the three loop level,  $\Delta\alpha_{\text{lept}}(M_Z^2) = 0.03149769$ . [58] It is conventional to separate the contribution  $\Delta\alpha_{\text{had}}^{(5)}(s)$  coming from the first five quark flavors. The contribution of the  $t$ -quark is estimated as  $\Delta\alpha_{\text{had}}^{\text{top}}(M_Z^2) = -0.000070(05)$  [59].

The quantity  $\Delta\alpha_{\text{had}}^{(5)}(s)$  at the  $Z$ -boson scale can be represented in the form of the dispersion integral (5). The total function  $R(s)$  is

$$R(s) = 3 \sum_f Q_f^2 \mathcal{R}_f(s), \quad (31)$$

where  $Q_f$  is the quark electric charge of flavour  $f$ . For the calculation of  $R(s)$  we use (31) with five quark flavors  $f = u, d, s, c, b$ . Varying the parameters as has been described above and using  $m_c = 1.3\text{--}1.5$  GeV, we get

$$\Delta\alpha_{\text{had}}^{(5)}(M_Z^2) = (279.9 \pm 4.0) \times 10^{-4}. \quad (32)$$

This value is to be compared with predictions extracted from a wide range of data describing  $e^+e^- \rightarrow \text{hadrons}$  [57]:

$$\Delta\alpha_{\text{had}}^{(5)}(M_Z^2) = (275.5 \pm 1.9_{\text{expt}} \pm 1.3_{\text{rad}}) \times 10^{-4}. \quad (33)$$

The result based on the analytic perturbation theory is  $\Delta\alpha_{\text{had}}^{(5)}(M_Z^2) = (278.2 \pm 3.5) \times 10^{-4}$  [26]. We see that our result (32) is consistent with previous theoretical/experimental evaluations, with comparable uncertainties.

The relative error in (32) is substantially less than the error that appears in the quantity  $a_\mu^{\text{had}}$  and therefore one can obtain a more exact result. In comparison with the  $a_\mu^{\text{had}}$  result, where the contribution of the  $c$ -quark was about 2%, now it is about 30%. The contribution of the  $b$ -quark is about 5% and the relative contribution of the  $t$ -quark is a fraction of a percent.

## 4 Summary

A method of performing QCD calculations in the nonperturbative domain has been developed. This method is based on the variational perturbation theory in QCD, takes into account the summation of threshold singularities and the involvement of nonperturbative light quark masses.

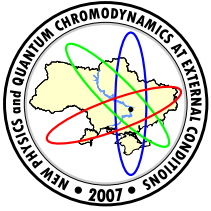
The following quantities have been analysed: the inclusive  $\tau$ -decay characteristic in the vector channel,  $R_\tau^V$ ; the light-quark Adler function,  $D(Q^2)$ ; the smeared  $R_\Delta$ -function; the hadronic contribution to the anomalous magnetic moment of the muon,  $a_\mu^{\text{had}}$ ; and the hadronic contribution to the fine structure constant,  $\Delta\alpha_{\text{had}}^{(5)}(M_Z^2)$ . We have demonstrated that the proposed method allows us to describe these quantities rather well.

*Acknowledgments.* It is a pleasure to thank D.V. Shirkov, A.N. Sissakian and O.P. Solovtsova for interest in the work and useful discussion. This work was supported in part by the International Program of Cooperation between the Republic of Belarus and JINR, the BRFBR, contract F06D-002.

## References

- [1] E. C. Poggio, H. R. Quinn and S. Weinberg, Phys. Rev. **D13**, 1958 (1976).
- [2] I.L. Solovtsov, Phys. Lett. **B327**, 335 (1994).
- [3] I.L. Solovtsov, Phys. Lett. **B340**, 245 (1994).
- [4] A.N. Sissakian and I.L. Solovtsov, Phys. Part. Nucl. **25**, 478 (1994).
- [5] A.N. Sissakian and I.L. Solovtsov, Phys. Part. Nucl. **30**, 461 (1999).

- [6] K. A. Milton and I. L. Solovtsov, Mod. Phys. Lett. **A16**, 2213 (2001).
- [7] K.A. Milton, I.L. Solovtsov and O.P. Solovtsova, Mod. Phys. Lett. **A21**, 1355 (2006).
- [8] W.E. Caswell, Ann. Phys. **123**, 153 (1979).
- [9] J. Killingbeck, J. Phys. **A14**, 1005 (1981).
- [10] P.M. Stevenson, Nucl. Phys. **B231**, 65 (1984).
- [11] H.F. Jones and I.L. Solovtsov, Phys. Lett. **B349**, 519 (1995).
- [12] D.V. Shirkov and I.L. Solovtsov, JINR Rapid Comm. No.2[76]-96, 5, hep-ph/9604363.
- [13] D.V. Shirkov and I.L. Solovtsov, Phys. Rev. Lett. **79**, 1209 (1997).
- [14] K.A. Milton and I.L. Solovtsov, Phys. Rev. **D55**, 5295 (1997).
- [15] K.A. Milton and O.P. Solovtsova, Phys. Rev. **D57**, 5402 (1998).
- [16] A.V. Radyushkin, Optimized Lambda-parametrization for the QCD running coupling constant in spacelike and timelike region, Preprint E2-82-159, JINR (1982), hep-ph/9907228.
- [17] N.V. Krasnikov and A.A. Pivovarov, Phys. Lett. **B116**, 168 (1982).
- [18] J. D. Bjorken, Two Topics In Quantum Chromodynamics, Preprint PUB-5103, SLAC (1989).
- [19] A. Sommerfeld, Atombau und Spektrallinien, Vol. 2 (Vieweg, Braunschweig, 1939).
- [20] A.D. Sakharov, Sov. Phys. JETP, **18**, 631 (1948).
- [21] R. Barbieri, P. Christillin and E. Remiddi, Phys. Rev. **D8**, 2266 (1973).
- [22] T. Appelquist and H.D. Politzer, Phys. Rev. Lett. **34**, 43 (1975).
- [23] T. Appelquist and H.D. Politzer, Phys. Rev. **D12**, 1404 (1975).
- [24] J. Schwinger, Particles, Sources and Fields, Vol. 2 (New York, Addison-Wesley, 1973, Perseus, 1998).
- [25] K. A. Milton, I. L. Solovtsov and O. P. Solovtsova, Phys. Rev. D **64**, 016005 (2001).
- [26] A.N. Sissakian, I.L. Solovtsov and O.P. Solovtsova, JETP Lett. **73**, 166 (2001).
- [27] I.L Solovtsov, O.P. Solovtsova and Yu.D. Chernichenko, Phys. Part. Nuclei Lett. **2**, No. 4, 199 (2005).
- [28] C.D. Roberts and S.M. Schmidt, Prog. Part. Nucl. Phys. **45**, S1 (2000).
- [29] C.S. Fisher and R. Alkofer, Phys. Lett. **B536**, 177 (2002).
- [30] C.S. Fisher and R. Alkofer, Phys. Rev. **D67**, 094020 (2003).
- [31] A.C. Aguilar, A.V. Nesterenko and J. Papavassiliou, hep-ph/0510117.
- [32] H.D. Politzer, Nucl. Phys. **B117**, 397 (1976).
- [33] N.V. Krasnikov and A.A. Pivovarov, Sov. Phys. J. **25**, 55 (1982).
- [34] V. Elias and M.D. Scadron, Phys. Rev. **D30**, 647 (1984).
- [35] L.J. Reinders and K. Stam, Phys. Lett. **B195**, 465 (1987).
- [36] Particle Data Group, S. Eidelman *et al.*, Phys. Lett. **B592**, 1 (2004).
- [37] ALEPH Collab., R. Barate *et al.*, Eur. Phys. J. **C4**, 409 (1998).
- [38] M. Davier and Ch. Yuan, Nucl. Phys. B (Proc. Suppl.) **123**, 47 (2003).
- [39] OPAL Collab., K. Ackerstaff *et al.*, Eur. Phys. J. **C7**, 571 (1999).
- [40] S. Peris, M. Perrottet and E. de Rafael, JHEP **9805**, 011 (1998).
- [41] A.E. Dorokhov, Phys. Rev. **D70**, 094011 (2004).
- [42] E. de Rafael, Phys. Lett. **B322**, 239 (1994).
- [43] S. Narison, Nucl. Phys. B (Proc. Suppl.) **96**, 364 (2001).
- [44] M.A. Shifman, A.I. Vainshtein and V.I. Zakharov, Nucl. Phys. **B147**, 385 (1979); Nucl. Phys. **B147**, 448 (1979); Nucl. Phys. **B147**, 519 (1979).
- [45] L.J. Reinders, H.R. Rubinstein and S. Yazaki, Phys. Rep. **127**, 1 (1985).
- [46] S. Eidelman, F. Jegerlehner, A.L. Kataev, O. Veretin, Phys. Lett. **B454**, 369 (1999).
- [47] A.I. Sanda, Phys. Rev. Lett. **42**, 1658 (1979).
- [48] J.J. Sakurai, K. Scilcher and M.D. Tran, Phys. Lett. **B102**, 55 (1981).
- [49] D.V. Shirkov and I.L. Solovtsov, in: Proc. Int. Workshop on  $e^+e^-$  Collisions from  $\phi$  to  $J/\Psi$ , eds. G. V. Fedotovich and S. I. Redin (Budker Inst. Phys., Novosibirsk, 2000) pp. 122-124, hep-ph/9906495.
- [50] A.E. Dorokhov, Acta Phys. Polon. **B36**, 3751 (2005).
- [51] A.E. Dorokhov and W. Broniowski, Eur. Phys. J. **C32**, 79 (2003).
- [52] K.A. Milton and O.P. Solovtsova, Int. J. Mod. Phys. **A17**, 3789 (2002).
- [53] K.A. Milton, I.L. Solovtsov and O.P. Solovtsova, Phys. Lett. **B415**, 104 (1997).
- [54] M. Davier, S. Eidelman, A. Hocker and Z. Zhang, Eur. Phys. J. **C31**, 503 (2003).
- [55] Muon  $g - 2$  Collab., G.W. Bennett *et al.*, Phys. Rev. Lett. **92**, 161802 (2004).
- [56] A. Hocker, in: Proc. the XXXII Int. Conf. ICHEP'04, eds. H. Chen *et al.* (World Scientific, 2005), Vol. 2., p. 710, hep-ph/0410081.
- [57] K. Hagiwara, A.D. Martin, D. Nomura, and T. Teubner, Phys. Rev. **D69**, 093003 (2004).
- [58] M. Steinhauser, Phys. Lett. **B429**, 158 (1998).
- [59] J.H. Kuhn and M. Steinhauser, Phys. Lett. **B437**, 425 (1998).



## ADVANTAGES OF APT IN QCD STUDY OF HADRONIC TAU DECAYS

O. P. Solovtsova<sup>a</sup>

Gomel State Technical University, Gomel, Belarus

A comparative analysis of different forms of approximations, which are applied to the description of the hadronic decays of the tau lepton, is given. Advantages and self-consistency of the method called analytic perturbation theory (APT) are demonstrated. It is shown that the use of the APT leads to the good description of certain inclusive functions associated with vector and axial-vector non-strange quark currents down to the lowest energy scale.

### 1 Introduction

The experimental data on the  $\tau$  lepton decay into hadrons obtained with a record accuracy for hadronic processes [1–3] give a unique possibility for testing QCD at low energy scale. The  $\tau$  lepton is the only lepton known at present whose mass,  $M_\tau = 1.777 \text{ GeV}$ , is large enough in order to produce decays with a hadronic mode. At the same time, in the context of QCD, the mass is sufficiently small to allow one to investigate perturbative and non-perturbative QCD effects. The theoretical analysis of the hadronic decays of a heavy lepton was performed Tsai [4] before the experimental discovery of the  $\tau$  lepton in 1975 and since then this process is intensively studied.

It is known, that perturbation theory (PT), which is a basic tool of calculations in quantum field theory, as a rule cannot be exhaustive in the low energy region of QCD. However, a structure of an initial perturbative approximation of some quantity is not a rigid construction fixed once and for all, but admits a considerable modification due to specific properties of quantum field theory. Such modification is based on further information of a general character about the sum of the series. In particular, the properties of renormalization-group (RG) invariance [5], which is lost in a finite order of the initial expansion, allow rearrangements of the perturbative series in terms of the invariant charge. In this case, the properties of the series change essentially. In distinction to the initial expression containing large logarithms, the expansion obtained within the RG method can be used for analyzing the ultraviolet region. However, the perturbative series so derived are ill-defined in the infrared region and the correct analytic properties of the series in the complex  $Q^2$ -plane are violated due to unphysical singularities of the perturbative running coupling, a ghost pole in the one-loop approximation (see discussion in [6, 7]). The difficulty associated with these unphysical singularities is overcome in the analytic approach proposed by Shirkov and Solovtsov [8]. This approach modifies the perturbative expansion on the basis of general properties of the theory so that the new approximations reflect fundamental principles of the theory—renormalization invariance, spectrality, and causality. In the new expansion the correct analytic properties are restored, and the property of RG invariance is preserved [8]. Further developments and applications of the Shirkov–Solovtsov analytic approach have been considered in many papers (see [9] as the recent review).

The original theoretical expression for the width  $\Gamma(\tau^- \rightarrow \text{hadrons} \nu_\tau)$  involves integration over small values of timelike momentum [4]. The perturbative description with the standard running coupling becomes ill-defined in this region and some additional ansatz has to be applied to get a finite result for the hadronic width. To this end, one usually transforms the initial expression, by using Cauchy's theorem, to a contour representation for  $R_\tau$  [10], which allows one to give meaning to the initial expression and, in principle, perform calculations in the framework of perturbative QCD. Assuming the validity of this transformation it is possible to present results in the form of a truncated power series with  $\alpha_s(M_\tau)$  as the expansion parameter [11, 12]. There are also other approaches to evaluating the contour integral. The Le Diberder and Pich prescription [13] allows one to improve the convergence properties of the approximate series and reduce the renormalization scheme (RS) dependence of theoretical predictions. The possibility of using different approaches in the perturbative description of  $\tau$  lepton decay leads to an uncertainty in the value of  $\alpha_s(M_\tau)$  extracted from the experimental data. Moreover, any perturbative description is based on this contour representation, *i.e.*, on the possibility of converting the initial expression involving integration over timelike momenta into a contour integral in the complex momentum plane. To carry out this transition by using Cauchy's theorem requires certain analytic properties of the hadronic correlator or of the corresponding Adler function. However, the occurrence of incorrect analytic properties in

e-mail: <sup>a</sup>solovtsova@gstu.gomel.by

the conventional perturbative approximation makes it impossible to exploit Cauchy's theorem in this manner and, therefore, prevents rewriting the initial expression for  $R_\tau$  in the form of a contour integral in the complex momentum-plane.

The method based on the Shirkov–Solovtsov analytic approach and called analytic perturbation theory (APT) [14] ensures the correct analytic properties of such important objects as the hadronic correlator or of the corresponding Adler function, leads to equality between the initial theoretical expression for the width  $\Gamma(\tau^- \rightarrow \text{hadrons} \nu_\tau)$  and the corresponding contour representation.

The aim of this paper is to reveal features of the application of PT and APT expansions in studying the process of  $\tau$  decay into hadrons, and in application the APT method for the description of hadronic widths associated with vector and axial-vector non-strange quark currents, and also for Adler functions, which are connected to these currents, down to the lowest energy scale.

## 2 Analytic perturbation theory

A main object in a description of hadronic decays of the  $\tau$  lepton and of many other physical processes is the correlator  $\Pi(q^2)$  or the corresponding Adler function  $D(Q^2)$ , which is connected to the correlator by the formula

$$D(Q^2) = -Q^2 \frac{d\Pi(-Q^2)}{dQ^2}. \quad (1)$$

We use the standard convention  $Q^2 = -q^2 > 0$  in the Euclidean region.

The integral representation for the  $D$ -function is given in terms of the function  $R(s) \equiv \text{Im } \Pi(s)/\pi$ :

$$D(Q^2) = Q^2 \int_0^\infty \frac{ds}{(s + Q^2)^2} R(s). \quad (2)$$

The representation (2) defines the function  $D(Q^2)$  as the analytic function in the complex  $Q^2$ -plane with the cut along the negative real axis.

It is convenient to separate QCD contributions,  $d(Q^2)$  and  $r(s)$ , in the functions  $D \propto 1 + d$  and  $R \propto 1 + r$ , respectively, which are related by the formulae

$$d(Q^2) = Q^2 \int_0^\infty \frac{ds}{(s + Q^2)^2} r(s), \quad (3)$$

$$r(s) = -\frac{1}{2\pi i} \int_{s-i\epsilon}^{s+i\epsilon} \frac{dz}{z} d(-z). \quad (4)$$

The integration contour in (4) lies in the region of analyticity of the integrand and encircles the cut of  $d(-z)$  on the positive real  $z$  axis.

In the APT the basic object is a spectral function  $\rho(\sigma)$  which enters into some integral representation. In particular, for two-point functions, it is the Källén–Lehmann representation; whereas for structure functions for inelastic lepton–hadron scattering, the integral representation is that of Jost–Lehmann–Dyson. The spectral function  $\rho(\sigma)$  for the objects under consideration here can be obtained by using the perturbative series as a initial approach. Truncated at the three-loop level, the perturbative  $d$ -function, rewritten in terms of the perturbative running coupling,  $a_{\text{pt}}(Q^2) = \bar{\alpha}_s(Q^2)/\pi$ , is

$$d_{\text{pt}}(Q^2) = a_{\text{pt}}(Q^2) + d_1 a_{\text{pt}}^2(Q^2) + d_2 a_{\text{pt}}^3(Q^2), \quad (5)$$

where in the  $\overline{\text{MS}}$  scheme for three active quarks ( $n_f = 3$ ) relevant in  $\tau$  decay, the expansion coefficients are  $d_1^{\overline{\text{MS}}} = 1.6398$  and  $d_2^{\overline{\text{MS}}} = 6.3710$  [15].

This expansion generates the following approximation to the spectral function  $\rho(\sigma)$ :

$$\rho(\sigma) = \varrho_0(\sigma) + d_1 \varrho_1(\sigma) + d_2 \varrho_2(\sigma), \quad (6)$$

where the coefficients  $d_1$  and  $d_2$  are the same as in the PT series (5) and the expansion functions are determined by the discontinuity of the corresponding power of the perturbative running coupling,  $\varrho_n(\sigma) = \text{Im}[a_{\text{pt}}^{n+1}(-\sigma - i\epsilon)]$ .

By using the spectral function (6), we obtain the  $d$ -function in the form of the expansion (not a power series in  $a$ )

$$d_{\text{an}}(Q^2) = \Delta_{\text{an}}^{(1)}(Q^2) + d_1 \Delta_{\text{an}}^{(2)}(Q^2) + d_2 \Delta_{\text{an}}^{(3)}(Q^2), \quad (7)$$

where the  $\Delta_{\text{an}}^{(n)}$  are analytic functions and  $\Delta_{\text{an}}^{(1)}(Q^2) = a_{\text{an}}(Q^2)$  (see [16] for details).

The Euclidean running coupling  $a_{\text{an}}(Q^2)$  and the running coupling  $\tilde{a}_{\text{an}}(s)$  defined in the Minkowskian region are expressed through the function  $\varrho_0(\sigma)$  [9, 17]. In the leading order

$$\varrho_0^{(1)}(\sigma) = \frac{1}{\beta_0} \frac{\pi}{\ln^2(\sigma/\Lambda^2) + \pi^2}, \quad \beta_0 = (11 - 2n_f/3)/4, \quad (8)$$

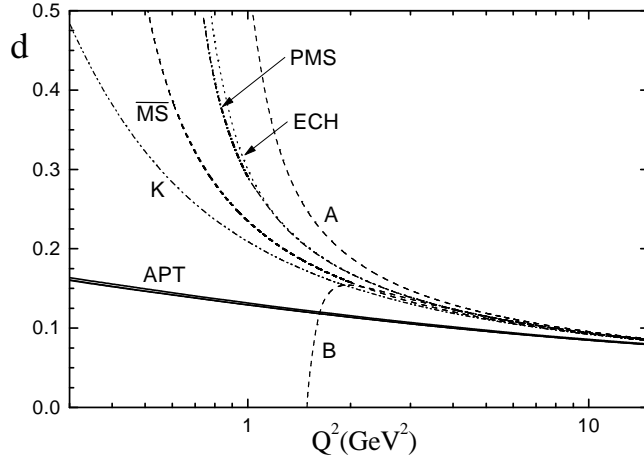


**Figure 1.** Renormalization scheme dependence of the  $d$ -function as a function of  $Q^2$  for the PT and APT approaches. The APT results are shown as solid lines which are very close to each other and practically merge into one curve.

$$a_{\text{an}}^{(1)}(Q^2) = \frac{1}{\beta_0} \left[ \frac{1}{\ln(Q^2/\Lambda^2)} + \frac{\Lambda^2}{\Lambda^2 - Q^2} \right], \quad (9)$$

$$\tilde{a}_{\text{an}}^{(1)}(s) = \frac{1}{\beta_0} \left[ \frac{1}{2} - \frac{1}{\pi} \arctan \frac{\ln(s/\Lambda^2)}{\pi} \right]. \quad (10)$$

The expression in the Euclidean region (9) contains the usual logarithmic term that coincides with the perturbation expression containing the ghost pole at  $Q^2 = \Lambda^2$ . The contribution of this pole is compensated by the second term in Eq. (9) of a power character in  $Q^2$ . Written in terms of the initial  $a_{\text{pt}}$ , this term is of the structure of  $\exp(-1/a_{\text{pt}})$  and therefore makes no contribution to the power series expansion in the coupling  $a_{\text{pt}}$ . That is, the  $Q^2$ -power contribution in the Euclidean running coupling (9), invisible in PT, is restored automatically on the basis of the analyticity principle. In contrast to the PT running coupling  $a_{\text{pt}}(Q^2)$ , the analytic function  $a_{\text{an}}(Q^2)$  has no unphysical singularities: the ghost pole and corresponding branch points (which appear in higher order) are absent. It should be stressed, the APT and PT coincide with each other in the asymptotic region of high energies. A value of the running coupling defined in the Minkowskian region,  $\tilde{a}_{\text{an}}(s)$ , is less than a value of the running coupling in the Euclidean region,  $a_{\text{an}}(Q^2)$ , at the same magnitude of argument [17, 18].

### 3 Renormalization scheme dependence

A significant source of theoretical uncertainty arises from the RS dependence of the results obtained due to the inevitable inclusion of only a finite number of terms in the PT series. In QCD, that uncertainty is the greater, than smaller a value of typical energy of the process.

There are no general principles that give preference to a particular RS, and in this sense, all schemes are equivalent. The APT method improves this situation and gives very stable results over a wide range of renormalization schemes. To demonstrate this fact, in Fig. 1 we plot functions  $d_{\text{pt}}(Q^2)$  and  $d_{\text{an}}(Q^2)$  in different RS. It is seen that predictions in the perturbative approach for  $d(Q^2)$  obtained within different RS diverge considerably (see dashed curves A and B). Note should be made of the fact that the schemes A and B are similar to each other and to the optimal PMS [19] and ECH [20] schemes in the sense of the cancellation index [21]:  $C_A \simeq C_B \simeq 2$ . For the ECH method, the cancellation index is minimal, equaling unity. The cancellation index for the  $\overline{\text{MS}}$  scheme turns out to be somewhat bigger,  $C_{\overline{\text{MS}}} \simeq 3.1$ . In Fig. 1, we also draw the curves representing PT results in the PMS, ECH,  $\overline{\text{MS}}$  and K schemes. For the same schemes, in Fig. 1 we also present results obtained in the APT approach. In this case the scheme arbitrariness is extremely small, and all the curves corresponding to the schemes A, B, PMS, ECH,  $\overline{\text{MS}}$ , and K merge into one thick solid curve. Thus, in the APT, the scheme arbitrariness is very dramatically reduced as compared to that in analogous PT calculations.

### 4 Ratio $R_\tau$

The total hadronic width of the  $\tau$  lepton is given by difference of its total width and the partial widths for the electronic and muonic decays  $\Gamma(\tau^- \rightarrow \text{hadrons} \nu_\tau) = \Gamma_{\text{tot}} - \Gamma_e - \Gamma_\mu$ . In an analogy to well-known Drell-ratio for the  $e^+e^-$  annihilation into hadrons, one can define a ratio  $R_\tau$

$$R_\tau \equiv \frac{\Gamma(\tau^- \rightarrow \text{hadrons} \nu_\tau)}{\Gamma(\tau^- \rightarrow \ell \bar{\nu}_\ell \nu_\tau)}.$$

The theoretical expression for  $R_\tau$  can be presented as follows

$$R_\tau = 3 (|V_{ud}|^2 + |V_{us}|^2) S_{\text{EW}} (1 + \delta_\tau), \quad (11)$$

where  $V_{ud}$  and  $V_{us}$  are elements of the CKM quark mixing matrix,  $S_{\text{EW}}$  is the electroweak factor, and the QCD contribution,  $\delta_\tau$ , is expressed via  $r(s)$  as

$$\delta_\tau = 2 \int_0^{M_\tau^2} \frac{ds}{M_\tau^2} \left(1 - \frac{s}{M_\tau^2}\right)^2 \left(1 + 2 \frac{s}{M_\tau^2}\right) r(s). \quad (12)$$

This expression is a starting point of our analysis. Within the PT the integral (12) cannot be evaluated directly due to unphysical singularities of the PT running coupling lying in the range of integration.

The most useful trick to rescue the situation is to appeal to analytic properties of the correlator  $\Pi(q^2)$ . The relations between the functions  $r(s)$  and  $d(Q^2)$  allow us to represent  $\delta_\tau$  as a contour integral in the complex  $z$  plane by choosing the contour to be a circle of radius  $|z| = M_\tau^2$  [11]

$$\delta_\tau = \frac{1}{2\pi i} \oint_{|z|=M_\tau^2} \frac{dz}{z} \left(1 - \frac{z}{M_\tau^2}\right)^3 \left(1 + \frac{z}{M_\tau^2}\right) d(-z). \quad (13)$$

It should be stressed that expressions (12) and (13) are equivalent only when the above-mentioned analytic properties are maintained.

It would seem that the transformation to the contour representation (13) allows one to avoid this difficulty, since in this case unphysical singularities of the running coupling lie outside of the contour, and the procedure of integration can formally be easily accomplished. However, in our opinion, this trick (“sweeping the difficulty under the rug”) does by no means solve the problem. Actually, incorrect analytic properties of the running coupling result in Eqs. (12) and (13) for  $\delta_\tau$  being no longer equivalent [14, 22], and, if one remains within PT, nothing can be said about the errors introduced by this transition. The APT may eliminate these problems.

The PT description is based on the contour representation and can be developed in the following two ways. In the Braaten’s (Br) method [12] the quantity (13) is represented in the form of truncated power series with the expansion parameter  $a_\tau = \bar{\alpha}_s(M_\tau^2)/\pi$ . In this case the three-loop representation for  $\delta_\tau$  is

$$\delta_\tau^{\text{Br}} = a_\tau + r_1 a_\tau^2 + r_2 a_\tau^3, \quad (14)$$

where the coefficients  $r_1$  and  $r_2$  in the  $\overline{\text{MS}}$  scheme with three active flavors are  $r_1 = 5.2023$  and  $r_2 = 26.366$  [12].

The method proposed by Le Diberder and Pich (LP) [13] uses the PT expansion of the  $d$ -function (5). It results to the following non-power representation

$$\delta_\tau^{\text{LP}} = A^{(1)}(a) + d_1 A^{(2)}(a) + d_2 A^{(3)}(a) \quad (15)$$

with

$$A^{(n)}(a) = \frac{1}{2\pi i} \oint_{|z|=M_\tau^2} \frac{dz}{z} \left(1 - \frac{z}{M_\tau^2}\right)^3 \left(1 + \frac{z}{M_\tau^2}\right) a^n(z). \quad (16)$$

Both these PT approaches, are widely used in the analysis of  $\tau$ -decay data. However, their status is different. The formula (14) can be obtained self-consistently. In expression (12) one has to use for  $r(s)$  the initial perturbative approximation with the expansion parameter  $a_\mu$ . Then, after integration over  $s$ , the logarithmic terms containing  $\ln(M_\tau^2/\mu^2)$  are removed by setting  $\mu^2 = M_\tau^2$ . The same result is obtained if the contour representation (13) is used and the  $d$ -function is taken in the form the initial perturbative approximation which preserves the required analytic properties. As for the representation (15), it will be consistent with expressions (12) and (13), if  $a(z)$  has analytic properties of the Källén–Lehmann type. The use of the standard PT running coupling with unphysical singularities in (16) breaks this consistency.

The APT description can be equivalently phrased either on the basis of the original expression (12), which involves the Minkowskian quantity  $r(s)$ , or on the contour representation (13), which involves the Euclidean quantity  $d(q^2)$ . Within the framework of the APT approach, both forms can be rewritten in terms of the spectral function  $\rho(\sigma)$  as [14]

$$\delta_\tau = \frac{1}{\pi} \int_0^\infty \frac{d\sigma}{\sigma} \rho(\sigma) - \frac{1}{\pi} \int_0^{M_\tau^2} \frac{d\sigma}{\sigma} \left(1 - \frac{\sigma}{M_\tau^2}\right)^3 \left(1 + \frac{\sigma}{M_\tau^2}\right) \rho(\sigma). \quad (17)$$

In Fig. 2, we illustrate the dependence of the  $R_\tau$ -ratio on the running coupling in the PT(Br) and APT approaches, comparing the convergence properties in the one-loop (dotted lines), two-loop (dashed lines), and three-loop (solid lines) approximations. Numbers above the curves specify the order of the approximation. The

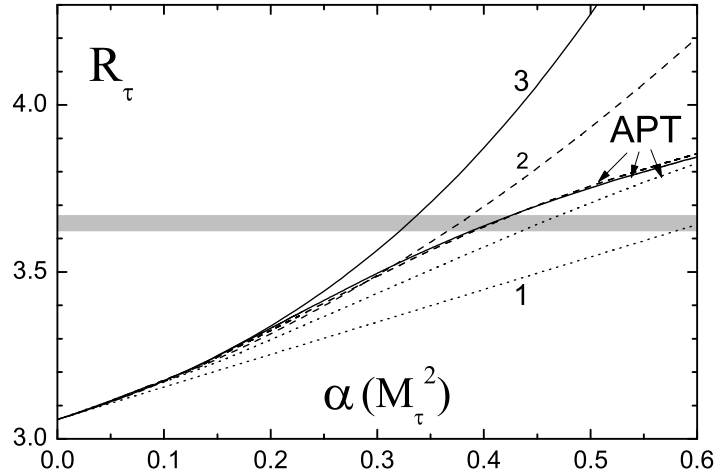


**Figure 2.** The PT(Br) and APT predictions for the  $R_\tau$  ratio vs. the running coupling in the  $\overline{\text{MS}}$  scheme. The numbers labelling the curves denote the level of the loop expansion used.

shaded area shows the corridor of experimental errors for  $R_\tau^{\text{expt}} = 3.646 \pm 0.022$  [23]. The convergence properties of the APT expansion seem to be much improved compared to those of the PT expansions.

The APT approach allows one to construct a series for which RS dependence is dramatically reduced. For the hadronic  $\tau$  decay it is easy for understanding if one takes into account the result which is shown in Fig. 1 for  $d$ -functions in different RS: instead of RS unstable and rapidly changing PT results, the APT predictions are practically RS independent.

In the case of massless quarks, the detailed APT analysis of the inclusive  $\tau$  decay on the three-loop level has been performed in [24]. This investigation together with other results allows us to formulate the following features of the APT method: (i) this approach maintains the correct analytic properties and leads to a self-consistent procedure of analytic continuation from the spacelike to the timelike region; (ii) it has much improved convergence properties and turns out to be stable with respect to higher-loop corrections; (iii) renormalization scheme dependence of the results obtained within this method is reduced dramatically.

## 5 Vector and axial-vector channels in $\tau$ decay

In this section we compare our theoretical result with results that we get from the  $\tau$ -data presented by the ALEPH Collaboration [3]. These data have been extensively used in various QCD studies including the determination of the strong coupling constant, the test of the conception of quark-hadron duality, the application in the evaluation of the anomalous magnetic moment of the muon and the determination of  $\rho$ -meson parameters.

From the complete analysis of the  $\tau$  branching ratios [3], it is possible to separate the non-strange vector and axial-vector hadronic  $\tau$  decay channels,  $V^- \nu_\tau$  and  $A^- \nu_\tau$ , respectively. The inclusive observable  $R_\tau$ -ratio can be written down as

$$R_\tau = R_{\tau,V} + R_{\tau,A} + R_{\tau,S}, \quad (18)$$

where  $R_{\tau,V}$  and  $R_{\tau,A}$  are contributions corresponding to the vector and axial-vector non-strange quark currents,  $\Gamma(\tau^- \rightarrow \text{hadrons}_{S=0})$ , and  $R_{\tau,S}$  includes strange decays,  $\Gamma(\tau^- \rightarrow \text{hadrons}_{S=-1})$ . Note, for the strange hadronic width vector and axial-vector contributions are not separated so far due to the lack of the corresponding experimental information for the Cabibbo-suppressed modes.

Within the perturbative approximation with massless quarks the vector and axial-vector contributions to  $R_\tau$  coincide with each other

$$R_{\tau,V} = R_{\tau,A} = \frac{3}{2} |V_{ud}|^2 (1 + \delta_\tau), \quad (19)$$

where  $\delta_\tau$  is given by the expression (12). However, the experimental measurements shown that these components are not equal to each other.

Figs. 3 and 4 show the ALEPH measurements for the vector and the axial-vector non-strange quark currents, functions  $R_V(s)$  and  $R_A(s)$ , respectively. These figures clearly demonstrate that the vector current function  $R_V(s)$  indicates a dominant large  $\rho^-(770)$  resonance and the axial-vector function  $R_A(s)$  indicates  $a_1(1260)$  resonance. Note that the normalization of the ALEPH functions  $v_1(s)$  and  $a_1(s)$  differ from that we use here: at the parton-level our function  $R(s)$  is equal to 1, therefore  $R_{V/A}(s) = 2v_1(s)/a_1(s)$ .

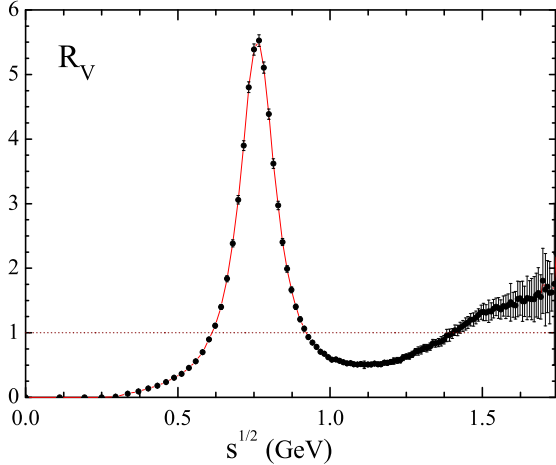


**Figure 3.** The total inclusive vector current function.

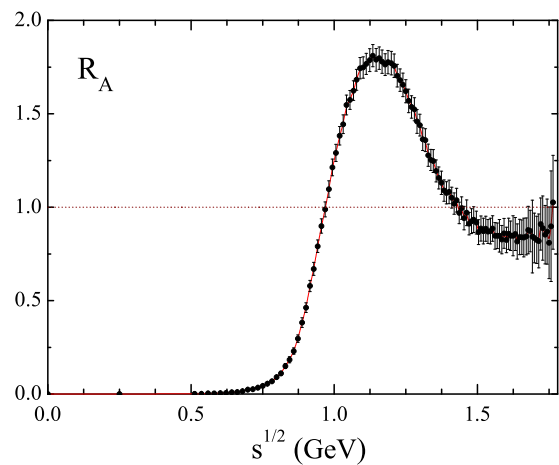


**Figure 4.** The inclusive  $\tau$  axial-vector function (without the pion pole).

The ratios  $R_{\tau,V}$  and  $R_{\tau,A}$  can be obtained through vector and axial-vector functions,  $R_V(s)$  and  $R_A(s)$ , as

$$R_{\tau,V/A}^{\text{exp/theor}} = R_0 \int_0^{M_\tau^2} \frac{ds}{M_\tau^2} \left(1 - \frac{s}{M_\tau^2}\right)^2 \left(1 + \frac{2s}{M_\tau^2}\right) R_{V/A}^{\text{exp/theor}}(s), \quad (20)$$

where  $R_0 \equiv 3|V_{ud}|^2 S_{\text{EW}}$ ,  $|V_{ud}| = 0.9752 \pm 0.0007$  and  $S_{\text{EW}} = 1.0194 \pm 0.0040$  (see [3] for details). The experimental value obtained by the ALEPH collaboration for the vector channel is

$$R_{\tau,V}^{\text{exp}} = 1.787 \pm 0.013. \quad (21)$$

Based on the APT, involving a summation of threshold singularities [25] and taking into account the nonperturbative character of the light quark masses, as it in details has been described in [26], we take as an input, the value of the running coupling defined in the Minkowskian region in  $\overline{\text{MS}}$  renormalization scheme  $\tilde{\alpha}_s(M_\tau^2) = 0.33$  and reproduce the central experimental value of the ALEPH data for the vector ratio

$$R_{\tau,V}^{\text{theor}} = 1.79 = R_{\tau,V}^{\text{exp,centr}}. \quad (22)$$

The experimental value obtained by the ALEPH collaboration for the total axial-vector channel is  $R_{\tau,A}^{\text{exp,tot}} = 1.695 \pm 0.013$ . The inclusive axial-vector function which show in Fig. 4 does not contain the pion pole. The branching fraction for the  $\pi^- \nu$  mode is given as  $(10.83 \pm 0.11)\%$  [3]. After subtraction of this pole contribution, we get

$$R_{\tau,A1}^{\text{exp}} = 1.087 \pm 0.015. \quad (23)$$

The ALEPH measurements allows us to study the  $D$ -function in the non-strange vector and axial-vector channels:

$$D_{V/A}^{\text{exp/theor}}(Q^2) = Q^2 \int_0^\infty ds \frac{R_{V/A}^{\text{exp/theor}}(s)}{(s + Q^2)^2}. \quad (24)$$

Although the function  $R_{V/A}(s)$  experimentally is not known for all values of  $s$ , it is possible to use the following expression

$$R_{V/A}(s) = R_{V/A}^{\text{exp}}(s) \theta(s_0 - s) + R_{V/A}^{\text{theor}}(s) \theta(s - s_0), \quad (25)$$

where, for example, the continuum threshold  $s_0$  can be found from the global duality relation [27], that usually gives  $s_0 = 1.35 \div 1.75$  GeV<sup>2</sup>.

Within the analytic approach the  $D_V$ -function has been analyzed in [16]. The improved studying has been done in [26]. These results are close to each other. In complete analogy to vector case [26], we consider the non-strange axial-vector  $D_A$ -function. As a first step, we use a simple model for the function  $R_A(s)$ , that usually used in the QCD sum rules

$$R_A^{\text{had}}(s) = \frac{2\pi}{g_A^2} m_A^2 \delta(s - m_A^2) + \left(1 + \frac{\alpha_s^{(0)}}{\pi}\right) \theta(s - s_0). \quad (26)$$

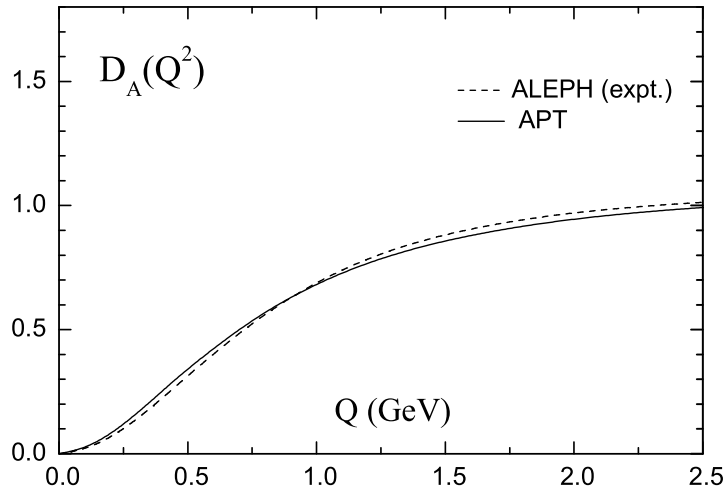


**Figure 5.** Experimental and theoretical  $D_A$ -functions for axial-vector channel.

This model expression leads to the function

$$D_A^{\text{had}}(Q^2) = \frac{2\pi}{g_A^2} \frac{Q^2 m_A^2}{(Q^2 + m_A^2)^2} + \left(1 + \frac{\alpha_s^{(0)}}{\pi}\right) \frac{Q^2}{Q^2 + s_0}, \quad (27)$$

which reproduces well the “experimental” curve  $D_A^{\text{exp}}(Q^2)$  constructed by using experimental data shown in Fig. 4 with the parameters:  $m_A = 1260$  MeV,  $g_A^{-2} = 1.65$ ,  $\alpha_s^{(0)} = 0.4$ , and  $s_0 = 1.75$  GeV $^2$ . The values of these parameters are close to the parameters that one usually uses in the sum rules method [28].

In Fig. 5 we plot the  $D_A$ -function obtained in the APT approach (solid curve) and the experimental curve (dashed line) constructed by using the ALEPH data. The  $D_A$ -function turns out to be a smooth function without any traces of resonance structure and, therefore, is useful to use in a theoretical analysis as the Euclidian characteristic of the inclusive process. Fig. 5 demonstrates a good agreement of our result with the experimental curve for whole interval of  $Q^2$ . Note here that an use of any finite order of the operator product expansion cannot adequately describe the  $D$ -function in the infrared region of low energy scale. The curve corresponding to model expression (27) coincides with the dashed line.

It is important to note, that we obtained the value of  $R_{\tau,V}^{\text{theor}}$  which agrees well with the experimental data (21) and, at the same time, within the the same theoretical framework, we obtained the value of  $R_{\tau,A}^{\text{theor}} = 1.045$  which is very close to the experimental value (23).

## 6 Conclusions

The analytic approach proposed by Shirkov and Solovtsov modifies the perturbative expansions such that the new approximations reflect basic principles of the theory, such as renormalization invariance, spectrality, and causality. Analytic perturbation theory, which was used here, gives a self-consistent description of both the spacelike and timelike regions. This method was applied to describe some physical quantities and functions an experimental information for which can be extracted from the  $\tau$  lepton decay data.

We performed a comparative analysis of the advantages and disadvantages of different forms of perturbative expansion both from the general standpoint and in the context of application to the inclusive  $\tau$  decay. We presented the arguments in favor of the APT, which not only agrees with the general principles of the theory but also has a number of practical advantages. In the analytic approach, the two methods for describing the inclusive  $\tau$  lepton decay in terms of timelike or spacelike variables are equivalent.

Within the APT, the dependence of the results on the choice of the renormalization prescription is essentially reduced, and we can speak of the practical independence of the three-loop expressions from the renormalization scheme. The calculations based on the APT thus considerably reduce the theoretical uncertainty of the results. Therefore, using it as the perturbative component increases the reliability of information about the QCD parameters obtained from the experimental data known with high accuracy for the  $\tau$  lepton decay.

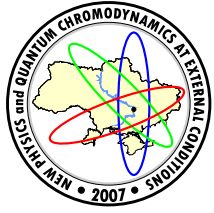
We considered the Adler function corresponding to the non-strange vector and axial-vector channels. These functions, defined in the Euclidean region, are smooth functions and represent a convenient testing ground for theoretical methods. The conventional method of approximating these function as a sum of perturbative terms and power corrections cannot describe the low energy scale region because both the logarithmic and power expansions diverge at small momenta. We have shown that our approach allows us to describe well the

experimental data for  $\tau$  decay in terms of the  $D_{V/A}$ -functions down to the lowest energy scale and for  $R_\tau$  in the non-strange vector axial-vector channels.

*Acknowledgments.* The author would like to thank the organizers of the NPQCD-2007 School-seminar for their warm hospitality, support, and the interesting scientific program. This work was supported in part by the BRFBR (contract F06D-002) and the grant of the Ministry of Education of Belarus.

## References

- [1] R. Barate *et al.* (ALEPH Collab.), Eur. Phys. J.C **4**, 409 (1998).
- [2] K. Ackerstaff *et al.* (OPAL Collab.), Eur. Phys. J. C **7**, 571 (1999).
- [3] S. Schael *et al.* (ALEPH Collab.), Phys. Rept. **421**, 191 (2005).
- [4] Y.S. Tsai, Phys. Rev. D **4**, 2821 (1971).
- [5] N.N. Bogoliubov, D.V. Shirkov, Introduction to the Theory of Quantized Fields (Wiley, New York, 1959 and 1980).
- [6] H.F. Jones and I.L. Solovtsov, Phys. Lett. B **349**, 519 (1995).
- [7] K.A. Milton and O.P. Solovtsova, Phys. Rev. D **57**, 5402 (1998).
- [8] D.V. Shirkov and I.L. Solovtsov, Phys. Rev. Lett. **79**, 1209 (1997).
- [9] D.V. Shirkov and I.L. Solovtsov, Theor. Math. Phys. **150**, 132 (2007).
- [10] C.S. Lam and T.M. Yan, Phys. Rev. D **16**, 703 (1977).
- [11] E. Braaten, Phys. Rev. Lett. **60**, 1606 (1988).
- [12] E. Braaten, S. Narison, and A. Pich, Nucl. Phys. B **373**, 581 (1992).
- [13] F. Le Diberder and A. Pich, Phys. Lett. B **286**, 147 (1992).
- [14] K.A. Milton, I.L. Solovtsov, and O.P. Solovtsova, Phys. Lett. B **415**, 104 (1997).
- [15] S.G. Gorishny, A.L. Kataev, S.A. Larin, and L.R. Surguladze, Phys. Rev. D **43**, 1633 (1991).
- [16] K.A. Milton, I.L. Solovtsov, and O.P. Solovtsova, Phys. Rev. D **64**, 016005 (2001).
- [17] K.A. Milton and I.L. Solovtsov, Phys. Rev. D **55**, 5295 (1997).
- [18] D.V. Shirkov, Eur. Phys. J. C **22**, 331 (2001).
- [19] P.M. Stevenson, Phys. Rev. D **23**, 2916 (1981).
- [20] G. Grunberg, Phys. Rev. D **29**, 2315 (1984).
- [21] P.A. Rączka, Z. Phys. C **65**, 481 (1995).
- [22] K.A. Milton and O.P. Solovtsova, Int J. Mod. Phys. A **26**, 3789 (2002).
- [23] D.E. Groom *et al.* (Particle Data Group), Eur. Phys. J. C **15**, 1 (2000); Yao W.-M. *et al.* (Particle Data Group), J. Phys. G **33**, 1 (2006).
- [24] K.A. Milton, I.L. Solovtsov, O.P. Solovtsova, and V.I. Yasnov, Eur. Phys. J. C **14**, 495 (2000).
- [25] K.A. Milton and I.L. Solovtsov, Mod. Phys. Lett. A **16**, 2213 (2001).
- [26] K.A. Milton, I.L. Solovtsov, O.P. Solovtsova, Mod. Phys. Lett. A **21**, 1355 (2006).
- [27] S. Peris, M. Perrottet, and E. de Rafael, JHEP **9805** 001 (1998).
- [28] L.J. Reinders, H.R. Rubinstein, and S. Yazaki, Phys. Rep. **127**, 1 (1985).



## ON THE ONE-LOOP RENORMALIZATION OF NONCOMMUTATIVE GAUGE THEORIES

Alexei Strelchenko<sup>a</sup>

Dnipropetrovsk National University, Dnipropetrovsk, Ukraine

The first three non-zero heat trace coefficients of the non-minimal  $U(N)$  gauge field kinetic operator on the Moyal plane taken in an arbitrary background are calculated. We show that the non-planar part of the heat trace asymptotics is determined by  $U(1)$  sector of the gauge model. The non-planar or mixed heat kernel coefficients are shown to be gauge-fixing dependent in any dimension of space-time. In the case of the degenerate deformation parameter the lowest mixed coefficients in the heat expansion produce non-local gauge-fixing dependent singularities of the one-loop effective action that destroy the renormalizability of the  $U(N)$  model at one-loop level.

### 1 Introduction

The heat kernel of (pseudo)differential operators has become one of the most powerful and actively developed tools in quantum field theory and spectral geometry (see [1–4] where the implementation of the heat kernel technique in a variety of physical and mathematical problems is discussed in details). Nowadays this topic has acquired particular interest in the context of noncommutative geometry and quantum field theories on noncommutative spaces [5–10]. The main result here is that the heat trace for a differential operator on a (flat) noncommutative manifold, e.g. so-called generalized star-Laplacian arising, for instance, in the noncommutative scalar  $\lambda\varphi^4$  theory, can be expanded in a power series in the “proper time” parameter that resembles, in some respect, the heat trace expansion for its commutative counterpart. This observation is of fundamental importance since makes it possible to employ the heat kernel machinery in many applications to noncommutative models such as the investigation of one-loop divergences or quantum anomalies [9].

Another interesting aspect of the heat kernel on noncommutative spaces is closely related to the UV/IR mixing phenomenon [11–13]. Namely, in the most general case when a star-differential operator involves both left and right Moyal multiplications (as it is for the generalized Laplacian mentioned above), its heat trace asymptotics contains a contribution produced by star-non-local terms that are singular when the deformation parameter vanishes. Clearly, it defines the non-planar part of the heat kernel expansion which is, in particular, responsible for the UV/IR mixing [7, 9]. The situation gets even more intriguing in the case when the deformation parameter is degenerate (that corresponds to space-like noncommutativity). In this case the non-planar contribution to the heat expansion becomes dangerous since it can affect the one-loop renormalization of a theory under consideration [10, 14].

The present talk is devoted to the investigation of renormalization properties of noncommutative gauge theories by means of the heat kernel technic. In particular, we will obtain the heat trace asymptotics for non-minimal operators appearing in the non-commutative  $U(N)$  gauge theory (on noncommutative non-compact flat manifolds) in the background field formalism. To be precise, we are concerned with gauge field kinetic operator on the Moyal plane taken in the covariant background gauge with an arbitrary gauge-fixing parameter. In the commutative case non-minimal operators (in various physical systems) were investigated by many authors [15–21]. In our study of the heat asymptotics we will follow the calculating method by Endo allowing to reduce the whole task to the computation of the heat trace coefficients for minimal operators by means of some algebraic relations between the heat kernel matrix elements [15, 19]. Indeed, this method turns out to be especially convenient within the background field formalism; at the same time, its purely algebraic nature allows one to generalize it easily to the noncommutative case.

### 2 Non-minimal operators in noncommutative gauge theories

Consider a self-adjoint second order non-minimal star-differential operator that corresponds to the kinetic operator of gauge particles propagating on Moyal plane in an external background. It can be represented in the

---

e-mail: <sup>a</sup>alexstrelch@yahoo.com

form

$$(D_{\mu\nu}^\xi)_{\alpha\beta} = -\left[\delta_{\mu\nu}\nabla^2 + \left(\frac{1}{\xi} - 1\right)\nabla_\mu\nabla_\nu + 2[\widehat{F}_{\mu\nu}, \cdot]_\star\right]_{\alpha\beta}, \quad (1)$$

where

$$\nabla_\mu = \partial_\mu + L(B_\mu) - R(B_\mu)$$

is an anti-Hermitian covariant-derivative operator in the background field  $B_\mu$ ,  $\xi$  is a numerical gauge-fixing parameter and  $F_{\mu\nu}$  is the curvature tensor of the gauge connection  $B_\mu$ . Such an operator naturally appears in the NC  $U(N)$  theory in the background field formalism; it defines, in particular, the quadratic in quantum gauge fields part of the total action written in a covariant background gauge:

$$S_2[Q] = -\frac{1}{2} \int_{R^n} d^n x \operatorname{tr}_N Q_\mu(x) D_{\mu\nu}^\xi Q_\nu(x),$$

where  $\operatorname{tr}_N$  means trace over internal indices (although we do not write them explicitly) and  $Q_\mu$  describes quantum fluctuations of the gauge fields. Functional integration of the expression  $\exp S_2[Q]$ , as known, gives the one-loop effective action,  $\Gamma_{\text{gauge}}[B] = \frac{1}{2} \ln \det(D^\xi)$ , that is invariant under the background field (star)gauge transformations of the form  $\delta B_\mu(x) = \nabla_\mu \lambda(x)$ . Some aspects of the background field formalism in NC field theories can be found, for instance, in Ref. [22].

We define also the operator  $D_0 := -\nabla^2$  which is a self-adjoint non-negative operator corresponding to the inverse propagator of ghost particles. In the following we assume that the operators  $D_0$  and  $D_{\mu\nu}^\xi$  have no zero-modes.

To simplify our analysis let us consider the case of  $U(1)$  gauge symmetry (generalization to the case of  $U(N)$  symmetry will be discussed in details in the next section). The heat trace for the kinetic operator (1) is defined as

$$K^\xi(t) = \operatorname{Tr}_{L^2} \exp(-tD^\xi), \quad (2)$$

where  $t$  is a (positive) spectral parameter and the trace is taken on the space of square integrable functions [3], [4]. Usually this expression is regularized by subtracting the heat trace of the Laplacian  $\Delta = -\partial_\mu \partial^\mu$  since the small  $t$  asymptotic expansion of the quantity  $\operatorname{Tr}_{L^2} \exp(-tD^\xi)$  contains a volume term that is divergent on a non-compact manifold.

We wish to compute the heat trace in the limit of small spectral parameter  $t \rightarrow 0$  by means of the Fock-Schwinger-DeWitt proper-time method. To this aim we introduce two abstract Hilbert spaces spanned by basis vectors  $|x\rangle$  and  $|\mu, x\rangle$ , respectively, and define "Hamiltonian" operators  $\widehat{D}_0$  and  $\widehat{D}^\xi$  associated with  $D_0$  and  $D_{\mu\nu}^\xi$  by<sup>1</sup>

$$\langle x|\widehat{D}_0|x'\rangle = D_0\langle x|x'\rangle, \quad \langle x, \mu|\widehat{D}^\xi|\nu, x'\rangle = D_{\mu\lambda}^\xi\langle x, \lambda|\nu, x'\rangle. \quad (3)$$

Operators on the right hand sides of these expressions are viewed as differential operators with respect to the variable  $x$ . The basis vectors satisfy the orthonormality conditions

$$\langle x|x'\rangle = \delta(x, x'), \quad \langle x, \mu|\nu, x'\rangle = \delta_{\mu\nu}\delta(x, x').$$

Note that, in the case of an arbitrary manifold, index of  $|\mu, x\rangle$  (as well as that of the conjugate  $\langle x, \mu|$ ) is regarded as that of a covariant vector density of weight 1/2 [23].

Next, the proper-time transformation functions, or heat kernels, for the operators  $D_0$  and  $D_{\mu\nu}^\xi$  are introduced by

$$K_0(x, x'; t) = \langle x|\exp[-t\widehat{D}_0]|x'\rangle, \quad K_{\mu\nu}^\xi(x, x'; t) = \langle x, \mu|\exp[-t\widehat{D}^\xi]|\nu, x'\rangle, \quad (4)$$

where  $t$  is interpreted as the proper-time parameter<sup>2</sup>. By making use of (3) it can be straightforwardly checked that the kernels  $K_0(x, x'; t)$  and  $K_{\mu\nu}^\xi(x, x'; t)$  satisfy the heat equations:

$$\begin{aligned} \left(\frac{\partial}{\partial t} + D_0\right) K_0(x, x'; t) &= 0, \\ \left(\delta_{\mu\lambda}\frac{\partial}{\partial t} + D_{\mu\lambda}^\xi\right) K_{\lambda\nu}^\xi(x, x'; t) &= 0, \end{aligned} \quad (5)$$

with the boundary conditions

$$\lim_{t \rightarrow 0} K_0(x, x'; t) = \delta(x, x'), \quad \lim_{t \rightarrow 0} K_{\mu\nu}^\xi(x, x'; t) = \delta_{\mu\nu}\delta(x, x'). \quad (6)$$

<sup>1</sup>In this paper we are dealing with flat Euclidean space and therefore the distinction between upper and lower indices is irrelevant.

<sup>2</sup>That is, the exponential operators on the right hand sides of (4) can be regarded as evolution operators of a "particle" in the proper time  $t$  [24].

From the kernels (4) one can obtain the one-loop effective action of pure NC Yang-Mills theory using the standard formal expressions:

$$\begin{aligned}\Gamma^{(1)}[B] &= \Gamma_{gauge}[B] + \Gamma_{ghost}[B], \\ \Gamma_{gauge}[B] &= \frac{1}{2} \ln \det(D^\xi) = -\frac{1}{2} \int_{R^n} dx \int_0^\infty \frac{dt}{t} \text{tr}_V K_{\mu\nu}^\xi(x, x; t), \\ \Gamma_{ghost}[B] &= -\ln \det(D) = \int_{R^n} dx \int_0^\infty \frac{dt}{t} \text{tr}_V K_0(x, x; t),\end{aligned}\tag{7}$$

where the first term,  $\Gamma_{gauge}[B]$ , describes a contribution to the effective action coming from the gauge sector of the model while the second term,  $\Gamma_{ghost}[B]$ , stands for the ghost contribution;  $\text{tr}_V$  means trace over Euclidean vector and, in general, internal indices. As is well-known, the expression for  $\Gamma^{(1)}[B]$  is divergent and must be regularized. This can be done, for instance, by replacing  $1/t$  in the integrands of (7) with  $\mu^{2\epsilon}/t^{1-\epsilon}$ , where  $\epsilon$  is a complex parameter and  $\mu$  is a dimensional quantity introduced to keep the total mass dimension of the expression unchanged. Now all information on the one-loop effective action contains in the heat traces which at  $t \rightarrow 0^+$  can be expanded in series over the spectral (proper time) parameter :

$$TrK(D; t) \simeq \sum_{k=0}^{\infty} t^{(k-n)/2} a_k(D).\tag{8}$$

The coefficients  $a_k(D)$  here define the asymptotics of the heat trace as  $t \rightarrow 0$ . On the manifold without boundary odd-numbered coefficients are equal to zero. From the expressions (7) and (8) one sees that terms with  $k \leq n$  in the heat kernel expansion can potentially give rise to divergences in the effective action.

In the commutative case the heat kernel coefficients  $a_k$ , known also as diagonal Seeley-Gilkey-DeWitt coefficients [23], [25], [26], are expressed only in terms of local gauge covariant quantities, such as matter fields, gauge field strength tensor and their covariant derivatives, and, hence, are manifestly gauge invariant objects (see review article [4]). However, on  $\theta$ -deformed manifolds, there appears another type of coefficients in the heat kernel expansion (8), so-called mixed coefficients, that reflect the non-local nature of NC field theories [7], [9]. As we have mentioned earlier, the contribution of these mixed terms is equivalent to the contribution of non-planar diagrams to the effective action. In particular, it can develop non-local singularities as  $\epsilon \rightarrow 0$  if the deformation parameter is degenerate [14].

### 3 Noncommutative Endo formula

Consider the heat trace for the operator (1),  $\text{Tr}K_{\mu\nu}^\xi(x, x; t)$ , and compute the first three non-zero heat kernel coefficients in the small  $t$  asymptotic expansion for this quantity. In the Feynman gauge ( $\xi = 1$ ) it can be done by means of the calculating procedure described in Refs. [5], [6], [9]. To apply it in the more general case of an arbitrary value of the gauge-fixing parameter we will reproduce in what follows the non-commutative version of the Endo formula [15], [19]. To simplify our computations we suppose that the background field satisfies the equation of motion:

$$\nabla_\mu F_{\mu\nu} = \partial_\mu F_{\mu\nu} + [B_\mu, F_{\mu\nu}]_\star = 0.\tag{9}$$

Then the following relation holds (see Ref [28] for details):

$$K_{\mu\nu}^\xi(x, x'; t) = K_{\mu\nu}^{\xi=1}(x, x'; t) - \int_t^{\frac{t}{\xi}} d\tau \nabla_\mu \nabla'_\nu K_0(x, x'; \tau),\tag{10}$$

where and prime over nabla indicates that this operator acts on  $x'$  variable. Accordingly, one can write down the similar relation for the corresponding heat traces<sup>3</sup>:

$$\begin{aligned}K^\xi(t, D^{(\xi)}) &= K^{\xi=1}(t, D^{(\xi=1)}) \\ &- \int_t^{t/\xi} d\tau \int_{\mathcal{M}} d^4x (\nabla_\mu \nabla'_\nu K_0(x, x'; \tau) - \partial_\mu \partial'_\nu K'_0(x, x'; \tau))|_{x=x'},\end{aligned}\tag{11}$$

where  $K'_0(x, x'; \tau) := \langle x | e^{-t\partial^2} | x' \rangle$ . Formula (11) is the starting point of our computations. More precisely, we are going to investigate the heat asymptotics for the trace of the kernel (11). In this connection it is necessary to note that the operators  $\exp(-tD^{\xi=1})$  and  $\exp(-tD_0)$  are trace-class for positive values of the spectral parameter  $t$  and, hence, the asymptotic expansions for the kernels in RHS of (11) are well-defined [5], [6], [9], [10].

<sup>3</sup>Notice that one has to eliminate volume divergences by adding appropriate terms.

#### 4 U(N) gauge symmetry

Let  $T^A$ ,  $A = 0, 1, \dots, N^2 - 1$ , be the generators of the  $U(N)$  group in the fundamental representation. The background potential is represented as  $B_\mu = B_\mu^A T^A$  that is a  $N \times N$  matrix in the group space. We normalize the  $U(1)$  generator as follows  $T^0 = \frac{1}{\sqrt{2N}}$ , so that

$$\text{tr}_N T^A T^B = \frac{1}{2} \delta^{AB}.$$

The generators of the  $SU(N)$  subgroup obey the algebra  $[T^a, T^b] = if^{abc}T^c$ , where  $f^{abc}$  are totally antisymmetric structure constants of the gauge group. One can also define an anticommutator as  $\{T^a, T^b\} = \frac{1}{N} \delta^{ab} + d^{abc} T^c$  with symmetric structure constants  $d^{abc}$ . The completeness relation is written in the form (here, as usual, the repeated indices are summed over)

$$T_{\alpha\beta}^a T_{\gamma\delta}^a = \frac{1}{2} \delta_{\alpha\delta} \delta_{\beta\gamma} - \frac{1}{2N} \delta_{\alpha\beta} \delta_{\gamma\delta}$$

which can be used to derive the following useful identities:

$$T_{\alpha\beta}^a T_{\beta\gamma}^a = \frac{N^2 - 1}{2N} \delta_{\alpha\gamma}, \quad T_{\alpha\beta}^A T_{\beta\gamma}^A = \frac{N}{2} \delta_{\alpha\gamma}. \quad (12)$$

It can be easily seen that the relations (9)-(10) remain unchanged with the only difference that now one looks at them as matrix relations. Similarly, to define heat kernels for the operators  $(D_0)_{\alpha\beta}$  and  $(D_{\mu\nu}^\xi)_{\alpha\beta}$  one can introduce two abstract Hilbert spaces spanned by basis vectors  $|x, A\rangle$  and  $|\mu, x, A\rangle$ , respectively, which satisfy the orthonormality conditions

$$\begin{aligned} \langle A, x | x', B \rangle &= \delta(x, x') \delta^{AB}, \\ \langle A, x, \mu | \nu, x', B \rangle &= \delta_{\mu\nu} \delta(x, x') \delta^{AB}. \end{aligned}$$

Then the heat kernels for the operators  $D_0$  and  $D_{\mu\nu}^\xi$  are defined by

$$\begin{aligned} K_0(x, x'; t) &= (x | \exp[-t\hat{D}_0] | x'), \\ K_{\mu\nu}^\xi(x, x'; t) &= (x, \mu | \exp[-t\hat{D}^\xi] | \nu, x'), \end{aligned} \quad (13)$$

where we denote  $(x | = T^A \langle A, x | := \sum_{A=1}^{N^2} T^A \langle A, x |$  and  $(x, \mu | = T^A \langle A, x, \mu |$ .

As an example, consider the planar contribution to the non-minimal ( $\xi$ -dependent) term of the quantity (11). In the  $U(N)$  case it reads

$$\int_{R^n} dx \text{tr}_N \left[ \{ \nabla_\mu^L \nabla_\mu^L e^{-tD_0^L} + \nabla_\mu^R \nabla_\mu^R e^{-tD_0^R} - 2\partial^2 e^{t\partial^2} \} (x | x') \right]_{x=x'}. \quad (14)$$

With the help of (12) and the orthonormality condition one has

$$(x | x')_{\alpha\beta} = T_{\alpha\gamma}^A \langle A, x | x', B \rangle T_{\gamma\beta}^B = T_{\alpha\gamma}^A T_{\gamma\beta}^A \langle x | x' \rangle = \frac{N}{2} \delta_{\alpha\beta} \langle x | x' \rangle.$$

By making use of the plane-wave basis and applying the calculating technique of the preceding section one obtains:

$$\begin{aligned} \tilde{a}_2^{planar}(\nabla^2, D_0) &= \frac{1}{(4\pi)^{\frac{n}{2}}} \frac{N}{2} \int_{R^n} dx \frac{4-n}{24} \text{tr}_N F_{\mu\nu} \star F_{\mu\nu}, \\ \tilde{a}_4^{planar}(\nabla^2, D_0) &= \frac{1}{(4\pi)^{\frac{n}{2}}} \frac{N}{2} \int_{R^n} dx \frac{n-6}{360} \text{tr}_N (6F_{\mu\nu} \star F_{\nu\lambda} \star F_{\lambda\mu} \\ &\quad + 2\nabla_\mu F_{\nu\lambda} \star \nabla_\mu F_{\nu\lambda} - \nabla_\mu F_{\mu\lambda} \star \nabla_\nu F_{\nu\lambda}). \end{aligned} \quad (15)$$

where  $\text{tr}_N$  means trace over internal indices. The mixed terms are treated in a similar way. One gets, in particular,

$$\tilde{a}_n^{mixed}(\nabla^2, D_0) = -2(\det \theta)^{-1} (2\pi)^{-n} \int_{R^n} dx \int_{R^n} dy \text{tr}_N B_\mu(x) T^D B_\mu(y) T^D. \quad (16)$$

Next,

$$\begin{aligned} \text{tr}_N T^A T^D T^C T^D &= \text{tr}_N \left( \frac{1}{2N} T^A T^C + T^A T^d T^C T^d \right) \\ &= \text{tr}_N \left( \frac{1}{2N} T^A T^C \right) + \frac{1}{2} T_{\alpha\alpha}^A T_{\beta\beta}^C - \frac{1}{2N} T_{\alpha\beta}^A T_{\beta\alpha}^C = \frac{1}{2} \text{tr}_N T^A \text{tr}_N T^C, \end{aligned}$$

where we used the completeness relation for the generators of the  $SU(N)$  group. Hence one arrived at the following expression for  $\tilde{a}_n^{mixed}$ :

$$\begin{aligned}\tilde{a}_n^{mixed}(\nabla^2, D_0) &= -\frac{(\det \theta)^{-1}}{(2\pi)^n} \int_{R^n} dx \int_{R^n} dy \operatorname{tr}_N B_\mu(x) \operatorname{tr}_N B_\mu(y) \\ &= -\frac{(\det \theta)^{-1}}{2(2\pi)^n} \int_{R^n} dx \int_{R^n} dy B_\mu^0(x) B_\mu^0(y).\end{aligned}\quad (17)$$

According to the formula (11), the planar heat kernel coefficients for the operator (1) are given by

$$\begin{aligned}a_4^{planar} &= \frac{1}{(4\pi)^{\frac{n}{2}}} \frac{N}{2} \int_{R^n} dx \left( \frac{n}{6} - 1 + \frac{1}{12}(1 - \xi^{\frac{n-4}{2}}) \right) \operatorname{tr}_N F_{\mu\nu} \star F_{\mu\nu}, \\ a_6^{planar} &= \frac{1}{(4\pi)^{\frac{n}{2}}} \frac{1}{360} \frac{N}{2} \int_{R^n} dx \operatorname{tr}_N \{ 120 F_{\mu\nu} \star F_{\nu\lambda} \star F_{\lambda\mu} \\ &\quad - 60 F_{\mu\nu} \star \nabla^2 F_{\mu\nu} - 2[n+1 - \xi^{\frac{n-6}{2}}](6 F_{\mu\nu} \star F_{\nu\lambda} \star F_{\lambda\mu} \\ &\quad + 2 \nabla_\mu F_{\nu\lambda} \star \nabla_\mu F_{\nu\lambda} - \nabla_\mu F_{\mu\lambda} \star \nabla_\nu F_{\nu\lambda}) \}.\end{aligned}\quad (18)$$

The first non-zero mixed coefficient is written as

$$a_{n+2}^{mixed} = \{2(n-1) + \xi^{-1}\} \frac{(\det \theta)^{-1}}{2(2\pi)^n} \int_{R^n} dx \int_{R^n} dy B_\mu^0(x) B_\mu^0(y).\quad (19)$$

This expression is manifestly gauge invariant and depends only upon zeroth component of the gauge potential.

## 5 Discussion

Let us make a few remarks about the obtained results. We consider the particular case of dimension  $n = 4$  for the purpose of definiteness. First, it is seen from (18) that the fourth heat kernel coefficient do not depend upon the gauge fixing parameter  $\xi$ . Thus, the one-loop  $\beta$ -function is a gauge-fixing independent object as it is in the commutative Yang-Mills theory (see, for instance, Refs. [16], [18]).

Second, in the case of a non-degenerate  $\theta$  matrix the one-loop renormalization of the theory is not affected by the mixed coefficients. Moreover, they are completely determined by  $U(1)$  sector of the model. In the diagrammatic approach this implies the known fact that non-planar one-loop  $U(N)$  diagrams contribute only to the  $U(1)$  part of the theory [12], [29]. As it was mentioned, such coefficients are responsible for the UV/IR mixing phenomenon [6], [9].

Third, in the case of a degenerate deformation parameter the first non-trivial mixed contribution appears already in  $a_4$ -coefficient (see also the recent paper [10]). To see this let us examine the space-like noncommutativity when components  $\theta^{0i}$ ,  $i = 1, 2, 3$  are equal to zero. For convenience, we adopt the same conventions as in Ref. [14] (see Appendix B for details). Then after simple manipulations one gets

$$a_4^{mixed} = \frac{(\det \theta_2)^{-1}}{32\pi^3} (8 + \ln \xi) \int_{R^2} d\tilde{x} \int_{R^2 \times R^2} d\bar{x} d\bar{y} \sum_{i=2,3} B_i^0(\tilde{x}, \bar{x}) B_i^0(\tilde{x}, \bar{y}),\quad (20)$$

where tensor  $\theta_2$  corresponds to the  $i = 2, 3$  plane. Note that, contrary to its planar counterpart, this coefficient itself is dependent on the gauge-fixing parameter. Next, it can be easily shown that a non-planar divergent part of the one-loop effective action for the  $U(1)$  sector of the model is presented by<sup>4</sup>

$$\begin{aligned}\Gamma_{NP}^{div.}[B^0] &= -\frac{\mu^{2\epsilon}}{32\pi^3 \det \theta_2} (8 + \ln \xi) \int_0^\infty \frac{dt}{t^\epsilon} \int_{R^2} d\tilde{x} \int_{R^2 \times R^2} d\bar{x} d\bar{y} \\ &\quad \times \sum_{i=2,3} B_i^0(\tilde{x}, \bar{x}) B_i^0(\tilde{x}, \bar{y}) \exp\left[-\frac{t(\bar{x} - \bar{y})^2}{\det \theta_2}\right],\end{aligned}$$

which gives the non-local, singular (as  $\epsilon \rightarrow 0$ ) and, in addition, gauge-fixing dependent contribution to the 1PI 2-point Green function of the form [14]

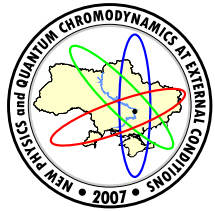
$$\Gamma_{ij U(1)}^{div.}(x_1 - x_2) = -\frac{\mu^{2\epsilon}}{16\pi^3 \det \theta_2} \delta_{ij} (8 + \ln \xi) \Gamma(\epsilon) \delta^2(\tilde{x}_1 - \tilde{x}_2) \left( \frac{(\bar{x}_1 - \bar{x}_2)^2}{\det \theta_2} \right)^{-\epsilon}.$$

Hence we come to the conclusion that the renormalization properties of NC  $U(N)$  theory are actually ruined by its  $U(1)$  sector in the degenerate case. It looks rather surprising but even this crucial drawback of the space-like noncommutative models may be bypassed in the context of so-called twisted gauge transformations considered in the next section.

<sup>4</sup>For the sake of brevity we do not consider the ghost contribution here. We remark only that this contribution does not change our conclusion.

## References

- [1] P. B. Gilkey, *Invariance Theory, the Heat Equation, and the Atiyah-Singer Index theorem* (CRC Press, Boca Raton, Florida, 1994).
- [2] N. Berline, E. Getzler and M. Vergne, *Heat Kernels and Dirac Operators* (Springer, Berlin, 1992).
- [3] K. Kirsten, *Spectral Functions in Mathematics and Physics*, (Chapman & Hall/CRC, Boca Raton, FL, 2001).
- [4] D. V. Vassilevich, Phys.Rept. **388**, 279-360 (2003) [hep-th/0306138].
- [5] D. V. Vassilevich, Lett.Math.Phys. **67**, 185-194 (2004) [hep-th/0310144].
- [6] V. Gayral and B. Iochum, J.Math.Phys. **46**, 043503 (2005) [hep-th/0402147].
- [7] V. Gayral, Ann. Henri Poincaré **6**, 991-1023 (2005) [hep-th/0412233].
- [8] D. V. Vassilevich, Nucl.Phys. **B715**, 695-712 (2005) [hep-th/0406163].
- [9] D. V. Vassilevich, JHEP **0508**, 085 (2005) [hep-th/0507123].
- [10] V. Gayral, B. Iochum and D. V. Vassilevich, hep-th/0607078.
- [11] I. Chepelev and R. Roiban, JHEP **0005**, 037 (2000) [hep-th/9911098].
- [12] S. Minwalla, M. Van Raamsdonk and N. Seiberg, JHEP **0002**, 020 (2000) [hep-th/9912072].
- [13] I. Y. Aref'eva, D. M. Belov and A. S. Koshelev, Phys.Lett. **B476**, 431 (2000) [hep-th/9912075].
- [14] V. Gayral, J. M. Gracia-Bondia and F. R. Ruiz, Phys.Lett. **B610**, 141-146 (2005) [hep-th/0412235].
- [15] R. Endo, Prog.Theor.Phys. **71**, 1366 (1984).
- [16] A. O. Barvinsky and G. A. Vilkovisky, Phys.Rep. **119** (1985).
- [17] V. P. Gusynin, E. V. Gorbar and V. V. Romankov, Nucl.Phys. **B362**, 449-471 (1991).  
V. P. Gusynin and E. V. Gorbar, Phys.Lett. **B270**, 29-36 (1991).
- [18] E. I. Guendelman, A. Leonidov, V. Nechitailo and D. A. Owen, Phys.Lett. **B324**, 160-163 (1994) [hep-th/9312138].
- [19] R. Endo, Class.Quant.Grav. **12**, 1157-1164 (1995) [hep-th/9407019].
- [20] S. Alexandrov and D. V. Vassilevich, J.Math.Phys. **37**, 5715 (1996) [hep-th/9601090].
- [21] I. G. Avramidi and T. Branson, Rev.Math.Phys. **13**, 847-890 (2001).  
I. G. Avramidi, math-ph/0509023.
- [22] L. Alvarez-Gaume and J. L. F. Barbon, Int.J.Mod.Phys. **A16**, 1123 (2001) [hep-th/0006209];  
A. Das, J. Frenkel, S. H. Pereira and J. C. Taylor, Phys.Lett. **B577**, 76-82 (2003) [hep-th/0309165].
- [23] B. S. DeWitt, *The dynamical theory of groups and fields* (Gordon and Breach, New York, 1965).
- [24] J. Schwinger, Phys.Rev. **82**, 664 (1951).
- [25] R. T. Seeley, Proc.Symp.Pure Math. **10**, 288-307 (1967).
- [26] P. B. Gilkey, J.Diff.Geom. **10**, 601-618 (1975).
- [27] R. I. Nepomechie, Phys.Rev. **D31**, 3291 (1985).
- [28] A. Strelchenko, Int.J.Mod.Phys. **A22**, 181 (2007) [hep-th/0608134].
- [29] A. Armoni, Nucl.Phys. **B593**, 229 (2001) [hep-th/0005208].



## THE LOGARITHMIC PERTURBATION THEORY FOR BOUND STATES IN SPHERICAL-SYMMETRIC POTENTIALS VIA THE $\hbar$ -EXPANSIONS

R. S. Tutik<sup>a</sup>, I. V. Dobrovolska<sup>b</sup>

Theoretical Physics Department  
Dnipropetrovsk National University, Dnipropetrovsk, Ukraine

The explicit semiclassical treatment of the logarithmic perturbation theory for the bound-state problem for the spherical anharmonic oscillator and the screened Coulomb potential is developed. Based upon the  $\hbar$ -expansions and suitable quantization conditions a new procedure for deriving perturbation expansions is offered. Avoiding disadvantages of the standard approach, new handy recursion formulae with the same simple form both for ground and excited states have been obtained. As examples, the perturbation expansions for the energy eigenvalues of the quartic anharmonic oscillator and the Debye potential are considered.

### 1 Introduction

The main task in application of the quantum mechanics is to solve the Schrödinger equations with different potentials. Unfortunately, realistic physical problems can practically never be solved exactly. Then one has to resort to some approximations. Most widely used among them is the perturbation theory. However, the explicit calculation with the Rayleigh–Schrödinger perturbation theory, described in most quantum mechanics textbooks, runs into the difficulty of the summation over all intermediate unperturbed eigenstates. To avoid this difficulty, various alternative perturbation procedures have been proposed [1–13].

Nevertheless up to now, one of the principal approximation techniques is the logarithmic perturbation theory [14–21]. Within the framework of this approach, the conventional way to solve a quantum-mechanical bound-state problem consists in changing from the wave function to its logarithmic derivative and converting the time-independent Schrödinger equation into the nonlinear Riccati equation.

In the case of ground states, the consequent expansion in a small parameter leads to handy recursion relations that permit us to derive easily the corrections to the energy as well as to the wave function for each order. However, when radially excited states are considered, the standard technique of the logarithmic perturbation theory becomes extremely cumbersome and, practically, inapplicable for describing higher orders of expansions.

Recently, a new procedure based on specific quantization conditions has been proposed to get series of the logarithmic perturbation theory via the  $\hbar$ -expansion technique within the framework of the one-dimensional Schrödinger equation [22]. Avoiding the disadvantages of the standard approach, this straightforward semiclassical procedure results in new handy recursion formulae with the same simple form both for the ground state and excited states.

The object of the present work is to extend the above mentioned formalism to the bound-state problems within the framework of the three-dimensional Schrödinger equation with central potentials, such as the anharmonic oscillator potential and the screened Coulomb one, which are widely used in practice.

### 2 Basic concepts of the method

We study the bound-state problem for a non-relativistic particle moving in a central potential admitted bounded eigenfunctions and having in consequence a discrete energy spectrum. Let us therefore consider the reduced radial part of the Schrödinger equation

$$-\frac{\hbar^2}{2m}U''(r) + \left[ \frac{\hbar^2 l(l+1)}{2mr^2} + V(r) \right] U(r) = EU(r), \quad (1)$$

with the effective potential having only one simple minimum.

Following usual practice, we apply the substitution,  $C(r) = \hbar U'(r)/U(r)$ , accepted in the logarithmic perturbation theory and go over from the Schrödinger equation (1) to the Riccati equation

$$\hbar C'(r) + C^2(r) = \frac{\hbar^2 l(l+1)}{r^2} + 2mV(r) - 2mE. \quad (2)$$

e-mail: <sup>a</sup>tutik@ff.dsu.dp.ua, <sup>b</sup>dobrovolska@resonance.zp.ua

© Tutik R.S., Dobrovolska I.V., 2007.

According to our assumption, we are seeking the eigenvalues and the eigenfunctions of this equation explicitly in a semiclassical manner with series expansions in powers of the Planck constant

$$E = \sum_{k=k1}^{\infty} E_k \hbar^k, \quad C(r) = \sum_{k=k2}^{\infty} C_k(r) \hbar^k, \quad (3)$$

where the order in  $\hbar$  of these quantities, i.e. the values of  $k1$  and  $k2$ , should be defined as a preliminary.

As in the standard approach, the substitution of these expansions into the Riccati equation leads to the simple recursion system. This system can be solved successively in the case of ground states, while the description of the excited states has some problems with taking into account the nodes of wave functions. For avoiding these problems, we shall attempt to use the quantization condition and the formalism of the theory of functions of a complex variable.

Remind that, in the complex plane, a number of zeros  $N$  of a regular function inside a closed contour is defined by the principle of argument known from the complex analysis. Being applied to the logarithmic derivative,  $C(r)$ , it means that

$$\frac{1}{2\pi i} \oint C(r) dr = \frac{1}{2\pi i} \sum_{k=0}^{\infty} \hbar^k \oint C_k(r) dr = \hbar N. \quad (4)$$

This quantization condition is exact and is widely used for deriving higher-order corrections to the WKB-approximation [23, 24] and the  $1/N$ -expansions [25–27]. There is, however, one important point to note. Because the radial and orbital quantum numbers,  $n$  and  $l$ , correspondingly, are specific quantum notions, the quantization condition (4) must be supplemented with a rule of achieving a classical limit for these quantities. It is this rule that stipulates the kind of the semiclassical approximation.

In particular, within the framework of the WKB-approach the passage to the classical limit is implemented using the rule

$$\hbar \rightarrow 0, \quad n \rightarrow \infty, \quad l \rightarrow \infty, \quad \hbar n = \text{const}, \quad \hbar l = \text{const}, \quad (5)$$

whereas the  $1/N$ -expansion requires the condition [25–27]

$$\hbar \rightarrow 0, \quad n = \text{const}, \quad l \rightarrow \infty, \quad \hbar n \rightarrow 0, \quad \hbar l = \text{const}. \quad (6)$$

The proposed semiclassical treatment of the logarithmic perturbation theory involves the alternative possibility:

$$\hbar \rightarrow 0, \quad n = \text{const}, \quad l = \text{const}, \quad \hbar n \rightarrow 0, \quad \hbar l \rightarrow 0. \quad (7)$$

With the last rule, the right-hand side of the equation (4) has the first order in  $\hbar$  and the quantization condition now takes the simple form

$$\frac{1}{2\pi i} \oint C_1(r) dr = N, \quad \frac{1}{2\pi i} \oint C_k(r) dr = 0, \quad k \neq 1. \quad (8)$$

However, this definition of the quantization condition is incomplete since we have not pointed out the path of integration. We shall now show that the suitable choice of the contour of integration and the consequent integration with application of the Cauchy residue theorem easily solves the problem of describing radially excited states.

### 3 The anharmonic oscillator

*Quantization conditions.* The discussion of details of the proposed technique we begin with the case of the anharmonic oscillator potential which is given by a symmetric function  $V(r)$  that can be written as a Taylor series expansion

$$V(r) = \frac{1}{2} m \omega^2 r^2 + \sum_{i \geq 1} f_i r^{2i+2}. \quad (9)$$

In the first place, let us consider the rule (7) of achieving the classical limit from the physical point of view. Since  $\hbar l \rightarrow 0$  as  $\hbar \rightarrow 0$ , the centrifugal term,  $\hbar^2 l(l+1)/r^2$ , has the second order in  $\hbar$  and disappears in the classical limit that corresponds to falling a particle into the center. This means that a particle drops into the bottom of the potential well as  $\hbar \rightarrow 0$  and its classical energy becomes  $E_0 = \min V(r) = 0$ . Hence, the series expansions in powers of the Planck constant for the energy eigenvalues and the  $C(r)$  must now read as  $E = \sum_{k=1}^{\infty} E_k \hbar^k$  and  $C(r) = \sum_{k=0}^{\infty} C_k(r) \hbar^k$ .

Upon inserting these expansions into the Riccati equation (2) and collecting coefficients of equal powers of  $\hbar$ , we obtain the following hierarchy of equations

$$\begin{aligned}
 C_0^2(r) &= 2 m V(r), \\
 C_0'(r) + 2 C_0(r) C_1(r) &= -2 m E_1, \\
 C_1'(r) + 2 C_0(r) C_2(r) + C_1^2(r) &= \frac{l(l+1)}{r^2} - 2 m E_2, \\
 &\dots \\
 C_{k-1}'(r) + \sum_{i=0}^k C_i(r) C_{k-i}(r) &= -2 m E_k, \quad k > 2.
 \end{aligned} \tag{10}$$

In the case of ground states, this recurrence system can be solved as straightforwardly as in the standard approach. For excited states, we intend to take into account the nodes of the wave function with the quantization condition (8) for which we must define the contour of integration.

It should be stressed that our technique is quite distinguished from the WKB method not only in the rule of achieving a classical limit but also in the choice of a contour of integration in the complex plane. With a view to elucidate the last difference let us now sketch out the WKB treatment of this bound-state problem. In the complex plane, because the potential is described by the symmetric function (9), there are two pairs of turning points, i.e. zeros of the classical momentum, on the real axis. Therefore we have two cuts between these points: in the region  $r > 0$  as well as in the region  $r < 0$ . In spite of only one cut lies in the physical region  $r > 0$ , the contour of integration in the WKB quantization condition has to encircle both cuts for the correct result for the harmonic oscillator to be obtained [28].

In our approach, when a particle is dropping into the bottom of the potential well these four turning points are drawing nearer and, at last, are joining together at the origin. Consequently, all zeros of the wave function are now removed from both positive and negative sides of the real axis into the origin and our contour of integration must enclose only this point and no other singularities.

Further, let us count the multiplicity of a zero formed in the wave function at  $r = 0$ . Imposed by the requirement of the regularity, the behavior  $r^{l+1}$  as  $r \rightarrow 0$  brings the value  $l + 1$ . The number of nodes in the physical region  $r > 0$  is equal to the radial quantum number  $n$ . But, because the potential (9) is a symmetric function, the same number of zeros must be in the region  $r < 0$ , too. Then the total number of zeros inside the contour becomes equal to  $N = 2n + l + 1$ .

For evaluation of the contour integrals in the quantization condition (8), let us consider the system (10) and investigate the behavior of the functions  $C_k(r)$ . From the first equation of this system, it follows instantly that the  $C_0(r)$  can be written as

$$C_0(r) = -[2mV(r)]^{1/2} = -m\omega r \left(1 + \frac{2}{m\omega^2} \sum_{i=1}^{\infty} f_i r^{2i}\right)^{1/2} = r \sum_{i=0}^{\infty} C_i^0 r^{2i}, \tag{11}$$

where the minus sign is chosen from the boundary conditions and coefficients  $C_i^0$  are defined by parameters of the potential through the relations

$$C_0^0 = -m\omega, \quad C_i^0 = \frac{1}{2m\omega} \left( \sum_{p=1}^{i-1} C_p^0 C_{i-p}^0 - 2m f_i \right), \quad i \geq 1. \tag{12}$$

At the origin, on account of the equality  $C_0(0) = 0$ , a simple pole arises for the function  $C_1(r)$ , while  $C_k(r)$  has a pole of the order  $(2k - 1)$ . Thus  $C_k(r)$  can be represented by the Laurent series

$$C_k(r) = r^{1-2k} \sum_{i=0}^{\infty} C_i^k r^{2i}, \quad k \geq 1. \tag{13}$$

Finally, with applying the residue theorem, the quantization condition (8) expressed explicitly in terms of the coefficients  $C_i^k$  takes the especially simple form

$$C_{k-1}^k = N \delta_{1,k}, \tag{14}$$

where  $N = 2n + l + 1$ .

It is this quantization condition that makes possible the common consideration of the ground and excited states and permits us to derive the simple recursion formulae.

*Recursion formulae and the example of application.* The substitution of the series (12) and (13) into the system (10) in the case  $i \neq k - 1$  yields the recursion relation for obtaining the Laurent-series coefficients of the logarithmic derivative of the wave function

$$C_i^k = -\frac{1}{2C_0^0} \left[ (3 - 2k + 2i)C_i^{k-1} + \sum_{j=1}^{k-1} \sum_{p=0}^i C_p^j C_{i-p}^{k-j} + \sum_{p=1}^i C_p^0 C_{i-p}^k - l(l+1)\delta_{2,k}\delta_{0,i} \right]. \quad (15)$$

If  $i = k - 1$ , by equating the expression (15) for  $C_{k-1}^k$  to the quantization condition (14) we arrive at the recursion formulae for the energy eigenvalues

$$2mE_k = -C_{k-1}^{k-1} - \sum_{j=0}^k \sum_{p=0}^{k-1} C_p^j C_{k-1-p}^{k-j}. \quad (16)$$

Derived in this way, first corrections to the energy eigenvalues of the spherical anharmonic oscillator take the form

$$\begin{aligned} E_1 &= \frac{1+2N}{2}\omega, \quad E_2 = \frac{(3-2L+6\eta)f_1}{4m^2\omega^2}, \\ E_3 &= \frac{1+2N}{8m^4\omega^5} [(-21+9L-17\eta)f_1^2 + m(15-6L+10\eta)\omega^2f_2], \\ E_4 &= \frac{1}{16m^6\omega^8} \left( [333+11L^2-3L(67+86\eta)+3\eta(347+125\eta)]f_1^3 \right. \\ &\quad \left. - 6m[60+3(-13+L)L+175\eta-42L\eta+55\eta^2]\omega^2f_1f_2 \right. \\ &\quad \left. + m^2[6L^2-12L(6+5\eta)+35(3+2\eta(4+\eta))]\omega^4f_3 \right), \\ E_5 &= -\frac{1+2N}{128m^8\omega^{11}} \left( [30885+909L^2-27L(613+330\eta) \right. \\ &\quad \left. + \eta(49927+10689\eta)]f_1^4 - 4m[11220+393L^2 \right. \\ &\quad \left. - 6L(1011+475\eta)+\eta(16342+3129\eta)]\omega^2f_1^2f_2 \right. \\ &\quad \left. + 16m^2[33L^2-L(501+190\eta)+63(15+\eta(19+3\eta))]\omega^4f_1f_3 \right. \\ &\quad \left. + 2m^2[3495+138L^2+4538\eta+786\eta^2-30L(63+26\eta)]\omega^4f_2^2 \right. \\ &\quad \left. - 4m^3[30L^2-20L(24+7\eta)+63(15+2\eta(8+\eta))]\omega^6f_4 \right), \end{aligned} \quad (17)$$

where  $N = 2n + l + 1$ ,  $\eta = N(N+1)$ ,  $L = l(l+1)$ .

As it was expected, the obtained expansion is indeed the series of the logarithmic perturbation theory in powers of the Taylor-series coefficients for the potential function, with the first approximation being equal to the energy of the three-dimensional harmonic oscillator

$$E_1 = \left( 2n + l + \frac{3}{2} \right) \omega. \quad (18)$$

Thus, the problem of obtaining the energy eigenvalues and eigenfunctions for the bound-state problem for the anharmonic oscillator can be considered solved. The equations (15)-(16) have the same simple form both for the ground and excited states and define a useful procedure for the successive calculation of higher orders of expansions of the logarithmic perturbation theory.

As an example, we examine eigenenergies for the anharmonic oscillator with the potential

$$V(r) = m\omega^2 r^2/2 + \lambda r^4, \quad \lambda > 0. \quad (19)$$

Then the equations (17) are rewritten as

$$\begin{aligned} E_1 &= \left( \frac{1}{2} + N \right) \omega, \quad E_2 = \frac{(3-2L+6\eta)}{4m^2\omega^2} \lambda, \quad E_3 = \frac{-(1+2N)(21-9L+17\eta)}{8m^4\omega^5} \lambda^2, \\ E_4 &= \frac{(333+11L^2-3L(67+86\eta)+3\eta(347+125\eta))}{16m^6\omega^8} \lambda^3, \\ E_5 &= \frac{-(1+2N)}{128m^8\omega^{11}} [30885+909L^2-27L(613+330\eta)+\eta(49927+10689\eta)] \lambda^4. \end{aligned} \quad (20)$$

We recall that here  $N = 2n + l + 1$ ,  $\eta = N(N + 1)$ ,  $L = l(l + 1)$ .

It is readily seen that the use of the  $\hbar$ -expansion technique does lead to the explicit perturbation expansion in powers of the small parameter  $\lambda$ .

In the case of ground states, obtained expansions for the energy eigenvalues coincide with those listed in Ref. [29]. In the case of excited states, our corrections coincide with corrections up to the second order which are just only calculated in Ref. [30].

As it is known, the expansions for the anharmonic oscillator are asymptotic and diverge for any finite value of the parameter  $\lambda$  that requires the use of some procedures of improving the convergence (for references see [31]). It should be noted, that the proposed technique is easily adapted to apply any scheme of the series renormalization [32].

#### 4 The screened Coulomb potential

*Quantization conditions.* Now let us consider the case of the screened Coulomb potential which in common practice has a form

$$V(r) = \frac{1}{r} F(\kappa, r). \quad (21)$$

where  $\kappa$  is a small parameter.

In what following, we do not single out explicitly the screening parameter, but incorporate it into coefficients  $V_i$  of the Taylor series expansion of this potential

$$V(r) = \frac{1}{r} \sum_{i=0}^{\infty} V_i r^i. \quad (22)$$

Note, that after performing the scale transformation  $r \rightarrow \hbar^2 r$  powers of the screening parameter appear in common with powers of Planck's constant squared. Hence, the perturbation series must be, as a matter of fact, not only  $\kappa$ -expansions but also the semiclassical  $\hbar^2$ -expansions, too.

In the classical limit, when a particle falls into the center, its energy eventually approaches infinity. Hence, the expansions (3) must be represented as  $E = \hbar^{-2} \sum_{k=0}^{\infty} E_k \hbar^{2k}$  and  $C(r) = \hbar^{-1} \sum_{k=0}^{\infty} C_k(r) \hbar^k$  that results in the recurrent system

$$\begin{aligned} C_0^2(r) &= -2mE_0, \\ C_0(r)C_1(r) &= m[V(r) - E_1], \\ C_1'(r) + 2C_0(r)C_2(r) + C_1^2(r) &= \frac{l(l+1)}{r^2} - 2mE_2, \\ \dots \\ C_{k-1}'(r) + \sum_{j=0}^k C_j(r)C_{k-j}(r) &= -2mE_k, \quad k > 2. \end{aligned} \quad (23)$$

which changes only in the first two equations in comparison with (10).

Now, let us consider the choice of the contour of integration in the quantization relation. Since in the classical limit a particle falls into center, the classical turning points again draw to the origin and the nodes of the wave function are joined together at  $r = 0$ . Then, as well as in the anharmonic oscillator case, the contour of integration must enclose only the origin. However, now the nodes of the function come into the origin only from the positive region of the real axis. Thus, with the number of nodes and the value  $l + 1$  included, the total number of zeros in the quantization condition (4) becomes equal to  $N = n + l + 1$ .

Further, from (23) it appears that  $C_0(r)$  is the constant and its Taylor-series coefficients are

$$C_0^0 = -\sqrt{-2mE_0}, \quad C_0^i = 0, \quad (24)$$

Owing to the Coulomb behavior of the potential at the origin, the  $C_1(r)$  has a simple pole at this point, while the function  $C_k(r)$  has a pole of the order  $k$  and may be represented as

$$C_k(r) = r^{-k} \sum_{i=0}^{\infty} C_i^k r^i, \quad (25)$$

that leads to the known quantization condition

$$C_{k-1}^k = N\delta_{1,k}, \quad (26)$$

where  $N = n + l + 1$ .

*Recursion formulae and the example of application.* After substitution (24)-(25) into (23), when ( $i \neq k$ ), we have:

$$\begin{aligned} C_i^1 &= \frac{m}{C_0^0} \left[ V_i - E_1 \delta_{i,1} \right], \\ C_i^k &= -\frac{1}{2C_0^0} \left[ (i-k+1)C_i^{k-1} + \sum_{j=1}^{k-1} \sum_{p=0}^i C_p^j C_{i-p}^{k-j} + 2mE_k \delta_{i,k} - l(l+1) \delta_{i,0} \delta_{k,2} \right], \quad k > 1. \end{aligned} \quad (27)$$

In the case  $i = k$ , from (26) and (27), we obtain

$$E_0 = -\frac{mV_0^2}{2N^2}, \quad E_1 = V_1, \quad E_k = -\frac{1}{2m} \left[ C_k^{k-1} + \sum_{j=1}^{k-1} \sum_{p=0}^k C_p^j C_{k-p}^{k-j} + 2C_0^0 C_k^k \right], \quad k > 1, \quad (28)$$

that, through the Taylor-series coefficients for the potential function, is

$$\begin{aligned} E_0 &= -\frac{mV_0^2}{2N^2}, \quad E_1 = V_1, \quad E_2 = \frac{(L-3N^2)V_2}{2mV_0}, \quad E_3 = \frac{N^2}{2m^2V_0^2} (1-3L+5N^2)V_3, \\ E_4 &= \frac{N^2}{8m^3V_0^4} ((3L^2-5N^2-7N^4)V_2^2 + (3L(2-L)-5N^2(5-6L)-35N^4)V_0V_4), \\ E_5 &= \frac{N^4}{8m^4V_0^5} ((-5L(2+3L)+7N^2(9-2L)+45N^4)V_2V_3 + \\ &\quad (12-50L+15L^2+35N^2(3-2L)+63N^4)V_0V_5), \end{aligned} \quad (29)$$

where  $N = n + l + 1$  and  $L = l(l+1)$ .

We see that the zero approximation gives the exact solution for the Coulomb problem.

As an example of application, we consider the case of the Debye potential, which is widely used in many branches of physics:

$$V(r) = -\frac{\alpha}{r} \exp(-\kappa r). \quad (30)$$

For this potential, the first corrections to the energy eigenvalues take the form

$$\begin{aligned} E_0 &= -\frac{m\alpha^2}{2N^2}, \quad E_1 = \alpha \kappa, \quad E_2 = \frac{(L-3N^2)}{4m} \kappa^2, \\ E_3 &= \frac{N^2}{12m^2\alpha} (1-3L+5N^2) \kappa^3, \\ E_4 &= \frac{N^2}{192m^3\alpha^2} [3L(2+5L)-5(11-6L)N^2+77N^4] \kappa^4, \\ E_5 &= \frac{N^4}{320m^4\alpha^3} [4-50L-45L^2+35(7-2L)N^2+171N^4] \kappa^5, \end{aligned} \quad (31)$$

where  $N = n + l + 1$ , and  $L = l(l+1)$ .

And again we recognize the explicit perturbation expansion in powers of the small parameter  $\kappa$ .

Typical results of the calculation with these formulae are presented in the Table I where the sequences of the partial sums of  $K$  corrections to the energy eigenvalues for the Debye potential  $V(r) = -\alpha \exp(-\kappa r)/r$  is compared with results of the numerical integration,  $E_{\text{num}}$ , in Coulomb units  $\hbar = m = \alpha = 1$ . It is seen that for small values of the screening parameter, the convergence of the series is quite sufficient for the use them without any renormalization.

## 5 Summary

In conclusion, a new useful technique for deriving results of the logarithmic perturbation theory has been developed. Based upon the  $\hbar$ -expansions and suitable quantization conditions, new handy recursion relations for solving the bound-state problem for a spherical anharmonic oscillator and a static screened-Coulomb potential have been obtained. These relations can be applied to excited states exactly in the same manner as to ground states providing, in principle, the calculation of the perturbation corrections of large orders in the analytic or numerical form. Besides this remarkable advantage over the standard approach to the logarithmic perturbation theory, our method does not imply knowledge of the exact solution for the zero approximation, which is obtained automatically. And at last, the recursion formulae at hand, having the same simple form both for the ground state and excited states, can be easily adapted to applying any renormalization scheme for improving the convergence of obtained series, as it is described in [32].

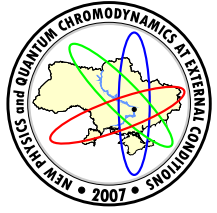
*Acknowledgments.* This research was supported by a grant N 0106U000782 from the Ministry of Education and Science of Ukraine which is gratefully acknowledged.

**Table 1.** The partial sums of  $K$  corrections to the energy eigenvalues for the Debye potential compared with results of the numerical integration,  $E_{\text{num}}$ , in Coulomb units  $\hbar = m = \alpha = 1$ .

$K$	$n = 0, l = 0,$ $\kappa = 0.2$	$n = 1, l = 0,$ $\kappa = 0.04$	$n = 1, l = 1,$ $\kappa = 0.02$
0	0.5000000000	0.1250000000	0.05555555556
1	0.3000000000	0.0750000000	0.03555555556
2	0.3300000000	0.0825000000	0.03805555556
3	0.3260000000	0.0816250000	0.03781555556
4	0.3271000000	0.0818140625	0.03786145556
5	0.3266800000	0.0817559375	0.03784969436
10	0.3268179839	0.0817715528	0.03785241171
15	0.3268059572	0.0817711705	0.03785238868
20	0.3268100537	0.0817711991	0.03785238922
25	0.3268067333	0.0817711961	0.03785238920
$E_{\text{num}}$	0.3268085112	0.0817711958	0.03785238920

## References

- [1] Sternheimer R., Phys.Rev. **84**, 244 (1951).
- [2] Sternheimer R. and Foley H., Phys.Rev. **102**, 731 (1956).
- [3] Dalgarno A. and Lewis J.T., Proc.R.Soc. **A233**, 70 (1955).
- [4] Schwartz C., Ann.Phys. **2**, 156 (1959).
- [5] Schwartz C. and Tiemann J.J., Ann.Phys. **2**, 178 (1959).
- [6] Mavromatis H.A., Am.J.Phys. **59**, 738 (1991).
- [7] Zel'dovich Ya.B., Zh.Eks.Teor.Fiz. **31**, 1101 (1956).
- [8] Baz A.I., Zel'dovich Ya.B. and Perelomov A.M., *Scattering, Reaction and Decay in Nonrelativistic Quantum Mechanics* (Jerusalem: Israel Program of Scientific Translation, 1969).
- [9] Coutinho F.A.B., Nogami Y. and Lauro Tomio, J.Phys.A: Math.Gen. **33**, 283 (2000).
- [10] Ciftci H., Hall R.L. and Saad, J.Phys.A: Math.Gen. **36**, 11807 (2003).
- [11] Bayrak O. and Boztosun I., J.Phys.A: Math.Gen. **39**, 6955 (2006).
- [12] Gonul B., Chin.Phys.Lett. **21**, 2330 (2004).
- [13] Gonul B., Celik N. and Olgar E., Mod.Phys.Lett. **A20**, 1683 (2005).
- [14] Polikanov V.S., Zh.Eks.Teor.Fiz. **52**, 1326 (1967).
- [15] Polikanov V.S., Teor.Mat.Fiz. **24**, 230 (1975).
- [16] Dolgov A.D. and Popov V.S., Phys.Lett. **B79**, 403 (1978).
- [17] Aharonov Y. and Au.C.K., Phys.Rev. **A20**, 2245 (1979).
- [18] Turbiner A.V., Usp.Fiz.Nauk **144**, 35 (1984).
- [19] Imbo T. and Sukhatme U., Am.J.Phys. **52**, 140 (1984).
- [20] Rogers G.M., J.Math.Phys. **26**, 567 (1985).
- [21] Mei W.N. and Chu D.S., Phys.Rev. **A58**, 713 (1998).
- [22] Dobrovolska I.V. and Tutik R.S., J.Phys.A: Math.Gen. **32**, 563 (1999).
- [23] Zwaan A., Arch.Nederland.Sci.Exact.Natur.Ser.3 **A12**, 1 (1929).
- [24] Dunham J.L., Phys.Rev. **41**, 713 (1932).
- [25] Stepanov S.S. and Tutik R.S., J.Phys.A: Math.Gen. **24**, L469 (1991).
- [26] Stepanov S.S. and Tutik R.S., Zh.Eks.Teor.Fiz. **100**, 415 (1991).
- [27] Stepanov S.S. and Tutik R.S., Teor.Mat.Fiz. **90**, 208 (1992).
- [28] Sergeenko M.N., quant-ph/9912069.
- [29] Dolgov A.D. and Popov V.S., Zh.Eks.Teor.Fiz. **75**, 2010 (1978).
- [30] Yukalova E.P. and Yukalov V.I., J.Phys.A: Math.Gen. **26**, 2011 (1993).
- [31] Yukalov V.I. and Yukalova E.P., Ann.Phys. **277**, 219 (1999).
- [32] Dobrovolska I.V. and Tutik R.S., Int.J.Mod.Phys. **A16**, 2493 (2001).



## PLASMA PHOTONS ARE ABLE TO EMIT AXIONS

V. S. Vanyashin

Dnipropetrovsk National University, Dnipropetrovsk, Ukraine

Hypothetical axions [1] have direct electromagnetic coupling similar to that of neutral pions:

$$\mathcal{L}_{A\gamma} = g_{A\gamma} \varphi_A \mathbf{E} \cdot \mathbf{H}. \quad (1)$$

Stellar plasma photons  $\tilde{\gamma}$  undergo the Primakoff conversion to axions  $A$ . The best upper limit for the axion-photon coupling constant  $g_{A\gamma}$  was obtained from the requirement that stellar evolution time scales are not appreciably affected by the axionic energy-loss channel [2]:

$$g_{A\gamma} < 0.6 \times 10^{-10} \text{ GeV}^{-1}. \quad (2)$$

It should be noted that the Primakoff conversion is complemented by another axion producing process which is caused by the two factors: the plasma photon instability and the axion mass smallness.

Photons in plasma are quasi-particles having limited lifetime. So they can emit low-mass particles within the range of their energy spreading. For the transversal photons in stellar interiors the energy spreading is orders of magnitude greater than the upper limit for the invisible axion mass [2]

$$m_A < 10^{-3} \text{ eV}. \quad (3)$$

The probability per unit time for the "decay" of a transversal plasma photon  $\tilde{\gamma} \rightarrow \tilde{\gamma} + A$  is given by the expression:

$$\frac{1}{\tau} = \frac{g_{A\gamma}^2}{16\pi E_p} \int_0^\infty dK K^2 \int_{-1}^1 dx \frac{1}{e^{\omega/T} - 1} \frac{1}{1 - e^{-\omega'/T}} \left[ \left( 1 + (\mathbf{n} \cdot \mathbf{n}')^2 \right) \left( \frac{k^2 \omega'}{\omega} + \frac{k'^2 \omega}{\omega'} \right) - 4(\mathbf{k} \cdot \mathbf{k}') \right] \times \frac{1}{\pi} \frac{\Gamma(\omega)/2 + \Gamma(\omega')/2}{(\omega - \omega' - E_p)^2 + [\Gamma(\omega) + \Gamma(\omega')]^2/4}, \quad (4)$$

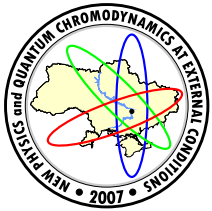
where

$$\omega \approx \sqrt{\omega_{\text{Le}}^2 + \mathbf{k}^2}, \quad \omega' \approx \sqrt{\omega_{\text{Le}}^2 + \mathbf{k}'^2}, \quad \mathbf{k} = \mathbf{K} + \frac{\mathbf{p}}{2}, \quad \mathbf{k}' = \mathbf{K} - \frac{\mathbf{p}}{2}, \quad x = \frac{\mathbf{K} \cdot \mathbf{p}}{K p}. \quad (5)$$

In this formula initial  $\mathbf{k}$  and final  $\mathbf{k}'$  plasma photon momenta are integrated over the Plank distribution, while the axion energy  $E_p = \sqrt{m_A^2 + \mathbf{p}^2}$  is kept fixed. That is adapted for calculating of the additional axionic flux, which, certainly, will diminish the existing stellar evolution [2] and laboratory [3] upper limits for the axion-photon coupling constant.

### References

- [1] R.Peccei and H.Quinn, Phys.Rev.Lett. **38**, 1440 (1977). S.Weinberg, Phys.Rev.Lett. **40**, 223 (1978). F.Wilczek, Phys.Rev.Lett. **40**, 279 (1978).
- [2] G.Raffelt, Physics Reports **198**, 1 (1990). G.Raffelt, hep-ph/0611350.
- [3] K. Zioutas *et al.* [CAST Collaboration], Phys.Rev.Lett. **94**, 121301 (2005) [hep-ex/0411033].



## MONOPOLE CONTRIBUTION TO THE WILSON LOOP IN THE 3D $SU(2)$ LATTICE GAUGE MODEL

S. Voloshin<sup>a</sup>, O. Borisenko<sup>b</sup>

N.N.Bogolyubov Institute for Theoretical Physics, National Academy of Sciences of Ukraine, Kiev, Ukraine

Using a plaquette formulation for lattice gauge models we describe monopoles of the 3D  $SU(2)$  theory which appear as configurations in the complete axial gauge and violate the continuum Bianchi identity. Furthermore we derive a dual representation for the Wilson loop in arbitrary representation and calculate the form of the interaction between generated electric flux and monopoles in the region of weak coupling relevant for the continuum limit. The effective theory which controls the interaction is a generalized version of the sine-Gordon model. The mechanism of confinement is proposed on the basis of the effective model obtained.

### 1 Introduction

The problem of the permanent confinement of quarks inside hadrons attracts attention of the theoretical physicists for the last three decades (see [1] and refs. therein for a recent review of the problem). Two of the most popular and the most elaborated mechanisms of confinement are based on the condensation of certain topologically nontrivial configurations - the so-called center vortices or monopoles. In this paper we are interested in the second of these configurations. It was proposed in [2] in the context of continuum compact three dimensional (3D) electrodynamics that the string tension is nonvanishing in this theory at any positive coupling constant, and the contribution of monopoles to the Wilson loop was estimated in the semiclassical approximation. Later this consideration was extended to  $U(1)$  lattice gauge theory (LGT) in 3D [3]. It turns out that these are precisely monopole configurations which make the string tension nonvanishing at all couplings. A rigorous proof of this property was done in [4]. While monopoles of abelian gauge models can be given a gauge invariant definition it is not the case for nonabelian models. The most popular approach consists in a partial gauge fixing such that some abelian subgroup of the full nonabelian group remains unbroken. Then, one can define monopoles in a nonabelian theory as monopoles of the unbroken abelian subgroup. Here we propose a different route to define monopoles in nonabelian models. Its main feature is complete gauge fixing. Monopoles appear as defects of smooth gauge fields which violate the Bianchi identity in the continuum limit, in the full analogy with abelian models. Our principal approach is to rewrite the compact LGT in the plaquette (continuum field-strength) representation and to find a dual form of the nonabelian theory. The Bianchi identity appears in such formulation as a condition on the admissible configurations. This allows to reveal the relevant field configurations contributing to the partition function and various observables. Such a program was accomplished for the abelian LGT in [3]. Here we are going to work out the corresponding approach for nonabelian models on the example of 3D  $SU(2)$  LGT.

### 2 Plaquette formulation and monopoles

The standard and possibly the only one available now tool of an investigation of such nonperturbative phenomenon like confinement is a quantization of the gauge fields on the lattice. Originally, LGT was formulated by K. Wilson in terms of group valued matrices on links of the lattice as fundamental degrees of freedom [5]. The partition function reads

$$Z = \int DU \exp\{-\beta S[U_\mu(x)]\}, \quad (1)$$

where  $S$  is the standard Wilson action and the integral is calculated over the Haar measure on the group at every link of the lattice.

The plaquette representation has been invented originally in the continuum theory by M. Halpern and extended to lattice models by G. Batrouni [6]. In this representation the plaquette matrices play the role of the dynamical degrees of freedom and satisfy certain constraints expressed through Bianchi identities in every cube of the lattice. In papers [7], [8], [9] we have developed a different plaquette formulation which we outline below.

e-mail: <sup>a</sup>sun-burn@yandex.ru, <sup>b</sup>oleg@bitp.kiev.ua

In the complete axial gauge

$$U_3(x, y, z) = U_2(x, y, 0) = U_1(x, 0, 0) = I \quad (2)$$

the partition function (1) can be identically rewritten on the dual lattice as

$$Z = \int \prod_l dV_l \exp[\beta \sum_l \operatorname{Re} \operatorname{Tr} V_l] \prod_{i=1}^4 \prod_{x(i)} J(V_x^{(i)}). \quad (3)$$

Here,  $V_l$  is a plaquette (dual link  $l$ ) matrix which satisfies constraint expressed through the group delta-function

$$J(V_x) = \sum_r d_r \chi_r(V_x), \quad (4)$$

where the sum over  $r$  is a sum over all representations of  $SU(N)$ ,  $\chi_r$  is character of  $r$ -th representation and  $d_r = \chi_r(I)$ .  $V_x$  is a certain product of plaquette matrices around a cube (dual site  $x$ ) of the lattice taken with the corresponding connectors. Connectors provide correct parallel transport of opposite sites of a given cube for nonabelian theory. In abelian models connectors are canceled out of group delta-functions. There appear four different types of connectors in our construction. E.g.,  $V_x$  for the first type is of the form

$$V_x^{(1)} = V_{l_5}^\dagger V_{l_1} V_{l_6}^\dagger C_{\vec{x}(1)} V_{l_2} V_{l_3} V_{l_4}^\dagger C_{\vec{x}(1)}^\dagger, \quad (5)$$

$$C_{\vec{x}(1)} = \prod_{k=z_i-1}^1 V_{n_2}(x_i, y_i - 1, k) \prod_{p=1}^{z_i-1} V_{n_1}(x_i - 1, y_i, p). \quad (6)$$

In what follows we consider the  $SU(2)$  gauge group. In this case it is easy to show that the constraint (4) expressed through elements of an algebra of  $SU(2)$  reads

$$\left[ \sum_k \omega_k^2(x) \right]^{1/2} = 2\pi m(x), \quad (7)$$

where  $m(x)$  is arbitrary integers and

$$\omega_k(x) = \sum_{i=1}^6 \theta_k(l_i) - \epsilon_{kmn} \left( \sum_{i < j}^6 \theta_m(l_i) \theta_n(l_j) + 2 \sum_{b \in C} \theta_m(b) \sum_{i=4}^6 \theta_n(l_i) + \dots \right). \quad (8)$$

In the continuum limit the last constraint reduces to the familiar Bianchi identity if one takes  $m(x) = 0$  for all  $x$ . However, when  $m(x)$  differs from zero one gets violation of the continuum Bianchi identity at the point  $x$ . This is genuine feature of compact gauge models. Below we want to clarify a role of these configurations in producing the string tension. Clearly,  $m(x) \neq 0$  configuration corresponds to the monopole configuration of nonabelian gauge field. Therefore, we may interpret the summation over  $m(x)$ , appearing below, as a summation over monopole charges which exist due to the periodicity of  $SU(2)$  delta-function (in close analogy with  $U(1)$  model).

Substituting (7) into (4) one can prove that the partition function (3) can be exactly rewritten to the following form [10]

$$Z_{SU(2)} = \int \prod_l \left[ \frac{\sin^2 W_l}{W_l^2} \prod_k d\omega_k(l) \right] \exp \left[ 2\beta \sum_l \cos W_l \right] \prod_x \frac{W_x}{\sin W_x} \prod_x \sum_{m(x)=-\infty}^{\infty} \int \prod_k d\alpha_k(x) \exp \left[ -i \sum_k \alpha_k(x) \omega_k(x) + 2\pi i m(x) \alpha(x) \right], \quad (9)$$

where  $\alpha(x) = (\sum_k \alpha_k^2(x))^{1/2}$ .

The Wilson loop of the size  $R \times T$  in some representation  $j$  gets the following form

$$W_j(C) = \operatorname{Tr} \prod_{n=R/2-1}^0 \left( \prod_{z_1=0}^{z+T-1} V_1^\dagger(x, y + 2n + 1, z_1) \prod_{z_2=z+T-1}^0 V_1^\dagger(x, y + 2n, z_2) \right). \quad (10)$$

We have supposed, for simplicity that the loop contour lies in the  $y - z$  plane, one side of the loop lies in the plane  $z = 0$  and  $R, T$  are even.

### 3 Effective monopole model for the Wilson loop

Here we would like to calculate the contribution of monopole configurations to the Wilson loop and estimate the string tension. We remind first the computations for the  $U(1)$  compact model and then proceed to the nonabelian theory.

#### 3.1 Monopoles in $U(1)$ LGT

The plaquette formulation of the  $U(1)$  LGT on the dual lattice reads

$$Z(h) = \int_0^{2\pi} \prod_l d\omega_l \exp [\beta \cos \omega_l] \int_{-\infty}^{\infty} \prod_x dr_x \sum_{m_x=-\infty}^{\infty} \exp \left[ i \sum_l \omega_l (r_x - r_{x+n}) + 2\pi i \sum_x r_x m_x + i \sum_l \omega_l h_l \right], \quad (11)$$

where the Bianchi identity has the form

$$\omega_x = \sum_{l \in x} \omega_l = 2\pi m_x. \quad (12)$$

Sources  $h_l$  have been introduced to represent the Wilson loop. Configurations with  $m_x \neq 0$  violate the continuum Bianchi identity in the same way as they do for the compact  $SU(2)$  model.

Consider the Wilson loop in the representation  $j$ . Let  $S_{xy}^d$  be some surface dual to the surface  $S_{xy}$  which is bounded by the loop  $C$  and consisting of links dual to plaquettes of the original lattice. Let  $b$  denote links from  $S_{xy}^d$ . Then, the expectation value of the Wilson loop takes the following form

$$\langle W(C) \rangle = \frac{1}{Z(0)} \exp \left[ -\frac{j^2}{4\beta} \sum_{b, b' \in S_{xy}^d} G_{bb'} \right] \sum_{m_x=-\infty}^{\infty} \exp \left[ -\pi^2 \beta m_x G_{x, x'} m_{x'} + i\pi j \sum_{b \in S_{xy}^d} D_b(x') m_{x'} \right], \quad (13)$$

where we have introduced the link Green functions  $G_{ll'}$  and  $D_l(x)$  (see [7]). Following strategy of [2], [3] one can use the dilute monopole gas approximation to perform summation over  $m_x$ . We skip all technical details which are well known. The resulting theory appears to be of the sin-Gordon type

$$\begin{aligned} \langle W(C) \rangle &= \exp \left[ -\frac{j^2}{4\beta} \sum_{bb' \in S_{xy}^d} G_{bb'} \right] \int \prod_x d\phi_x \exp \left[ -\frac{1}{2\beta} \sum_{x, n} (\phi_x - \phi_{x+n})^2 \right] \\ &\times \exp \left[ 2m^2 \sum_x \cos \left( \pi \phi_x + \pi j \sum_{b \in S_{xy}^d} D_b(x) \right) \right] \frac{1}{Z(0)}, \end{aligned} \quad (14)$$

where  $m^2$  is a mass of the dual photons (it is exponentially small in  $\beta$ ). To analyze this theory one can use the semiclassical approximation. The saddle-point equation is

$$\Delta \alpha(x) = 2\pi j \delta'(x) - m^2 \sin \alpha(x). \quad (15)$$

Far from the boundaries of the contour  $C$  the saddle-point equation (15) is essentially one dimensional and has the solution for  $j = 1$

$$\alpha(z) = \begin{cases} 4 \arctan(e^{-mz}), & z > 0 \\ -4 \arctan(e^{mz}), & z < 0. \end{cases}$$

Substituting this solution into (14) one can easily get the area law for the Wilson loop

$$\langle W_j(C) \rangle = e^{-\sigma(j=1)S}$$

with the string tension given by

$$a^2 \sigma(j=1) = \frac{8}{\sqrt{2\pi^2 \beta}} \exp \left[ -\frac{1}{2} \pi^2 \beta G_0 \right]. \quad (16)$$

Here,  $\beta = 1/(g^2 a)$  is dimensionless coupling constant and  $G_0 \approx 0.5054$  is zero-distance Green function. A rigorous proof of permanent confinement was given in [4]. It was shown that the semiclassical expression (16) gives lower bound on the string tension.

### 3.2 $SU(2)$ LGT. Representation for the Wilson loop

Here we would like to extend calculations of the previous section to  $SU(2)$  gauge theory. In doing this we use three approximations. First of all, we neglect connectors of the Bianchi identity because they do not contribute to the string tension in the leading orders of the strong coupling expansion. We thus assume that at weak couplings connectors produce smooth corrections to spin waves. The second approximation consists in an expansion of the Wilson loop in a power series  $1/\beta$ . Finally, we restrict ourselves to monopole configurations  $m = 0, \pm 1$ , precisely like for the  $U(1)$  model. At large  $\beta$ , and using first of our approximations one obtains from (9) the following expression

$$Z_{SU(2)} = \sum_{m(x)=-\infty}^{\infty} \int_{-\infty}^{\infty} \prod_{l,k} d\omega_k(l) \int_{-\infty}^{\infty} \prod_{x,k} d\alpha_k(x) \times \exp\left[-\frac{1}{2}\omega_k^2(l) - i\omega_k(l)(\alpha_k(x+e_n) - \alpha_k(x)) + 2\pi i\sqrt{2\beta} \sum_x \alpha(x)m(x)\right]. \quad (17)$$

Obviously, the last expression is an analog of the formula (11) for the  $U(1)$  model. However, even in this case all integrations cannot be done exactly due to non-linear couplings of monopoles with auxiliary fields.

As before,  $S_{xy}^d$  denotes some surface dual to the surface  $S_{xy}$  which is bounded by the loop  $C$ . Then, the expectation value of  $W(C)$  at  $\beta \rightarrow \infty$  we present in the form

$$\langle W_j(C) \rangle = \prod_{l \in S} \int_0^\pi \sin \alpha_l d\alpha_l \int_0^{2\pi} \frac{\varphi_l}{\sqrt{4\pi}} \text{TR}(C) H_j ,$$

where

$$H_j \equiv H_j(\alpha_l, \varphi_l) = \left\langle \prod_{l \in S} Q_j(l) \right\rangle \quad (18)$$

and

$$\text{TR}(C) = \sum_{m_l=-j}^j \prod_{l=1}^{\nu[S]} \frac{1}{2j+1} \sum_{\lambda, k} \sqrt{2\lambda+1} C_{jm}^{jn} {}_{\lambda k} Y_{\lambda k}(\alpha, \varphi) .$$

Here  $C_{a\alpha}^{c\gamma} {}_{b\beta}$  is the Clebsch-Gordan coefficient,  $Y_{\lambda k}$  is the spherical function and  $\nu(S)$  is a number of dual links that belong to the Wilson loop. Since at large  $\beta$  the plaquette matrix fluctuates smoothly around unit matrix  $\omega(l) \approx 0$  it is allowed to use asymptotics of  $Q_j(l)$  in (18) at  $\omega \approx 0$  uniformly valid in  $j$ . This asymptotics is

$$Q_j(l) = \exp[-ij_k(l)\omega_k(l)] ,$$

where

$$\omega_1 = \omega \cos \theta, \omega_2 = \omega \sin \theta \cos \phi, \omega_3 = \omega \sin \theta \sin \phi$$

and

$$j_1 = \sqrt{j(j+1)} \cos \alpha, j_2 = \sqrt{j(j+1)} \sin \alpha \cos \varphi, j_3 = \sqrt{j(j+1)} \sin \alpha \sin \varphi .$$

Introducing sources like

$$J_k(l) = \begin{cases} j_k(l)/\sqrt{2\beta}, & l \in S \\ 0, & l \notin S \end{cases} \quad (19)$$

the effective monopole theory can be written down as

$$H_j = \frac{1}{Z} \sum_{m(x)=-\infty}^{\infty} \int_{-\infty}^{\infty} \prod_{l,k} d\omega_k(l) \exp \left[ -\frac{\omega_k^2(l)}{2} - i\omega_k(l)[\alpha_k(x+e_n) - \alpha_k(x)] + 2\pi i\sqrt{2\beta} \sum_x \alpha(x)m(x) - iJ_k(l)\omega_k(l) \right]. \quad (20)$$

We use the following representation to perform the integration over  $\alpha_k(x)$

$$\begin{aligned} \sum_{m(x)=-\infty}^{\infty} \exp[2\pi i\sqrt{2\beta} \sum_x \alpha(x)m(x)] &= \sum_{m(x)=-\infty}^{\infty} \sqrt{m(x)} \left( 1 + \xi \frac{\partial}{\partial \xi} \right) \\ &\times \int \prod_{k=1}^3 d\sigma_k(x) \frac{\delta(m^2(x) - \sum_k \sigma_k^2(x))}{V(S^2)} \exp[i\xi \alpha_k(x)\sigma_k(x)] , \end{aligned} \quad (21)$$

where  $\xi = 2\pi\sqrt{2\beta}$ . Integration over  $\omega_k(l)$  and  $\alpha_k(x)$  gives

$$\begin{aligned} H_j &= H_j^{gl} H_j^{mon}, \\ H_j^{gl} &= \exp\left[-\frac{1}{4}J_k(l)G_{ll'}J_k(l')\right], \\ H_j^{mon} &= \frac{1}{Z} \sum_{m(x)=-\infty}^{\infty} \sqrt{m_x} \left(1 + \xi \frac{\partial}{\partial \xi}\right) \int \prod_{k=1}^3 d\sigma_k(x) \frac{\delta(\sum_k \sigma_k^2(x) - 1)}{V(S^2)} \exp[S_{eff}] \end{aligned} \quad (22)$$

where the effective action  $S_{eff}$  is of the form

$$S_{eff} = -\frac{1}{4}\xi_x m(x)\sigma_k(x)G_{xx'}\sigma_k(x')m(x')\xi_{x'} + \frac{i}{2}D_l(x)\xi_x m(x)\sigma_k(x)J_k(l).$$

Derivatives are calculated at  $\xi_x = \xi = 2\pi\sqrt{2\beta}$ . One proves that at large  $j$  this leads to the representation

$$\langle W_j(C) \rangle = \int_0^\pi \sin \alpha d\alpha \int_0^{2\pi} \frac{d\varphi}{\sqrt{4\pi}} H_j(\alpha, \varphi).$$

As is known the dual photon contribution  $H_j^{gl}$  produces only the perimeter law. In the next subsection we evaluate in the semiclassical approximation contribution of  $H_j^{mon}$  to the Wilson loop.

### 3.3 $SU(2)$ LGT. Sine-Gordon type model

In order to perform the summation over monopole configurations  $m_x = 0, \pm 1$  we follow the strategy of Refs.[4], [11]. Using decomposition

$$G_{xx'} = B_{xx'} + G_{xx'}(M),$$

where

$$\begin{aligned} G_{xx'}(M) &= \frac{1}{L^3} \sum_{k_n} \frac{e^{\frac{2\pi}{L}k_n(x-x')_n}}{3 - \sum_n \cos[\frac{2\pi}{L}k_n] + \frac{1}{2}M^2}, \\ G_{xx'} &= G_{xx'}(M=0), \quad B_{xx'} = G_{xx'} - G_{xx'}(M) \end{aligned}$$

we rewrite the effective action in the form ( $\eta_k(x) = \xi_x m(x)\sigma_k(x)$ )

$$\begin{aligned} S_{eff} &= -\frac{1}{4}\eta_k(x)B_{xx'}\eta_k(x') - \frac{1}{4}G_0 \sum_x \xi_x^2 m_x^2 \\ &\quad - \frac{1}{4} \sum_{x \neq x'} \eta_k(x)G_{xx'}(M)\eta_k(x') + \frac{i}{2}D_l(x)\eta_x J_k(l). \end{aligned} \quad (23)$$

The first term in (23) is presented as

$$\begin{aligned} \exp\left[-\frac{1}{4}\eta_k(x)B_{xx'}\eta_k(x')\right] &= (\det B_{xx'}^{-1})^{3/2} \\ &\times \int_{-\infty}^{\infty} \prod_{x,k} d\alpha_k(x) \exp[-\alpha_k(x)B_{xx'}^{-1}\alpha_k(x') + i\alpha_k(x)\eta_k(x)]. \end{aligned} \quad (24)$$

The behaviour of  $G_{xx'}(M)$  in the thermodynamic and continuum limits is well known

$$G_{xx'}(M) = \frac{2}{\pi R} e^{-MR/2}, \quad R = \left[ \sum_k (x_k - x'_k)^2 \right]^{1/2}. \quad (25)$$

This behaviour allows us to keep only self-energy of monopoles if  $MR \gg 1$ , i.e. the term

$$S_{eff}^{SE} = -\frac{1}{4}G_0(M)\xi^2 \sum_x m_x^2. \quad (26)$$

Inserting (24) into (23) and taking into account (26) one can integrate out  $\sigma_k(x)$ . After taking all derivatives we keep in the sums over monopoles only configurations  $m = 0, \pm 1$ . This finally gives the effective model which appears to be of the sine-Gordon type

$$H_j^{mon} = \int_{-\infty}^{\infty} \prod_{x,k} d\alpha_k(x) \exp \left[ -\alpha_k(x)B_{xx'}^{-1}\alpha_k(x') + \gamma \sum_x V[\alpha(x)] \right],$$

where

$$V[\alpha(x)] = \cos \xi \mu(x) - \frac{1}{2} G_0(M) \xi \frac{\sin(\xi \mu(x))}{\xi \mu(x)},$$

$$\gamma = 2 \exp[-2\pi^2 \beta G_0(M)], \quad \mu(x) = \left( \sum_k \mu_k^2(x) \right)^{1/2},$$

$$\mu_k(x) = \alpha_k(x) + \frac{1}{2} D_l(x) J_k(l).$$

Collecting all formulae together we get for the Wilson loop

$$\langle W_j(C) \rangle = \exp \left[ -\frac{1}{4} J_k(l) G_{ll'} J_k(l') \right] \int_0^\pi \sin \alpha d\alpha \int_0^{2\pi} \frac{d\varphi}{\sqrt{4\pi}} H_j^{mon}. \quad (27)$$

Making use of the fact that  $B_{xx'}^{-1}(M) \approx G_{xx'}^{-1}$  for  $M$  sufficiently large, one obtains after a shift

$$\alpha_k(x) \rightarrow \alpha_k(x) - \frac{1}{2} \sum_l D_l(x) J_k(l) \equiv \alpha_k(x) - h_k(x) \quad (28)$$

the following expression for the monopole contribution

$$H_j^{mon} = \int_{-\infty}^{\infty} \prod_{x,k} d\alpha_k(x) \exp[-S_{eff}^m], \quad (29)$$

where

$$S_{eff}^{mon}[\alpha_k(x)] = -[\alpha_k(x) - h_k(x)] G_{xx'}^{-1} [\alpha_k(x') - h_k(x')] + \gamma \sum_x V[\alpha(x)], \quad (30)$$

$$V[\alpha(x)] = \cos \xi \alpha(x) - \frac{1}{2} G_0(M) \xi \frac{\sin(\xi \alpha(x))}{\alpha(x)}. \quad (31)$$

To make semiclassical calculations we take the continuum limit. In this limit the saddle-point equation reads

$$\Delta \alpha_k(x) = 2\pi \mu_k(x) - m^2 \frac{\alpha_k(x)}{\alpha(x)} W[\alpha(x)], \quad (32)$$

$$\mu_k(x) = \sum_{l \in S} j_k(l) \theta(l) = \sum_{y \in S} j_k(y, n) \theta_n(x - y),$$

where  $n$  is fixed and orthogonal to  $S$  and

$$\theta_n(x - y) = \begin{cases} -1, & x = y \\ +1, & x = y + n \\ 0, & \text{otherwise} \end{cases}.$$

Here we have introduced the Debye mass

$$m^2 = 16\pi^2 \beta \exp[-2\pi^2 \beta G_0(M)]. \quad (33)$$

In the continuum limit one has

$$W[\alpha(x)] = \sin \alpha(x) + 4\pi^2 \beta G_0(M) \left[ \frac{\cos \alpha(x)}{\alpha(x)} - \frac{\sin \alpha(x)}{\alpha^2(x)} \right],$$

$$\mu_k(x) = \int_{y \in S} dy j_k(y, n = 3) \delta'_3(x - y).$$

To find a solution of the saddle-point equation we insert the anzatz

$$\alpha_k(x) = j_k(z, n = 3) \alpha(z).$$

This gives

$$\Delta \tilde{\alpha}(z) = \pi(2j + 1) \delta'_z(z) - m^2 \left( \sin \tilde{\alpha}(z) + 4\pi^2 \beta G_0(M) \left[ \frac{\cos \tilde{\alpha}(z)}{\tilde{\alpha}(z)} - \frac{\sin \tilde{\alpha}(z)}{\tilde{\alpha}^2(z)} \right] \right),$$

where

$$\tilde{\alpha}(z) = (2j+1)\alpha(z) .$$

One can easily construct the approximate solution if one takes  $\beta G_0(M) \approx 0$ . Then for  $j = 1/2$  the saddle-point equation reduces to the form (15). It leads to the desirable area law

$$\langle W_j(C) \rangle = e^{-\sigma(j=1/2)S}$$

with the string tension

$$\sigma = \frac{4m}{\pi^2 \beta} .$$

The mass of dual photons are given in (33). This result coincides with that quoted in [11].

#### 4 Conclusion

In this paper we calculated nontrivial 2D theory for the expectation value of the Wilson loop at large values of  $\beta$  valid for all values of representations  $j$  and which takes into account both the dual photon and the monopole contributions. For the fundamental representation in the semiclassical approximation we have found that the Wilson loop obeys the area law and  $\sigma(j = 1/2) \sim m$ . The most important conclusion is that the monopole contribution is sufficient to produce the area law and thus to explain confinement in 3D nonabelian models. It remains unclear at the moment if this contribution is also necessary condition of confinement. Another open problem is to compute the Wilson loop in the adjoint representation. It is well known that the adjoint string tension vanishes at large distances therefore it is important to understand if the proposed mechanism of confinement is able to reproduce this essential feature of the theory.

#### References

- [1] J. Greensite, *Prog.Part.Nucl.Phys.* **51**, 1 (2003).
- [2] A.M. Polyakov, *Nucl.Phys.* **B120**, 429 (1977).
- [3] T. Banks, J. Kogut, R. Myerson, *Nucl.Phys.* **B121**, 493 (1977).
- [4] M. Göpfert, G. Mack, *Commun.Math.Phys.* **82**, 545 (1982).
- [5] K. G. Wilson, *Phys.Rev.* **D10**, 2445 (1974).
- [6] M.B. Halpern, *Phys.Rev.* **D19**, 517 (1979); *Phys.Lett.* **B81**, 245 (1979); G. Batrouni, *Nucl.Phys.* **B208**, 467 (1982).
- [7] O. Borisenko, S. Voloshin, M. Faber, *Proc. of NATO Workshop *Confinement, Topology and Other Non-perturbative Aspects of QCD**, Ed. by J. Greensite and S. Olejnik, Kluwer Academic Publishers, 2002, 33 [hep-lat/0204028].
- [8] O. Borisenko, S. Voloshin, M. Faber, "Perturbation Theory for Non-Abelian Gauge Models in The Plaquette Formulation", Preprint of University of Technology of Vienna, IK-TUW-Preprint 0312401, 2003.
- [9] O. Borisenko, S. Voloshin, M. Faber, hep-lat/0508003.
- [10] O. Borisenko, V. Kushnir, A. Velytsky, *Phys.Rev.* **D62**, 025013 (2000).
- [11] F. Conrady, hep-th/0610238.